
Characterization, optimization and stabilization of the lighting quality aspects of high qualitative hybrid LED-lamps by development of transient LED models

Vom Fachbereich Elektrotechnik und Informationstechnik

der Technischen Universität Darmstadt

zur Erlangung des akademischen Grades eines

Doktor-Ingenieurs (Dr.-Ing)

genehmigte Dissertation

von

Quang Vinh Trinh, M.Sc.

Geboren am 04. Januar 1982

in Haiphong / Vietnam

Referent: Prof. Dr.-Ing. habil. Tran Quoc Khanh

Korreferent: Prof. Dr. rer. nat. Wolfgang Erich Elsässer

Tag der Einreichung: 10. 4. 2013

Tag der mündlichen Prüfung: 10. 9. 2013

D17

Darmstadt 2013

Erklärung zur Dissertation

Hiermit versichere ich, die vorliegende Dissertation ohne Hilfe Dritter nur mit den angegebenen Quellen und Hilfsmitteln angefertigt zu haben. Alle Stellen, die aus Quellen entnommen wurden, sind als solche kenntlich gemacht. Diese Arbeit hat in gleicher oder ähnlicher Form noch keiner Prüfungsbehörde vorgelegen.

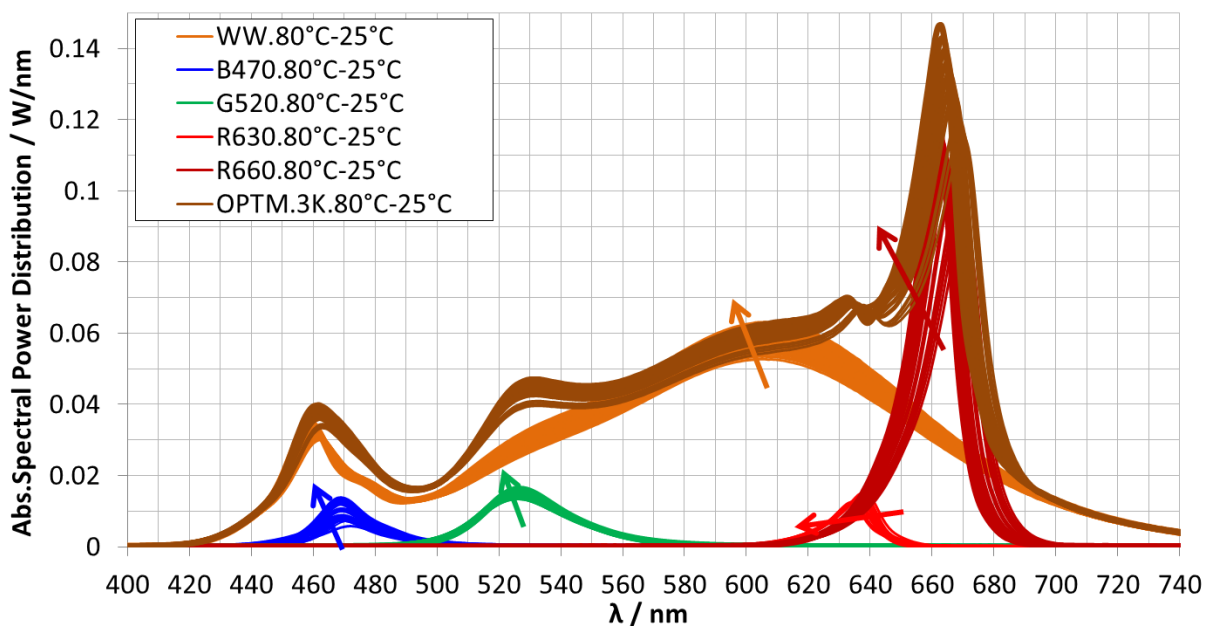
Darmstadt, den 10. April 2013

(Trinh Quang Vinh)

Abstract

Since year 1996, when NAKAMURA demonstrated his first InGaN blue LEDs that can be combined with luminescent materials to create high brightness phosphor converted LEDs (PC-LEDs), the third revolution of lighting with LEDs had begun officially. Nowadays, the luminous efficacy of some cold white PC-LEDs can achieve a value of about 140 lm/W. Moreover, by an appropriate combination of color semiconductor LEDs and white PC-LEDs in hybrid LED-lamps, their spectra can be controlled dynamically. However, unfortunately the optical, radiant and colorimetric properties of LEDs vary strongly according to their forward current and their operating temperature. Consequently, it will be impossible to manufacture good and stable quality solid state luminaires, as well to optimize and stabilize their spectra, if LED properties are not characterized appropriately by transient LED models.

Therefore, in this thesis the variation of LED properties must be investigated practically and the intrinsic physical and chemical phenomena taking place inside LEDs must be studied entirely. Hence, the difficulties in the applying, control and operation of LEDs will also be recognized. As well, the accurate characterization for the properties of LEDs by the development of the transient LED models will be carried out. Then, these transient LED models will be applied for the optimization and stabilization of the lighting quality aspects of high qualitative hybrid LED-lamps adapted to the colored surface objects. In that, an available LED combination with optimized / stabilized algorithms in the microcontrollers of hybrid LED-lamps will make the solid state luminaires achieve the high and stable lighting quality with the high luminous efficacy and the optimal spectra possible. In addition, color objects in the lighting application must also be identified specifically by their spectral reflectance distributions. As a result, the adaptive and optimal control factors will create the high qualitative hybrid LED-lamps that can satisfy the lighting demand of the color objects. Finally, high quality solid state lighting systems with these hybrid LED-lamps are the main aim of the thesis.

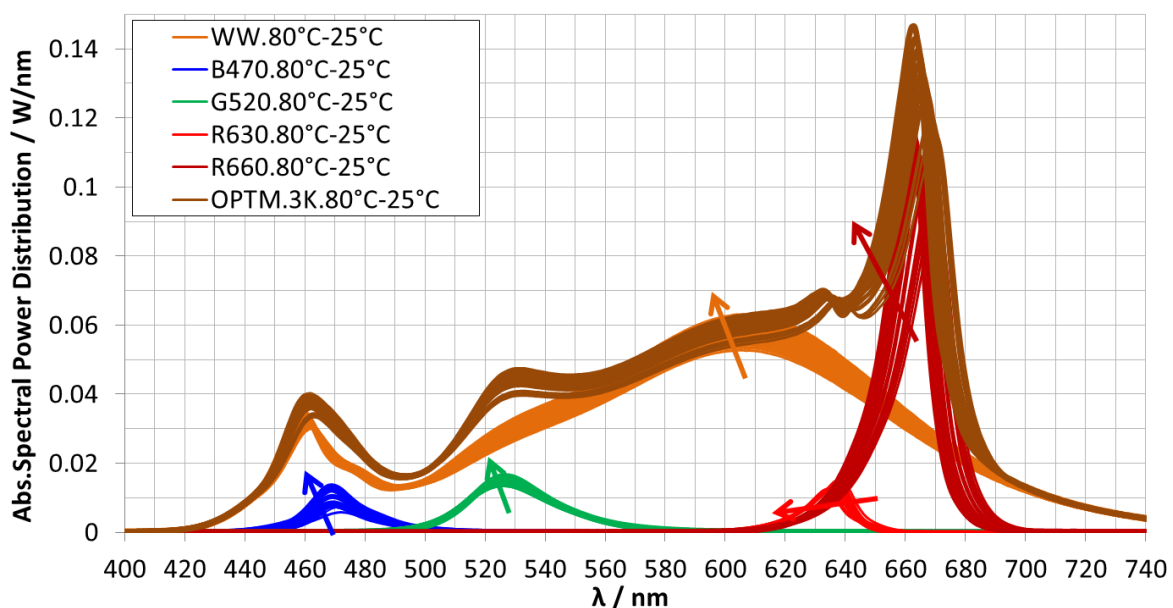


The optimization and stabilization for a hybrid LED-lamp in the shop lighting with operating temperatures from 25 °C to 80 °C

Kurzfassung

Seit 1996, als NAKAMURA seine ersten InGaN blauen LEDs demonstrierte, die mit lumineszierenden Materialien kombiniert werden können, um die weißen leuchtstoff-basierten Hochleistungs-LEDs (PC-LEDs) herzustellen, begann die dritte weltweite Revolution der Beleuchtung mit LEDs. Derzeit kann die Lichtausbeute von kaltweißen PC-LEDs einen Wert von etwa 140 lm/W erreichen. Außerdem können ihre Spektren dynamisch durch eine geeignete Kombination von farbigen LEDs und weißen PC-LEDs in hybriden LED-Lampen gesteuert werden. Doch variieren die optischen, lichttechnischen und farbtechnischen Eigenschaften der LEDs stark mit ihren Strömen und Betriebstemperaturen. Folglich wird es unmöglich, gute und stabile Halbleiter-Lichtquellen herzustellen sowie ihre Spektren zu optimieren und zeitlich zu stabilisieren, wenn die LED-Eigenschaften nicht vorher angemessen durch transiente LED Modelle charakterisiert wurden.

Deshalb müssen die Variationen der LED-Eigenschaften praktisch in dieser Arbeit untersucht werden und die intrinsischen physikalischen und chemischen Phänomene der LEDs vollständig studiert werden. Dadurch werden die Schwierigkeiten bei der Anwendung, Steuerung und Bedienung der LEDs auch erkannt. Auch wird die genaue Charakterisierung der Eigenschaften von LEDs durch Entwicklung der transienten LED-Modelle durchgeführt werden. Dann werden diese transienten LED-Modelle zur Optimierung und Stabilisierung der Lichtqualität-Aspekte der qualitativen hybriden LED-Lampen angewendet werden, um die Farbobjekte anzupassen. Dies führt zu einem Aufbau einer LED-Kombination mit optimierten / stabilisierten Algorithmen in den Mikrokontrollern hybrider LED-Lampen bezüglich hoher und stabiler Lichtqualität, die eine hohe Lichtausbeute und optimale Spektren aufweisen. Zusätzlich müssen die farbigen Oberflächenobjekte in den Beleuchtungsanwendungen speziell durch ihre spektralen Reflexionsgrade betrachtet werden. Folglich werden die adaptiven und optimalen Einstellungsfaktoren für die LED-Lichtquellen hergeleitet, so dass die LED-Lichtquellen die Anforderungen bezüglich hoher Farbqualität der Beleuchtung vorher definierter Farbobjekte erfüllen können. Die theoretische und praktische Auslegung hochwertiger Halbleiter-Beleuchtungssysteme mit hybriden LED-Lampen bildet das Hauptziel dieser Arbeit.



Optimierung und Stabilisierung für eine hybride LED-Lampe in der Shop-Beleuchtung für Betriebstemperaturen von 25 °C bis 80 °C

Preface

This dissertation is the result of my 4-year study and research in the LABORATORY OF LIGHTING TECHNOLOGY - TECHNISCHE UNIVERSITÄT DARMSTADT. Beside the personal attempts, the results are achieved by the direct and indirect contribution of many people to the dissertation. Therefore, I would like to express my deep gratitude to them.

Firstly, I would like to express my gratitude to Prof. Dr.-Ing. habil. TRAN QUOC KHANH, the supervisor and leader of the Laboratory. I would thank for his greatest support all through my dissertation with his scientific supervision, inspiration and effective working plan throughout the 4-years. As well, I am very grateful for his support in formalities and finance for my study in Germany.

I thank Prof. Dr. rer. nat. WOLFGANG ERICH ELSÄBER for his interest and for acting as the co-advisor.

I thank the 322-PROJECT of the VIETNAMESE MINISTRY OF EDUCATION AND TRAINING (MOET) for the financial support for my basic living cost and the WORLD UNIVERSITY SERVICE - DEUTSCHES KOMITEE E.V. (WUS) on behalf of MOET and the HESSEN STATE MINISTRY OF HIGHER EDUCATION, RESEARCH AND THE ARTS (HMWK) for the formality support at the beginning of and during my study.

I would like to express my gratitude to all my colleagues in the LABORATORY OF LIGHTING TECHNOLOGY for their helps and comments, a very efficient team-working culture and many useful discussions. Especially, I would like to thank Dr. -Ing. habil. PETER BODROGI for his important advice for my dissertation.

I am very grateful to my parents and my wife for their support, encouragement and especially take care of my son and daughter during my study.

After all the support, I had been given, it was really happy in my preface to be able to express my gratitude one more time, especially to my great supervisor who had shared his immeasurable knowledge and precious time with me, and to my tolerant family members who had supported me through every step of the progress!

Darmstadt, April 10th 2013

Trinh Quang Vinh

Table of Contents

Erklärung zur Dissertation	I
Abstract	II
Kurzfassung	III
Preface	IV
Table of Contents	V
Table of Figures	VIII
Tables	XIV
1. Introduction	1
1.1. Brief classification and development history of LEDs	1
1.1.1. Classification of LEDs	1
1.1.2. Overview history of LEDs	3
1.2. Current development status of LEDs in solid state lighting applications,	5
problems and motivations	5
1.2.1. Current development status of LEDs.....	6
1.2.2. Problems and motivations	8
1.3. Concept and structure of the thesis	8
1.3.1. Concept of the thesis	8
1.3.2. Structure of the thesis	9
1.4. Summary.....	11
2. Basic knowledge of LEDs	12
2.1. Basic knowledge about the intrinsic phenomena inside color semiconductor LEDs	12
2.1.1. Injection luminescence	12
2.1.2. Homo - junction, hetero-junction and quantum well	13
2.1.3. Recombination	17
2.1.4. Efficiency	20
2.1.5. Input condition and output spectrum of color semiconductor LEDs	22
2.2. Input condition and output spectrum of phosphor converted LEDs.....	26
2.2.1. Brief explanation about the basic principle.....	27
of the spectral conversions inside a luminescent material layer	27
2.2.2. Phosphor temperature and output spectrum of PC-LEDs.....	27
with a thermal quenching mechanism.....	27
2.2.3. Excitation spectrum and output spectrum of PC-LEDs.....	29
2.2.4. Summary	30
2.3. General summary	31
3. Optical, radiant and colorimetric properties of LEDs	32
3.1. Motivation.....	32
3.2. Concepts of lighting qualities and their limited range in the thesis	32
3.3. Optical, radiant and colorimetric properties of typical color semiconductor LEDs	34
3.3.1. General Consideration	34

3.3.2. Temperature and current dependence of the color semiconductor LED spectra	35
3.3.3. Temperature and current dependence of peak wavelengths.....	37
and full width at half maximum wavelengths of the color semiconductor LEDs	37
3.3.4. Temperature and current dependence of radiant fluxes.....	38
and radiant efficiencies of the color semiconductor LEDs	38
3.3.5. Temperature and current dependence of color differences.....	41
of the color semiconductor LEDs	41
3.4. Optical, radiant and colorimetric properties of warm white PC-LEDs	43
3.4.1. General Consideration.....	43
3.4.2. Temperature and current dependence of warm white PC-LED spectra.....	44
3.4.3. Current limits of color rendering indexes, luminous efficacies.....	46
and whiteness of warm white PC-LEDs	46
3.4.4. Temperature and current dependence of luminous fluxes.....	49
and luminous efficacies of warm white PC-LEDs.....	49
3.4.5. Temperature and current dependence of color differences of warm white PC-LEDs	51
3.4.6. Temperature and current dependence of correlated color temperatures.....	53
of warm white PC-LEDs.....	53
3.4. Summary.....	55
4. A minimization solution to parameter differences between LED-	57
and LED-luminaire manufacturers.....	57
4.1. Motivation.....	57
4.2. A demonstration example for a simple minimization solution	58
4.2.1. Definition of essential quality categories in the real performance	58
4.2.2. Parameters of the energy category	59
4.2.3. Parameters of the color quality category	64
4.2.4. Further development	68
4.3. Summary.....	70
5. Junction temperature determination, thermal transient identification.....	71
and thermal map decoding of LEDs.....	71
5.1. General Consideration.....	71
5.2. Determination of LED junction temperature	78
5.2.1. Measurement methods and procedures of the LED junction temperature determination ...	78
5.2.2. Comparison between the cooling and heating measurement procedures	80
5.2.3. Causes of inaccuracy and improvement proposals.....	83
5.3. Thermal transient identification and thermal map decoding of LEDs.....	85
5.3.1. Mathematical background for thermal circuits	85
5.3.2. Study and analysis of the current well-known identification and decoding solution	89
5.3.3. A demonstration example for the thermal transient identification.....	93
and the thermal map decoding of some cold white PC-LEDs based on a new solution.....	93
5.4. Summary.....	99
6. Transient LED Model	101
6.1. Motivation.....	101
6.2. General Consideration.....	102
6.3. Electrical transient LED model	103
6.3.1. Theoretical approach for an ideal diode	103

6.3.2. Modern and experimental approaches.....	105
6.3.3. Experimental proposal of the limited electrical transient LED model	109
6.4. Optical transient LED model	113
6.4.1. General Consideration.....	113
6.4.2. Overview of the optical transient LED models of color semiconductor LEDs.....	114
and white PC-LEDs.....	114
6.4.3. Investigations and proposals for the optical transient LED models.....	121
of color semiconductor LEDs	121
6.4.4. Investigation and proposal for the optical transient LED models of white PC-LEDs.....	130
6.5. General Summary	135
7. Optimization and stabilization for some lighting quality aspects.....	136
of hybrid LED-lamps adapted to color objects	136
7.1. Motivation and general consideration.....	136
7.1.1. Motivation	136
7.1.2. General Consideration.....	137
7.2. Demonstration example of the optimization for some lighting quality aspects.....	138
of the hybrid LED-lamp adapted to the color objects.....	138
7.2.1. LED combination and LED selection of the LED-lamps	138
7.2.2. The optimization for the oil color index of the hybrid LED-lamp.....	140
adapted to oil color paintings.....	140
7.2.3. Establishment of new standard reflectance curves for the museum lighting.....	148
7.3. Demonstration example of the stabilization.....	161
for some lighting quality aspects of the hybrid LED-lamp adapted to the color objects.....	161
7.3.1. Temperature dependence of some lighting quality parameters of the hybrid LED-lamps ..	161
7.3.2. Description of a control system structure for the stabilization.....	166
of some lighting quality parameters and the improvement.....	166
of other lighting quality parameters	166
7.3.3. Results.....	168
7.4. Summary.....	170
8. Conclusions	171
List of Symbols.....	A
Abbreviation	G
Bibliography.....	J
Appendix A – Calculation of CIE Color Rendering Index.....	S
Appendix B – Calculation of CIECAM02	T
Appendix C – Name of oil color objects	U
Appendix D – Basic design for the 3000 K hybrid LED-Lamp.....	V
Appendix E – Basic design for the 4000 K hybrid LED-Lamp	Y
Appendix F – Investigation for neutral white PC-LEDs.....	BB
Appendix G – Investigation for cold white PC-LEDs	FF
Appendix H – Data for the comparison between the cooling and heating procedure.....	JJ
Veröffentlichungen.....	MM
Lebenslauf	NN

Table of Figures

Figure 1.1 - Available semiconductor materials for high brightness color LEDs ([4]).....	5
Figure 1.2 - Progress of the luminous efficacy of white PC-LEDs in several recent years	6
Figure.1.3 - Progress of white OSRAM PC-LEDs in 2012 ([2])	7
Figure 2.1 - Energy diagram of an ideal color semiconductor LED in unbiased state.....	12
Figure 2.2 - Energy diagram of an ideal color semiconductor LED in biased state.....	13
Figure 2.3 - Structure of a single hetero - junction with the increase.....	15
of potential barrier ΔE_v for p-carriers and the decrease.....	15
of potential barrier ΔE_c for n-carriers ([14])	15
Figure 2.4 - Double hetero - junction with bidirectional injection ([14])	15
Figure 2.5 - A quantum well with an electron trapped in its structure ([14])	16
Figure 2.6 - Direct recombination in a material with a direct band-gap (GaN) ([125])	17
Figure 2.7 - Indirect recombination in a material with an indirect band-gap (SiC) ([125])	18
Figure 2.8 - Radiative (a) and non-radiative recombination (b) in the host lattice of LEDs ([1]).....	18
Figure 2.9 - a) Non-radiative recombination at the deep level, b) Auger recombination and	19
c) Radiative recombination ([1])	19
Figure 2.10 - Carrier density of n and p particles as functions of time in the recombination ([1])	20
Figure 2.11 - Total reflections in a LED material layer ([14])	21
Figure 2.12 - Some structural forms of LED capsules in order to improve output light ([14])	21
Figure 2.13 - Radiative recombination mechanics of electron-hole pairs ([1]).....	24
Figure 2.14 - Theoretical emission spectrum of a color semiconductor LED ([1]).....	26
Figure 2.15 - Thermal quenching and its mechanism in $Y_3Al_5O_{12}:Ce^{3+}$ and $CaAlSiN_3:Eu^{2+}$ ([17])	28
Figure 2.16 - An example in case of donor-acceptor pair luminescence.....	30
of GaP doped with ZnS ([18])	30
Figure 3.1 - Current lighting situation ([30])	33
Figure 3.2 - New concepts for lighting quality ([30])	33
Figure 3.3 - Temperature dependence of the spectra of four color semiconductor LEDs at 350 mA.....	36
Figure 3.4 - Current dependence of the spectra of four color semiconductor LEDs at 80 °C.....	37
Figure 3.5 - Temperature dependence of color LED radiant fluxes.....	39
and radiant efficiencies at 350 mA.....	39
Figure 3.6 - Current dependence of color LED radiant fluxes and radiant efficiencies at 80 °C	40
Figure 3.7 - Color differences of the color semiconductor LEDs as a function of temperature	41
Figure 3.8 - Color differences of color semiconductor LEDs as a function of current.....	42
Figure 3.9 - Temperature dependence of six typical warm white LEDs.....	44
(2700 K < CCT < 3500 K) of different LED manufacturers at 350 mA.....	44
Solid lines correspond with 40 °C, dashed lines with 80 °C, respectively.	44
Figure 3.10 - Current dependence of six typical white warm white LEDs.....	45
(2700 K < CCT < 3500 K) of different LED manufacturers at 80 °C.....	45
Solid lines correspond with 350 mA, dashed lines with 700 mA, respectively.	45
Figure 3.11 - Color rendering indexes (R_a , R_9 and AVR_{1-14}).....	47
and luminous efficacies of some current warm white PC-LEDs.....	47
(2700 K < CCT < 3000 K) at 350 mA and 80 °C.....	47

Figure 3.12 - Color rendering indexes (R_a , R_9 and AVR_{1-14}) and luminous efficacies.....	47
of some current warm white PC-LEDs ($3000\text{ K} < CCT < 3500\text{ K}$).....	47
at 350 mA and 80 °C.....	47
Figure 3.13 - Whiteness of some current warm white PC-LEDs ($2700\text{ K} < CCT < 3000\text{ K}$).....	48
at 350 mA and 80 °C.....	48
Figure 3.14 - Whiteness of some current warm white PC-LEDs ($3000\text{ K} < CCT < 3500\text{ K}$).....	49
at 350 mA and 80 °C.....	49
Figure 3.15 - Temperature dependence of luminous fluxes and luminous efficacies.....	50
of six typical warm white PC-LEDs of different LED manufacturers at 350 mA.....	50
Figure 3.16 - Current dependence of luminous fluxes and luminous efficacies.....	51
of six typical warm white PC-LEDs of different LED manufacturers at 80 °C.....	51
Figure 3.17 - Temperature dependence of color differences.....	52
of six typical warm white PC-LEDs at 350 mA.....	52
Figure 3.18 - Current dependence of color differences of six typical warm white PC-LEDs at 80 °C.....	53
Figure 3.19 - CCT change of some warm white PC-LEDs at different temperatures and 350 mA.....	54
Figure 3.20 - CCT change of some warm white PC-LEDs at different forward currents and 80 °C.....	55
Figure 4.1 - Relative luminous fluxes as functions of operating temperature.....	59
at different forward currents.....	59
Figure 4.2 - Relative luminous fluxes as functions of forward current.....	60
at different operating temperatures.....	60
Figure.4.3- Relative luminous flux as a three-dimensional function.....	61
of operating temperature and current.....	61
Figure.4.4- Verification for the correct characterization of the luminous flux function.....	61
and the binning quality.....	61
Figure.4.5- Relative radiant flux as a three-dimensional function.....	63
of operating temperature and current.....	63
Figure.4.6- Relative forward voltage as a three-dimensional function.....	64
of operating temperature and current.....	64
Figure.4.7- Relative CCT as a three-dimensional function of operating temperature and current.....	65
Figure.4.8 - CRI_a as a three-dimensional function of operating temperature and current.....	66
Figure 4.9 - $R_1 - R_{14}$, R_a and AVR_{1-14} as functions of operating temperature and current.....	66
Figure 4.10 - Chromaticity u' and v' as functions of operating temperature and current.....	67
Figure 4.11 - Color differences as functions of operating temperature.....	68
in the cold binning at different currents.....	68
Figure 4.12 - Color differences as functions of operating temperature.....	69
in the hot binning at different currents.....	69
Figure 5.1 - Multi-input multi-output system model of a solid state lighting structure.....	72
Figure 5.2 - Color mixing principle and conservation law of energy in PC-LEDs.....	73
Figure 5.3 - Thermal transient LED model as a single-input single-output system (SISO system).....	74
Figure 5.4 - Thermal structure of an OSRAM GOLDEN DRAGON LED ([40]).....	75
Figure 5.5 - Equivalent thermal circuit of a GOLDEN DRAGON LED ([40]).....	76
Figure 5.6 - Structure of single layer MCPCB and structure of a heat sink component of LEDs ([40]).....	76
Figure 5.7 - Substrate area dependence of $R_{th,BA}$ ([40]).....	77
Figure 5.8 - Heating measurement procedure.....	79
Figure 5.9 - Cooling measurement procedure.....	79
Figure 5.10 - Measurement system in TECHNISCHE UNIVERSITÄT DARMSTADT.....	80

Figure 5.11 - Direct comparison of the $V_f(T_j)$ properties measured.....	81
by the heating and cooling procedures	81
Figure 5.12 - Procedures of an indirect comparison	82
Figure 5.13 - System structure diagram of simple static thermal models of the cooling and heating ...	83
Figure 5.14 - Properties $V_f(T_s)$ of the cooling and heating thermal models.....	83
and practical DC measurement results	83
Figure 5.15 - First order equivalent thermal circuit for a general material layer	85
Figure 5.16 - Second order equivalent thermal circuit for two material layers in a serial connection...	87
Figure 5.17 - n^{th} order equivalent thermal circuit for n material layers in a serial connection.....	88
Figure 5.18 - Absolute spectral power distributions of the cold white PC-LED (5000 K)	93
Figure 5.19 - Thermal impedance functions of three cold white LEDs (5000 K) at 700 mA and 40 °C .	94
Figure 5.20 - Thermal impedance functions of three cold white LEDs (5000 K) at 700 mA and 80 °C .	95
Figure 5.21 - Derivative functions of the thermal impedances.....	96
of three cold white LEDs (5000 K) at 700 mA.....	96
Figure 5.22 - A simulated two stage thermal RC circuit as a demonstration example.....	97
for the evaluation of the accuracy of the exponential interpolation.....	97
and the EUCLIDEAN decoding method	97
Figure 5.23 - The transient thermal response of the simulated two stage thermal RC circuit	98
Figure 6.1 - System structure diagram of a suggested LED system.....	101
with a very good color sensor for the control and the optimization.....	101
of some lighting quality parameters in ([63]) as a reference example.....	101
Figure 6.2 - Spectral comparison between color spectra of a MTCS sensor.....	102
and the referent standard color curves (CIE, 1964) under the angle of 10°	102
at TECHNISCHE UNIVERSITÄT DARMSTADT.....	102
Figure 6.3 - A multi-input single-output subsystem model for electrical transient LED models	102
Figure 6.4 - A multi-input multi-output subsystem model for optical transient LED models.....	103
Figure 6.5 - a) Bending of dislocation b) Surface V-defect (left).....	108
and “internal” V-defect (right) ([85])	108
Figure 6.6 - Small signal equivalent circuit matching an InGaAlP LED.....	109
at the forward current of 0.9 mA ([66])	109
Figure 6.7 - Nearly linear functional relationship between forward voltage.....	111
and junction temperature with minimal, average, maximal values.....	111
and 95 % confidence offset of 20 similar cold white LEDs (5000 K)	111
Figure 6.8 - Logarithmic functional relationship between forward voltage.....	111
and junction temperature with minimal, average, maximal value.....	111
and 95 % confidence offset of 20 similar cold white LEDs (5000 K).....	111
Figure 6.9 - Three-dimensional electrical transient LED model and measured values.....	112
of cold white LEDs	112
Figure 6.10 - Spectral changes and influence factors in PC-LEDs	113
Figure 6.11- Description of the double GAUSSIAN model for the green semiconductor LED (a).....	115
and the white PC-LED (b) at $T_j=25$ °C and $I_f=350$ mA. For the LED,.....	115
the blue and phosphor spectral components were individually considered.....	115
by two double functions G_B and G'_B and G_F and G'_F , respectively according to ([105])	115
Figure 6.12 - Comparison between simulated and measured spectral results.....	118
of the color semiconductor LED for the case of 10 mA and 76.8 °C (a).....	118
and the case of 20 mA and 104.7 °C (b) according to ([103])	118

Figure 6.13 - Absolute spectral power distributions of the investigated blue semiconductor LED.....	121
at forward currents of 350 mA, 700 mA and 1000 mA and temperatures.....	121
of 25 °C, 55 °C, 85 °C and 100 °C	121
Figure 6.14 - Fitting of the spectrum of the blue semiconductor LED at the current of 350 mA.....	122
and the PCB temperature of 25 °C as a demonstration example.....	122
with different high order GAUSSIAN functions	122
Figure 6.15 - Interface of the program with imagines of many spectra.....	124
at different operating conditions.....	124
Figure 6.16 - Interface of the program for the import, interpolation and export of data	126
Figure 6.17 - Spectral comparison between measured and simulated absolute SPDs.....	127
of the blue LED 450 nm of Manufacturer C with the same current of 350 mA.....	127
and different sensor temperatures of 25 °C - 95 °C.....	127
as the first demonstration example of the influence of temperature factor.....	127
Symbols “Me.” and “Mo.” are to denote measured and modeled spectra, respectively.....	127
Figure 6.18 - Spectral comparison between measured and simulated absolute SPDs.....	128
of the blue LED 450 nm of Manufacturer C at the same sensor temperature of 80 °C.....	128
and different forward currents of 50 mA - 700 mA.....	128
as the second demonstration example of the influence of forward current factor.....	128
Symbols “Me.” and “Mo.” denote measured and modeled spectra, respectively.....	128
Figure 6.19 - Spectral comparison between measured and simulated absolute SPDs.....	129
of the deep red, red, royal blue, blue and green semiconductor LEDs.....	129
of three manufacturers (A, B and C) as a demonstration example.....	129
“Me.” and “Mo.” denote measured and modeled spectra respectively.....	129
“350.80.” denotes for 350 mA and 80 °C. And ”450”, “470”, “530”, “630” and.....	129
“660” denote LED peak wavelengths published in datasheets.....	129
Figure 6.20 - The chosen cold white PC-LED (5000 K) for the investigation.....	130
as a demonstration example	130
Figure 6.21 - Investigation for mathematical functions of horizontal spectral LED models.....	131
as an example	131
Figure 6.22 - Interface of the evaluating program for the cold white PC-LED.....	133
as a demonstration example	133
Figure 6.23 - Spectral comparison between measured and simulated absolute SPDs.....	134
of a typical low warm white (2700 K - B2.7K), high warm white (3000 K - C3K),.....	134
neutral white (4000 K - C4K) and cold white (5000 K - B5K).....	134
of two different manufacturers (B and C) as demonstration examples.....	134
Symbols “Me.” and “Mo.” denote measured and modeled spectra, respectively.....	134
And symbol “350.80.” denotes 350 mA and 80 °C.	134
Figure 7.1 - RAPHAEL’s “THE SCHOOL OF ATHENS”, 1510 - 11, VATICAN palace,.....	136
ROME published by HAAS, R. in ([109])	136
Figure 7.2 - Seventy nine well-known oil colors $RO_1 - RO_{79}$ of the oil paintings ([108]).....	141
Figure 7.3 - Spectral reflectance curves of some different types of the human skin ([154]).....	142
Figure 7.4 - Spectral reflectance curves of some different types of the human hair ([154]).....	143
Figure 7.5 - Spectral reflectance curves of some varied colored textiles ([154])	143
Figure 7.6 - Spectral reflectance curves of some different clothes ([154])	144
Figure 7.7 - Control system structure for the optimization of the hybrid LED-lamp	145

Figure 7.8 - Optimized absolute SPDs of cases 3000 K, 4000 K, 5000 K and 6500 K.....	146
for the museum lighting.....	146
Figure 7.9 - CRI quality of the optimized spectra	147
Figure 7.10 - CQS quality of the optimized spectra	148
Figure 7.11 - Classification of the oil color objects by CAM02-UCS and comparison with CIE CRIs ...	149
Figure 7.12 - Establishment principle for the new candidate reflectance curve of each color group...	151
Figure 7.13 - Deep red group, its deep red candidate (ROG_1) and the matching R_1 (TCS_1)	152
Figure 7.14 - Strong red group, its strong red candidate (ROG_2) and matching R_9 (TCS_9).....	153
Figure 7.15 - Light yellowish pink group, its light yellowish pink candidate (ROG_3).....	153
and matching R_{13} (TCS_{13}).....	153
Figure 7.16 - Skin color group, its skin color candidate (ROG_4) and no matching CIE TCS	153
Figure 7.17 - Yellow group, its yellow candidate (ROG_6) and no matching CIE TCS	154
Figure 7.18 - a) Dark grayish yellow group - its candidate (ROG_5) - matching R_2 (TCS_2),.....	154
b) Strong yellow green group - its candidate (ROG_7) - matching R_3 (TCS_3),.....	154
c) Strong yellow group - its candidate (ROG_8) - matching R_{10} (TCS_{10}),.....	154
d) Moderate olive green group - its candidate (ROG_9) - matching R_{14} (TCS_{14})	154
Figure 7.19 - a) Permanent green group - its candidate (ROG_{10}) - No matching CIE TCS,.....	155
b) Emerald green group - its candidate (ROG_{12}) - No matching CIE TCS,.....	155
c) Chromium oxide green group - its candidate (ROG_{12}) - R_4 (TCS_4) and R_{11} (TCS_{11}),...	155
d) Phthalate green group - its candidate (ROG_{13}) - No matching CRI,.....	155
e) Cobalt turquoise group - candidate (ROG_{14}) - R_5 (TCS_5),.....	155
f) Violet group - its candidate (ROG_{18}) - R_7 (TCS_7)	155
Figure 7.20 - Strong blue group, its strong blue candidate (ROG_{15}) and matching R_{12} (TCS_{12})	155
Figure 7.21 - Light blue group, its light blue candidate (ROG_{15}) and matching R_6 (TCS_6)	156
Figure 7.22 - Dark blue group, its dark blue candidate (ROG_{17}) and no matching CIE TCS	156
Figure 7.23 - Fourteen CIE standard reflectance curves	157
Figure 7.24 - Eighteen new candidate reflectance curves of TECHNISCHE UNIVERSITÄT DARMSTADT	157
Figure 7.25 - First offset between average new specific CRIs.....	160
(AVR.i.TUD-3K, AVR.i.TUD-4K, AVR.i.TUD-5K and AVR.i.TUD-65K).....	160
and new candidate CRIs (ROGi.TUD-3K, ROGi.TUD-4K, ROGi.TUD-5K.....	160
and ROGi.TUD-65K) in the cases of 3000 K, 4000 K, 5000 K and 6500 K, respectively ...	160
Figure 7.26 - Second offset between average new specific CRIs.....	160
(AVR.i.TUD-3K, AVR.i.TUD-4K, AVR.i.TUD-5K and AVR.i.TUD-65K).....	160
and CIE standard CRIs (Ri.TUD-3K, Ri.TUD-4K, Ri.TUD-5K and Ri.TUD-65K).....	160
in the cases of 3000 K, 4000 K, 5000 K and 6500 K, respectively.....	160
Figure 7.27 - Red objects in general shop lighting applications ([154])	162
Figure 7.28 - Optimized spectra for the red color index.....	163
of the warm white hybrid LED-lamp (3000 K).....	163
adapted to the red objects in general shop lighting applications.....	163
with varied LEDs of three different manufacturers (A, B and C).....	163
as well as their combinations at 80 °C and 700 mA.....	163
and three original warm white spectra	163
Figure 7.29 - Color quality of six optimized LED-lamps at 80 °C and 700 mA.....	164
and three original warm white LEDs at 80 °C.....	164
and 350 mA (A.3000K and B.2700K) or 700 mA (C.3000K).....	164

Figure 7.30 - Luminous flux and luminous efficacy of six optimized LED-lamps at 80 °C.....	164
and 700 mA and three original warm white LEDs at 80 °C.....	164
and 350 mA (A.3000K and B.2700K) or 700 mA (C.3000K).....	164
Figure 7.31 - Temperature stability of CCTs and whiteness at different operating temperatures.....	165
Figure 7.32 - Temperature stability of the red color index and R_9	166
at different operating temperatures	166
Figure 7.33 - Control system structure	167
to stabilize some lighting quality parameters and improve.....	167
some other lighting quality parameters of the hybrid LED-lamp.....	167
Figure 7.34 - Control of the componential color spectra to stabilize.....	169
some lighting quality parameters	169

Tables

Table 3.1 - Temperature dependence of $\lambda_p / \lambda_{FWHM}$38 of red, green, blue and orange LEDs at 350 mA..... 38	38
Table 3.2 - Current dependence of $\lambda_p / \lambda_{FWHM}$ of red, green, blue and orange LEDs at 80 °C 38	38
Table 4.1 - Comparison between the calculated and measured results of luminous flux 62	62
Table 4.2 - Confidence 95 % of the LED binning group 62	62
Table 4.3 - The ratios of maximal/average and average/minimal of luminous flux 63	63
Table 4.4 - Comparison between the calculated and measured results of <i>CCT</i> 65	65
Table 4.5 - Color differences with different operating regions.....68 in the cold binning (350 mA and 25 °C) 68	68
Table 4.6 - Color differences with different operating regions.....70 in the hot binning (350 mA and 80 °C) 70	70
Table 5.1 - Parameters of some PCB substrates in a GOLDEN DRAGON LED ([40]) 76	76
Table 5.2 - $R_{th,SB}$ of substrate technologies with the standard geometry and size77 of a GOLDEN DRAGON LED ([40]) 77	77
Table 5.3 - FOSTER model parameters of the three cold white LEDs at 700 mA and 40 °C..... 94	94
Table 5.4 - FOSTER model parameters of three cold white LEDs at 700 mA and 80 °C..... 95	95
Table 5.5 - The FOSTER - CAUER transformation by means of the EUCLIDEAN algorithm.....98 for the simulated two stage thermal circuit as a demonstration example 98	98
Table 5.6 - Comparison and evaluation of the accuracy of the EUCLIDEAN algorithm.....99 and the exponential interpolation as a demonstration example..... 99	99
Table 5.7 - Decoded thermal maps of three cold white LEDs (5000 K).....99 at 700 mA and 40 °C as an example..... 99	99
Table 5.8 - Decoded thermal maps of three cold white LEDs (5000 K).....99 at 700 mA and 80 °C as an example..... 99	99
Table 6.1 - Parameters of the BAUREIS LED model established by means.....109 of the high frequency technique ([66])..... 109	109
Table 6.2- Parameters of the standard model and approximated model..... 112	112
Table 6.2 - Examined approximation functions by the authors in ([103])..... 117	117
Table 6.3 - Comparison between simulated and measured results at 350 mA.....120 and 340 K for the color semiconductor LEDs given by the authors in ([106]) 120	120
Table 6.4 - Fitting constants of the second order GAUSSIAN function 122	122
Table 6.5 - Fitting parameters for the constants of the second GAUSSIAN function..... 123	123
Table 6.6 - Color differences between simulated and measured spectra.....124 at different operating conditions..... 124	124
Table 6.7 - Color differences between measured and simulated spectra.....127 of the blue LED 450 nm of Manufacturer C at the same forward current.....127 of 350 mA and different sensor temperatures of 25 °C - 95 °C.....127 as the first demonstration example of the influence of temperature factor 127	127
Table 6.8 - Color differences between measured and simulated spectra.....128 of the blue LED 450 nm of Manufacturer C.....128	128

	at the same sensor temperature of 80 °C and different forward currents.....	128
	of 50 mA - 700 mA as the second example of the influence of forward current factor	128
Table 6.9 -	Color differences between measured and simulated SPDs.....	129
	of the deep red, red, royal blue, blue and green semiconductor LEDs.....	129
	of three manufacturers (A, B, C) at 350 mA and 80 °C as a demonstration example	129
Table 6.10 -	Fitting parameters of the ninth GAUSSIAN function for the cold white PC-LED.....	132
	as an example	132
Table 6.11 -	Color differences between the simulated and measured spectra.....	133
	in different operating conditions.....	133
Table 6.12-	Color differences, CCTs, AVR. ₁₋₁₄ between measured and simulated spectra.....	135
	of the white PC-LEDs	135
Table 7.1 -	Relative quantitative evaluation of some possible LED combinations	139
Table 7.2 -	Eighteen oil color groups with matching oil color objects.....	150
	and fourteen CIE standard TCSs.	150
Table 7.3 -	Eighteen comparing groups ($Gr_{.1} - Gr_{.18}$) for the first offsets ($Offset_1$).....	159
	between 18 average new specific CRIs ($AVR_{Gr.1} - AVR_{Gr.18}$).....	159
	of 18 oil color groups and 18 new candidate CRIs.....	159
	and for the second offsets ($Offset_2$) between 18 average new specific CRIs.....	159
	and 14 matching CIE standard CRIs in the case.....	159
	of optimized warm white light source (3000 K).....	159
Table 7.4 -	Lighting quality parameters of the hybrid LED-lamp.....	169
	after applying the control algorithm	169

1. Introduction

The lighting industry has reached significant achievements in several recent years. In this progress, the solid state lighting played an essential role and dedicated huge benefits for the human life. Although the first light-emitting diodes (LEDs) had been invented and manufactured since early years in the 20th century with the discovery of electroluminescence and of appropriate semiconductor compounds, only low brightness color LEDs were able to be manufactured at the beginning. Consequently, these LEDs were mostly used in display and indicator applications. In the last 10 years, the high brightness LEDs became available, because the illumination and the efficiency of LEDs were improved considerably. However, the lighting quality of LEDs such as the short term stability and long term stability in different conditions of operating temperature and forward current, lifetime, color rendering indexes (CRIs), whiteness ($\Delta u'v'_{CT}$), correlated color temperature (CCT / K), circadian stimulus (CS), scotopic - photopic ratio (S/P) and other quality parameters of LEDs has not been considered appropriately in general lighting applications and especially in high quality lighting applications. In order to characterize, optimize and stabilize some quality aspects for LED - luminaires in high quality lighting applications adapted to color objects, the chapter 1 will classify the LEDs, summarize briefly about the history of LEDs, establish the general problems and propose the structure of the thesis.

1.1. Brief classification and development history of LEDs

In order to have a general overview of LEDs, in this section, LEDs will be briefly classified. Then, the development history of LEDs will be reviewed corresponding to the non-stopped revolutionizing of semiconductor materials. Thus, the entire framework of the development progress of LEDs will be recognized. As well, the current quality of LEDs and their development tendency will be updated to have a correct perception on the state-of-the-art LED technology for further researches in successive sections.

1.1.1. Classification of LEDs

Before the development history of LEDs is reviewed, it is necessary to classify LEDs briefly. Particularly, LEDs should be sorted into different groups or different types based on some criteria or the combination of some criteria. These criteria can be power aspect, color aspect and semiconductor material aspect.

* **Power aspect:** Regarding the power aspect, the LED family can be classified into three different types including low power LEDs, medium power LEDs and high power LEDs. If the low power LEDs were used worldwide in indicator and display applications for a long time ago, the high power LEDs have been just available for lighting applications as an excellent achievement of the human kind in the lighting industry since 1999. Hence, a new era of the solid state lighting was opened for modern lighting applications. Otherwise, in recent several years, some LED manufacturers fabricated a new generation LED with medium power. Astonishingly, these medium power LEDs have become especially suitable due to both their cost and their technique in the television and display industry. Thus, it can be recognized obviously, that low power LEDs, medium power LEDs and high power LEDs could be combined together to fulfill all tasks of different applicable segments in the lighting industry.

* **Color aspect:** About color aspect, LEDs can be also classified into three different types including invisible semiconductor LEDs, visible color semiconductor LEDs and white PC-LEDs. Particularly, in invisible wavelength range, invisible semiconductor LEDs can be ultraviolet semiconductor LEDs with short wavelengths or infrared semiconductor LEDs with long wavelengths. In real applications, ultraviolet LEDs are usually used much in the process of drinking-water manufacturers for normal life activities or sterilized water manufacturers in health services. In addition, they are used in applications that require sterilization, in chip process or in some special biology and health fields. Otherwise, ultraviolet LEDs can be sometimes used in the fabrication of white phosphor converted LEDs (PC-LEDs). In another applicable segment, infrared LEDs are often applied in remote control devices, short distance communications, in some security or military applications or in some special biology and health fields.

In visible light wavelength range, conventional visible color LEDs can be violet, royal blue, blue, cyan, green, yellow, orange, red or deep red semiconductor LEDs. Since long time ago, these LEDs have been used mostly in indicators, displays, architectural lighting applications, decorative lighting applications or in general entertainment industry. Only in recent times, visible LEDs are also used much more in lighting applications in general and in high quality lighting applications in particular. Otherwise, blue semiconductor LEDs can be used to fabricate PC-LEDs, yellow, amber, orange and red semiconductor LEDs can be used for rear lamps or parking lamps in the automobile industry, and red, yellow, green LEDs are used in transport controlling signal lamps. As well, they can be also mixed with PC-LEDs in order to have high quality hybrid lighting solutions flexibly.

On the other hand, white LEDs can be classified into three primary groups following to how to manufacture them. The first group gives white impression for human eyes by the combination of three individual colors (red - R, green - G and blue - B) called as RGB white LEDs or multi - color LEDs. In real designs and operations, there are significant problems for this group. Indeed, electrical power circuits, controlling circuits, feedback signal buses and homogeneous optical mixing systems for RGB white LEDs become more difficult and complicated. In addition, the changes of their properties over the operating temperature, forward current and burning time are inhomogeneous. Therefore, they must often be mixed according to the changes of operating temperature, forward current and burning time. Nonetheless, with higher efficiency and better flexibility in the adjustment of optical properties compared with other groups, this group is still interested in high quality lighting applications such as the shop lighting, the film and TV lighting, the architectural lighting or the museum lighting. The second type is phosphor converted LEDs (PC-LEDs) or phosphor-based LEDs. In this group, the blue semiconductor LEDs or ultraviolet LEDs are coated by a determined phosphor layer. The used phosphor types may be yellow phosphors such as YAG:Ce³⁺ (Y₃Al₅O₁₂:Ce³⁺), GdAG ((Y_{1-x}Gd_x)Al₅O₁₂:Ce^{3+y}), TAG ((Y,Tb)₃Al₅O₁₂:Ce³⁺) or yellow Ortho-Silicates (Ba_{2-x-y-z}Sr_xCa_ySiO₄:Eu^{2+z}) or may be the compound of several phosphors such as green, yellow or orange Ortho Silicates (Ba_{2-x-y-z}Sr_xCa_ySiO₄:Eu^{2+z}), Thiogallate (SrGa₂S₄:Eu²⁺), Calcium Sulfides (Ca,Sr)S:Eu²⁺, Nitrides ((Ba,Sr)₂Si₅N₈:Eu²⁺), Oxy Nitride Silicate (SrSi₂N₂O₂:Eu²⁺), Ca₃Sc₂Si₃O₁₂:Ce³⁺, LuAG (Lu_{3-x}Al₅O₁₂:Ce_x) or LuGaAG (Lu_{3-x}(AlGa)₅O₁₂:Ce_x). Particularly, blue semiconductor chips or ultra violet chips pump the original blue or ultraviolet spectra. Then, a phosphor or a phosphor system absorbs an amount of the original blue or ultraviolet spectra and radiate their own green, yellow or red spectra. Successively, these color phosphor spectra are mixed with the rest amount of blue or ultraviolet radiation and also give a white impression for human eyes. In fact, the second group is preferred because it is simple giving high color rendering indexes (CRIs) and has a relatively good luminous efficacy depending on used phosphor types. The third group is a hybrid LED-lamp type, where PC-LEDs can be combined with

royal blue, blue, cyan, green, yellow, amber, orange, red or deep red semiconductor LEDs, or green, yellow, amber, orange, red or deep red full converted phosphor LEDs, or both of them in order to achieve desired lighting quality parameters. Otherwise, white PC-LEDs can be also classified according to the color impression of human eyes. In this approach, white PC-LEDs can be grouped into the warm white PC-LEDs ($2500\text{ K} < \text{CCT} < 3500\text{ K}$), neutral white PC-LEDs ($3800\text{ K} < \text{CCT} < 4500\text{ K}$) and cold white PC-LEDs ($5000\text{ K} < \text{CCT} < 6500\text{ K}$). In another approach, the white PC-LEDs can be also sorted into low quality CRI PC-LEDs ($R_a < 70$), moderate CRI PC-LEDs ($R_a < 80$), good CRI PC-LEDs ($80 < R_a < 85$), very good CRI PC-LEDs ($86 < R_a < 92$) and excellent CRI PC-LEDs ($R_a > 92$). Finally, they can be also classified based on both of the above approaches to become different groups such as very bad CRI - warm white PC-LEDs, bad CRI - warm white PC-LEDs, good CRI - warm white PC-LEDs, very good CRI - warm white PC-LEDs and excellent CRI PC-LEDs and so on.

* **Material aspect:** In fact, there are only some semiconductor materials that can be used to fabricate LEDs. They can be Gallium Arsenide (GaAs), Aluminum Gallium Arsenide (AlGaAs), Gallium Arsenide Phosphide (GaAsP), Aluminum Gallium Indium Phosphide (AlGaInP), Gallium (III) Phosphide (GaP), Indium Gallium Nitride (InGaN), Gallium (III) Nitride (GaN), Zinc Selenide (ZnSe), Silicon Carbide (SiC), Aluminum Nitride (AlN) and Aluminum Gallium Indium Nitride (AlGaInN). For instance, in case of blue semiconductor LEDs ($400\text{ nm} < \lambda_p < 470\text{ nm}$), their blue chips can be manufactured by ZnSe, InGaN, SiC or GaN. Therefore, they can be recognized as InGaN blue semiconductor LEDs or GaN blue semiconductor LED. Likewise, other color semiconductor LEDs such as infrared, red, orange, yellow, amber, green or ultraviolet semiconductor LEDs can be also classified and called following to their constituent material compositions.

1.1.2. Overview history of LEDs

Based on the above classifications of LEDs, it can be recognized, that there is diversification in the grouping process of LEDs. In that, manufacturing and material factors play a very significant role. Even it can be assumed, that the development history of LEDs based on non-stopped inventions and improvements of the semiconductor material technology. Regarding this theme, SCHUBERT in [1] had a very good review and very valuable comments about the history of LEDs. In this section, his main ideas are summarized briefly combining with a few comments of the author about the period of time and the applicability at each phase.

* **Silicon carbide (SiC) ([1]):** Silicon carbide is assumed as the first semiconductor material discovered for LEDs. In 1907, ROUND discovered the electroluminescence. Particularly, he used crystal SiC and a cat's - whisker detector ([2]). However, SiC was not processed and controlled much. As well, the knowledge about inside emission processes was quite limited. According to [1], the minority carriers were injected into semiconductor layers by tunneling through a surface potential barrier and the voltage required for minority carrier injection in SHOTTKY diode must be higher than a typical p - n junction LED voltage equaling about between 10 V and 110 V. Moreover, following to [3] twenty years later a Russian researcher, LOSEV, reported on his creation of the first LED in 1927. Unfortunately, although his report was printed in Russian, German and British scientific journal, there was no practical use of this discovery because SiC had an indirect band gap with a very low efficiency. Even, its converting efficiency was only 0.005 % in 1969 and 0.03 % at the top in 1993 after 66 years of non-stopped improving.

* **Gallium Arsenide (GaAs) and Aluminum Gallium Arsenide (AlGaAs) ([1]):** A group of researchers in IBM Corporation including WOODALL, RUPPRECHT, PILKUHN, NATHAN and others developed GaAs and AlGaAs in the early 1960s. GaAs and AlGaAs were found later than SiC, because they do not exist in nature like SiC. Fortunately, this group had gotten the liquid phase epitaxy technique of NELSON at RADIO CORPORATION OF AMERICA (RCA). Therefore, GaAs and AlGaAs red LEDs came into real uses very quickly. Even they have still been used widely until now for remote control devices of televisions, videos or audios and short distance communications. Moreover, SCHUBERT in [1] showed that red AlGaAs/AlGaAs LEDs were used as red visible high brightness LEDs with a higher efficiency than that of GaAsP/GaAs red LEDs but lower than that of the AlGaInP/GaAs red LEDs. As a record, anyhow the IBM research group created practical red LEDs quite well.

* **Gallium Arsenide Phosphide (GaAsP) ([1]):** In 1962, HOLONYAK invented a GaAsP junction. Particularly, he used vapor-phase epitaxy of GaAsP on GaAs substrates that was appropriate for the large-volume growth of wafers. However, although this LED type was good at its electrical property, its optical property was limited because of direct-indirect transitions and high dislocation densities.

* **Gallium Phosphide (GaP) and Gallium Arsenide Phosphide (GaAsP) doped with an active impurity ([1]):** ALLEN, GRIMMEISS and SCHOLZ reported about their GaP junction in 1963 and 1964. This junction type emitted a red light but with a better efficiency than others. But until 1965, THOMAS recognized that although GaP with an indirect band gap does not emit light much because of the momentum conservation in an optical transition, it will have a strong optical transition if it is doped with an optically active isoelectronic impurity such as N ([1]). Seven years later, in 1967 LOGAN formed a new junction with a n-type GaP layer onto Zn-P-doped wafers increasing the efficiency of LEDs. Then, other active impurities such as Zn, O, N or their alloy were developed at later 1960s and early 1970s. This LED type was used early in numeric display applications such as calculators or watches.

* **Gallium Nitride (GaN) Zn - doped, Mg - doped ([1]):** Based on the above steps, it can be recognized, that high efficient red GaAsP LEDs and high efficient green GaP doped N were found and used in varied applications. Successively, if the LEDs are desired to design color televisions, high efficient blue LEDs are necessary to produce. Then, all color objects with enough colors by the combination of three red, green and blue colors will be able to be created in the real operation of color televisions. In 1968, TIETJEN thought similarly and wanted to fabricate a single crystal film of GaN emitting a blue light. A young man in his team, MARUSKA, had to perform on this duty and he gave the first single-crystal film of GaN in 1969. Until 1970, PANKOVE of RCA was interested in the GaN film of MARUSKA and invented the electroluminescence based on GaN in 1971. Particularly, an insulating Zn-doped layer was contacted with two surface probes and the LED emitted a blue wavelength of 475 nm. Successively, he made a new device containing an undoped n-type region, an insulating Zn-doped layer and an indium surface contact. As a result, these products were the first GaN LED emitting green and blue light. Later 1972, this group of RCA changed Zn-doped by Mg-doped and dedicated blue and violet emissions at 430 nm. However, unfortunately these LEDs had still no good enough efficiency.

* **Indium Gallium Nitride (InGaN) ([1]):** Although PANKOVE published his results in 1982, AKASAKI and his team refused it. Seven years later in 1989, they invented the first true p-type doping and p-type conductivity in GaN. In that, Mg acceptors were activated by an electron-beam irradiation ([1]). As well, a high temperature post-growth-anneal of Mg-doped GaN activated Mg also dopants in GaN following to NAKAMURA (1994). This invention opened a new era of high efficiency LEDs, although the efficiency was only 1 % in 1992. NAKAMURA and his team developed a two-flow organometallic vapor-

phase epitaxy growth system, demonstrated for the first blue and green InGaN double hetero-structure LEDs with the efficiency of 10 % and InGaN/GaN current injection blue lasers operating at room temperature (NAKAMURA, 1996) ([1]). As a result, green InGaN LEDs replaced for green GaPN LEDs, because of their better brightness. As well, blue InGaN LEDs played a very important role in the white PC-LED fabrication. Moreover, very big potential of white PC-LEDs based on blue InGaN LEDs was forecasted previously at that time.

* **Aluminum Gallium Indium Phosphide (AlGaInP)** ([1]): Beside GaN and InGaN were useful inventions for high power blue LEDs, AlGaInP was also an available material for high power red, orange and yellow LEDs. In the beginning, this material was only developed for lasers in Japan in the late 1980s. In the 1990s, AlGaInP was widened following the direction of LEDs so that the entire junction can emit light. Particularly, a system that uses multiple quantum well active regions was built up. Finally, all available semiconductor materials for high brightness color LEDs were invented and fulfilled the complete visible wavelength range like the description in Figure 1.1.

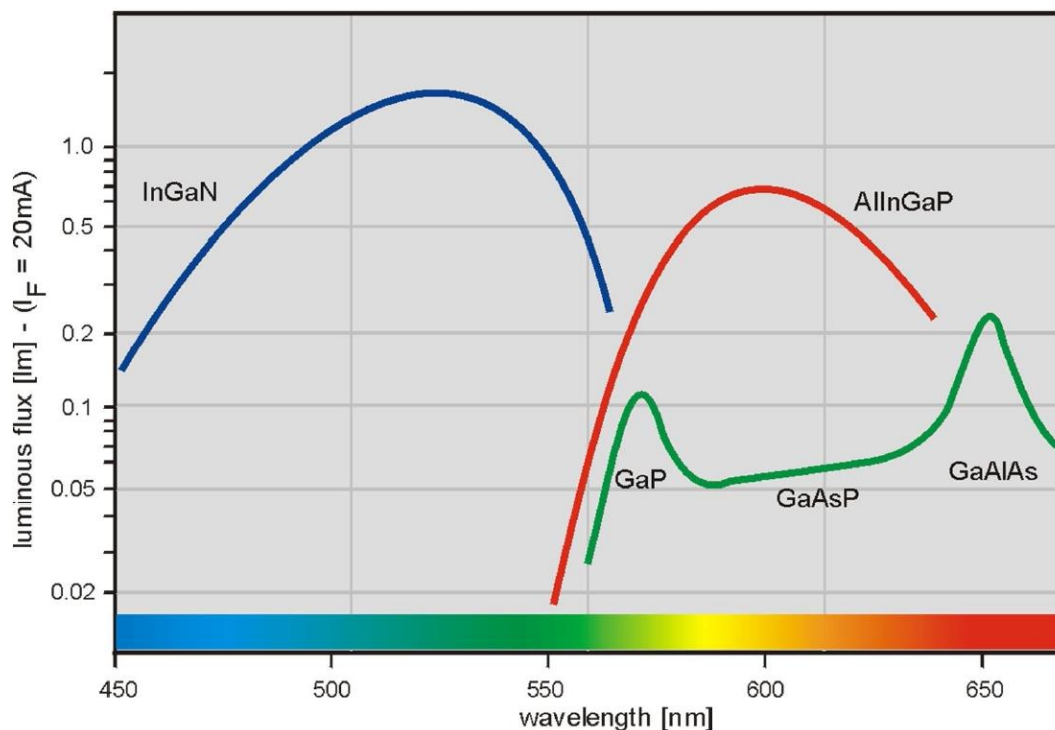


Figure 1.1 - Available semiconductor materials for high brightness color LEDs ([4])

1.2. Current development status of LEDs in solid state lighting applications, problems and motivations

In Section 1.1, LEDs were classified into different groups or types according to criteria of power, color and constituent semiconductor material. Simultaneously, the non-stopped evolution of LEDs and semiconductor materials during a long time were summarized quite entirely. In that, the efficiency and the brightness of LEDs were always treated as important factors. In this section, the current development status of the LEDs in solid state lighting applications including the light output and the lighting quality will be reviewed briefly. Hence, the advantages and the disadvantages of current LED development status will be recognized. As a result, problems and motivation will be determined and established for successive investigations and researches of the author in this thesis.

1.2.1. Current development status of LEDs

* **Current state of the lighting output of LEDs:** According to [5] and [6], in 2001 and 2002 the process of growing GaN LEDs on silicon were demonstrated successfully and applied to manufacture high power LEDs reported in January 2012. Therefore, the high epitaxy cost could be reduced down to 90 % by using a six-inch silicon wafer instead of two-inch sapphire wafers ([7]). On the other hand, following to the investigation of TECHNISCHE UNIVERSITÄT DARMSTADT described in Figure 1.2, until April 2011 the luminous efficacy of cold white PC-LEDs reached about 140 lm/W. Likewise, this parameter of warm white PC-LEDs also achieved approximately 110 lm/W. Moreover, the datasheets of OSRAM, LUMILED, CREE and other LED manufacturers ([8]) published that the color semiconductor LEDs with 640 MW optical power at 1 W input electrical power have been ready on the market.

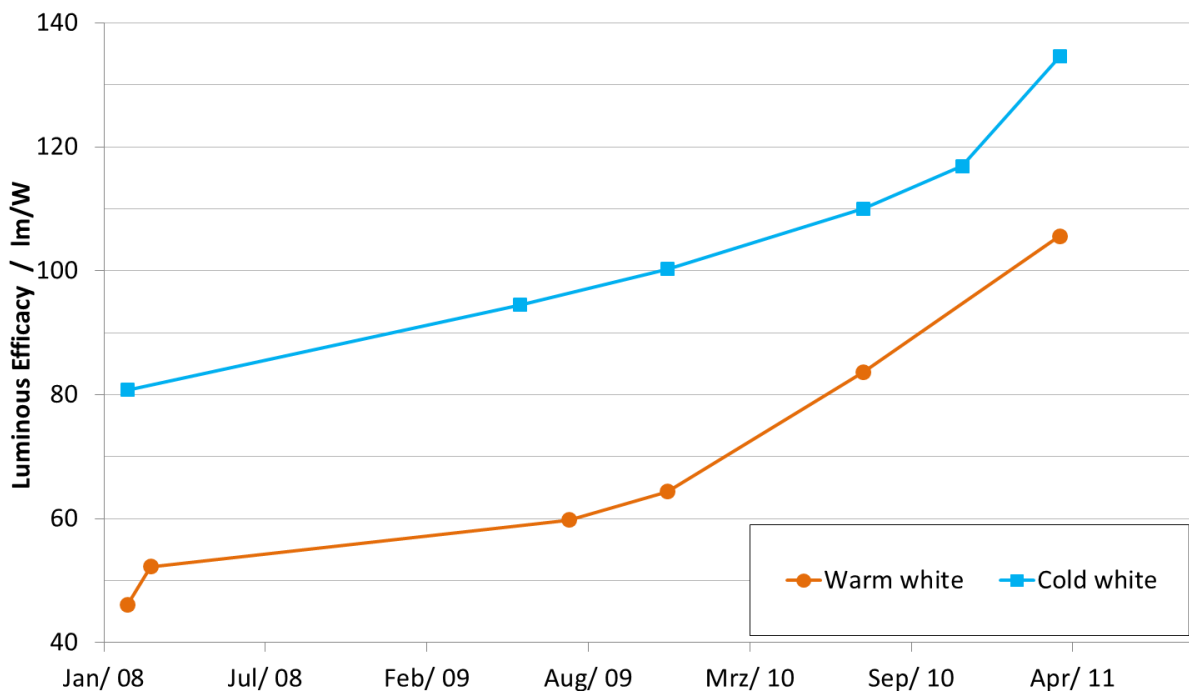


Figure 1.2 - Progress of the luminous efficacy of white PC-LEDs in several recent years

* **Current state of the lighting quality of LEDs:** About lighting quality aspect, MÜLLER in [9] mentioned to excellent high color rendering index LEDs ($R_a > 90$) in 2008. Two years later, BAUMANN in [10] reported about very high color rendering index LEDs. In 2012, the manufacturer OSRAM published about its very high color rendering index LED-lamps described in Figure 1.3 ([11]). In that, their luminous fluxes achieved about 3000 lm to 5000 lm, their general color rendering index R_a for the first eight standard CIE test color samples was always higher than 90, their ninth CIE color rendering index R_9 for the CIE strong red test color sample was higher than 80, and their luminous efficacy reached around 100 lm/W.

The American standards for LEDs, ENERGY STAR, mentioned that the correlated color temperature CCT in K must be within 8 specified regions (2700 K = 2725 K \pm 145 K, 3000 K = 3045 K \pm 175 K, 3500 K = 3465 K \pm 245 K, 4000 K = 3985 K \pm 275 K, 4500 K = 4503 K \pm 243 K, 5000 K = 5028 K \pm 283 K, 5700 K = 5665 K \pm 355 K, 6500 K = 6530 K \pm 510 K), the tolerance of CCT must be in 7-step chromaticity quadrangles, the variation of chromaticity in different directions shall be within 0.004 from the weighted average point on the CIE 1976 (u' , v') diagram; the color maintenance over burning time shall be within 7 MAC ADAM ellipses, and the general CRI (R_a) for indoor lighting (nominal

2700 K, 3000 K, 3500 K and 4000 K) shall have the minimum value of 70 in the version 1.1 (2008) and 80 in the version 1.0 (2010) ([12]). Beside the definitions of ENERGY STAR STANDARDS, the regions of CCT and CRI should be investigated furthermore and should be determined more appropriately according to the real physiological and biological sensitivity of the human eyes. Moreover, in parallel to the limits of CCT and general CRI (R_a) mentioned above, many other important lighting quality aspects such as whiteness, color preference, color harmony, color memory, color gamut, light source brightness, object brightness, brilliance, circadian stimulus, scotopic and photopic ratio, short term stability, long term stability and their limits are very essential to be paid a reasonable attention in solid state lighting applications. Especially, the short term and long term stability over operating temperature, forward current and burning time have been not yet considered appropriate in published literatures, data sheets or other publications. Some published literatures (the typical one as [33]) mentioned about the short term stability of LEDs over operating temperature and forward current have just played the role of warnings, but there was no good enough improvement solution for them. Some other ones like [105] described the current compensation solutions to stabilize the correlated color temperature of LEDs, but they did not recognize and solve entirely that when the forward current increases or decreases, all color quality parameters (including correlated color temperature) also change simultaneously. Therefore, an acceptable solution should be treated on three dimension spaces of operating temperature, forward current and LED properties. Regarding long term stability aspect, the measurement method, the measurement procedure and the data process were described in some published literatures such as in standards LESNA LM-79, LESNA LM-80 or TM-21 ([13]). However, an entire consideration of all optical properties as functions of the operating temperature, the forward current and the burning time in the long term has been not yet published. Obviously, about the quality lighting of LEDs, there are very large gaps that are necessary to be studied and fulfilled in order to achieve new advancements for solid state lighting applications.

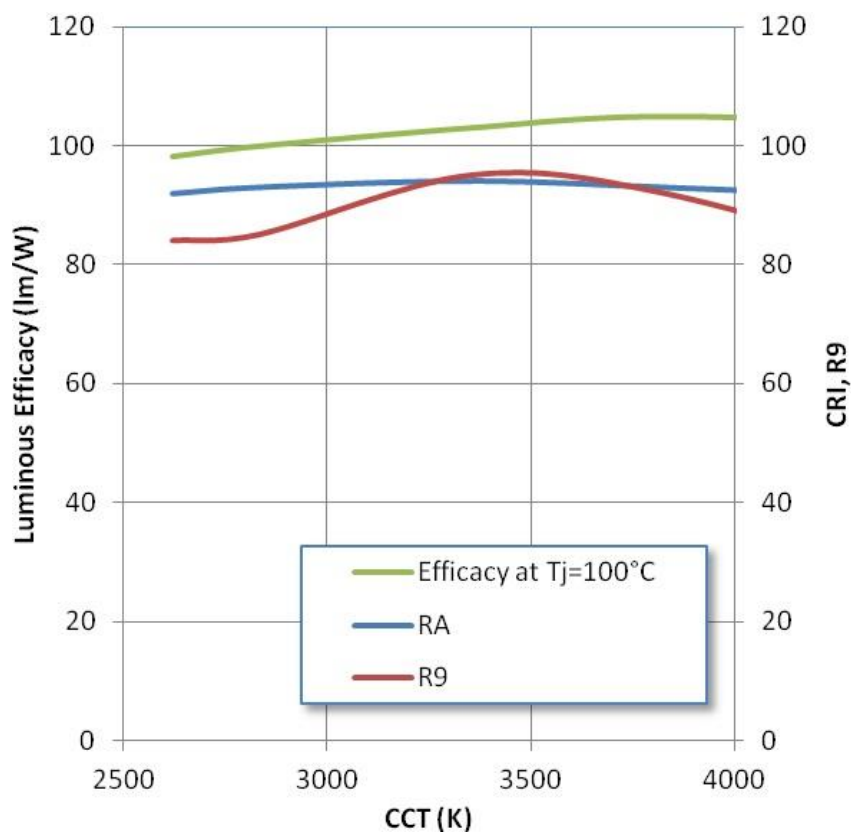


Figure.1.3 - Progress of white OSRAM PC-LEDs in 2012 ([2])

1.2.2. Problems and motivations

Based on investigations of the current development status of LEDs mentioned in Section 1.2.1, it can be recognized, that the light output of LEDs has been improved significantly. However, the lighting quality of LEDs was carried out in real solid state lighting applications quite limitedly on some basic parameters such as correlated color temperature and color rendering indexes including the general color rendering index. As well, in Section 1.2.1 the gaps in lighting quality were also determined and shown specifically. Nonetheless, in the framework of this thesis it is impossible to characterize, optimize and stabilize all lighting quality parameters mentioned in the above section. Thus, meaningfully this thesis should focus on some lighting quality aspects that are important and have direct influences on the design, the control and the operation of solid state lighting systems in high quality lighting applications such as the shop lighting, the film and TV lighting, the architectural lighting or the museum lighting. Particularly, there are four pressing categories that should be studied appropriately: The first category is the short term stability of lighting quality parameters of LEDs over operating temperature and forward current. The second category is the parameter differences between LED-manufacturers and LED-luminaire manufacturers and a solution for them. The third category is the characterization of thermal, electrical and optical properties of LEDs. The fourth category is the optimization and the stabilization of some lighting quality aspects adapted to color objects in high quality solid state lighting applications. As a result, the above four categories are problems that are necessary to be solved in this thesis.

1.3. Concept and structure of the thesis

1.3.1. Concept of the thesis

The fundamental concept of this thesis can be generalized into five basic steps in a process progress from theory to real operations, from a simple solution to complicated characterizations and from mathematical modeling to real creative applications including,

* **Step 1:** The first step is the essential theoretical description of intrinsic phenomena inside LEDs. Particularly, in this step the background of semiconductor physics, quantum physics and luminescent material chemistry will be studied and combined together in order to establish the correlations between inputs and outputs of LEDs and to explain the intrinsic phenomena of spectral and energy conversions inside LEDs with appropriate mathematical formulations.

* **Step 2:** The second step is the necessary practical description of properties of LEDs. In this step, typical color semiconductor LEDs and typical white PC-LEDs will be investigated in different operating conditions of the forward current and operating temperature. From that, the temperature dependence and current dependence of properties of LEDs will be described by means of experimental three-dimensional functions. As well, limits of lighting quality parameters will be recorded as desired targets for successive study steps.

* **Step 3:** The third step is the formulation of problems in LED applications and the attempt for a simple solution. In that, experiences of LED applications combining with practical properties of LEDs will be used to determine difficulties of the LED application for LED-luminaire manufacturers. Then, a simple solution is important to solve the difficulties directly.

* **Step 4:** The fourth step is the comprehensive understanding of a solid state lighting system as a multi-input multi-output system (MIMO system), the appropriate separation of the MIMO system into thermal, electrical and optical sub-systems, and the accurate characterization of these sub-systems. In this step, the knowledge of system identification, control system structure, data sampling, analysis and synthesis of a system and the corresponding mathematical formulations have to be applied appropriately and creatively.

* **Step 5:** The fifth step is the meaningful application of the above characterizations for high quality solid state lighting systems. Particularly, the knowledge of automatic control system, optimal control, dynamic stability control and adaptive control will be used in order to create optimized / stabilized algorithms and appropriate control system structures for high quality solid state lighting applications adapted to color objects. Moreover, the investigation of color objects in desired solid state lighting applications and their qualification are essential to supply necessary parameters for the color object adaptive control and the color quality optimization. Otherwise, the deep knowledge of color and color evaluation should be studied specifically. Hence, the supports or critics for the current color qualification as well as new improvement approaches to it will be offered. In addition, new definitions for color objects and their applications will be created in order to have useful and appropriate tools in designs and evaluations. Finally, high and stable quality solid state lighting systems are the targets that must be achieved in this thesis.

1.3.2. Structure of the thesis

In order to realize all targets mentioned above, the thesis will be organized according to the following structure.

* **Chapter 1 - Introduction:** In this chapter, the classification and the overview history of LEDs will be described briefly and the current development status of the LEDs in solid state lighting applications for both light output and lighting quality will be updated. As a result, their advantages and disadvantages can be recognized. Successively, the disadvantages will be analyzed so that the problems are determined and established in more details. The desired solutions for the established problems are the motivations of the author in the entire framework of the thesis. Finally, the appropriate concept and structure of the thesis will be established and organized in order to solve problems and achieve the desired targets.

* **Chapter 2 - Basic knowledge of LEDs:** The task of the chapter 2 is to have correct and comprehensive knowledge about LEDs on aspects of semiconductor physics, quantum physics and luminescent material chemistry in order to describe intrinsic phenomena inside both color semiconductor LEDs and white PC-LEDs with corresponding mathematic forms. In that, the correlations between inputs and outputs with spectral and energy conversions in LEDs will be the central objects of this chapter.

* **Chapter 3 - Optical, radiant and colorimetric properties of LEDs:** The task of the chapter 3 is to investigate the optical, radiant and colorimetric properties of both typical color semiconductor LEDs and typical white PC-LEDs. In that, the energy quality aspect such as radiant flux and radiant efficiency for color semiconductor LEDs or luminous flux and luminous efficacy for white pc-LEDs and the color quality aspects such as the shift of peak wavelength, the widening of full width at the half maximum and color difference for color semiconductor LEDs or color rendering indexes, correlated color

temperature and color difference for white PC-LEDs will be considered specifically in different conditions of the operating temperature and forward current. In addition, the total changes of their spectra will be observed and analyzed for each spectral component. Hence, the changes of LED properties in three-dimensional relationships of operating temperature and forward current will be summarized to have a practical perception of LED behaviors for successive chapters. On the other hand, the limit of luminous efficacy of white PC-LEDs with different color rendering index levels will be recorded in order to support the chapter 7 in the establishment of the most available combination between color semiconductor LEDs and white PC-LEDs in hybrid LED-lamps. The combination will have to satisfy both better lighting quality and higher luminous efficacy comparing with original white PC-LEDs.

* **Chapter 4 - A minimization solution to parameter differences between LED- and LED-luminaire manufacturers:** This chapter refers to parameter differences between LED manufacturers and LED-luminaire manufacturers. Hence, the difficulties of LED-luminaire manufacturers will be recognized. Consequently, a simple technique solution will be established to solve the problems for LED-luminaire manufacturers and eliminate barriers that prevent a dynamic development of LEDs in all solid state lighting applications. In the framework of the thesis, the given solution should be just a core idea playing the role of a demonstration example methodically. A realistic and entire performance should be developed furthermore by LED-manufacturers or/and LED-luminaire manufacturers.

* **Chapter 5 - Junction temperature determination, thermal transient identification and thermal map decoding of LEDs:** Since this chapter, LEDs will be investigated and researched on advanced levels with their intrinsic phenomena. Particularly, in Chapter 5 the thermal property of LEDs characterized by junction temperature, the total thermal resistor and capacitor will be measured and determined by different methods. Consequently, the comparison between methods is necessary to find out an applicable solution. Otherwise, inaccuracies of the measurement will be recognized in order to give suggestions for important improvements. Finally, a reasonable identification and decoding solution will be offered for the analysis of LED thermal property. Hence, a thermal map with a series of partial thermal resistors and partial thermal capacitors will be identified and decoded for several typical LEDs as a methodical demonstration example for the proposed solution.

* **Chapter 6 - Transient LED model:** The thermal property is very important and difficult to be determined and characterized. Therefore, it is separated and described in Chapter 5. Consequently, the electrical and optical transient LED models will be described and characterized in Chapter 6. About electrical transient LED models, different approaches published in different literatures in many years will be discussed so that a feasible approach in a conventional operating region will be proposed. Consequently, a useable limited electrical model will be established as a three-dimensional function of forward current and junction temperature. In this framework of this thesis, electrical LED transient models just play a role as links between thermal, electrical and optical components of LEDs. Whereas, the optical transient LED models are special important components in this thesis and are the key contents of Chapter 6. These optical transient LED models will be treated as LED spectral models with some different forms. Therefore, the published spectral LED models will be analyzed and evaluated for their accuracy and then a new approach for the establishment of better LED spectral models for both color semiconductor LEDs and white PC-LEDs with a higher accuracy will be proposed. As well, new spectral LED models will be investigated and evaluated to prove for their accuracy.

* **Chapter 7 - Optimization and stabilization for some lighting quality aspects of hybrid LED-lamps adapted to color objects:** High quality lighting applications may be the shop lighting, the film

and TV lighting, the architectural lighting or the museum lighting. In the framework of the thesis, not all high quality lighting applications can be investigated and researched, but two applications such as the shop lighting and the museum lighting with determined lighting spaces will be carried out as methodical demonstration examples. In these particular lighting spaces, a determined amount of color objects will be measured and characterized by spectral reflectance curves and then be quantified by new object specific color rendering indexes based on standardized definitions and equations about CIE color rendering indexes. Applying the best spectral LED models (established according to the most accurate method that was investigated and proved in Chapter 6) of color semiconductor LEDs and white PC-LEDs belonging to the most available LED combination of hybrid LED-lamps and output lighting quality parameters characterized for color objects, control system structures for high quality solid state lighting systems will be established appropriately. As a result, optimization algorithms will be applied to create componential currency control laws for each LED component so that output lighting quality parameters of hybrid LED-lamps will be optimized for the museum lighting as the first methodical demonstration example. On the other hand, main and subordinate conditions are necessary to be classified, prioritized and assigned specifically. Finally, the stabilization for some main lighting quality parameters, the optimization of some other important quality parameters as well as the improvement of some subordinate quality parameters adapted to color objects will be carried out in the general shop lighting application as the second methodical demonstration example.

Chapter 8 - Conclusions: In this chapter, the general summary of the work in the thesis is presented, and suggestions for the future works are quoted.

1.4. Summary

In this chapter, the short classification for LEDs was performed, the brief summary of the LED development history was carried out, and the current development status of the LEDs was updated in order to achieve a comprehensive description of the light output and the lighting quality of current LEDs. Therefore, the problems and motivations of this thesis were determined and established. Consequently, the concept and the structure of this thesis were proposed and described. In that, the tasks were arranged and organized for each chapter specifically.

On the basic level, the theoretical explanation based on the semiconductor physics, quantum physics and luminescent material chemistry as well as the practical investigation of the properties for both color semiconductor LEDs and white PC-LEDs were assigned for Chapter 2 and Chapter 3.

On the advanced level, the identification and modeling of the thermal, electrical and optical properties of LEDs with different priority levels and varied approaches, the consideration of the color objects of high quality lighting applications, and the optimization and stabilization with available algorithms and control system structures were assigned for Chapter 5, Chapter 6 and Chapter 7. Moreover, as a link for two levels above, Chapter 4 is arranged to solve the difficulties of LED-luminaire manufacturers by means of a simple solution.

As a result, in the role of an introduction chapter, the framework of this thesis with explicit platforms was established particularly so that successive chapters can be researched and developed synchronously in this general structure.

2. Basic knowledge of LEDs

Based on established problems, the tasks for each chapter were assigned particularly in Chapter 1. The main aims of Chapter 2 are to review briefly the intrinsic phenomena inside LEDs on the theoretical background of the semiconductor physics, quantum physics and luminescent material chemistry, and to satisfy two important inquiries. The questions are how the input electrical energy (indicated by a forward current) is converted into the optical energy (indicated by the primary absolute spectral power distribution of color semiconductor LEDs) and how the primary absolute spectral power distribution of blue semiconductor LEDs is transferred into the secondary absolute spectral power distribution of luminescent materials. In addition, each stage and each constituent component have particular parameters to describe their intrinsic phenomena. Consequently, two derivative queries are how mathematical relationships between these parameters are and how these parameters change when the inputs of the operating temperature and the forward current change. Theoretically, the above problems will be studied and solved in this chapter.

2.1. Basic knowledge about the intrinsic phenomena inside color semiconductor LEDs

2.1.1. Injection luminescence

A color semiconductor LED is a type of diode that can emit light under appropriate bias conditions. Thus, color semiconductors LEDs include an abundant semiconductor material layer with positive carriers and another with negative carriers. Positive carriers (called holes) are particles that lack of electrons due to their chemical composition. Thus, the positive material layer is called p-layer. Contrarily, negative carriers are electrons belonging to a negative material layer called n-layer because its chemical compound creates electrons in excess. Normally there are two main states in operation of color semiconductor LEDs including an unbiased state and a bias state.

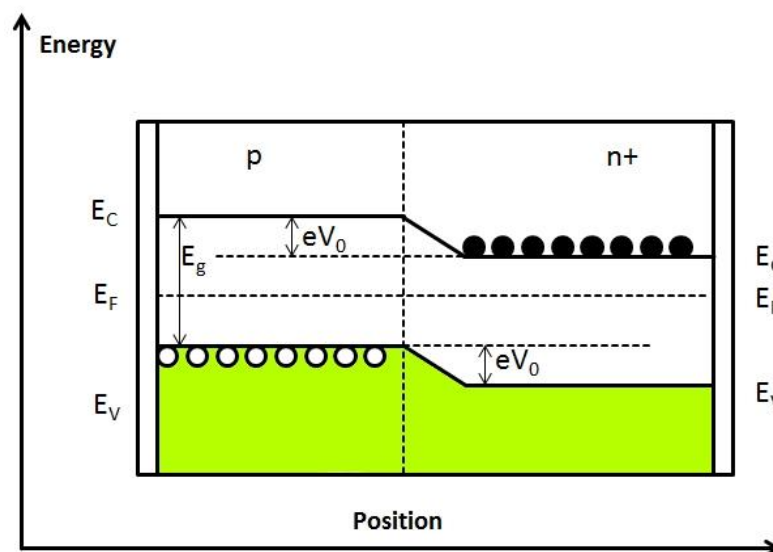


Figure 2.1 - Energy diagram of an ideal color semiconductor LED in unbiased state

* **Unbiased state:** Under an unbiased condition, a depletion region is created and extends mainly into the p-side causing to an insulating state like a lock with a very tiny leakage current (10^{-9} - 10^{-12} A) described in Figure 2.1. This state is ensured and determined by a built-in voltage V_0 in V.

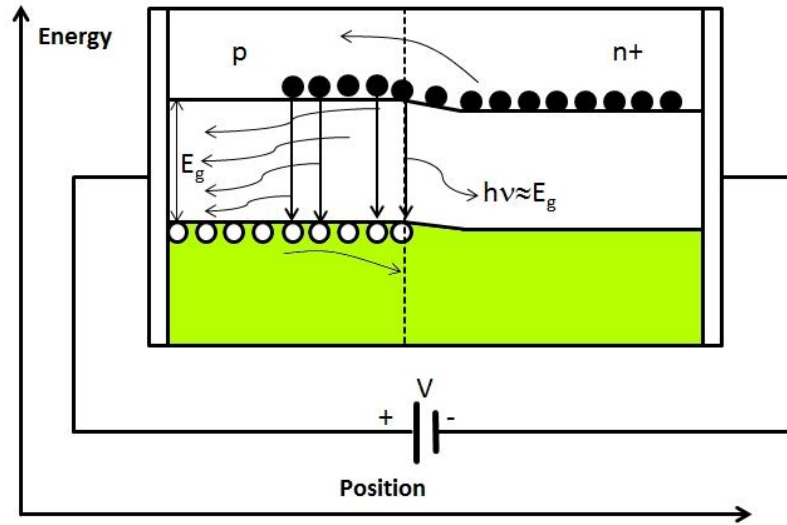


Figure 2.2 - Energy diagram of an ideal color semiconductor LED in biased state

* **Bias state:** When an appropriate forward voltage V is applied to a junction of a color semiconductor LED, the built-in voltage reduces down to $V_0 - V$ in V. Therefore, the corresponding barrier energy reduces down to $e(V_0 - V)$ in eV. Consequently, electrons can flow from the n-side into the p-side of the color semiconductor LED and reversely for holes. Successively, if a hole and an electron have the same momentum, they can recombine together and emit an optical radiation with a wavelength depending on the energy band gap E_g in eV of the semiconductor material described in Figure 2.2. This process is characterized by the equilibrium of photon energy described by Equation PLANCK-EINSTEIN and band-gap energy E_g in eV according to the energy conservation law as the following equation.

$$E = h\nu = \frac{hc}{\lambda} \approx E_g \text{ (eV)} \quad (2.1)$$

Whereby, h is the PLANCK's constant ($\sim 6.626 \cdot 10^{-34}$ m²kg/s), c is the speed of light ($\sim 3 \cdot 10^8$ m/s) and λ (nm) is the wavelength of an emitted light. Solving Equation 2.1 gives Equation 2.2 of an emitted wavelength,

$$\lambda \approx \frac{hc}{E_g} = \frac{1.24}{E_g} \text{ (}\mu\text{m)} \quad (2.2)$$

The above process is the most important mechanism in color semiconductor LEDs. It is called “*Injection luminescence*”.

2.1.2. Homo - junction, hetero - junction and quantum well

In the real operation of commercial color semiconductor LEDs on the world market, their injection luminescence is much more complicated. And intrinsic phenomena occurring inside color semiconductor LEDs depend on chemical composition and physical structure of their junctions. Generally, there are three structural levels of LED junctions including homo - junction (conventional no fabrication for real LEDs), hetero - junction and quantum well.

* **Homo - junction [14]:** The authors ZUKAUSKAS, SHUR and GASKA in [14] defined that a mono - junction like the description in Figure 2.1 and Figure 2.2 is composed of a p-type semiconductor and a n-type semiconductor belonging to the same semiconductor type with similar band-gap parameter. Thus, name “*homo - junction*” is to reflect this meaning. Theoretically, homo - junctions can create one or both conductivity regions, where radiative recombination can occur. In order to supply materials for recombination, electrons and holes diffuse into two sides of mono - junctions. Under a bias state like the mention in 2.1.1, majority carriers diffuse due to an external electric field creating an excess density of minority carriers on both sides of a junction layer. Successively, in that junction layer injected carriers can recombine both radiatively and non-radiatively. Hence, injection currents can be characterized as follows.

$$I_n = I_{n0} \left[\exp \left(\frac{V}{V_T} \right) - 1 \right] \quad (2.3)$$

$$I_p = I_{p0} \left[\exp \left(\frac{V}{V_T} \right) - 1 \right] \quad (2.4)$$

Where, I_n and I_p in A are the forward currents for electrons and holes at carrier temperature T_c in K, respectively; I_{n0} and I_{p0} in A are the forward currents for electrons and holes at a reference temperature T_{c0} in K, respectively. In addition, the thermal voltage at carrier temperature T_c is $V_T = \frac{k_B T_c}{e}$ in V with the BOLTZMANN’s constant k_B ($\sim 1.38 \cdot 10^{-23}$ J/K) and the electric charge e ($1.602 \cdot 10^{-19}$ C). In fact, the decrease of potential barrier by an applied voltage is lower, because of voltage dropped in series resistances R_s in Ω and a current added due to non-radiative recombination at a junction region. Therefore, the real current is presented in Equation 2.5.

$$I = I_n + I_p + I_{nr} = (I_{n0} + I_{p0}) \left[\exp \left(\frac{V - IR_s}{V_T} \right) - 1 \right] + I_{nr0} \left[\exp \left(\frac{V - IR_s}{n_{ideal} V_T} \right) - 1 \right] \quad (2.5)$$

Where, I_{nr0} in A is reverse non-radiative recombination current at a reference temperature $T_{c,0}$ and n_{ideal} is an ideality factor for a recombination current ($1 \leq n_{ideal} \leq 2$). Unfortunately, the injection efficiency of the homo - junction LED was normally very low in a range of 0.3 - 0.8 according to BERGH and DEAN (1976) mentioned in [14]. Therefore, the homo - junction was almost not fabricated for real LEDs.

* **Hetero - junction [14]:** Based on practical investigation, semiconductor physicists confirmed that there were many disadvantages with homo - junction structures such as the high reabsorption due to low light extraction efficiency. Thus, their internal efficiency can be only enhanced at one conductive region (for example, p-region, $I_n \gg I_p$), if doping is carried out much more with donors than acceptors. However, doping much more with donors makes the reabsorption of lights increasing and creates many non-radiative centers. Consequently, only changing of material compositions as a function of the distance can help to adjust carrier injection, radiative recombination and reabsorption in the junction layers of color semiconductor LEDs. As a result, a new junction structure established from dissimilar semiconductors with different band gaps due to different chemical compositions was created to satisfy the above requirement. Therefore, the difference of semiconductor material is reflected by the name “*hetero - structure*”. Conventionally, there are two types of hetero - structures including single hetero - structure and double hetero - structure. In the single hetero - structure described in Figure 2.3, a conductive region is composed of two semiconductor types so that the energy level of the n-type layer with band gap $E_{g,1}$ in eV is lower than that of p-type layer with band gap $E_{g,2}$ in eV, and the n-type conductivity region is wider than that of the p-type. This band discontinuity increases potential barrier for holes that diffuse to n-region by energy barrier ΔE_v in eV.

Moreover, depending on interface abruptness, potential barrier for electrons can decrease by a value in a range of $0 - \Delta E_c$ in eV. Accordingly, the rate of injection currents I_n/I_p can increase proportionately to $e^{\frac{\Delta E}{k_B T}}$, where $\Delta E_v \leq \Delta E \leq \Delta E_v + \Delta E_c$. In addition, another important advantage is, n-type is usually transparent for photons generated in the p - region. For this reason, the photons can escape outside easily in order to minimize the reabsorption of lights coming toward n-side.

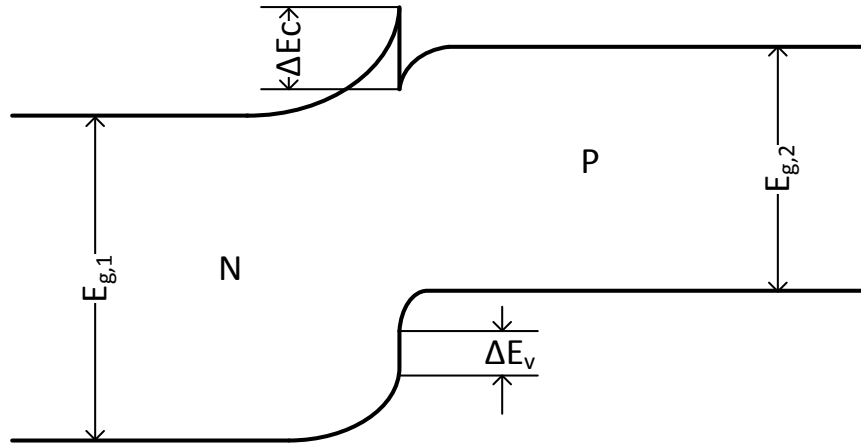


Figure 2.3 - Structure of a single hetero - junction with the increase of potential barrier ΔE_v for p-carriers and the decrease of potential barrier ΔE_c for n-carriers ([14])

On the other hand, in Figure 2.4 a “double hetero - structure” is made of a narrow gap active p-type layer kept between two wide-gap conductive regions of n- and p-types. This special structure allows for the bidirectional injection of excess carriers into the active layer, where electrons and holes can recombine together to emit light. In addition, minority carriers that diffuse through one side of hetero - interfaces are trapped in the active layer by the rest hetero - interface and cannot diffuse away. For this reason, the excess carrier density is increased. Therefore, the rate of radiative recombination also increases. Moreover, both conductive layers should be transparent so that the reabsorption effect is minimized in both two directions, although reabsorption can still occur in the active layer.

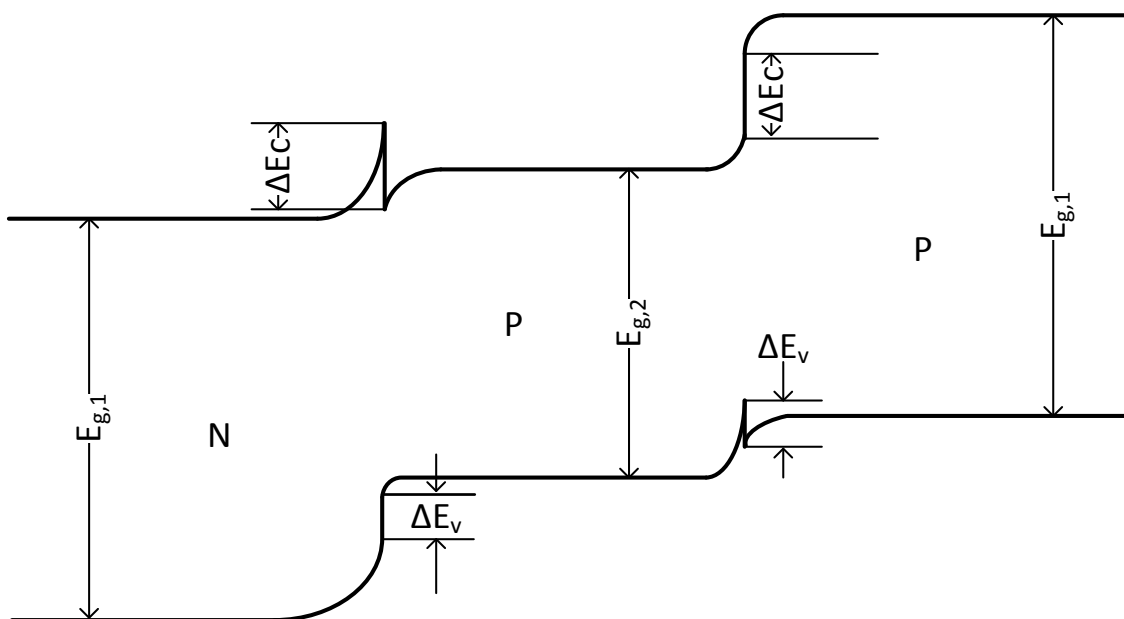


Figure 2.4 - Double hetero - junction with bidirectional injection ([14])

* **Quantum well [14]:** Quantum well is a special case of hetero - structures, where its specific structure helps to enhance the ability of carrier trapping. As a simple level, a double hetero - structure is also a single quantum well (SQW). However, the junction of high brightness LEDs is not only made of this single quantum well, but double quantum wells (DQWs) or multiple quantum well (MQWs). The optical properties of QWs are different from those of a normal semiconductor material volume. Particularly, instead of free motion along the perpendicular direction to a hetero - interface (x), discrete energy levels (E_n / ev) occur there. For an infinite deep rectangular quantum well, these discrete energy levels separated from its bottom of its conduction band (E_c / ev) can be described mathematically as the following equation.

$$E_n - E_c = \frac{\pi^2 \hbar^2 n^2}{2m_e a^2} \quad (2.6)$$

Where, $n=1, 2, 3, \dots$ is the quantum number, constant a in nm is the width of the quantum well and m_e in mg is the effective electron mass. In addition, in a y-z plane, which is parallel to the hetero - interface, the electron motion is not quantized so that the electron energy within a sub-band n is given by the following equation.

$$E = E_n - E_c + \frac{\hbar^2 k^2}{2m_e} = \frac{\pi^2 \hbar^2 n^2}{2m_e a^2} + \frac{\hbar^2 k^2}{2m_e} \quad (2.7)$$

Where, k is the two-dimensional wavenumber.

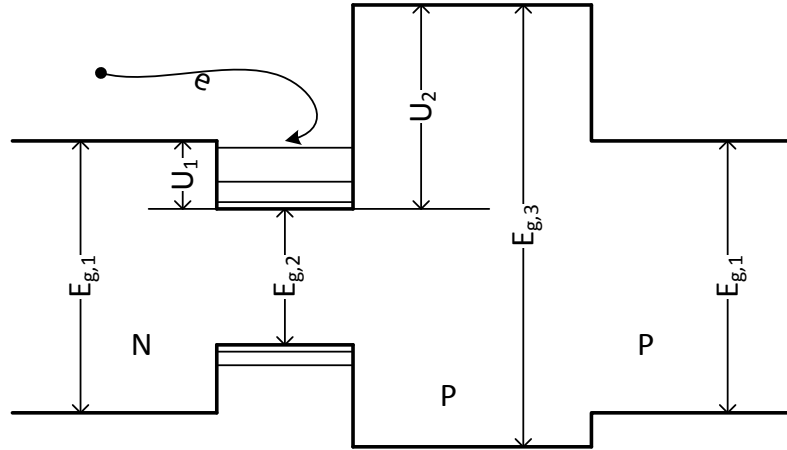


Figure 2.5 - A quantum well with an electron trapped in its structure ([14])

For a quantum well structure, which is almost used to fabricate in the color semiconductor LEDs in the reality, the forward current-voltage characteristics can be described more complicatedly by three current components including the diffusion current, the recombination (both radiative and non-radiative) and the temperature-independent tunnel current as the following equation.

$$I_f(V_f) = I_D(V_f) + I_R(V_f) + I_T(V_f) \quad (2.8)$$

Respectively, according to [14] the diffusion, recombination and tunnel currents were characterized by the following mathematical descriptions.

$$I_D(V_f) = I_{D0} \left[\exp\left(\frac{V - IR_s}{V_T}\right) - 1 \right] \quad (2.9)$$

$$I_R(V_f) = I_{R0} \left[\exp\left(\frac{V - IR_s}{n_{\text{ideal}} V_T}\right) - 1 \right] \quad (2.10)$$

$$I_T(V_f) = I_{T0} \left[\exp\left(\frac{V - IR_s}{\frac{E_t}{e}}\right) - 1 \right] \quad (2.11)$$

Where, E_t is the characteristic energy constant with the magnitude ~ 0.1 eV according to the author PERLIN (1996) mentioned in [14]. Current amplitudes (I_{D0} , I_{R0} and I_{T0} in A) were not yet described and explained explicitly, but were fitted experimentally and very differently depending on the various chemical compositions and physical structures of varied color semiconductor LEDs.

2.1.3. Recombination

Section 2.1.1 described about injection luminescence in a simple homo - junction. Section 2.1.2 treated to different junction structures of color semiconductor LEDs with different trapping abilities for carriers leading to different recombining abilities and different internal quantum efficiency. In fact, recombination of electrons and holes in the junctions occurs more complicatedly than what was described in the above sections. Phenomena are due to chemical compositions and physical structures inside the semiconductor LEDs. In this section, recombination will be classified and described according to intrinsic phenomena occurring in semiconductor structures including direct and indirect recombination, radiative and non-radiative recombination and some their simple theoretical qualifications

* **Direct and indirect recombination:** According to intrinsic structure of semiconductor materials, recombination can be classified into direct and indirect recombination. Indeed, direct recombination takes place in direct band gap semiconductor materials, where the minimum energy of their conduction band lies directly above the maximum energy of their valence band in a momentum-energy coordinate shown in Figure 2.6. Therefore, electrons at the bottom of conduction band can recombine directly with holes at the top of the valence band in order to emit light efficiently. In this case, the probability of band-to-band transitions is high leading to more radiative recombinations than others, because carriers have approximate similar momentums at the best energy position of the conduction band and valence band, where the energy level offset is lowest.

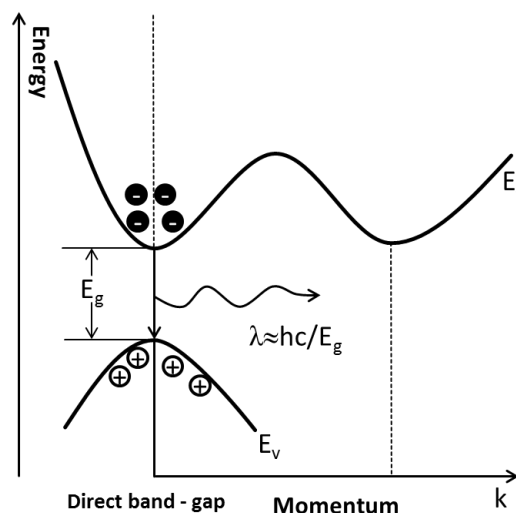


Figure 2.6 - Direct recombination in a material with a direct band-gap (GaN) ([125])

On the other hand, indirect recombination occurs in indirect band-gap semiconductor materials. In that, minimum energy of their conduction band shifted a distance from the maximum energy of their valence band shown in Figure 2.7. Therefore, there is a dissimilar momentum of electrons at the minimum energy position of conduction band and four holes at the maximum energy position of the valence band causing troubles for radiative recombination. Thus, in order to emit light electrons must have a way to change their momentum. And phonons are necessary to be added into junctions in order

to establish the same momentum state for both electrons and holes. In fact, this establishment is carried out by adding of impurities or dopants in order to form shallow donor/acceptor states. And then, these formed donor/acceptor states play role of recombination substations, where electrons are captured and supplemented an appropriate amount of momentum for their recombination. Originally, self-indirect recombination is worse than direct recombination in emitting light. However, if indirect band-gap semiconductor material is doped with an available impurity, indirect band-gap doped semiconductor material can even emit more lights than direct band-gap semiconductor materials in some cases.

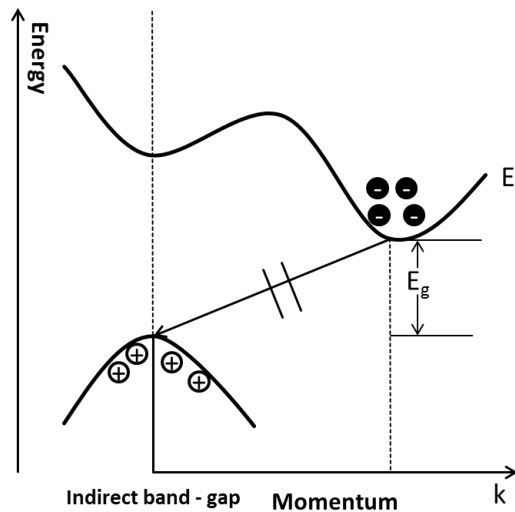


Figure 2.7 - Indirect recombination in a material with an indirect band-gap (SiC) ([125])

* **Radiative, non-radiative recombination and their simple theoretical quantification:** In order to investigate what takes place inside LEDs, many researchers assumed that there are two recombination types including radiative recombination and non-radiative recombination. If radiative recombination helps LEDs have more light output by radiation of photons, non-radiative recombination is only harmful for LEDs due to their thermal radiation. Particularly, it consumes input electrical energy of LEDs, but does not convert this electrical energy into optical energy and creates new vibrations and increases old vibrations of particles causing the increase of carrier temperature and total temperature of the semiconductor structure of LEDs. These vibration atoms are called “*phonons*” described in Figure 2.8.

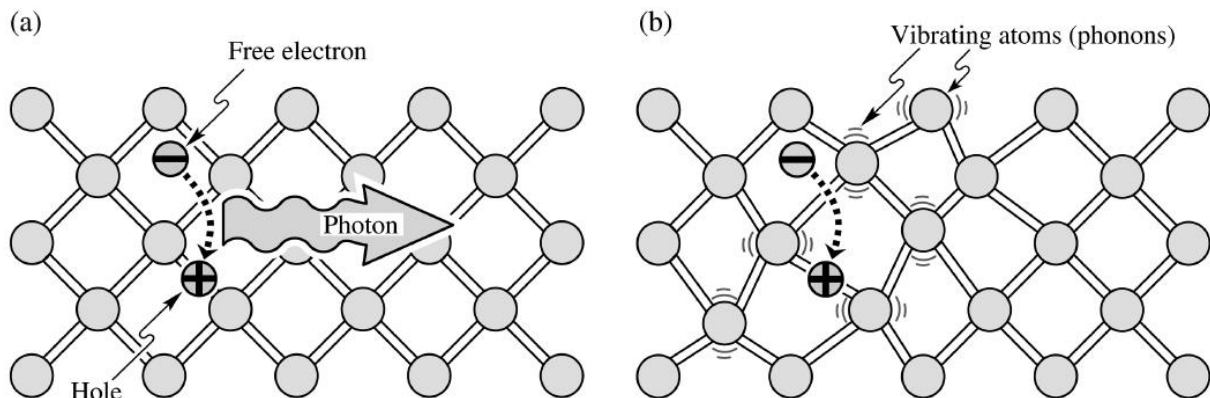


Figure 2.8 - Radiative (a) and non-radiative recombination (b) in the host lattice of LEDs ([1])

There are some reasons for non-radiative recombination such as auger recombination, recombination at defect areas or simply multi-phonon emission at deep impurity sizes illustrated in Figure 2.9.

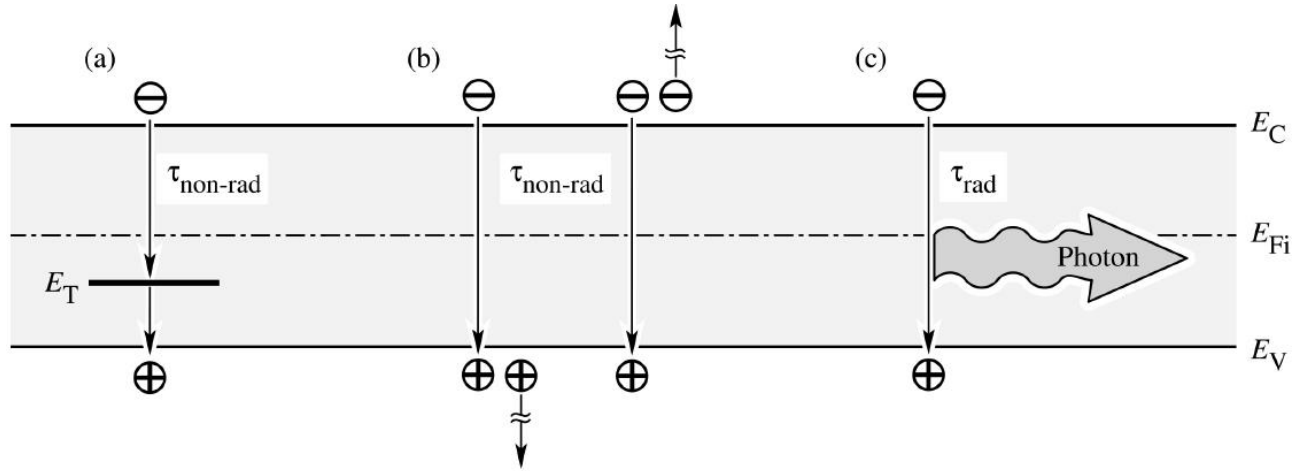


Figure 2.9 - a) Non-radiative recombination at the deep level, b) Auger recombination and c) Radiative recombination ([1])

Both radiative recombination and non-radiative recombination always occur concurrently. Therefore, it is necessary to consider them simultaneously in the investigation. According to [1] and [125], the successive carrier injection process causes excess carrier density in semiconductor layers. Therefore, in order to have neutral statuses, after each injection cycle, the excess carrier density of n-particles (Δn) and the one of the p-particles (Δp) must return to neutral statuses in a time cycle (τ / ns). In more detail, the excess carrier density decreases exponentially over time like the mathematical description in Equation 2.12 and Equation 2.13 and the graphical description in Figure 2.10.

$$\Delta n = \Delta n_0 e^{-\frac{t}{\tau}} \quad (2.12)$$

$$\Delta p = \Delta p_0 e^{-\frac{t}{\tau}} \quad (2.13)$$

Where Δn_0 and Δp_0 are the initial excess carrier densities of p- and n-particles and τ in ns is the recombination lifetime. This recombination lifetime includes both the radiative recombination lifetime τ_r and the non-radiative recombination lifetime τ_{nr} in ns according to the relationship described in Equation 2.14. These lifetimes are quite different between the low excitation case ($\tau = \text{constant}$) and the high excitation case ($\tau(t) = t + (B\Delta n_0)^{-1}$). As a result, the luminescence intensity may be a stretched exponential decay function in the case of high excitation ($\Delta n \gg N_A$) or become an exponential decay function in the case of low excitation ($\Delta n \ll N_A$), where N_A in cm^{-3} is the doping concentration. Then, the total probability of a recombination is determined by the sum of radiative and non-radiative probabilities as the following equation.

$$\frac{1}{\tau} = \frac{1}{\tau_r} + \frac{1}{\tau_{nr}} \quad (2.14)$$

The radiative recombination rate and non-radiative recombination rate in the relationship with the excess carrier density and the radiative recombination lifetime or non-radiative recombination lifetime can be also defined simply as shown in Equation 2.15 and Equation 2.16, respectively.

$$R_r = \frac{\Delta n}{\tau_r} \quad (2.15)$$

$$R_{nr} = \frac{\Delta n}{\tau_{nr}} \quad (2.16)$$

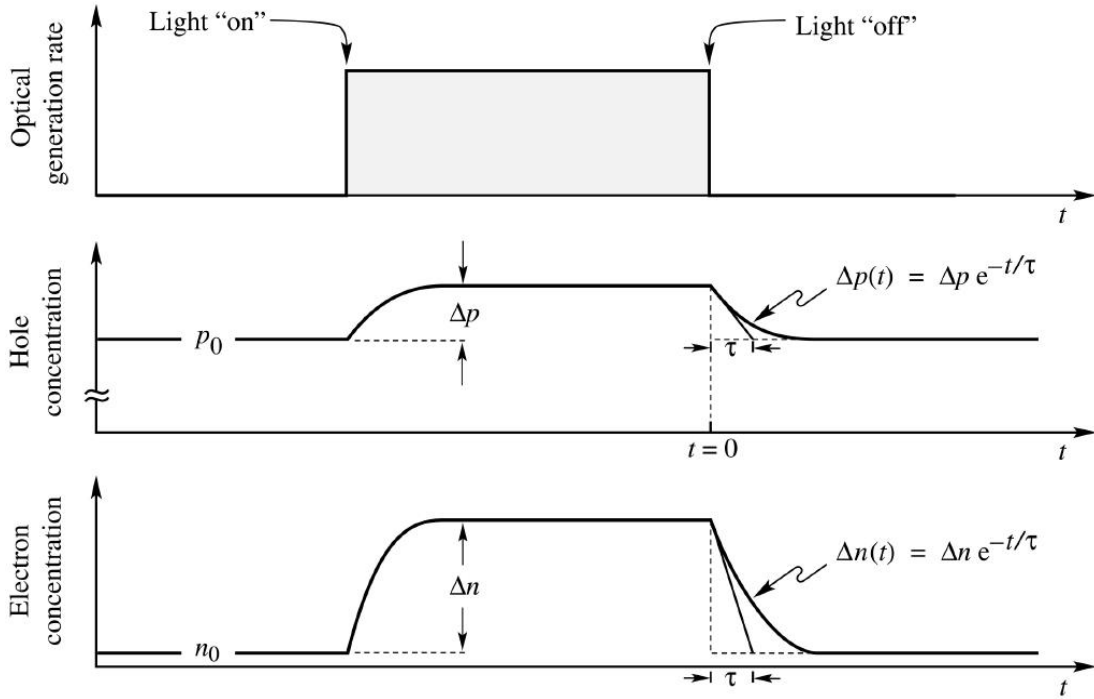


Figure 2.10 - Carrier density of n and p particles as functions of time in the recombination ([1])

2.1.4. Efficiency

From the inside to outside of LEDs, there are some different concepts of the efficiencies of LEDs such as the internal quantum efficiency (η_i), the injection efficiency (η_{inj}), the light extraction efficiency ($\eta_{extraction}$), the external quantum efficiency (η_{ext}), the radiative energy efficiency (η_e) and the luminous efficiency (η_v). These concepts can be described as follows.

* **Internal quantum efficiency (η_i):** The internal quantum efficiency is the ratio of the radiative recombination rate to the total recombination rate as shown in Equation 2.17.

$$\eta_i = \frac{R_r}{R_r + R_{nr}} = \frac{1/\tau_r}{1/\tau_r + 1/\tau_{nr}} = \frac{1}{1 + 1/\tau_{nr}/\tau_r} \quad (2.17)$$

In the 1960s, the internal efficiency was very low (about 1%). Gradually, the lower defect density and better impurity material were developed leading to a higher efficiency.

* **Injection efficiency (η_{inj}):** The injection of carriers into an active region is not easy. If the total forward current density is called as J_f in A/m^2 , the electron-current density injected into an active region is only J_e in A/m^2 and the hole-current density injected into an active region is only J_h in A/m^2 with the much lower value compared with the original forward current density J_f . Therefore, the injection efficiency for p-semiconductor can be determined as the following equation.

$$\eta_{inj,p} = \frac{J_h}{J_e + J_h} \quad (2.18)$$

In addition, since 1950 SHOCKLEY defined that,

$$\eta_{inj,p} = \frac{D_n n L_p}{D_n n L_p + D_p p L_n} \quad (2.19)$$

Where, D_n and D_p are the diffusion coefficients for electrons and holes, respectively. L_p and L_n are the minority carrier diffusion lengths. Parameters n and p are the net electron and hole concentrations on two sides of a junction layer.

* **Light extraction efficiency ($\eta_{\text{extraction}}$):** Optical radiations are necessary to escape out from the radiative recombination centers taking place in a junction layer. However, the physical structure and geometry of material layers can cause total reflections or barriers for the escapement. Particularly, some emitted lights have their own incident angles that are higher than the limited angle of a material layer causing total reflections illustrated in Figure 2.11. Then, these lights return into the inside of the junction layer and can be reabsorbed.

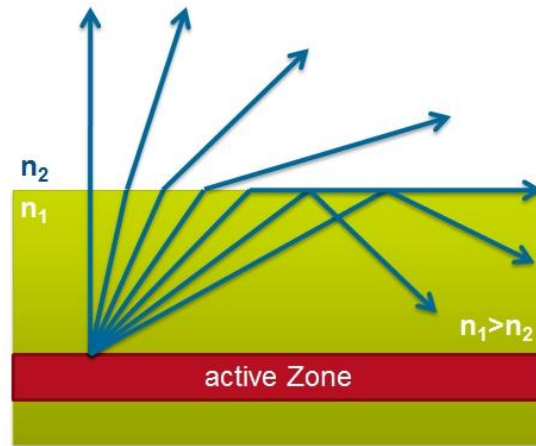


Figure 2.11 - Total reflections in a LED material layer ([14])

Therefore, many LED manufacturers attempted with the varied structural forms and diverse materials of LED capsules in order to improve their output radiation as shown in Figure 2.12. Consequently, the extraction efficiency can be defined as the rate of light leaving out from an optical surface and total light emitted in a junction layer.

$$\eta_{\text{extraction}} = \frac{\text{Output radiation on an optical surface}}{\text{Radiation emitted in a junction layer}} \quad (2.20)$$

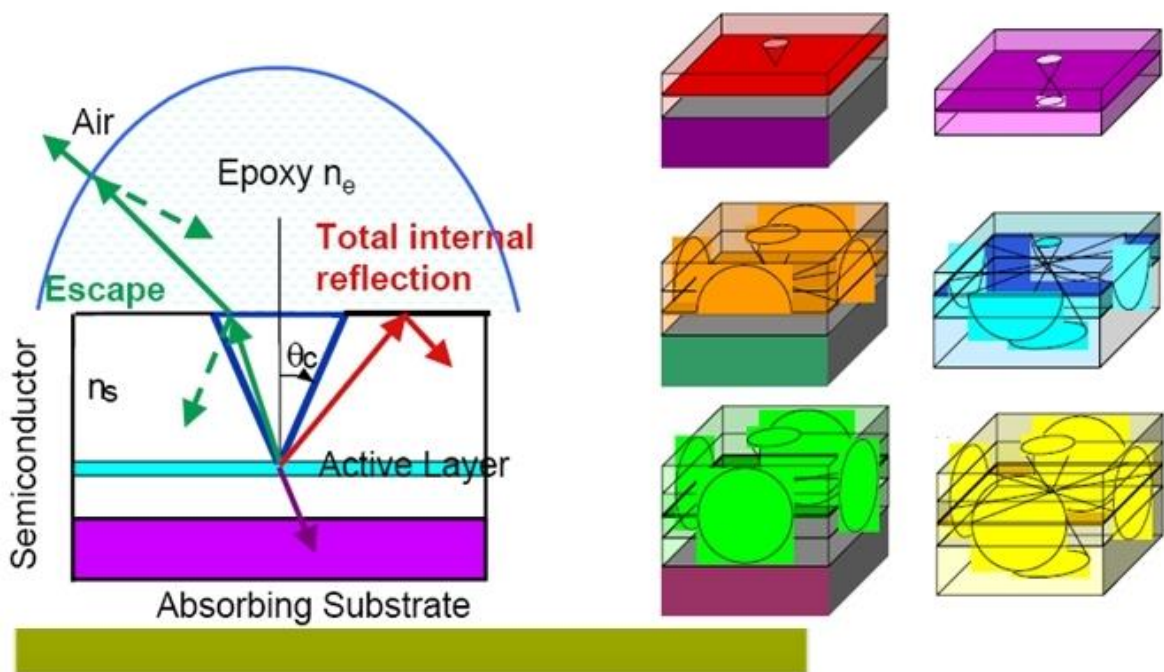


Figure 2.12 - Some structural forms of LED capsules in order to improve output radiation ([14])

* **External quantum efficiency (η_{ext}):** The external efficiency η_{ext} is defined as the rate of out photons and injected electrons. It can be calculated as the product of the internal efficiency η_i , the injection efficiency η_{inj} and the light extraction efficiency $\eta_{\text{extraction}}$.

$$\eta_{\text{ext}} = \eta_i \cdot \eta_{\text{inj}} \cdot \eta_{\text{extraction}} \quad (2.21)$$

External efficiency can be enhanced if the current of electrons dominates the current of holes. In addition, in order to have a high external efficiency, semiconductor materials must be processed so as to have much more radiative recombination than non-radiative recombination by means of an appropriate band gap, an available doping in n-layers and p-layers with the lowest resistivity or an optimal geometry of the capsule with less total reflection and less re-absorption.

* **Energy efficiency (η_e):** The energy efficiency η_e is the rate between optical power P_{opt} (or called radiative flux Φ_e in W) measured at a output surface and input electrical power P_e in W. Respectively, if V_f and I_f denote for the forward voltage in V and the forward current in A of LEDs, the energy efficiency can be determined as the following equation.

$$\eta_e = \frac{P_{\text{opt}}}{P_e} = \frac{P_{\text{opt}}}{V_f I_f} \quad (2.22)$$

This efficiency is the top level of total efficiency, when the internal efficiency, the injection efficiency and the extraction efficiency were accounted in the progress. As well, it is also an important parameter to evaluate the energy quality of LEDs.

* **Luminous efficacy (η_v in lm/W):** Optical radiation can be emitted with different peak wavelengths. However, the human eyes can only have an efficient sensitivity in a specific region determined by the average spectral sensitivity of the human visual perception of brightness ($V(\lambda)$ for the photopic vision). Therefore, the real efficient sensitivity of the human eyes is defined by means of the luminous flux Φ_v in lm calculated by Equation 2.23, where $\Phi(\lambda)$ is the absolute spectral power distribution of a LED.

$$\Phi_v = 683 \frac{\text{lm}}{\text{W}} \int_{380}^{780} V_\lambda(\lambda) \Phi(\lambda) d\lambda \quad (2.23)$$

As a result, the luminous efficacy is the rate between the luminous flux and the input electric power determined by Equation 2.24.

$$\eta_v = \frac{\Phi_v}{P_e} = \frac{683 \frac{\text{lm}}{\text{W}} \int_{380}^{780} V_\lambda(\lambda) \Phi(\lambda) d\lambda}{V_f I_f} \quad (2.24)$$

This parameter is used conventionally and very important for the design and evaluation for solid state lighting applications. In addition, it also plays an essential role to estimate the cost and quality of LEDs on the energy quality aspect.

2.1.5. Input condition and output spectrum of color semiconductor LEDs

The input energy of LEDs represented by forward current I_f in mA and influence factor of the operating temperature are treated commonly as input conditions. Consequently, the first problems established in the beginning of this chapter are a determination of the relationship between the input condition and an output spectrum or an absolute spectral power distribution of color semiconductor LEDs. Conventionally, an absolute spectral power distribution was characterized by three parameters including peak wavelength λ_p nm, full width at half maximum λ_{FWHM} in nm and peak intensity S_p in W/nm. Fortunately, the relationship between these parameters and the input condition can be

explained by the band structure theory. In that, both the forward current and operating temperature play important roles in change of carrier density, the BOLTZMANN distribution, the joint density of states and carrier temperature as well as the probability of recombination (both radiative and non-radiative recombination) in an active region. However the operating temperature T_s in °C always has a complicated relationship with the junction temperature T_j in °C and carrier temperature T_c °C. This relationship will be researched further in Chapter 5. In this section, the carrier temperature or carrier temperature converted from junction temperature will be used in mathematical descriptions. Generally, many literatures were published about the band structure theory and its application. Practically, the following knowledge is really necessary to theoretically solve the given problems in LEDs.

* **Concepts of matter waves of BROGLIE:** The band structure theory is started with concepts of matter waves or BROGLIE waves reflecting wave-particle duality of matter proposed by BROGLIE in 1924. In that, their wavelength is inversely proportional to momentum, and their frequency is directly proportional to the kinetic energy of particles. The oscillation of a particle is described by Equation 2.25.

$$\psi = Ae^{px-\omega t} \quad (2.25)$$

Where, ψ is the intensity of the oscillation, p is the momentum of a particle, and $\omega = 2\pi f$ is the angular frequency. As well, BROGLIE offered that,

$$f = \frac{p}{h} = \frac{\gamma m_0 \vartheta}{h} = \frac{m_0 \vartheta}{h \sqrt{1 - \frac{\vartheta^2}{c^2}}} \quad (2.26)$$

$$p = \hbar k = \frac{h}{2\pi} \frac{2\pi}{\lambda} = \frac{h}{\lambda} \quad (2.27)$$

Where, m_0 is the particle's rest mass, ϑ is the particle's velocity, γ is the LORENTZ factor, c is the speed of light in a vacuum, and $k = \frac{2\pi}{\lambda}$ is the angular wavenumber.

* **The physical mechanism of the emitting of a photon:** The physical mechanism of the emitting of a photon in LEDs is the spontaneous recombination of an electron and a hole illustrated in Figure 2.13. Electrons in a conduction band and holes in a valence band are distributed in two different parabolic forms in the same energy diagram. Equations for their energy band distributions are characterized as follows.

$$E_e = E_C + \frac{\hbar^2 k^2}{2m_e^*} \quad (2.28)$$

$$E_h = E_V - \frac{\hbar^2 k^2}{2m_h^*} \quad (2.29)$$

Where, m_e^* and m_h^* are the effective masses of electrons and holes, respectively, \hbar is the PLANCK's constant divided by 2π , k is the carrier wave number, E_C and E_V are the conduction band edge and valence band edge, respectively.

Likewise, a hole with the hole effective mass m_h^* and other similar parameters has the following momentum.

$$p_h = m_h^* \vartheta = \sqrt{(2m_h^*) \left(\frac{1}{2} m_h^* \vartheta^2 \right)} = \sqrt{(2m_h^*) (kT_j \sigma)} \quad (2.30)$$

The momentum of a photon with the energy E_g can be calculated by,

$$p_{\text{ph}} = \hbar k = \frac{h}{\lambda} \approx \frac{hE_g}{hc} = \frac{E_g}{c} \quad (2.31)$$

After the recombination process, if a new particle does not oscillate more, the momentum conservation law can be applied as follows.

$$p_{\text{ph}} = p_e + p_h \quad (2.32)$$

$$\frac{E_g}{c} = \sqrt{(2m_e^*)(kT_j\alpha)} + \sqrt{(2m_h^*)(kT_j\sigma)} \quad (2.33)$$

Therefore, in the transition from a conduction band to a valence band, an electron cannot change significantly its momentum. Moreover, an electron can only recombine with a hole, if they have the same momentum. Consequently, the photon energy can be written as follows,

$$E_{\text{ph}} = h\nu = h \frac{c}{\lambda} = E_e - E_h = E_C + \frac{\hbar^2 k^2}{2m_e^*} - E_V + \frac{\hbar^2 k^2}{2m_h^*} = E_g + \frac{\hbar^2 k^2}{2m_r^*} \quad (2.34)$$

$$\frac{1}{m_r^*} = \frac{1}{m_e^*} + \frac{1}{m_h^*} \quad (2.35)$$

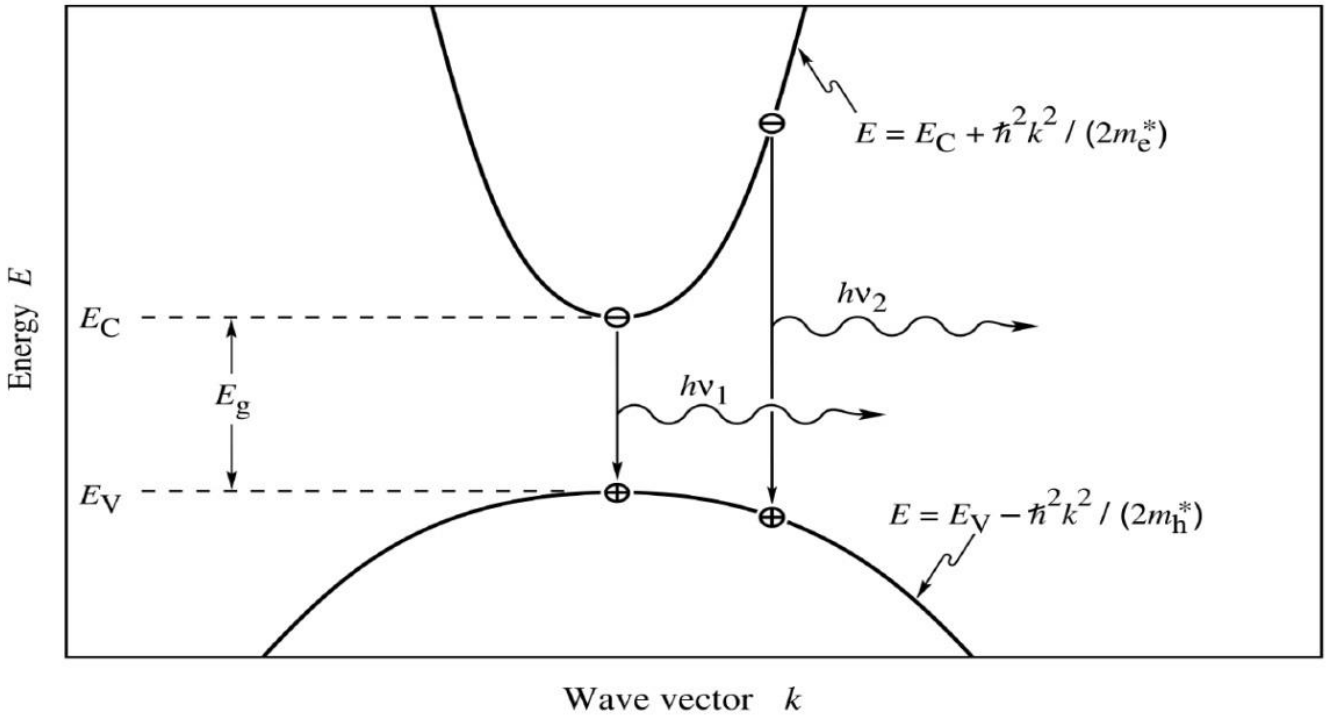


Figure 2.13 - Radiative recombination mechanics of electron-hole pairs ([1])

* **Theoretical absolute spectral power distribution of a color semiconductor LED:** By using the joint dispersion relation, the joint density of states can be calculated,

$$\rho(E) = \frac{1}{2\pi^2} \left(\frac{2m_r^*}{\hbar^2} \right)^{3/2} \sqrt{E - E_g} \quad (2.36)$$

Otherwise, the distribution of carriers in allowing bands is given by the BOLTZMANN distribution,

$$f_B(E) = e^{-E/(kT_j\sigma)} \quad (2.37)$$

Based on Equation 2.36 and Equation 2.37, a theoretical emission intensity distribution of a color semiconductor LED is proportional to the product of the joint density of states and the BOLTZMANN distribution of carriers as shown in Equation 2.38 with the energy variable E in eV or the one in Equation 2.39 with the wavelength variable λ in nm.

$$S(E) = a \left\{ \frac{1}{2\pi^2} \left(\frac{2m_r^*}{\hbar^2} \right)^{\frac{3}{2}} \sqrt{E - E_g} \right\} \left\{ e^{-\frac{E}{\sigma k T_j}} \right\} \quad (2.38)$$

$$S(\lambda) = a \left\{ \frac{1}{2\pi^2} \left(\frac{2m_r^*}{\hbar^2} \right)^{\frac{3}{2}} \sqrt{\frac{hc}{\lambda} - E_g} \right\} \left\{ e^{-\frac{hc}{\lambda \sigma k T_j}} \right\} \quad (2.39)$$

* **Characteristic parameters of an absolute spectral power distribution:** Three characteristic parameters of a spectrum mentioned in the above sections are peak wavelength, full width at half maximum and peak intensity. If the mathematical function in Equation 2.39 is drawn in a graphic form, the theoretical absolute spectral power distribution of a color semiconductor LED is presented visually in Figure 2.14. In that, its intensity is maximal at a specific energy and this energy is determined as,

$$E = E_g + \frac{1}{2} k T_j \sigma \quad (2.40)$$

Likewise, based on the curves in Figure 2.14, the peak wavelength, the full width at half maximum and the peak intensity can be also determined successively as follows.

$$\lambda_p = \frac{hc}{E_g + \frac{1}{2} k \sigma T_j} \quad (2.41)$$

$$\lambda_{FWHM} = \frac{hc}{1.8 k \sigma T_j} \quad (2.42)$$

$$S_p = a \left\{ \frac{1}{2\pi^2} \left(\frac{2m_r^*}{\hbar^2} \right)^{\frac{3}{2}} \sqrt{\frac{hc}{\lambda_p} - E_g} \right\} \left\{ e^{-\frac{hc}{\lambda_p \sigma k T_j}} \right\} \quad (2.43)$$

* **Role of the input forward current:** The simple theory about the forward current of the color semiconductor LEDs was mentioned in Section 2.1.2 and was described mathematically by equations 2.3, 2.4, 2.5, 2.8, 2.9, 2.10 and 2.11. Following to MÜLLER in [15], the relationship between currents and effective masses should be described by Equation 2.44.

$$\frac{\frac{I_h}{A_h}}{\frac{I_e}{A_e}} = \frac{J_h}{J_e} = \left(\frac{D_h N_h}{L_h} \right) \left(\frac{L_e}{D_e N_e} \right) \left(\frac{(m_e^* m_h^*)_n}{(m_e^* m_h^*)_p} \right)^{\frac{3}{2}} \exp\left(\frac{\Delta E_g}{k_B \sigma T_j} \right) \quad (2.44)$$

Where, J_e and J_h are the injected electron and hole current densities, D_e and D_h and L_e and L_h are the minority electron and hole diffusion coefficients and diffusion lengths, respectively, A_e and A_h are the cross-sectional areas of electrons and holes, N_e and N_h are the electron and hole doping densities, m_e^* and m_h^* are the electron and hole effective masses (on the n-side in the numerator and the p-side in the denominator), and ΔE_g is the energy gap difference between the upper confining layer and the active layer.

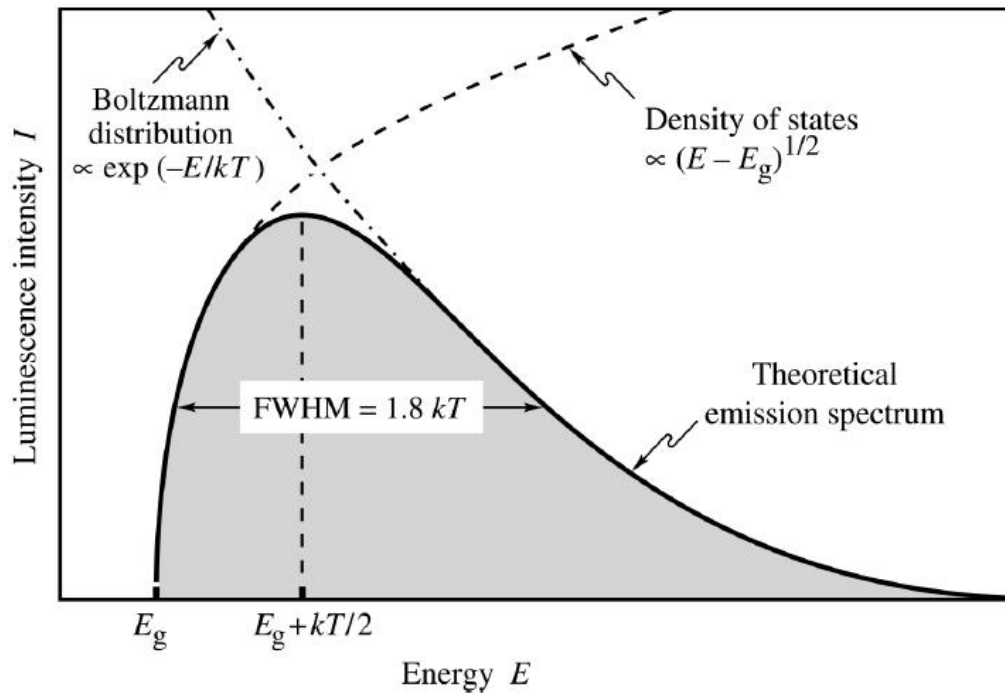


Figure 2.14 - Theoretical emission spectrum of a color semiconductor LED ([1])

* **Summary:** The equation system 2.28 - 2.44 is the mathematical description of the relationships between three characteristic parameters of the primary spectral power distribution of a color semiconductor and the operating condition including the forward current and the junction temperature based on the band structure theory, the concepts of BROGLIE, the energy conservation law, the momentum conservation law, the joint dispersion relation and the BOLTZMANN distribution. Consequently, it can be recognized, that theoretically these relationships can be described mathematically as three-dimensional functions such as $\lambda_p(I_f, T_j)$, $\lambda_{FWHM}(I_f, T_j)$ and $S_p(I_f, T_j)$. However, unfortunately many parameters are very difficult to measure and determine explicitly. Therefore, based on the above fundamental knowledge, more feasible and practical mathematical forms should be investigated and offered for real spectral power distributions of color semiconductor LEDs, experimentally. Moreover, it is also really necessary to analyze and examine whether the three above characteristic parameters are really good enough to describe the real absolute spectral power distributions of color semiconductor LEDs.

2.2. Input condition and output spectrum of phosphor converted LEDs

In Section 2.1, the basic knowledge about the intrinsic phenomena inside color semiconductor LEDs was discussed particularly. In that, beside the review of the basic concepts of color semiconductor LEDs based on the semiconductor physics, the band structure theory was used to describe and explain the relationships between input conditions and the theoretical absolute spectral power distribution of color semiconductor LEDs. They are very important knowledge for the practical investigations of LED properties in Chapter 3, for the analysis of the thermal reactions between LED components in Chapter 5 and for the establishment of the electrical and optical transient models in Chapter 6.

Successively, a luminescent material layer of PC-LEDs is the central object in the study of this section. However, regarding LED modeling and LED model applications, not all intrinsic phenomena occurring inside a luminescent material layer such as the absorption (or excitation), the radiative transition

(or emission), the relaxation, the Beer-Lambert material absorption, the Mie light scattering, as well as not all basic chemical concepts such the host lattice (or matrix), the activator and the sensitizer are necessary to be explained specifically and entirely in this section like that done for semiconductor LEDs in Section 2.1, because these systematic factors are only possible to be improved or changed by chemistry and packaging technologies that are not researched in the framework of this thesis. Therefore, the most important theme in Section 2.2 is the relationship between the input condition and the output spectrum for a luminescent material layer. Particularly, the input condition in case of a luminescent material layer of PC-LEDs are neither the junction temperature nor the carrier temperature, as well as no the forward current, but are the primary absolute spectral power distribution of a blue semiconductor LED (called “*original blue spectrum*”) and the inside temperature of a luminescent material layer (called “*phosphor temperature*”). And the output is the secondary absolute spectral power distribution of a luminescent material layer (called “*phosphor spectrum*”).

2.2.1. Brief explanation about the basic principle of the spectral conversions inside a luminescent material layer

The input condition for a luminescent material layer of PC-LEDs consists of the phosphor temperature T_{ph} in °C and the original blue spectrum. Under these input conditions, a luminescent layer can absorb the original blue spectrum and then emit its own spectrum called phosphor spectrum or emission spectrum. This emission spectrum plays a role as a secondary absolute spectral power distribution created derivatively from the primary absolute spectral power distribution of the blue semiconductor LED. Depending on the nature of the blue semiconductor LED, the chemical composition, geometry and concentration of the luminescent material layer, the material and shape of the capsule containing both the luminescent material and the blue chip, the chemical and physical internal reactions between components, and the luminescent material temperature in the operating process, the final absolute spectral power distribution (called “*final spectrum*” or “*output spectrum*”) of pc-LEDs, which is the sum of the rest blue absolute spectral power distribution of the blue semiconductor LED (called “*rest blue spectrum*”) and the phosphor spectrum, will have different shapes and amplitudes. In more detail, the general composition and structure of a luminescent material layer of PC-LEDs and its energy conversion following to the energy conservation law will be explained specifically in Section 5.1 in Chapter 5. As well, two spectral conversions inside a PC-LEDs with many influential factors will be described specifically in Section 6.4.1 in Chapter 6.

2.2.2. Phosphor temperature and output spectrum of PC-LEDs with a thermal quenching mechanism

The author LIN and co-authors in [16] and [17] published the investigation of thermal quenching and its mechanism for $Y_3Al_5O_{12}:Ce^{3+}$ and $CaAlSiN_3:Eu^{2+}$. These authors described the optical intensity reduction and peak wavelength shift of $Y_3Al_5O_{12}:Ce^{3+}$ and $CaAlSiN_3:Eu^{2+}$ over the phosphor temperature of 25 °C - 300 °C like the description in Figure 2.15.a. In Figure 2.15.b the authors illustrated and explained for the mechanism of thermal quenching of luminescent materials. In that, GS is the ground state, ES_2 is the excited state at the phosphor temperature $T_{ph,2}$ corresponding with energy level T_2 of electron level 5d, ES_1 is the excited state at the phosphor temperature $T_{ph,1}$ corresponding with energy level E of the same electron level 5d, ΔE_1 is the thermal excitation energy due to the non-radiative transition from original excited state ES_0 to new excited state ES_1 and ΔE_2 is the thermal excitation energy due to the non-radiative transition from original excited state ES_0 to new

excited state ES_2 . In addition, the original excited state ES_0 is due to absorbed external energy Ex corresponding with an original phosphor temperature $T_{ph,0}$. As well, E_m is the energy for a radiative transition (called “radiative transient energy”). Moreover, the new excited state of $YAG:Ce^{3+}$ at a new phosphor temperature caused a shift down to a lower radiative transition energy level. As a result, the peak wavelength emission of $YAG:Ce^{3+}$ was shifted 10 nm (from 560 nm - 570 nm) into the right side (called “red shift”).

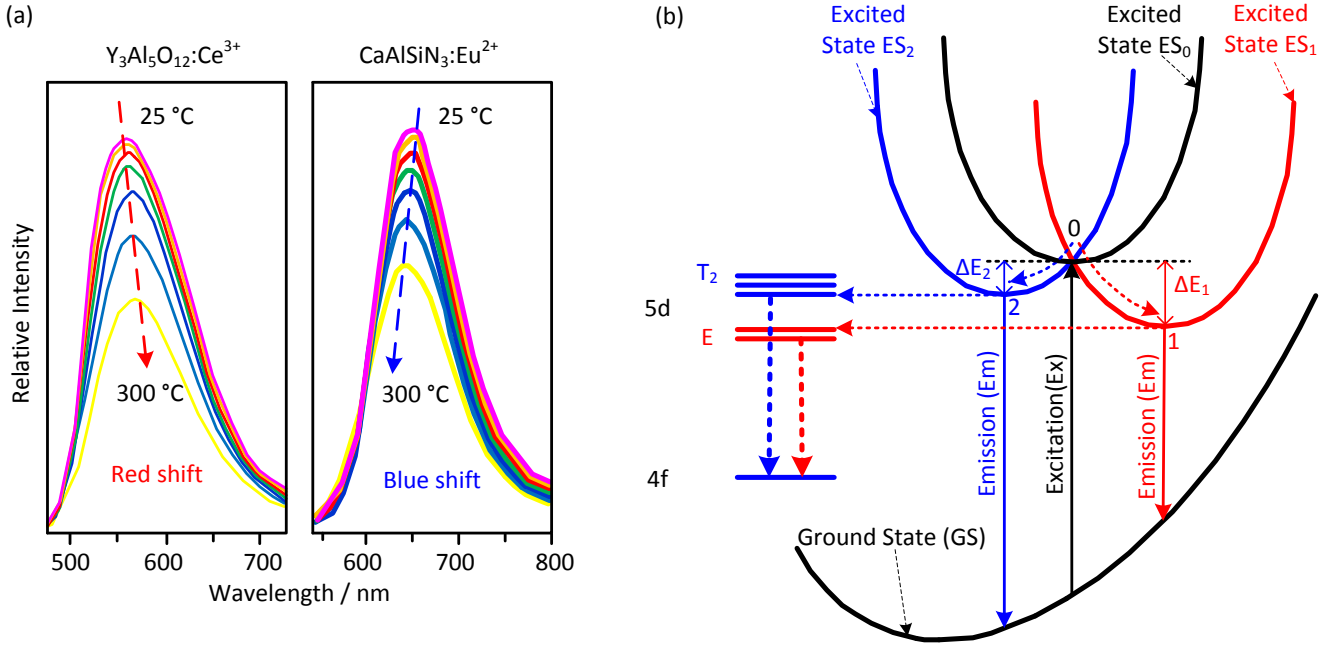


Figure 2.15 - Thermal quenching and its mechanism in $Y_3Al_5O_{12}:Ce^{3+}$ and $CaAlSiN_3:Eu^{2+}$ ([17])

This shift can be explained by the VARSHNI equation 2.45 for the temperature dependence of the energy difference between an excited state and a ground state of a luminous material as follows,

$$E(T_{ph}) = E_0 - \frac{aT_{ph}^2}{T_{ph}+b} \quad (2.45)$$

Where, $E(T_{ph})$ is the energy difference between an excited state and a ground state at temperate T_{ph} in K, E_0 is the initial energy difference at a low phosphor temperature and a and b are fitting parameters. When the phosphor temperature increases, $E(T_{ph})$ decreases. Consequently, the peak wavelength of phosphor spectrum ($\lambda_{peak} = \frac{hc}{E(T_{ph})}$) increases causing a red shift for the output spectrum of PC-LEDs. This is the principle of the peak wavelength shift of a phosphor spectrum in a thermal quenching mechanism.

Likewise, for a reduction of the peak intensity of a phosphor spectrum, the ARRHENIUS equation 2.46 is ideal to determine its temperature dependence in a thermal quenching mechanism.

$$S_p(T_{ph}) \approx \frac{S_{p,0}}{1+d\exp\left(\frac{-E}{k_B T_{ph}}\right)} \quad (2.46)$$

Where, $S_{p,0}$ is the initial peak intensity of the phosphor emission spectrum at a low temperature, $S_p(T_{ph})$ is the peak intensity at phosphor temperature T_{ph} in K, d is a fitting constant, E is the activation energy for the thermal quenching, and k_B is the BOLTZMANN's constant. Furthermore, the authors in [16] determined that the thermal activation energies were 0.25 eV and 0.21 eV for $Y_3Al_5O_{12}:Ce^{3+}$ and $CaAlSiN_3:Eu^{2+}$, respectively.

Similarly, the idea of the equation ARRHENIUS is also used to determine the luminescence decay time depending on a phosphor temperature as in Equation 2.47.

$$\tau(T_{\text{ph}}) = \frac{\tau_0}{1 + e \cdot \exp\left(\frac{-E}{k_B T_{\text{ph}}}\right)} \quad (2.47)$$

Where, $\tau(T_{\text{ph}})$ is the luminescence decay time at the phosphor temperature T_{ph} in K, τ_0 is the initial decay time at a low temperature, and e is a fitting constant. Finally, the above results and analyses showed that the thermal quenching is not good for PC-LEDs at both the energy efficacy factor and color quality factor. Therefore, the thermal quenching should be improved as well as possible by appropriate chemical compositions.

2.2.3. Excitation spectrum and output spectrum of PC-LEDs

In Section 2.2.2, all analyses mentioned to the temperature dependence of the characteristic parameters of an emission spectrum based on initial values such as the initial energy E_0 in eV, the initial intensity $S_{p,0}$ in W/nm and the initial luminescence decay time τ_0 in ns. Experimentally, these initial values were measured at a low phosphor temperature that was defined by the researchers. Therefore, it was always assumed that the initial parameters were already determined. However, a spectral conversion from an input excitation spectrum of a blue semiconductor LED into a phosphor emission spectrum or an output PC-LED spectrum (a phosphor emission and an output PC-LED spectra can be treated commonly as an output PC-LED spectrum in mathematical descriptions, if packaging factors are processed as a systematic constant or a converted constant) is not yet described explicitly by means of mathematical formulas. Consequently, in this section the relationship between the input excitation blue spectrum and the output PC-LED spectrum will be attempted to study furthermore.

Particularly, if the energy factor E in eV in Equation 2.46 is substituted by the expression determined by Equation 2.45, a new equation for the peak intensity of an output PC-LED spectrum can be rewritten as,

$$S_p(T_{\text{ph}}) \approx \frac{S_{p,0}}{1 + d \exp\left(\frac{-E_0 + \frac{aT_{\text{ph}}^2}{T_{\text{ph}} + b}}{k_B T_{\text{ph}}}\right)} \quad (2.48)$$

Then, the relationship between the primary absolute spectral power distribution of a blue semiconductor LED described in Equation 2.38 or Equation 2.39 and the final absolute spectral power distribution of a PC-LED described in Equation 2.48 can be solved via the energy conservation law and the intrinsic structure parameters of a luminescent material indicated by the initial energy E_0 in eV and the initial intensity $S_{p,0}$ in W/nm. However, unfortunately not all spectral components of the spectral power distribution of blue chips can be absorbed similarly in a luminescent material. In some spectral regions, spectral components can be absorbed much more and in other spectral regions, spectral components can be absorbed less or even not absorbed.

In more detail, the absorbed energy must correspond to the band gap energy of luminescent materials ($E_{g,\text{ph}}$ / eV). In addition, according to [18], in a neutralization of the ionized donor, the involved energy is $-E_D + e^2 / (4\pi\epsilon_0\epsilon R)$, where R is the distance between a donor and an acceptor concerned in the emission process, and ϵ and ϵ_0 are the dielectric constants of luminescent materials. And the COULOMB term originates from the electrostatic interaction between ionized donors and

acceptors. As well, in the neutralization of the ionized acceptor, the involved energy is $-E_A$. Finally, the involved energy for the luminescence process can be determined by,

$$E_0 = E_{g,ph} - (E_D + E_A) + \frac{e^2}{4\pi\epsilon_0\epsilon R} \quad (2.49)$$

In fact, the distribution of E_0 in an energy diagram is the complicated distribution specified by the chemical nature of each phosphor structure with many donor-acceptor pairs like an example in Figure 2.16. Therefore, the mathematical description of the distribution of E_0 in front of different excitation spectra of blue semiconductor LEDs for varied luminescent materials is really difficult to realize specifically.

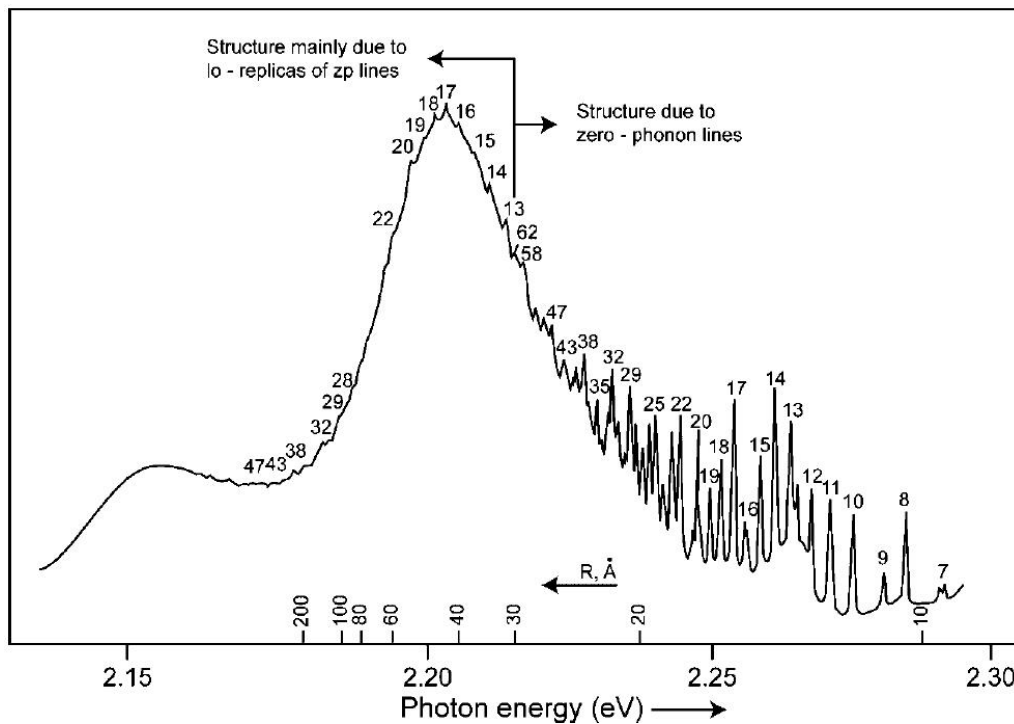


Figure 2.16 - An example in case of donor-acceptor pair luminescence of GaP doped with ZnS ([18])

2.2.4. Summary

From the above analyses, it can be recognized, that the establishment of explicit equations with very specific descriptions of the relationship between the primary absolute spectral distributions of blue semiconductor LEDs and the secondary absolute spectral power distributions of luminescent materials is still unpractical and infeasible. Therefore, theoretical explanations about a basic principle of the spectral conversion inside a luminescent material layer of PC-LEDs or practical investigations and experimental characterizations about a temperature dependence of emission spectra are only enough to confirm that three characteristic parameters of emission spectra or output spectra of PC-LEDs have mathematical relationships as “three-dimensional functions” of a blue excitation spectrum and a phosphor temperature. Moreover, the concept “three-dimensional functions” here is even not completely correct, because a blue excitation spectrum is also described by at least its own three characteristic parameters. In addition, systematic factors relating chemistry and packaging technologies are difficult to determine fully and exactly. As well, the phosphor temperature is not easy to measure and calculate from the operating temperature, because their relationship must be determined accurately in a spatial thermal equilibrium with few different thermal transport mechanisms such as thermal conduction,

thermal convection and thermal radiation on each material gradient and the packaging of the PC-LEDs is very tiny and always blocked completely. Consequently, an experimental and feasible approach in the establishment of optical transient LED models for PC-LEDs is really necessary to be investigated and offered furthermore in Chapter 6.

2.3. General summary

In the role of a background chapter, the basic knowledge about the essential intrinsic phenomena inside semiconductor LEDs such as the injection luminescence, the physical semiconductor structure of a junction layer (homo-junction, hetero-junction and quantum well) with corresponding mathematical descriptions, direct / indirect recombination, radiative / non-radiative recombination and efficiency concepts were described briefly. On the other hand, the basic principle of a spectral conversion inside a luminescent material layer of PC-LEDs was also explained. Especially, the key problems about relationships between the input conditions and the output spectra of color semiconductor LEDs and PC-LEDs were studied specifically. Finally, the main contents of this chapter can be summarized by the following points.

In the first place, the forward current and the operating temperature were treated as the input conditions of color semiconductor LEDs. Moreover, the carrier temperature or the carrier temperature converted from a junction temperature was the official temperature parameter used in the mathematical relationships. As well, an output spectrum of a color semiconductor LED was explained and described by a combination between the joint density of states and the thermal BOLTZMANN distribution. Consequently, the mathematical characterization for an absolute spectral power distribution of color semiconductor LEDs was understood fully. Nevertheless, many parameters in this characterization are very difficult to measure and determine accurately. Therefore, this characterization should be only used to explain the properties of the color semiconductor LEDs in the practical investigations in Chapter 3 and to suggest the appropriate mathematical forms of color the semiconductor LED models in Section 6.4.2 and Section 6.4.3 in Chapter 6, but the modeling of color semiconductor LEDs for solid state lighting applications needs a more practical and feasible approach, which will be offered in Section 6.4.3 in Chapter 6.

In the second place, a luminescent material layer was the key object of PC-LEDs. However, in the context of LED modeling and LED model applying, inside intrinsic phenomena, chemical compositions, physical structures, geometrical forms and concentrations of luminescent materials, as well as physical and chemical reactions between them were not studied in the framework of this thesis. But the biggest consideration in this chapter was the relationship between the input conditions of the phosphor temperature and the original blue spectrum and the output spectrum of PC-LEDs. Thus, the basic principles of the spectral conversions and the temperature dependence of the output spectrum of PC-LEDs in the thermal quenching mechanism were studied. Consequently, the mathematical descriptions of the relationships were recognized. Nonetheless, it is not easy to apply these descriptions in real performances, because the initial parameters at a low phosphor temperature, the correlation between these initial parameters with the reactions of the excitation blue spectrum and the chemical nature of a luminescent material layer, as well as the phosphor temperature measurement are big barriers in practical performances. Therefore, meaningfully the experimental investigations and the practical offers for the transient LED models of PC-LEDs should be researched according to a more available approach in Section 6.4.4 in Chapter 6.

3. Optical, radiant and colorimetric properties of LEDs

3.1. Motivation

In Chapter 1, brief classification and overview history of LEDs were described. Especially, the current development state of LEDs of both the light output and the lighting quality was also updated. Consequently, it could be recognized, that light output of LEDs was improved considerably. Contrarily, lighting quality of LEDs has been not yet considered appropriate. Therefore, in this chapter, lighting quality has to be investigated and discussed furthermore for both color semiconductor LEDs and white PC-LEDs. Particularly, concepts of lighting quality and its limited range in this thesis will be analyzed specifically in order to define key quality aspects of research. Successively, color semiconductor LEDs and white PC-LEDs will be investigated regarding the temperature dependence and current dependence of optical, radiant and calorimetric properties. Finally, the achieved results will give necessary suggestions for minimization of parameter differences between the LED manufacturers and LED-luminaire manufacturers in Chapter 4, the characterization of thermal, electrical and optical transient LEDs in Chapter 5 and Chapter 6, as well as the optimization and stabilization in Chapter 7.

3.2. Concepts of lighting qualities and their limited range in the thesis

The determination of lighting quality parameters for lighting applications in general and lighting quality for solid state lighting applications in particular is not simple, because it relates to many different scientific and technical fields such as semiconductor physics, quantum physics, luminescent material chemistry, psychology and physiology of the human eyes or lighting technique. In addition, demand of lighting quality depends particularly on lighting objects, lighting fields and lighting application types such as indoor lighting or outdoor lighting, office lighting or architecture lighting. Until now the lighting estimation has almost based on the average spectral sensitivity of the human visual perception of brightness such as $V(\lambda)$ for the photopic vision and $V'(\lambda)$ for the scotopic vision, although it is not accurate perfectly for every case. Based on this estimation, some basic concepts were defined for the lighting industry such as radiant flux Φ_e in W, radiant intensity I_e in W/sr, irradiance E_e in W/m^2 , luminous flux Φ_v in lm, luminous intensity I_v in cd, luminance E_v in lx and luminance L_v in cd/m^2 like the description diagram in Figure 3.1. Otherwise, some more complicated concepts were established relating to the light intensity distribution such as radiant intensity distribution, vertical luminous intensity distribution, horizontal luminous intensity distribution, cylindrical luminous intensity distribution, half cylindrical luminous intensity distribution and iso-lux-line luminous intensity distribution. Or some other complicated concepts, which are applied much in the automotive lighting industry, relate to psychology and physiology aspects of the human eyes such as glare and contrast behavior. Therefore, it can be recognized, that almost current concepts of the lighting evaluation have been usually to use for outdoor lighting applications, while advance concepts for indoor lighting applications were mentioned quite limitedly.

Fortunately, in recent time new achievements about evaluation of lighting quality were published in some literatures such as [19] - [35]. Based on these new advancements, the collection of new quality parameters for evaluation of lighting quality can be established like the description diagram in Figure 3.2. In that, lighting technique does not only consist of parameters for a weighting of light output such as luminous flux, radiant flux, luminous efficacy or radiant efficiency, but also includes parameters for evaluation of color quality such as chromaticity, correlated color temperature CCT in K, whiteness $\Delta u'v'_{CCT}$, color rendering indexes (R_a , R_9 or AVR_{1-14}), color preference, color harmony, color memory, color gamut, light source brightness, object brightness, brilliance, circadian stimulus CS and scotopic - photopic ratio S/P . In more detail, definitions and mathematical descriptions of these concepts were explained specifically in the literatures [19] - [35].

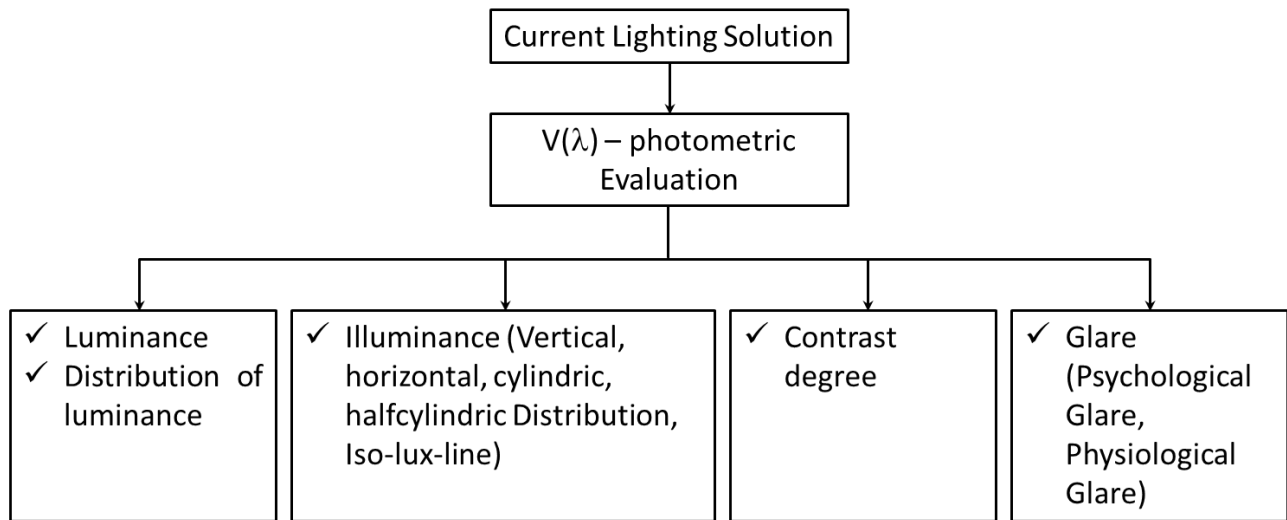


Figure 3.1 - Current lighting situation ([30])

On the other hand, short term stability and long term stability of light sources in different operating conditions of the forward current and operating temperature as well as the burning time must be taken account into lighting quality as special important parameters for solid state lighting applications like content published in [33], [36], [127] and [153] by the author, because if a high quality solid state lighting system is only able to operate in a very short time and/or its quality parameters change intensively according to the variation of operating condition, this system will be impossible to be used in lighting applications.

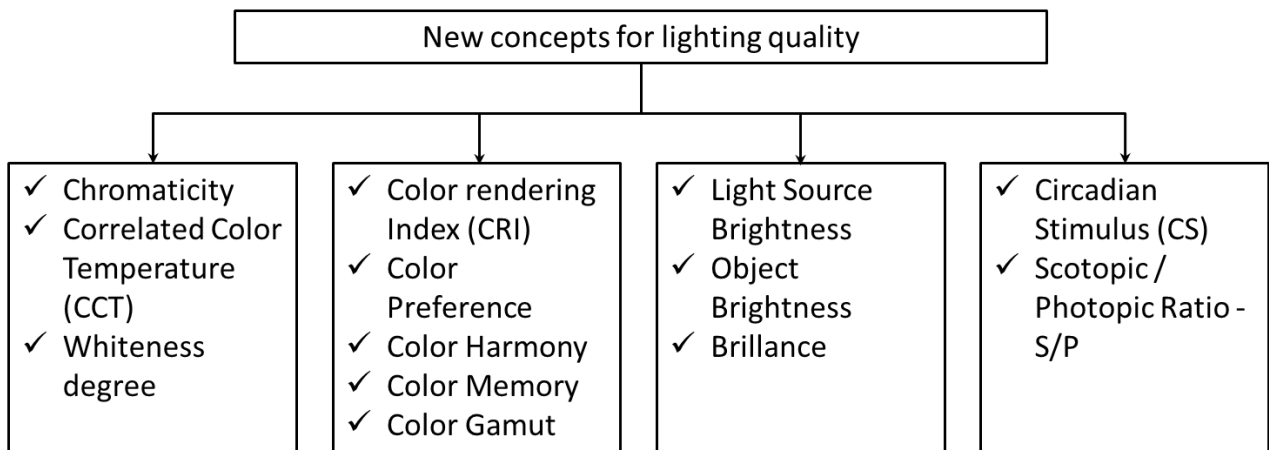


Figure 3.2 - New concepts for lighting quality ([30])

However in the framework of this thesis, it is impossible to research all lighting quality aspects like the above mentioned. Instead of that, the focus should be laid on some key aspects such as chromaticity, correlated color temperature, whiteness, color rendering indexes, luminous flux, luminous efficacy and short term temperature stability of hybrid LED-lamps in high quality solid state lighting applications. Therefore, in the next sections in this chapter, optical, radiant and colorimetric properties of color semiconductor LEDs and white PC-LEDs will be investigated regarding their temperature and current dependence. Particularly, these dependencies will be researched for LED spectra previously in order to have an intrinsic perception. Then, more detailed analyses will be carried out for the temperature dependence and the current dependence of peak wavelength, full width at half maximum wavelength, radiant flux, radiant efficiency and color difference of color semiconductor LEDs, and the temperature dependence and the current dependence of luminous flux, luminous efficacy, color difference and CCT of white PC-LEDs. Especially, color rendering indexes, luminous efficacy and whiteness of current commercial PC-LEDs on the worldwide market should be investigated at a binning condition (350 mA and 80 °C) in order to determine their limits for LED selection, LED combination, optimization and stabilization in Chapter 7.

3.3. Optical, radiant and colorimetric properties of typical color semiconductor LEDs

3.3.1. General Consideration

In Session 3.2, the lighting quality from basic concepts to advance concepts was discussed. Hence, disadvantages of the current concepts and advantages of the new concepts of lighting quality were determined. In addition, necessary lighting quality aspects of short term stability and long term stability for the solid state lighting applications were supplemented. In order to carry out practical investigations, a general consideration is necessary to determine representations for color semiconductor LEDs and to establish the desired targets.

* **Representations for color semiconductor LEDs in investigation:** In Section 1.1.2 in the chapter 1, many different types of color semiconductor LEDs were discussed following to varied semiconductor materials such as Silicon carbide (SiC), Gallium Arsenide (GaAs), Aluminum Gallium Arsenide (AlGaAs), Gallium Arsenide Phosphide (GaAsP), Gallium Phosphide (GaP), Gallium Nitride (GaN), Indium Gallium Nitride (InGaN) and Aluminum Gallium Indium Phosphide (AlGaInP). However, up to now only some of them can be usually used to fabricate color semiconductor LEDs worldwide, because of their limit of efficiency and technology. Particularly, these semiconductor materials can be grouped into three groups including the first group with Indium Gallium Nitride (InGaN), the second group with Aluminum Indium Gallium Phosphide (AlInGaP) and the third group with Gallium Phosphide (GaP), Gallium Arsenide Phosphide (GaAsP) and Gallium Aluminum Arsenide (GaAlAs). In that, the first group (InGaN) is usually used to fabricate ultraviolet, royal blue, blue and green semiconductor LEDs with a high radiant efficiency and a good stability, the second group (AlInGaP) is usually used to fabricate yellow, amber, orange and red semiconductor LEDs with a worse radiant efficiency and a bad stability and the last group (GaP, GaAsP and GaAlAs) is also used to fabricate yellow, amber, orange and red semiconductor LEDs with a bad radiant efficiency and a bad stability. Therefore, in fact almost current semiconductor LEDs are fabricated by Thin-GaN technology for royal blue ($440 \text{ nm} \leq \lambda_p \leq 450 \text{ nm}$), blue ($460 \text{ nm} \leq \lambda_p \leq 470 \text{ nm}$) and green ($510 \text{ nm} \leq \lambda_p \leq 535 \text{ nm}$) semiconductor

LED, and by InGaAlP-Thin-film technology for red ($610 \text{ nm} \leq \lambda_p \leq 630 \text{ nm}$) and deep red ($630 \text{ nm} \leq \lambda_p \leq 680 \text{ nm}$). However, in the framework of this thesis, it is impossible to investigate all color semiconductor LED types with all semiconductor materials, but meaningfully it should focus on some typical semiconductor LEDs that can represent well for other conventional color semiconductor LEDs and their results are also possible to serve directly for further researches in the next chapters. Consequently, in this chapter, four typical color semiconductor LEDs including red (R with $\lambda_p \sim 640 \text{ nm}$), green (G with $\lambda_p \sim 510 \text{ nm}$), blue (B with $\lambda_p \sim 460 \text{ nm}$) and orange (O with $\lambda_p \sim 600 \text{ nm}$) semiconductor LEDs of three well-known manufacturers (A, B and C) are selected in investigations.

* **Determination of desired targets:** Desired targets in this section include the investigation of optical, radiant and colorimetric properties of four typical color semiconductor LEDs and determination of the temperature and current dependence of the spectra, peak wavelength λ_p in nm, full width at half maximum wavelength λ_{FWHM} in nm, radiant efficiency Φ_e in W/W or %, radiant flux Φ_v in W and color difference $\Delta u'v'$. In addition, based on practical experiences, the operating region, which is available for investigations, should be from $40 \text{ }^\circ\text{C}$ to about $80/85 \text{ }^\circ\text{C}$ of the operating temperature and from 350 mA to 700 mA of the forward current. Specially, for the current dependence of color difference, the operating current range should be widened from 100 mA to 700 mA in order to have a better view on the current dependence in the low forward current region.

3.3.2. Temperature and current dependence of the color semiconductor LED spectra

In order to have an intrinsic perception and deep explanation about temperature dependence and current dependence of optical, radiant and colorimetric properties of color semiconductor LEDs in the next sections, their temperature and current dependence of color semiconductor LED spectra will be investigated and discussed as follows.

* **Temperature dependence of color semiconductor LED spectra:** In Figure 3.3, the temperature dependence of the chosen color semiconductor LEDs is described in the operating region from $40 \text{ }^\circ\text{C}$ to $80 \text{ }^\circ\text{C}$ of operating temperature and at the forward current of 350 mA . Based on investigating results in Figure 3.3, it can be recognized, that when the operating temperature increased from $40 \text{ }^\circ\text{C}$ to $80 \text{ }^\circ\text{C}$, spectra of the orange and red semiconductor LEDs (InGaAlP LEDs) shifted into the right side of the average spectral sensitivity of the human visual perception of brightness ($V(\lambda)$ for the photopic vision and $V'(\lambda)$ for the scotopic vision) making their luminous flux lower. Otherwise, some spectral component of the blue and green semiconductor LED spectra (InGaN LEDs) shifted into the right side, while fewer low spectral components widened a little into the left side. Therefore, in order to evaluate the energy quality aspect fairly, in Section 3.3.4 radiant flux and radiant efficiency should be chosen to substitute for luminous flux and luminous efficacy. In addition, the results also illustrated, that the spectral shift of the red and orange semiconductor LEDs (InGaAlP LEDs) are stronger than that of the blue and orange semiconductor LEDs (InGaN LEDs) causing their big color differences like mentioned in Section 3.3.5.

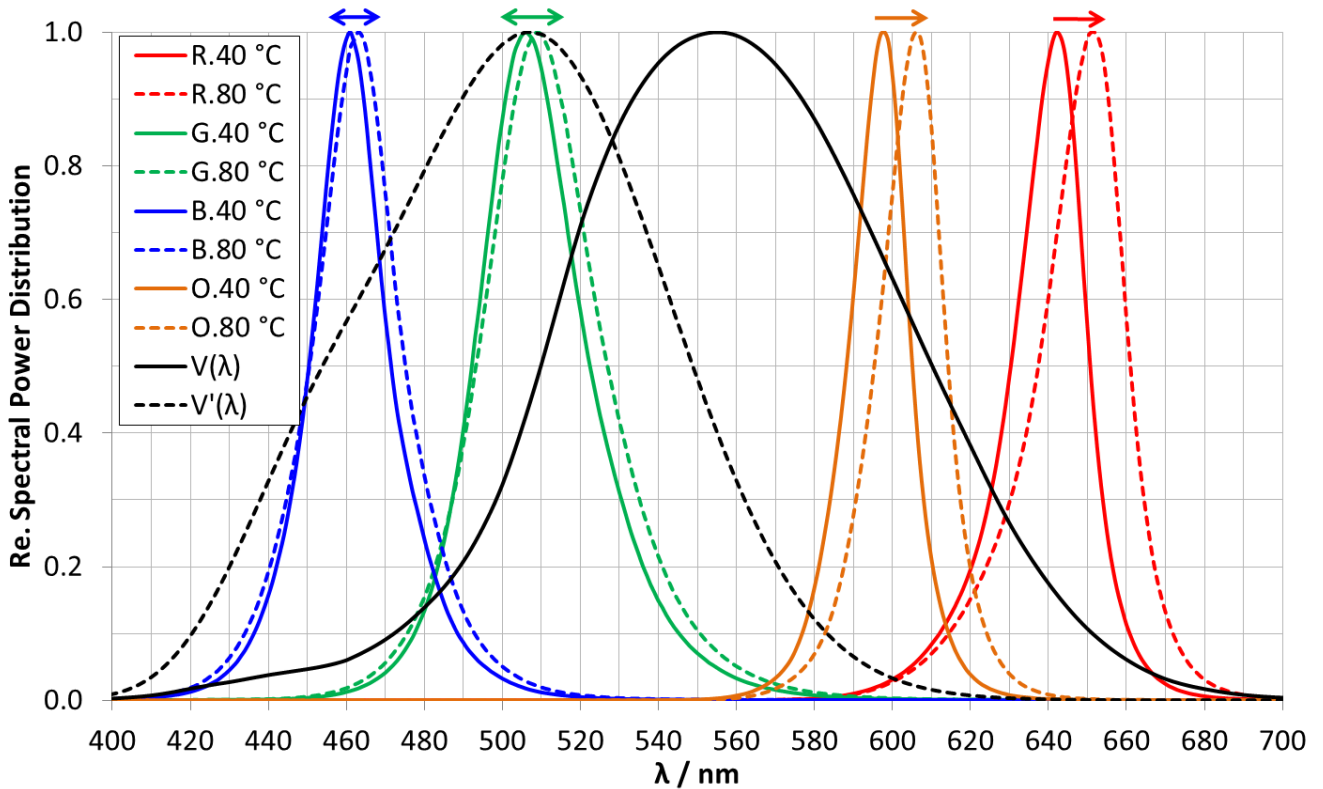


Figure 3.3 - Temperature dependence of the spectra of four color semiconductor LEDs at 350 mA

* **Current dependence of color semiconductor LED spectra:** On the other hand, in Figure 3.4 the current dependence of four typical color semiconductor LEDs is described in the operating region from about 350 mA to 700 mA of the forward current and at operating temperature of 80 °C. The investigated results in Figure 3.4 showed that when forward current increased from 350 mA to 700 mA, spectra of the red and orange semiconductor LEDs (InGaAlP LEDs) shifted strongly into the right side. Otherwise, there was nearly no spectral shift for the blue and green semiconductor LEDs (InGaN LEDs), but the bandwidth of their spectra spread wider a little into the left side. These results are only possible to confirm that the color difference of InGaAlP LEDs was much more than that of InGaN LEDs, but they cannot conclude about the radiant flux, the radiant efficiency, the luminous flux or the luminous efficacy of these semiconductor LEDs. Particularly, when forward current increases, the carrier density is higher in the active region in a junction layer, but the carrier distribution is also changed causing the change in spectral shape of color semiconductor LEDs asymmetrically like the theory described in Section 2.1.5 in Chapter 2. Therefore, theoretically more radiative recombination due to higher carrier density makes color semiconductor LEDs having more brightness. Contrarily, more non-radiative recombination and the change of carrier distribution make color semiconductor LEDs have less brightness. Two opposite processes take place concurrently and differently between InGaN LEDs and InGaAlP LEDs. Consequently, when forward current increases, the InGaN LEDs are brighter, but their brightness are not linearly proportional to the increase of forward current and oppositely some InGaAlP LEDs sometimes are even darker like the description in Section 3.3.4.

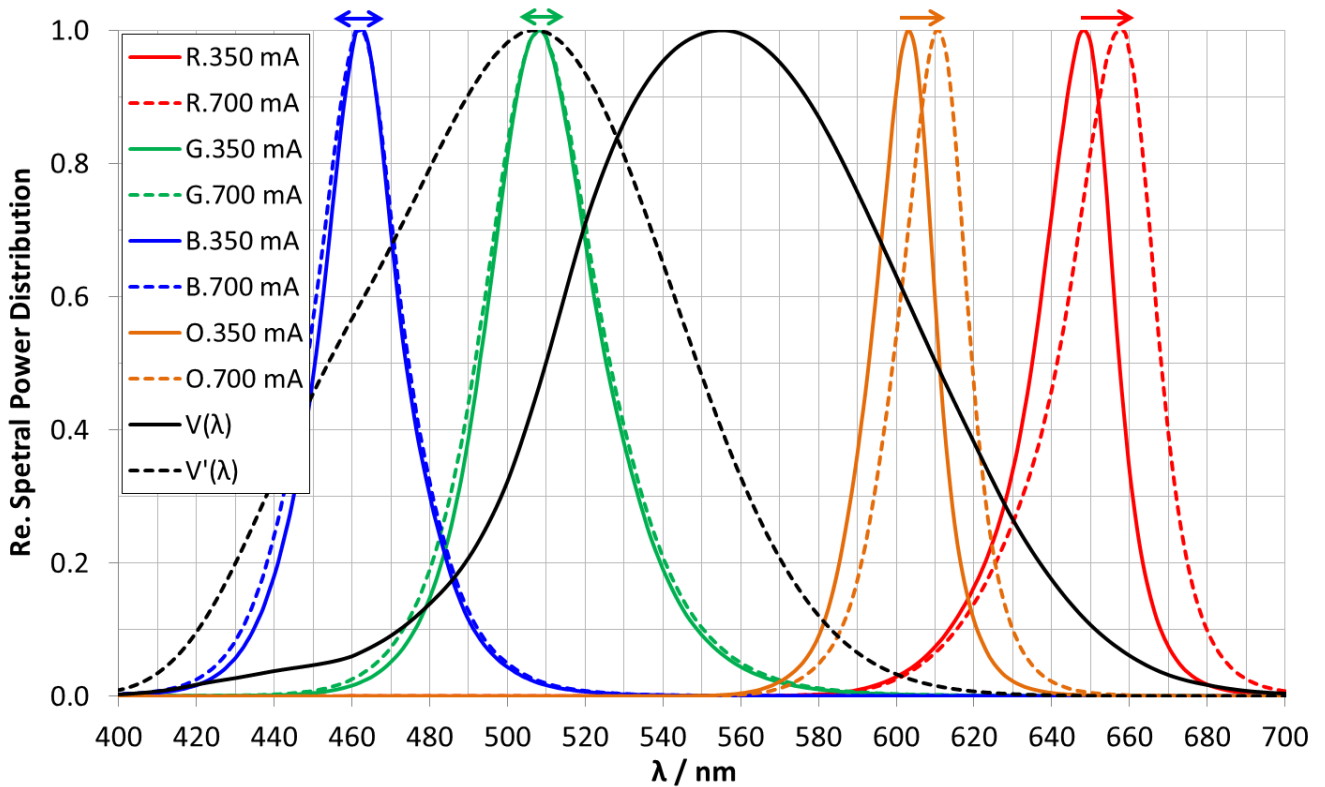


Figure 3.4 - Current dependence of the spectra of four color semiconductor LEDs at 80 °C

3.3.3. Temperature and current dependence of peak wavelengths and full width at half maximum wavelengths of the color semiconductor LEDs

In Section 3.3.2, the temperature dependence and the current dependence of four typical color semiconductor LED spectra were described in general. In this section, the change of those spectra will be determined in more detail by means of three-dimensional relationships of peak wavelength λ_p in nm for spectral shift and full width at half maximum λ_{FWHM} in nm for spectral spread with operating temperature and forward current.

* **Description for detailed comparisons:** Quantitatively, the value of $\lambda_{FWHM} / \lambda_p$ is quite different between different color semiconductor LEDs. Particularly, the peak wavelength of InGaAlP LEDs is usually about 600 nm or longer, while the one of InGaN LEDs is always about 540 nm or shorter. Similarly, the full width at half maximum of green semiconductor LEDs is usually about 30 nm or wider, while the one of orange, red and blue semiconductor LEDs is only from about 18 nm to 25 nm. Therefore, their relative form should be not used in comparisons, but their absolute values are necessary in the use. In following descriptions, the asterisk in two Table 3.1 and Table 3.2 is to denote for the binning condition (350 mA and 80 °C). Hence, the comparison between $\lambda_{FWHM} / \lambda_p$ at any operating point and that at the binning point can be determined such as the comparison between $\lambda_{FWHM} / \lambda_p$ at 40 °C and that at 80 °C with constant current of 350 mA in Table 3.1 or the comparison between $\lambda_{FWHM} / \lambda_p$ at 350 mA and that at 700 mA with constant operating temperature of 80 °C in Table 3.2.

* **Temperature dependence of peak wavelengths and full width at half maximum wavelengths of the color semiconductor LEDs:** In Table 3.1, when operating temperature increases from 40 °C to

80 °C, peak wavelengths change strongly in the case of the red semiconductor LED (7 nm) and of the orange semiconductor LED (5 nm) causing a significant color shift for these LEDs. Otherwise, the change of peak wavelength was only 2 nm for the green and blue semiconductor LEDs leading to their good color stability under different operating temperatures. Contrarily, also in a similar range of operating temperature change, full width at half maximum wavelengths often change moderately for all four typical color semiconductor LEDs (1 nm - 2 nm). These values correspond completely with the temperature dependence of four typical color semiconductor LED spectra at 350 mA shown in Figure 3.3.

Table 3.1 - Temperature dependence of $\lambda_p / \lambda_{FWHM}$ of red, green, blue and orange LEDs at 350 mA

Order	Temperature / °C	40	80*
1	$\lambda_p / \lambda_{FWHM}$ in nm - Red LED	642/20	649/22
2	$\lambda_p / \lambda_{FWHM}$ in nm - Green LED	506/30	508/32
3	$\lambda_p / \lambda_{FWHM}$ in nm - Blue LED	461/21	463/23
4	$\lambda_p / \lambda_{FWHM}$ in nm - Orange LED	598/17	603/18

* **Current dependence of peak wavelengths and full width at half maximum wavelengths of the color semiconductor LEDs:** In Table 3.2, when forward current increases from 350 mA to 700 mA, the peak wavelengths change near similarly for the red and the orange semiconductor LEDs (8 nm for the red semiconductor LED and 5 nm for the orange semiconductor LED), oppositely they do not nearly change for the green and blue semiconductor LED. On another side, the change of the full width at half maximum wavelengths can be classified for all LEDs conducted in the descending order by the first position of the red (5 nm), the second one of the green and blue (3 nm), and the third one of the orange semiconductor LED (2 nm). These values also correspond completely with the current dependence of four typical color semiconductor LED spectra at 80 °C shown in Figure 3.4.

Table 3.2 - Current dependence of $\lambda_p / \lambda_{FWHM}$ of red, green, blue and orange LEDs at 80 °C

Order	Current / mA	350*	700
1	$\lambda_p / \lambda_{FWHM}$ in nm - Red LED	649/22	657/27
2	$\lambda_p / \lambda_{FWHM}$ in nm - Green LED	508/32	508/35
3	$\lambda_p / \lambda_{FWHM}$ in nm - Blue LED	463/23	462/26
4	$\lambda_p / \lambda_{FWHM}$ in nm - Orange LED	603/18	611/20

3.3.4. Temperature and current dependence of radiant fluxes and radiant efficiencies of the color semiconductor LEDs

The energy quality aspects of color semiconductor LEDs, the concepts of luminous flux Φ_v in lm and luminous efficacy η_v in lm/W are not used, but should be substituted by the radiant flux Φ_e in W and the radiant efficiency η_r in W/W or %, because the values of luminous flux and luminous efficiency are weighted by the average spectral sensitivity of the human visual perception of brightness ($V(\lambda)$ for the photopic vision). Therefore, they are always unfair for very different positions of the red, the orange,

the yellow, the green and the blue semiconductor LED spectra in calculations and comparisons like analyzed in Section 3.3.2. In addition, in this section radiant flux and radiant efficiency should be converted into the relative form so that their difference and their change of the color semiconductor LEDs can be recognized more obviously.

*** Temperature dependence of radiant fluxes and radiant efficiencies of the color semiconductor LEDs:** Figure 3.5 describes the temperature dependence of radiant flux and radiant efficiency of the four typical color semiconductor LEDs at the forward current of 350 mA, relatively. The results in Figure 3.5 showed that when the operating temperature increases from 40 °C to 80 °C at 350 mA, radiant fluxes change near similarly to radiant efficiencies. Particularly, the losses of both radiant flux and radiant efficiency of the orange semiconductor LED are about 95 %, the ones of the red semiconductor LED are about 28 %, and the ones of both the blue and green semiconductor LED are about 10 %. Thus, relatively the losses of the orange semiconductor LEDs are equal 3.39 times compared with the ones of the red semiconductor LED and 9.5 times compared with the ones of the blue and green semiconductor LEDs. Therefore, the very big losses of both radiant flux and radiant efficiency of the orange semiconductor LEDs comparing with other semiconductor LEDs must be paid a special attention in the LED selection and the LED combination in the establishment of hybrid LED-lamps in Chapter 7.

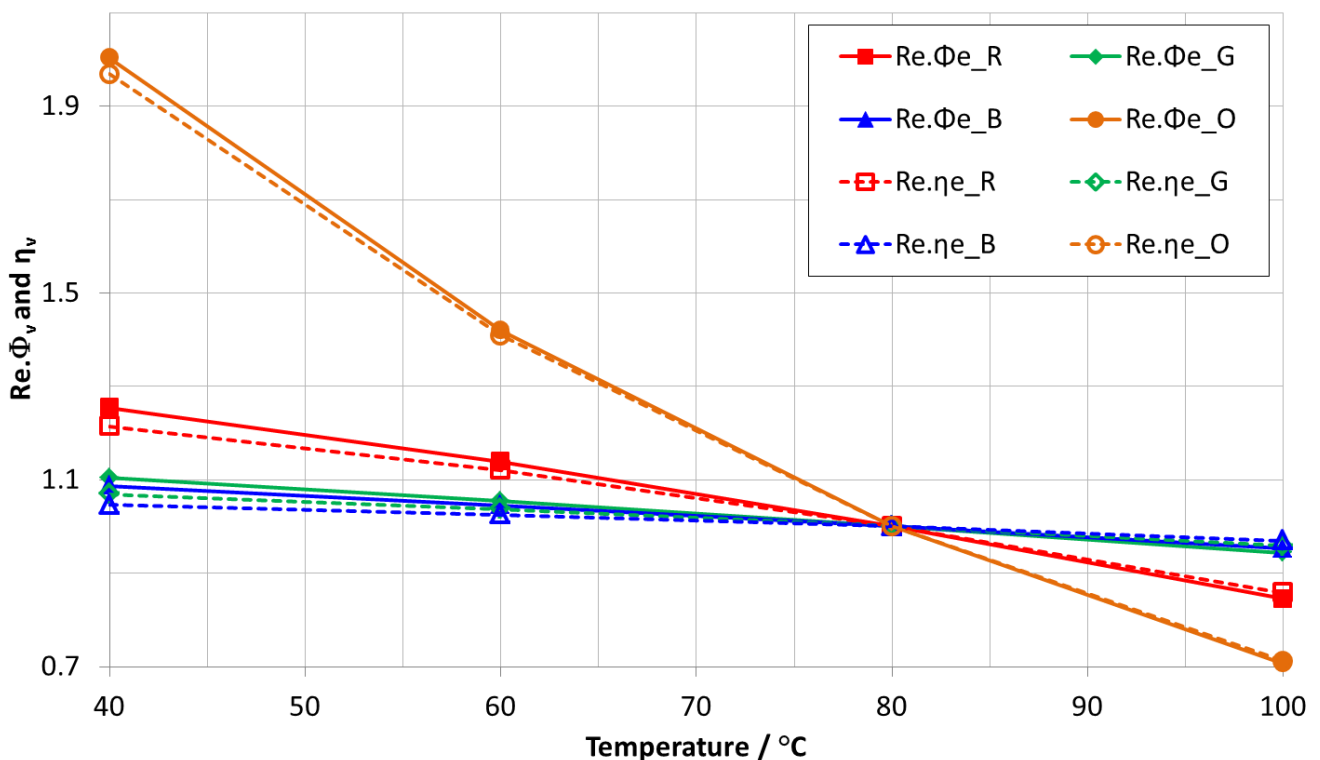


Figure 3.5 - Temperature dependence of color LED radiant fluxes and radiant efficiencies at 350 mA

*** Current dependence of radiant fluxes and radiant efficiencies of the color semiconductor LEDs:** Figure 3.6 describes the current dependence of radiant flux and radiant efficiency at operating temperature of 80 °C, relatively. Based on the results in this diagram, it can be recognized, that when the forward current increased from 350 mA to 700 mA at operating temperature of 80°C, the radiant fluxes of the blue and the green semiconductor LED increased about 65 % and 50 %, respectively. Contrarily, the radiant efficiency decreased about 25 % for the blue semiconductor LED and decreased about 30 % for the green semiconductor LED. Especially, with the similar increase of forward current

(350 - 700 mA) at the operating temperature of 80 °C, the radiant flux of the red semiconductor LED increased insignificantly and the one of the orange semiconductor LED did not increase. Whereas, there was a big reduction of the radiant efficiency of both the red semiconductor LED (about 60 %) and the orange semiconductor LED (about 70 %). These results supplemented for the relative spectral evaluation in Section 3.3.2 so that the instability of the orange and red color semiconductor LEDs over the operating forward current was brought into relief.

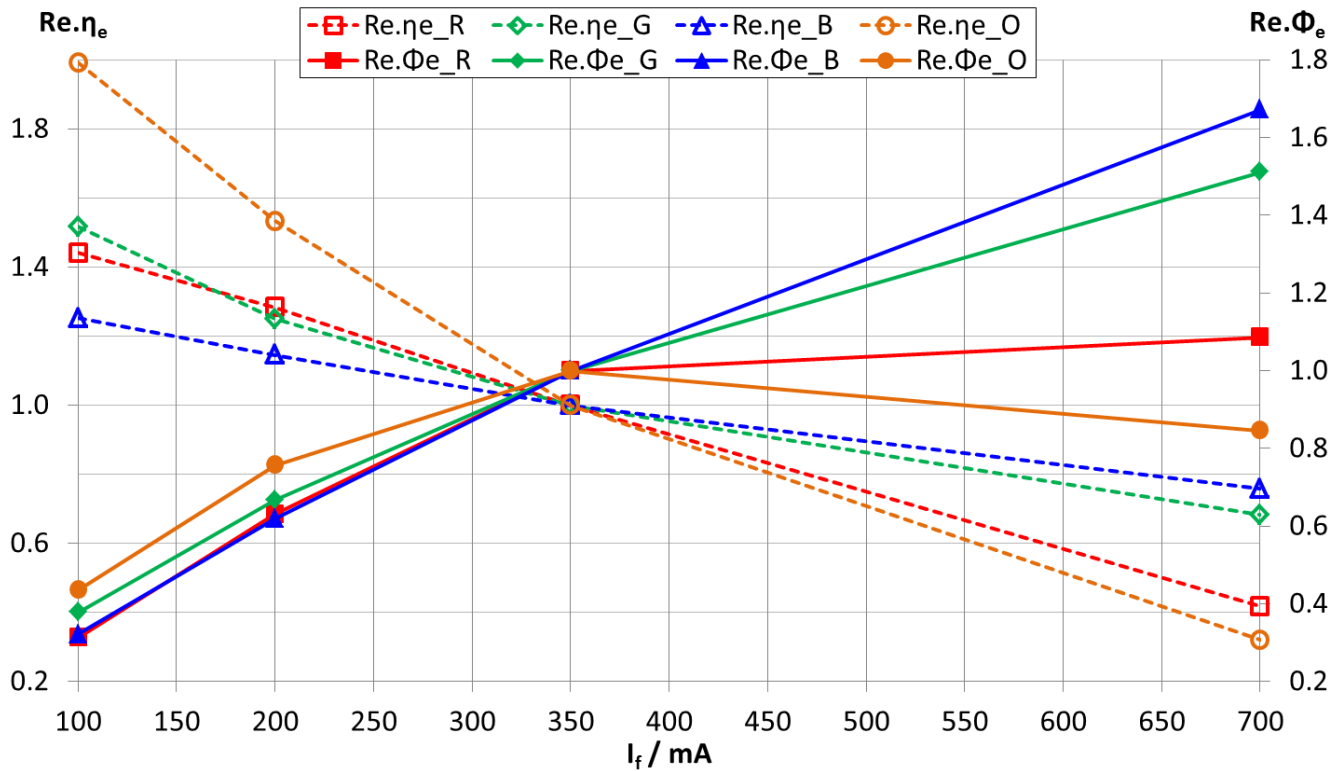


Figure 3.6 - Current dependence of color LED radiant fluxes and radiant efficiencies at 80 °C

* **Conclusion:** From the above analyses, it can be concluded that both temperature dependence and current dependence of the red and the orange semiconductor LEDs are very high, while these dependencies of the blue and green LEDs can be accepted in small operating regions. Therefore, if these LEDs are really essential in some solid state lighting applications because of the reasons of color mixing, a compensation solution for their temperature dependence and their current dependence must be issued. In that, except that operating temperature cannot be adjusted, forward current must be chosen at an appropriate low level so that their radiant flux is as high as the desire, while their radiant efficiency does not reduce down to a too low level. For this problem, it can take the case of the above orange semiconductor LED as a very good demonstration example. When the forward current of the orange semiconductor LED increased from 350 mA to 700 mA, its radiant flux did not increase but decreased to about 85 % at the forward current of 700 mA comparing with that at 350 mA, and its efficiency decreased very intensively to about 30 % at the forward current of 700 mA comparing with that at 350 mA. In another word, 70 % energy was lost with no benefit (15 % loss of the radiant flux).

3.3.5. Temperature and current dependence of color differences of the color semiconductor LEDs

If the binning point (350 mA and 80 °C) is established as a reference point and the concept of color difference ($\Delta u'v'$, 1976) is applied to calculations and evaluations, the temperature dependence and the current dependence of color differences between any operating point and the referent point can be determined. The color difference will be the new aspect of color quality stability supplementing and quantifying for the relative spectral evaluation in Section 3.3.2.

* **Temperature dependence of color differences of the color semiconductor LEDs:** In Figure 3.7, the temperature dependence of color difference of the four typical color semiconductor LEDs is shown, when operating temperature changes from 40 °C to 100 °C with the forward current of 350 mA. The results showed that the color difference was gradually worse in the order of the green, red, blue and orange semiconductor LEDs, successively. Indeed, the color difference of the orange semiconductor LED is the worst case. If the three MAC ADAM ellipses are assumed as the acceptable limit of color difference for the human eyes according to the researched results mentioned in [37], the permitted region on the operating temperature of the orange semiconductor LED is about 80 ± 2.5 °C, the one of the blue semiconductor LED is from about 70 °C to about 90 °C, and the one of the green semiconductor LED and the red semiconductor LED is about from about 60 °C to about 100 °C. Thus, it can be recognized, that the stabilization for color difference of the orange semiconductor LED at an acceptable limit in its operating process is nearly impossible, unless a high cost temperature control system is applied to adjust operating temperature for this color semiconductor LED type. Otherwise, the blue semiconductor LED is also only allowed to operate in a quite narrow region. Whereas, the color difference of the green and the red semiconductor LEDs can be ensured in a wide operating temperature range. Therefore, the orange semiconductor LED should be avoided in the LED combination for hybrid LED-lamps in Chapter 7.

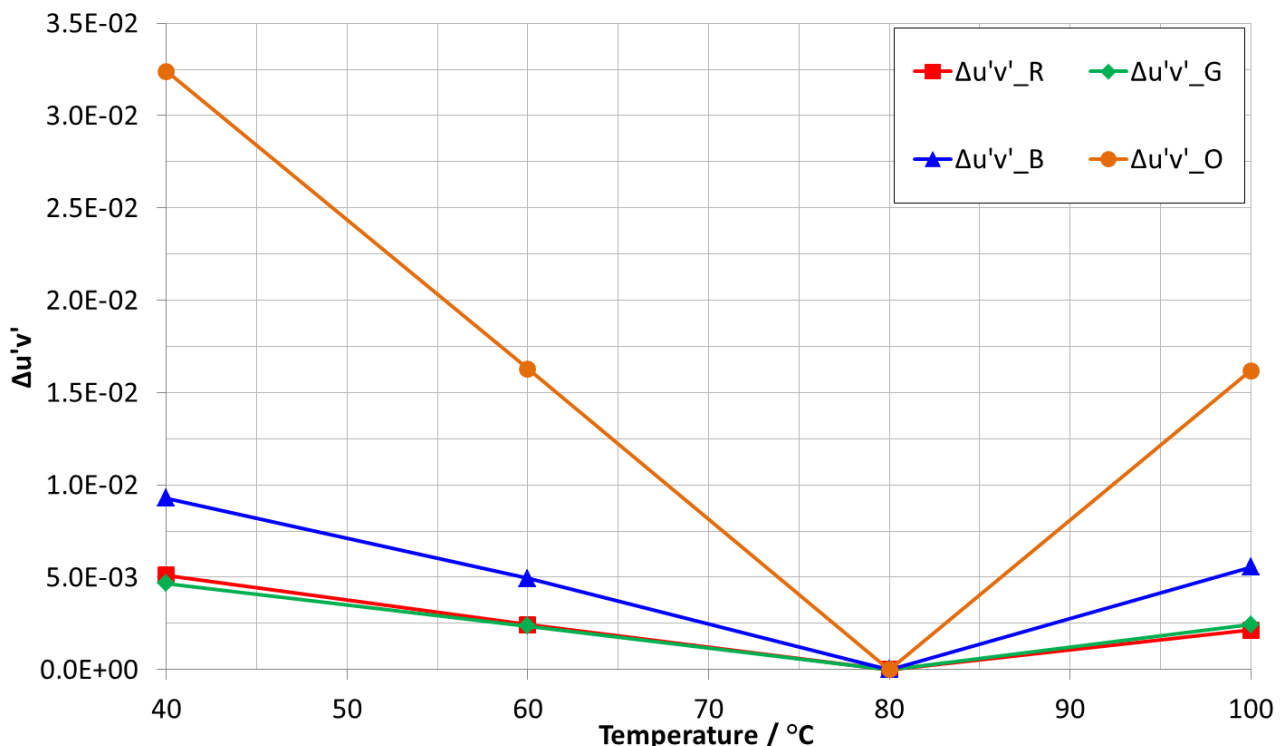


Figure 3.7 - Color differences of the color semiconductor LEDs as a function of temperature

* **Current dependence of color differences of the color semiconductor LEDs:** In Figure 3.8, the current dependence of color differences of four typical color semiconductor LEDs is shown. Similarly, if three MAC ADAM ellipses are still set as the permitted limit of color difference for the human eyes, their color difference was gradual better according to the order of the orange, blue, green and red semiconductor LEDs.

Following this order, the best operating current region around the binning point (350 mA and 80 °C) was from 100 mA to 600 mA for the red semiconductor LED approaching forward to the lower current regions. Oppositely, the worst operating current region was only about 350 ± 20 mA for the orange semiconductor LEDs. And the quite wide one was about from 220 am to 600 am for the green semiconductor LED. Finally, the best one is about from 220 mA to 700 mA for the blue semiconductor LED approaching forward to high forward current regions. Obviously, based on these results, it can be confirmed, that the blue semiconductor LED was the best selection for its operation in high current regions, and the orange semiconductor was the worst case due to its color difference in its entire operating current region. Therefore, blue semiconductor LEDs are the most appropriate color semiconductor LEDs for fabrication of PC-LEDs on high brightness demand, because of their good color stability and their spectra lie in the high excitation range of almost luminescent materials. Whereas, the orange semiconductor should be substituted by yellow or orange spectral components of appropriate luminescent materials in the color mixing of hybrid LED-lamps for high quality solid state lighting applications in order to avoid its very high color instability. Moreover, an available substitution solution for orange semiconductor LEDs in signaling lamps on automobile vehicles is necessary to be researched furthermore.

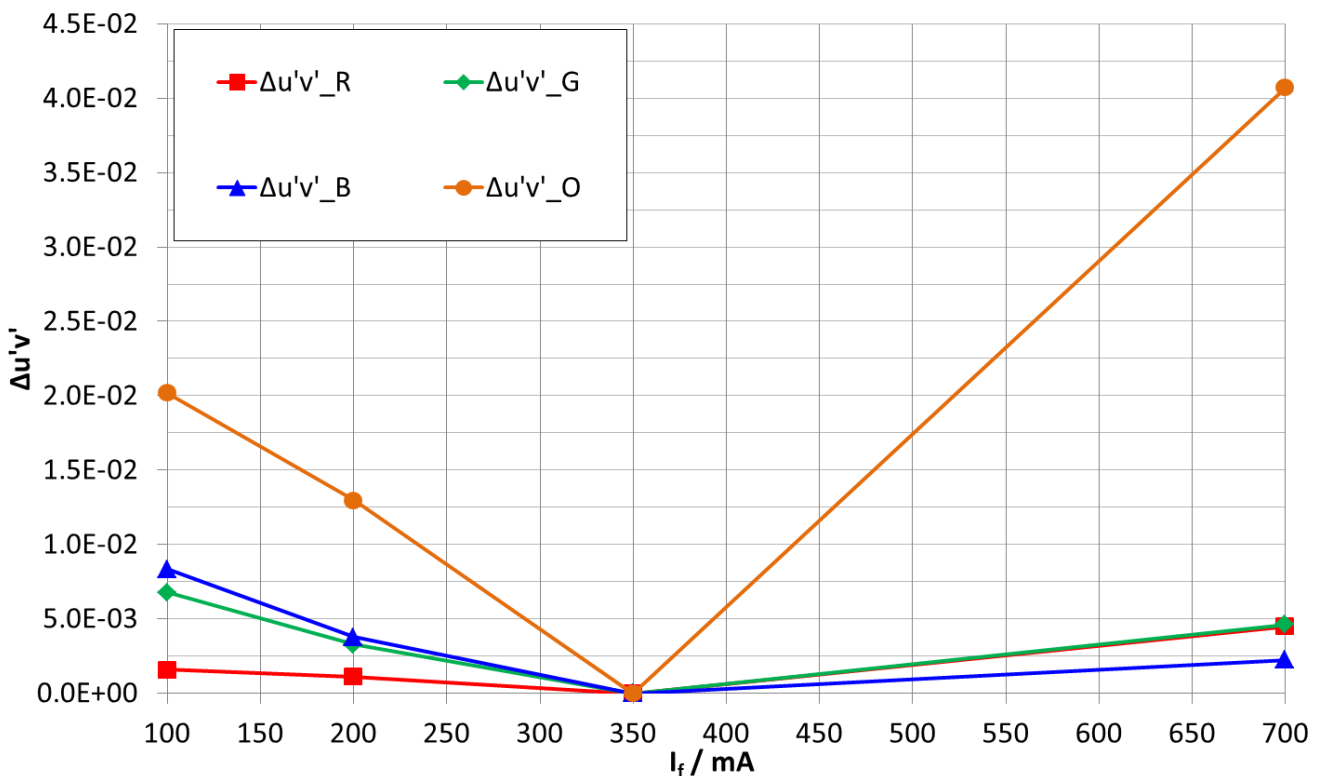


Figure 3.8 - Color differences of color semiconductor LEDs as a function of current

3.4. Optical, radiant and colorimetric properties of warm white PC-LEDs

3.4.1. General Consideration

* **Limit in the investigation:** Section 3.3 investigated the optical, radiant and colorimetric properties of some typical color semiconductor LEDs. The measured results showed that the blue semiconductor LED is really appropriate for fabrication of PC-LEDs on high brightness demand and the orange semiconductor LED should be avoided in high-end solid state lighting applications because of its very low quality on all aspects of color difference, radiant flux, radiant efficiency and spectral change when the operating temperature or/and forward current change. Similarly, in this section radiant quality and color quality parameters of white PC-LEDs will be investigated and discussed for solid state lighting applications. In fact, on the best way, chosen white PC-LEDs for the investigation should cover entirely conventional applicable regions of the white light perception on the human eyes including warm white ($2700\text{ K} < CCT < 3500\text{ K}$), neutral warm white ($3500\text{ K} < CCT < 5000\text{ K}$) and cold white ($5000\text{ K} < CCT < 6500\text{ K}$) with color rendering index R_a higher than 80. Low CRI LEDs are no objects of this thesis for high quality solid state lighting applications. However, methodically and meaningfully warm white PC-LEDs ($2700\text{ K} < CCT < 3500\text{ K}$) should be described in this chapter previously, because warm white hybrid LED-lamps will be proved as the best lighting solution for the first demonstration example of museum lighting and will be chosen as the second demonstration example of shop lighting for stabilization in the chapter 7. In addition, similar procedures of the investigation in cases of neutral white ($4000\text{ K} < CCT < 4800\text{ K}$) and cold white ($5000\text{ K} < CCT < 6500\text{ K}$) should be not repeated many times in this thesis, but will be described as experimental/referent results in Appendix F and in Appendix G, respectively.

* **Determination for desired targets:** In more detail, the key lighting quality aspects of the investigation should be the temperature dependence and the current dependence of the spectra, luminous flux Φ_v / lm , luminous efficacy η_v in lm/W , color rendering indexes (R_a , R_9 and AVR_{1-14}), whiteness $\Delta u'v'_{CT}$, color difference $\Delta u'v'$ and correlated color temperature CCT in K of warm white PC-LEDs. Whereas, the radiant flux and the radiant efficiency are not really necessary for the investigation, because the evaluation for high brightness and luminous efficacy of warm white PC-LEDs with different luminescent materials and different blue chips are more important for high quality solid state lighting application. Moreover, according to practical experiences, the available conventional operating region of warm white PC-LEDs should be from 350 mA to 700 mA for forward current at operating temperature of about 80/85 °C, when the current dependence is investigated; and the one should be from 40 °C to about 80/85 °C for operating temperature at the forward current of 350 mA, when the temperature dependence is investigated. Otherwise, the investigated region of forward current should be widened a little from 100 mA to 700 mA for the investigation of color difference, luminous flux and luminous efficacy because then the range of an available current region will be determined more obviously from the original current region ($100\text{ mA} < I_f < 700\text{ mA}$) in order to compare and evaluate accurately for varied warm white PC-LEDs.

3.4.2. Temperature and current dependence of warm white PC-LED spectra

In Section 3.4.1, the necessary range and desired targets for the investigation was defined. The achieved results of the spectral change over operating temperature and forward current are very important, by which the variations of all other optical and calorimetric parameters can be explained qualitatively and determined quantitatively. In this section, six typical cases, which can represent for spectral behaviors of other warm white PC-LEDs, are selected to illustrate for spectral changes over operating temperature in Figure 3.9 and over forward current in Figure 3.10.

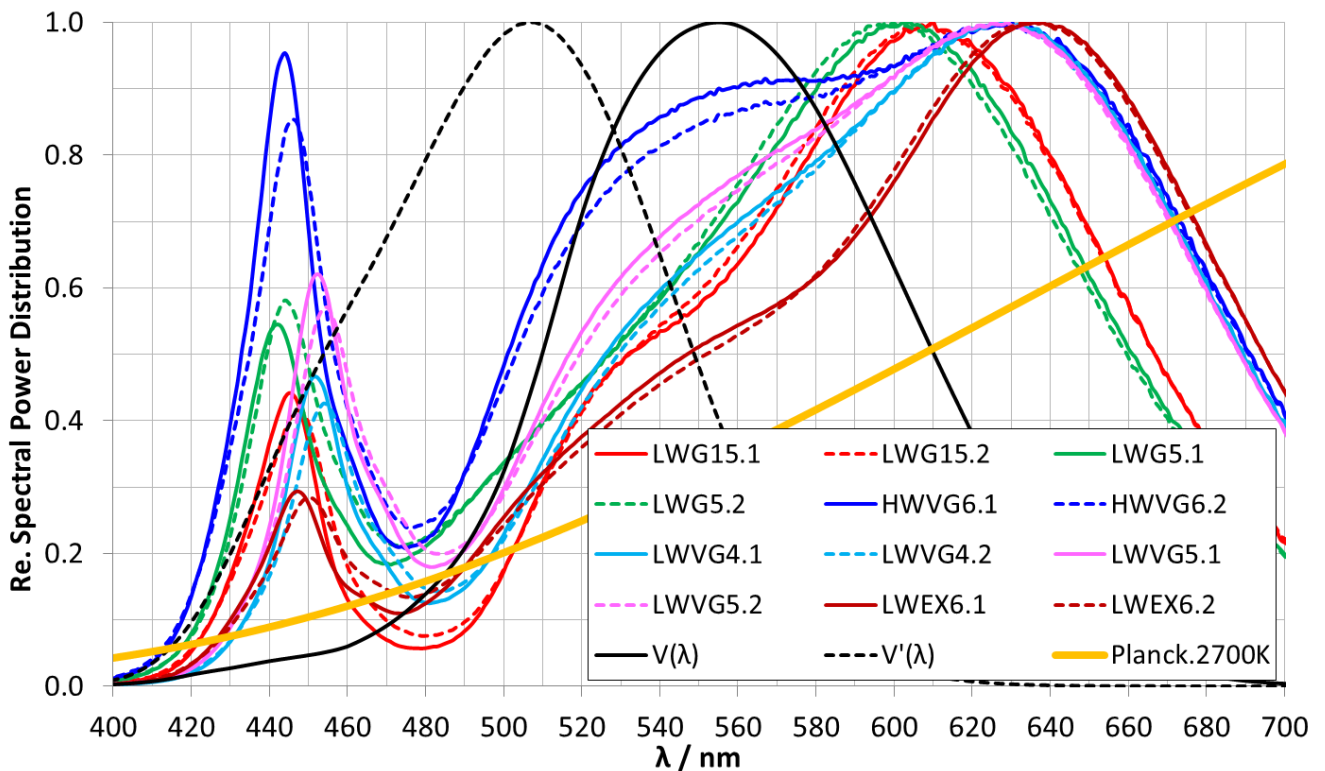


Figure 3.9 - Temperature dependence of six typical warm white LEDs ($2700\text{ K} < \text{CCT} < 3500\text{ K}$) of different LED manufacturers at 350 mA. Solid lines correspond with 40 °C, dashed lines with 80 °C, respectively.

* **Temperature dependence of PC-LED spectra:** Particularly, in Figure 3.9 the temperature dependence of warm white PC-LED spectra is shown in the operating region from 40 °C to 80 °C for operating temperature at the forward current of 350 mA. In that, indexes “1” and “2” (attached to the name of each LED in Figure 3.9) are to indicate for spectra at 40 °C and 80 °C, respectively. Fundamentally, in warm white PC-LEDs, a luminescent material system with two different phosphor types (such as the mixture of a green phosphor and a red phosphor or the one of a yellow / orange phosphor and a red phosphor) is usually built-on a blue chip. Therefore, in the investigation of warm white PC-LED spectra, three spectral components (the left spectral component of blue chip, the middle spectral component of green / orange / yellow phosphor and the right spectral component of red phosphor) must be considered concomitantly. Hence, based on measured spectra of warm white PC-LEDs in Figure 3.9, it can be recognized, that the peak wavelength of the red phosphor component of almost very good CRI LEDs (such as LWVG4 and HWVG6) and the one of excellent CRI LED (such as LWEX6) are always very high (about 630 nm - 640 nm). And, the one of the lower CRI LEDs was only about 600 nm (for LWG5) or about 610 nm (for LWG15). In addition, the comparison between solid curves (denoted for spectra at 40 °C) and broken curves (denoted for spectra at 80 °C) in Figure 3.9

showed that the temperature stability of the right spectral components (belonging to red phosphors) in short term operation was much better than that of the middle spectral components (belonging to green, yellow or orange phosphors). Successively, the one of the middle spectral components was better than that of the left spectral components (belonging to blue chip). Indeed, it can take four LEDs (HWVG6, LWG5, LWVG5 and LWEX6) as very obvious examples for the very bad temperature stability of warm white PC-LEDs. For cases of HWVG6, LWVG5 and LWEX6, the left spectral components and the middle spectral components reduced very strongly comparing with the right spectral components. Therefore, their white point shifted into the red direction much (called red shift) causing the strong decrease of CCT like described in Figure 3.19. Whereas in the case of LWG5, there was nearly no change for the middle spectral component, while the left spectral component increased strongly and the right spectral component shifted into the left side in a very wide range. As a result, its white point has shifted into the blue direction (called blue shift) causing the strong increase of CCT like described in Figure 3.19. Furthermore, spectral change also caused HWVG6, LWG5 and LWEX6 big color differences compared with the binning point excepting case LWVG5 like the illustration in Figure 3.17. Especially, the less spectral change of LWVG5 in the blue gap (450 nm - 490 nm) made its color difference better than that of cases HWVG6, LWG5 and LWEX6.

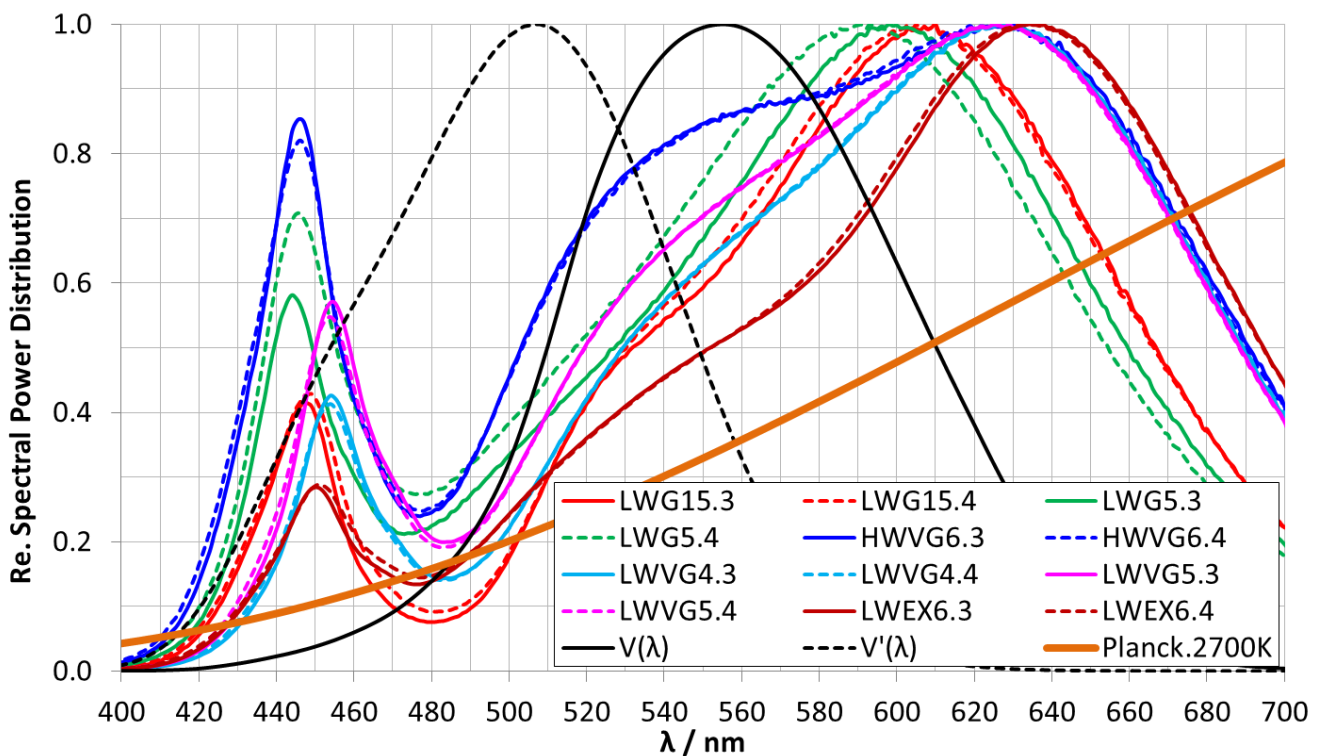


Figure 3.10 - Current dependence of six typical white warm white LEDs ($2700\text{ K} < \text{CCT} < 3500\text{ K}$) of different LED manufacturers at $80\text{ }^\circ\text{C}$. Solid lines correspond with 350 mA , dashed lines with 700 mA , respectively.

* **Current dependence of white PC-LED spectra:** Figure 3.10 describes the current dependence of warm white PC-LED spectra in the operating region from 350 mA to 700 mA for forward current at the operating temperature of $80\text{ }^\circ\text{C}$. In that, indexes “3” and “4” in Figure 3.10 are to denote for spectra at 350 mA and 700 mA , respectively. In a relative comparison, the most important point is to recognize the synchronous increase of three spectral components, when the forward current increases. Particularly, if their increase is proportional to the one of the forward current, there is neither color difference nor CCT change of warm white PC-LEDs. Indeed, in almost cases of the investigated warm white PC-LEDs, the spectral increase of their spectral components is proportional to forward current

excepting cases LWG5 and LWG15. Therefore, their relative spectral change are quite small, when forward current increases from 350 mA (denoted by solid curves) to 700 mA (denoted by broken curves) like the description in Figure 3.10. In the worst case of LWG5, the big spectral change happens to all spectral components (the left, middle and right spectral components). Thus, this is an obvious demonstration example of a low quality warm white LED, where both the blue chip and the phosphor system have neither good temperature stability nor current stability. In addition, although the spectral change of LWG15 is less than that of LWG5, it happens with sensitive spectral regions such as the blue gap (450 nm - 490 nm) and the amber - red region (550 nm - 600 nm) causing undesired color differences for this PC-LED like the illustration in Figure 3.18. Otherwise, there is very bad CCT instability for some warm white PC-LEDs, if the forward current increases. In six chosen typical candidates for the spectral evaluation, the worst case of CCT instability is LWG5 and the other bad case is LWG15 like the description in Figure 3.20. Spectral evaluations about temperature and current dependences in the above mentions will be proved in more detail by determining values in Section 3.4.5 and in Section 3.4.6.

3.4.3. Current limits of color rendering indexes, luminous efficacies and whiteness of warm white PC-LEDs

* **General consideration:** Section 3.4.2 had the valuable discussion and evaluation about the temperature and current dependence of six LED types with typical spectra. In this section with column charts, the color rendering indexes, luminous efficacy and white degree of a bigger sample amount of warm white PC-LEDs will be investigated in order to determine their current limits as desired targets for optimization and stabilization in Chapter 7. About color rendering index (*CRI*), although in many cases the general *CRI* (R_a) of white PC-LEDs is high, their specific *CRI*s (such as the ninth *CRI* - R_9) are low. Therefore, the average *CRI* for the fourteen CIE standard test color samples ($AVR_{.1-14}$) should be used and/or combined with other specific *CRI*s in order to evaluate the color quality more accurately. In addition, experimentally *CRI*s of the warm white PC-LEDs can be classified into three levels including “good *CRI*” ($80 < R_a < 85$), “very good *CRI*” ($86 < R_a < 90$) and “excellent *CRI*” ($90 < R_a < 100$). Otherwise, warm white PC-LEDs can be also classified into two smaller groups including warm white ($2700\text{ K} < CCT < 3000\text{ K}$) and warm white PC-LEDs ($3000\text{ K} < CCT < 3500\text{ K}$). Hence, in Figure 3.11 and Figure 3.12 *CRI*s (R_a , R_9 and $AVR_{.1-14}$) on the left ordinate axis and luminous efficacy η_v in lm/W on the right ordinate axis of diagrams will be shown together. In that, all results are measured at the hot binning point (350 mA and 80 °C).

* **The opposition of the color rendering indexes and luminous efficacy:** The investigated results in Figure 3.11 and Figure 3.12 show that there is always opposition between color rendering indexes and luminous efficacy for warm white PC-LEDs. Particularly, when *CRI*s are high, luminous efficacy is low and in converse. Indeed, the luminous efficiency of almost current excellent *CRI* warm white LEDs ($2700\text{ K} < CCT < 3500\text{ K}$) is always lower than 60 lm/W. Moreover the one of very good *CRI* warm white LEDs is usually lower than 70 lm/W. Only a few good *CRI* warm white LEDs have a high luminous efficacy level of about 105 / lm/W such as LWG13 and HWG1, but their $AVR_{.1-14}$ and R_9 only reach about 77 and 17, respectively. These values are really important so that an available LED combination solution between color semiconductor LEDs and white PC-LEDs for hybrid LED-lamps can be established for better lighting quality at both *CRI*s and luminous efficacy in Chapter 7. In that, achieved lighting quality of hybrid LED-lamps should be higher or in an acceptable compromise comparing with that of warm white PC-LEDs investigated in this section.

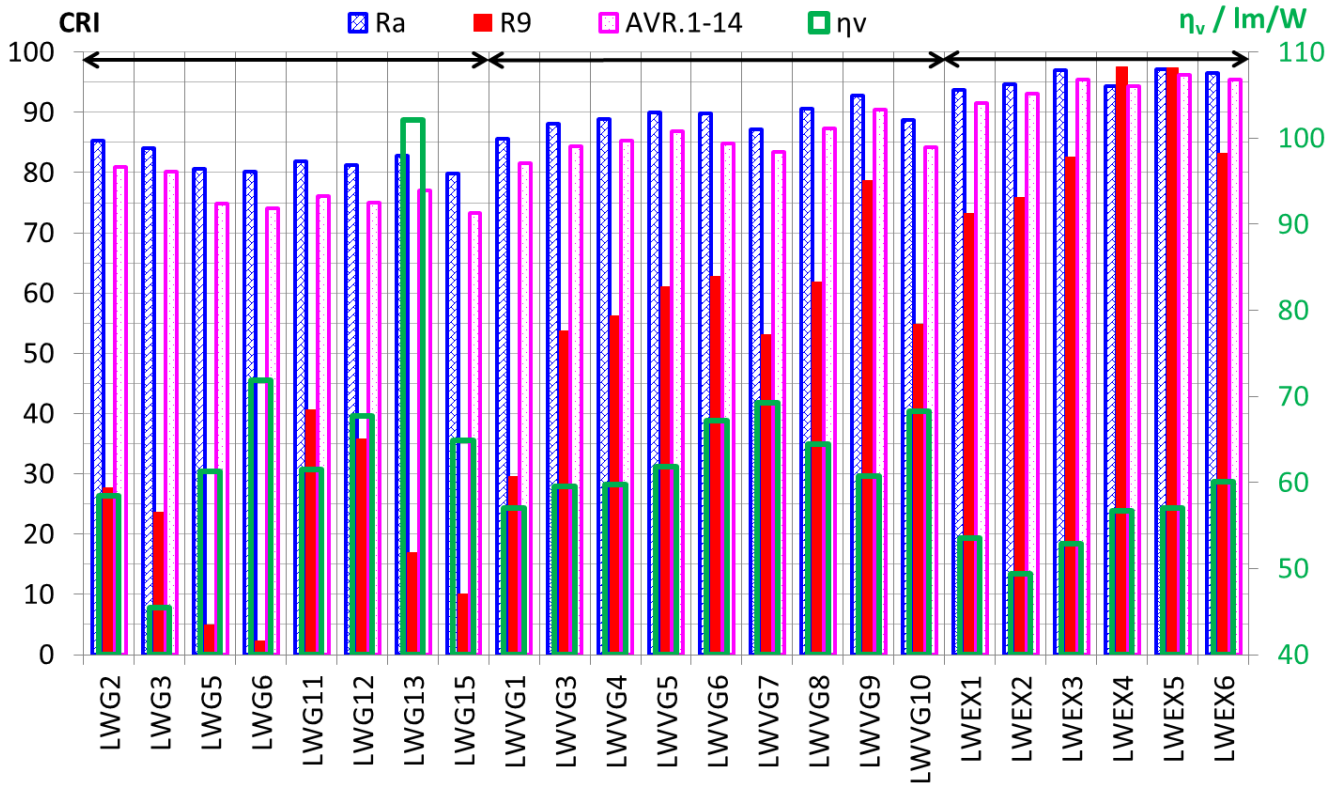


Figure 3.11 - Color rendering indexes (R_a , R_9 and AVR_{1-14}) and luminous efficacies of some current warm white PC-LEDs ($2700\text{ K} < CCT < 3000\text{ K}$) at 350 mA and 80 °C

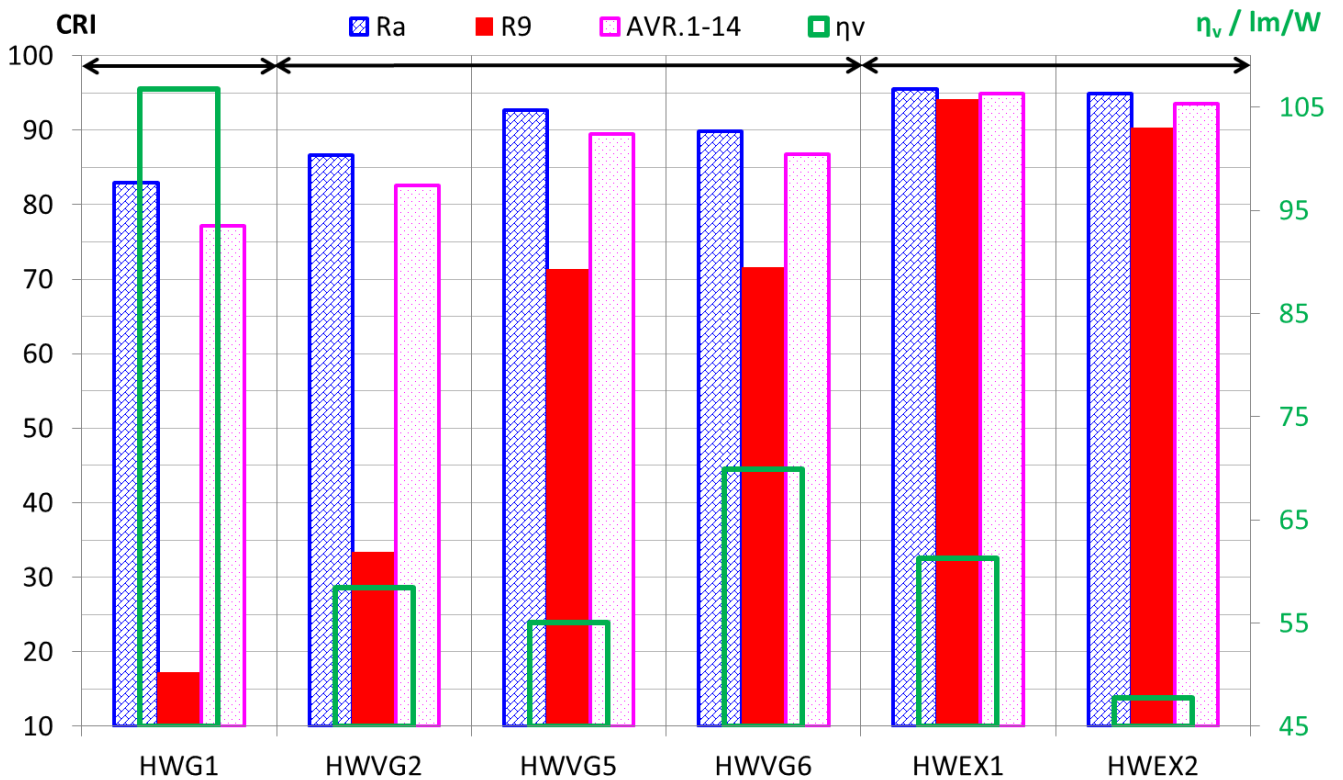


Figure 3.12 - Color rendering indexes (R_a , R_9 and AVR_{1-14}) and luminous efficacies of some current warm white PC-LEDs ($3000\text{ K} < CCT < 3500\text{ K}$) at 350 mA and 80 °C

* **The whiteness of warm white PC-LEDs:** In Figure 3.13 and Figure 3.14, the whiteness for warm white LEDs ($2700\text{ K} < CCT < 3000\text{ K}$) and warm white LEDs ($3000\text{ K} < CCT < 3500\text{ K}$) are shown, respectively. The concept of whiteness $\Delta u'v'_{CCT}$ is defined as the shortest distance between the chromaticity of LEDs and the corresponding referent white point on the black body locus. The shorter the distance is, the better the whiteness is. The results investigated in Figure 3.13 and Figure 3.14 showed that if the acceptable whiteness is lower than three MAC ADAM ellipses for the perception threshold limit of the human eyes like the researched results mentioned in [37], there were many unaccepted LEDs such as LWG2, LWG3, LWVG1, LWEX2, LWEX4, LWEX6, HWVG2, HWEX1 and HWEX2. For these LEDs, achieved light sources are no warm white light source ($2700\text{ K} < CCT < 3500\text{ K}$) furthermore, but become yellow / orange / amber or purple light sources depending on the derivative between the white point of these light sources and the matching white point on the black body locus. If the derivative is positive and big enough, it will become a yellow / orange / amber light source. Contrarily, if it is negative and big enough, it will become a purple light source. And both of them are not good for high quality solid state lighting applications. Therefore, for the optimization and stabilization in Chapter 7, the whiteness must be paid an attention so that the hybrid LED-lamps become true warm white, neutral white or cold white light sources. Particularly, based on the suggestions of the author in [37], the whiteness of hybrid LED-lamps should be zero on the black body locus or lower than 1 MAC ADAM ellipses as an acceptable limit for the demand of high quality solid state lighting applications.

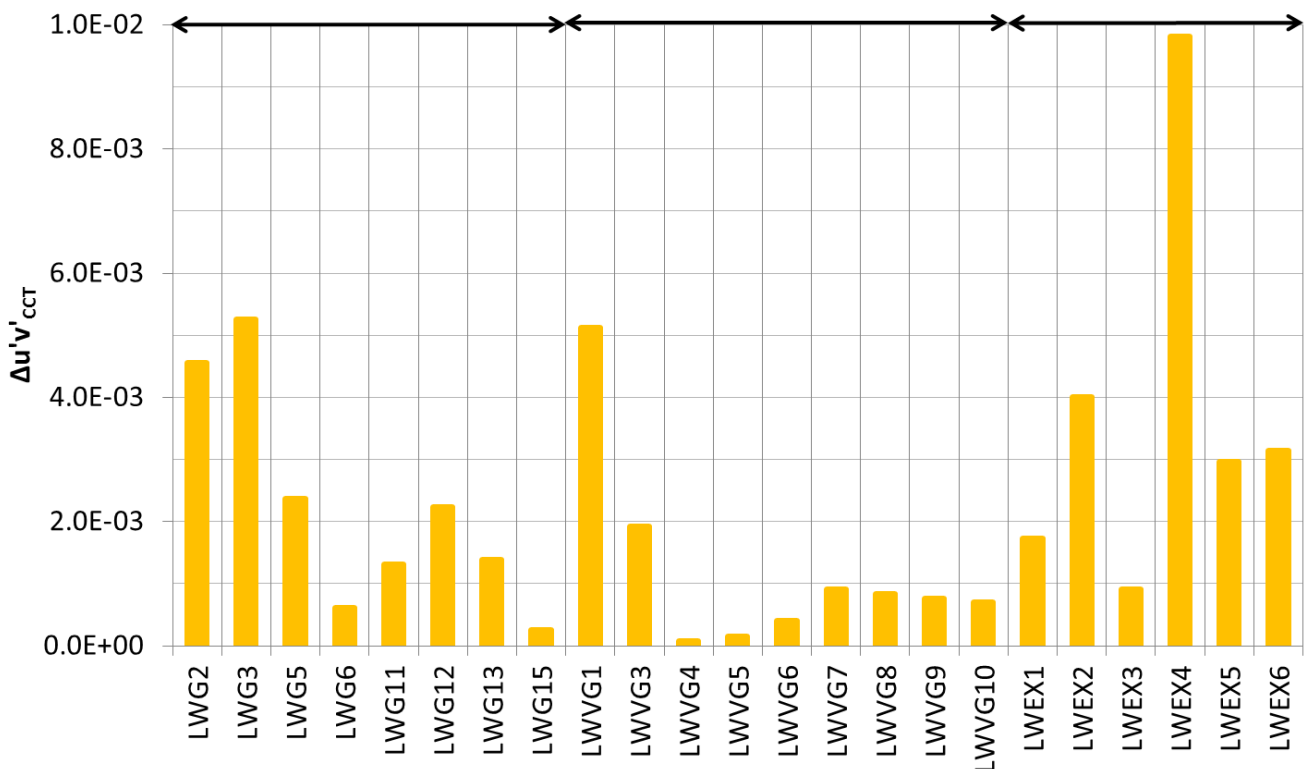


Figure 3.13 - Whiteness of some current warm white PC-LEDs ($2700\text{ K} < CCT < 3000\text{ K}$) at 350 mA and 80 °C

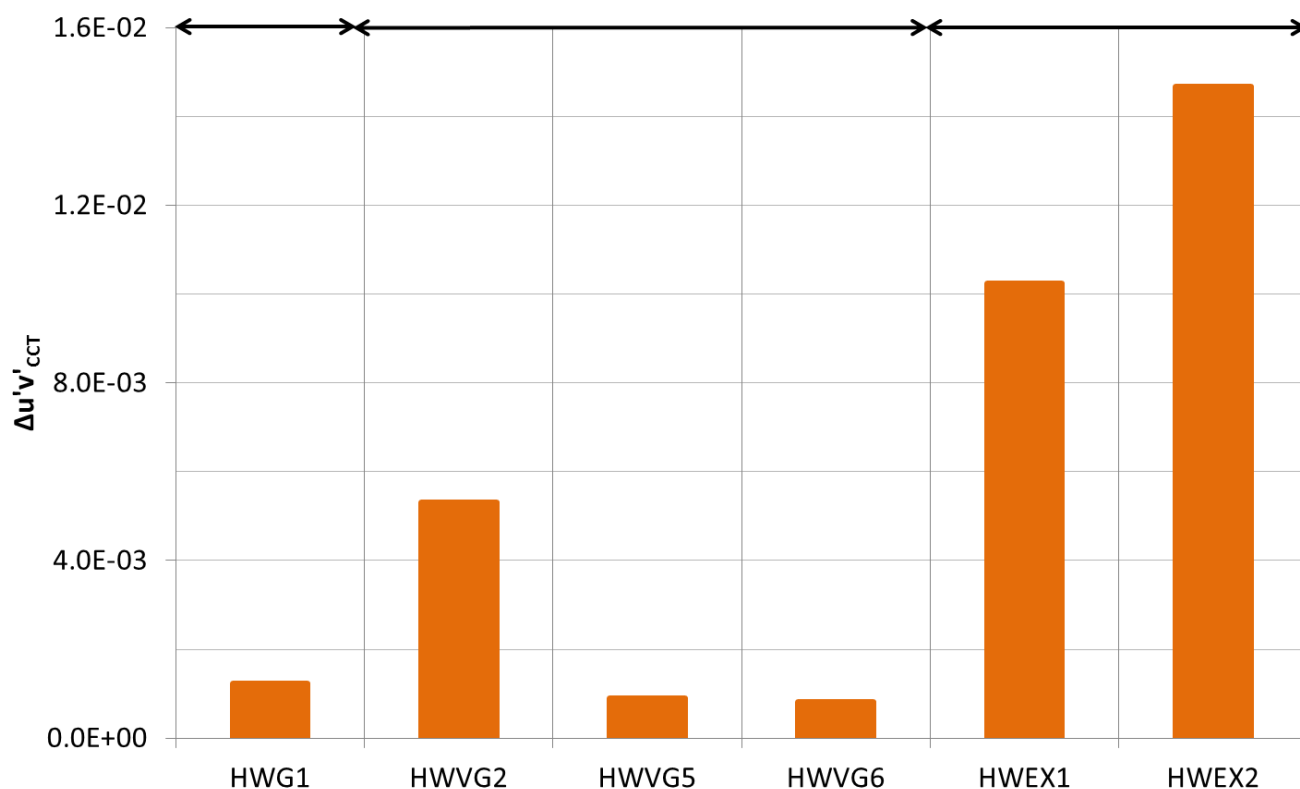


Figure 3.14 - Whiteness of some current warm white PC-LEDs ($3000\text{ K} < \text{CCT} < 3500\text{ K}$) at 350 mA and $80\text{ }^\circ\text{C}$

3.4.4. Temperature and current dependence of luminous fluxes and luminous efficacies of warm white PC-LEDs

Lighting quality limits such as luminous efficacy and whiteness were determined with a high sample number of warm white PC-LEDs by column charts in Section 3.4.3. However, similarly to Section 3.4.2, in order to avoid too complicated diagrams, only six typical candidates of warm white PC-LEDs will be chosen to investigate the temperature dependence and current dependence of luminous flux and luminous efficacy of warm white PC-LEDs. The achieved results are important to determine the demand of minimization for parameter differences between LED manufacturers and LED-luminaire manufacturers in Chapter 4, to select an available operating forward current for hybrid LED-lamps, to stabilize their color quality and as well improve their luminous flux and luminous efficacy in Chapter 7.

* Temperature dependence of luminous fluxes and luminous efficacies of warm white PC-LEDs:

In Figure 3.15, the temperature dependence of the luminous flux and luminous efficacy of six warm white PC-LEDs is described in the operating region from $40\text{ }^\circ\text{C}$ to $80\text{ }^\circ\text{C}$ of operating temperature at the forward current of 350 mA . In that, the relative form of parameters is used to make the comparison between them more obvious and the binning state (350 mA and $80\text{ }^\circ\text{C}$) corresponds to 100 %, relatively. Quantitatively, the measured results of temperature dependence described in Figure 3.15 showed that the luminous flux decrease was from about 4.6 % for LWG15 (as the minimal case) to about 14.6 % for LWVG4 (as the maximal case), and the luminous efficacy also decreased from about 1.8 % for LWG15 (as the minimal case) to about 12.3 % for LWVG4 (as the maximal case), when the operating temperature increased from $40\text{ }^\circ\text{C}$ to $80\text{ }^\circ\text{C}$. Hence, it can be recognized, that with 14.6% luminous flux decrease and 12.3% luminous efficacy decrease in the worst case, LED-luminaire

manufacturers, which buys LWVG4 from the LED manufacturers, cannot describe true operating parameters in their guide books, because their changes are too much when an unavoidable variation of operating temperature takes place. In addition, if PC-LEDs of LED manufacturers are grouped at the cold binning state (350 mA and 25 °C in 25 microseconds), the designed parameters will deviate so much comparing with the operating parameters of LED-luminaires in real solid lighting applications, because their operating temperature will be never at 25 °C. This problem is really a big trouble for LED-luminaire manufacturers for their products as well as main motivation for Chapter 4.

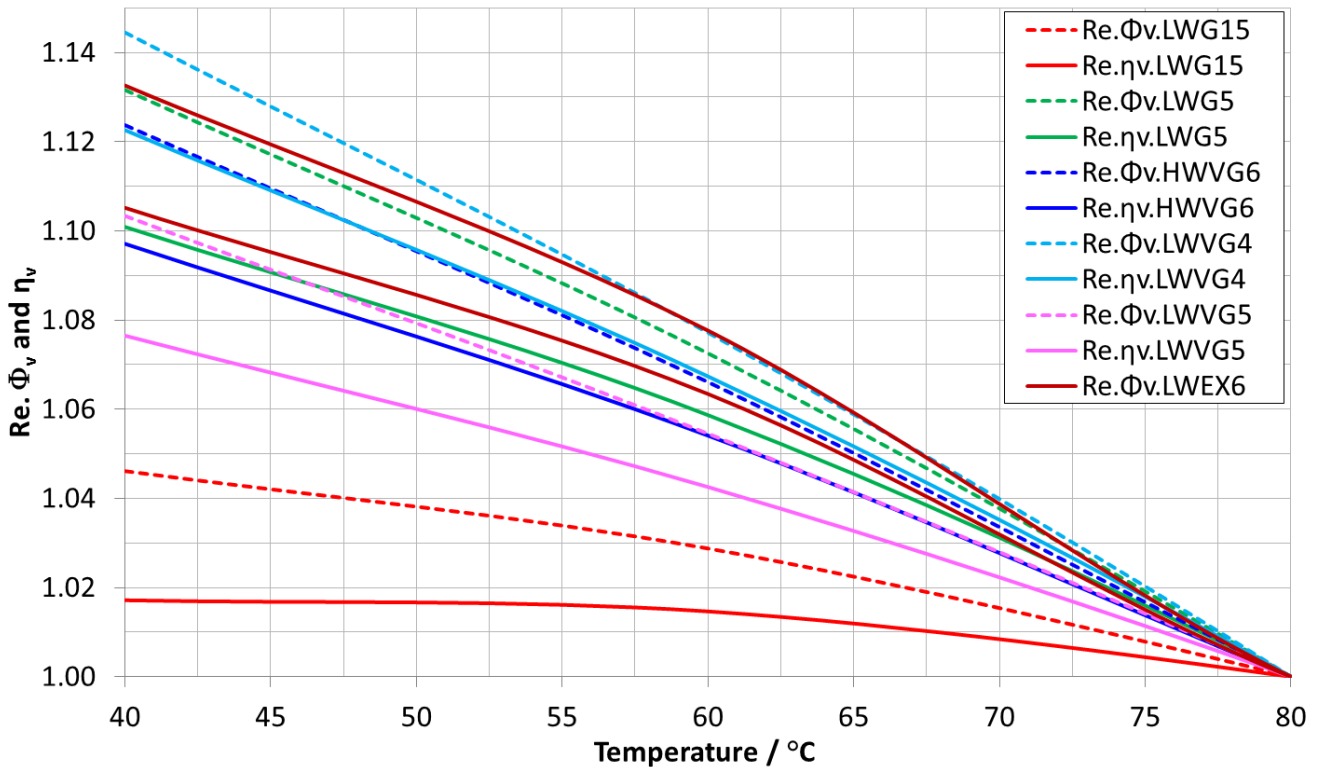


Figure 3.15 - Temperature dependence of luminous fluxes and luminous efficacies of six typical warm white PC-LEDs of different LED manufacturers at 350 mA

* **Current dependence of luminous fluxes and luminous efficacies of warm white PC-LEDs:** In Figure 3.16, the current dependence of the luminous flux and luminous efficacy of six typical warm white PC-LEDs is described in the operating region from 100 mA to 700 mA of forward current at the operating temperature of 80 °C. In that, the luminous flux and the luminous efficacy are described relatively on the right and on the left ordinate of the same diagram in Figure 3.16, respectively. Based on the measured results, it can be recognized, that there are opposite changes between the luminous flux and luminous efficacy, when the forward current increases from 100 mA to 700 mA. Particularly, the luminous flux increases following the increase of forward current, and contrarily the luminous efficacy decreases correspondingly. However, both the increase and the decrease are not linear directly proportional or inversely proportional to the forward current, respectively. Indeed, although the forward current increases two times from the binning point (350 mA and 80 °C) to the derivative operating point (700 mA and 80 °C), the luminous flux of warm white PC-LEDs is only able to increase up to 1.4 times as the minimal case and up to 1.9 times as the maximal case. Whereas, the luminous efficacy decreases down to 65 % (35 % energy loss) as the worst case and down to 89 % (11 % energy loss) as the best case. This problem depends on the chemical and physical intrinsic nature of blue chips, luminescent material system and internal reactions between them like described in Chapter 2.

Sometimes, although the forward current is supplied much more, blue chips cannot radiate light output much more. Or although blue chips can radiate light output much more, luminescent material systems may not absorb that blue radiation much more. Even though this luminous material system can absorb that light much more, it also may not re-radiate its own light output much more, but almost radiate much thermal energy causing phosphor layers and a complete PC-LED warmer. Therefore, meaningfully it is necessary to get an available compromise between the increase of luminous flux and the decrease of luminous efficacy so that an optimal balance between them can be achieved by an appropriate selection of a white PC-LED and its forward current. This issue is an important criterion for LED combination and LED selection of hybrid LED-lamps in chapter 7.

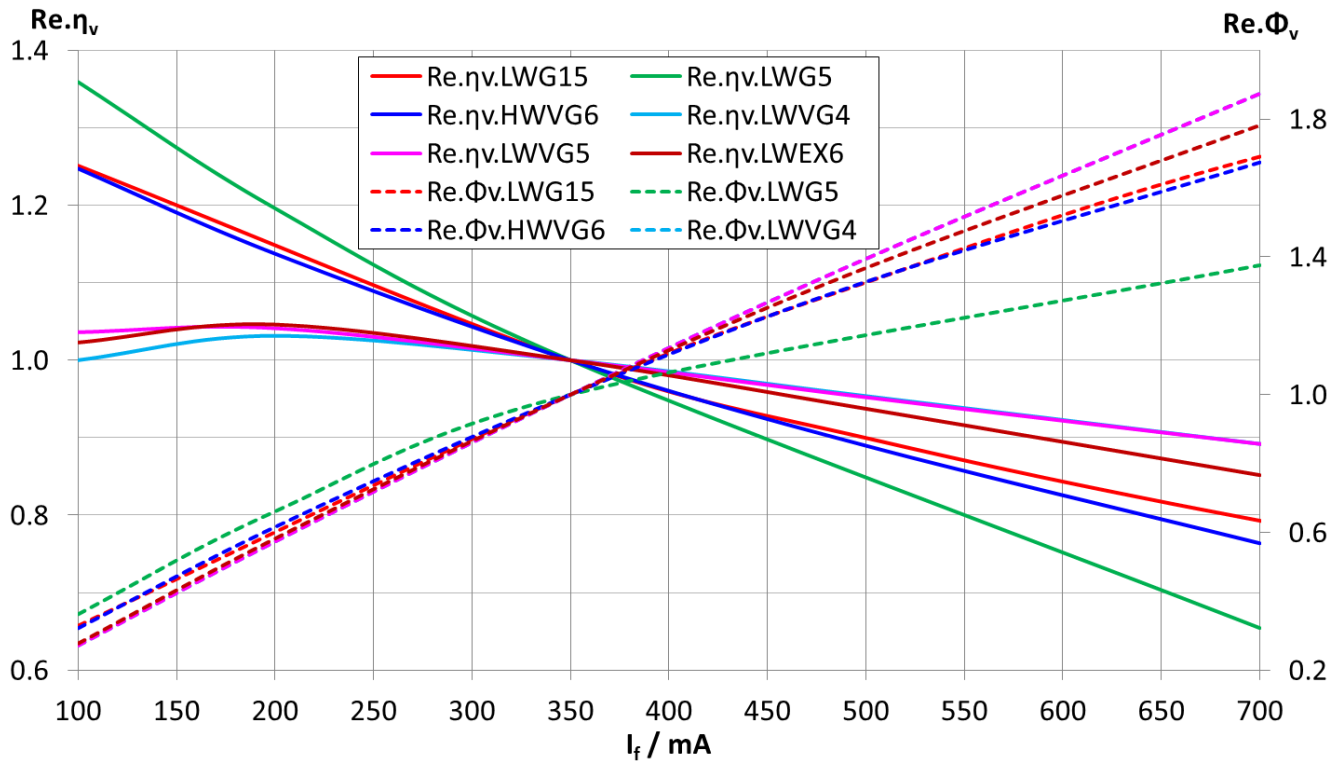


Figure 3.16 - Current dependence of luminous fluxes and luminous efficacies of six typical warm white PC-LEDs of different LED manufacturers at 80 °C

3.4.5. Temperature and current dependence of color differences of warm white PC-LEDs

* **General consideration:** About color quality aspect, color rendering indexes of warm white PC-LEDs at the binning state (350 mA and 80 °C) were also discussed in Section 3.4.3. About energy quality aspect, luminous efficacy and luminous flux of warm white PC-LEDs was investigated partially for their limit in Section 3.4.3 and more entirely for their current and temperature dependence in Section 3.4.4. In this section, the temperature and the current dependence of color difference of warm white PC-LEDs will be described as supplement factors for color quality aspect regarding the short term stability of warm white PC-LEDs. Particularly, if the hot binning point (350 mA and 80 °C) is assumed as the referent point and the concept of color difference (Δu^*v^* , 1976) is applied to calculations and evaluations, the color difference between the reference point and operating points can be determined.

* **Temperature dependence of color differences of warm white PC-LEDs:** Particularly, in Figure 3.17, the temperature dependence of color difference of warm white LEDs is described in the operating region from 40 °C to 80 °C of operating temperature at the forward current of 350 mA. The results of the temperature dependence described in Figure 3.17 show that if the color difference is always necessary to be kept at the acceptable level of lower than 3 MAC ADAM ellipses according to the author in [37], the permitted operating temperature must be always higher than about 45 °C for LWEX6, LWG5 and HWVG6. Moreover, there is nearly no color difference for other LEDs, when operating temperature increases from 40 °C to 80 °C. With the knowledge on the temperature dependence of warm white PC-LED spectra, the explanation for the color difference of these six cases was given very specifically in Section 3.4.2. As well, these investigated results corresponded very well with spectral changes over operating temperature in Figure 3.9 and are important to determine desired targets for the optimization and stabilization in Chapter 7.

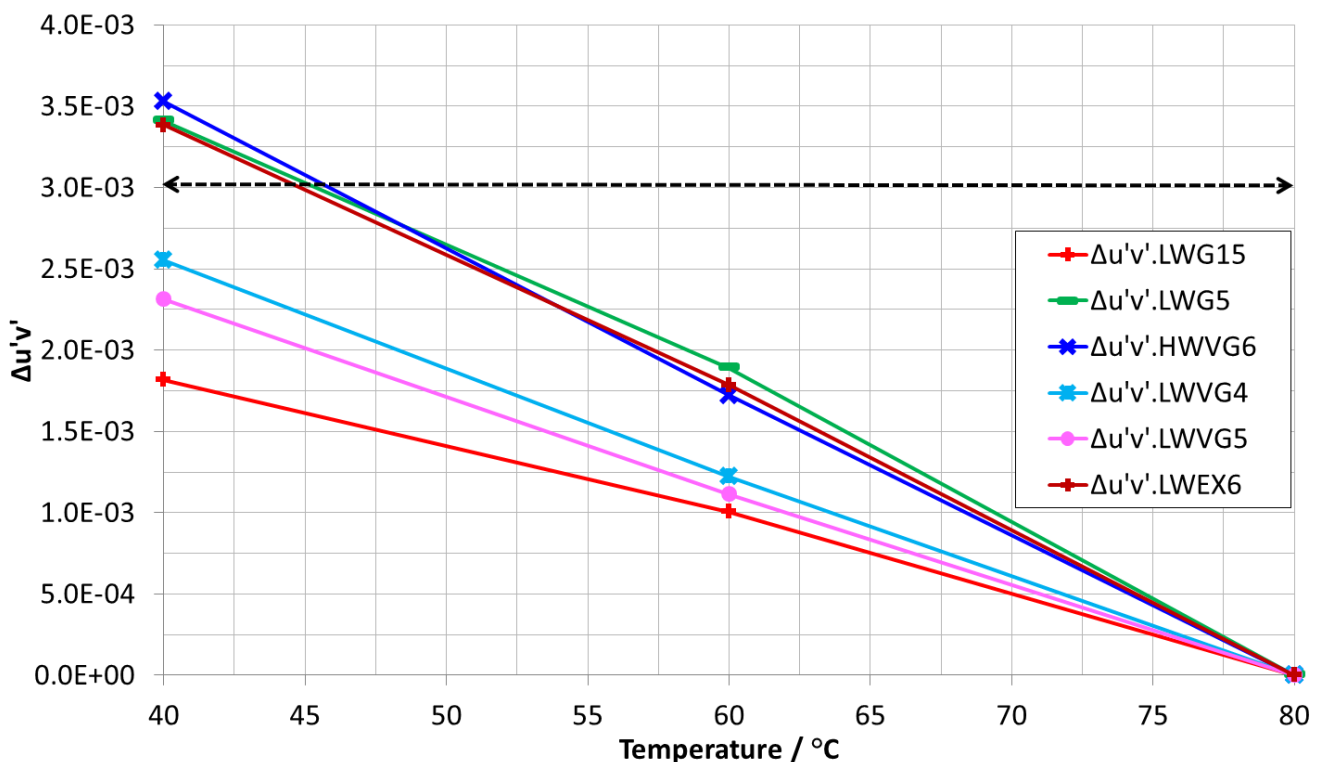


Figure 3.17 - Temperature dependence of color differences of six typical warm white PC-LEDs at 350 mA

* **Current dependence of color differences of warm white PC-LEDs:** In Figure 3.18, the current dependence of the color difference of warm white LEDs is described in the operating region from 100 mA to 700 mA of forward current at the operating temperature of 80 °C. Based on the results of the current dependence in Figure 3.18, it can be recognized, that the available operating current range was the entire region from 100 mA to 700 mA for almost warm white PC-LEDs. In other words, when the forward current increased from 100 mA to 700 mA, there was nearly no color difference for the almost warm white PC-LEDs excepting LWG5 and LWG15. Particularly, the permitted forward current region was only from about 100 mA to about 650 mA for LWG15 as a bad case and was from about 275 mA to about 425 mA for LWG5 as the worst case. These results corresponded very well with the current dependence of warm white PC-LED spectra investigated in Section 3.4.2. In that, the explanation for the bad color stability of LWG5 and LWG15 were discussed obviously.

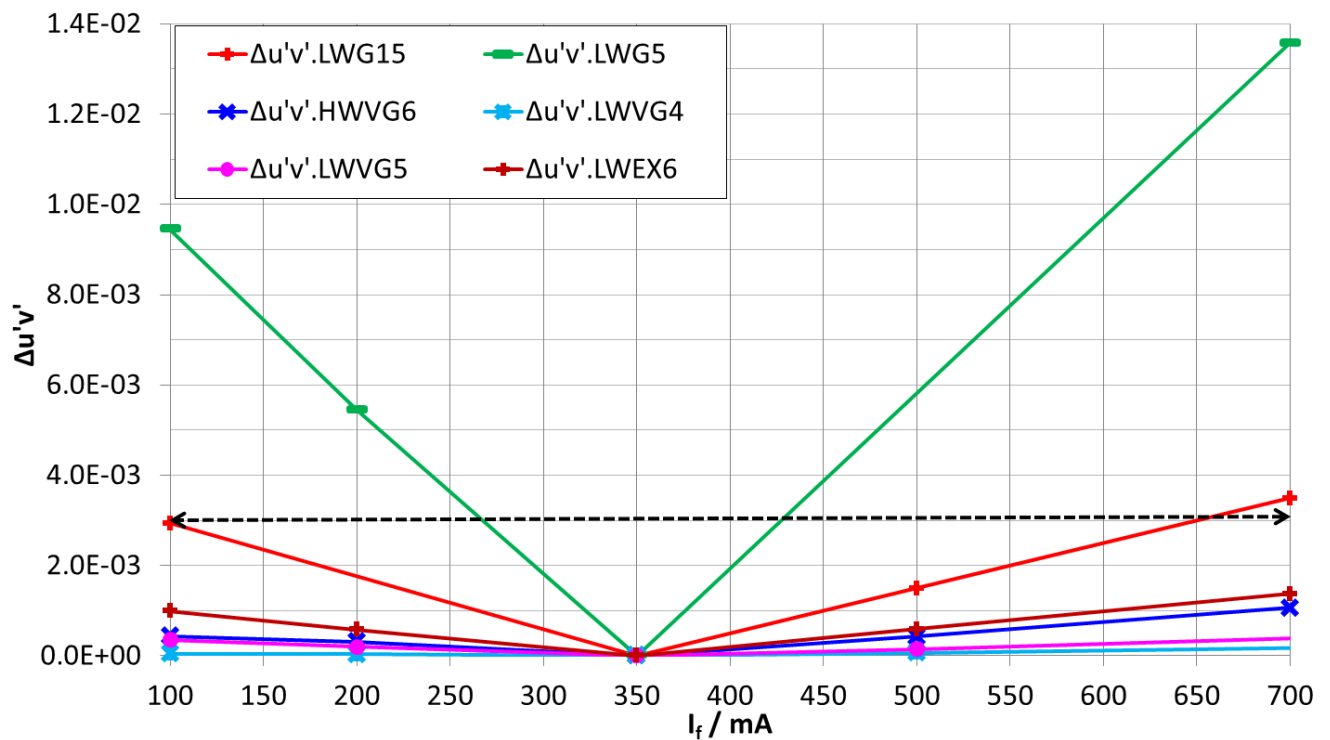


Figure 3.18 - Current dependence of color differences of six typical warm white PC-LEDs at 80 °C

3.4.6. Temperature and current dependence of correlated color temperatures of warm white PC-LEDs

* **Temperature dependence of correlated color temperatures of warm white PC-LEDs:** In Figure 3.19, the correlated color temperature variation of a high sample number of warm white PC-LEDs at the operating temperatures 40 °C, 60 °C and 80 °C at the forward current of 350 mA are described in the form of a column chart similarly to that in Section 3.4.3. The measured results show that there are two shift types of white points of warm white PC-LEDs. The first type is the blue shift with the CCT increase according to the increase of operating temperature in cases LWG15, LWG6, LWG5, LWG2, LWVG1 and LWVG2. The second type is the red shift with the CCT decrease according to the increase of operating temperature in cases LWG12, LWG11, LWVG4, HWVG6, LWVG4, LWVG5, LWEX6 and LWEX3. The reasons for these shifts were explained in Section 3.4.2 based on the opinion of spectral changes.

In this section, the most important points are the accurate determination for the shifts and their tendency. Particularly, the offsets between CCTs are from 11 K to 38 K for the temperature change from 60 °C to 80 °C, and from 28 K to 80 K for the temperature change from 40 °C to 80 °C. In that, the minimal CCT offset for LWG12 and the maximal CCT offset for HWVG6 corresponding its intensive spectral change described in Figure 3.9 in Section 3.4.2. Moreover, the determination for the maximal CCT offset (80 K) is very important so that the stabilization in Chapter 7 must be carried out to overcome this limit. As well, the CCT change over operating temperature gives the suggestion of a three-dimensional relationship between CCT, forward current and operating temperature in Chapter 4.

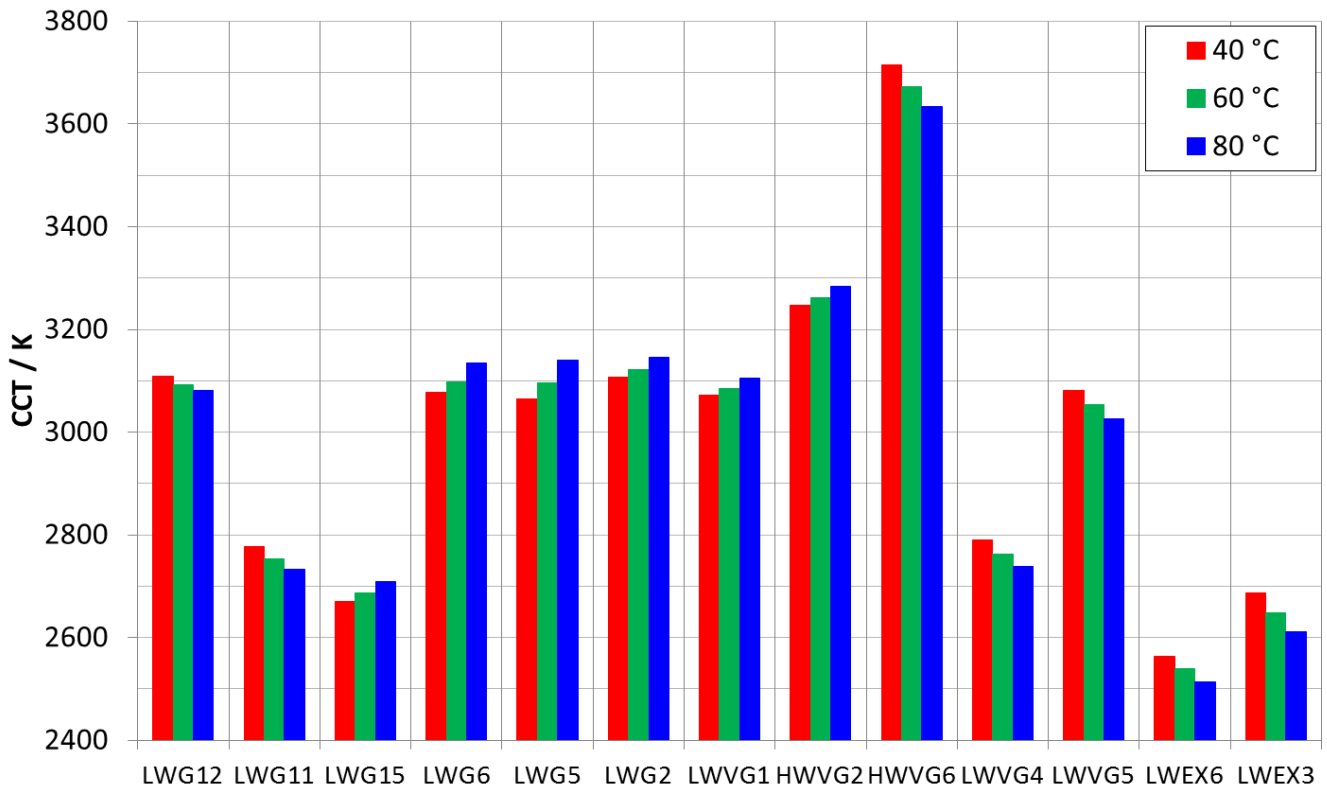


Figure 3.19 - CCT change of some warm white PC-LEDs at different temperatures and 350 mA

* **Current dependence of correlated color temperatures of warm white PC-LEDs:** In Figure 3.20, the correlated color temperature change of warm white PC-LEDs between the binning point (350 mA and 80 °C) and the derivate operating point (700 mA and 80 °C) is described. The investigated results suggest that warm white PC-LEDs can be classified into two LED groups based on the current dependence of their CCT including a bad CCT stability group and a good CCT stability group. Particularly, big CCT shifts can be seen for LWG15, LWG6, LWG5, LWG2, LWVG1 and HWVG2 of the bad CCT stability group with values of 72 K, 338 K, 417 K, 170 K, 174 K and 181 K, respectively. Contrarily, small offsets are achieved for LWG12, LWG11, HWVG6, LWVG4, LWVG5, LWEX6 and LWEX3 of the good CCT stability group with different values of 6 K, 2 K, 8 K, 4 K, 10 K, 5 K and 8 K, respectively. However, in Figure 3.10 in Section 3.4.2, only some typical candidates for these two groups were used to describe for their spectra in order to avoid a too complicated spectral diagram. Indeed, typical candidates of the bad CCT stability group in Figure 3.10 were LWG5 ($\Delta CCT=417$ K) and LWG15 ($\Delta CCT=73$ K), and the typical candidates of the good CCT stability group were HWVG6 ($\Delta CCT=8$ K), LWVG4 ($\Delta CCT=4$ K), LWVG5 ($\Delta CCT=10$ K) and LWEX6 ($\Delta CCT=5$ K). Based on the spectral diagram in Figure 3.10, it can be recognized, that the deep red phosphors (630 nm - 640 nm) and the wide spectrum green phosphor (about 520 nm - 530 nm) were usually used to fabricate very good and excellent CRI warm white PC-LEDs such as HWVG6, LWVG4, LWVG5 and LWEX6. Intrinsically, besides the appropriate combination between luminescent materials in a phosphor mixture and the appropriate combination between a phosphor mixture and a blue chip, the own specific properties of red phosphors and green phosphors play very important role for the CCT stability of very good and excellent CRI warm white PC-LEDs. Particularly, although red phosphors always absorb optical energy and radiate their thermal energy very intensively, the absorption and the radiation of red phosphors as well as the ones of green phosphors change proportionally to forward current. Therefore, they had a quite good CCT stability over forward current. Whereas there are

different problems happening with bad CCT stability warm white PC-LEDs such as LWG15 and LWG5. For LWG15, although the proportional spectral change of the red phosphor to the forward current is quite good, the one of the yellow phosphor (about 550 nm - 560 nm) and the one of the blue chip (about 450 nm) are not really good. Otherwise, LWG5 is a typical demonstration example for the inappropriate combination between luminous materials in a phosphor mixture and the one between a phosphor mixture and a blue chip. As a result, its right spectral component shifted strongly into the left side. As well, both its left and its middle spectral component increased intensively up to the above side. Consequently, LWG5 became the worst CCT instability case.

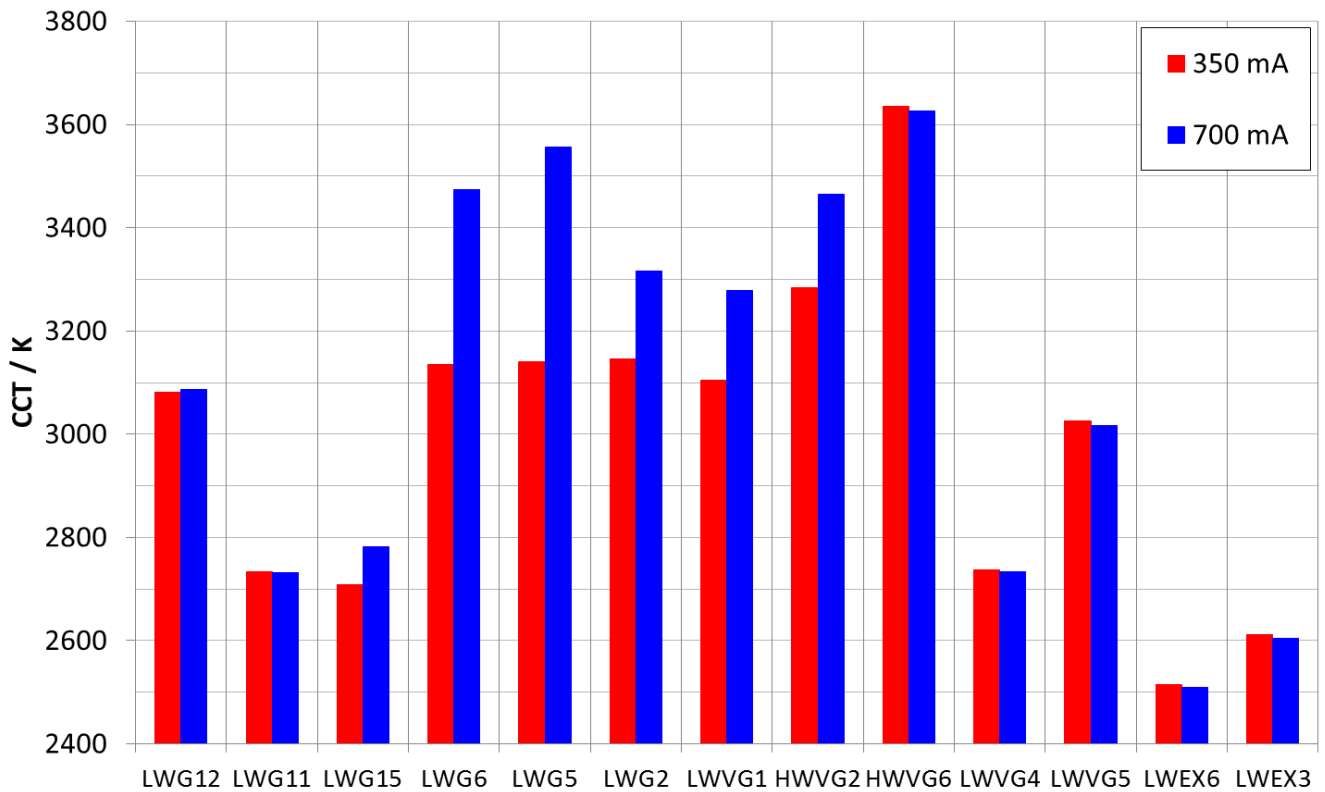


Figure 3.20 - CCT change of some warm white PC-LEDs at different forward currents and 80 °C

3.4. Summary

In Section 3.2, the basic and advanced concepts about current lighting quality as well as the new lighting quality were generalized and discussed. Hence, the key quality aspects were defined for further researches in this thesis including chromaticity, correlated color temperature, whiteness, color rendering indexes, luminous flux, luminous efficacy and their short term temperature stability in high quality solid state lighting applications. Then, in Section 3.3 four typical commercial color semiconductor LEDs on the worldwide market (belonging two conventional LED groups including InGaN LED group and InGaAlP LED group) were selected for the investigation. Hence, the spectral shifts over operating temperature and forward current of the InGaN LEDs and InGaAlP were determined and explained. Consequently, more detailed parameters such as peak wavelength, full width at half maximum wavelength, radiant flux, radiant efficiency and color difference were measured and analyzed comprehensively. As a result, the orange semiconductor LED was recommended to be avoided in the LED combination for hybrid LED-lamps in chapter 7. Special

attention must be paid for the red semiconductor LED in applications in order to limit and stabilize its radiant efficiency appropriately in real operations. Finally, the blue semiconductor LED was confirmed for its appropriateness in the high current operating region and for the fabrication of white PC-LEDs. The investigated results about the temperature dependence and current dependence also give essential suggestions for the characterization of color semiconductor LEDs in Chapter 6.

On the other hand, warm white PC-LEDs were investigated very specifically in Section 3.4. In that, their typical spectral candidates were analyzed into three partial spectral components including the shorter spectral component of the blue chips, the middle spectral component of green / yellow / orange phosphors and the longer spectral component of red phosphors. Good / bad combinations among luminescent materials in a phosphor mixture and the ones between a phosphor mixture and a blue chip for warm white PC-LEDs with their good / bad temperature stability and current stability of the color difference, correlated color temperature, luminous flux and luminous efficacy were investigated and explained. These results are very important suggestions for the minimization in Chapter 4, the characterization for white PC-LEDs in Chapter 6, the appropriate operating current selection, the stabilization and the improvement of the lighting quality of hybrid LED-lamps in Chapter 7. As well, the current limits of white PC-LEDs regarding the color rendering indexes, luminous efficacy and whiteness of warm white PC-LEDs determined at the binning point are the desired targets for the optimization and the stabilization of the hybrid LED-lamps in Chapter 7.

4. A minimization solution to parameter differences between LED- and LED-luminaire manufacturers

4.1. Motivation

* **Demands and tasks of LED-luminaire manufacturers:** In design of LED-luminaires and LED-luminaires, accurate parameters of color semiconductor LEDs and PC-LEDs are necessary to be accounted in each stage of the LED-luminaire development such as the calculation of one or many available optical combinations with a specific geometrical form of LEDs for a desired light intensity distribution, the determination of a suitable spatial distribution and configuration of a printed circuit board, the improvement for effective operation for the LED-luminaire and the arrangement of each electrical component matching its function. In addition, LED-luminaire manufacturers must consider appropriately the heat sink and the mechanical structure of the case, gasket, mounting platform and shape of the finished LED-luminaires. Finally, the LED-luminaire manufacturers must publish a datasheet or a guide book with full required information such as luminous flux Φ_v in lm, curves of luminous intensity distribution, radiant flux Φ_e in W, power factor ($\cos\phi$), chromaticity (x, y, u, v or u' and v'), correlated color temperature CCT in K, chromaticity and CCT as functions for emission angle of light, color rendering indexes (R_a, R_9 and AVR_{1-14}), lifetime as a function of operating condition (current and temperature), dimming curves, safe parameters and the total operating voltage V_f in V.

* **Parameter differences between LED manufacturers and LED-luminaire manufacturers:** In order to avoid the deviation of luminaire data, LED-luminaire manufacturers should select similar LEDs belonging to the same binning group and take care, whether the published parameters in their datasheets or guide books are still correct during the LED-luminaire operation within the limits defined previously or not. This problem should mean not small difficulties for LED-luminaire manufacturers. Indeed, like well-known information, a binning process for commercial LEDs is always performed at 25 °C and 350 mA in 25 microseconds in the case of cold binning or 80/85 °C in 25 microseconds in the case of hot binning by LED manufacturers. Contrarily, finished LED-luminaires of LED-luminaire manufacturers will operate a long time each day like from 8 o'clock to 18 o'clock for an office lighting system or from 18 o'clock to 6 o'clock for a street lighting system in an extremely hard operating condition. Depending on measured positions in the case of LED-luminaires, daytime, nighttime, season and dimming status, the operating temperature of LED-luminaires can be between 40 °C to 120 °C. Even in good air-conditioned rooms, the junction temperature of LEDs can be about 70 °C to 100 °C. Thus, there were big differences between the sorting temperature at LED fabrication and the real operating temperature of LED-luminaires at LED-luminaire applications. In addition, the original forward current of LEDs in a binning process at LED manufacturers is a current of 350 mA. Oppositely, the operating current at LED-luminaire manufacturers is often a PWM current between 250 mA and 1000 mA. Therefore, luminous flux, luminous efficacy, CCT, CRI, chromaticity, lifetime and other parameters will be quite much different comparing with their original parameters in binning conditions. In more detail, investigations in Chapter 3 showed that the lighting technique and calorimetric parameters of both color semiconductor LEDs and PC-LEDs always depend strongly on forward current and operating temperature as three-dimensional functions. That is why the parameters of LED-luminaires are usually different to those in guidebooks for LED-luminaires of LED-luminaire manufacturers.

* **A simple minimization solution and the know-how for its demonstration:** In order to minimize parameter differences and make current datasheets of LEDs more serious for the real operation of LED-luminaires, parameters of LEDs at different forward currents and varied operating temperatures should be measured, characterized and published fully. Therefore, this chapter has to describe methodically an example about a new characterization for photometric and colorimetric parameters of a warm white LED type. Their chosen parameters will be established as simple three-dimensional functions of forward current and operating temperature limited in a conventional operating region (about 100 mA-1000 mA and about 25 °C - 100 °C). Moreover, all twenty warm white LEDs belonging to the same binning group ($CCT \sim 2700$ K) of a well-known LED manufacturer C will be measured. However, only fifteen LEDs will be used for the characterization. The five other LEDs will be used to evaluate the accuracy of characterization for chosen parameters. These procedures are used to demonstrate for a simple minimization solution for parameter differences in order to reduce difficulties for LED-luminaire manufacturers and enhance the applicability for commercial LEDs on the worldwide market in solid state lighting applications.

4.2. A demonstration example for a simple minimization solution

In Section 4.1, the demand and task of LED-luminaire manufacturers were studied specifically. Consequently, the problem of parameter differences between LED manufacturers and LED-luminaire manufacturers was recognized. Then, a simple minimization for parameter differences and know-how for its demonstration was offered. Therefore, this section has to realize the simple minimization solution by means of new characterizations with three-dimensional functions for a specific demonstration example.

4.2.1. Definition of essential quality categories in the real performance

In fact, not all parameters of LEDs should be measured, characterized and supplied to customers, but only just full amount of really necessary parameters should be published so that users can apply the given information to calculate correlated parameters. Particularly, the parameters of LEDs should be classified into three categories including energy category, color quality category and the rest category.

Firstly, the rest category relating to safe operation parameters, soldering temperature tolerance, mechanical and structure parameters (size, shape and dimension), positive / negative poles and symbols will not be mentioned in this thesis.

Secondly, the energy category includes the luminous flux Φ_v in lm, radiant power Φ_e in W and forward voltage V_f in V as three-dimensional functions of the forward current I_f in mA and the operating temperature T_s in °C. In fact, based on these parameters, the electrical power $P_{el}=I_fV_f$ in W, luminous efficacy $\eta_v=\Phi_v/P_{el}$ in lm/W and radiant efficiency $\eta_e=\Phi_e/P_{el}$ in W/W or % can be calculated easily for any derivate operating point.

Thirdly, the color quality category includes the correlated color temperature CCT in K, the chromaticity (u', v' , CIE1976), the color difference between an operating point and a binning point at LED manufacturers ($\Delta u'v'$, CIE1976) and color rendering indexes (R_1-R_{14} , R_a and AVR_{1-14}) as three-dimensional functions of forward current I_f and operating temperature T_s . Moreover, whiteness $\Delta u'v'_{CT}$ can be also calculated from the above given chromaticity. Otherwise, some special quality parameters such ratio S/P , circadian stimulus CS and others, which have been not yet considered and applied much in current solid state lighting applications, will not be studied in this chapter. In the next sections, the energy category, the color quality category and offers for further development will be described successively.

4.2.2. Parameters of the energy category

In the defined energy category in Section 4.2.1, there are three parameters including luminous flux, radiant flux and forward voltage. In the role of a methodical demonstration example, the luminous flux of LEDs will be investigated and characterized specifically. Indeed, firstly two dimension functions between luminous flux and operating temperature at different forward currents and the ones between luminous flux and forward current at different operating temperatures will be investigated and characterized. Secondly, two above functions will be combined into a three-dimensional function of luminous flux, operating temperature and forward current. Thirdly, the verification of the accuracy of characterizations will be carried out by means of the maximal, average and minimal measured luminous fluxes of 15 warm white PC-LEDs and the measured luminous fluxes of 5 rest PC-LEDs. As well, the binning quality of the LED binning group of the LED-manufacturer C for luminous flux will be evaluated by means of confidence 95 % at different operating temperatures and forward currents. The lower the confidence offset is, the higher the binning quality is. Finally, four above steps are the full procedure for the new characterization of luminous flux according to the simple minimization solution. The other meaningful parameters will be only performed with the second step as the key characterization by means of complete three-dimensional functions of operating temperature and forward current in order to avoid unnecessary repeated procedures.

* **Luminous flux:** In order to realize the above steps for luminous flux, firstly binning condition is selected at 350 mA and 25°C. Therefore, all parameters will be characterized as relative parameters compared to that at the binning condition. Particularly, in Figure 4.1 characteristics of the relative luminous flux of the chosen warm white LED type are described. In that, the broken curves are characterized properties and the solid curves are average measured properties of fifteen warm white LEDs as functions of operating temperature at five forward currents 100 mA, 350 mA, 500 mA, 700 mA and 1000 mA. Based on achieving results, it can be recognized, that the shape of both characterized and measured curves is quite similar and the higher the operating temperature is, the lower the luminous flux is. Moreover, at higher forward currents, the reduction of luminous flux is stronger.

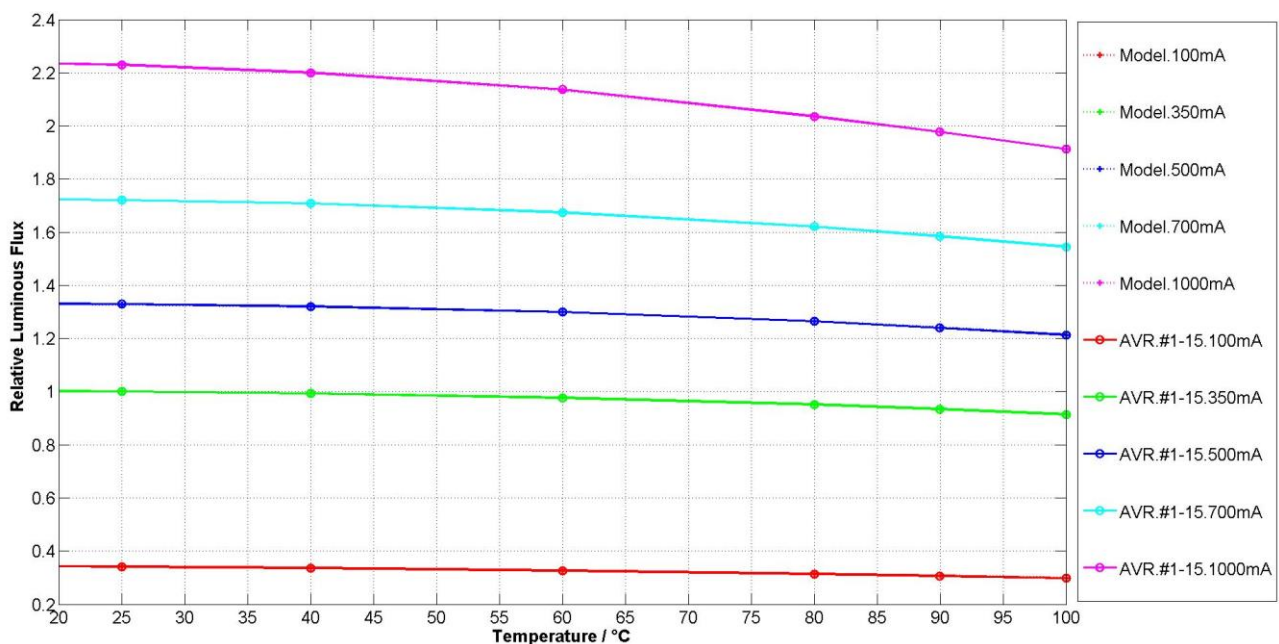


Figure 4.1 - Relative luminous fluxes as functions of operating temperature at different forward currents

On the other hand, the property of the relative luminous flux of the warm white PC-LED type is described as the function of forward current at six operating temperatures 25°C, 40°C, 60°C, 80°C,

90°C and 100 °C) in Figure 4.2. In that, the broken curves and solid curves are to denote for the characterized and measured properties, respectively. Visually, the results in Figure 4.2 show that the behavior of two curve types is similar and they increase non-linearly following the increase of forward current. Indeed, at 350 mA and 25 °C the relative luminous flux is 100 %, but at 700 mA and 25 °C (the forward current increased 2 times), it is only about 175 %. Even when the operating temperature increases up to 100 °C, the relative luminous flux at 700 mA is lower (only about 158 %) compared with that at the binning point.

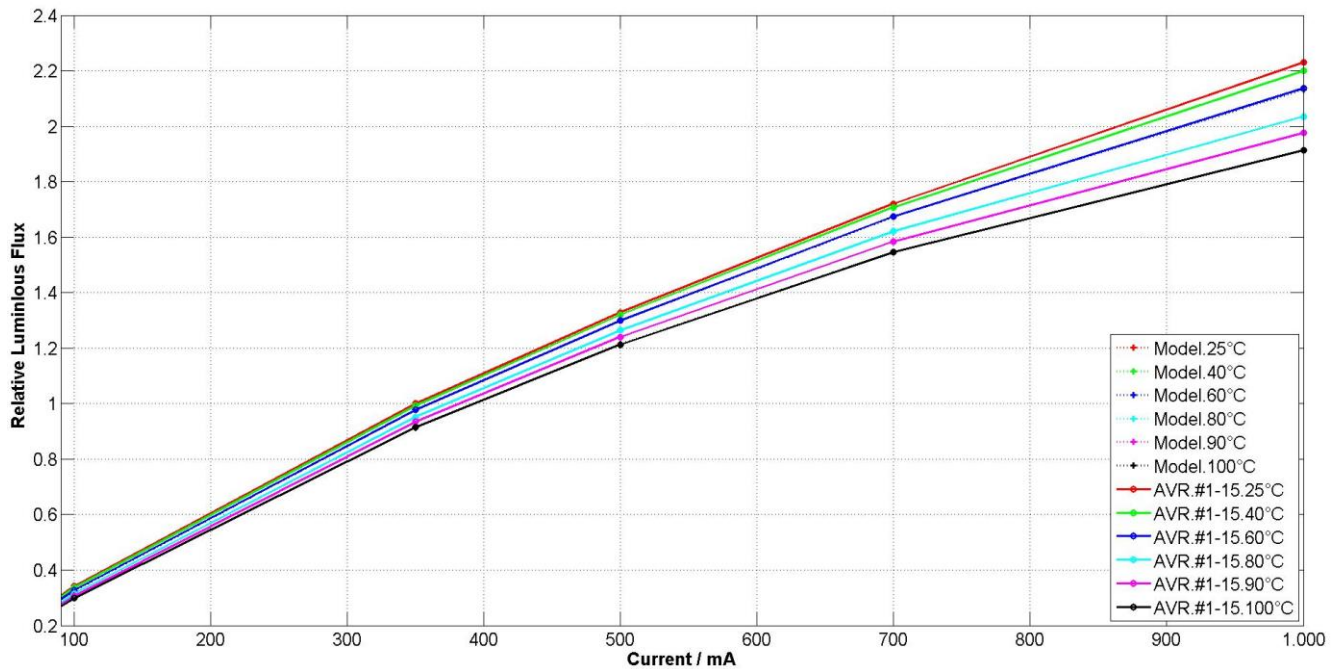


Figure 4.2 - Relative luminous fluxes as functions of forward current at different operating temperatures

Successively, combining functions in Figure 4.1 and Figure 4.2 gives the LED-luminaire manufacturers a three-dimensional function of relative luminous flux described in Figure 4.3. With this three-dimensional function, the LED-luminaire developers can determine the tendency, the level and the value of luminous flux at any desired operating points / regions. As well, in a conventional operating region, LED-luminaire manufacturers can define an accurate limit of the luminous flux of their final LED-luminaries.

Finally, the verification of the accuracy of characterization and the evaluation of the binning quality of the PC-LED binning group are really very essential in order to ensure that the characterization is correct and the offset between similar LEDs belonging to the same binning group is within an acceptable limit. Therefore, in Figure 4.4 the maximal, average and minimal measured luminous fluxes of the fifteen similar LEDs are described and then the measured luminous fluxes of five rest similar PC-LEDs are described in the same diagram at different forward currents and different operating temperatures. Hence, the results in in Figure 4.4 show that the luminous fluxes of five rest PC-LEDs lie between the maximal and minimal limits and distribute around the average curves. Moreover, the higher the forward current and the operating temperature are, the wider the distribution is. However, the derivate of luminous flux is still in the permitted boundary of the maximal and minimal measured values. Therefore, it can be verified, that the characterized curves of luminous flux had eligibility to reflect the practical behaviors of the entire warm white PC-LED binning group regarding the luminous flux. As well, the binning quality of the binning group about luminous flux is good enough for the establishment of LED-luminaires without taking care about their homogeneity.

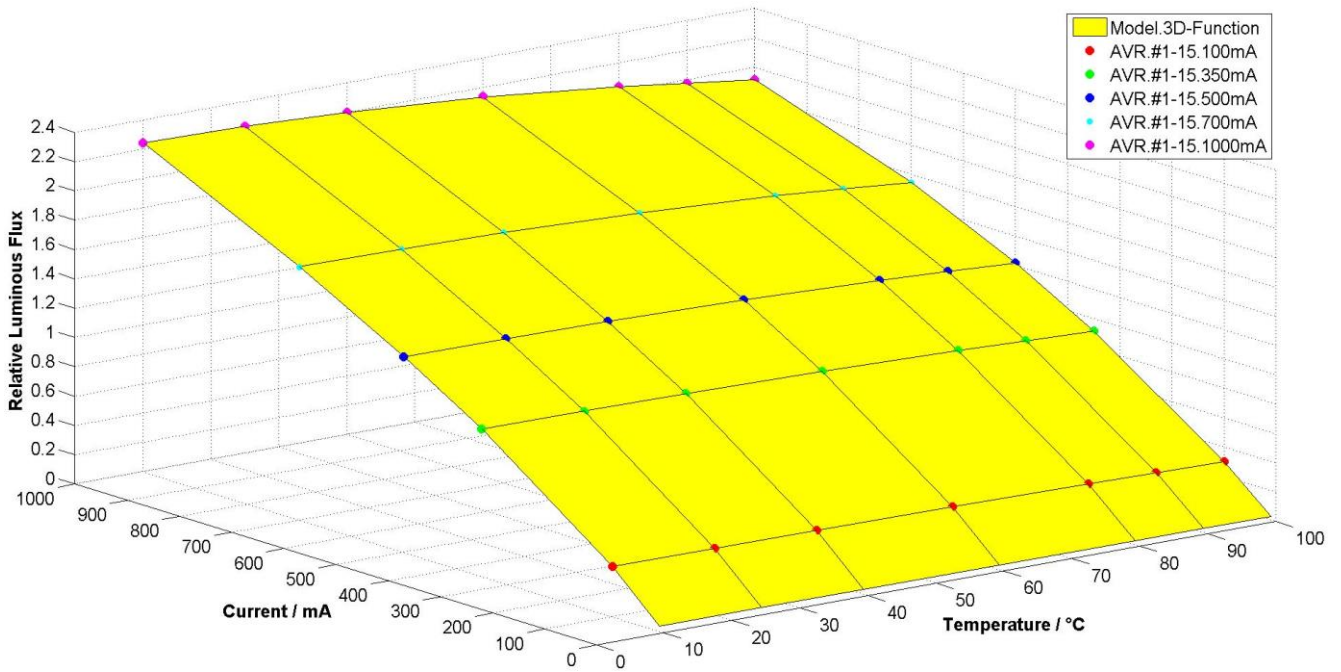


Figure.4.3- Relative luminous flux as a three-dimensional function of operating temperature and current

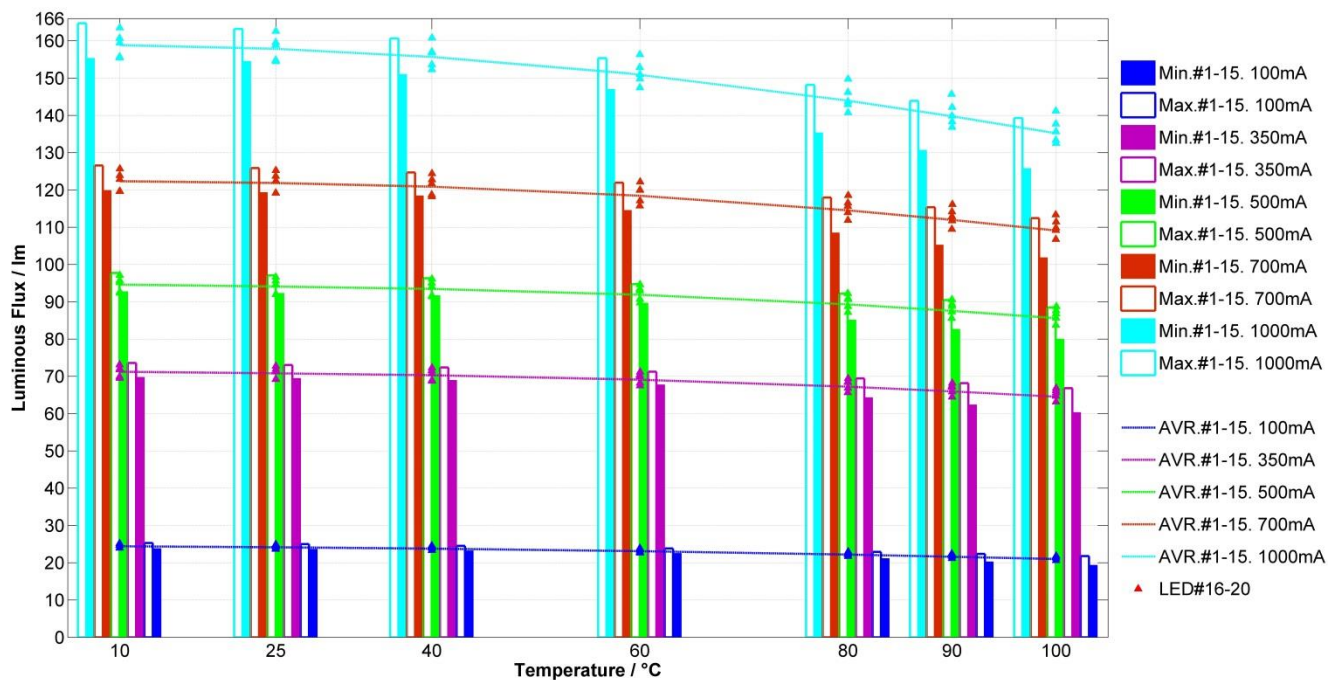


Figure.4.4- Verification for the correct characterization of the luminous flux function and the binning quality

In more detail, average luminous flux $\Phi_{v,avr-1-15}$ in lm of the fifteen LEDs, calculated luminous flux $\Phi_{v,cal}$ in lm of the above characterization and offset $\Delta\Phi_v$ in % between them at five forward currents 100 mA, 350 mA, 500 mA, 700 mA and 1000 mA and six operating temperatures 25 °C, 40 °C, 60 °C, 80 °C, 90 °C and 100 °C are listed in Table 4.1. The results show that the maximal offset between average and calculated luminous fluxes is 0.336 % and the minimal offset between them is 0.005 %. Obviously, it can be recognized, that these offsets can be accepted in the calculation and the design for LED-luminaire manufacturers. On another side, in order to evaluate the distribution quality of similar LEDs belonging to the same warm white PC-LED binning group, the confidence offsets (95 %) for the

distribution are listed in Table 4.2. Particularly, with 95 % confidence of the distribution, the maximal luminous flux offset is 1.422 lm and the minimal luminous flux offset is 0.21 lm. In fact, these very small offsets confirmed for LED-luminaire manufacturers that the distribution of the chosen warm white PC-LED binning group is very homogenous and this binning group is valuable enough to pay a corresponding cost for it. As well, LED-luminaire manufacturers can determine and publish self-confidently the accuracy limit of the luminous flux of finished LED-luminaries that are built from these LEDs in their guidebooks. In addition, in Table 4.3 the ratios of maximal/average and average/minimal (called Max/AVR. and AVR./Min or Max./AVR./Min shortly) of the luminous flux of the fifteen LEDs are published in order to illustrate for the curves in Figure 4.4, quantitatively. Normally, the luminous flux offset between LEDs is always small at the binning point (350 mA and 25 °C) and bigger at higher forward currents and operating temperatures. Specifically, the maximal value and minimal value of the ratio Max/AVR. are 3.8 % and 2.7 % at 100°C and 100 mA and at 60 °C and 1000 mA, respectively. And the maximal value and minimal value of the ratio AVR./Min are 8.7 % and 1.9 % at 100 °C and 100 mA and 350 mA and 25 °C, respectively.

Table 4.1 - Comparison between the calculated and measured results of luminous flux

$\Phi_{v.cal.} / \text{lm}$	100 mA	350 mA	500 mA	700 mA	1000 mA
25 °C	24.108	70.872	94.100	121.899	157.864
40 °C	23.728	70.315	93.464	120.888	155.739
60 °C	23.085	69.134	91.934	118.441	150.965
80 °C	22.201	67.211	89.354	114.516	143.991
90 °C	21.663	65.934	87.638	112.002	139.791
100 °C	21.077	64.458	85.662	109.169	135.238
$\Phi_{v.avr.1-15} / \text{lm}$	100 mA	350 mA	500 mA	700 mA	1000 mA
25 °C	24.155	70.826	94.117	121.875	157.891
40 °C	23.788	70.306	93.480	120.902	155.716
60 °C	23.121	69.119	91.900	118.471	151.307
80 °C	22.193	67.238	89.324	114.554	143.977
90 °C	21.617	65.971	87.591	112.008	139.801
100 °C	21.007	64.547	85.630	109.158	135.244
$\Delta\Phi_v / \%$	100 mA	350 mA	500 mA	700 mA	1000 mA
25 °C	-0.194	0.065	-0.018	0.020	-0.017
40 °C	-0.251	0.013	-0.017	-0.012	0.015
60 °C	-0.159	0.023	0.037	-0.025	-0.226
80 °C	0.037	-0.040	0.033	-0.033	0.010
90 °C	0.212	-0.057	0.054	-0.006	-0.007
100 °C	0.336	-0.137	0.037	0.010	-0.005

Table 4.2 - Confidence 95 % of the LED binning group

$\Phi_{v.confidence.0.95} / \text{lm}$	25 °C	40 °C	60 °C	80 °C	90 °C	100 °C
100 mA	0.225	0.219	0.210	0.216	0.282	0.324
350 mA	1.365	1.363	1.442	1.256	1.778	1.832
500 mA	0.594	0.577	0.570	0.600	0.740	0.817
700 mA	0.781	0.760	0.764	0.825	0.997	1.083
1000 mA	1.010	0.998	1.025	1.138	1.327	1.404

Table 4.3 - The ratios of maximal/average and average/minimal of luminous flux

Max/AVR./Min	25 °C	40 °C	60 °C	80 °C	90 °C	100 °C
100 mA	1.035	1.031	1.031	1.033	1.035	1.038
	1.023	1.024	1.027	1.051	1.068	1.087
350 mA	1.031	1.030	1.031	1.033	1.033	1.035
	1.019	1.020	1.020	1.045	1.058	1.070
500 mA	1.032	1.030	1.031	1.032	1.033	1.034
	1.020	1.020	1.025	1.049	1.060	1.070
700 mA	1.033	1.031	1.029	1.030	1.030	1.030
	1.021	1.021	1.034	1.056	1.064	1.072
1000 mA	1.034	1.032	1.027	1.029	1.029	1.030
	1.022	1.031	1.029	1.064	1.070	1.075

* **Radiant flux and forward voltage:** Likewise, in Figure 4.5 and 4.6 the relative radiant flux and forward voltage are characterized by three-dimensional functions of forward current and operating temperature, respectively. In that, yellow dimension surfaces are images of three-dimensional functions and red, green, blue, blue and violet solid circles are to denote for average measured values of fifteen warm white PC-LEDs at 100 mA, 350 mA, 500 mA, 700 mA and 1000 mA, respectively. The achieved results show that characterized surfaces contain all average measured points. Therefore, they can be used in the calculation and design of LED-luminaire manufacturers. Otherwise, the verification of the confidence and the accuracy of the calculated radiant flux and forward voltage must be performed and supplied fully like that described in Figure 4.4 and Tables 4.1-4.3. Finally, based on these characterized surfaces, LED-luminaire developers can determine exactly the tendency, the level and the value of the radiant power and forward voltage at different forward currents and different operating temperatures. As well, they can also design and calculate easily for any necessary values or limits of quality parameters at each specific operating condition.

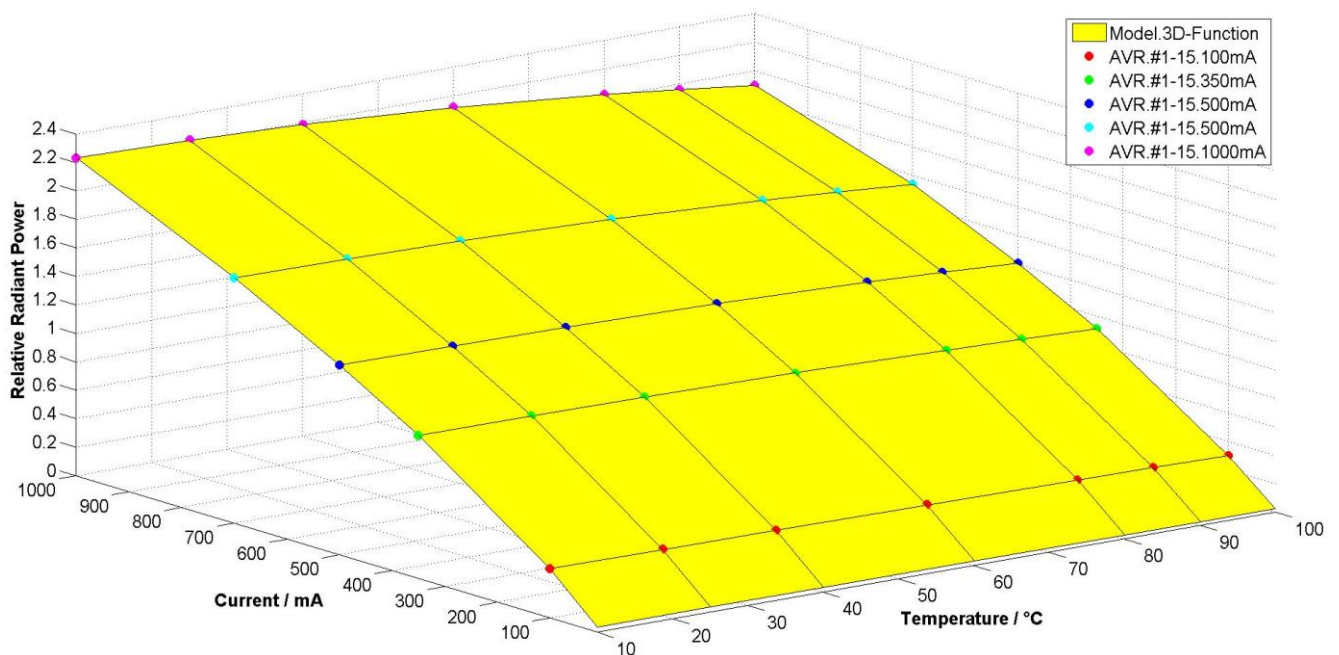


Figure.4.5- Relative radiant flux as a three-dimensional function of operating temperature and current

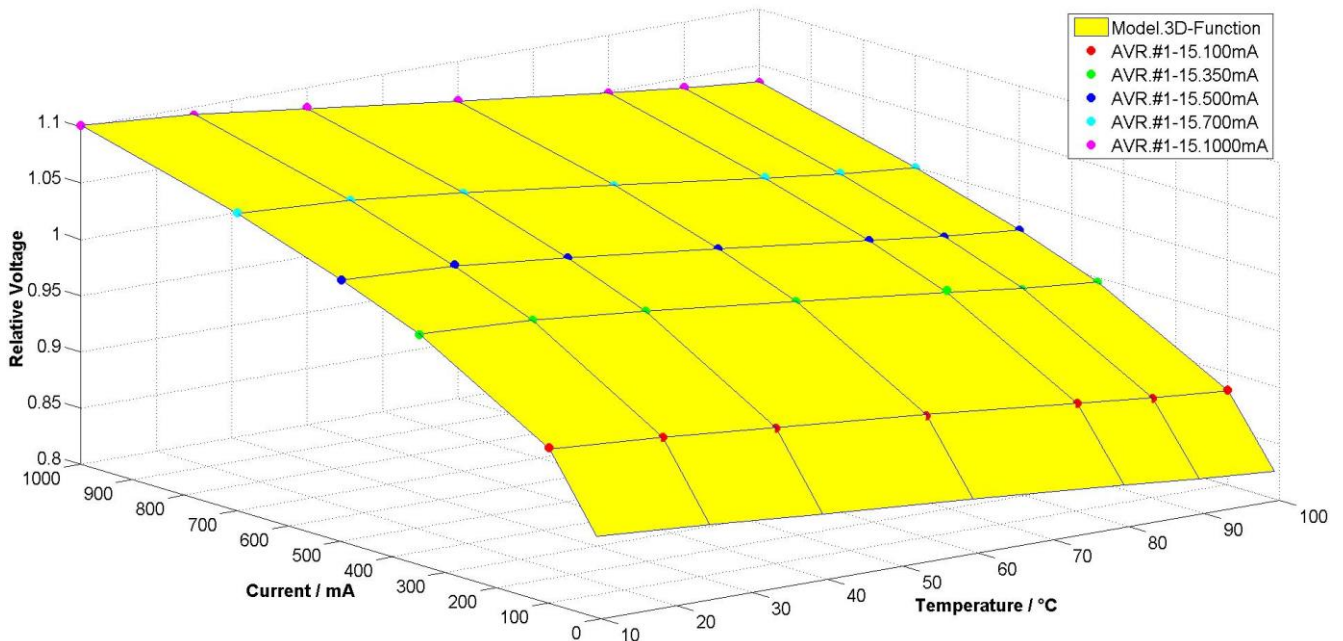


Figure.4.6- Relative forward voltage as a three-dimensional function of operating temperature and current

4.2.3. Parameters of the color quality category

In Section 4.2.1, the color quality category was defined with four main parameters including correlated color temperature CCT in K, color rendering indexes (R_1 - R_{14} , R_a and AVR_{1-14}), chromaticity (u', v' , CIE1976) and color difference between an operating point and the binning point ($\Delta u'v'$, CIE1976). In this section, in order to minimize parameter differences for four main above parameters, the new characterization by means of three-dimensional functions will be carried out with only key factors.

* **Correlated color temperature:** Similar to the performance in Section 4.2.2 with luminous flux, in Figure 4.7 a three-dimensional key relationship between correlated color temperature CCT of the warm white PC-LED with forward current and operating temperature is characterized, relatively. In that, the yellow surface is to describe the characterized property of CCT and the color solid circles are to indicate the average measured values of the fifteen similar warm white PC-LEDs. Consequently, the attachment between characterized and measured properties confirms that the characterization is applicable in the calculation and the design of LED-luminaire manufacturers with high accuracy. In fact, this characterized surface of CCT is very important so that LED-luminaire developers can determine the tendency, the level and the value of the correlated color temperature of LED-luminaires at any operating point / region. As well, limited values / regions of the correlated color temperature of finished LED-luminaires can be published accurately in guide books of LED-luminaire manufacturers.

In more detail, the calculated absolute correlated color temperature CCT_{cal} in K based on the above characterized surface, the average absolute correlated color temperature $CCT_{AVR,1-15}$ in K determined by the measured results of the 15 warm white PC-LEDs and the relative offset ΔCCT_{re} between them are listed in Table 4.4. In that, the maximal ΔCCT_{re} and the minimal ΔCCT_{re} are 0.03 % (0.8 K) at 100 mA and 40 °C, and 0 % (0 K) at 350 mA and 100 °C, respectively. Otherwise, the maximal and minimal offsets between CCT s at an operating point and at the binning point can be also calculated from the data in Table 4.4. Particularly, the maximal offset is about 7.9 % (213.2 K) at 1000 mA and 100 °C, and the minimal offset is 0.17 % (4.7 K) at 100 mA and 90 °C. In addition, the verification of the accuracy between characterized and measured CCT s and the evaluation of the binning quality of CCT

of the warm white PC-LED binning group are very important for the design of LED-luminaire manufacturers. Thus, in the reality they must be carried out similarly like that done in Section 4.2.2 for luminous flux.

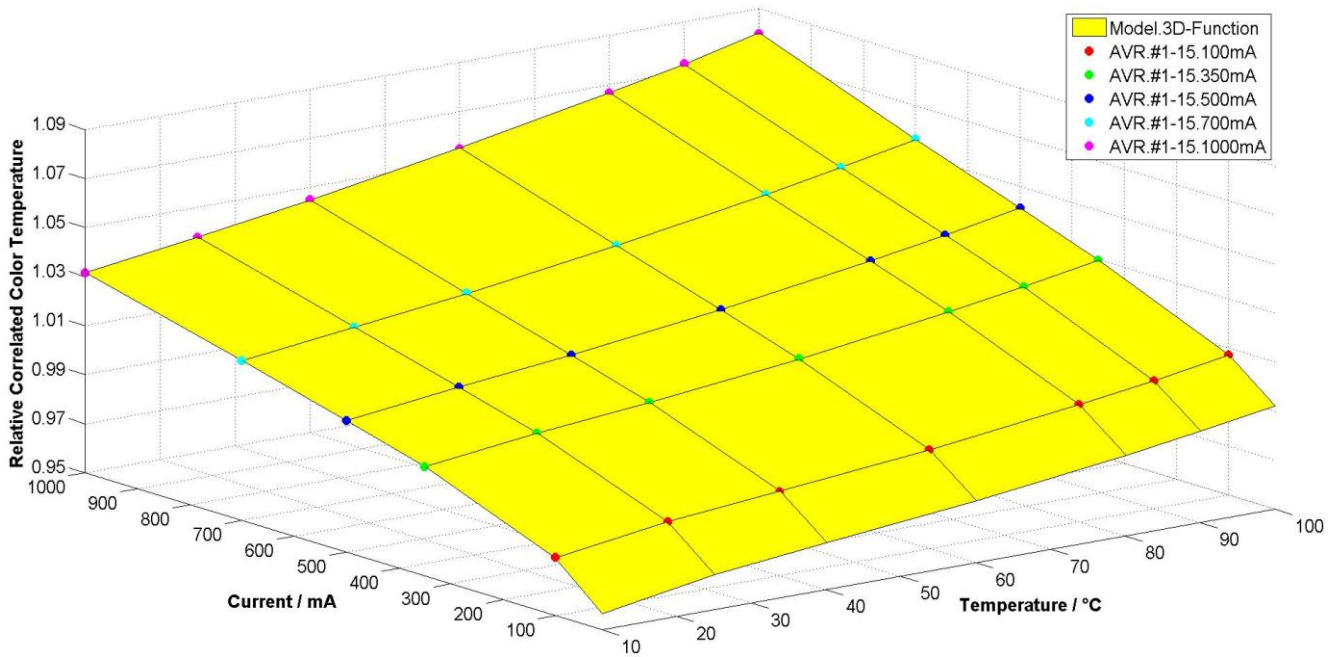


Figure.4.7- Relative CCT as a three-dimensional function of operating temperature and current

Table 4.4 - Comparison between the calculated and measured results of CCT

$CCT_{cal.} / K$	100 mA	350 mA*	500 mA	700 mA	1000 mA
25 °C	2639.5	2693.2	2717.3	2747.9	2794.2
40 °C	2651.0	2704.9	2730.3	2762.8	2812.6
60 °C	2666.5	2722.6	2750.3	2785.7	2840.1
80 °C	2686.3	2744.6	2774.3	2811.9	2870.3
90 °C	2697.9	2757.1	2787.7	2826.3	2887.0
100 °C	2710.7	2771.0	2802.5	2842.5	2906.4
$CCT_{AVR.1-15} / K$	100 mA	350 mA*	500 mA	700 mA	1000 mA
25 °C	2639.3	2692.8	2717.3	2747.7	2794.1
40 °C	2650.2	2704.8	2730.7	2762.9	2812.8
60 °C	2666.7	2723.0	2750.5	2785.5	2838.3
80 °C	2686.5	2744.7*	2773.9	2811.4	2870.2
90 °C	2697.8	2757.3	2787.6	2826.6	2887.5
100 °C	2710.6	2771.0	2802.4	2842.7	2906.1
$\Delta CCT_{re.} / \%$	100 mA	350 mA*	500 mA	700 mA	1000 mA
25 °C	0.008	0.015	0.000	0.007	0.004
40 °C	0.030	0.004	-0.015	-0.004	-0.007
60 °C	-0.007	-0.015	-0.007	0.007	0.063
80 °C	-0.007	-0.004	0.014	0.018	0.003
90 °C	0.004	-0.007	0.004	-0.011	-0.017
100 °C	0.004	0.000	0.004	-0.007	0.010

* **Color rendering index:** General color rendering index (R_a or CRI_a) is often mentioned in current datasheets and in some standards. However, in fact CRI_a is only the average value of the first eight CIE standard test color samples (TCS) of the total fourteen CIE standard TCSs. Therefore, CRI_a does not

reflect entirely abundant colors of color objects in real lighting applications. Nonetheless, in Figure 4.8 a three-dimensional relationship between CRI_a , forward current and operating temperature, which is characterized as a demonstration example, can also show the changing limits of CRI_a at different operating points / regions. In real applications, this characterized surface of CRI_a is necessary for LED-luminaire manufacturers to determine accurately the limit of CRI_a in their designs. Likewise, other three-dimensional functions can also be established for other color rendering indexes.

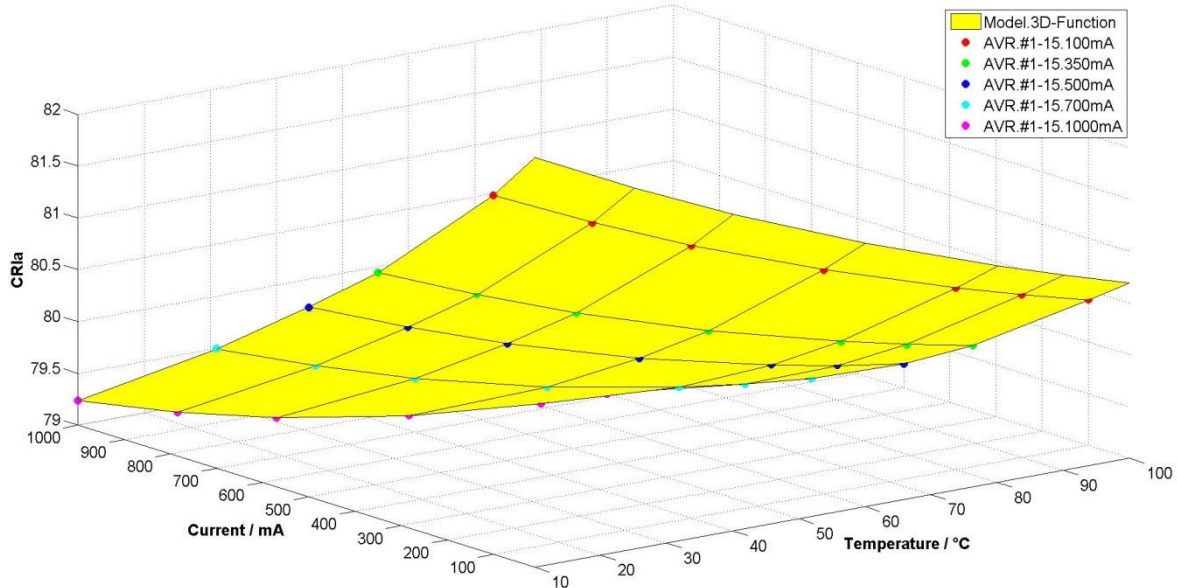


Figure.4.8 - CRI_a as a three-dimensional function of operating temperature and current

In more detail, color rendering indexes ($R_1 - R_{14}$) should be supplied fully like described in Figure 4.9. Consequently, LED-luminaire manufacturers can recognize that the warm white PC-LED has a very low color quality of red objects (R_9), a low color quality of blue objects (R_{12}) and purple objects (R_8), a very high color quality of green and olive green objects (R_{14} and R_3), and quite high color quality for the other rest color objects. Moreover, the higher temperature and forward current cause color rendering indexes worse. As a result, these warm white PC-LEDs should be only designed for lighting applications with the low color quality demand for red, purple and blue objects. As well, the limit of the CRI changes can be recognized and determined in desired operating regions.

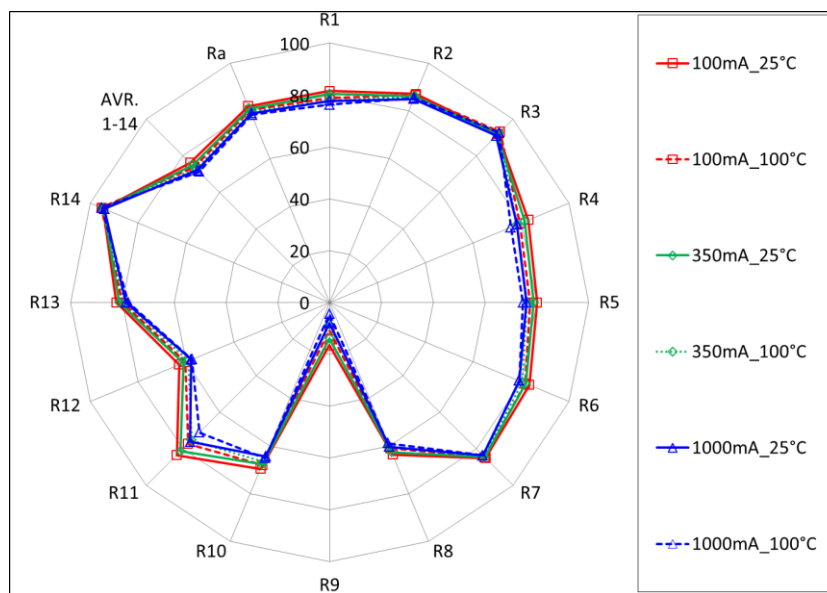


Figure 4.9 - $R_1 - R_{14}$, R_a and AVR.1-14 as functions of operating temperature and current

* **Chromaticity:** The changes of the chromaticity (u', v' , CIE1976) should be characterized and supplied entirely in different operating regions of forward current and operating temperature like the description in Figure 4.10. In that, the solid curves are to indicate for average measured properties of the chromaticity of the warm white PC-LED. Moreover, color arrows are to determine the tendency of color changes when operating temperature increases. Based on the color diagram in Figure 4.10, LED-luminaire developers will have good perception where the color region of finished LED-luminaires in a specific operating point / region is. Consequently, a quite accurate color region can be determined and published for LED-luminaire applications.

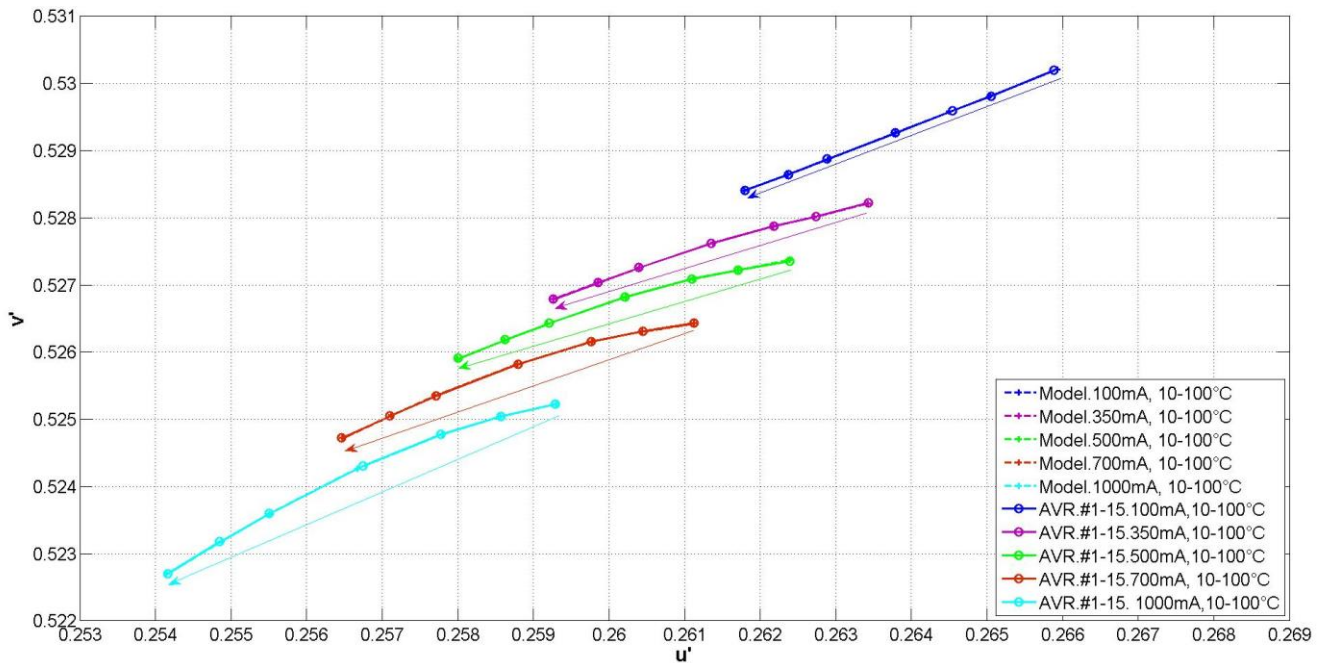


Figure 4.10 - Chromaticity u' and v' as functions of operating temperature and current

* **Color differences between operating points and the binning point:** When the chosen binning point is chosen at 350 mA and 25 °C (the cold binning), the color differences between operating points and the binning point can be determined and shown like the description in Figure 4.11. In addition, if the region of three MAC ADAM ellipses is selected as the standard limit of color difference for the human eyes like the researched results published in [37], the operating temperature is limited at above 25 °C in the case of 100 mA, at below 90 °C in the case of 350 mA and at below about 64 °C in the case of 500 mA. As well, the warm white PC-LED are nearly not allowed to operate at 700 mA and are prohibited completely at higher currents.

In more detail, the color differences are listed specifically in Table 4.5. In that, yellow cells are to indicate the very low color difference region, where the human eyes cannot recognize color differences between operating points and the binning point. Blue cells are to determine the acceptable color difference region, where color differences are tolerant and it is difficult for the human eyes to differentiate them. Successively, bright orange cells are the moderate color difference regions, where the human eyes can differentiate color differences quite obviously. Finally, orange cells and dark orange cells are high and very high color difference regions, respectively, where the color of the PC-LEDs is shifted into a completely new color. In real applications, the results in Table 4.5 are important so that LED-developers can recognize that the operating regions with low and tolerant color difference are around 100 mA, at 350 mA with the operating temperature below 100 °C, at 500 mA with the

operating temperature below 60 °C, and at 700 mA with the operating temperature below 25 °C. Moreover, the PC-LEDs are prohibited completely for the high current 1000 mA. Consequently, LED-developers can select appropriately designing materials, electrical and mechanical elements, forward currents and operating temperatures so that color differences between operating points and the binning point in a specific operating region is always below an acceptable limit.

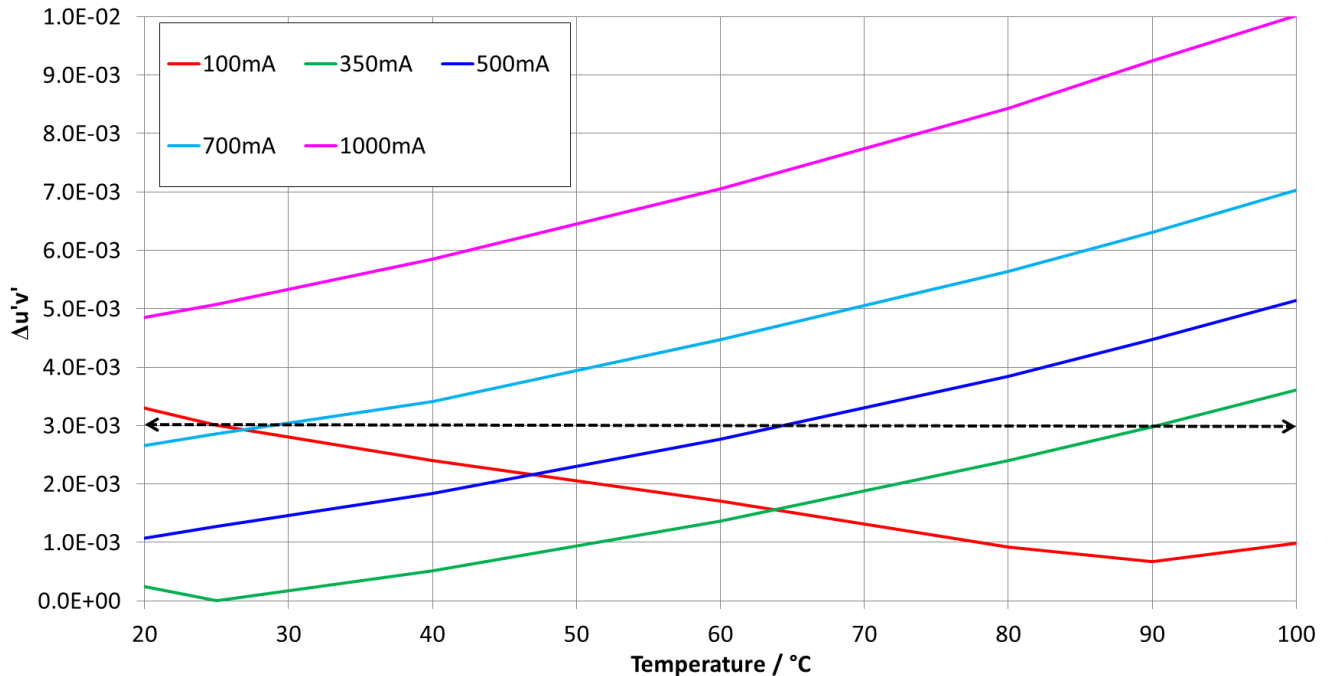


Figure 4.11 - Color differences as functions of operating temperature in the cold binning at different currents

Table 4.5 - Color differences with different operating regions in the cold binning (350 mA and 25 °C)

$\Delta u'v' / 10^{-3}$	100 mA	350 mA	500 mA	700 mA	1000 mA
25 °C	2	0	1	3	5
40 °C	2	1	2	3	6
60 °C	2	1	3	4	7
80 °C	1	2	4	6	8
90 °C	1	3	4	6	9
100 °C	1	4	5	7	10

4.2.4. Further development

Naturally, for the full characterization in reality, other properties such as the distribution of luminous intensity, the correlated color temperature and the chromaticity as the functions of emission angles must be established and supplied moreover. However, in the role of a demonstration example for the simple minimization solution, the performance mentioned above is only to describe core points of the new characterization for one typical warm white PC-LED type that is usually applied in indoor lighting applications in the European area. In the lighting industry, other white PC-LEDs in the warm white region ($2500 \text{ K} < CCT < 3000 \text{ K}$), warm white region ($3000 \text{ K} < CCT < 3500 \text{ K}$), neutral white region ($3800 \text{ K} < CCT < 4200 \text{ K}$), cold white region ($4500 \text{ K} < CCT < 5500 \text{ K}$) and cold white region ($6000 \text{ K} < CCT < 6500 \text{ K}$) or color semiconductor LEDs such as royal blue, blue, green, yellow, amber,

orange, red and deep red LEDs are also necessary to be described furthermore. Especially, although the energy category for color semiconductor LEDs is similar to that for PC-LEDs, their color quality category has some differences excepting the color difference parameter. Particularly, instead of three-dimensional functions of the correlated color temperature and color rendering indexes in the characterization, the similar functions of the peak wavelength and full width at half maximum are necessary in the description.

Furthermore, the binning point in the above example is only the cold binning condition at 350 mA and 25 °C in 25 microseconds. Nowadays, some LED manufacturers applied several hot binning conditions such as 350 mA and 80/85 °C or 700 mA and 80/85 °C in 25 microseconds. Specifically, in Figure 4.12 color differences of the above warm white PC-LEDs in form of the hot binning condition (350 mA and 80 °C). In that, the achieved results show that the operating region in the case of the hot binning is widened very much. Particularly, for forward currents 350 mA and 500 mA, the allowable operating temperature region is from 20 °C to 100 °C. In addition, for forward current 700 mA the PC-LED is permitted to operate until about 75 °C. Conventionally, forward currents 100 mA and 1000 mA (too low and too high currents) should be not considered in designs of LED-luminaire manufacturers, because the operation at a low current region requests a high number of the built-in LEDs and causes a high cost for final LED-luminaires and contrarily the operation at a high current region forces the degradation of finished LED-luminaires quickly.

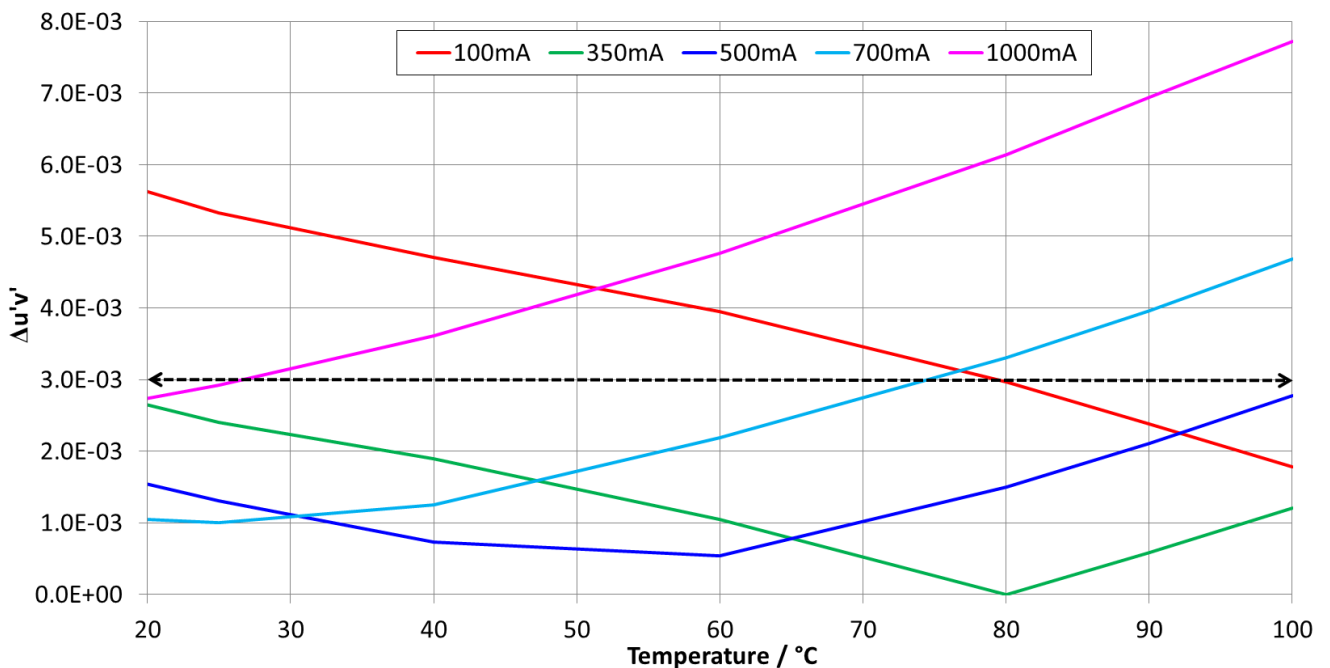


Figure 4.12 - Color differences as functions of operating temperature in the hot binning at different currents

In more detail, color differences for the hot binning are listed in Table 4.6. The definitions of cell colors are similar to those in Section 4.2.3. The results show that almost blue and yellow regions cover the map of color difference. Moreover, bright orange and orange cells concentrate at 700 mA with very high operating temperatures or at 1000 mA with low and middle operating temperatures. As well, bright orange and orange cells also happen for 100 mA at low operating temperatures. However, like the above mentioned, the forward current 100 mA is an unfeasible current in real applications. Finally, dark orange regions only occur in extreme hard operating conditions of 1000 mA and 100 °C.

Table 4.6 - Color differences with different operating regions in the hot binning (350 mA and 80 °C)

$\Delta u'v' / 10^{-3}$	100 mA	350 mA	500 mA	700 mA	1000 mA
25 °C	5	2	1	1	3
40 °C	5	2	1	1	4
60 °C	4	1	1	2	5
80 °C	3	0	2	3	6
90 °C	2	1	2	4	7
100 °C	2	1	3	5	8

4.3. Summary

Properties of both PC-LEDs and color semiconductor LEDs always change as three-dimensional functions of the forward current and the operating temperature that were investigated and described in the chapter 3. Thus, there are very big difficulties for LED-luminaire manufacturers. Even the difficulties become worse when there are usually parameter differences between LED manufacturers and LED-luminaire manufacturers. Normally, LED manufacturers always perform their binning at 350 mA and 25 °C in 25 microseconds for the cold binning or 350/700 mA and 80/85 °C in 25 microseconds for the hot binning. Contrarily, LED-luminaire manufacturers must operate their LED-luminaires in harder conditions such as operating temperatures of about 40 °C - 100 °C and PWM forward currents of about 500 mA - 700 mA. As a result, calculations and designs of LED-luminaire developers based on current datasheets of LED manufacturers are not accurate. Therefore, the data of guide books of LED-luminaire manufacturers are not ensured and LED-luminaire manufacturers must face the problems of guarantee, reputation and engagement with their customers.

In order to solve these problems, Chapter 4 proposed a simple minimization solution to the parameter differences between LED manufacturers and LED-luminaire manufacturers by means of the new characterization of the parameters with three-dimensional functions of operating temperature and forward current. In that, a warm white type (2700 K) PC-LED type was chosen as a demonstration example. Then, the parameters belonging to the energy category and the color quality category were established as three-dimensional functions of operating temperature and forward current. As well, the conventional operating region was limited from 100 mA to 1000 mA for the forward current and from 25 °C to 100 °C for the operating temperature. Moreover, in the performance twenty PC-LEDs were measured, but only fifteen PC-LEDs were used to build three-dimensional functions. In addition, the verification of the accuracy of the characterization and the evaluation of the binning quality of the similar PC-LEDs belonging to the same binning group by means of the confidence were performed in order to ensure that three-dimensional functions can be accepted in the calculations and designs of LED-luminaire developers. Beside the well-known parameters such as luminous flux, radiant flux, forward voltage, correlated color temperature and color rendering indexes and chromaticity, the color differences between operating points and the binning point were investigated and characterized as the new color quality parameter. As well, the maps of color differences with color indicators were established for both the cold binning and the hot binning. Finally, with the important core content above, the simple minimization solution was described fundamentally. Hence, the simple and direct solution was offered so that commercial color semiconductor LEDs and PC-LEDs of LED manufacturers on the worldwide market can be used widely and quickly in real solid state lighting applications and LED-luminaire manufacturers can fabricate best LED-luminaires, as well ensure the quality of their products for customers.

5. Junction temperature determination, thermal transient identification and thermal map decoding of LEDs

Overview description about history and classification of LEDs were carried out in Chapter 1. As well, current data about light output and lighting quality of LEDs was also updated in that chapter in order to establish problems and motivations for the thesis. Successively, in Chapter 2 background knowledge of LEDs was described in order to fundamentally understand both color semiconductor LEDs and white PC-LEDs. Then, their optical, radiant and calorimetric properties were investigated particularly in Chapter 3. Accordingly, investigated results confirmed that their properties always changed as three-dimensional functions of operating temperature and forward current. These changes and parameter differences between LED manufacturers and LED-luminaire manufacturers caused problems for LED-luminaire calculations. Therefore, in Chapter 4 a simple minimization solution to the parameter differences was offered by means of new characterization with three-dimensional relationships. However the new characterization was quite simple and limited. Consequently, in Chapter 5 and Chapter 6, more comprehensive characterization will be studied at an advanced level. Particularly, in this chapter the thermal transient processes will be captured appropriately. Then, based on thermal transient properties, the junction temperature of LEDs will be determined, identification of the processes will be carried out and the thermal map of LEDs with an array of partial thermal resistances and partial thermal capacitances will be decoded, specifically.

5.1. General Consideration

In order to carry out thermal transient capture, junction temperature determination, thermal transient identification and thermal map decoding of LEDs, general consideration in this section is very important to have knowledge about LEDs in the context of control system identification. Hence, the identified object in a correlation with entire system will be determined obviously. Successively, color mixing principle and conservation law of energy in PC-LEDs are necessary to be understood fully so that essential practical compositions and their energy relationships in PC-LEDs will be separated and converted appropriately into a single mathematical task for system identification of a thermal system structure. As well, a very specific description of an LED structure with thermal relationships will be collected directly from manufacturer OSRAM in order to have correct and practical information about the thermal objects, which will be identified in successive sections.

a. Multi-Input Multi-Output system model of a solid state lighting structure

Figure 5.1 describes a multi-input multi-output system (called MIMO system) model of a solid state lighting structure. In that, there are four main parts including “power” part, “sensor” part, “set and feedback signal” part and “control signal” part. Their inputs and outputs always twist together.

* **“Power” part:** “Power” part describes a phosphor converted LED manufacturing process. Different phosphor components (Element A_1) are mixed together with appropriate phosphor mass m_{ph} in mg, phosphor rate R/G , phosphor concentration c_{ph} in % and a matching silicon type. A finished semiconductor blue chip (Element A_2) with specific wavelength peak λ_p in nm is selected. Then, they are established together in a specific geometrical structure (Element A_3). Successively, the finished phosphor converted LED must be processed by optical imaging elements such as optical lenses and others (Element A_4). Finally, the completed product (Element A_5) with layout components and other added electrical components radiates an output spectrum (Element A_6).

* **“Sensor” part and “set and feedback” part:** “Sensor” part is human eyes (Element A_7). The task of the human eyes is to evaluate the quality of an output spectrum and give the feedback signals. Particularly, the feedback signals can be classified into four categories including energy quality, durability (or long term stability), color quality and short term stability of quality parameters. Firstly, energy quality category can be assigned to luminous flux Φ_v in lm, luminous efficacy η_v in lm/W, radiant flux Φ_e in W and radiant efficiency η_e in W/W or %. Secondly, durability can be appointed to lifetime L_{70} of LEDs in hour defined by standard LM80 or some other standards. This category can be extended for more parameters in long term stability. However, this category is not studied in this thesis. Thirdly, color quality aspects can include correlated color temperature CCT in K, color rendering indexes (R_a , R_9 and AVR_{1-14}) and whiteness $\Delta u'v'_{CT}$. Fourthly, the last category is the short term stability of quality parameters over operating temperature and forward current. In addition, set signals are the target values of feedback or output signals.

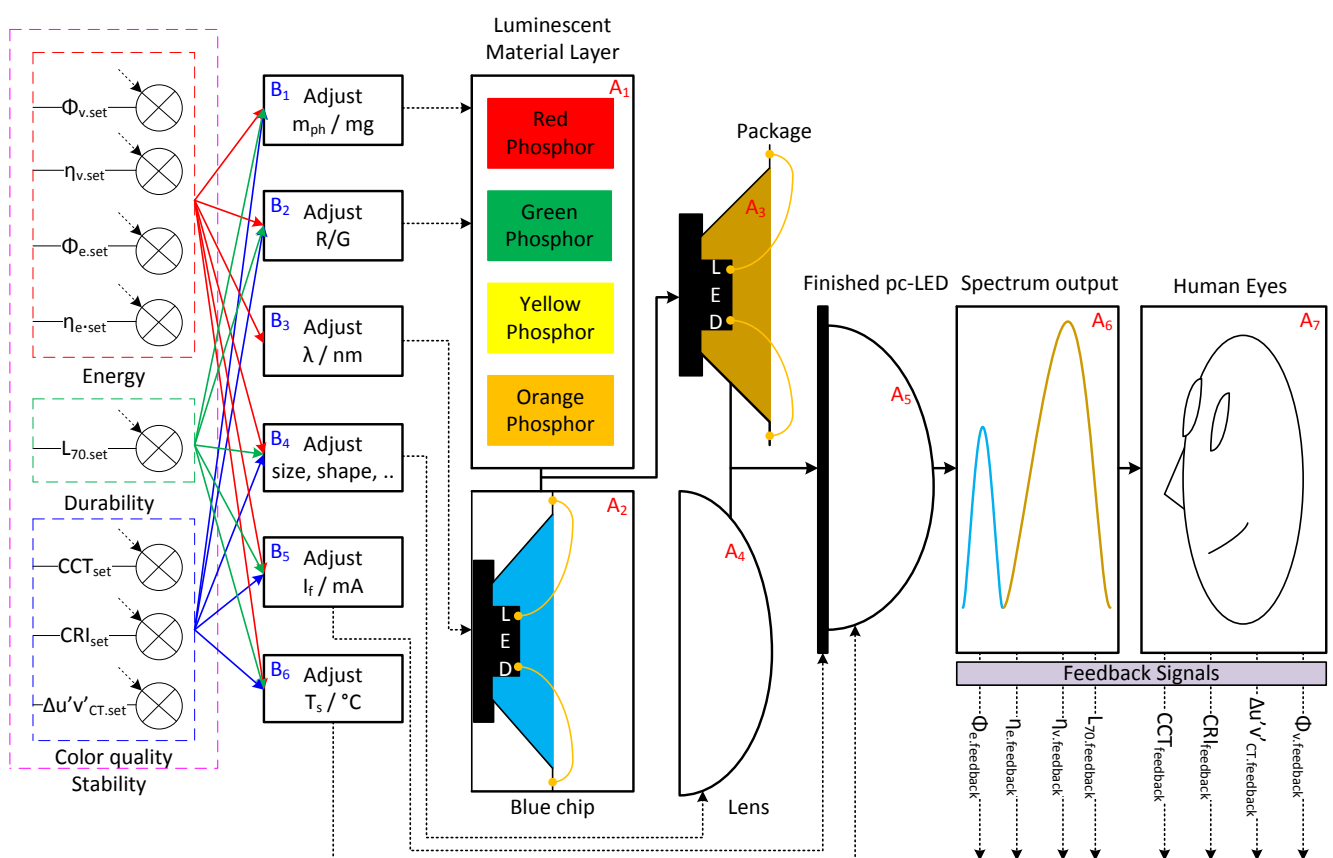


Figure 5.1 - Multi-input multi-output system model of a solid state lighting structure

* **“Control signal” part:** “Control signal” part includes four main categories relating to phosphor, blue chip, optical conduction factor and operating condition. Firstly, phosphor category includes phosphor mass, phosphor rate, phosphor concentration, phosphor composition and used silicon type. However, in Figure 5.1 only phosphor mass (Element B_1) and phosphor rate (Element B_2) were described. Secondly, blue chip factor (Element B_3) has taken account into “control signal” part in Figure 5.1 by means of peak wavelength parameter λ_p and full width at half maximum λ_{FWHM} in nm (called in a general name λ in nm). Thirdly, optical conduction factor (Element B_4) includes size, shape and material of optical lens, capsule and others having influences to the output spectrum. These three categories depend on luminescent material, blue semiconductor chip and packaging technology of LED manufacturers. Therefore, they are not assumed as inputs in this thesis, but considered as systematic constants given by manufacturers. Hence, the last category about the operating condition of LEDs

including forward current (Element B₅) and operating temperature (Element B₆) plays a role of inputs in the MIMO system. While forward current factor was identified obviously, operating temperature factor is still a complicated problem. Indeed, the used temperature in the MIMO system may be the temperature of a LED printed circuit board (PCB), a capsule temperature or a junction temperature. As well, the relationship between these temperatures, their influences to a MIMO system and the characterization of them are really important to be determined specifically. In fact, these problems will be only solvable, when a thermal system block diagram with the color mixing principle and the conservation law of energy in PC-LEDs is analyzed and established in Section 5.1.b and the element A₅ in Figure 5.1 is investigated in more detail in Section 5.1.c.

b. Color mixing principle and conservation law of energy in PC-LEDs

* **Color mixing principle in PC-LEDs:** After the manufacturing process described by compositions from Element A₁ to Element A₅ in Figure 5.1, the finished PC-LED is supplied with a forward current, and its blue chip “pumps” an original blue spectrum indicated by the blue curve 1 in Figure 5.2.b playing the role of a primary light source. Successively, depending on many different factors such as phosphor mass, phosphor rate, phosphor concentration, phosphor chemical composition, blue chip type, and their shape, their size, their operating condition (forward current and operating temperature) as well as chemical and physical interactions between them, one amount of the original blue spectrum is converted into a color phosphor spectral component (such as red, green, yellow or orange spectrum) indicated by red curves 1 - 5 in Figure 5.2.b playing the role of a secondary light source. The blue broken curves (1→5) and the red broken curves (1→5) in Figure 5.2.b are to illustrate for intensity decrease of the blue spectral component and corresponding intensity increase of the color phosphor spectral component according to the increase of phosphor mixture (silicon and phosphor) amount, respectively. This was known as the concept of the specific conversion law of each luminescent material. Both the decrease and increase are nonlinear, because of many reasons such as spectral changes (including both their shape and their amplitude) due to physical and chemical reactions between luminescent materials of phosphor mixture or due to the interactions between phosphor mixture and blue chip. Finally, the spectral rest of the primary light source is mixed with just occurring secondary light source spectrum to create a desired white point.

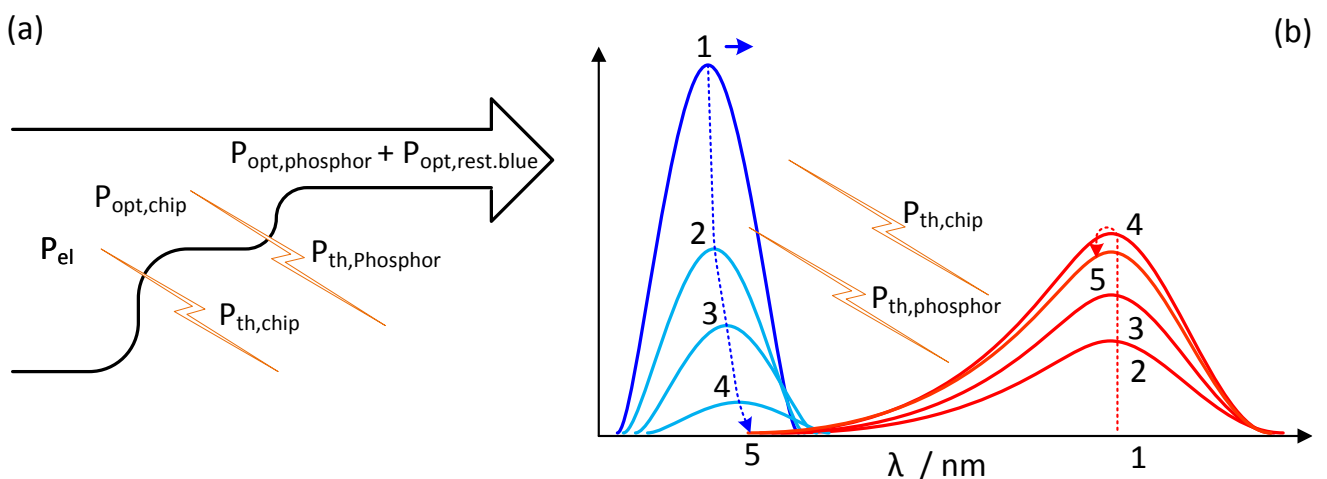


Figure 5.2 - Color mixing principle and conservation law of energy in PC-LEDs

***The conservation law of energy in PC-LEDs:** According to conservation law of energy described by the energy diagram shown in Figure 5.2.a, original electrical power P_{el} in W is converted firstly by an internal semiconductor structure into optical power $P_{opt,chip}$ in W of a blue chip represented by the

original blue spectrum and the first chip thermal power $P_{th,chip}$ in W. And then, $P_{opt,chip}$ is converted secondly by a luminescent material structure into optical power $P_{opt,phosphor}$ in W of the luminescent material corresponding to the color phosphor spectral component and the second phosphor thermal power $P_{th,phosphor}$ in W. Finally, output optical power $P_{opt,out}$ in W is the sum of optical power $P_{opt,rest.blue}$ in W of the rest blue spectral component and optical power $P_{opt,phosphor}$ in W of the luminescent material. Particularly, these relationships can be described mathematically by four following equations.

$$P_{el} = P_{opt,chip} + P_{th,chip} \quad (5.1)$$

$$P_{opt,chip} = P_{th,phosphor} + P_{opt,phosphor} + P_{opt,rest.blue} \quad (5.2)$$

$$P_{opt,out} = P_{opt,rest.blue} + P_{opt,phosphor} \quad (5.3)$$

$$P_{el} = (P_{th,chip} + P_{th,phosphor}) + (P_{opt,rest.blue} + P_{opt,phosphor}) \quad (5.4)$$

In that, three power components $P_{th,phosphor}$, $P_{opt,blue.rest}$ and $P_{opt,phosphor}$ depend on phosphor mixture mass m_{ph} in mg, phosphor rate R/G (when there are many phosphors in the mixture), chemical composition α_{ch} , phosphor concentration c_{ph} in %, particle shape and size ss in μm , forward current I_f in mA and temperature T in $^{\circ}C$ as functions $P_{th,phosphor}(m_{ph}, \alpha_{ch}, c_{ph}, ss, I_f, T, R/G)$, $P_{opt,blue.rest}(m_{ph}, \alpha_{ch}, c_{ph}, ss, I_f, T, R/G)$ and $P_{opt,phosphor}(m_{ph}, \alpha_{ch}, c_{ph}, ss, I_f, T, R/G)$. Moreover, different chemical compositions such varied lattice, activator and their concentration in a luminescent material have different abilities of radiative transition and non-radiative transition leading to different thermal losses, optical radiations, shapes and positions of color spectral components. In addition, different concentrations, shapes and sizes of phosphor cause different thermal losses like mathematical descriptions of the Mie scattering law and the Beer-Lambert law. In fact, the forward current is only possible to decide the original blue spectral component. On the other hand, temperature T in $^{\circ}C$ in the above relationships is a complicated concept. Indeed, the junction temperature T_j in $^{\circ}C$ influences the optical conversion of internal semiconductor layers of blue chips. Then, this temperature is transferred out in varied directions by many heat transport mechanisms such as heat conduction, radiation and convection influencing directly to phosphor temperature T_{ph} in $^{\circ}C$. Individually, this phosphor temperature is caused by the thermal energy of phosphor and silicon. Hence, the temperature T_{ph} depends on the junction temperature T_j , ambient temperature T_a and phosphor thermal power $P_{th,phosphor}$. Obviously, there are very complicated interactions between the above factors. In order to analyze, identify and decode a thermal map of LEDs, the author of this thesis assumed that the total effective thermal power $P_{th,in}$ in W influences on the junction temperature T_j as follows,

$$P_{th,in} = \alpha P_{th,chip} + \beta P_{th,phosphor} \quad (5.5)$$

Where, α and β is the effective percentage of blue chip thermal power and phosphor thermal power on junction temperature T_j , respectively. Thus, a thermal component or a thermal object of an entire LED structure can be separated into a thermal transient LED model like a single-input single-output system (called SISO system) illustrated by a structure block diagram in Figure 5.3. In that, an input is the effective thermal power $P_{th,in}$ and an output is the temperature difference between the junction temperature T_j and ambient temperature T_a .

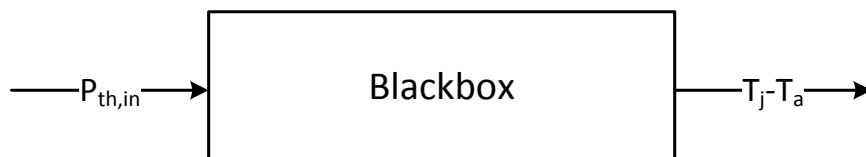


Figure 5.3 - Thermal transient LED model as a single-input single-output system (SISO system)

c. LED structure in thermal relationships

In order to identify and establish a thermal transient LED model of high power LEDs, the finished element A_5 in Figure 5.1 has to be investigated in more detail. Fortunately, some well-known LED manufacturers in [38], [39] and [40] introduced about the LED structure in thermal relationships very specifically. Based on practical and experimental knowledge of the element A_5 in these literatures, the main contents of these publications are collected and generalized again in this section.

* **The thermal structure of a typical LED:** LEDs of many LED manufacturers with varied materials have different thermal properties. However, data of GOLDEN DRAGON LEDs of OSRAM in [38], [39] and [40] can be used as a demonstration example for a thermal structure of a typical LED like described in Figure 5.4. Based on the description in Figure 5.4, it can be recognized, that a typical LED is composed of dielectric, heat sink, solder, solder pads, molding compound, die, bond wire, die attach, aluminum plate and leads. Particularly, the authors in [38], [39] and [40] explained that thermal power $P_{th,chip}$ in W from a junction layer of a chip is firstly transported via a package and a substrate by heat conduction mechanism and then is transported successively from the free surfaces to the outside environment by radiation and convection mechanisms. Compositely, GOLDEN DRAGON LEDs consists of a chip mounted on a chip carrier (called “heat spreader”) by a soldering or a bonding adhesive. As well, the heat spreader is made of a high conductive material such as copper. In this LED structure, a phosphor layer did not appear here, because it is only a color semiconductor LED.

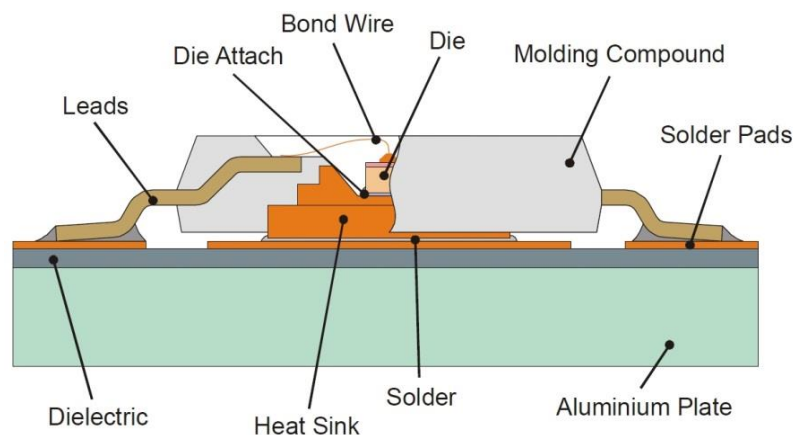


Figure 5.4 - Thermal structure of an OSRAM GOLDEN DRAGON LED ([40])

* **Typical equivalent thermal circuit:** Based on the above structure of GOLDEN DRAGON LEDs, the authors established an associated static equivalent thermal circuit diagram described in Figure 5.5. As well, power dissipation $P_D = P_{th,chip}$ in W occurring close to the chip surface is denoted by a current source. Essentially, the resistance network of the LED is a serial connection to ambient temperature T_a in °C. Approximately, a parallel-connected thermal resistance of the plastic housing can be neglected. In more detail, the thermal circuit can be analyzed as follows: Firstly, there is thermal power dissipation P_D playing the role of a current source and indicated by junction temperature T_j or temperature offset $\Delta T = T_j - T_a$ between junction temperature T_j and ambient temperature T_a . Secondly, thermal resistances of die, die attach, heat sink and the solder point with very small values play the role as internal thermal resistances $R_{th,JS}$ in K/W. Thirdly, thermal resistances of solder pad and board with bigger values play the role as application partial thermal resistance $R_{th,SA}$. Practically, $R_{th,SA}$ should be even specified into two more detailed thermal resistances as $R_{th,SB}$ from the solder point to board and $R_{th,BA}$ from board to ambient. In fact, $R_{th,SB}$ is usually strongly influenced by various factors such as solder pad design, component placement, a printed board material and board construction. Finally, the above thermal resistances should be collected into three thermal resistance types including internal

thermal resistance $R_{th,JS}$ from junction to solder point, middle thermal resistance $R_{th,SB}$ from the solder point to board and external thermal resistance $R_{th,BA}$ from board to ambient. Or they can be assumed as only one external thermal resistance that is the sum of $R_{th,SB}$ and $R_{th,BA}$.

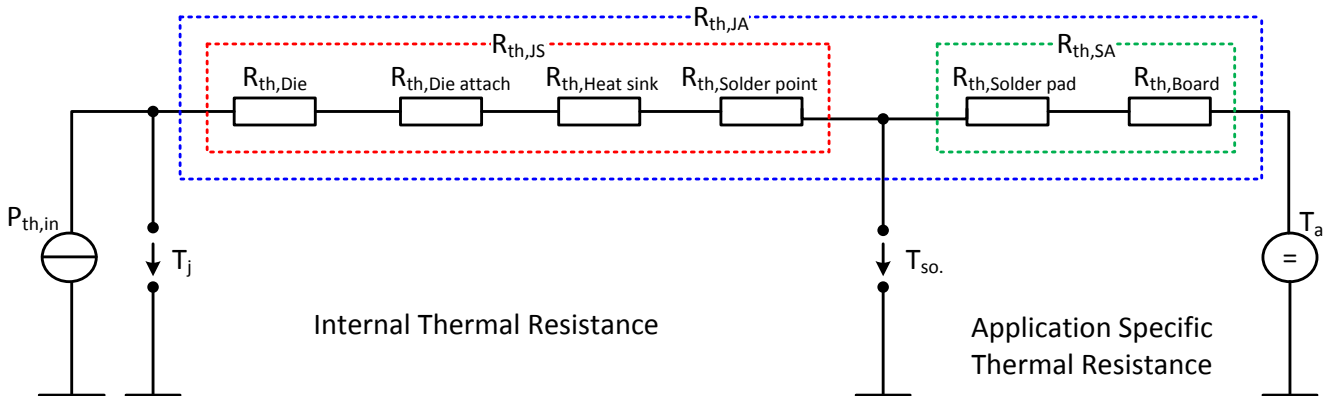


Figure 5.5 - Equivalent thermal circuit of a GOLDEN DRAGON LED ([40])

* **External thermal resistance:** Based on the above analyses, two thermal resistance components ($R_{th,SB}$ and $R_{th,BA}$) should be described deeply.

Firstly, thermal resistance $R_{th,SB}$ has always depended on the substrate technology strongly. In order to ensure the best efficiency and a good thermal management, $R_{th,SB}$ has to be optimized. Particularly, the used printed circuit board (PCB) technology has to be considered appropriately. Indeed, besides standard substrates such as FR4 PCB material, new thermal enhanced substrate technologies have been found. Some of these technologies such as MCPCB (the metal core printed circuit board), flexible PCB laminated on aluminum and enhanced FR4 PCB glued to aluminum were established in GOLDEN DRAGON LEDs as the following table,

Table 5.1 - Parameters of some PCB substrates in a GOLDEN DRAGON LED ([40])

Composition	Outer OCB Dimensions (L x W)	Board Material	Material for Solder Pads	Power distribution	Reference Temperature
GOLDEN DRAGON LED	25 x 25 mm ²	- FR4 on Aluminum MCPCB - FPC on Aluminum	35 μm Cu	1 W	25 °C

In more detail, a structure of a single MCPCB was shown in Figure 5.6.a. In that, the typical thickness of copper layer was about 35 μm - 200 μm, the one of dielectric layer was about 75 μm - 100 μm and the one of the metal layer was about 1 mm - 3 mm.

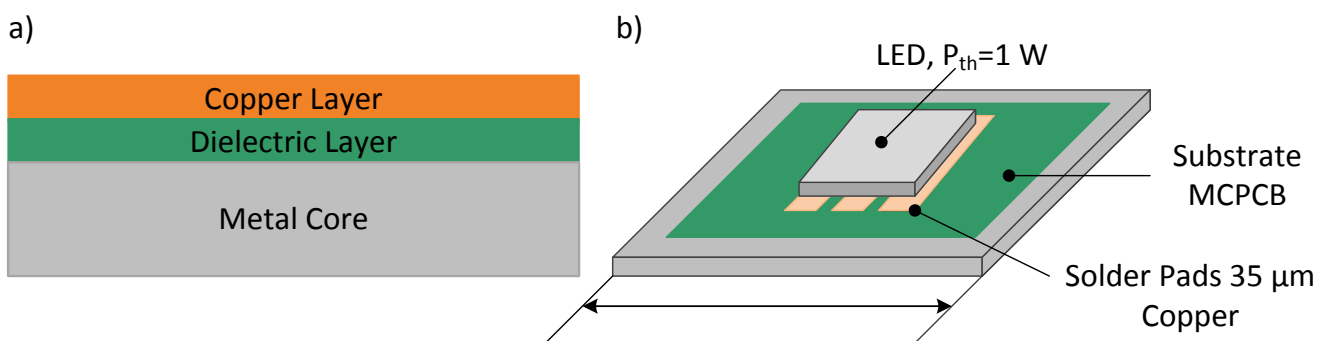


Figure 5.6 - Structure of single layer MCPCB and structure of a heat sink component of LEDs ([40])

For thickness of 100 μm for dielectric layer, the one of 1.5 mm for metal core of an aluminum alloy and the one of 35 μm for copper layer, the lowest thermal resistance can be reached with an enhanced thermal dielectric layer. In the simulation of the authors in [129], the thermal conductivity of substrate was about 1.3 W/mK. Moreover, analyses of other structures, which are only valid for mentioning PCB constructions and boundary conditions, published as in the following table,

Table 5.2 - $R_{\text{th,SB}}$ of substrate technologies with the standard geometry and size of a GOLDEN DRAGON LED ([40])

Substrate Technology	MPCB with enhanced dielectric	MPCB with FR4 dielectric	FPC on aluminum with standard PSA	FPC on aluminum with thermal enhanced PSA	FR4 - PCB on aluminum with thermal vias
$R_{\text{th,SB}}$	3.4 K/W	7.3 K/W	9.5 K/W	7.6 K/W	9.7 K/W

Secondly, thermal resistance $R_{\text{th,BA}}$ from board to ambient depends strongly on heat sink considerations. The heat transfer from a solid body in a fluid can be enhanced by extending the surface of the solid body. In fact, for a given heat dissipation, the temperature difference is controlled by a heat transfer coefficient h_{tr} and a heat surface area A . However, unfortunately, increasing for the heat transfer coefficient h_{tr} is always not easy. Therefore, the heat transfer surface area A is more feasible to achieve a desired thermal improvement. Particularly, in order to increase the surface area A , a conventional method is the use of heat sinks. In Figure 5.6.b, a structure of heat sink for GOLDEN DRAGON LEDs was described. In that, the surface area A of the underlying heat sink layer can be extended by increasing distance variable L . Practical results in Figure 5.7 showed that the wider substrate area A is, the lower thermal resistance $R_{\text{th,BA}}$ is.

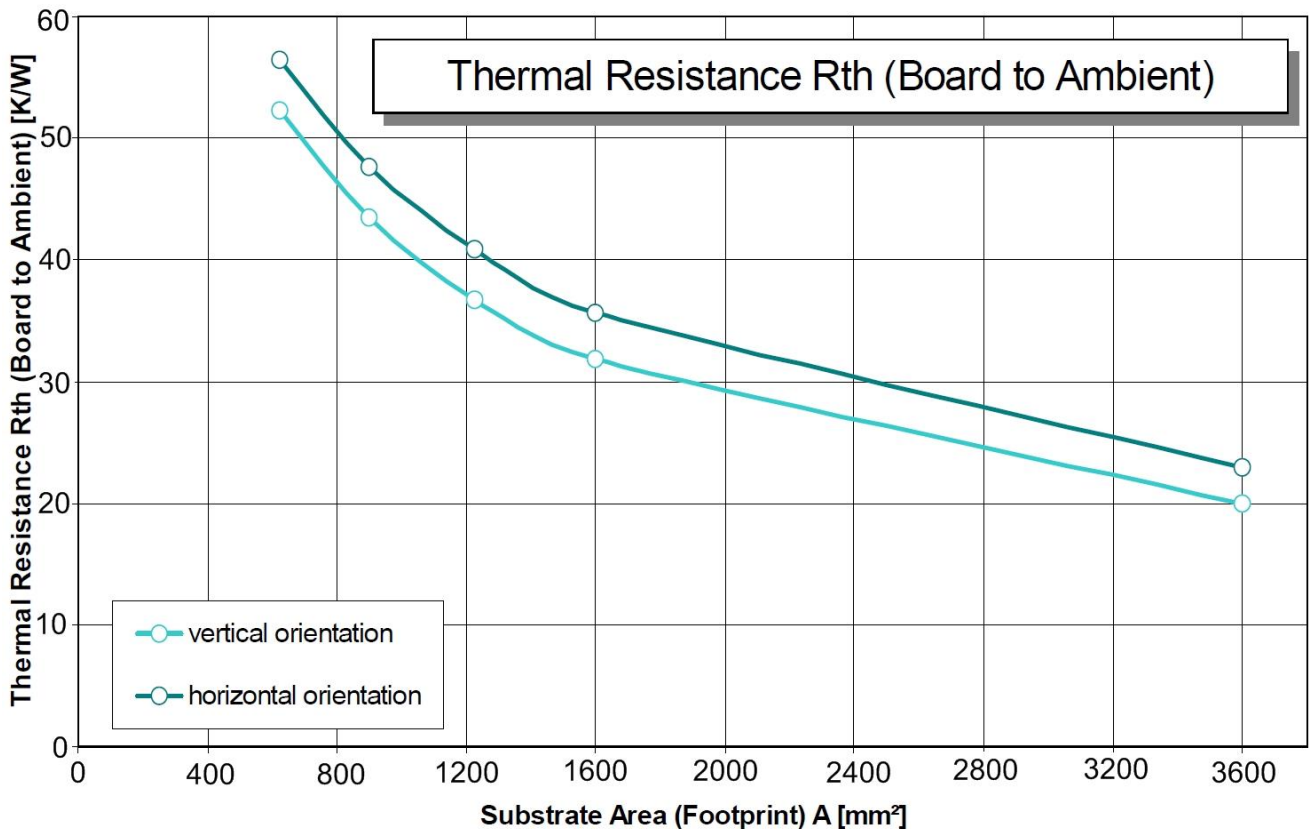


Figure 5.7 - Substrate area dependence of $R_{\text{th,BA}}$ ([40])

5.2. Determination of LED junction temperature

In the section 5.1, the color mixing principle and conservation law of energy in PC-LEDs, the knowledge of a multi input - multi output system model of a solid state lighting structure, the practical LED structure with thermal relationships were described specifically. As well, a thermal object and its system structure were analyzed in details. Moreover, the system structure diagram of a thermal transient LED model in Figure 5.3, the theoretical description of an absolute spectral power distribution in Section 2.1.5 and the horizontal LED models in Section 6.4.3 and Section 6.4.4 need the junction temperature. Therefore, in this section the methods of the LED junction temperature determination will be reviewed briefly and selected into two available solutions. Successively, with these solutions the thermal transient capture and the necessary procedures for the LED junction temperature determination will be carried out and compared together in order to select a more available solution with a better accuracy. Finally, the causes of inaccuracy and improvement offers in the LED junction temperature determination will be also explained and proposed.

5.2.1. Measurement methods and procedures of the LED junction temperature determination

* **Selection of an available measurement method:** There were some LED junction temperature measurement and determination methods. As the simplest method, a thermal camera can be used to measure junction temperature. However its measurement result is only qualitative and not accurate. Consequently, other options for the LED junction temperature determination can be based on indirect optical test methods (OTMs) such as light power method (POP) with relationship $P_{opt}=f(T_j)$ between optical power P_{opt} in W and junction temperature T_j in °C, wavelength shift method (WSM) with relationship $\lambda_p=g(T_j)$ between peak wavelength λ_p in nm and junction temperature T_j or relationship $\lambda_{FWHM}=h(T_j)$ between full width at half maximum wavelength λ_{FWHM} in nm and junction temperature T_j . The LED junction temperature can also be determined based on electrical test methods (ETMs) such as the single current method (SCM) and the dual current method (DCM) discussed by SIEGAL in [41]. Especially, GU and NARENDRAN in [42] offered a non-contact method for the junction temperature determination of white PC-LEDs based ratio W/B of spectral white component W in W and blue spectral component B in W of white PC-LEDs. As well, these authors criticized the accuracy of method WSM. Likewise, SCHUBERT and co-authors in [1] and [43] also explained and compared some items of methods WSM and ETMs.

Based on the above brief review, it can be recognized, that the measurement and determination of LED junction temperature were approached very variously. However, generally in all above methods, the method based on a forward voltage (belonging to ETMs) is very well known and preferred in practical applications because of its accuracy, simplicity and feasibility. Particularly, linear relationship $V_f=aT_j+b$ between forward voltage V_f in V and junction temperature T_j was proved in [1], [44], [45] and [46]. Thus, based on measured voltage V_f , the junction temperature T_j can be determined easily by means of relationship $T_j=(V_f-b)/a$. Nevertheless, problems occurred in the determination of the constants a and b . Therefore, in order to achieve these constants, two measurement procedures for thermal transient captures were discovered including “*heating procedure*” and “*cooling procedure*”. In more detail, the heating procedure was described specifically in [1], [44], [47] and [48], and the idea of the cooling procedure appeared generally in [41] and [49]. Names “*heating procedure*” and “*cooling procedure*” are called again in this thesis according to the intrinsic phenomena of thermal transient processes. Other names were also used in other documents. Successively, in order to understand and evaluate the accuracy of the heating and cooling procedures, descriptions and practical investigations with the same measuring hardware structure will be carried out in the next section.

* **Description for the heating and cooling measurement procedures:** The heating procedure is to determine indirectly junction temperature T_j in $^{\circ}\text{C}$ based on forward voltage V_f in V. Particularly, the heating procedure is described in Figure 5.8 including a transient measurement and a DC measurement. In the transient measurement, current pulses with a suitable duty cycle are supplied for a LED at case temperatures $T_{s,i}$ in $^{\circ}\text{C}$. At a small enough time point, forward voltages $V_{f\text{-heating},i}$ in V can be captured. Then, temperature offsets $\Delta T_i = T_{j,i} - T_{s,i}$ in K are approximately equal zero and junction temperatures are equal approximately case temperatures, because heating processes have just taken place. Thus, relationship $V_f = a_n T_j + b_n$ can be approximated by $V_f = a_n T_s + b_n$ for a specific forward current $I_f = n$ mA. Successively, based on this relationship, forward voltage V_f in V and thermal power P_{th} in W measured by the DC measurement at T_s $^{\circ}\text{C}$, junction temperature T_j and thermal resistance R_{th} in K/W can be determined by the relationships $T_j = (V_f - b_n) / a_n$ and $R_{th} = (T_j - T_s) / P_{th}$, respectively.

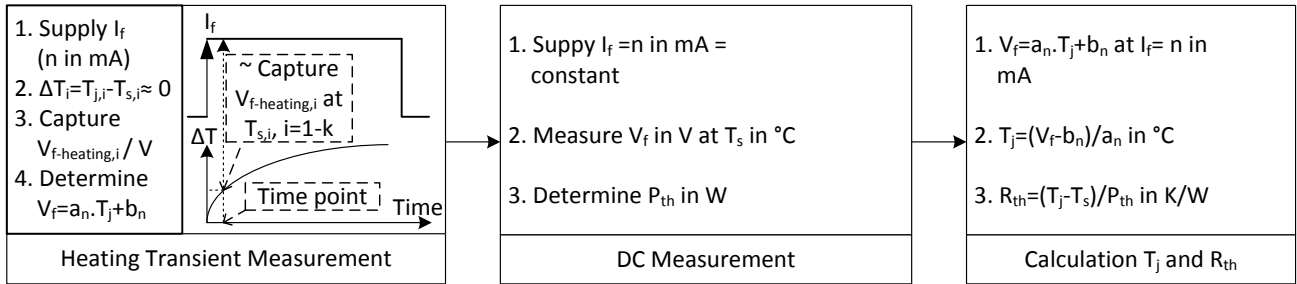


Figure 5.8 - Heating measurement procedure

On the other hand, the cooling procedure is to determine indirectly junction temperature T_j in $^{\circ}\text{C}$ based on voltage difference $\Delta V_f = (V_{f\text{-cooling-beginning}} - V_{f\text{-cooling-end}})$ in V captured in cooling processes. Particularly, the cooling procedure is described in Figure 5.9 including a transient measurement and a DC measurement. In the transient measurement, firstly a specific forward current $I_f = m$ mA is supplied for a LED in a long enough time in order to reach a full thermal charge. Successively, a step down current pulse is created by shutting from current m mA down to a low current (eg. 1 mA). At this low current, there is nearly no more supplied thermal power and a cooling process takes place gradually. Then, previous charged thermal energy P_{th} in W is transported from the LED junction layer into the external environment. This cooling process is denoted by means of the change of the forward voltage $V_{f\text{-cooling}}$ or the forward voltage difference ΔV_f in V. Otherwise, thermal power P_{th} in W, case temperature T_s in $^{\circ}\text{C}$ and constant a_0 of voltage relationship $V_f = a_0 T_j + b_0$ at the low current can be determined easily in the DC measurement. Therefore, temperature difference $\Delta T = T_j - T_s$ in K can be calculated from the relationship $\Delta T = \Delta V_f / a_0$. This difference is an important characteristic parameter of the LED thermal property. Finally, junction temperature T_j in $^{\circ}\text{C}$ and thermal resistance $R_{th,\Sigma}$ in K/W can be determined by means of the relationships $T_j = T_s + \Delta T$ and $R_{th,\Sigma} = \Delta T / P_{th}$, respectively. In addition, a theory of identification system can be applied to identify entirely this thermal transient process. Based on the identified functions, partial thermal parameters such system time $T_{sys,i}$ in s, thermal resistance $R_{th,i}$ in K/W and thermal capacitance $C_{th,i}$ in Ws/K can be decoded (the index $i = 1-k$, k depends on each LED). Or simply the total system time τ_{sys} in s can be also determined to help for the calculation of total equivalent thermal capacitance $C_{th,\Sigma}$ in Ws/K based on the relationship $C_{th,\Sigma} = \tau_{sys} / R_{th,\Sigma}$.

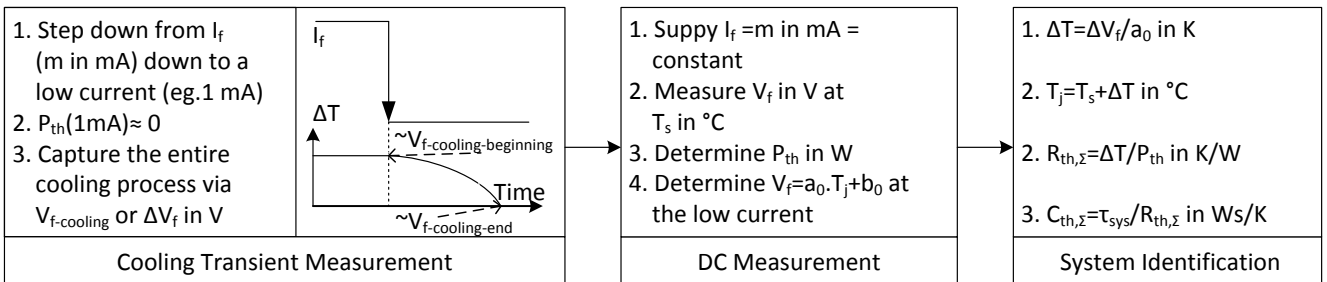


Figure 5.9 - Cooling measurement procedure

5.2.2. Comparison between the cooling and heating measurement procedures

Section 5.2.1 discussed about different methods of measurement and determination of LED junction temperature. Based on varied published literatures, the method based on the forward voltage (belonging to ETMs) was assumed as the most available method in practical applications. Successively, the cooling and heating procedures were described. In this section, the measurement system in TECHNISCHE UNIVERSITÄT DARMSTADT will be described. Then, this system will be applied for both measurement procedures. Finally, measured results will be compared together directly and indirectly in order to determine a better measurement procedure for next research steps.

a. Description of the measurement system

A measurement system is established in TECHNISCHE UNERSITÄT DARMSTADT and illustrated in the figure 5.10. In that, a 300 mm optical integrating sphere with an auxiliary lamp, a baffle and an optical detector is used to measure absolute spectral power distributions (SPDs) of the LEDs. Moreover, LEDs are soldered to a printed circuit board (PCB) with a star form. As well, under this star a temperature sensor is established to touch directly to it. Then, the entire metal star and the temperature sensor are positioned on a copperhead that is attached on the cold side of a PELTIER module. And the hot side of the PELTIER module is connected to a PELTIER cooler system including a heat sink and an electrical fan so that it can transfer quickly the thermal energy P_{th} in W into the surrounding environment. Otherwise, a THORLAB controller connected to a host computer is used to control the PELTIER module in order to keep the temperature at under the metal star constant at any desired level. In addition, spectral radiometer CAS120 of INSTRUMENT SYSTEM is used to measure and convert electrical signals from the optical detector (oriented optically by a baffle) and then sends them to the host computer. Furthermore, Model 2651A high power / high current system source / meter instrument is to supply desired current pulses and measure voltage of the LEDs. As well, the measured results are also sent to the computer. Finally, in the host computer, the special software owned by TECHNISHCE UNIVERSITÄT DARMSTADT is used to control THORLAB-controller, KEILTHLEY 2651A instrument and spectral radiometer CAS120 synchronously in order to measure LEDs at any desired current and temperature on demands of measurement procedures.

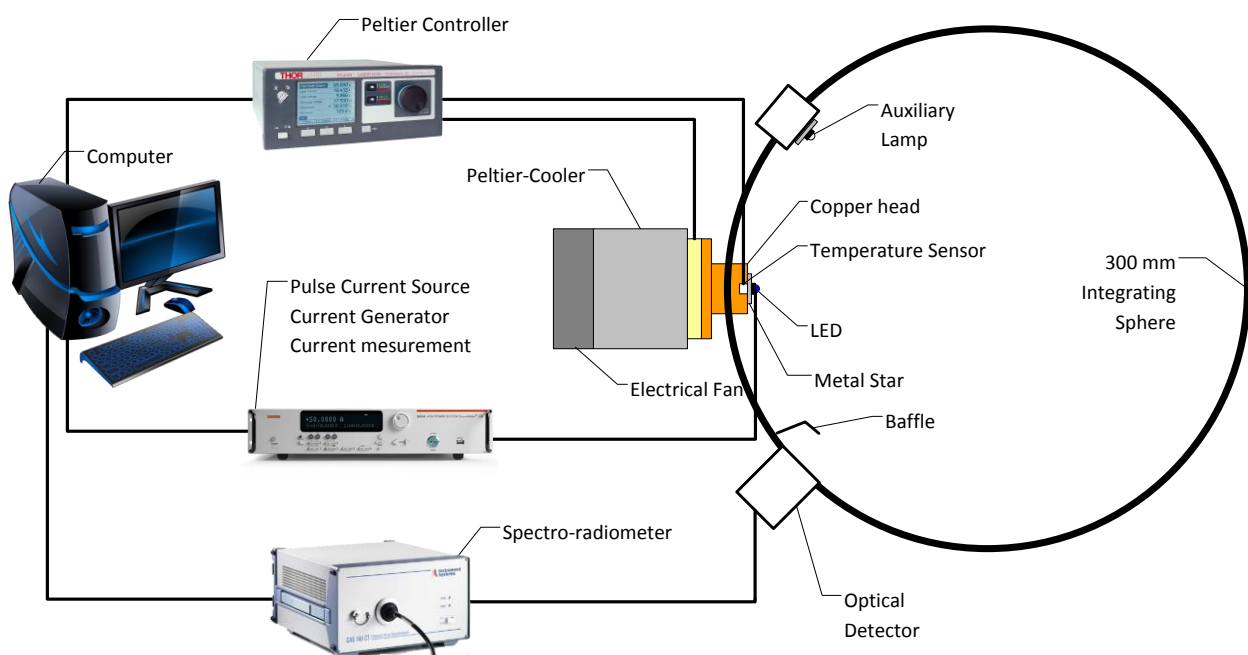


Figure 5.10 - Measurement system in TECHNISCHE UNIVERSITÄT DARMSTADT

b. Direct comparison between heating and cooling measurement procedures

In Section 5.2.1, two measurement procedures (heating and cooling) were discussed specifically. Successively, in Section 5.2.2.a, a measurement system was described. In this section, the heating and cooling measurement procedures will be carried out with the same above measurement system for a typical blue semiconductor LED in order to have the most objective measured results. Then, these measured results will be compared directly together in Figure 5.11.

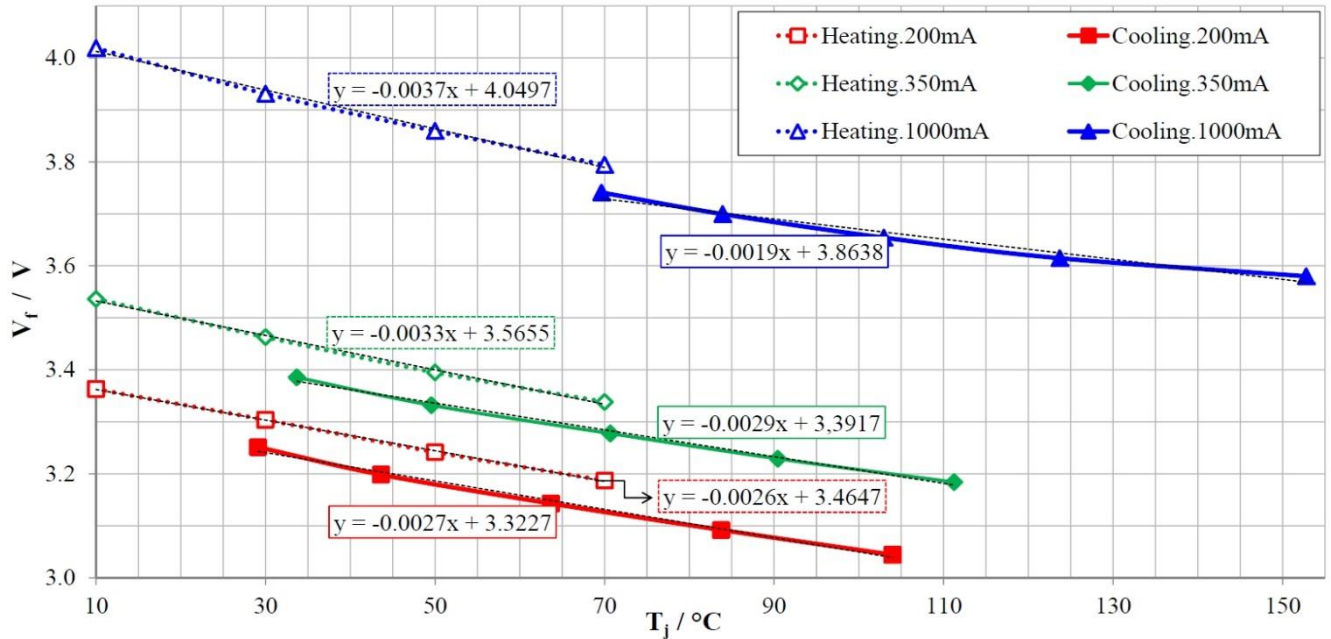


Figure 5.11 - Direct comparison of the $V_f(T_j)$ properties measured by the heating and cooling procedures

Particularly, firstly similar DC measurements for both measurement procedures are carried out to give optical power $P_{opt,i}$ in W, electrical power $P_{el,i}$ in W and DC forward voltage $V_{f-DC,i}$ in V at forward currents $I_{f,i}=200$ mA, 350 mA and 1000 mA and case temperatures $T_{s,i} = 15$ °C, 30 °C, 50 °C, 70 °C and 90 °C. The index i is the indicator for the measurement order corresponding with used forward current i in mA. Secondly, transient measurements of the cooling procedure are applied to determine constant a_0 , forward voltage $V_{f-cooling-beginning}$ in V at the beginning and forward voltage $V_{f-cooling-end}$ in V at the end of the cooling transient process. Then, based on these measured results, junction temperature T_j can be determined indirectly. Thirdly, other transient measurements of the heating procedure are also applied to determine directly the relationships $V_f(T_s) \approx V_f(T_j)$ at three forward currents $I_f=200$ mA, 350 mA and 1000 mA.

Finally, relationships $V_f = aT_j + b$ between the forward voltage and the junction temperature determined by the heating and cooling procedures are drawn in the same diagram in Figure 5.11. Based on the voltage properties described together in Figure 5.11, it can be recognized, that the higher forward current is, the higher the difference of constant a is (0.0001 at 200 mA, 0.0004 at 350 mA and 0.0018 at 1000 mA), and the higher the difference of constant b is (0.142 at 200mA, 0.1738 at 350 mA and 0.1859 at 1000 mA). However, unfortunately although the direct comparison in Figure 5.12 is able to confirm that there was a big difference between two measurement procedures, it is impossible to determine which procedure is more accurate. Therefore, an indirect comparison is necessary to investigate furthermore in Section 5.2.2.c.

c. The indirect comparison between heating and cooling measurement procedures

In order to determine the more accurate measurement procedure, an indirect comparison between the heating and cooling measurement procedure is performed like the procedures described in Figure 5.12.

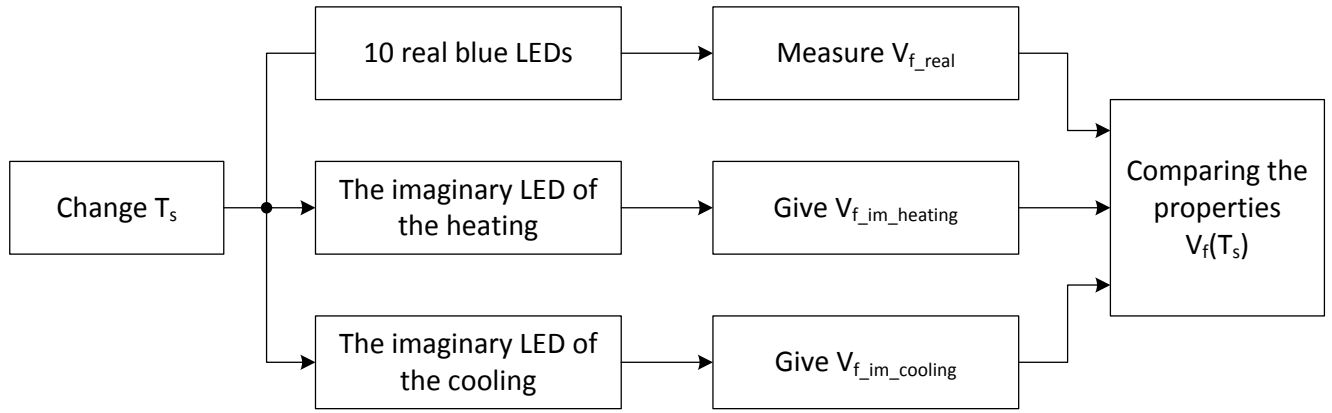


Figure 5.12 - Procedures of an indirect comparison

Particularly, in Section 5.2.2.b forward voltage $V_{f-DC,i}$ and thermal power $P_{th,i}=P_{el,i}-P_{opt,i}$ were measured by the DC measurements and then junction temperatures $T_{j-heat,i}$ and $T_{j-cool,i}$ in °C were determined by the transient measurements of the heating and cooling measurement procedures, respectively. Thus, three-dimensional relationships $P_{th,i}=f_{11}(T_{j-heat,i},I_{f,i})$ and $V_{f,i}=f_{12}(T_{j-heat,i},I_{f,i})$ for the heating and the ones $P_{th,i}=f_{21}(T_{j-cool,i},I_{f,i})$ and $V_{f,i}=f_{22}(T_{j-cool,i},I_{f,i})$ for the cooling are possible to be interpolated by the MATLAB surface fitting toolbox. In addition, two dimension relationship $R_{th,i}=f_{13}(I_{f,i})$ between the thermal resistance $R_{th,i}$ and forward current $I_{f,i}$ for the heating and the one $R_{th,i}=f_{23}(I_{f,i})$ for the cooling can be also interpolated by the MATLAB curve fitting toolbox, because the thermal resistances of blue LEDs changed inconsiderable according to ambient temperatures and changed strongly according to forward currents like the experiences of authors JAYASINGLE, DONG and NARENDRAN in [107]. Hence, simple static thermal models for the heating and cooling can be established like the system structure diagram in Figure 5.13. In the modeling process, in order to ensure a good accuracy, the interpolation is performed with the DC measurement data of 10 blue LEDs belonging to the same binning group and with 25 measurement points at case temperatures $T_s=15\text{ °C}$, 30 °C , 50 °C , 70 °C and 90 °C and at forward currents $I_f=100\text{ mA}$, 200 mA , 350 mA , 700 mA and 1000 mA . Then, maximal, average and minimal values of parameters are calculated for 10 blue LEDs and their average values are used for the interpolation.

Successively, similar conditions of forward current I_f and case temperature T_s are supplied for two thermal models like 25 real investigated points of DC measurements. Finally, the relationships $V_f=f(T_s)$ between forward voltages and case temperatures of two models and the measured results of 10 typical blue LEDs at three forward currents are drawn in the same diagram in Figure 5.14 in order to compare them together. The results show that the cooling procedure achieved a better accuracy than the heating procedure. Particularly, the curves $V_f(T_s)$ of the cooling model are always between the minimal and maximal curves of measured results and attached strongly on the average measured curves, while there was a remarkable offset between the curves $V_f(T_s)$ of the heating model and the average measured curves, especially at high temperatures and high currents such as 1000 mA and 90 °C . The reason for the inaccuracy of the heating procedure can be explained that while the time point of the voltage captures in the transient measurement of the heating procedure is always kept constant, temperature difference $\Delta T=T_j-T_a$ between junction temperature T_j and case temperature T_s increases

higher for high forward currents. In fact, the adjustment to achieve small enough time points corresponding with the forward currents is very difficult and unfeasible in the real performances.

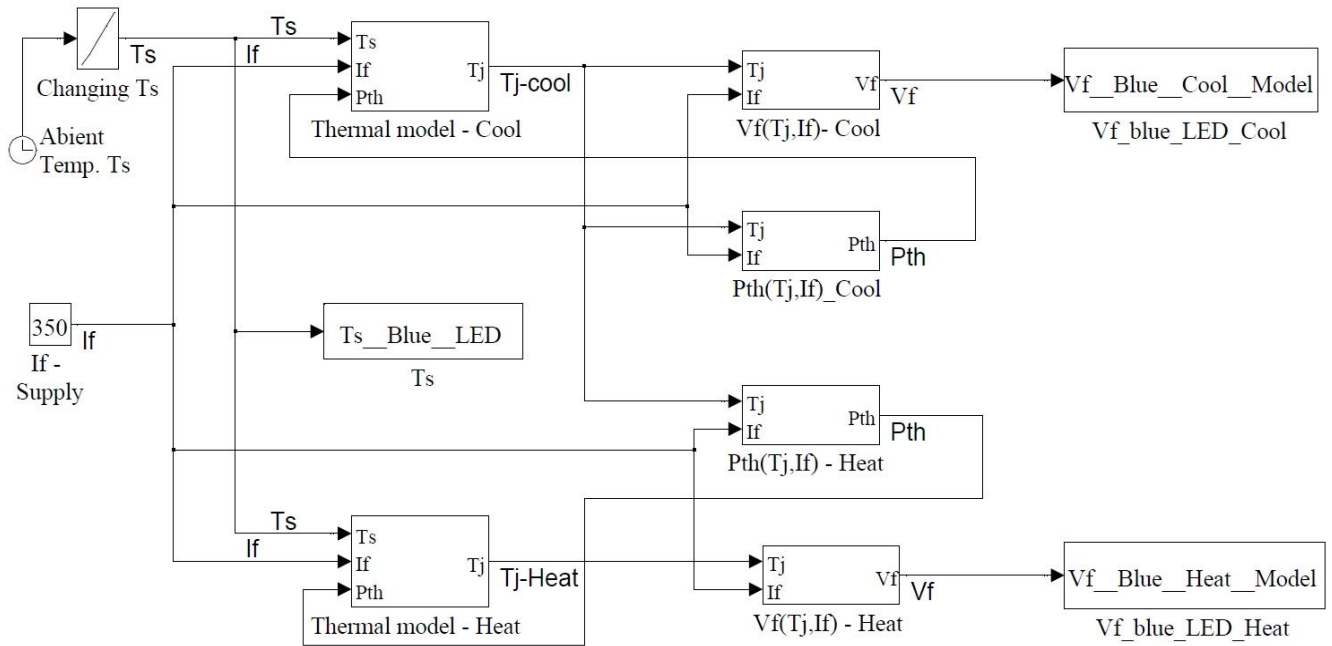


Figure 5.13 - System structure diagram of simple static thermal models of the cooling and heating

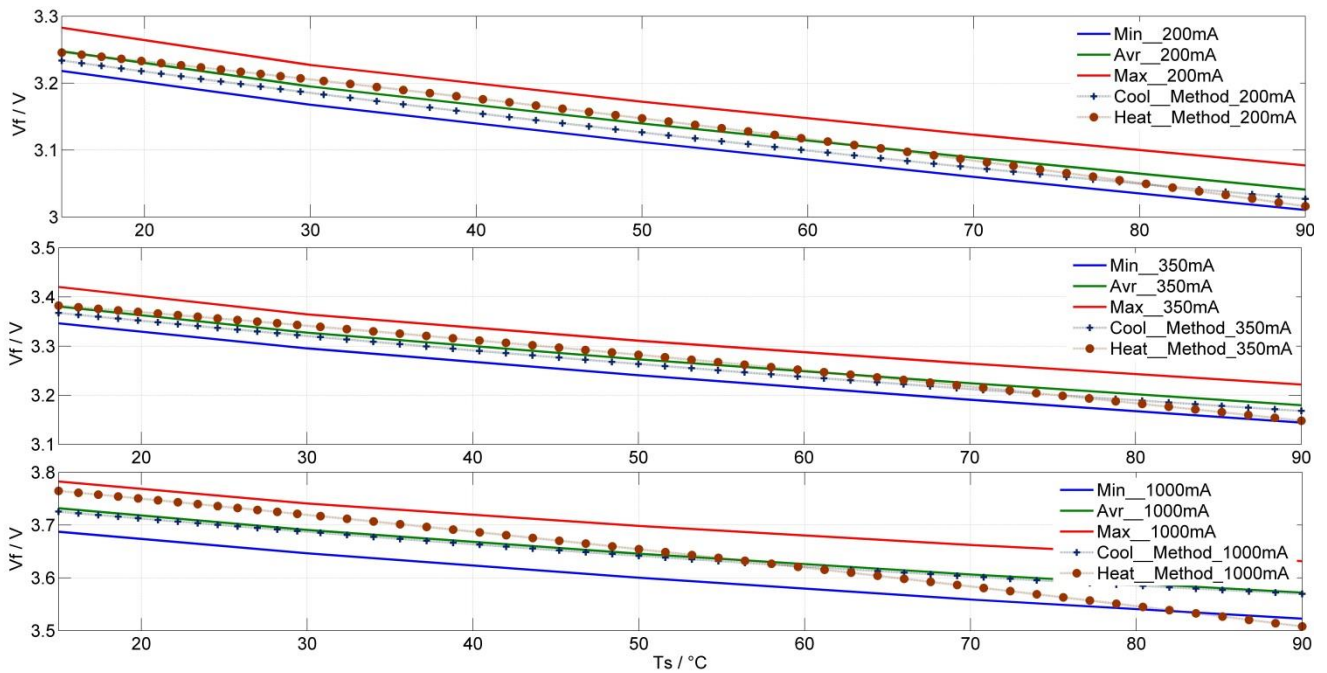


Figure 5.14 - Properties $V_f(T_s)$ of the cooling and heating thermal models and practical DC measurement results

5.2.3. Causes of inaccuracy and improvement proposals

In order to measure accurately, the factors that influence the total accuracy must be considered and improved as well as possible. In this section, these factors will be analyzed and explained.

Firstly, the capture for the transient thermal processes mentioned in section 5.2.1 influences directly and strongly the total accuracy. The comparison between the heating and cooling as well as their

necessary procedures were described in Section 5.2.2 and in more detail with the corresponding data in Appendix H. In that, the cooling procedure was proved that it achieved a higher accuracy than that of the heating method. In [51], the cooling method was also preferred in the real performance. Therefore, the cooling method is the available measurement procedure used in this thesis. Moreover, the lower the forward current at the low level in the cooling is, the higher the accuracy is, because at the very low current, relationship $V_f(T_s)$ between forward voltage V_f and sensor temperature T_s is approximately equal relationship $V_f(T_j)$ between forward voltage V_f and junction temperature T_j . However, if the forward current is too low, the noises of the own measurement instrument can influence strongly the measured results depending on ability of varied specific instruments. In the measurement system of this thesis, KEITHLEY 2651A used with a pA and V resolution is a good reason to set the low current of about 1 mA (in [51], it was 10 mA). In addition, in order to transform from forward voltage difference ΔV in V into temperature difference ΔT in K, an appropriate converted coefficient a_0 in mV/K (or called a sensitivity factor in some documents) is very important. Particularly, this coefficient was set by -1.84 mV/K for the case of a specific LED in [51], but was always determined again for each LED in [50] of the author and also in this thesis, because the coefficient always depends differently on varied LEDs. Therefore, this repeated determination plays an essential role in the accuracy.

Secondly, sampling time of measuring instruments must be considered appropriately. Particularly, the authors in [51] and [52] agreed together that sampling time has a very important meaning on the accuracy. As well, the authors in [51] noted that there were many tiny thermal processes occurring below 1 ms and therefore high sampling time was really essential. However, the problem is recognized, how high sampling time is good enough. Thus, in order to solve this problem, the authors in [52] offered a number 6 μ s and the authors in [51] published a thermal transient measurement with about 10 μ s as the minimal system time constant of the process. Fortunately, the solution in more detail lies in the SHANNON sampling theorem. Indeed, the main idea of SHANNON sampling theorem in [53] proposed that sampling frequency f_{sampling} in Hz of a measurement instrument should be higher than maximal sampling frequency $f_{\text{sys,max}}$ in Hz of measured objects two times in order to assure a good interpolation, identification or reconstruction. It means that if the minimal system time constant $T_{\text{sys,min}}$ in [51] was about 10 μ s (or the maximum frequency system $f_{\text{sys,max}}$ is about 0.1 MHz), the sampling time T_{sampling} of the equipment should be 4 - 5 μ s or shorter (or its sampling frequency f_{sampling} should be about 0.2 MHz - 0.25 MHz or higher). Therefore, the sampling time of 6 μ s in [52] was also nearly good enough. In this thesis, KEITHLEY 2651A with sampling time of 1 μ s can ensure for a good accuracy. In addition, according to the experiences of WESCOTT in [54], if the mathematical form of a process is understood obviously and an available operating region is selected specifically for an application, the requirement of sampling time will be less hard leading to a cheaper instrument cost. For thermal systems in the LEDs, it depends on the order of thermal processes, which is necessary to be identified. This order was 5th order in [51]. For the practical data of OSRAM collected in Section 5.1.c, the order could be only 3rd in order to avoid too small values of internal thermal resistors and thermal capacitors in the LEDs.

Thirdly, the rising time and the falling time of measurement instrument should be well-thought-out. Particularly, if the rising time is a very important parameter for the heating procedure, the falling time is also an essential parameter for the cooling procedure. Indeed, if the falling time of a pulse is too long, a captured cooling process will be not completely due to the nature of materials, but also due to the specific falling process of a measurement instrument. The shorter the specific falling process is, the higher the measurement accuracy is. Therefore, the falling time should be shorter than the minimal

system time about two times or even shorter. Moreover the falling process of the measurement instrument should be removed from the captured cooling data. In the framework of this thesis, KEITHLEY 2561A has only about $100\ \mu\text{s}$ (depending on the used high current) of the falling time. Thus, the beginning process of $100\ \mu\text{s}$ must be removed from the captured cooling process. As a result, the minimal system time must be higher or equal to $2 \cdot 10^{-4}\ \text{s}$. Then, according to SHANNON sampling theory, the semantic sampling time for this system is only about $10^{-4}\ \text{s}$, although the ability of instrument KEITHLEY 2561A is $1\ \mu\text{s}$ at the best sampling time. Even, in despite of having better instrument, it is also very difficult to identify exactly for the regions of tiny thermal resistors and thermal capacitors, if these small values are really valuable to be accounted into LED thermal systems.

5.3. Thermal transient identification and thermal map decoding of LEDs

In Section 5.2, some thermal transient captures and junction temperature determinations of LEDs were described and compared together. As a result, the better capture and determination method are proposed. As well, the causes of inaccuracy and improvement proposals were discussed. In this section, thermal transient identification and thermal map decoding of LEDs will be researched furthermore. Particularly, the mathematical background for thermal circuits will be studied and described. Moreover, the current well-known identification and decoding method via a structure function will be analyzed in order to recognize its advantages and its disadvantages. Finally, the identification of LED thermal transient processes and an available solution for decoding LED thermal maps will be proposed and carried out for some cold white PC-LEDs as a demonstration example.

5.3.1. Mathematical background for thermal circuits

In this section, the mathematical background for thermal circuits will be analyzed in order to establish explicit equations for the mathematical description of thermal transient LED models. Hence, the feasibility of the classical modeling method will be evaluated in more detail.

* **First order thermal circuit:** In Figure 5.15, a first order equivalent thermal circuit is described. In that, the thermal property of a general material layer can be quantified by two parameters including thermal resistance R_{th} in K/W and thermal capacitance C_{th} in Ws/K .

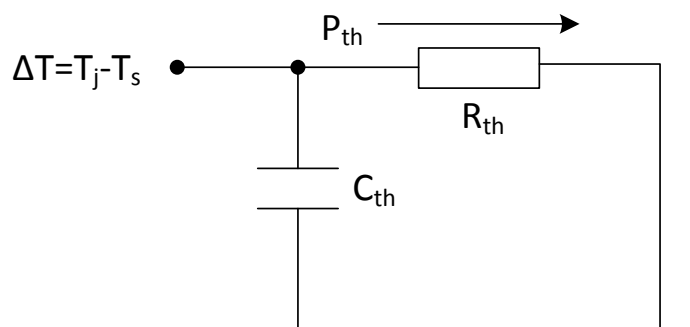


Figure 5.15 - First order equivalent thermal circuit for a general material layer

Thermal resistance R_{th} is a parameter to characterize the ability of a material layer that resists a heat flow P_{th} in W through it, when a temperature difference $\Delta T = T_j - T_s$ in K occurs between two sides of this material layer. In that, T_j in $^{\circ}\text{C}$ is the temperature of the hot side of a general material layer or the junction temperature in the case of LEDs, T_s in $^{\circ}\text{C}$ is the temperature of the cold side of a general material layer or the capsule temperature in case of LEDs, and P_{th} in W is the thermal power that has to be transported from the hot side into the cold side.

$$R_{th} = \frac{\Delta T}{P_{th}} = \frac{T_j - T_s}{P_{th}} \quad (5.6)$$

On the other hand, in order to heat a mass m of a specific material layer from T_s up to T_j , it is necessary to feed a thermal energy Q_{th} into the material layer described in Equation 5.7,

$$Q_{th} = mC(T_j - T_s) = \rho V_{vol} C(T_j - T_s) \quad (5.7)$$

$$C_{th} = \rho V_{vol} C = \frac{Q_{th}}{\Delta T} = \frac{\int P_{th} dt}{\Delta T} \quad (5.8)$$

Hence, thermal capacitance C_{th} in Ws/K can be defined as a parameter that quantifies for the heat accumulation ability of a material volume like the description in Equation 5.8. As well, the specific property of a material can be characterized by three parameters including volume V_{vol} in m^3 , mass m in kg, specific heat capacity C in J/kgK and bulk density ρ in kg/m^3 .

Based on the above definitions of thermal resistance and thermal capacitance, for a specific material layer, thermal processes including heating and cooling can be described mathematically. Particularly, if an initial thermal energy Q_{th_int} in J has to sink from a hot side to a cold side, the reduced thermal energy in a unit of time will be P_{th} in J/s. Then, heat sink process over time can be described as follows,

$$Q_{th}(t) = Q_{th_int} - \int_0^t P_{th}(t) dt \quad (5.9)$$

$$P_{th} = -\frac{dQ_{th}(t)}{dt} = -C_{th} \frac{d\Delta T(t)}{dt} = \frac{\Delta T(t)}{R_{th}} \quad (5.10)$$

$$\Delta T(t) + R_{th} C_{th} \frac{d\Delta T(t)}{dt} = 0 \quad (5.11)$$

Solving Equation 5.10, cooling process can be determined like the description in Equation 5.12 (called cooling equation) with the thermal system time τ_{sys} or T_{sys} described by Equation 5.13.

$$\Delta T = \Delta T_0 \left[\exp\left(\frac{-t}{\tau_{sys}}\right) \right] \quad (5.12)$$

$$\tau_{sys} = T_{sys} = R_{th} C_{th} \quad (5.13)$$

The similar performance gives out the heating equation 5.14 describing for the reverse process of the above cooling process.

$$\Delta T = \Delta T_{\infty} \left[1 - \exp\left(\frac{-t}{\tau_{sys}}\right) \right] \quad (5.14)$$

The maximal amplitude of two processes shown in two equations 5.12 and 5.14 ($\Delta T_{\infty} = \Delta T_0 = \Delta T_{max}$ in K) is the saturation value of a heating process and the initial value of a cooling process.

* **Second order thermal circuit:** If two material layers are in a series connection, a second order equivalent thermal circuit with two stage RCs are illustrated in Figure 5.16. In that, ΔT_i , C_{thi} , R_{thi} and P_{thi} are the i^{th} temperature difference, the i^{th} thermal capacitance, the i^{th} thermal resistance and the i^{th} thermal power at the stage i . The index i is from 1 to 2.

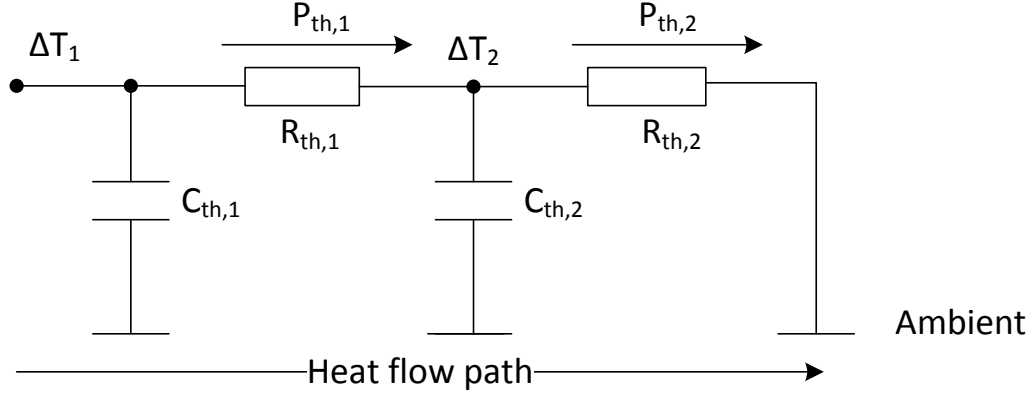


Figure 5.16 - Second order equivalent thermal circuit for two material layers in a serial connection

Analyzing the thermal circuit in Figure 5.17 with variables of temperature differences gives the following equations,

$$\begin{cases} \Delta T_1 = \Delta T_2 + R_{th,1} P_{th,1} \\ \Delta T_2 = R_{th,2} P_{th,2} \end{cases} \quad (5.15)$$

$$\begin{cases} \Delta T_1 = R_{th,1} P_{th,1} + R_{th,2} P_{th,2} \\ \Delta T_2 = R_{th,2} P_{th,2} \end{cases} \quad (5.16)$$

$$\begin{bmatrix} \Delta T_1 \\ \Delta T_2 \end{bmatrix} = \begin{bmatrix} R_{th,1} & R_{th,2} \\ 0 & R_{th,2} \end{bmatrix} \begin{bmatrix} P_{th,1} \\ P_{th,2} \end{bmatrix} \quad (5.17)$$

$$\begin{bmatrix} P_{th,1} \\ P_{th,2} \end{bmatrix} = \begin{bmatrix} 1/R_{th,1} & -1/R_{th,1} \\ 0 & 1/R_{th,2} \end{bmatrix} \begin{bmatrix} \Delta T_1 \\ \Delta T_2 \end{bmatrix} \quad (5.18)$$

$$\begin{bmatrix} P_{th,1} \\ P_{th,2} \end{bmatrix} = \begin{bmatrix} g_1 & -g_1 \\ 0 & g_2 \end{bmatrix} \begin{bmatrix} \Delta T_1 \\ \Delta T_2 \end{bmatrix} \quad (5.19)$$

Or,

$$\begin{cases} P_{th,1} = -C_{th,1} s \Delta T_1 + P_{th,in} \\ P_{th,2} = -C_{th,1} s \Delta T_1 - C_{th,2} s \Delta T_2 + P_{th,in} \end{cases} \quad (5.20)$$

$$\begin{bmatrix} P_{th,1} \\ P_{th,2} \end{bmatrix} = \begin{bmatrix} -C_{th,1} s & 0 \\ -C_{th,1} s & -C_{th,2} s \end{bmatrix} \begin{bmatrix} \Delta T_1 \\ \Delta T_2 \end{bmatrix} + \begin{bmatrix} P_{th,in} \\ P_{th,in} \end{bmatrix} \quad (5.21)$$

$$\begin{bmatrix} P_{th,1} \\ P_{th,2} \end{bmatrix} = \begin{bmatrix} -1/f_1 & 0 \\ -1/f_1 & -1/f_2 \end{bmatrix} \begin{bmatrix} \Delta T_1 \\ \Delta T_2 \end{bmatrix} + \begin{bmatrix} P_{th,in} \\ P_{th,in} \end{bmatrix} \quad (5.22)$$

Combining the equation 5.19 and the equation 5.22, we have the following derivative equations,

$$\begin{bmatrix} P_{th,1} \\ P_{th,2} \end{bmatrix} = \begin{bmatrix} g_1 & -g_1 \\ 0 & g_2 \end{bmatrix} \begin{bmatrix} \Delta T_1 \\ \Delta T_2 \end{bmatrix} = \begin{bmatrix} -1/f_1 & 0 \\ -1/f_1 & -1/f_2 \end{bmatrix} \begin{bmatrix} \Delta T_1 \\ \Delta T_2 \end{bmatrix} + \begin{bmatrix} P_{th,in} \\ P_{th,in} \end{bmatrix} \quad (5.23)$$

$$\begin{bmatrix} g_1 + 1/f_1 & -g_1 \\ 1/f_1 & g_2 + 1/f_2 \end{bmatrix} \begin{bmatrix} \Delta T_1 \\ \Delta T_2 \end{bmatrix} = \begin{bmatrix} P_{th,in} \\ P_{th,in} \end{bmatrix} \quad (5.24)$$

$$\begin{bmatrix} g_1 + 1/f_1 & -g_1 \\ 1/f_1 & g_2 + 1/f_2 \end{bmatrix} \begin{bmatrix} T f_1 \\ T f_2 \end{bmatrix} = \begin{bmatrix} 1 \\ 1 \end{bmatrix} \quad (5.25)$$

$$\begin{bmatrix} T f_1 \\ T f_2 \end{bmatrix} = \begin{bmatrix} g_1 + 1/f_1 & -g_1 \\ 1/f_1 & g_2 + 1/f_2 \end{bmatrix}^{-1} \begin{bmatrix} 1 \\ 1 \end{bmatrix} \quad (5.26)$$

Solving the equation 5.26 gives out transfer functions between i^{th} output temperature difference ΔT_i in K and the input thermal power $P_{\text{th,in}}$ in W as follows,

$$Tf_1 = \frac{\Delta T_1}{P_{\text{th,in}}} = \frac{g_1 + g_2 + C_{\text{th},2}s}{(g_1 + C_{\text{th},1}s)(g_2 + C_{\text{th},2}s) + g_1 C_{\text{th},1}s} \quad (5.27)$$

$$Tf_1 = \frac{\Delta T_1}{P_{\text{th,in}}} = \frac{(R_{\text{th},1} + R_{\text{th},2}) + R_{\text{th},1}R_{\text{th},2}C_{\text{th},2}s}{1 + (R_{\text{th},1}C_{\text{th},1} + R_{\text{th},2}C_{\text{th},2} + R_{\text{th},2}C_{\text{th},1})s + R_{\text{th},1}R_{\text{th},2}C_{\text{th},1}C_{\text{th},2}s^2} \quad (5.28)$$

$$Tf_2 = \frac{\Delta T_2}{P_{\text{th,in}}} = \frac{g_1}{(g_1 + C_{\text{th},1}s)(g_2 + C_{\text{th},2}s) + g_1 C_{\text{th},1}s} \quad (5.29)$$

$$Tf_2 = \frac{\Delta T_2}{P_{\text{th,in}}} = \frac{R_{\text{th},2}}{1 + (R_{\text{th},1}C_{\text{th},1} + R_{\text{th},2}C_{\text{th},2} + R_{\text{th},2}C_{\text{th},1})s + R_{\text{th},1}R_{\text{th},2}C_{\text{th},1}C_{\text{th},2}s^2} \quad (5.30)$$

Similarly, the transfer functions between i^{th} output local thermal power $P_{\text{th},i}$ in W and input thermal power $P_{\text{th,in}}$ in W can be solved as follows.

$$Tg_1 = \frac{P_{\text{th},1}}{P_{\text{th,in}}} = \frac{(R_{\text{th},2} + f_2)f_1}{(R_{\text{th},1} + f_1)(R_{\text{th},2} + f_2) + R_{\text{th},2}f_2} \quad (5.31)$$

$$Tg_1 = \frac{P_{\text{th},1}}{P_{\text{th,in}}} = \frac{1 + R_{\text{th},2}C_{\text{th},2}s}{1 + (R_{\text{th},1}C_{\text{th},1} + R_{\text{th},2}C_{\text{th},2} + R_{\text{th},2}C_{\text{th},1})s + R_{\text{th},1}R_{\text{th},2}C_{\text{th},1}C_{\text{th},2}s^2} \quad (5.32)$$

$$Tg_2 = \frac{P_{\text{th},2}}{P_{\text{th,in}}} = \frac{f_1 f_2}{(R_{\text{th},1} + f_1)(R_{\text{th},2} + f_2) + R_{\text{th},2}f_2} \quad (5.33)$$

$$Tg_2 = \frac{P_{\text{th},2}}{P_{\text{th,in}}} = \frac{1}{1 + (R_{\text{th},1}C_{\text{th},1} + R_{\text{th},2}C_{\text{th},2} + R_{\text{th},2}C_{\text{th},1})s + R_{\text{th},1}R_{\text{th},2}C_{\text{th},1}C_{\text{th},2}s^2} \quad (5.34)$$

* n^{th} order thermal circuit: Figure 5.17 describes a n^{th} order equivalent thermal circuit for n RC stages matching with n material layers in a serial connection. In that, ΔT_i , $C_{\text{th},i}$, $R_{\text{th},i}$ and $P_{\text{th},i}$ are the i^{th} temperature difference, the i^{th} thermal capacitance, the i^{th} thermal resistance and the i^{th} thermal power at the stage i . In this case, the index i is from 1 to n .

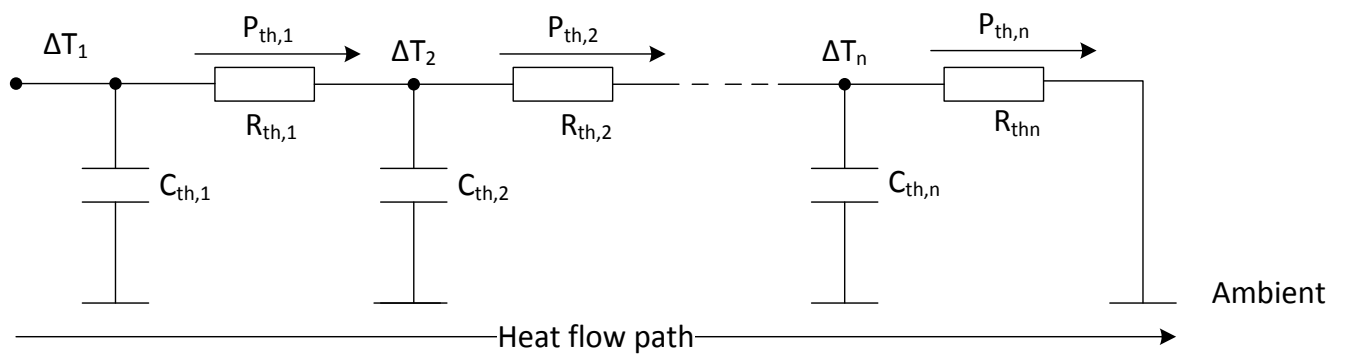


Figure 5.17 - n^{th} order equivalent thermal circuit for n material layers in a serial connection

Applying similar analyses of the second order equivalent thermal circuit into the n^{th} order equivalent thermal circuit in Figure 5.17, a general matrix of transfer functions between the output temperature difference ΔT_i in K and the input thermal power $P_{\text{th,in}}$ in W and between the output local thermal power $P_{\text{th},i}$ in W and the input thermal power input $P_{\text{th,in}}$ W are described by Equation 5.35 and Equation 5.36, respectively as follows,

$$\begin{bmatrix} Tf_1 \\ Tf_2 \\ Tf_3 \\ \dots \\ Tf_{n-1} \\ Tf_n \end{bmatrix} = \begin{bmatrix} g_1 + 1/f_1 & -g_1 & 0 & 0 & \dots & 0 \\ 1/f_1 & g_2 + 1/f_2 & -g_2 & 0 & \dots & 0 \\ 1/f_1 & 1/f_2 & g_3 + 1/f_3 & -g_3 & \dots & 0 \\ \dots & \dots & \dots & \dots & \dots & \dots \\ 1/f_1 & 1/f_2 & 1/f_3 & 1/f_4 & \dots & -g_{n-1} \\ 1/f_1 & 1/f_2 & 1/f_3 & 1/f_4 & \dots & g_n + 1/f_n \end{bmatrix}^{-1} \begin{bmatrix} 1 \\ 1 \\ 1 \\ \dots \\ 1 \\ 1 \end{bmatrix} \quad (5.35)$$

$$\begin{bmatrix} Tg_1 \\ Tg_2 \\ Tg_3 \\ \dots \\ Tg_{n-1} \\ Tg_n \end{bmatrix} = \begin{bmatrix} R_{th,1} + f_1 & R_{th,2} & R_{th,3} & R_{th,4} & \dots & R_{th,n} \\ -f_2 & R_{th,2} + f_2 & R_{th,3} & R_{th,4} & \dots & R_{th,n} \\ 0 & -f_3 & R_{th,3} + f_3 & R_{th,4} & \dots & R_{th,n} \\ \dots & \dots & \dots & \dots & \dots & \dots \\ 0 & 0 & 0 & 0 & \dots & R_{th,n} \\ 0 & 0 & 0 & 0 & \dots & R_{th,n} + f_n \end{bmatrix}^{-1} \begin{bmatrix} f_1 \\ 0 \\ 0 \\ \dots \\ 0 \\ 0 \end{bmatrix} \quad (5.36)$$

* **Transient function and weighting function:** In the time domain, for the n stage thermal circuit in Figure 5.17, combining the solution in Equation 5.14 and property of a linear system, transient function $h(t) = \frac{\Delta T_1(t)}{P_{in}(t)}$ of the temperature difference $\Delta T_1(t)$ according to time can be determined as,

$$h(t) = A_1 \left[1 - e^{-\frac{t}{T_1}} \right] + A_2 \left[1 - e^{-\frac{t}{T_2}} \right] + \dots + A_n \left[1 - e^{-\frac{t}{T_n}} \right] \quad (5.37)$$

Then, the weighting function $g(t) = \frac{dh(t)}{dt}$ can be solved,

$$g(t) = \frac{A_1}{T_1} e^{-\frac{t}{T_1}} + \frac{A_2}{T_2} e^{-\frac{t}{T_2}} + \dots + \frac{A_n}{T_n} e^{-\frac{t}{T_n}} \quad (5.38)$$

As a result, the transfer function $G(s)$ between the output temperature difference ΔT_1 in K and the input thermal power P_{in} in W can be determined,

$$G(s) = \frac{\Delta T_1(s)}{P_{in}(s)} = \frac{A_1}{T_1 s + 1} + \frac{A_2}{T_2 s + 1} + \dots + \frac{A_n}{T_n s + 1} \quad (5.39)$$

* **Conclusion:** Based on the above analyses, it can be confirmed, that the thermal object in a LED system is a high order and linear system with no overshoot, no derivation component (D) and no integration component (I), but with only one proportion component (P). Therefore, the thermal system will approach to a saturation status, when the time runs to infinity. Otherwise, it can also be recognized, that with the equations 5.35, 5.36 and 5.37, it is very difficult to determine explicitly values of partial thermal resistances and partial thermal capacitances for a n stage thermal circuit. In addition, the order of the total system is also not easy to determine accurately. Therefore, another better theory of identification and decoding for this high order thermal transient LED model has to be investigated and proposed. The theory should be as simple as possible so that the establishment of thermal transient LED models can be carried out easily.

5.3.2. Study and analysis of the current well-known identification and decoding solution

In Section 5.3.1, mathematical background for thermal circuits was described and discussed. The mathematical form of the high order linear thermal object in a LED system was determined. However, this classical approach leads to a complicated equation system that is difficult to be determined

explicitly. Therefore, it is necessary to have another theory for this problem. Fortunately, the basic theory of non-uniform RC lines was described in [55] and [56]. As well, fundamental analyses of one dimensional heat path were discussed in [57]. Based on [55], [56] and [57], the authors in [52] proposed and performed a powerful identification and decoding solution for the thermal object in LED systems by the structure function method. This solution is the well-known identification and decoding solution currently. Therefore, in this section the main ideas of the solution will be generalized and analyzed in order to determine its advantages and its disadvantages. Consequently, its advantages will be inherited and its disadvantages will be improved by the other available solution in Section 5.3.3.

* **Thermal transient process:** The thermal transient process captured from cooling or heating procedure has their specified mathematical forms like the simple description in Equation 5.12 and Equation 5.14, respectively. In despite of cooling or heating transient process, the preferred mathematical form in practical performance is the heating equation. Therefore, Equation 5.37 can be written as,

$$\Delta T = \sum_{i=1}^n A_i [1 - e^{-\frac{t}{T_i}}] \quad (5.40)$$

If both sides of Equation 5.40 are divided by thermal power input $P_{th,in}$ in W, the thermal impedance of the thermal object in a LED system can be determined,

$$Z_{th} = \frac{\Delta T}{P_{th,in}} = a(t) = \sum_{i=1}^n R_{th,i} [1 - e^{-\frac{t}{T_i}}] \quad (5.41)$$

Where,

ΔT is the temperature difference between junction temperature and sensor temperature (K).

A_i is the magnitude of each thermal transient component (K).

T_i is the partial subsystem time of each thermal transient element (s).

Z_{th} is the total thermal impedance (K/W).

$R_{th,i}$ is the partial thermal resistance of the Foster circuit model (K/W).

$C_{th,i} = T_i / R_{th,i}$ is the partial thermal capacitance of the Foster circuit model (Ws/K).

The mathematical form of Equation 5.41 should be fitted well enough for further processes, because fitting has strong influences the accuracy of both identification and decoding later. As well, decoding depends on the used algorithms or software. In this thesis, the MATLAB curve fitting toolbox is used to fit for exponential equations. Otherwise, the order of the system is a difficult problem. The classical identification theory has some theorems to determine the order of the systems. However, unfortunately these theorems are only to use for some specific models such as PT_1 , IT_1 , IT_n , PT_2 , PT_n , lead/lag model or second order oscillating component model. Moreover, according to the classical identification theory, its theorems cannot be used for very fast systems with system time of below $1 \mu s$. Therefore, in this thesis the order of the systems is selected from one to an available maximal stage, where the least square error is minimal. Up to now, by an available fitting tool, the thermal transient process of LEDs can be completely identified with the explicit mathematical form described by Equation 5.41 and it can be used as a simple thermal transient LED model. In addition, the total thermal resistance $R_{th,\Sigma}$, the total thermal capacitance $C_{th,\Sigma}$ and the junction temperature T_j can be also determined. However, in order to decode a LED thermal map with partial thermal resistances and partial thermal capacitances, more complicated mathematical tools must be applied.

* **Transformation from a thermal transient process into a structure function:** In order to determine a LED thermal map with an array of partial thermal resistances and partial thermal capacitances, the transformation from a thermal transient process into a structure function is a very powerful but also very complicated solution described in [51] and [52]. In that, necessary steps must be carried out as follows,

$$\xi = \ln(T_i) \text{ or } T_i = e^\xi \quad (5.42)$$

$$z = \ln(t) \text{ or } t = e^z \quad (5.43)$$

Then,

$$Z_{th}(z) = \sum_{i=1}^n R_{th}(\xi) [1 - e^{-\frac{e^z}{e^\xi}}] \rightsquigarrow \int_{-\infty}^{+\infty} R_{th}(\xi) [1 - e^{-e^{(z-\xi)}}] d\xi \quad (5.44)$$

$$\frac{dZ_{th}(z)}{dz} = \int_{-\infty}^{+\infty} R(\xi) [-e^{-e^{(z-\xi)}} \cdot -e^{(z-\xi)}] d\xi \quad (5.45)$$

$$\frac{dZ_{th}(z)}{dz} = \int_{-\infty}^{+\infty} R(\xi) [e^{(z-\xi)-e^{(z-\xi)}}] d\xi \quad (5.46)$$

Based on the definition of convolution, it can be determined,

$$(f * g)(t) \stackrel{\text{def}}{=} \int_{-\infty}^{+\infty} f(\tau) g(t - \tau) d\tau \rightsquigarrow f(j\omega) g(j\omega) = f(s) g(s) \quad (5.47)$$

$$\frac{dZ_{th}(z)}{dz} = R(z) * W(z) = R(z) * \exp(z - e^z) \quad (5.48)$$

From Equation 5.48, thermal resistance equation $R(z)$ can be converted as follows,

$$R(z) = \frac{dZ_{th}(z)}{dz} *^{-1} \exp[z - \exp(z)] = \frac{dZ_{th}(z)}{dz} *^{-1} W(z) \quad (5.49)$$

The deconvolution in Equation 5.49 can give the mathematical form of $R(z)$ matching directly to FOSTER network and as well it also causes a very bad inaccuracy for the transformation. Then, a FOSTER to CAUER transformation successively causes worse inaccuracy in numerous components and a wide range of the time constant. In real performance, these inaccuracies can only be improved by a good enough numerical algorithm of deconvolution and numerical transformation. Some approximation methods of the FOSTER to CAUER transformation were discussed in [58], [59] and [60]. In that, the determination for a structure function needed for the theory of one-dimensional heat-flow model in [57]. Thus, the authors in [52] proposed that a reasonable approximation for a given structure based on this theory would show the correspondence between the different sections of CAUER network and the different parts of a physical structure of LEDs. According to [57], the heat flow equation for a one dimensional structure can be calculated as follows,

$$\frac{\partial T}{\partial t} = \frac{1}{c(x)} \frac{\partial}{\partial x} \left(\frac{1}{r(x)} \frac{\partial T}{\partial x} \right) \quad (5.50)$$

Where, $r(x)$ is the thermal resistance per unit length, c was the thermal capacitance per unit length. Replacing a special ‘‘arc-length parameter’’ $\rho(x)$ for x , we have another form of Equation 5.50 with $K(x) = \frac{c(x)}{r(x)}$,

$$\frac{\partial T}{\partial t} = \frac{1}{K} \frac{\partial^2 T}{\partial \rho^2} \quad (5.51)$$

For a material layer, coefficient K is proportional to its squared cross area A (for example, $K_{\text{silicon}}=2.58 \cdot 10^8 \text{A}^2 / \text{W}^2 \text{s}/^\circ\text{C}^2$ and $K_{\text{kovar}}=0.7 \cdot 10^8 \text{A}^2 / \text{W}^2 \text{s}/^\circ\text{C}^2$). Approximate plotting K -value as a function of thermal resistance would give us a decoding map of partial thermal resistances R_n and partial thermal capacitances C_n based on the following equations,

$$K_n = \frac{2C_n}{R_{n-1}+R_n} \text{ and } \rho_n = \sum_{i=1}^{n-1} R_i \quad (5.52)$$

* **Evaluation and summary:** Unfortunately, characteristic parameters of tiny material layers in LEDs such thickness, width and heat conductivity are difficult to determine explicitly, especially in the role of LED users. Therefore, in the condition of an application laboratory, the above approximation is not feasible and is difficult to perform as accurately as LED manufacturers like the descriptions in Section 5.1.c. In addition, the accuracy of the above approximations is in the first query. On another side, the second query is, whether specific decoding with very high order of very tiny material layers is really necessary, or an explicit thermal impedance function is enough to describe a thermal transient process for other modeling components, as well also enough to calculate both total thermal resistance and junction temperature of LEDs.

These two queries were shared by the authors in [61]. Indeed, the most criticized point for the structure function method is the numerical deconvolution. Particularly, with different levels of the numerical deconvolution accuracy, deconvolution can give completely different solutions of thermal resistance $R(z)$. Consequently, based on these solutions of thermal resistances $R(z)$, values of partial thermal resistances and partial capacitances will be determined very differently. The second criticized point is the inaccuracy of separation of partial thermal resistances and partial capacitances from a differential structure function. This work required both good experiences of users and full information about characteristics parameters and material compositions of LED chips. The third criticized point is that there is no much new and useful information from a structure function comparing with original thermal impedance function $Z_{\text{th}}(t)$, while we have to face its inaccuracy.

Moreover, the authors in [61] proposed that if it is necessary to estimate thermal transient processes of LEDs, thermal impedance function $Z_{\text{th}}(t)$ is the most available, and if it is necessary to estimate very small differences between different material layers or different impacting factors, derivative function of thermal impedance $dZ_{\text{th}}/dz(t)$ is also good and accurate enough. Successively, these authors also conclude that the comparison of derivative function $dZ_{\text{th}}/dz(t)$ instead of structure functions might be an alternative way to determine a total thermal resistance from dual interface measurements that is less error-prone than the structure function approach. In addition, it does not require an experienced user but can be performed automatically in evaluation software. Even, one of the original authors of the structure function method in [52] and the co-authors wrote another paper about a procedure to correct errors in structure functions based on thermal measurement methods shown in [62]. In this paper, a quite complicated procedure with five steps was offered to improve structure functions.

Therefore, in the next section, thermal transient identification of cold white PC-LEDs by means of exponential interpolation and then establishment of their thermal impedance functions will be carried out as a demonstration example of an available approach. Successively, the transformation of thermal impedance functions into their derivative functions will be also performed for the comparison of material differences. Finally, a more available solution for the thermal map decoding of LEDs will be proposed and proved for cold white PC-LEDs.

5.3.3. A demonstration example for the thermal transient identification and the thermal map decoding of some cold white PC-LEDs based on a new solution

a. Objects in the performance

In this section, three cold white PC-LEDs belonging to the same binning group (5000 K) are used as a demonstration example for transient thermal identification and thermal map decoding based on a new solution. In this example, the selected forward current is 700 mA and the sensor temperature is kept constant for two cases 40 °C and 80 °C. In Figure 5.18, absolute spectral power distributions of the cold white PC-LED at two different temperatures are described. When the temperature increased from 40 °C to 80 °C, the average optical power of the three cold white PC-LEDs decreased from 0.56 W down to 0.47 W and contrarily their average thermal power increased from 1.47 W to 1.51 W.

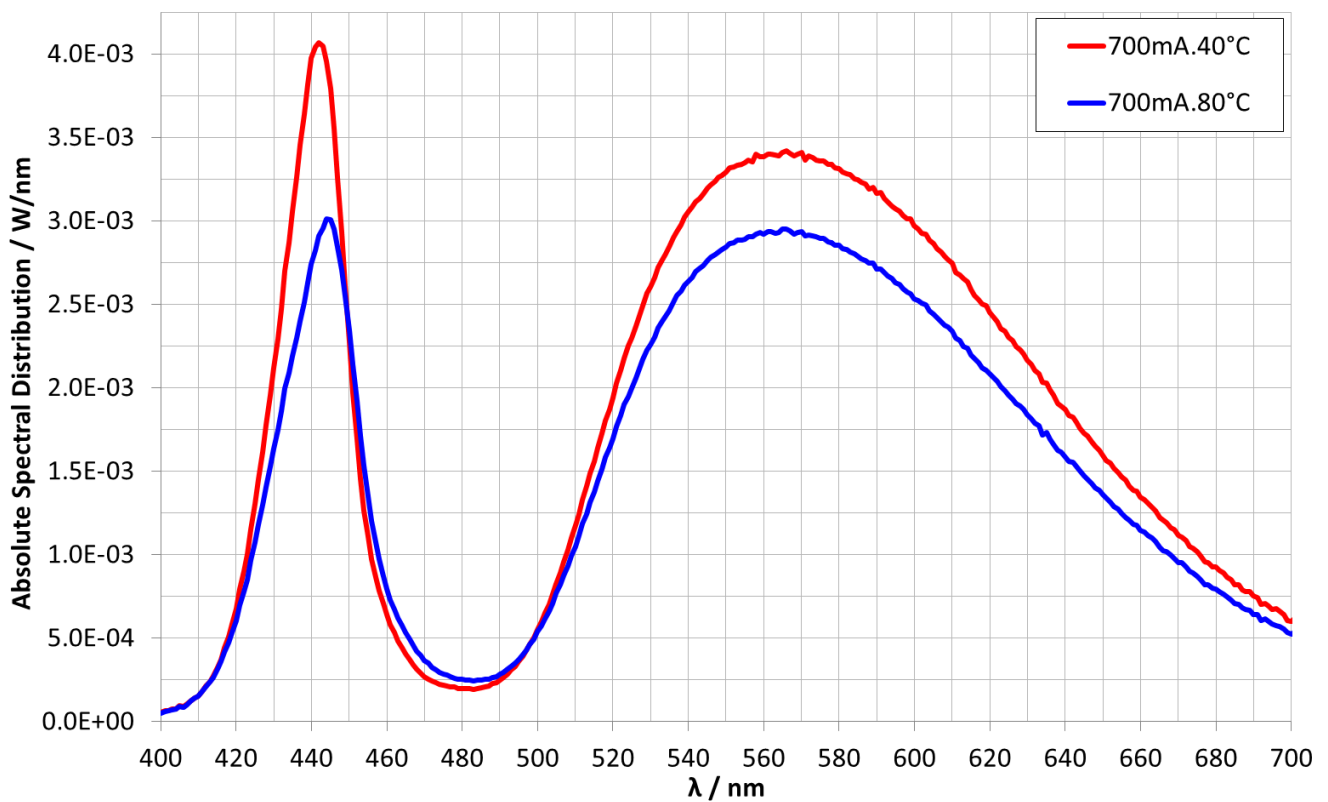


Figure 5.18 - Absolute spectral power distributions of the cold white PC-LED (5000 K)

b. Thermal transient identification of the three cold white PC-LEDs as a demonstration example

* **Identification of thermal transient process of three cold white PC-LEDs at 700mA and 40°C:** In the first case, the sensor temperature is kept constant 40 °C by the THORLAB controller. The forward current I_f of 700 mA is supplied for the three cold white LEDs in a long enough time to charge fully thermal power P_{th} in W for them. After this procedure, forward current I_f is turned off suddenly down to 1 mA. As a result, a cooling process occurs to transfer thermal power P_{th} from the inside of LEDs to the ambient. Similarly to the cooling measurement procedure in Section 5.2.1, forward voltage difference ΔV in V of the three PC-LEDs are transformed into temperature different ΔT in K by means of relationship $\Delta T = \Delta V / a_0$. Moreover, relationship $V_f = a_0 T_s + b_0 \approx V_f = a_0 T_j + b_0$ was determined previously at 1 mA in order to achieve constant a_0 for the calculation. In addition, the thermal power P_{th} was also

calculated from a DC measurement. Therefore, the thermal transient process described by a thermal impedance function can be determined for the three PC-LEDs like the description in Figure 5.19 with corresponding parameters in Table 5.3. Based on Figure 5.19, it can be recognized, that at the beginning of the thermal transient process, there were considerable offsets for thermal impedances of the three PC-LEDs, but at the end of the thermal transient process, curves focused gradually on quite similar saturated magnitudes. Otherwise, quantitatively, their total thermal resistances of about 15 K/W - 16 K/W are quite appropriate to the data, the composition and the structure published by OSRAM in Section 5.1.c.

Table 5.3 - FOSTER model parameters of the three cold white LEDs at 700 mA and 40 °C

LED	LED ₂₁ - FOSTER Model			LED ₃₁ - FOSTER Model			LED ₄₁ - FOSTER Model		
Order	$R_{th,i}/$ K/W	$C_{th,i}/$ Ws/K	$\tau_i/$ s	$R_{th,i}/$ K/W	$C_{th,i}/$ Ws/K	$\tau_i/$ s	$R_{th,i}/$ K/W	$C_{th,i}/$ Ws/K	$\tau_i/$ s
1	5.51	0.011	0.061	6.29	0.01	0.063	2	0.02	0.04
2	3.67	0.081	0.297	2.93	0.09	0.264	8.50	0.016	0.136
3	3.62	$1.03 \cdot 10^{-6}$	$3.73 \cdot 10^{-6}$	2.84	$7.7 \cdot 10^{-6}$	$22 \cdot 10^{-6}$	3.05	$1.2 \cdot 10^{-6}$	$3.66 \cdot 10^{-6}$
4	3.05	0.098	0.299	3.58	0.075	0.269	3.88	0.25	0.97
$R_{th,total}$	15.85	$R_{square,21}$	99.63 %	15.64	$R_{square,31}$	99.9 %	17.43	$R_{square,41}$	99.88 %

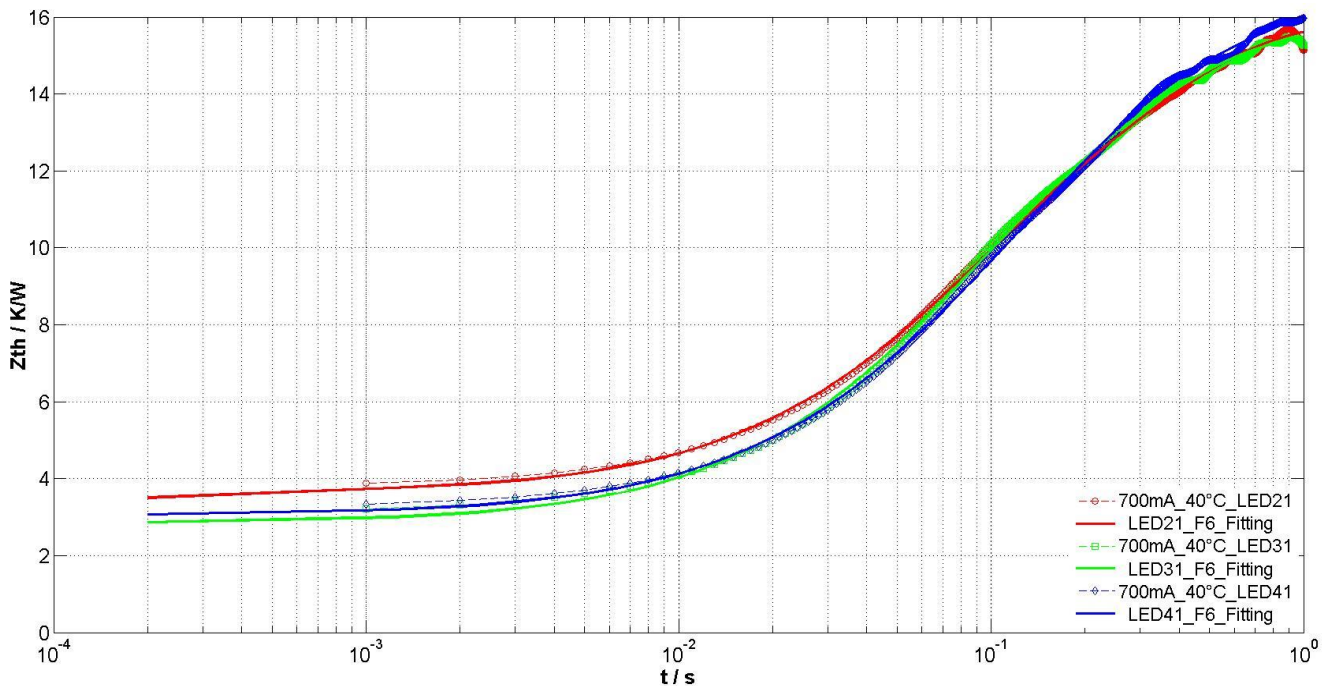


Figure 5.19 - Thermal impedance functions of three cold white LEDs (5000 K) at 700 mA and 40 °C

* Identification for the thermal transient processes of three cold white PC-LEDs at 700mA and 80°C and transformation into derivative functions of their thermal impedances: In the second case, the similar forward current I_f of 700 mA is still supplied for the three PC-LEDs, but the sensor temperature is increased up to 80 °C. Then, the results of the fitting according to Equation 5.41 are

described in Figure 5.20 and corresponding parameters are listed in Table 5.4. The results showed that at the beginning of the thermal transient process, there was nearly no offset between curves, but at the end of the thermal transient process, their magnitudes were separated from about 16 K/W to about 17.5 K/W. These values are still quite available with the analyses mentioned in Section 5.1.c by OSRAM. Successively, in Figure 5.21, derivative functions of thermal impedance dZ_{th}/dZ were shown so that very small differences between different materials and different impacting factors can be observed more obviously. In that, it can be recognized, that the increase of temperature caused a slight increase of the thermal impedances.

Table 5.4 - FOSTER model parameters of three cold white LEDs at 700 mA and 80 °C

LED	LED ₂₁ - FOSTER Model			LED ₃₁ - FOSTER Model			LED ₄₁ - FOSTER Model		
Order	$R_{th,i} /$ K/W	$C_{th,i} /$ Ws/K	$\tau_i /$ s	$R_{th,i} /$ K/W	$C_{th,i} /$ Ws/K	$\tau_i /$ s	$R_{th,i} /$ K/W	$C_{th,i} /$ Ws/K	$\tau_i /$ s
1	6.68	0.038	0.254	4.80	0.046	0.22	5.85	0.01	0.0585
2	4.96	0.018	0.089	4.91	0.010	0.049	4.27	0.06	0.256
3	3.13	$0.69 \cdot 10^{-6}$	$2.16 \cdot 10^{-6}$	3.21	$3.89 \cdot 10^{-6}$	$12 \cdot 10^{-6}$	3.15	$8.8 \cdot 10^{-6}$	$27.7 \cdot 10^{-6}$
4	1.1	0.038	0.042	4.03	0.054	0.22	4.41	0.057	0.2514
$R_{th,total}$	15.87	$R_{square,21}$	99.8 %	16.95	$R_{square,31}$	99.9 %	17.68	$R_{square,41}$	99.85 %

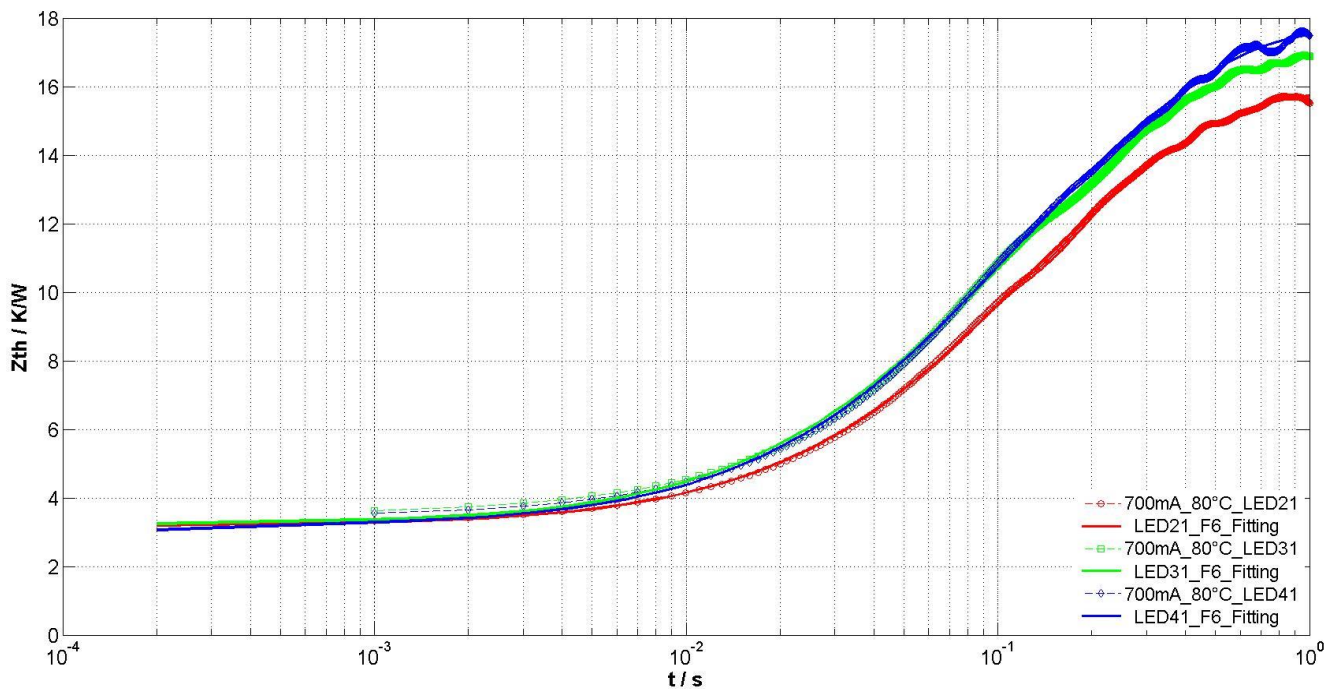


Figure 5.20 - Thermal impedance functions of three cold white LEDs (5000 K) at 700 mA and 80 °C

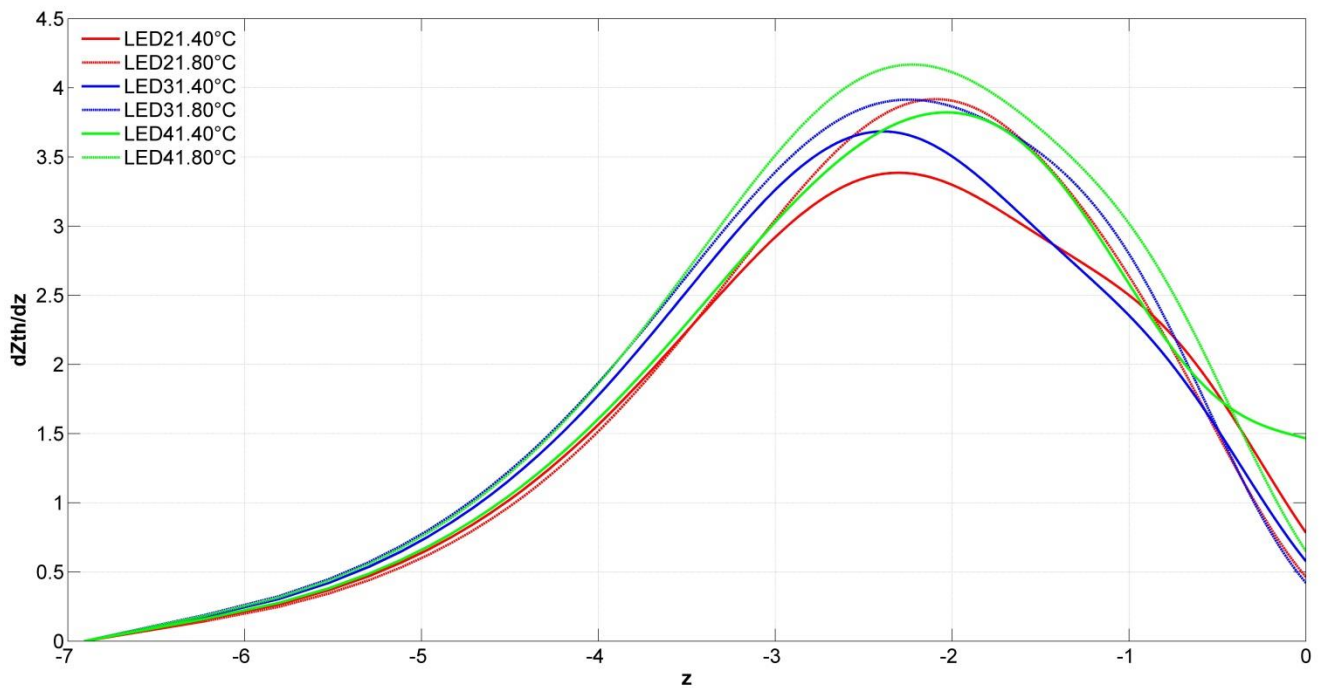


Figure 5.21 - Derivative functions of the thermal impedances of three cold white LEDs (5000 K) at 700 mA

* **Summary:** In fact, inhomogeneity between similar LEDs belonging to the same binning group and slight change of partial thermal resistances following to temperature are unavoidable factors in a LED manufacturing process. Depending on physical and chemical properties of compositions in LED structures, partial thermal resistances and partial thermal capacitances can have different changes according to local temperatures at each material layer. These changes are very difficult to be able to be determined specifically and accurately. In addition, both figures 5.19 and 5.20 also illustrated for influences of sampling time and falling time on the accuracy of system identification. Particularly, the falling time of 100 s reduced the resolution of the instrument significantly. As a result, there was no information on high frequency regions (0.1 MHz - 1 MHz). Therefore, the transient thermal process in regions under about 3.5 K/W was not able to be investigated and determined exactly, although total thermal resistances and junction temperatures were still able to be calculated. Furthermore, because there was no information of K_n coefficients like the description in Equation 5.52, and no characteristic parameter and no chemical composition of material layers established in the white PC-LEDs like requirements in [94], the transformation from the determined thermal transient processes into structure functions was not able to be carried out. Consequently, a LED thermal map with partial CAUER thermal resistances and partial CAUER thermal capacitances was also not able to be decoded by the structure function method. Hence, another more suitable solution will be supposed in the next section in order to substitute for the structure function method and become easier in the real performance.

c. Proposal of an available solution for thermal map decoding of LEDs

In the figures 5.19 - 5.21 and the tables 5.3 - 5.4, the important properties of the cold white PC-LEDs such as thermal impedance functions $Z_{th}(t)$ and derivative functions of thermal impedance $dZ_{th}/dz(t)$ were determined satisfying the characterization and establishment of thermal transient LED models like the requirements in [61]. As well, the performance has avoided the inaccuracy due to numerical transformations such as numerical deconvolution, FOSTER - CAUER transformation or approximation of

the differentiate structure functions. However, the own FOSTER partial thermal resistances and FOSTER partial thermal capacitances in the tables 5.3 - 5.4 do not reflect the physical nature of the real material layers in LED structures. Therefore, in this section a more available solution for LED thermal map decoding of LEDs will be investigated and proposed. In order to realize the solution, the authors in [60] suggested the EUCLIDEAN algorithm and the authors in [59] also offered a nearly similar algorithm. As a result, the EUCLIDEAN algorithm (called EUCLIDEAN decoding method) will be applied to decode thermal maps of the three white cold white PC-LEDs in an array of CAUER partial thermal resistances and CAUER partial thermal capacitances as a demonstration example for a substituting method of the structure function method.

*** Investigation and evaluation of the accuracy of the EUCLIDEAN decoding method and the exponential interpolation in Section 5.3.3.b:** In this section, a demonstration example of a simulated two stage CAUER thermal circuit is established like the system structure diagram in Figure 5.22 with $R_{th,1}=1$ K/W, $C_{th,1}=1$ Ws/K, $R_{th,2}=2$ K/W and $C_{th,2}=2$ Ws/K. By means of the MATLAB simulation, this example is to investigate and evaluate the accuracy of the EUCLIDEAN decoding method as well as the exponential interpolation used for the thermal transient identification of the three cold white PC-LEDs in Section 5.3.3.b.

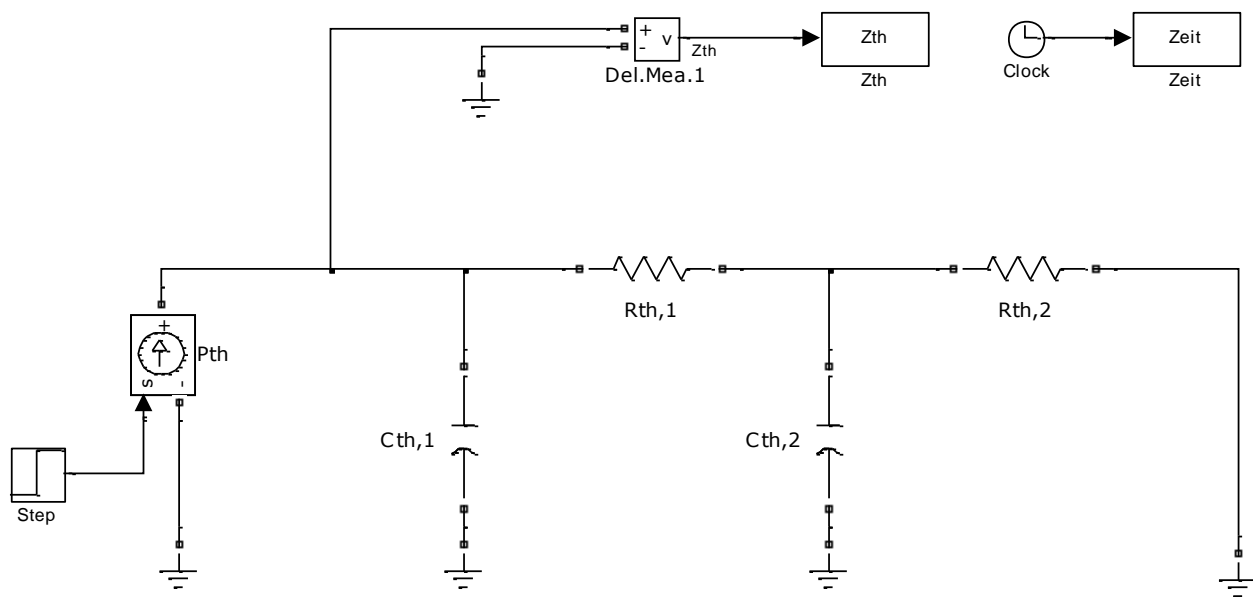


Figure 5.22 - A simulated two stage thermal RC circuit as a demonstration example for the evaluation of the accuracy of the exponential interpolation and the EUCLIDEAN decoding method

Particularly, a MATLAB SIMULINK thermal circuit in Figure 5.23 is simulated with the given structure parameters of partial thermal resistances and partial thermal capacitances and input thermal power pulse $P_{th,in}$ of 1 W. And then, the simulation gives a thermal transient process like the description in Figure 5.23. Successively, the MATLAB curve fitting toolbox is used to establish a mathematical description for the thermal transient process shown in Equation 5.53. As well, a LAPLACE transformation is carried out to convert from the thermal transient function into the LAPLACE thermal impedance function and the LAPLACE thermal conductivity function shown in Equation 5.54 and Equation 5.55, respectively.

$$Z_{th}(t) = 0.3685 \left(1 - e^{-\frac{t}{0.6277}}\right) + 2.632 \left(1 - e^{-\frac{t}{6.372}}\right) \quad (5.53)$$

$$Z_{th}(s) = \frac{4.0002s + 3.0005}{3.9997s^2 + 6.9997s + 1} \quad (5.54)$$

$$Y_{th}(s) = \frac{1}{Z_{th}(s)} = \frac{3.9997s^2 + 6.9997s + 1}{4.0002s + 3.0005} \quad (5.55)$$

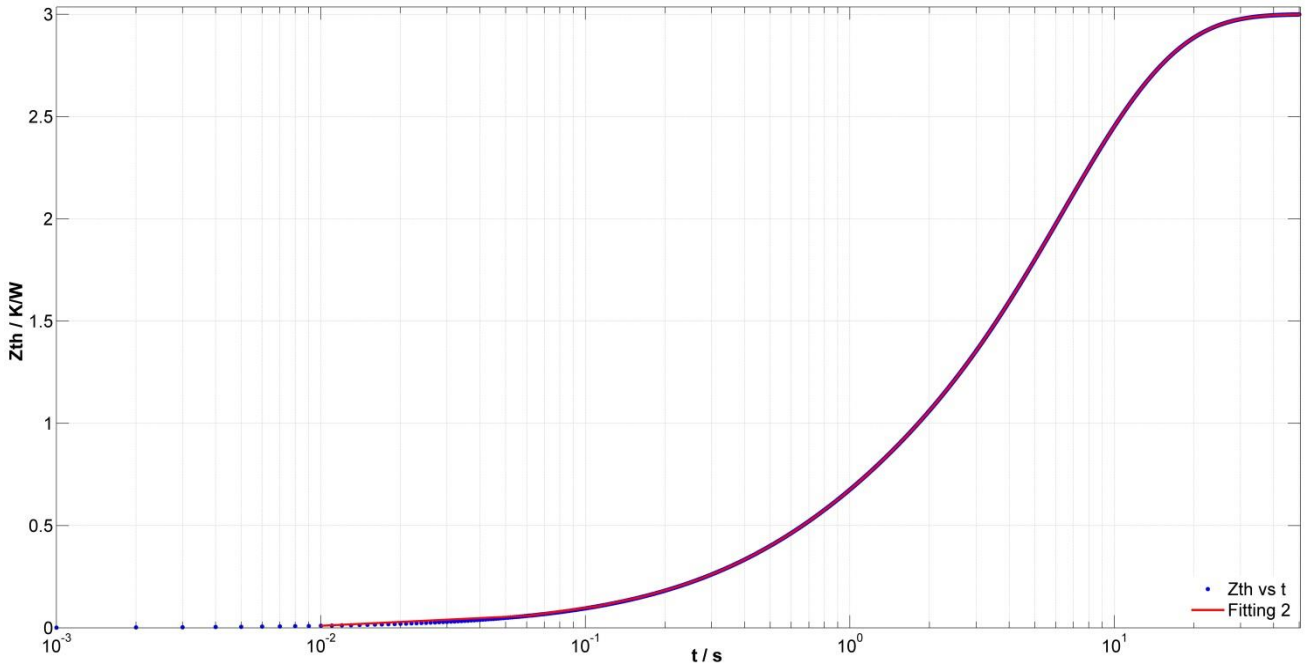


Figure 5.23 - The transient thermal response of the simulated two stage thermal RC circuit

Finally, the FOSTER - CAUER transformation is undertaken by means of the EUCLIDEAN algorithm with particular steps described in Table 5.5. The archived results are compared directly with original values and evaluated via offsets in percent between them as in Table 5.6. Based on the results in Table 5.6, it can be recognized, that the identification with the exponential interpolation by the MATLAB curve fitting toolbox and the decoding for LED thermal map by the EUCLIDEAN algorithm were very accurate. Indeed, the offsets between calculated values and original values of partial thermal resistances and partial thermal capacitances were very small from 0.02 % to 0.05 %. Therefore, it can be confirmed, that the exponential interpolation and the EUCLIDEAN algorithm should be used for the identification of the thermal transient processes and the thermal map decoding of LEDs. As well, they are also good proposals in order to avoid the inaccuracies of the numerical deconvolution and other complicated procedures of the structure function method.

Table 5.5 - The FOSTER - CAUER transformation by means of the EUCLIDEAN algorithm for the simulated two stage thermal circuit as a demonstration example

Step	Y of shunt elements	$3.9997s^2 + 6.9997s + 1$	$4.0002s + 3.0005$	Z of series element
1	$(3.9997/4.0002) = 0.9999s$	$3.9997s^2 + 3.0002s$		
		$3.9995s + 1$	$4.0002s + 3.0005$	
2			$4.0002s + 1.0002$	$4.0002/3.9995 = 1.0002$
		$3.9995s + 1$	2.0003	
3	$(3.9995/2.0003)s = 1.9995s$	$3.9995s$		
		1	2.0003	$2.0003/1 = 2.0033$
4			2.0003	
			0	

Table 5.6 - Comparison and evaluation of the accuracy of the EUCLIDEAN algorithm and the exponential interpolation as a demonstration example

Parameters	Original	FOSTER Model Identification	CAUER Model Identification	Offset / %
$R_{th,1} / K/W$	1	0.3685	1.0002	0.02
$C_{th,1} / Ws/K$	1	2.632	0.9999	0.01
$R_{th,2} / K/W$	2	1.7034	2.0003	0.03
$C_{th,2} / Ws/K$	2	2.4210	1.9995	0.05

* **Application of the EUCLIDEAN decoding method for three cold white LEDs at 700 mA and 40 °C and 700 mA and 80 °C:** Practically, the thermal map decoding with a four stage CAUER thermal circuit or higher stage CAUER thermal circuit will be also performed similarly on the steps in Table 5.5. Consequently, the thermal maps with CAUER partial thermal resistances and CAUER partial thermal capacitances for the above cold white LEDs at 700 mA and 40 °C and at 700 mA and 80 °C were decoded by the EUCLIDEAN algorithm and their corresponding results listed in Table 5.7 and Table 5.8, respectively.

Table 5.7 - Decoded thermal maps of three cold white LEDs (5000 K) at 700 mA and 40 °C as an example

LED	LED ₂₁ - CAUER Model		LED ₃₁ - CAUER Model		LED ₄₁ - CAUER Model	
Order	$R_{th,i} / K/W$	$C_{th,i} / Ws/K$	$R_{th,i} / K/W$	$C_{th,i} / Ws/K$	$R_{th,i} / K/W$	$C_{th,i} / Ws/K$
1	3.6224	$1.034 \cdot 10^{-6}$	2.8430	$7.710 \cdot 10^{-6}$	3.0481	$1.199 \cdot 10^{-6}$
2	8.2374	$8.984 \cdot 10^{-3}$	9.1096	$7.838 \cdot 10^{-3}$	7.8163	$8.616 \cdot 10^{-3}$
3	3.9779	$6.285 \cdot 10^{-2}$	3.6762	$6.197 \cdot 10^{-2}$	3.9812	$2.257 \cdot 10^{-2}$
4	0.0023	$1.317 \cdot 10^2$	0.0011	$2.479 \cdot 10^2$	2.5843	$3.405 \cdot 10^{-1}$
$R_{th,total}$	15.84		15.63		17.43	

Table 5.8 - Decoded thermal maps of three cold white LEDs (5000 K) at 700 mA and 80 °C as an example

LED	LED ₂₁ - CAUER Model		LED ₃₁ - CAUER Model		LED ₄₁ - CAUER Model	
Order	$R_{th,i} / K/W$	$C_{th,i} / Ws/K$	$R_{th,i} / K/W$	$C_{th,i} / Ws/K$	$R_{th,i} / K/W$	$C_{th,i} / Ws/K$
1	3.1301	$6.914 \cdot 10^{-7}$	3.2159	$3.883 \cdot 10^{-6}$	3.1569	$8.799 \cdot 10^{-6}$
2	8.6164	$9.330 \cdot 10^{-3}$	9.0061	$7.338 \cdot 10^{-3}$	9.8820	$7.577 \cdot 10^{-3}$
3	2.8224	$2.797 \cdot 10^{-2}$	4.7370	$3.584 \cdot 10^{-2}$	4.6399	$4.349 \cdot 10^{-2}$
4	1.2911	$1.170 \cdot 10^{-1}$	0.0011	$2.079 \cdot 10^2$	0.0011	$2.324 \cdot 10^2$
$R_{th,total}$	15.86		16.96		17.68	

5.4. Summary

Chapter 5 described phenomena taking place in the PC-LEDs and a MIMO system of a solid state lighting structure, intrinsically. Thus, a system structure block diagram for the thermal LED transient model was separated from the MIMO system. Then, a finished LED structure and its characterization in thermal relationships were collected and described from the published data of OSRAM in order to have

practical information about a real LED structure and its thermal compositions. Successively, the junction temperature determination of LEDs was discussed specifically. In that, different measurement methods were generalized and the measurement method based on forward voltages was chosen as the most suitable method. With this measurement method, two different measurement procedures including the heating and the cooling procedures were carried out in the practical comparison and evaluation with a direct mode and an indirect mode. Hence, the early results proved that the cooling procedure can achieve a better accuracy than the heating procedure. Moreover, the causes of inaccuracy and the improvement proposals were explained and offered.

On the other hand, the thermal transient identification and the thermal map decoding of LEDs are very important to establish thermal transient LED models. Therefore, the mathematical background for thermal circuits was described in order to establish thermal transient LED models by explicit mathematical equations, classically. The system is linear with no overshoot, no derivation component (D) and no integration component (I), but only with one proportion component (P). However, unfortunately thermal objects in LED systems are high-order objects. Thus, the classical explicit determination of their order and their parameters are very difficult to perform in the reality. Therefore, the structure function method was analyzed on the role of current well-known identification and decoding solution. The analyses showed that the structure function method faced four problems including complicated procedures, inaccuracies by numerical transformations, dependences on the experience of users and the published data of LED manufacturers, and not much new and useful information comparing with original thermal transient processes.

Finally, the exponential interpolation based on the MATLAB curve fitting toolbox was carried out to identify the thermal transient processes of three cold white PC-LEDs with their explicit mathematical equations as a demonstration example. Basically, these mathematical equations can play the full role of thermal transient LED models. Furthermore, the EUCLIDEAN decoding method was proposed to substitute the structure function method in thermal map decoding of LEDs. By simulation, the achieved results confirmed that both the exponential interpolation and the EUCLIDEAN decoding method had very high accuracy. Therefore, they are also available solutions for the measurement, identification and establishment of thermal transient LED models. Hence, the established problems at the beginning of this chapter of junction temperature determination, thermal transient identification and thermal map decoding of LEDs were solved entirely.

However, the performances with three cold white LEDs have just played a role as a methodical demonstration example of junction temperature determination, thermal transient identification and thermal map decoding in this thesis. As well, the comparison between the cooling and heating method has achieved early results with a limited amount of measured samples. In future, the junction temperature determination, the thermal transient identification and the thermal map decoding can be carried out better by the improvement of the measurement system and its software. Then, the achieved results will become more accurate, especially for partial thermal resistances and partial thermal capacitances. Moreover, the demonstration with a big enough amount of diverse measured samples is really necessary so that a higher accuracy of the cooling method and the EUCLIDEAN decoding method can be confirmed more persuadable by practical results.

6. Transient LED Model

6.1. Motivation

The investigations in Chapter 3 showed that LED properties always change as three-dimensional functions of operating temperature and forward current. Therefore, it is essential to control, optimize and stabilize LED properties for high quality solid state lighting applications such as the film and TV lighting, the shop lighting, the architectural lighting and the museum lighting. In order to achieve desired targets, a suggested LED system with a very good color sensor for the control and the optimization of some lighting quality parameters was carried out and published by HAILER and NIMZ in [63]. In that, a MAZeT true color sensor (MTCS) was applied to determine the chromaticity and other parameters such as correlated color temperature (CCT / K) of the LED system (including red, green, blue, warm white, cold white and amber LEDs called RGBWW). In addition, the controller of this LED system was able to stabilize its CCT. As well, the MTCS was calibrated by a JETI SPECBOS 1211 spectrometer as a reference. And then, the entire system was optimized for cases 2700 K, 4500 K and 6500 K at temperatures 20 °C, 50 °C and 80 °C. Finally, by means of the optimization with 108 - 114 mixed colors, the achievable accuracy of the MTCS was $\Delta u'v' < 0.0021$ for 4500 K and 6500 K, and $\Delta u'v' < 0.0057$ for 2700 K.

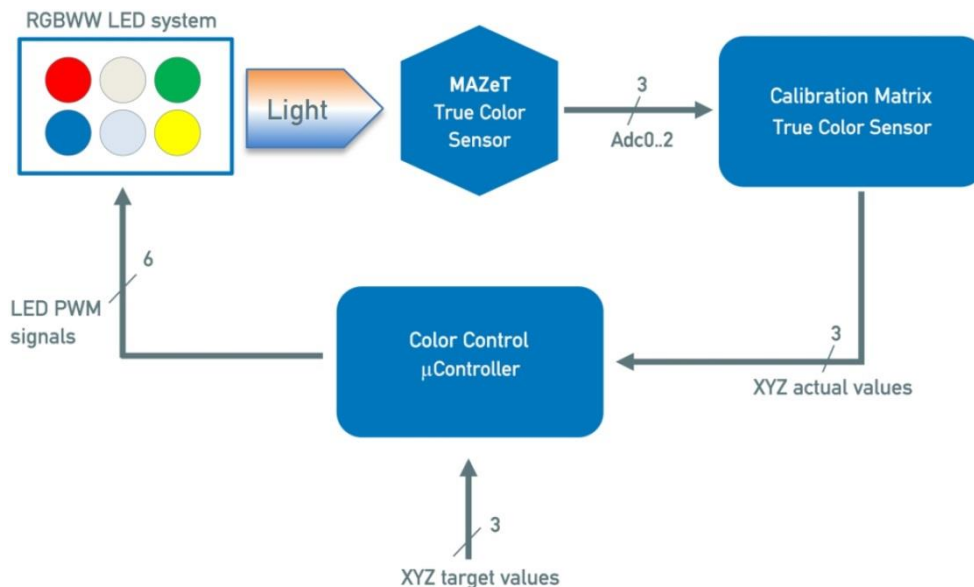


Figure 6.1 - System structure diagram of a suggested LED system with a very good color sensor for the control and the optimization of some lighting quality parameters in ([63]) as a reference example

In order to check the accuracy and the applicable ability of the MTCS for high quality solid state lighting applications, a MTCS was measured again under the angle of 10 ° and operating temperature of 25 °C. Successively, it was compared with the standard color spectra of CIE (1964). Unfortunately, the results described in Figure 6.2 showed that the difference was significant in the case of the X-curve and of the Z-curve. In more detail, the offset was really not good at the blue spectral region (380 nm - 490 nm), the green - yellow region spectral region (490 nm - 560 nm) and the deep red region (680 nm - 780 nm). The difference was only small at the orange - red spectral region (570 nm - 680 nm). Therefore, other ideas about sensorless LED systems are necessary to avoid not good enough

accuracy of color semiconductor sensors and their complicated calibration procedures, as well to enhance the reliability of the total system in a wide region of operating temperature and forward current. In addition, it can help to optimize much more LED parameters with higher accuracy and reduce the total cost of LED systems. However, sensorless LED systems need transient LED models such as electrical transient LED models or optical transient LED models with an acceptable accuracy. Consequently, in this chapter the investigation and the establishment of electrical transient LED models and optical transient LED models will be carried out in order to contribute best LED models for the above sensorless LED systems.

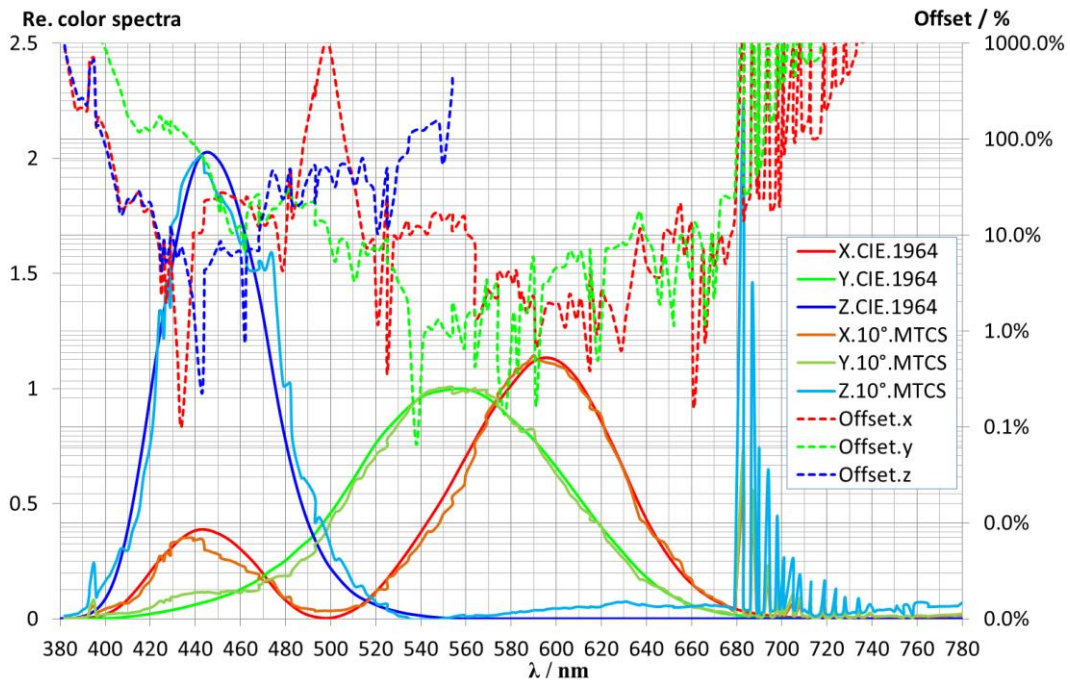


Figure 6.2 - Spectral comparison between color spectra of a MTCS sensor and the referent standard color curves (CIE, 1964) under the angle of 10° at TECHNISCHE UNIVERSITÄT DARMSTADT

6.2. General Consideration

The figures 5.1 and 5.2 in the part 5.1 of Chapter 5 described clearly about intrinsic phenomena taking place in the PC-LEDs. Consequently, the LED junction temperature and LED thermal map with an array of componential thermal resistances and componential thermal capacitances of the three cold white LEDs were measured, identified and decoded as a demonstrated example. The results are very important to be able to decouple the very complicated MIMO system structure diagram in Figure 5.1 into two simpler system structure diagrams including the multi-input single-output subsystem model (MISO subsystem) for electrical transient LED models described in Figure 6.3 and the multi-input multi-output subsystem (MIMO subsystem) for optical transient LED models described in Figure 6.4.

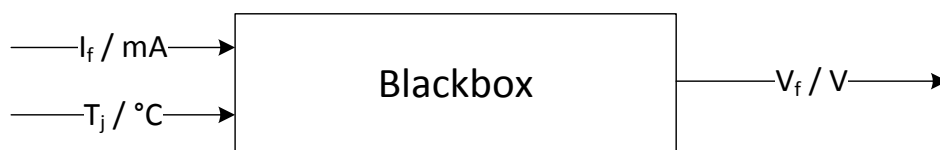


Figure 6.3 - A multi-input single-output subsystem model for electrical transient LED models



Figure 6.4 - A multi-input multi-output subsystem model for optical transient LED models

The inputs of the new subsystem models are forward current and junction temperature of LEDs, similarly. However, the output of electrical transient LED models is the forward voltage of LEDs and the output of the optical transient LED models is the absolute output spectrum of LEDs. In more detail, the electrical transient LED models and the optical transient LED models will be established in Section 6.3 and Section 6.4, respectively.

6.3. Electrical transient LED model

Electrical transient LED models were investigated and established on many aspects published in the literatures [64] - [99]. Particularly, before 1956 the main interest of electrical LED models only focused on the homo-junction in early stages of the transistor theory. Thus, the famous SHOCKLEY equation and SHOCKLEY model were also published for normal diodes in [67], [68], [69] and [70]. Since 1956, the electrical characteristics of hetero - junctions were considered much more in some reports, because the method for the growing of large area epitaxial layers of Germanium on Gallium Arsenide and Silicon substrates was discovered and proposals about wide band-gap emitters were contributed. Successively, in a long time period since 1956 to now with non-stopped technology development, approaches of transient electrical models have been always improved continuously. Therefore, in this section the theoretical approach will be described as the background knowledge for a homo - junction. Then, the modern and experimental approaches will be discussed such as the determination of hetero - junction models based on semiconductor parameters, the one of quantum well models taking account of their defect, dislocation and impurity and the one of another experimental model based on the circuit technology. Consequently, their advantages and their disadvantages will be verified. Finally, a more available modeling solution for LEDs in conventional operating regions of many solid state lighting applications will be proposed and carried out as a demonstration example.

6.3.1. Theoretical approach for an ideal diode

The theoretical approach is to mention the ideal abrupt junction that described in section 2.1.2 of Chapter 2. Particularly, it's assumed that there was no the compensation of dopants caused by unintentional impurities and defects. Thus, the ideality factor n_{ideal} equals 1 for an ideal diode. On mathematical modeling aspect, it starts with the well-known SHOCKLEY equation as follows,

$$I_f = AJ_f = I_s \left[\exp\left(\frac{eV}{n_{\text{ideal}}k_B T}\right) - 1 \right] = AJ_s \left[\exp\left(\frac{eV}{n_{\text{ideal}}k_B T}\right) - 1 \right] \quad (6.1)$$

$$J_s = e \left[\sqrt{\frac{D_n}{\tau_n}} \frac{n_i^2}{N_D} + \sqrt{\frac{D_p}{\tau_p}} \frac{n_i^2}{N_A} \right] \quad (6.2)$$

where I_f is the forward current in mA, I_s is the saturated current in mA, A is the cross-sectional area in m^2 , e is the electron charge ($\sim 1.6 \cdot 10^{-19}$ C), n_{ideal} is the ideal constant, k_B is the BOLTZMANN's constant ($\sim 1.38 \cdot 10^{-23}$ J/K), T is the absolute temperature in K, D_n is the diffusion constant of free electrons in m^2/s , D_p is the diffusion constant of free holes in m^2/s , τ_n is the lifetime of electron minority in s, τ_p is the lifetime of hole minority in s, N_D is the density of donors in cm^{-3} , N_A is the density of acceptors in cm^{-3} , $n_i = \sqrt{pn}$ is the intrinsic concentration in cm^{-3} , p is the concentration of free holes in cm^{-3} , n is the concentration of free electrons in cm^{-3} , V is the voltage at a junction in V. The space charge region has a potential called built-in voltage or diffusion voltage in V (denoted by V_0 , V_{bi} or V_D in many parts of the thesis).

$$V_0 = V_D = \frac{kT}{e} \ln\left(\frac{N_A N_D}{n_i^2}\right) \quad (6.3)$$

The width (W_D / m) of the depletion region is determined by the POISSON equation for reverse current bias state and low current forward bias state,

$$W_D = \sqrt{\frac{2\varepsilon}{e} (V_D - V_A) \left(\frac{1}{N_A} + \frac{1}{N_D}\right)} \quad (6.4)$$

Where, $\varepsilon = \varepsilon_r \varepsilon_0 = (1 + \chi) \varepsilon_0$ is the dielectric permittivity in F/m, ε_0 is the vacuum permittivity ($\varepsilon_0 \sim 8.85 \cdot 10^{-12}$ F/m), χ is the electric susceptibility of a material and V_A is the applied voltage in V into a junction. Thus, the free electron concentration (n / cm^{-3}) and the free hole concentration (p / cm^{-3}) can be determined,

$$n = N_C \text{Exp}\left(\frac{E_C - E_F}{k_B T}\right) \text{ and } p = N_V \text{Exp}\left(-\frac{E_V - E_F}{k_B T}\right) \quad (6.5)$$

Where, N_C is the effective density of states of conduction band edge in cm^{-3} , N_V is the effective density of states of valence band edge in cm^{-3} , E_C is the energy level of a conduction band in eV and E_V is the energy level of a valence band in eV. Consequently, these effective number of states can be calculated as follows,

$$N_C = 2 \left(\frac{2\pi m_{en} k_B T}{h^2}\right)^{\frac{3}{2}} M_C \quad (6.6)$$

$$N_V = 2 \left(\frac{2\pi m_{ep} k_B T}{h^2}\right)^{\frac{3}{2}} \quad (6.7)$$

Where, m_{en} and m_{ep} are the effective mass of electrons and the one of holes for each state, respectively, h is the PLANCK's constant, M_C is the number of the equivalent minima in a conduction band. Therefore, the intrinsic concentration n_i can be computed by,

$$n_i = \sqrt{N_C N_V \left\{ \exp\left(\frac{E_C - E_V}{k_B T}\right) \right\}} = \sqrt{N_C N_V \left\{ \exp\left(\frac{E_g - eV_D}{k_B T}\right) \right\}} \quad (6.8)$$

According to the conservation law of energy, the energy equivalent can be considered as,

$$eV_D - E_g + (E_F - E_V) + (E_C - E_F) = eV_D - E_g + E_C - E_V = 0 \text{ or } E_C - E_V = E_g - eV_D \quad (6.9)$$

Under the reverse bias condition, the LED current saturates and this saturation current is given by the factor preceding the exponential function in the SHOCKLEY equation 6.1 (n_{ideal} is assumed equal 1),

$$I_r = I_s [\exp(\frac{eV}{k_B T}) - 1] \text{ with } I_s = eA [\sqrt{\frac{D_n}{\tau_n}} \frac{n_i^2}{N_D} + \sqrt{\frac{D_p}{\tau_p}} \frac{n_i^2}{N_A}] \quad (6.10)$$

Under the typical forward bias condition, the LED voltage is $V_f \gg k_B T/e$ and n_{ideal} is assumed equal 1, it can be approximated by,

$$\left[\exp\left(\frac{V}{\frac{k_B T}{e}}\right) - 1 \right] \approx \exp\left(\frac{eV}{k_B T}\right) = \exp\left[\frac{e(V_A - V_D)}{k_B T}\right] \quad (6.11)$$

$$I_f = eA \left(\sqrt{\frac{D_p}{\tau_p}} N_A + \sqrt{\frac{D_n}{\tau_n}} N_D \right) \exp\left[\frac{e(V_A - V_D)}{k_B T}\right] \quad (6.12)$$

The current starts its very strong increment, when the applied voltage is equal approximately to the built-in voltage or the diffusion voltage V_D in V. Therefore, the diffusion voltage is also called threshold voltage (V_{th}/V). If the energy distance between a conduction band and a valence band ($E_C - E_V$) ~ 0 , the relationship between the band-gap energy of the semiconductor material and the diffusion voltage can be determined by,

$$V_{th} \approx V_D \approx \frac{E_g}{e} \quad (6.13)$$

The equation system from Equation 6.1 to Equation 6.13 can entirely describe and quantify the electrical phenomena taking place inside an ideal diode. However the above approximations ignored many important factors that influencing strongly the operation of real LEDs. In addition, many parameters such as diffusion constants, lifetime of hole minority and electron minority, effective masses, acceptor concentration, donor concentration, free electron concentration, free hole concentration, the number of the equivalent minima in a conduction band, dielectric permittivity and others are very difficult to be determined explicitly in the real operating conditions of LEDs. As a result, the classical and theoretical approach is to supply the fundamental perception about the electrical intrinsic nature of LEDs, but is impossible to apply good enough measures for the establishment of electrical transient LED models in reality.

6.3.2. Modern and experimental approaches

a. Correlating between semiconductor parameters of hetero - junctions and their measured V - I characteristics

In order to establish electrical transient LED models for real applications, the theoretical approach in Section 6.3.1 is not appropriate, because it only mentioned the ideal LEDs with the homo - junction with many ignored factors. In fact, almost modern LEDs are made of an abrupt junction with the form of multiple hetero - junctions in the structure of multiple quantum wells. Therefore, the phenomena taking place in the modern LEDs are very different and complicated. Therefore, at earlier attempts almost LED experts concentrated on the correlating between semiconductor parameters of hetero - junctions (also called hetero - junction models) and measured V - I characteristics of different operating regions such as reverse bias, low forward bias and low temperature, and high forward bias and high temperature.

* **An example about the correlation of the forward current model and the reverse current model with the measured V - I characteristics in different conditions for hetero - junctions:** Although many immeasurable parameters were big barriers to the establishment of hetero - junction models, the reports about this theme were published very copious in [66] and [71] - [99]. In that, the reports [72] in 1965, [74] on March 1966, [73] on September 1966, [95] in 1967, [85] and [86] in 2002, and [66] in 2005 were the valuable reports. Particularly, RIBEN and FEUCHT in [74] published their investigation and demonstration about the reverse current model and the forward current model in nGe - pGaAs hetero - junctions. The measured capacitance and the V-I characteristic of nGe-pGaAs hetero - junctions proved that the basic energy band diagram for abrupt hetero - junctions as the proposal of Anderson in [96] was essentially correct. These authors also determined the values of energy offsets ΔE_c of 0.11 eV and ΔE_v of 0.56 eV. However, unfortunately in the investigation of forward current property, Anderson model was not correct furthermore. Therefore the authors assumed that the observed functional behavior in the forward direction could be explained qualitatively on the basis of the band-to-band tunneling coupled with recombination processes. Otherwise, the reverse voltage in the report of the authors was also greater than approximately 0.5 V comparing with the calculated value of ZENER tunneling model in [97].

* **Comparison and evaluation of different hetero - junction models and proposal of available models matching current transport mechanisms:** Based on the above analysis of RIBEN and FEUCHT in [74], it can be recognized, that a hetero - junction model prediction can be correct at some points, but incorrect at some other points. Therefore, CALOW and his co-authors in [95] as well as DONNELLY and his co-authors in [73] attempted to compare between different hetero - junction models. If CALOW just reviewed theoretical aspects of four hetero - junction models such as ANDERSON's theory, PERLMAN and FEUCHT's theory, OLDHAM and MILNE's theory and VARUYVEN, PAPHENHUIJZN and VERHOVEN's theory, DONNELLY and his colleagues investigated very meticulously for real hetero - junctions and contributed many worthwhile evaluations. Indeed, six possible current transport mechanisms in n-p hetero - junctions offered by these authors were 1 - ANDERSON's model, 2 - REDIKER's model, 3 - DOLEGA's Model, 4 - Model applicable for nGe-pGaAs junction, 5 - Model applicable for pGe-nGaAs, nGe-pSi and pG-nSi junctions and 6- another form of the 5-Model. Successively, based on the practical investigations, the authors assumed that the models from 1 - 4 for nGe-pGaAs were only explained successfully for different aspects of the forward characteristics of pGe-nGaAs diodes by means of a multistep recombination - tunneling model form. Consequently, these authors proposed the fifth model for cases of pGe-nGaAs, nGe-pSi and pGe-nSi junctions. Based on these models, the tunneling current flowed in the Germanium, while the diffusion current that recombines at the interface flowed in the wide-gap material. In addition, these currents that flowed in series are related by interface-state parameters.

However, up to that time no available mathematical model was proved practically so that it was really good enough for reverse current models, low forward current models and high forward current models. For that reason, DUMIN and PEARSON in their report about the properties of Gallium Arsenide diodes between 4.2 K and 300 K in [72] measured the forward and reverse current characteristics in zinc-diffused GaAs diodes. The range of the doping density of the parent varied from $6.1 \cdot 10^{15} \text{ cm}^{-3}$ to $9.4 \cdot 10^{18} \text{ cm}^{-3}$. And the various dopants on the n-side were also controlled. As a result, the investigation of these authors proved that with the temperature range of 4.2 K - 300 K the reverse current had the functional form of a tunneling current defined by MOLL in [98].

$$I_r = A \frac{\sqrt{2}e^3 m_T^{1/2} V_A \bar{E}}{4\pi^3 \hbar^2 e^{1/2} V_g^{1/2}} \exp\left(-\frac{\pi m_T^{1/2} \epsilon_g^{3/2}}{2\sqrt{2}e\hbar \bar{E}}\right) \quad (6.14)$$

where, J_r is the reverse current density, e is the electronic charge, m_T is the effective tunneling mass, V_A is the applied voltage, \bar{E} is the electric field of a junction region, \hbar is the PLANCK's constant divided by 2π , V_g is the energy gap and \mathcal{E}_g is the height of an energy barrier in electron volts which under reverse bias is the energy gap. The effective tunneling mass was suggested by KELDYSH in [99] that $m_T^{-1} = m_{en}^{-1} + m_{ep}^{-1}$. The electric field of a step junction was written as its maximum value of $E = 2(V_g - V_A)/\varepsilon$, where ε is dielectric constant ($\sim 12.5\varepsilon_0$ in the case of GaAs). Otherwise, forward current was generally dominated by thermal recombination in a space charge region at high temperatures and low doping densities like that determined by Equation 6.12. Contrarily, at lower temperatures and higher doping densities forward current also has a functional form of a tunneling current by a tunneling mechanism. This approach was also prompted by observation of the direct band-to-band tunneling at low voltages and low temperatures. The determination of the tunneling current in these cases was described by the following equations.

$$I_T = AB \exp(\delta V_A) \quad (6.15)$$

$$B = J_T \exp\left[(-\pi m_T^{\frac{1}{2}} V_D \varepsilon^{\frac{1}{2}}) / (4\hbar N_D^{\frac{1}{2}})\right] \quad (6.16)$$

$$\delta = (\pi m_T^{\frac{1}{2}} \varepsilon^{\frac{1}{2}}) / (4\hbar N_D^{\frac{1}{2}}) \quad (6.17)$$

Finally, these authors contributed a definition with matching mathematical equation of the effective low temperature (T_{eff}/K) for step junctions. And at a fixed diode current the variation in voltage across the step junction GaAs diodes of the doping density of 10^{18} cm^{-3} or greater was almost linear with the temperature from 4.2 K to the effective low temperature. In addition, the effective temperature was near room temperature (25 °C) for this specific diode type.

* **Conclusion:** Based on the progress of hetero - junction models in the above mentions, it can be concluded that: Firstly, a reverse current is dominated by a tunneling current transport mechanism and quantified quite well by the equation of MOLL in 6.14. Secondly, at a low bias and a low temperature, a forward current is also dominated by a tunneling current and can be determined in the form of Equation 6.15. In this case, its property depends very poorly on temperature and its symptom can be observed by means of ideality constant. Particularly, an ideality constant becomes an unrealistic number if the property V - I is fitted following to the mathematical form like Equation 6.1. Thirdly, at high biases and high temperatures, thermal diffusion recombination is the main process. And it is characterized like Equation 6.12 with the ideality constant in the range of 1 and 2. Fourthly, different hetero - junction models with different current transport mechanisms are strongly dependent on the inside semiconductor compositions and outside operating conditions.

b. Defect, dislocation and impurity in multiple quantum wells of modern LEDs and their V-I characteristics

The above results have still not been completed, because the researched objects were only single or double hetero - junctions, and influences of the defect, the dislocation and the impurity were not contemplated. Consequently, assuredly the current transport mechanism through an abrupt junction of modern LEDs with multiple quantum well structures must be much more complicated. Fortunately, until the end of 1990s and the beginning of 2000s the atomic force microscope (AFM) and the cross-sectional transmission electron microscopy (TEM) were developed and used widely in the investigation of semiconductor LED properties. Indeed, the authors CAO, STOKES and co-authors in [85] and [86] published the results about diffusion and tunneling currents in GaN/InGaN multiple quantum well LEDs and influences of defects on the electrical characteristics of GaN/InGaN-based LEDs. Particularly, their TEM images of two different LEDs were published like described in Figure 6.5. Based on these

images, bending of the dislocation, the surface V-defect or the “internal” V-defect in the semiconductor layers of the LEDs was observed visually supporting conveniently for analysis of current transport mechanisms. Hence, by the combination between the mathematical indication by means of ideality constant and the visual observation of AFM and TEM images, the strong correlation between the epitaxial quality of GaN/InGaN LEDs and their performance was able to be discovered. Likewise, the relationship between the high density of microstructural defects and the radiate / non-radiate tunneling current transport across a p-n junction was also able to be verified. In addition, these authors also confirmed that the thermal diffusion - recombination was still the main carrier injection mechanism in these LEDs. As well, the non-radiate recombination centers of these LEDs were saturated at the very low current level. The Screw and mixed dislocation as the non-radiate centers in the InGaN/GaN quantum wells mentioned in [82] or the pit formation in the GaInN quantum well mentioned in [80] were assumed to have their contributions to some carrier tunneling and recombination channels in defective LEDs.

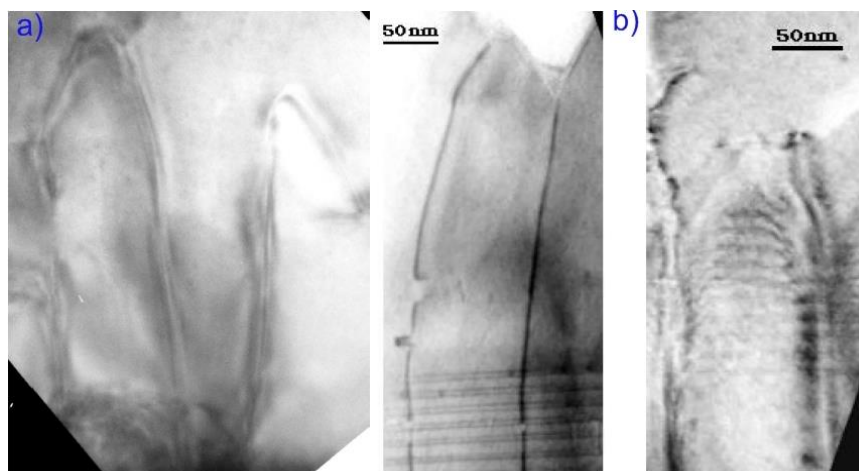


Figure 6.5 - a) Bending of dislocation b) Surface V-defect (left) and “internal” V-defect (right) ([85])

c. An experimental model for the LED applications based on the circuit technology

The above researches outlined in abundance about electrical operations in the semiconductor layers inside LEDs. However, accurate qualification was really very difficult, because there were too many immeasurable parameters about minority carriers in too tiny charge spaces. Contrarily, only two applicable measures were measured $V-I$ characteristics and EFM / TEM images. Therefore, the attempt for correlating between captured results by two above measures and prediction hetero-junction models were unfeasible. Therefore, the above researches should be only used to orientate for more feasible modeling methods. As good agreement with this idea, BAUREIS in [66] applied the above orientation of the tunneling current model for low bias, the one of the defect, dislocation and impurity with unrealistic ideality constants for low currents and low temperatures, and the one of the diffusion-recombination current model for high biases and high temperatures with the ideality constant of 1 for the diffusion component and 2 for the limited space-charge recombination. Particularly, small signal scattering (S) parameters with the high frequency technique (> 50 MHz) was used in the accurate determination for model parameters. Thus, the transient electrical model was established based on this idea described in Figure 6.6, where parameters C_1 and C_2 were to quantify for the capacitive coupling of the diode under the test to ground plane of the test fixture, parameter L_s was to describe for the bond wire and package inductance, parameter R_s was for the series resistance, parameter C_j was for combination of the diffusion and junction capacitance, parameter R_j was for the differential junction resistance, and parameters L_{skin} , R_{skin} and k were to take account for the skin effect. Based on the measured and simulated results, the author could determine model parameters listed in Table 6.1.

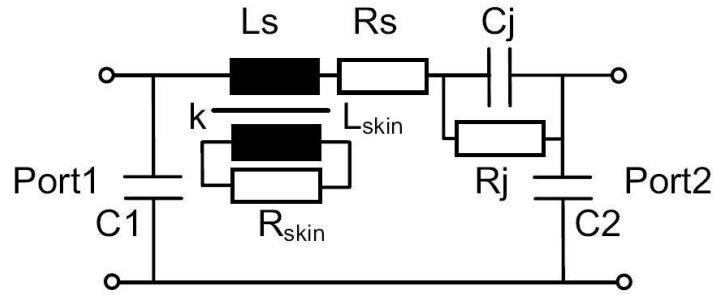


Figure 6.6 - Small signal equivalent circuit matching an InGaAlP LED at the forward current of 0.9 mA ([66])

Table 6.1 - Parameters of the BAUREIS LED model established by means of the high frequency technique ([66])

R_s / Ω	1.59	C_1 / fF	150	$L_{\text{skin}} / \text{nH}$	1.00
L_s / nH	1.72	C_2 / fF	330	R_{skin} / Ω	15.0
C_j / pF	76.2	R_j / Ω	72.3	K	0.25

d. Summary

A big number of electrical LED models for forward current, reverse current and influences of the inside defect/dislocation/impurity of LEDs in different operating regions were investigated and published. But unfortunately, there was generally no good agreement for them in practical operations. Some of them were correct for some points, but were incorrect for other points. Consequently early attempts for the correlation between mathematical parameters with poor measured results were really unfeasible for solid state lighting applications. Finally, in order to achieve applicable models, the electrical transient LED model with the small signal equivalent circuit form was established by the BAUREIS. Despite the high frequency small signal measurement was not easy, the idea of the small signal equivalent circuit for the electrical transient LED model was also very meaningful in LED modeling progress. However, the region covered by this model was quite narrow and not available in the reverse direction and in the high current region. Therefore, a more available proposal for electrical transient LED models in a conventional limited operating region of forward current and junction temperature is really necessary to be established in the next section.

6.3.3. Experimental proposal of the limited electrical transient LED model

Section 6.3.1 started with the theoretical approach for an ideal diode with homo - junctions in order to have background knowledge about LED electrical property. Successively, Section 6.3.2 discussed about modern and experimental approaches with tunneling models, the defect/dislocation/impurity inside LEDs and the high frequency small signal equivalent circuit LED model. However, unfortunately the above approaches are difficult to apply to solid state lighting applications, because of their immeasurable parameters and feasibility. Therefore, in this section the experimental proposal of the limited transient LED models will be described and carried out.

* **Limited operating region:** The conventional operating region of high power LEDs should be practically defined. Particularly, for normal LEDs in solid state lighting applications, their operating current is usually about 150 mA - 1000 mA and their operating temperature is about 40 - 100 °C. In order to achieve a higher accuracy for LED modeling, this operating region can widen a little including the operating current region of 100 - 1000 mA and the operating temperature region of 25 - 100 °C. And the reverse region, low voltage region (below 100 mA) and low temperature region (under 25 °C) are not necessary to be contemplated for the modeling in this section.

* **Mathematical description of the LED forward current in the limited operating region:** Like the content described in Section 6.3.2.a, in the above defined operating region the thermal diffusion - recombination is the predominant carrier transport mechanism. Other mechanisms can be ignored. Thus, the matching mathematical descriptions for the LED forward current in the limited operating region in Equation 6.1 and Equation 6.12 are available and can be rewritten as follows,

$$I_f = eA \left(\sqrt{\frac{D_p}{\tau_p}} N_A + \sqrt{\frac{D_n}{\tau_n}} N_D \right) \left\{ \exp \left[\frac{e(V_A - V_D)}{n_{ideal} k_B T} \right] \right\} \quad (6.18)$$

$$I_f = I_s \left\{ \exp \left[\frac{e(V_A - V_D)}{n_{ideal} k_B T} \right] \right\} \quad (6.19)$$

Processing Equation 6.19, its new mathematical form can be achieved,

$$V_A = \left[\frac{n_{ideal} k_B}{e} \right] T_j \ln(I_f) + \left[\frac{273.15 \ln(I_s) n_{ideal}}{e} \right] \ln(I_f) - \left\{ \left[\frac{n_{ideal} k_B}{e} \right] \ln(I_s) \right\} T_j + \{V_D - \left[\frac{273.15 \ln(I_s) n_{ideal}}{e} \right] \ln(I_s)\} \quad (6.20)$$

$$V_f = V_A = a T_j \ln(I_f) + b \ln(I_f) - c T_j + d \quad (6.21)$$

$$a = \left[\frac{n_{ideal} k_B}{e} \right] \quad (6.22)$$

$$b = \left[\frac{273.15 \ln(I_s) n_{ideal}}{e} \right] \quad (6.23)$$

$$c = \left\{ \left[\frac{n_{ideal} k_B}{e} \right] \ln(I_s) \right\} \quad (6.24)$$

$$d = \{V_D - \left[\frac{273.15 \ln(I_s) n_{ideal}}{e} \right] \ln(I_s)\} \quad (6.25)$$

The meaning of the symbols in the above equations was explained in Section 6.3.1. In addition, for the determined specific semiconductor structure in the defined operating region, the parameters a , b , c and d can be assumed as constants. Moreover, based on Equation 6.20, it can be recognized, that the forward voltage of LEDs had a linear mathematical form with junction temperature T_j in °C, a logarithmic mathematical form with forward current I_f in mA and a first order twisted term with both T_j and $\ln(I_f)$.

* **An example for the establishment of the limited electrical transient LED model:** In order to prove for above conclusions, 20 cold white LEDs (5000 K) belonging to the cold white LED type that has described in Section 5.3.3.a in Chapter 5, were used again here to measure and determine their junction temperature, their forward voltage and their forward current. From this measurement, the relationship between the forward voltage and the junction temperature of 20 cold white LEDs with the minimal, average, maximal values and the 95 % confidence offset was shown in Figure 6.7. Likewise, the functional coupling between the forward voltage and the forward current of the 20 cold white LEDs with the minimal, average, maximal values and 95 % confidence offset was illustrated in Figure 6.8.

Visually, the results shown in Figure 6.7 and Figure 6.8 had a very good agreement with mathematical forms in Equation 6.21. Thus, it can be confirmed, that the concentration on a simple mathematical form with a feasible measurement in the defined operating region was really a good solution to solve

troubles, which happened in many approaches mentioned in the above sections. Finally, based on measured results of junction temperature, forward current and forward voltage, and the mathematical form described in Equation 6.21, the experimental electrical transient LED model for the cold white LEDs can be established for the real performance and limited in the defined operating region. Particularly, the experimental electrical transient LED model for the cold white LEDs in the three-dimensional form was carried out and shown in Figure 6.9. As well, its parameters were listed in Table 6.2.

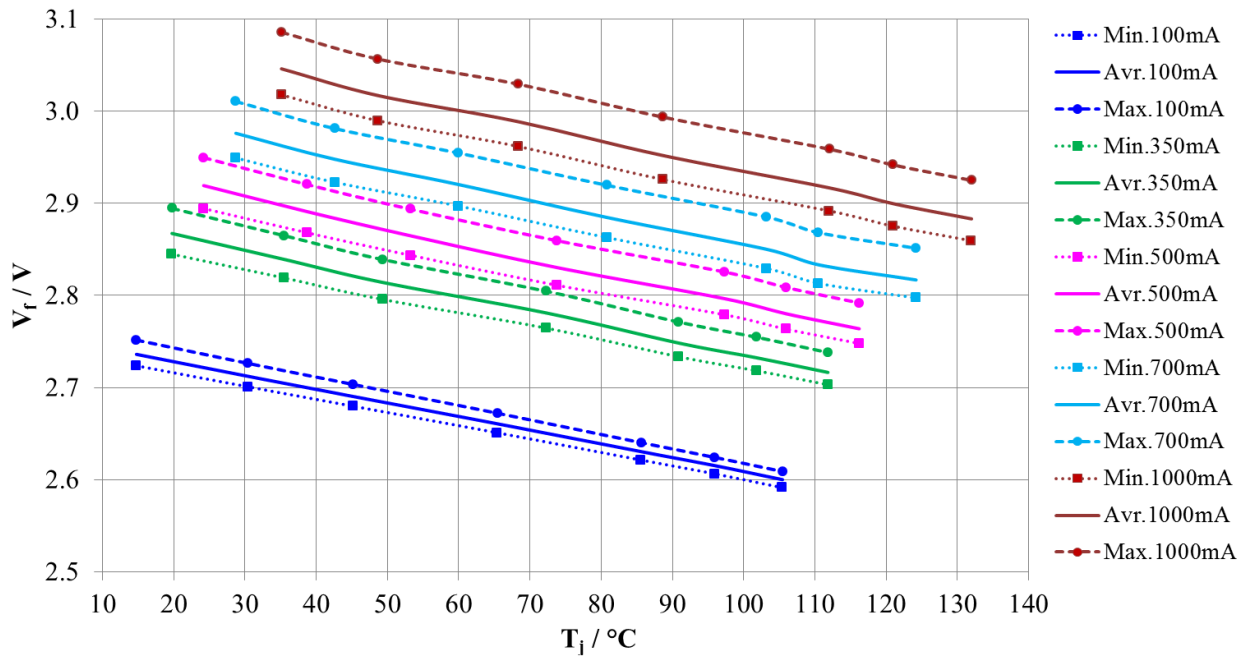


Figure 6.7 - Nearly linear functional relationship between forward voltage and junction temperature with minimal, average, maximal values and 95 % confidence offset of 20 similar cold white LEDs (5000 K)

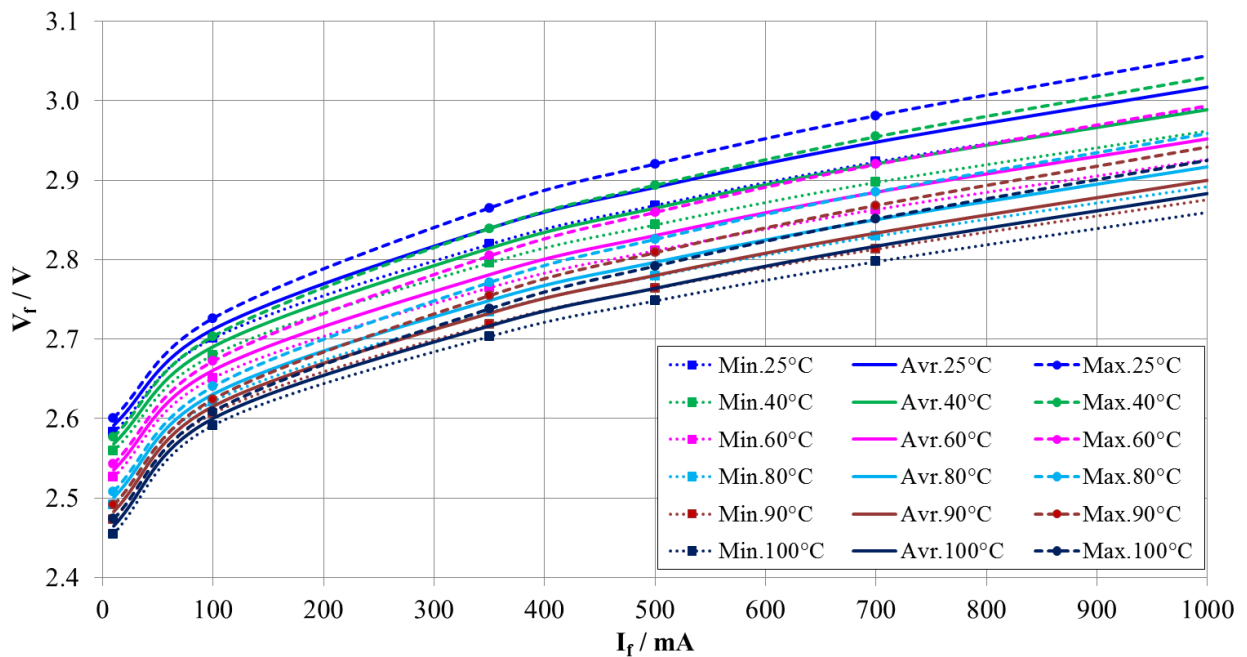


Figure 6.8 - Logarithmic functional relationship between forward voltage and junction temperature with minimal, average, maximal value and 95 % confidence offset of 20 similar cold white LEDs (5000 K)

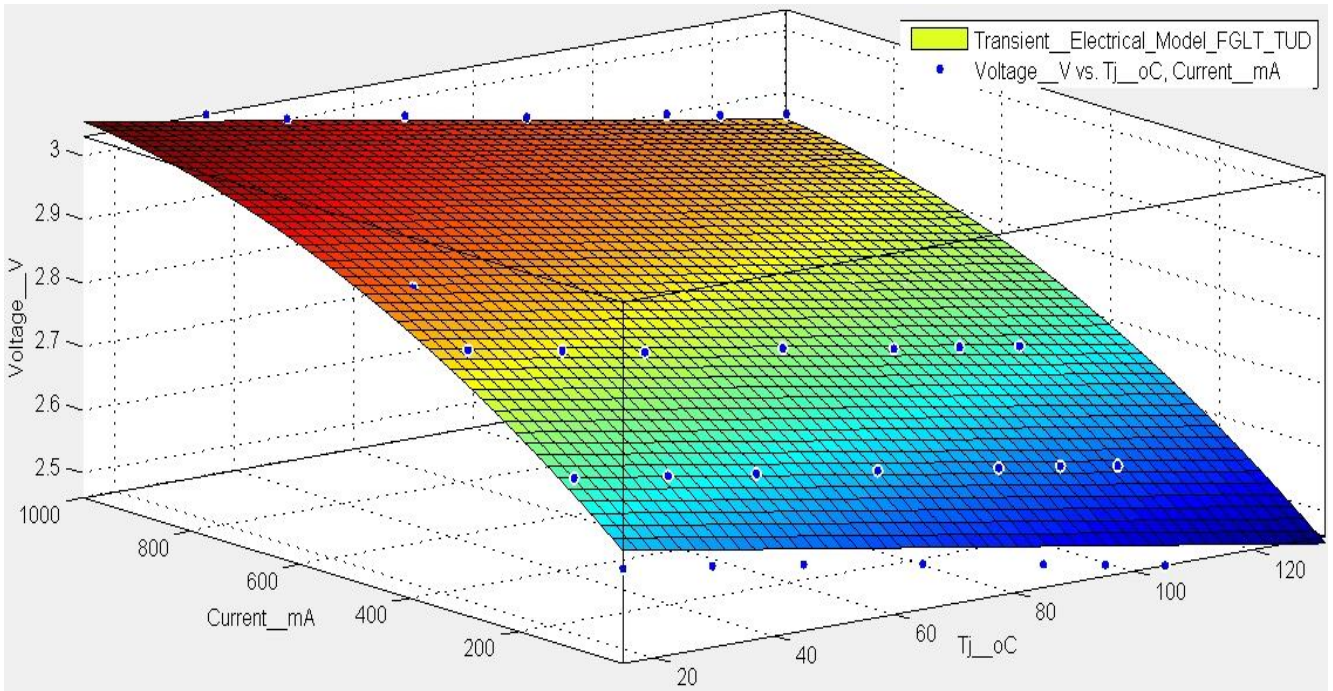


Figure 6.9 - Three-dimensional electrical transient LED model and measured values of cold white LEDs

* **Evaluation and improvement of the experimental electrical transient LED model:** Based on the result in Figure 6.9, it can be recognized, that the logarithmic relationship between forward voltage and forward current as well as the twisted term with both T_j and $\ln(I_f)$ of the cold white LEDs were quite small. Therefore, the twisted term can be ignored and the logarithmic relationship can be approximated by a simple second order polynomial equation. Consequently, Equation 6.21 can be replaced by the approximated and decoupled equation, which is more convenient for control algorithms in microcontrollers, as follows,

$$V_f = aT_j + bI_f^2 + cI_f + d \quad (6.26)$$

Parameters of the experimental electrical transient LED model for the cold white LEDs in the defined operating region with the standard form described in Equation 6.21 and in the approximated form described in Equation 6.26 were listed in the following table.

Table 6.2- Parameters of the standard model and approximated model

Parameters	Standard model parameters	Approximated model parameters
a	$1.134 \cdot 10^{-4}$	$-1.637 \cdot 10^{-3}$
b	$8.329 \cdot 10^{-2}$	$-3.287 \cdot 10^{-7}$
c	$2.077 \cdot 10^{-3}$	$7.465 \cdot 10^{-4}$
d	2.421	2.657
R_{square}	0.9238	0.9807

The results in Table 6.2 showed that the approximated electrical transient LED model with the simple second order polynomial equation had the R-square quality of 98.07 %, which was even better than that of the standard transient LED model, because strong influences of the electrical circuit factors such as the serial resistance and others mentioned in the LED model of BAUREIS in Figure 6.6 were not taken into account and treated appropriately in the standard transient LED model. Finally, the above experimental proposal of the limited electrical transient LED model with the approximated model form can be applied similarly to other LED types in solid state lighting applications.

6.4. Optical transient LED model

Similarly to the content mentioned in Section 6.3.1, the predominant carrier transport in the defined operating region is diffusion-recombination. Queries are how the relationship between diffusion-recombination current and radiant spectra of blue semiconductor LEDs is and consequently, how the relationship between these original spectra with final output white spectra of PC-LEDs is? Particularly, two successive spectral conversions in PC-LEDs are necessary to be studied and quantified appropriately. Then, based on these described relationships, optical transient models will be able to be established for solid state lighting applications.

6.4.1. General Consideration

If Figure 5.1 in Chapter 5 is separated into smaller and more particular components, Figure 6.10 is a good component to describe the spectral changes and influencing factors in PC-LEDs. In addition, the system block diagram for the separated optical transient LED model in Figure 6.4 showed that an optical transient LED model is a MIMO system. In that, its two inputs are forward current and junction temperature. Its outputs are spectral components of PC-LEDs. Conventionally, an output spectrum can be characterized by three parameters including peak wavelength (λ_p / nm), full width at half maximum (λ_{FWHM} / nm) and peak intensity (S_p / W/nm).

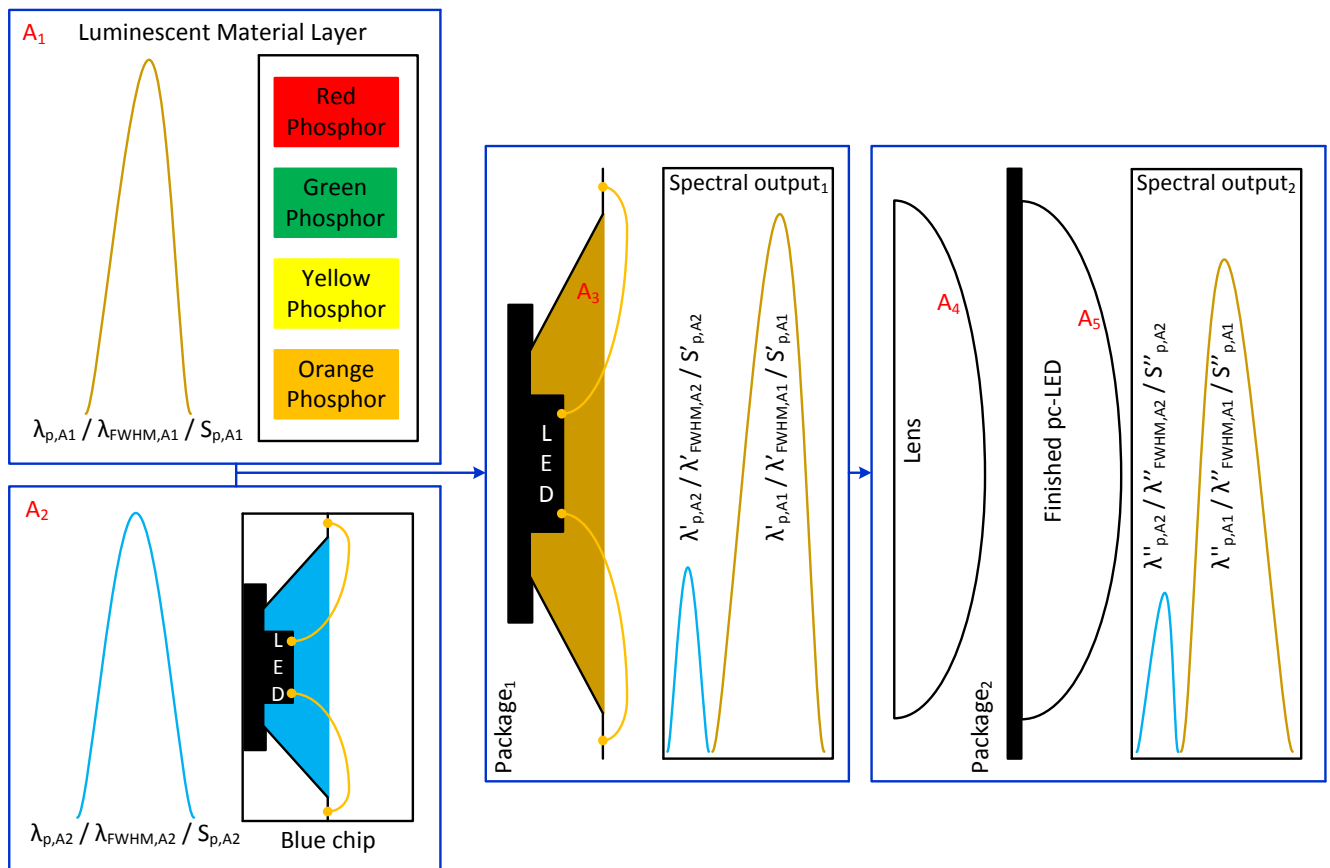


Figure 6.10 - Spectral changes and influence factors in PC-LEDs

However, in reality phenomena take place more complicatedly. Firstly, blue semiconductor LED chips play a role as a primary light source to “pump” an original blue spectrum described by three parameters peak wavelength ($\lambda_{p,A2}$ / nm), full width at half maximum ($\lambda_{FWHM,A2}$ / nm) and peak intensity ($S_{p,A2}$ / W/nm). The first spectral conversion of electrical energy in these blue chips into optical energy is the first MIMO sub-system. Secondly, the radiant spectra of phosphors play a role as a

secondary light source indicated by three other parameters ($\lambda_{p,A1}$, $\lambda_{FWHM,A1}$ and $S_{p,A1}$). In the phosphor layer, the second spectral conversion from the original blue spectrum into the phosphor spectrum is the second MIMO sub-system. Successively, at the first package step, the phosphors are mixed together and packed with the blue chips with a specific capsule geometry. Therefore, the output white spectrum is the sum of the rest blue spectrum and the new radiate spectra of phosphors. Due to internal chemical, physical, mechanical reactions between phosphors each other, and between phosphors and the blue chip, the original blue spectrum and the original phosphor spectra are changed into the new spectral forms indicated by three new parameters ($\lambda'_{p,A2}$, $\lambda'_{FWHM,A2}$ and $S'_{p,A2}$) for the new blue spectral component and three other new ones ($\lambda'_{p,A1}$, $\lambda'_{FWHM,A1}$ and $S'_{p,A1}$) for the new phosphor spectral component. Consequently, this process can be assumed as the third MIMO sub-system. Thus, at this third step the total white spectrum must be described by six parameters $\lambda'_{p,A1}$, $\lambda'_{FWHM,A1}$, $S'_{p,A1}$, $\lambda'_{p,A2}$, $\lambda'_{FWHM,A2}$ and $S'_{p,A2}$. Fourthly, the total white spectrum must go through an optical conduction system such as lens and other optical elements. As a result, the final output white spectrum becomes another spectral form specified by six other parameters $\lambda''_{p,A1}$, $\lambda''_{FWHM,A1}$, $S''_{p,A1}$, $\lambda''_{p,A2}$, $\lambda''_{FWHM,A2}$ and $S''_{p,A2}$. Hence, we have the fourth MIMO sub-system. Finally, the conversion of input electrical energy to final output white spectrum are very complicated including several electrical, thermal and optical processes influenced by diverse chemical, physical and geometrical factors.

Practically, if packaging technology factors at the third and fourth spectral conversion steps are assumed as system constants, the MIMO system of optical transient LED models only includes the first MIMO sub-system and the second MIMO sub-system. As well, the first MIMO sub-system is the first spectral conversion from input conditions (forward current and junction temperature) to the original blue spectral form that was described in Section 2.1.5 in Chapter 2. The second MIMO sub-system is the second spectral conversion from the original blue spectrum to the white spectrum under a specific operating condition that was described in Section 2.2.3 in Chapter 2. Individually, in a color semiconductor LED, only the first MIMO sub-system takes place and its output spectrum is a specific color spectral form such as red, green, blue, orange or amber spectrum.

6.4.2. Overview of the optical transient LED models of color semiconductor LEDs and white PC-LEDs.

The spectral power distribution of LEDs is the important characteristic to determine luminous flux, chromaticity, color quality and many other optical parameters. Therefore, since about 2005, there were some publications studying this theme. Until now there were two main approaches including a purely mathematical approach and a combination approach between mathematical descriptions and the physical nature of LEDs.

a. Mathematical approach

* **GAUSSIAN function:** At the beginning on purely mathematical approach, the authors in [101] and [102] assumed that the first order GAUSSIAN function could describe LED spectra. This function related peak wavelength (λ_p / nm) and full width at half maximum (λ_{FWHM} / nm) as follows,

$$S(\lambda_p, \lambda_{FWHM}, \lambda) = \exp\left\{\frac{-2.7725(\lambda - \lambda_p)^2}{\lambda_{FWHM}^2}\right\} \quad (6.27)$$

This GAUSSIAN function has been used continuously until now in many documents writing about LED spectra, although its simulating quality is not good enough. In addition, the current dependence and temperature dependence of the parameters of spectral LED models were not completely reflected in this approach.

* **Developing approaches from the original idea of GAUSSIAN function:** Theoretical background about a LED spectral power distribution was described in Section 2.1.5 in Chapter 2. In that, the equations 2.38 and 2.39 determined qualitatively that a spectral LED power distribution is asymmetric. Indeed, there was a big difference between the left-side and the right-side of a LED spectrum. If the left-distribution has the form of a square root ($S_{\text{left}}(E) \sim \sqrt{E - E_g}$), the right-distribution has an exponential form ($S_{\text{right}}(E) \sim e^{-E/(kT_j\alpha)}$). Thus, the rising edge of the left-distribution is faster, while the falling edge of the right-distribution is slower. Oppositely, the GAUSSIAN functions were always symmetric mathematical forms. Therefore, the authors in [103], [104] and [105] attempted to develop from the original idea of the GAUSSIAN function into new more realistic forms. Particularly, the authors in [105] supported a double GAUSSIAN function with two sets of parameters including the first set of the first spectral power (P/W), the first peak wavelength (λ_p/nm) and the first full width at half maximum ($\lambda_{\text{FWHM}}/\text{nm}$) and the second set of the second spectral power (P'/W), the second peak wavelength (λ'_p/nm) and the second full width at half maximum ($\lambda'_{\text{FWHM}}/\text{nm}$). All the parameters were functions of both junction temperature and forward current. The estimated $M \times N$ spectral matrix \tilde{S} for color semiconductor LEDs can be described as follows,

$$\tilde{S} = G + G' \quad (6.28)$$

where, $G = (gg_1, gg_2, \dots, gg_M)^T$ and $G' = (gg'_1, gg'_2, \dots, gg'_M)^T$ are GAUSSIAN spectral matrices. And the matrix G had M spectral vectors gg with N sampling wavelengths. From the n^{th} point of m^{th} row vector gg_m (denoted by gg_{mn}), its value could be determined as,

$$gg_{mn} = p_m \exp\left\{-\frac{[\lambda_n - (\lambda_p)_m]^2}{(\lambda_{\text{FWHM}})_m^2}\right\} \quad (6.29)$$

Parameters p_m , $(\lambda_p)_m$, and $(\lambda_{\text{FWHM}})_m$ mentioned to the m^{th} power, the m^{th} peak wavelength and the m^{th} full width at half maximum, whose values could be obtained by satisfying the minimization in Equation 6.30.

$$\arg \min [|S_m - \tilde{S}_m|^2, \{p_m, (\lambda_p)_m, (\lambda_{\text{FWHM}})_m, p'_m, (\lambda'_p)_m, (\lambda'_{\text{FWHM}})_m\}] \quad (6.30)$$

Where, s_m and $\tilde{s}_m = gg_m + gg'_m$ are the m^{th} row vectors of S and \tilde{S} , respectively. In order to evaluate the accuracy in this approach, the simulated and measured spectra of the green semiconductor LED (a) and the PC-LED (b) were compared together in Figure 6.11.

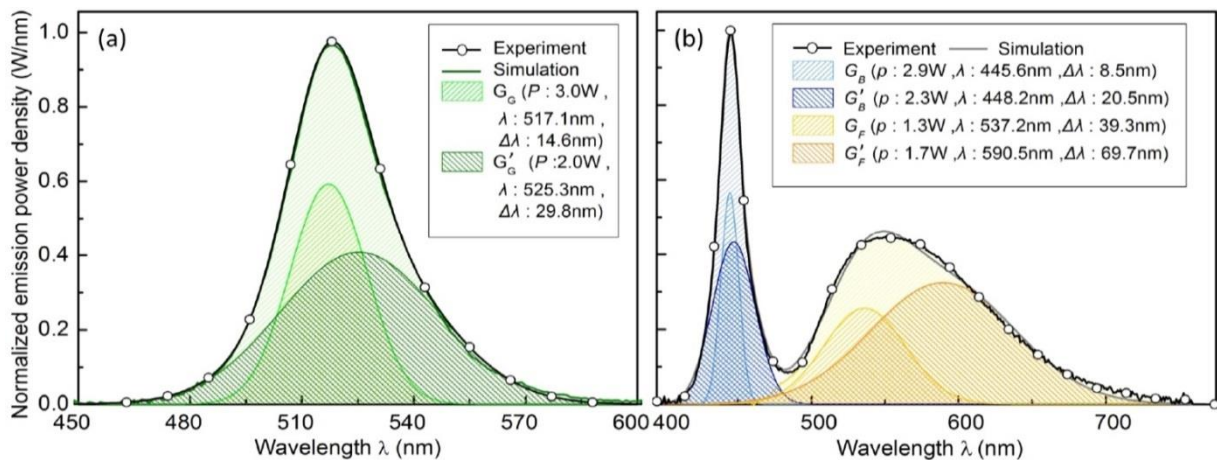


Figure 6.11- Description of the double GAUSSIAN model for the green semiconductor LED (a) and the white PC-LED (b) at $T_j=25^\circ\text{C}$ and $I_f=350\text{ mA}$. For the PC-LED, the blue and phosphor spectral components were individually considered by two double functions G_B and G'_B and G_F and G'_F , respectively according to ([105])

In Figure 6.11, it can be recognized, that the authors performed the idea of spectrum matrix with 12 data sampling points for the green semiconductor LED and 20 data sampling points for the PC-LED. Particularly, in Figure 6.11.a, the spectrum of the green semiconductor LED at T_j of 25 °C and I_f of 350 mA was described by two GAUSSIAN elements. The first GAUSSIAN element G_G had a power of 3 W, peak wavelength of 517.1 nm and full width at half maximum of 14.6 nm. The second GAUSSIAN element G'_G had a power of 3 W, peak wavelength of 525.3 nm and full width at half maximum of 29.8 nm. Otherwise, in Figure 6.11.b, the spectrum of the PC-LED at T_j of 25 °C and I_f of 350 mA was described by fours GAUSSIAN components. In fact, the original spectrum of the PC-LED was separated into two main spectral components. The first component was blue spectral component modeled by two GAUSSIAN elements (G_B with power of 2.9 W, peak wavelength of 445.6 nm and full width at half maximum of 8.5 nm, and G'_B with power of 2.2 W, peak wavelength of 448.2 nm and full width at half maximum of 20.5 nm). The second component was the phosphor spectral component modeled by two other GAUSSIAN elements (G_F with power of 1.3 W, peak wavelength of 537.2 nm and full width at half maximum of 39.3 nm, and G'_F with power of 1.7 W, peak wavelength of 590.5 nm and full width at half maximum of 69.7 nm). Finally, the results in Figure 6.11 showed visually that the offset between the simulated and measured spectrum for the green semiconductor LED could be accepted, but the difference for the PC-LED was remarkable.

Furthermore, in [105] the authors approached to the matrix solution of LED spectra, because there was sometime no functional correlation between parameters of double GAUSSIAN functions and junction temperature and forward current, experimentally. However, the query was established how big the spectrum matrix ($M \times N$) good enough for the LED spectral approximation is, was not contemplated appropriately. But in the performance of these authors, the 12 data sampling points for the green semiconductor LED and the 20 data sampling point for the PC-LEDs only played the role as the demonstration examples. In order to solve this trouble, the other authors in [103] approached to the split GAUSSIAN function with different exponential behaviors on each side of LED spectra. And the chosen objects were color semiconductor LEDs. Moreover, these authors assumed that the possible functions should meet several requirements. Particularly, they must have appropriate shapes and parameterizations, available measured spectral values with a good accuracy and can be evaluated easily. As well, their parameters must be simply interpreted from a spectral measurement. Thus, the main target of these authors was that model parameters of spectral functions should have a functional correlation with the junction temperature and forward current. Consequently, the mathematical forms compared by the authors were listed in Table 6.2.

For the mathematical forms in Table 6.2, the authors in [103] assumed that the functions 1 - 4 should be ignored because they were symmetric. The function 10 approximated the spectra very well, but its parameters could not be interpreted directly. In addition, this function was defined piecewise and could not be extended for varying temperatures and currents. Thus, it was not suitable to be selected for the modeling. Other forms, which considered to the asymmetry of LED spectra, were split equations with two ranges - one for the left side and one for the right side of LED spectra like that done with Function 2 and Function 8. However, unfortunately these mathematical forms were too cumbersome for the optimization and they were not continuously uniform. Otherwise, in Function 9 two skew parameters were used, but these parameters could not be also interpreted. Experimentally, the authors confirmed mathematically that only functions 5, 6 and 7 were eligible. Especially, their parameters A and C could be interpreted directly as intensity and peak wavelength, respectively. Then, varied LEDs with different semiconductor material systems were investigated practically for these mathematical forms. Finally, the authors concluded that the function 5 was the most suitable for the approximation

of color semiconductor LED spectra. Particularly, the function 5 with its extension can be rewritten as follows,

$$f(\lambda) = \frac{A}{S} \left(1 + e^{\frac{\lambda-C+W \ln(S)}{W}}\right)^{\frac{-S-1}{S}} \left\{e^{\frac{\lambda-C+W \ln(S)}{W}}\right\} (S+1)^{\frac{S+1}{S}} \quad (6.31)$$

$$A(T_j, I_f) = a_0 T_j^{a_T} I_f^{a_I} \quad (6.32)$$

$$C(T_j, I_f) = c_0 + c_T T_j + c_I \log(I_f) \quad (6.33)$$

$$S(T_j, I_f) = s_0 + s_T T_j + s_I \log(I_f) \quad (6.34)$$

$$W(T_j, I_f) = w_0 + w_T T_j + w_I I_f \quad (6.35)$$

The accuracy of the experimental equation 6.31 was proved by the comparison between the simulated and measured spectral results at 10 mA and 76.8 °C, and 20 mA and 104.7 °C in Figure 6.12. Consequently, the spectral results in Figure 6.12 showed that the mathematical form in Equation 6.31 was very good for the spectral approximation of color semiconductor LEDs. However, similar to [103], [104] and [105] the approximation of LED spectra were carried out pure mathematically. Therefore, Section 6.4.2.b will describe the combination approach between the mathematical form and physical nature of color semiconductor LEDs in order to test for a more available solution.

Table 6.2 - Examined approximation functions by the authors in ([103])

Ord.	Name	Function f(λ)
1	GAUSSIAN	$f(\lambda) = A e^{-\left(\frac{\lambda-C}{W}\right)^2}$
2	Split GAUSSIAN	$f(\lambda) = A e^{-\left(\frac{\lambda-C}{W}\right)^2}$ with $W=W_1$, for $\lambda < C$ and $W=W_2$ otherwise
3	Sum of GAUSSIAN	$f(\lambda) = A_1 e^{-\left(\frac{\lambda-C_1}{W_1}\right)^2} + A_2 e^{-\left(\frac{\lambda-C_2}{W_2}\right)^2}$
4	Second Oder LORENTZ	$f(\lambda) = \frac{A}{\left(1 + \left(\frac{\lambda-C}{W}\right)^2\right)^2}$
5	Logistic Power Peak	$f(\lambda) = \frac{A}{S} \left(1 + e^{\frac{\lambda-C+W \ln(S)}{W}}\right)^{\frac{-S-1}{S}} \left\{e^{\frac{\lambda-C+W \ln(S)}{W}}\right\} (S+1)^{\frac{S+1}{S}}$
6	Asymmetric Logistic Peak	$f(\lambda) = A \left(1 + e^{\frac{\lambda-C+W \ln(S)}{W}}\right)^{-S-1} \left\{e^{\frac{\lambda-C+W \ln(S)}{W}}\right\} S^{-S} (S+1)^{S+1}$
7	Pearson VII	$f(\lambda) = \frac{A}{\left(1 + \left(\frac{\lambda-C}{W}\right)^2 (2^{\frac{1}{S}} - 1)\right)^S}$
8	Split Pearson VII	$f(\lambda) = \frac{A}{\left(1 + \left(\frac{\lambda-C}{W}\right)^2 (2^{\frac{1}{S}} - 1)\right)^S}$ with $W=W_1, S=S_1$ for $\lambda < C$ and $W=W_2, S=S_2$ otherwise
9	Asymmetric Double Sigmoidal	$f(\lambda) = \frac{A}{1 + e^{-\frac{\lambda-C+\frac{W}{2}}{S_1}}} \left(1 - \frac{1}{1 + e^{-\frac{\lambda-C+\frac{W}{2}}{S_2}}}\right)$
10	Piecewise 3 rd Oder Polynomial (Spline)	Piecewise: $f(\lambda) = a_3 x^3 + a_2 x^2 + a_1 x^1 + a_0$, piecewise defined for n range $x_{k-1} \leq x < x_k, k=1 \dots n$

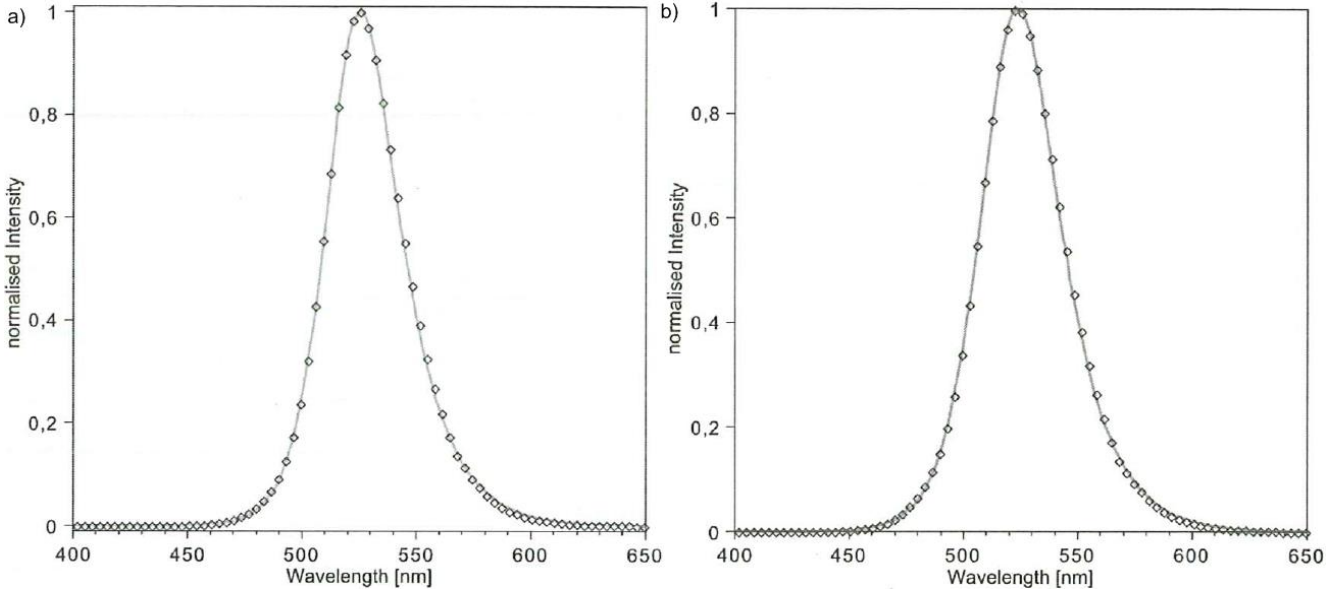


Figure 6.12 - Comparison between simulated and measured spectral results of the color semiconductor LED for the case of 10 mA and 76.8 °C (a) and the case of 20 mA and 104.7 °C (b) according to ([103])

b. Combination approach between mathematical descriptions and physical nature of color semiconductor LEDs

Inheriting previous achievements and improving weak points in [103], [104] and [105], the authors in [106] proposed the combination approach between the mathematical description and physical nature of color semiconductor LEDs. The physical nature of color semiconductor LEDs is not only considered via the distribution of the joint density of states and the BOLTZMANN distribution, but also via the relationship between the junction temperature (T_j / K) and the carrier temperature (T_c / K), the band gap energy shift and the increment in the non-radiative recombination rate with the junction temperature. These authors started with the mathematical form containing the combination of two exponentials as follows,

$$\Phi_{e,\lambda} = \frac{2S_{p0}}{\exp\left[\frac{\lambda-\lambda_p}{B(\lambda)}\right] + \exp\left[-\frac{\lambda-\lambda_p}{B(\lambda)}\right]} \quad (6.36)$$

Where, S_{p0} was spectral intensity at peak wavelength λ_p and $B(\lambda)$ was a piecewise defined by asymmetrical line width. Then, the authors inserted the BOLTZMANN behavior into Equation 6.36 to have,

$$\Phi_{e,v} = \frac{1}{S_1 \exp[-a(v-v_p)] + S_2 \exp\left[\frac{h}{kT_c}(v-v_p)\right]} \quad (6.37)$$

Where, the v_p was experimental peak wavelength and S_1 , S_2 , a and T_c were the four positive fitting parameters. The equation 6.37 was simulated to confirm that it was not able to model the complete spectrum shape. Therefore, the authors improved it by the addition of a GAUSSIAN function as follows,

$$\Phi_{e,v} = \frac{1}{S_1 \exp[-a(v-v_p)] + S_2 \exp\left[\frac{h}{kT_c}(v-v_p)\right] + S_3 \exp\left[-\left(\frac{v-v_G}{b}\right)^2\right]} \quad (6.38)$$

where, S_3 , b and the peak frequency of the GAUSSIAN function (ν_G) acted as three additional parameters. Successively, the authors assumed that Equation 6.38 can be accepted, because the most fitting at only 25 °C and 350 mA for typical red, green and blue semiconductor LEDs had the R^2 values exceeding 0.99 and the carrier temperature was higher than the junction temperature as expected. Then, the authors attempted to equip three temperature dependence terms into Equation 6.38 including the carrier temperature, the peak wavelength and the absolute power. In the first term, the carrier temperature could be determined by Equation 6.39.

$$T_C(T_j) \approx c(T_j - T_{\text{ref}}) + T_{C,\text{ref}} = c\Delta T + T_{C,\text{ref}} \quad (6.39)$$

where, T_{ref} was 300 K, $T_{C,\text{ref}}$ was the reference temperature of the carrier, and c was a positive fitting parameter. In the second term, based on the VARSHNI's equation 2.45 in Chapter 2, the temperature dependence of the energy band gap could be rewritten as follows,

$$E_g(T_j) = E_g(0) - \frac{\alpha T_j^2}{T_j + b} \quad (6.40)$$

$$E_g(T_j) \approx E_{g,\text{ref}} - \alpha'(T_j - T_{\text{ref}}) \quad (6.41)$$

where, $E_{g,\text{ref}}$ was the band gap energy at 300 K and α' was a positive fitting constant. From that, the authors could determine the temperature dependence of the peak wavelength and the GAUSSIAN peak wavelength by Equation 6.42 and 6.43, respectively.

$$\nu_p(T_j) \approx \nu_{p,\text{ref}} - \gamma_p(T_j - T_{\text{ref}}) = \nu_{p,\text{ref}} - \gamma_p\Delta T \quad (6.42)$$

$$\nu_G(T_j) \approx \nu_{G,\text{ref}} - \gamma_G(T_j - T_{\text{ref}}) = \nu_{G,\text{ref}} - \gamma_G\Delta T \quad (6.43)$$

where, $\gamma_p = \frac{\alpha'}{h}$, the γ_G played a similar role to γ_p for the GAUSSIAN element, $\nu_{p,\text{ref}}$ and $\nu_{G,\text{ref}}$ were the peak wavelength and the GAUSSIAN peak wavelength at 300 K. At the third term, the authors continued to quantify the temperature dependence of the spectral radiant power at a constant forward current based the energy relationship as follows,

$$\Phi_e(T) \propto \exp\left(-\frac{T_j - T_{\text{ref}}}{T_0}\right) = \exp\left(-\frac{\Delta T}{T_0}\right) \quad (6.44)$$

where, the T_{ref} was the reference temperature and the denominator T_0 was called the characteristic temperature. By equipping the three above temperature dependences, the spectral power distribution of color semiconductor LED described in Equation 6.38 could be converted into the new form in Equation 6.45.

$$\Phi_{e,v}(T) = \left\{ \frac{1}{S_{1,\text{ref}} \exp[-a(\nu - \nu_{p,\text{ref}} + \gamma_p \Delta T)] + S_{2,\text{ref}} \exp\left[\frac{h(\nu - \nu_{p,\text{ref}} - \gamma_p \Delta T)}{k(c\Delta T + T_{C,\text{ref}})}\right] + S_{3,\text{ref}} \exp\left[-\left(\frac{\nu - \nu_{G,\text{ref}} + \gamma_G \Delta T}{b}\right)^2\right]} \right\} \exp\left(-\frac{\Delta T}{T_0}\right) \quad (6.45)$$

where, $\nu_{p,\text{ref}}$, $S_{1,\text{ref}}$, a , $S_{2,\text{ref}}$, $T_{C,\text{ref}}$, $\nu_{G,\text{ref}}$, $S_{3,\text{ref}}$ and b were determined from one referent spectrum at the reference temperature T_{ref} and $\Delta T = T_j - T_{\text{ref}}$, and for the determination of γ_p , γ_G , c and T_0 , a spectrum obtained at an additional temperature had to become available. Finally, the authors assumed that Equation 6.45 was the best equation, which combined between the available mathematical form and physical nature of semiconductor LEDs. However, the current dependence was not considered completely in this model. The evaluation of the accuracy of the simulation was indicated by the color difference ($\Delta u'v'$, CIE 1976) and the luminous flux difference between simulated and measured results at 350 mA and 340 K listed in Table 6.3.

Table 6.3 - Comparison between simulated and measured results at 350 mA and 340 K for the color semiconductor LEDs given by the authors in ([106])

Name	Measured			Simulated			Deviation	
LED	Φ_v / lm	CIE x	CIE y	Φ_v / lm	CIE x	CIE y	$\Delta\Phi_v / \%$	$\Delta u'v' / 10^{-3}$
R ₁	20.1	0.6939	0.3055	19.6	0.6935	0.3064	2.4	1.5
R ₂	26.9	0.6941	0.3053	24.5	0.7037	0.2962	8.9	20.7
G ₁	29.2	0.2045	0.6714	28.7	0.2049	0.6844	1.7	2.8
G ₂	55.4	0.1671	0.6679	54.7	0.1709	0.6649	1.3	1.7
B ₁	4.5	0.1513	0.0284	4.5	0.1511	0.0270	0.0	3.8
B ₂	18.0	0.1367	0.0537	17.9	0.1363	0.0534	0.5	0.7

c. Summary

In Section 6.4.2 some approaches of optical transient LED models of some well-known publications on the world in the last years were described. As well, most of them only simulated pure mathematically for color semiconductor LED spectra such as [103], [104] and [105]. At advanced level, the authors in [105] established a purely mathematical spectral LED model for a cold white PC-LED by a fourth order GAUSSIAN function, and the authors in [106] attempted to correlate between the physical nature of color semiconductor LEDs and available mathematical equipment. However, in almost publications the accuracy was only evaluated and published at one or several currents and temperatures. Based on these poor data and explanations of authors, it can be confirmed, that the correlation between the physical nature of LEDs and mathematical descriptions was only carried out at quite simple levels with the temperature dependence and for several semiconductor LEDs, while the current dependence was not yet contemplated fully. Moreover, unfortunately with the combination approach, the accuracy of the LED models in [106] was bad for the red semiconductor LEDs and tolerable for the green semiconductor LEDs at 350 mA and 340 K. Although the luminous flux offset was low for the blue semiconductor LEDs, the color difference was high for blue LED B₁ at 350 mA and 340 K. Likewise, it can be recognized visually, that the early simulated result of a cold white PC-LED in [105] with a fourth order GAUSSIAN function was also not good enough. Otherwise, although the double GAUSSIAN spectrum matrix approach in [105] contributed a good accuracy for a green semiconductor LED, the logistic power peak equation in [103] was more feasible for the establishment of optical transient LED models of color semiconductor LEDs, because of the functional correlations of their parameters with the forward current and junction temperature.

Successively, based on the above investigations and analyses, some suggestions can be offered as follows: Firstly, an available combination approach between mathematical descriptions and the physical nature of both color semiconductor LEDs and white PC-LEDs has been not yet really ready until now. Thus, more scrupulous research of physicists and chemists about it is really an urgent need, and this approach should be left for future works. Secondly, about optical modeling for color semiconductor LEDs, the double Gaussian spectrum matrix approach is rejected by the author, because the size of the matrix was not determined and proved appropriately in order to ensure the accuracy of LED models, while its procedures were complicated. Otherwise, the idea of the authors in [103] with logistic power peak equation was only proved in the cases of 10 mA and 76.8 °C and 20 mA and 104.7 °C. Oppositely, the author of this thesis contemplates to high current regions and simplified mathematical equations. Consequently, a complicated logistic power peak equation system with the low current region will be also not applied in this thesis. However, the idea of mathematical LED models with their parameters as the functions of junction temperature and forward current will be inherited and developed. Thirdly, a new and suitable approach of optical transient LED models for both color semiconductor LEDs and PC-LEDs should be researched, tested and offered in the next sections.

6.4.3. Investigations and proposals for the optical transient LED models of color semiconductor LEDs

The section 6.4.2 discussed about two approaches for color semiconductor LED models and white PC-LED models with some well-known mathematical models. As well, the studied results of the published LED models were collected and compared. Consequently, their advantage, disadvantages, accuracy, objects and applicable regions were recognized. In this section, the multi - GAUSSIAN equation with their parameters as three-dimensional functions of junction temperature and forward current (called horizontal spectral LED model) will be investigated and tested for a typical blue semiconductor LED type. Successively, a new idea of a polynomial function model of LED spectral intensity (called vertical spectral LED model) will be carried out and evaluated for its accuracy. Finally, modeling solutions will be compared together in order to offer more available mathematical models for color semiconductor LEDs.

a. Experiments for horizontal spectral LED models of color semiconductor LEDs

* **Description of the investigated object:** The blue semiconductor LED with dominant wavelength of 450 nm (according to the datasheet) is used in the investigation. Particularly, this LED is measured at forward currents 350 mA, 700 mA and 1000 mA and layout temperatures 25 °C, 55 °C, 85 °C and 100 °C. Then, its measured spectra are shown in Figure 6.13. In addition, applying the measuring procedures described in Chapter 5, its junction temperature can be determined. Consequently, the model parameters of the optical transient LED model for this blue semiconductor LED can be established with inputs of forward current and junction temperature as three-dimensional functions.

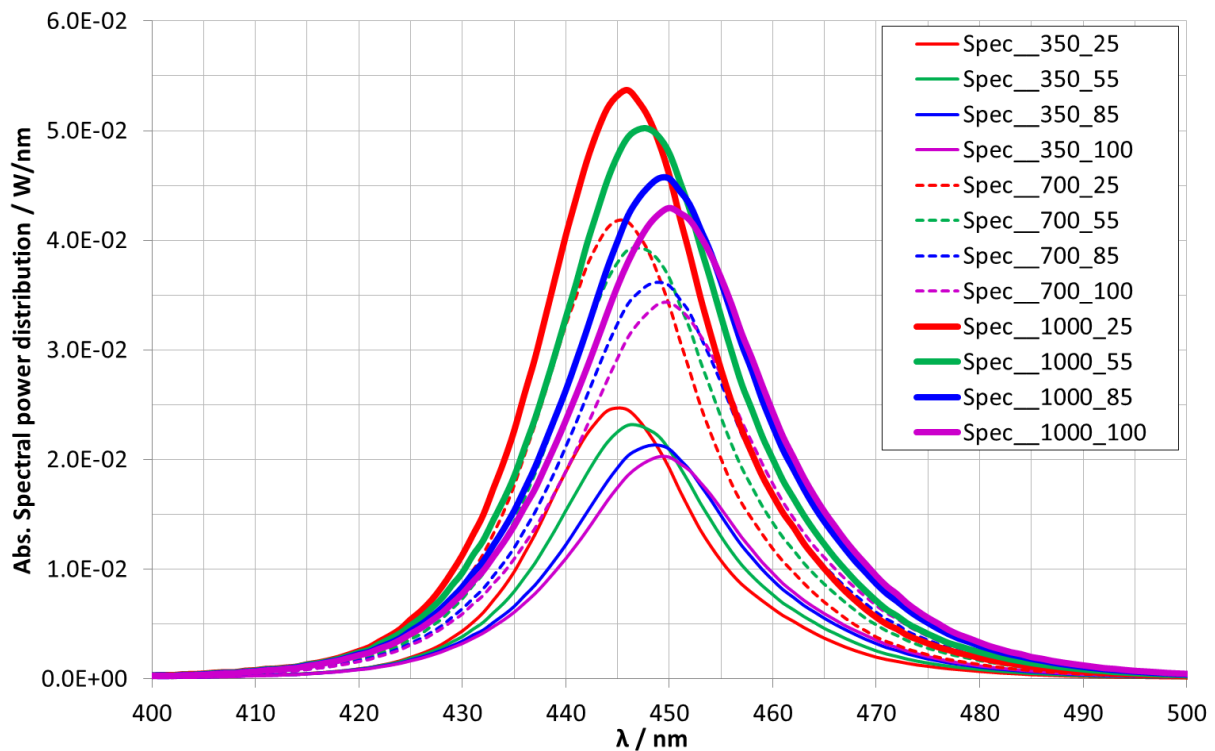


Figure 6.13 - Absolute spectral power distributions of the investigated blue semiconductor LED at forward currents of 350 mA, 700 mA and 1000 mA and temperatures of 25 °C, 55 °C, 85 °C and 100 °C

* **Selection of available mathematical forms, establishment of LED models and results:** In this section, the multi GAUSSIAN mathematical equation system will be investigated from the first order to sixth order. Fitting for the blue spectrum with the forward current of 350 mA and the layout

temperature of 25°C was shown in Figure 6.14 as a demonstration example. Fitting results showed that the first order was not optimal, because the difference between measured and fitted curves was too big. Contrarily, there was nearly no big difference of the fitting quality in the cases of the second GAUSSIAN to the sixth GAUSSIAN function. Hence, the selection of the second or higher GAUSSIAN order only depends of their fitting constants. If the constants of a function have a good functional correlation with junction temperature and forward current, the function will be selected.

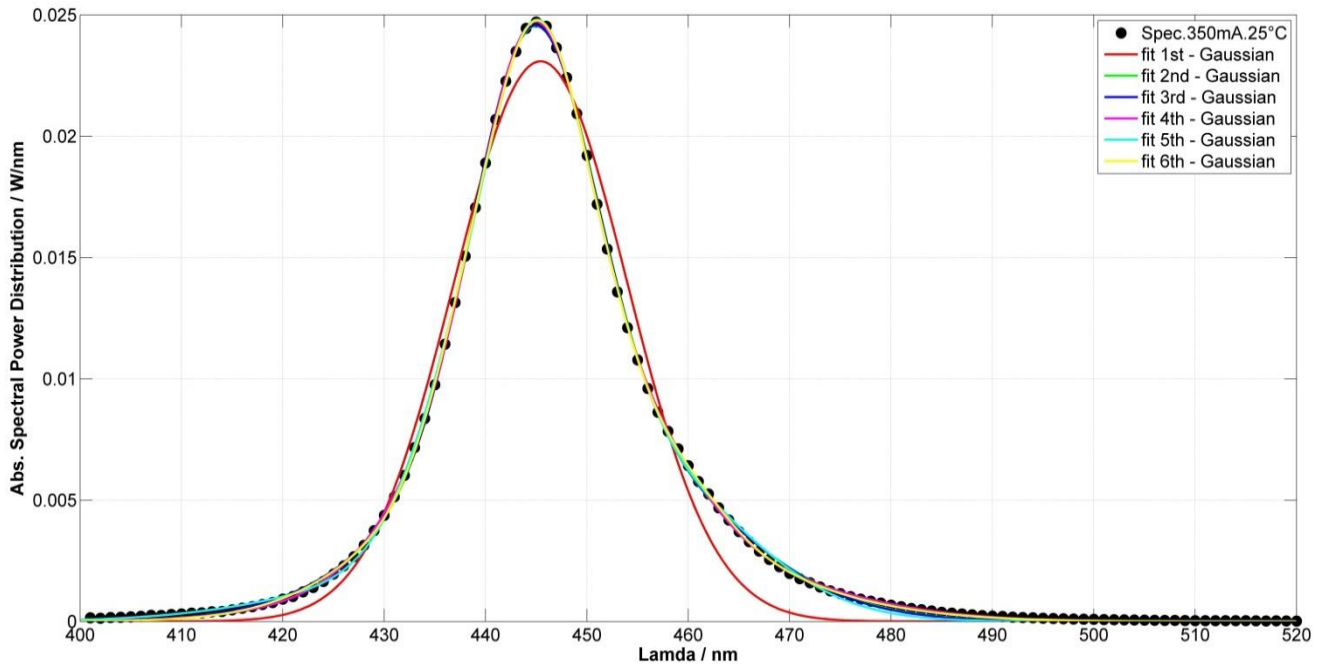


Figure 6.14 - Fitting of the spectrum of the blue semiconductor LED at the current of 350 mA and the PCB temperature of 25 °C as a demonstration example with different high order GAUSSIAN functions

Particularly, in the performance the fitting by MATLAB curve fitting toolbox gave fitting constants (or model parameters) for the second to sixth order GAUSSIAN function. Their R^2 quality was always higher than 0.99. However, only constants of the second GAUSSIAN function had a good functional correlation with forward current and junction temperature like the results demonstrated in Table 6.4. Therefore, the second order GAUSSIAN function should be selected to establish the optical transient LED model of the blue semiconductor LED.

Table 6.4 - Fitting constants of the second order GAUSSIAN function

$a_1 / 10^{-3}$	16	14	13	12	27	24	21	20	34	30	27	25
$a_2 / 10^{-3}$	8.56	9.04	8.77	8.65	14.9	15.4	15.4	14.2	19.7	19.9	18.8	17.8
b_1	444.7	446.3	448.1	448.9	444.9	446.6	448.4	449.3	445.4	447.1	448.9	449.8
b_2	447.8	448.8	450.1	450.7	447.7	448.9	450.2	451.0	447.9	449.3	450.7	451.4
c_1	8.3	8.5	8.9	9.1	8.8	9.0	9.3	9.8	9.1	9.4	9.9	10.3
c_2	19.0	19.4	20.2	20.5	19.7	20.2	20.7	21.5	20.2	20.8	21.7	22.2
I_f / mA	350	350	350	350	700	700	700	700	1000	1000	1000	1000
$T_j / \text{°C}$	35	64	95	110	41	70	103	120	54	80	112	128
$T_s / \text{°C}$	25	55	85	100	25	55	85	100	25	55	85	100
V_f / V	2.905	2.856	2.806	2.783	3.034	2.980	2.927	2.901	3.114	3.057	3.002	2.977

Technically, micro-controllers will be able to perform its function easier, if functional correlations of the constants are described by polynomial equations. Therefore, the correlations were fitted by polynomial functions as follows,

$$a_1 = p_{00,a1} + p_{10,a1} I_f + p_{01,a1} T_j + p_{20,a1} I_f^2 + p_{11,a1} I_f T_j + p_{02,a1} T_j^2 \quad (6.46)$$

$$a_2 = p_{00,a2} + p_{10,a2} I_f + p_{01,a2} T_j + p_{20,a2} I_f^2 + p_{11,a2} I_f T_j + p_{02,a2} T_j^2 \quad (6.47)$$

$$b_1 = p_{00,b1} + p_{10,b1} I_f + p_{01,b1} T_j + p_{20,b1} I_f^2 + p_{11,b1} I_f T_j + p_{02,b1} T_j^2 \quad (6.48)$$

$$b_2 = p_{00,b2} + p_{10,b2} I_f + p_{01,b2} T_j + p_{20,b2} I_f^2 + p_{11,b2} I_f T_j + p_{02,b2} T_j^2 \quad (6.49)$$

$$c_1 = p_{00,c1} + p_{10,c1} I_f + p_{01,c1} T_j + p_{20,c1} I_f^2 + p_{11,c1} I_f T_j + p_{02,c1} T_j^2 \quad (6.50)$$

$$c_2 = p_{00,c2} + p_{10,c2} I_f + p_{01,c2} T_j + p_{20,c2} I_f^2 + p_{11,c2} I_f T_j + p_{02,c2} T_j^2 \quad (6.51)$$

Fitting parameters of the above equations were listed in Table 6.5.

Table 6.5 - Fitting parameters for the constants of the second GAUSSIAN function

Parameters	$P_{00} / 10^0$	$P_{10} / 10^{-4}$	$P_{01} / 10^{-4}$	$P_{20} / 10^{-7}$	$P_{11} / 10^{-7}$	$P_{02} / 10^{-6}$
a_1	0.005	0.421	-0.561	-0.055	-1.051	0.225
a_2	-0.002	0.251	0.844	-0.060	-0.087	-0.546
b_1	442.9	-9.034	594.3	0.8182	60.14	-41.09
b_2	447.1	-19.44	333.1	4.379	112.3	8.056
c_1	7.98	16.39	-94.65	-3.704	6.286	131.6
c_2	18.22	18.88	-6.104	-2.415	3.282	144.8

* **Evaluation of the accuracy of the model:** In order to evaluate the accuracy of the model, the above equation system and measured results are programmed into a specific program. In that, input parameters are forward current and layout temperature and output parameters are absolute spectral power distributions, established constants of LED models, forward voltage, electrical power, optical power, junction temperature, thermal resistance, luminous flux, luminous efficiency, radiative efficiency and chromaticity. In addition, the program must calculate and compare the offset between simulated and measured spectral power distributions by two different forms. In the first form, the offset is represented visually by an absolute spectral power distribution offset. In the second form, the offset is indicated by color difference ($\Delta E = \Delta u'v'_{Me.-Mo.} = \sqrt{(u'_{model} - u'_{measure})^2 + (v'_{model} - v'_{measure})^2}$). Particularly, the interface with the results of the program was described in Figure 6.15. In more detail, specific results of color differences between simulated and measured spectra are listed in Table 6.6. In that, the minimal color difference was 4.18 MAC ADAM ellipses at the forward current of 350 mA and the layout temperature of 25 °C and the maximal color difference was 5.15 MAC ADAM ellipses at the forward current of 1000 mA and the layout temperature of 85 °C. In addition, although in the operating region of 350 mA - 1000 mA and 25 °C- 100 °C, the spectral shape and intensity of simulated and measured spectra were quite similar, their color differences of 4 and 5 MAC ADAM ellipses were big compared with the requirement of color difference researched by the author in [37] (the acceptable maximal level was only 3 MAC ADAM ellipses). Therefore, if applications do not require a very high accuracy for color difference, this optical transient LED model will be still used possibly.

Table 6.6 - Color differences between simulated and measured spectra at different operating conditions

I_f / mA	350	350	350	350	700	700	700	700	1000	1000	1000	1000
$T_s / ^\circ\text{C}$	25	55	85	100	25	55	85	100	25	55	85	100
$\Delta u'v'_{\text{Me.-Mo.}} / 10^{-3}$	4.18	4.2	4.7	5.01	4.2	4.6	5.06	5.14	4.4	4.9	5.15	4.9

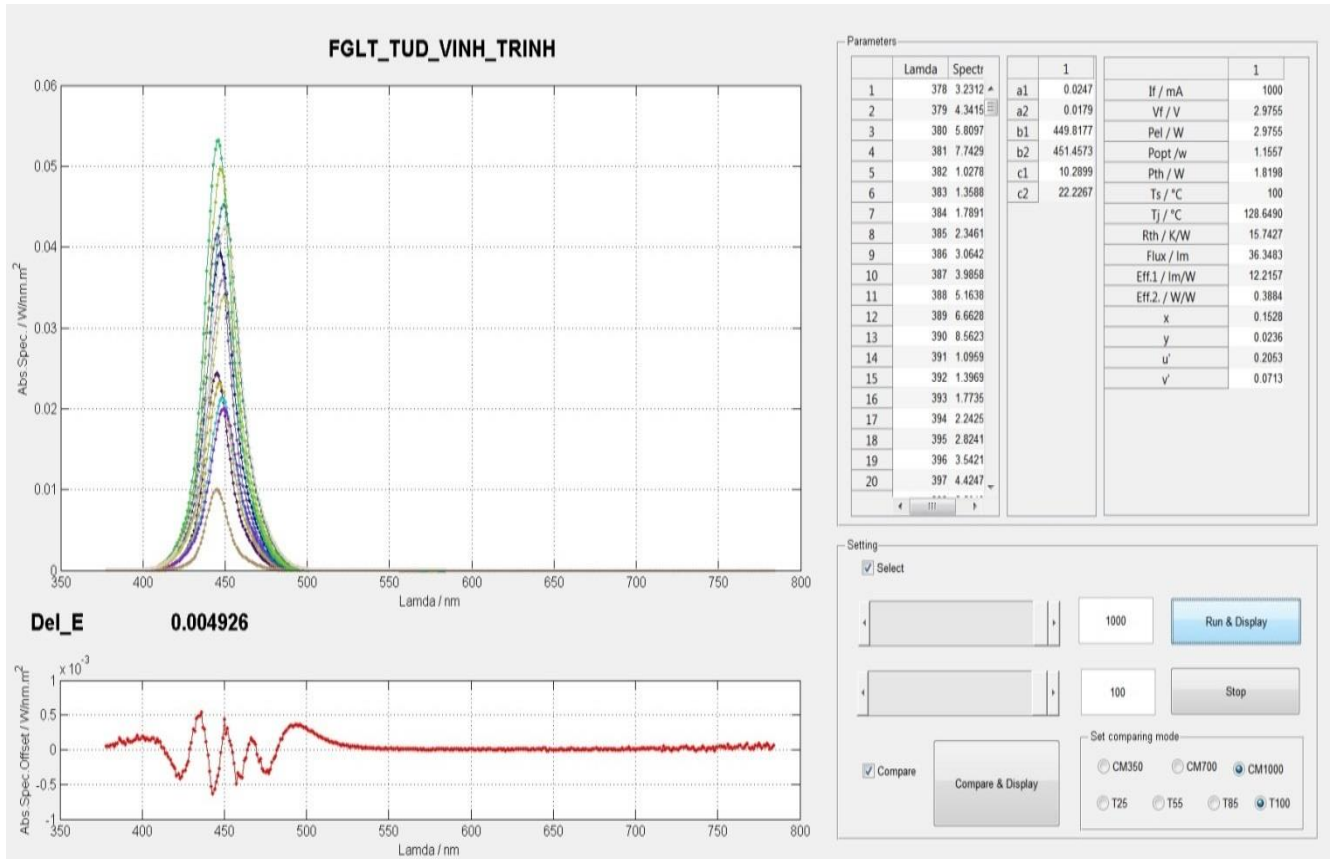


Figure 6.15 - Interface of the program with imagines of many spectra at different operating conditions

b. Proposal and establishment for vertical spectral LED models of color semiconductor LEDs

In Section 6.4.3.a, the approach of multi GAUSSIAN functions with which their parameters had functional correlations with junction temperature and forward current was attempted. However, the above results showed that this approach will be only used, if applications do not require a very high accuracy of color difference. Therefore, in this section, another approach will be offered and carried out in order to enhance the accuracy of LED models for high quality solid state lighting applications.

* **Physical nature, mathematical description and feasibility of the new approach:** Equation 2.39 in Section 2.1.5 in Chapter 2 described the theoretical absolute spectral power distribution of color semiconductor LEDs, intrinsically. If the junction temperature is not used, but it is substituted by any sensor temperature that can be measured by a normal temperature sensor and this temperature sensor can be placed anywhere on a printed circuit board, the measurement, control and regulation of the color semiconductor LEDs will become much easier, because the determination of junction temperature has sometime no high accuracy. Indeed, the thermal transport in LEDs is not only carried out by thermal conduction, but also by thermal convection and thermal radiation. And the percentage of thermal conduction, thermal convection and thermal radiation must be determined by a very complicated thermal balance in tiny three-dimensional space of LEDs. Consequently, parameters α and

β in Equation 5.5 in Chapter 5 have to be determined accurately in order to give the effective thermal power that influences directly on the junction temperature. Hence, the equation system for the description of the theoretical absolute spectral power distribution of LEDs can be rewritten as follows,

$$P_{th,in} = \alpha P_{th,chip} + \beta P_{th,phosphor} \quad (6.52)$$

$$T_j = T_s + R_{th\Sigma} P_{th,in} \quad (6.53)$$

$$S(\lambda) = a \left\{ \frac{1}{2\pi^2} \left(\frac{2m_r^*}{\hbar^2} \right)^{\frac{3}{2}} \sqrt{\frac{hc}{\lambda} - E_g} \right\} \left\{ e^{-\frac{hc}{\sigma k_B T_j}} \right\} \quad (6.54)$$

$$S(\lambda) = a \left\{ \frac{1}{2\pi^2} \left(\frac{2m_r^*}{\hbar^2} \right)^{\frac{3}{2}} \sqrt{\frac{hc}{\lambda} - E_g} \right\} \left\{ e^{-\frac{hc}{\sigma k_B (T_s + R_{th\Sigma} P_{th,in})}} \right\} \quad (6.55)$$

If the LED was already determined and the wavelength λ_i was kept constant, intensity S_i at specific wavelength λ_i only depends on sensor temperature and forward current. In addition, the relationship between forward current (I_f / mA) and total effective mass (m_r^* / mg) is very complicated and is not yet determined explicitly, because it relates to series resistors, carrier concentrations, the BOLTZMANN distribution of carriers inside semiconductor LEDs and other effects. However, based on the form of Equation 6.55, the relationship can be assumed as $S(\lambda_i) \propto \exp\left(\frac{-d}{eT_s + f}\right)$ and $S(\lambda_i) \propto gI_f^x$, where d , e , f , g and x are fitting constants. Otherwise, according to the theory of TAYLOR series, any multi variable function can be also converted by a TAYLOR series, as follows,

$$T(x_1, x_2, \dots, x_d) = \sum_{n_1=0}^{\infty} \sum_{n_2=0}^{\infty} \dots \sum_{n_d=0}^{\infty} \frac{(x_1 - a_1)^{n_1} \dots (x_d - a_d)^{n_d}}{n_1! \dots n_d!} \left(\frac{\partial^{n_1 + \dots + n_d}}{\partial x_1^{n_1} \dots \partial x_d^{n_d}} \right) (a_1, \dots, a_d) \quad (6.56)$$

Therefore, although the temperature dependence of intensity $S(\lambda_i)$ is an exponential function and its forward current dependence is a power function or any other form, the three-dimensional relationship between $S(\lambda_i)$ and sensor temperature and forward current can be interpolated into two variable polynomial functions. The order of these functions depends on the desired accuracy of LED models. Indeed, if a specific operating region is defined by certain temperature and current values and the accuracy of a LED model with a chosen order of the mathematical functions is ensured in an acceptable tolerance, the chosen order of the functions can be accepted. The spectral LED model established by this approach is called as a vertical polynomial model or vertical spectral LED model by the author of this thesis. In the visible light region (380 nm - 780 nm) and for the chosen resolution of 1 nm, the LED vertical polynomial model can be recognized as follows,

$$S(\lambda) = \sum_{i=380}^{i=780} S_{\lambda_i}(T_s, I_f) \quad (6.57)$$

However, in fact the number of equations is less and depends on each specific color semiconductor LED type, because the visible light region of color semiconductor LEDs is narrower such as about 400 nm - 500 nm for blue semiconductor LEDs, about 460 nm - 560 nm for green semiconductor LEDs, about 560 nm - 610 nm for orange and amber semiconductor LEDs and about 590 nm - 700 nm for red semiconductor LEDs. In addition, if the accuracy is required lower and the chosen resolution is wider, the number of equations will be also less. In this aspect, in order to interpolate for a huge number of equations, a specific program is necessary to be programmed for the automatic interpolation.

*** The establishment for vertical spectral models of some typical deep red, red, green, blue and royal semiconductor LEDs of three different manufacturers (called A, B and C):** If the new idea is

applied for the above blue LED type with only three forward current points and four layout temperature points, the accuracy of new model established for it will be ensured perfectly. Indeed, by selecting of the fighting style of the second polynomial function for forward current and the one of the third polynomial function for layout temperature, the model will correspond completely the measured results. Therefore, in order to have the most objective evaluation of the new idea, the author will establish spectral models for varied color semiconductor LEDs (deep red, red, green, blue and royal LEDs) of three different manufacturers (called by A, B and C) with big enough data samples (layout temperatures of 25 °C, 35 °C, 45 °C, 55 °C, 65 °C, 75 °C, 80 °C, 85 °C and 95 °C and forward currents of 50 mA, 100 mA, 200 mA, 300 mA, 350 mA, 400 mA, 500 mA, 600 mA and 700 mA). However, the data samples of 350 mA and 80 °C will be not used in the establishment of the LED models so that they can be used for evaluation of the accuracy of LED models later. Moreover, the specific program for the interpolation and establishment of LED models is programmed and has the interface described in Figure 6.16. Based on this program, the high sample number of measured EXCEL-data can be imported into the program. Then, the data are interpolated by the program automatically with an optional fitting style. Successively, the parameters of the LED models are exported into a new EXCEL-file. As well, any desired spectrum at a specific condition of sensor temperature and forward current can also be calculated and exported into an Excel-file for later other calculations and comparisons.

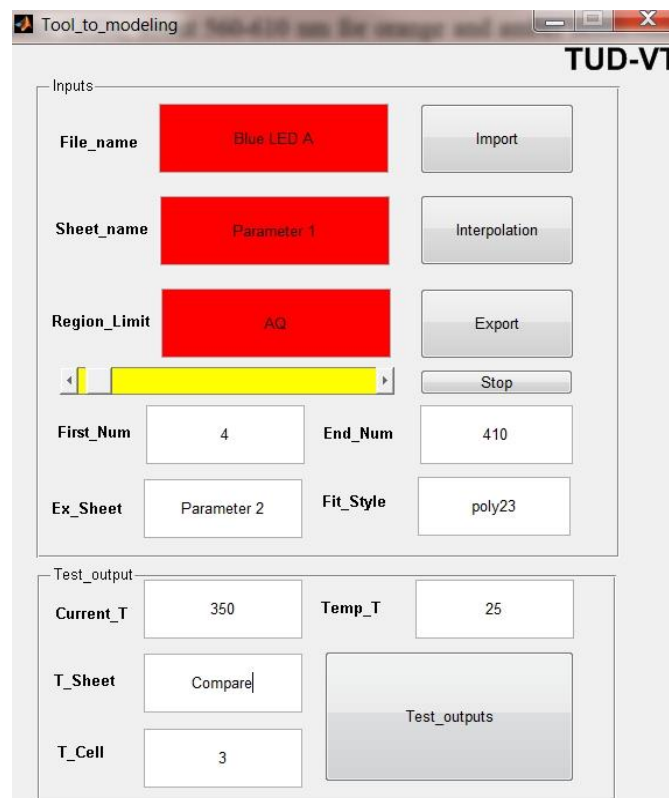


Figure 6.16 - Interface of the program for the import, interpolation and export of data

Finally, the program is used to establish spectral LED models for varied color semiconductor LEDs. Successively, as the first detailed demonstration example of the influence of temperature factor on the accuracy of LED model establishment, the spectral comparison between the measured and simulated absolute spectral power distributions (SPDs) of the blue LED (445 nm) of Manufacturer C at the same forward current of 350 mA and the different sensor temperatures of 25 °C - 95 °C, which were not used in the previous interpolation, is shown in Figure 6.17. The results revealed that the simulated SPDs (solid curves) were completely similar to the measured SPDs (open circle curves).

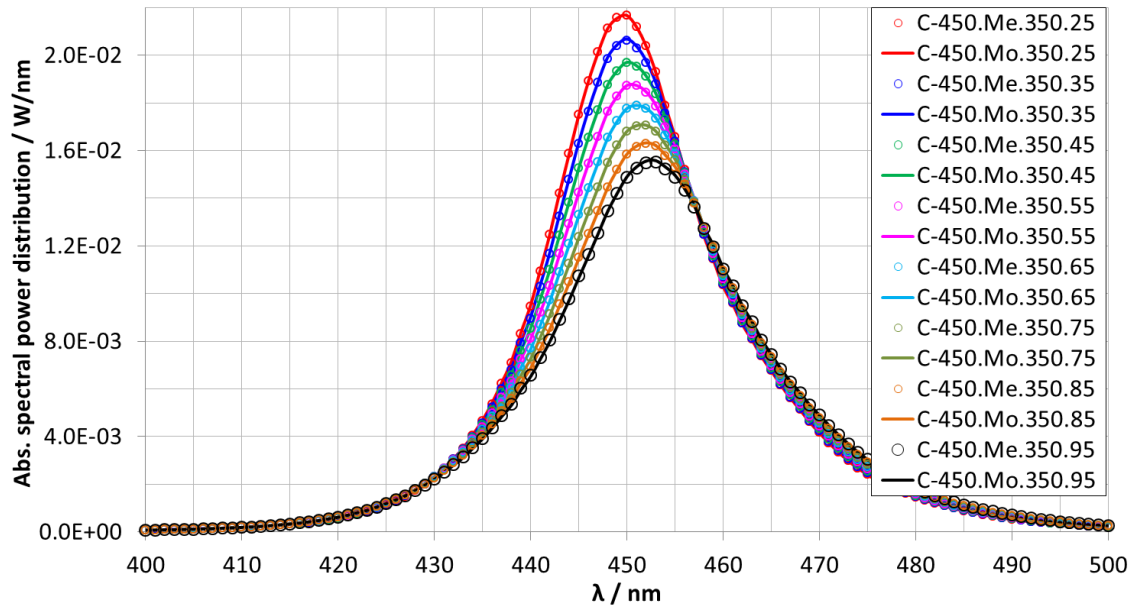


Figure 6.17 - Spectral comparison between measured and simulated absolute SPDs of the blue LED 450 nm of Manufacturer C with the same current of 350 mA and different sensor temperatures of 25 °C - 95 °C as the first demonstration example of the influence of temperature factor. Symbols “Me.” and “Mo.” are to denote measured and modeled spectra, respectively.

In more detail, in order to evaluate the accuracy of the spectral LED model under the influence of temperature factor, color differences ($\Delta u'v'_{Me.-Mo.}$) between the above measured and simulated SPDs are calculated and listed in Table 6.7. In that, all color differences were always lower than 1 MAC ADAM ellipses. Thus, these good results confirmed that the vertical spectral LED model for the blue semiconductor LED under the influence of temperature factor can be accepted for solid state lighting applications that require the high color accuracy.

Table 6.7 - Color differences between measured and simulated spectra of the blue LED 450 nm of Manufacturer C at the same forward current of 350 mA and different sensor temperatures of 25 °C - 95 °C as the first demonstration example of the influence of temperature factor

Order	Name	I_f / mA	$T_s / ^\circ\text{C}$	u'_{Measure}	v'_{Measure}	u'_{Model}	v'_{Model}	$\Delta u'v'_{Me.-Mo.} / 10^{-3}$
1	C-450	350	25	0.2033	0.0764	2.034	0.0763	0.12
2	C-450	350	35	0.2025	0.0775	0.2025	0.0776	0.09
3	C-450	350	45	0.2016	0.0789	0.2016	0.0790	0.16
4	C-450	350	55	0.2006	0.0804	0.2005	0.0806	0.16
5	C-450	350	65	0.1996	0.0821	0.1994	0.0822	0.21
6	C-450	350	75	0.1984	0.0839	0.1983	0.0840	0.15
7	C-450	350	85	0.1971	0.0858	0.1971	0.0859	0.11
8	C-450	350	95	0.1958	0.0879	0.1958	0.0879	0.05

Otherwise, as the second demonstrated example of the influence of forward current factor on the accuracy of the LED model establishment, spectral comparison between measured and simulated absolute SPDs of the above similar blue LED at the same sensor temperature of 80 °C and different forward currents of 50 mA - 700 mA, which were not used in the previous interpolation, is shown in Figure 6.18. Based on the spectra in Figure 6.18, it can be recognized, that the simulated (solid curve) and measured curves (open circle) had also completely similar shapes and intensities.

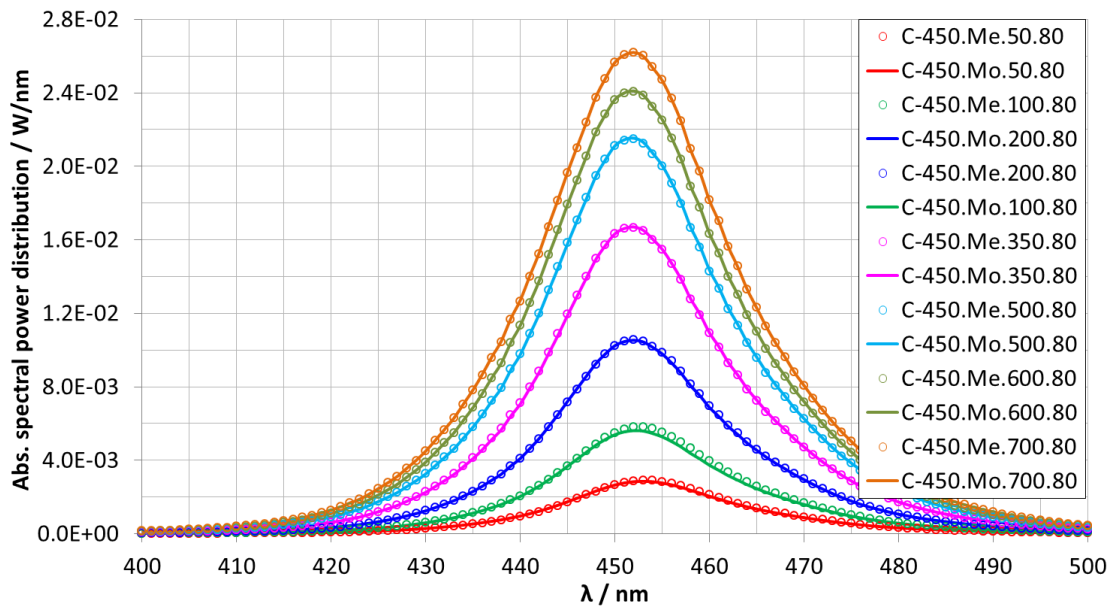


Figure 6.18 - Spectral comparison between measured and simulated absolute SPDs of the blue LED 450 nm of Manufacturer C at the same sensor temperature of 80 °C and different forward currents of 50 mA - 700 mA as the second demonstration example of the influence of forward current factor. Symbols “Me.” and “Mo.” denote measured and modeled spectra, respectively.

Specifically, color differences between measured and simulated LED spectra of the blue semiconductor LED were calculated and listed in Table 6.8. And the results showed that color differences were always lower in high forward current region and higher in the low forward current region. Nonetheless, the maximal color difference was only 1.18 MAC ADAM ellipses. Consequently, this color difference is impossible to be identified by the human eyes according to published results of the author in [37]. As a result, the established LED model under the influence of forward current factor is still appropriate for high quality solid state lighting applications that require a high color accuracy.

Table 6.8 - Color differences between measured and simulated spectra of the blue LED 450 nm of Manufacturer C at the same sensor temperature of 80 °C and different forward currents of 50 mA - 700 mA as the second example of the influence of forward current factor

Order	Name	I_f / mA	T_s / °C	u'_{Measure}	v'_{Measure}	u'_{Model}	v'_{Model}	$\Delta u'v'_{\text{Me.-Mo.}} / 10^{-3}$
1	C-450	50	80	0.1937	0.0901	0.1944	0.0892	1.16
2	C-450	100	80	0.1957	0.0873	0.1964	0.0863	1.18
3	C-450	200	80	0.1970	0.0856	0.1972	0.0853	0.34
4	C-450	350	80	0.1978	0.0848	0.1977	0.0849	0.15
5	C-450	500	80	0.1979	0.0850	0.1978	0.0851	0.16
6	C-450	600	80	0.1977	0.0854	0.1977	0.0855	0.07
7	C-450	700	80	0.1974	0.0861	0.1974	0.0861	0.07

Successively, in order to attain more firm confirmation for vertical spectral LED models, spectral comparison between simulated and measured SPDs of five color semiconductor LEDs including deep red ($\lambda_p \sim 660$ nm), red ($\lambda_p \sim 630$ nm), green ($\lambda_p \sim 530$ nm), blue ($\lambda_p \sim 470$ nm) and royal blue ($\lambda_p \sim 445$ nm - 450 nm) semiconductor LEDs of three different manufacturers (A, B and C) is exposed in Figure 6.19. In that, selected forward current of 350 mA and sensor temperature of 80 °C were not used in the establishment of these LED models previously. Thus, the results confirmed fairly that there was nearly no offset between simulated and measured SPDs of the varied color semiconductor LEDs.

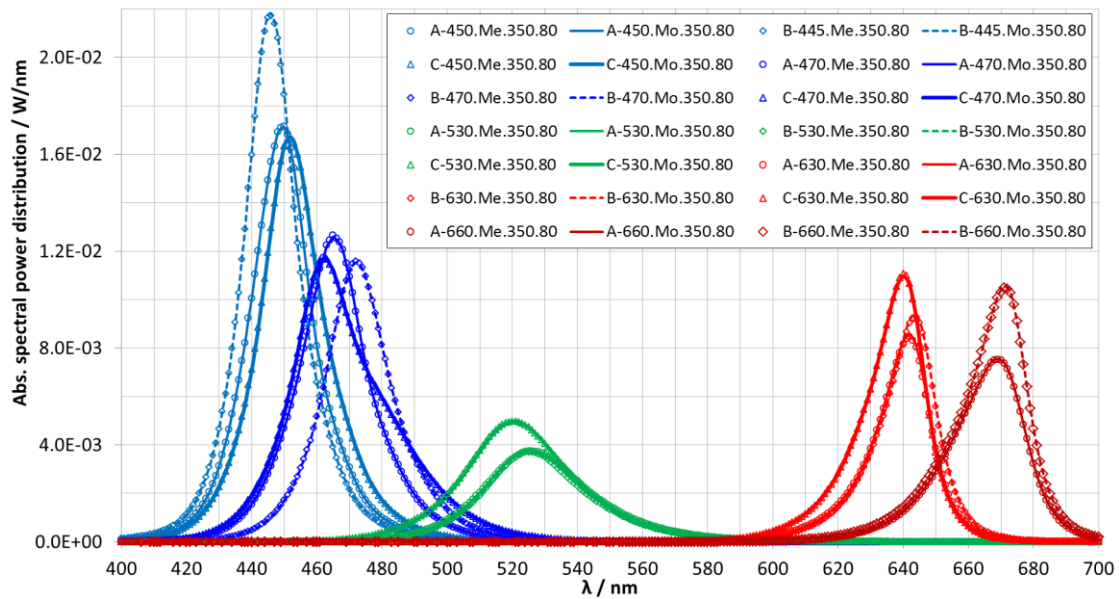


Figure 6.19 - Spectral comparison between measured and simulated absolute SPDs of the deep red, red, royal blue, blue and green semiconductor LEDs of three manufacturers (A, B and C) as a demonstration example. “Me.” and “Mo.” denote measured and model spectra respectively. “350.80.” denotes for 350 mA and 80 °C. And “450”, “470”, “530”, “630” and “660” denote LED peak wavelengths published in datasheets.

Particularly, chromaticity (u', v'_{Measure} and u', v'_{Model}) and color differences ($\Delta u'v'_{\text{Me.-Mo.}}$) between simulated and measured SPDs of five different LEDs are listed in Table 6.9. In that, all color differences were always lower than 1 MAC ADAM ellipses. Consequently, these results proved that models of different semiconductor LEDs belonging to three manufactures (A, B and C) satisfied the demand of high color accuracy for high quality solid state lighting applications. Hence, combining with previous results in the first and the second demonstration examples, it can be confirmed, that the new idea of establishment of vertical optical transient LED models achieved so much better accuracy than that of the idea of horizontal optical transient LED models. Therefore, the author proposes that the vertical spectral modeling should be used and expanded for establishment of optical LED models.

Table 6.9 - Color differences between measured and simulated SPDs of the deep red, red, royal blue, blue and green semiconductor LEDs of three manufacturers (A, B, C) at 350 mA and 80 °C as a demonstration example

Order	Name	I_f / mA	$T_s / \text{°C}$	u'_{Measure}	v'_{Measure}	u'_{Model}	v'_{Model}	$\Delta u'v'_{\text{Me.-Mo.}} / 10^{-3}$
1	A-450	350	80	0.2073	0.0714	0.207	0.0706	0.84
2	A-470	350	80	0.1567	0.1517	0.1567	0.1517	0.06
3	A-530	350	80	0.0720	0.5758	0.0719	0.5757	0.11
4	A-630	350	80	0.5473	0.5177	0.5473	0.5179	0.19
5	A-660	350	80	0.5880	0.5116	0.5883	0.5117	0.26
6	B-445	350	80	0.2150	0.0604	0.2151	0.0605	0.13
7	B-470	350	80	0.1235	0.2161	0.1236	0.2160	0.10
8	B-530	350	80	0.0700	0.5757	0.0702	0.5758	0.33
9	B-630	350	80	0.5531	0.5168	0.5531	0.5170	0.16
10	B-660	350	80	0.5858	0.5118	0.5864	0.5121	0.68
11	C-450	350	80	0.1978	0.0848	0.1977	0.0849	0.15
12	C-470	350	80	0.1439	0.1882	0.1437	0.1888	0.67
13	C-530	350	80	0.0616	0.5696	0.0619	0.5699	0.37
14	C-630	350	80	0.5387	0.5190	0.5388	0.5191	0.14

6.4.4. Investigation and proposal for the optical transient LED models of white PC-LEDs

Section 6.4.3 investigated and offered for optical transient LED models of color semiconductor LEDs. In that, establishment of horizontal transient spectral LED models with double GAUSSIAN form, where its parameters were three-dimensional functions of forward current and junction temperature, was suggested for applications with relatively moderate color difference accuracy. In addition, establishment of vertical spectral LED models with polynomial forms was investigated and proposed for applications with high color difference accuracy. Especially, in vertical spectral LED models the used temperature was not the junction temperature, but the temperature that a normal temperature sensor can measure it such as layout temperature or capsule temperature. Thus, it was easier to design, monitor and control for LED-lamps in solid state lighting applications. Likewise, in this section multi GAUSSIAN function system will be also investigated and tested for optical transient LED models of white PC-LEDs. And then, the new idea for vertical transient optical LED models will be suggested and carried out for white PC-LEDs.

a. Experiments for horizontal spectral LED models of white PC-LEDs

* **Description of the investigated object:** A typical cold white PC-LED (5000 K) was chosen for the investigation. The blue chip in the cold white PC-LED had the peak wavelength of about 445 nm. When the phosphor was built-up on the blue chip, its peak wavelength was shifted a little into the right side, because of inside chemical, physical and geometrical reactions between the phosphor and the chip structure. Moreover, the used phosphor for the cold white PC-LED was YAG phosphor with a peak wavelength of about 560 nm. However, in fact the peak wavelength of the YAG phosphor in the cold white PC-LED was also shifted into the right side due to the inside reactions between the phosphor and the chip structure. In addition, with different operating conditions of forward current and temperature, blue spectral component of the blue chip and yellow spectral component of the YAG phosphor changed their shape and intensity. Indeed, Figure 6.20 shows spectral changes of the cold white PC-LED with different operating conditions. Particularly, the operating conditions in this investigation are forward currents of 350 mA, 700 mA and 1000 mA and sensor temperatures 25 °C, 55 °C, 85 °C and 100 °C. Otherwise, applying procedures described in Chapter 5, the junction temperature of the cold white PC-LEDs could be determined. Consequently, three-dimensional functions of the model parameters of the spectral LED model for the cold white PC-LED could be established with inputs of forward current and junction temperature.

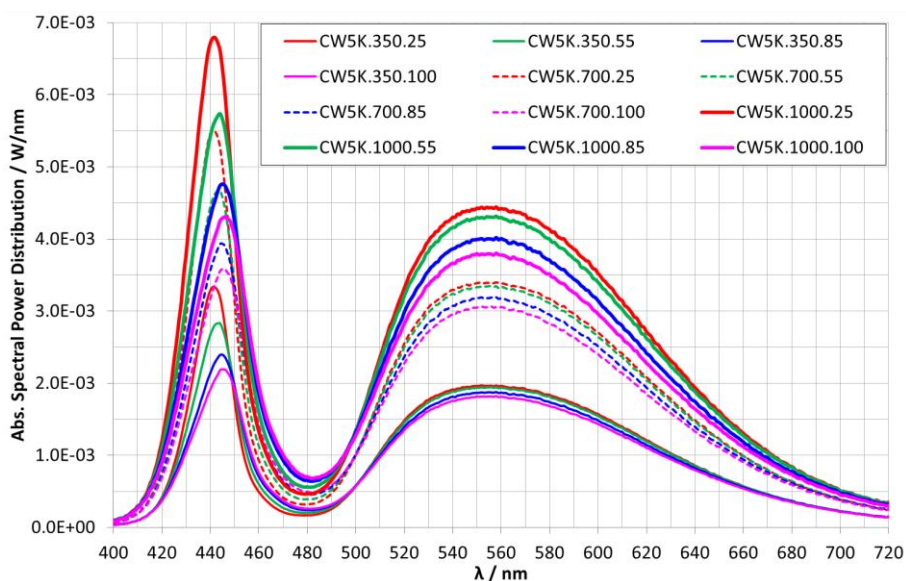


Figure 6.20 - The chosen cold white PC-LED (5000 K) for the investigation as a demonstration example

* **Selection of available mathematical forms, establishment of LED models and results:** In order to establish the horizontal spectral models for the cold white PC-LED described in the above section, there were two approaches. In the first approach, the spectrum of the cold white PC-LED can be separated into smaller spectral pieces such as blue spectral piece ($400 \text{ nm} < \lambda_p < 450 \text{ nm}$) and YAG phosphor spectral piece ($450 \text{ nm} < \lambda_p < 740 \text{ nm}$), or blue spectral piece ($400 \text{ nm} < \lambda_p < 450 \text{ nm}$), cross spectral piece ($450 \text{ nm} < \lambda_p < 500 \text{ nm}$), green-amber spectral piece ($500 \text{ nm} < \lambda_p < 620 \text{ nm}$) and red spectral piece ($620 \text{ nm} < \lambda_p < 740 \text{ nm}$). In the mathematical aspect, the blue, cross and red spectral pieces can be simulated by double GAUSSIAN, polynomial and power functions, respectively. Individually, the green spectral pieces or YAG phosphor spectral pieces can be also modeled by polynomial, GAUSSIAN or FOURIER functions. As a good agreement with this approach, the authors in [105] offered a LED model for a cold white PC-LED with a four-GAUSSIAN-component function (or called the fourth order GAUSSIAN function in this thesis) including the first two-GAUSSIAN-component function (or called double GAUSSIAN function) for the blue spectral piece and the second two-GAUSSIAN-component function for the YAG phosphor spectral piece like described in Figure 6.11.b.

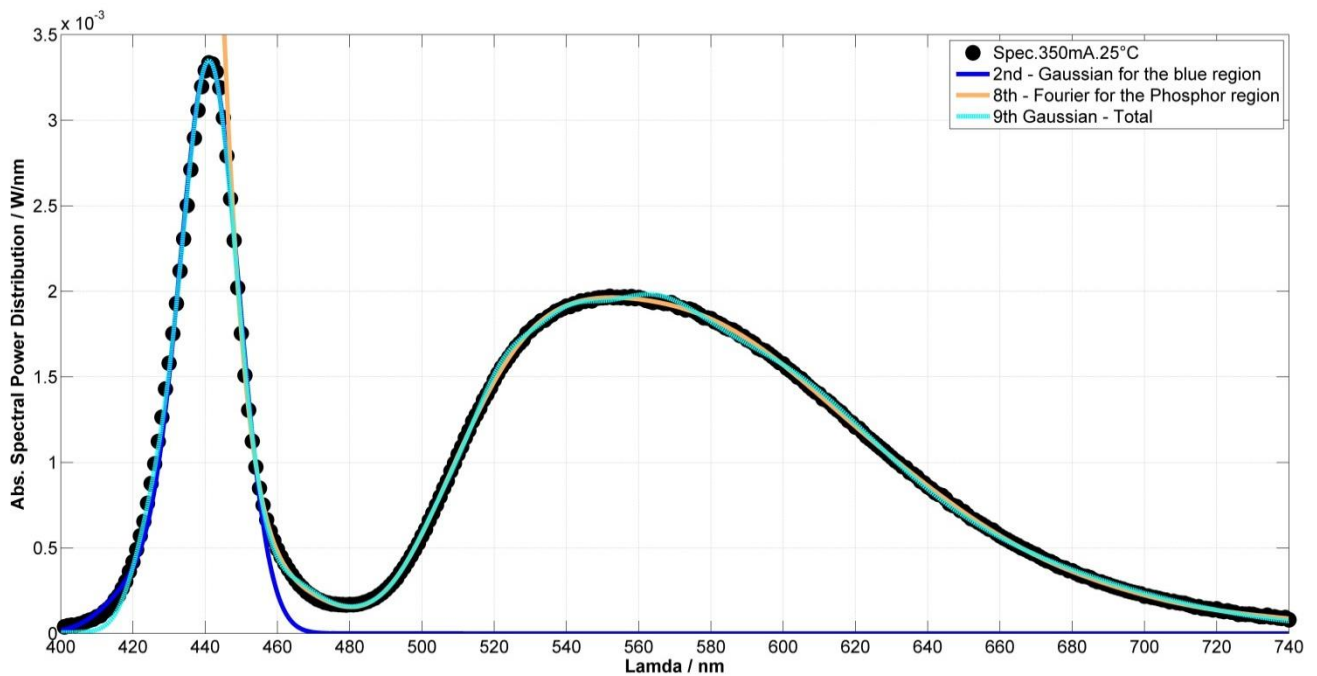


Figure 6.21 - Investigation for mathematical functions of horizontal spectral LED models as an example

Nevertheless, in the real investigation of the author, the fitting for the YAG phosphor spectral piece with two-GAUSSIAN-component function was not completely available. Moreover, the attempt with other higher order GAUSSIAN functions for this spectral piece did also not achieve the desired accuracy. Furthermore, the effort with other spectral piecewise separations and with other mathematical forms of polynomial, GAUSSIAN and FOURIER functions were impossible to be accepted, because their constants had no functional correlations with the junction temperature and forward current. Finally, based on many experiments with the diverse combinations of spectral separations and mathematical functions, only spectral separation with a blue spectral piece and a YAG phosphor spectral piece are possible to be accepted. Correspondingly, the mathematical description of double GAUSSIAN and the eighth order FOURIER functions are appropriate for them, respectively. Visually, in Figure 6.21 they are described by the blue curve and the orange curve in the case of 350 mA and 25 °C as an example. However, unfortunately with this piecewise approach, the horizontal spectral LED model always faced the problem of the limited point 450 nm between spectral pieces. Particularly, the left-450 nm belonging to the blue horizontal spectral model and the right-450 nm belonging to the YAG phosphor

horizontal spectral model change dissimilarly under different operating conditions. In addition, the model parameters of spectral functions had no good functional correlations with forward current and junction temperature. Therefore, this approach should also not be used for the LED modeling. Thus, in order to avoid problems in the first approach, in the second approach the author of this thesis fits the total measured spectrum by the high GAUSSIAN order function. Fortunately, the ninth GAUSSIAN order function (denoted by the cyan curve in Figure 6.21) can play its role quite well because of both the best fitting quality and best satisfaction for the functional correlations with forward current and junction temperature. A well, the parameters of this fitting were listed in Table 6.10.

Table 6.10 - Fitting parameters of the ninth GAUSSIAN function for the cold white PC-LED as an example

$a_1 / 10^{-4}$	5.68	5.32	3.88	3.63	10.7	8.32	7.05	5.16	9.19	17.3	8.83	6.31
$a_2 / 10^{-3}$	3.25	2.70	2.31	1.89	5.25	4.46	3.38	3.32	6.62	4.86	4.47	4.18
$a_3 / 10^{-4}$	2.82	2.93	2.88	2.88	4.37	4.22	5.21	3.54	5.90	6.50	5.47	5.87
$a_4 / 10^{-5}$	37.7	67.0	38.1	18.0	0.005	85.9	67.6	53.9	51.3	14.4	71.8	11.4
$a_5 / 10^{-4}$	4.18	10.3	9.61	4.41	14.5	15.5	16.0	4.90	21.5	7.80	14.8	14.5
$a_6 / 10^{-4}$	6.40	6.30	5.81	5.20	5.90	5.32	9.20	13.8	18.1	6.15	10.0	8.88
$a_7 / 10^{-4}$	8.42	7.66	9.12	7.31	11.1	12.2	18.5	7.36	13.1	14.3	14.0	13.4
$a_8 / 10^{-4}$	9.02	11.6	9.82	9.10	16.1	13.8	12.0	16.6	27.5	24.8	17.9	21.7
$a_9 / 10^{-4}$	6.82	6.54	8.05	5.57	8.68	16.1	9.61	6.91	7.10	8.15	15.6	94.9
b_1	426.4	427	425.4	428.8	426.8	425.5	427.7	424.6	424.2	429.8	426.5	424.9
b_2	441.2	442.6	443.6	444.8	441.5	442.5	444.3	444.2	441	443.9	444.9	445.4
b_3	461	465.1	468.2	460.1	462.4	465.9	461.2	465.9	461.7	462.2	472.6	480.6
b_4	505.9	507.8	500.1	503.3	501.5	506.9	506.9	506.1	502.1	505.3	502	508.4
b_5	518.9	525.7	518.8	517.5	521.5	524.8	524.7	519.3	522.1	518.7	519.7	524.8
b_6	533.6	541.6	535.4	533.9	543.6	540.7	544	536.6	543.3	536.6	536.8	541.2
b_7	554	556.9	551	553.1	561.6	552.2	562.1	565	565.7	550.1	553.3	555.6
b_8	588.1	582.9	580.3	584.3	591.5	580.3	601	587.1	592.9	582.7	581.8	583.6
b_9	613.4	628.1	620.6	623.2	606.8	605.8	621	606.5	611.6	619.8	608.8	626.7
c_1	9.659	11.6	11.51	10.35	11.24	11.4	10.73	11.4	10.99	13.68	14.88	15.9
c_2	10.56	11.52	13.1	12.82	11.22	12.48	13	14.6	12.09	11.97	14.79	16.24
c_3	14.69	18.98	17.12	45.79	11.19	21.21	42.56	23.48	13.37	16.16	14.23	18.63
c_4	17.21	15.7	13.86	11.24	20.17	13.6	12.93	14.05	16.1	13.72	14.36	12.49
c_5	13.99	13.13	13.75	14.66	22.39	13.85	15.37	12.79	16.26	17.68	14.4	12.27
c_6	17.9	11.51	12.34	19.32	20.45	11.46	15.13	20.69	16.02	20.39	15.21	13.5
c_7	29.16	20.78	22.25	32.42	32.8	22.54	30.06	24.84	21.27	39.7	26.18	27.96
c_8	44.93	42.7	37.2	49.6	54.21	39.3	40.13	57.49	54.66	63.57	45.75	53.18
c_9	84.16	70.45	68.02	80.78	102.7	79.19	85.33	111.4	127	101.5	85.9	87.08
I_f / mA	350	350	350	350	700	700	700	700	1000	1000	1000	1000
$T_j / ^\circ\text{C}$	36	65	101	115	44	82	110	124	60	90	122	137
$T_s / ^\circ\text{C}$	25	55	85	100	25	55	85	100	25	55	85	100
V_f / V	3.015	2.963	2.914	2.890	3.173	3.117	3.067	3.043	3.273	3.216	3.165	3.141

* **Evaluation of the accuracy of LED models:** From the parameters in Table 6.10, three-dimensional functions $a_1=f_{a1}(I_f, T_j) \dots a_9=f_{a9}(I_f, T_j)$, $b_1=f_{b1}(I_f, T_j) \dots b_9=f_{b9}(I_f, T_j)$ and $c_1=f_{c1}(I_f, T_j) \dots c_9=f_{c9}(I_f, T_j)$ are buildable.

As well, a specific program is programmed in order to describe the operation of the LED model and to compare between simulated and measured spectra. The interface of this program is described in Figure 6.22. Particularly, its inputs are forward current and sensor temperature, and its outputs are an output spectrum with a visual image and a corresponding data table, constants of the horizontal spectral LED model, forward voltage, electrical power, optical power, thermal power, junction temperature, thermal resistance, luminous flux, luminous efficacy, radiative efficiency, color correlated temperature, whiteness, chromaticity (x, y, u', v'), color rendering indexes ($R_1-R_{14}, R_a, AVR_{1-14}$), peak wavelength and full width at half maximum (parameters about color quality can be displayed by pressing on button “Calculate & Display CRI & Others”). Additionally, in more detail color differences between simulated and measured spectra at different operating conditions were listed in Table 6.11. Based on these results, it can be recognized, that the biggest color difference was 3.70 MAC ADAM ellipses and the smallest color difference was 0.62 MAC ADAM ellipses. Moreover, according to researched results published by the author in [37], these color differences between measured and simulated LED spectra in different operating conditions can be accepted for solid state lighting applications that require quite high color accuracy. However, the spectra at some operating points such as 350 mA and 55 °C or 350 mA and 85 °C have dissimilar shapes to the measured spectra in the spectral region of YAG phosphor visually, although their color differences are still quite small and their operating condition is similar. As a result, it can cause a little offset about color rendering indexes between measured and simulated spectra. Therefore, another new idea should be investigated and offered for applications that required higher accuracy for many aspects such as color difference, color rendering index and others.

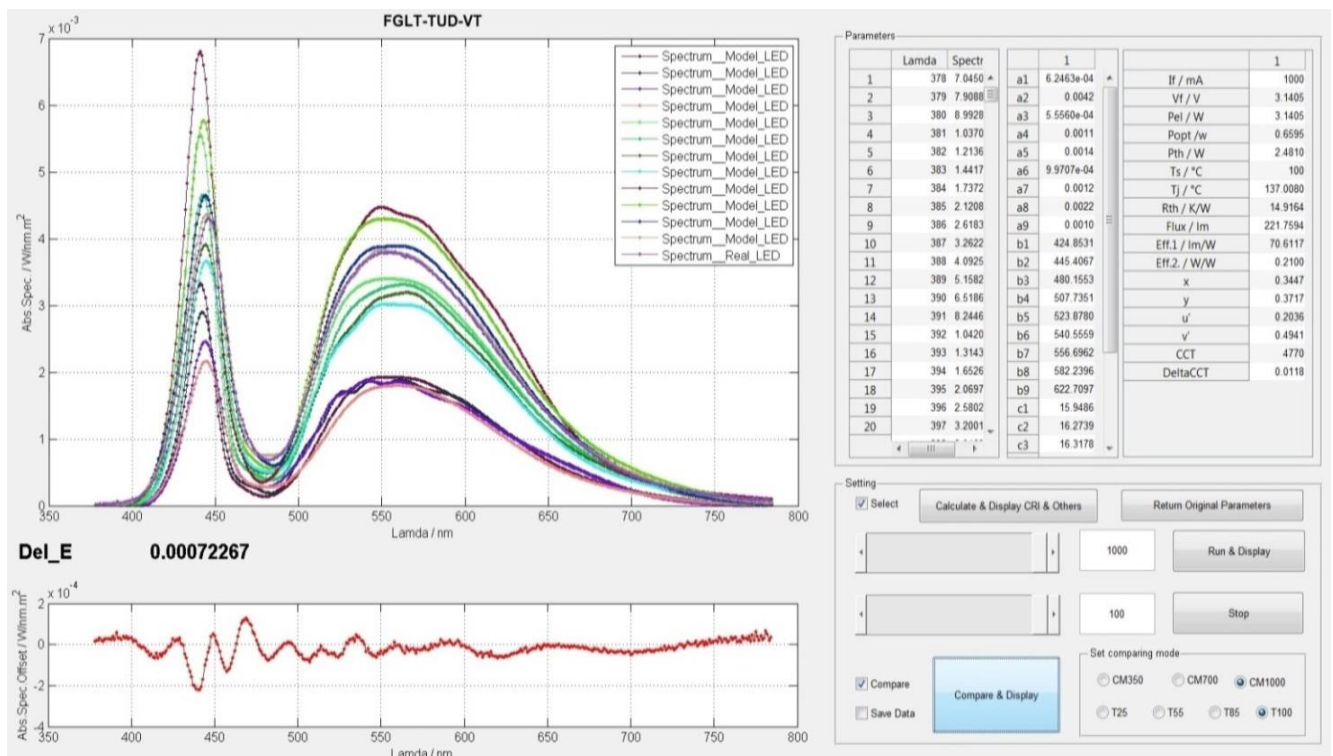


Figure 6.22 - Interface of the evaluating program for the cold white PC-LED as a demonstration example

Table 6.11 - Color differences between the simulated and measured spectra in different operating conditions

I_f / mA	350	350	350	350	700	700	700	700	1000	1000	1000	1000
$T_s / \text{°C}$	25	55	85	100	25	55	85	100	25	55	85	100
$\Delta u'v'_{\text{Me.-Mo.}} / 10^{-3}$	2.39	2.67	2.99	3.70	1.05	2.66	2.09	2.29	1.68	1.48	0.62	0.72

b. Proposal and establishment for vertical spectral LED models of white PC-LEDs

In Section 6.4.4.a, the horizontal spectral LED model was investigated and established for the cold white PC-LED. Therefore, its available mathematical forms, advantages, disadvantages and applicable regions were determined obviously. Otherwise, the new idea of vertical spectral LED models was described in Section 6.4.3.b and was pointed out, that vertical spectral LED models achieved the higher color accuracy than horizontal spectral LED models in the modeling of color semiconductor LEDs.

In this section, this new idea is carried out successively for a typical warm white PC-LED (2700 K) of Manufacturer B (called B2.7K), a other typical warm white PC-LED (3000 K) of Manufacture C (called C3K), a typical neutral white PC-LED (4000 K) of Manufacturer C (called C4K) and a typical cold white PC-LED (5000 K) of Manufacturer B (called B5K). The appropriate operating region is defined by the forward current of 100 mA - 1000 mA and the sensor temperature of 25 °C - 100 °C. Furthermore, the operating point of 350 mA and 80 °C is not used in the interpolation and establishment of vertical spectral LED models so that it can be used for objective comparisons. The used temperature in the establishment of vertical spectral LED models is the sensor temperature that is measurable by a normal temperature sensor at any point on printed circuit boards of PC-LEDs. Finally, the specific program, which was programmed and described in Figure 6.16, is used to establish vertical spectral LED models for four white PC-LEDs B2.7K, C3K, C4K and B5K of the manufacturers B and C.

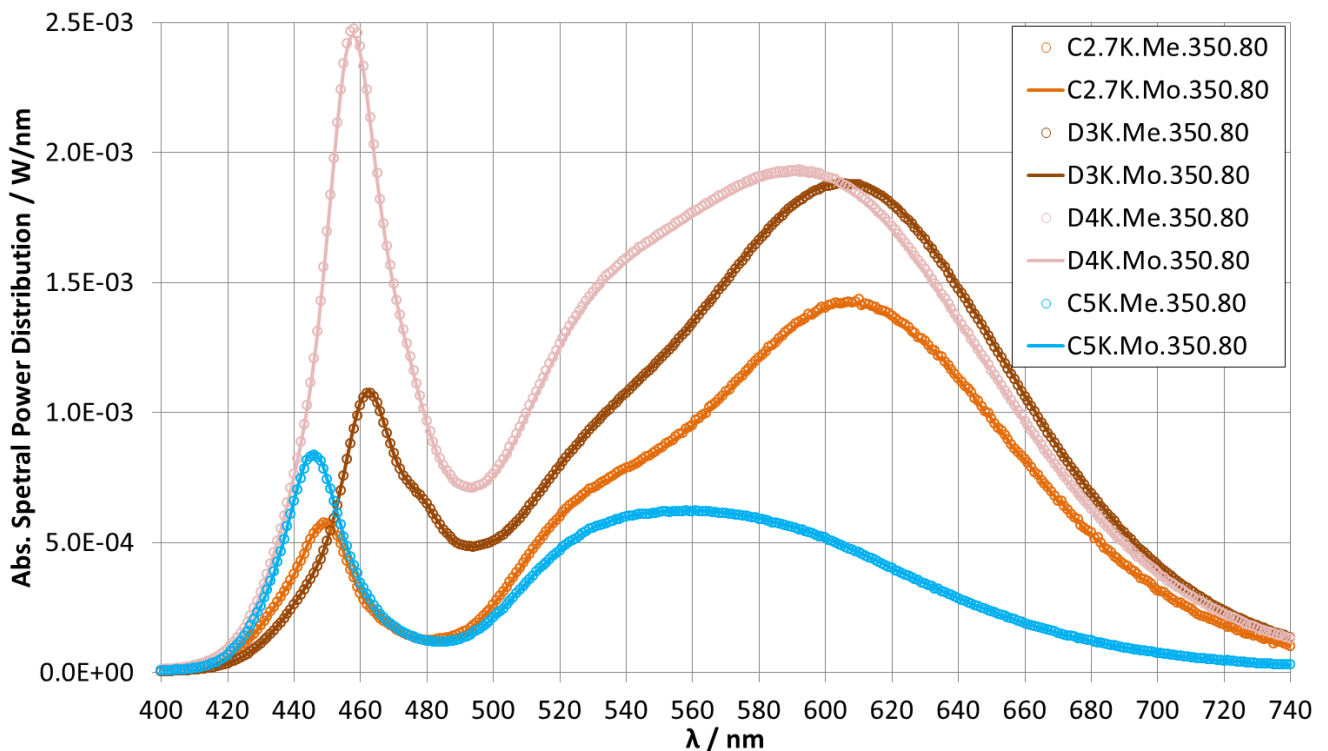


Figure 6.23 - Spectral comparison between measured and simulated absolute SPDs of a typical low warm white (2700 K - B2.7K), high warm white (3000 K - C3K), neutral white (4000 K - C4K) and cold white (5000 K - B5K) of two different manufacturers (B and C) as demonstration examples. Symbols "Me." and "Mo." denote measured and modeled spectra, respectively. And symbol "350.80." denotes 350 mA and 80 °C.

Successively, the spectral comparison between the measured and simulated LED spectra is shown in the figure 6.23. Visually, it can be recognized, that there was nearly no offset between the measured and simulated spectra of the white PC-LEDs. In more detail, the comparison results of color differences ($\Delta u'v'_{Me-Mo}$), correlated color temperatures (CCT_{Me} and CCT_{Mo}) and average color rendering indexes for fourteen standard CIE test color samples ($AVR_{1-14.Me.}$ and $AVR_{1-14.Mo.}$) between the measured and simulated LED spectra are revealed in Table 6.12. Based on these results, it can be identified, that the

maximal color difference ($\Delta u'v'_{Me-Mo}$), correlated color temperature offset (ΔCCT_{Me-Mo}) and average color rendering index offset ($\Delta AVR_{.1-14 Me-Mo}$) between the measured and simulated spectra are 0.14 MAC ADAM ellipses, 3.89 K and 0.07, respectively. Likewise, the minimal $\Delta u'v'_{Me-Mo}$, ΔCCT_{Me-Mo} and $\Delta AVR_{.1-14 Me-Mo}$ are 0.04 MAC ADAM ellipses, 1.06 K and 0.03, respectively. These differences are very small compared with the LED models published previously. Therefore, the vertical spectral LED models of white PC-LEDs can be accepted as the applicable optical transient LED models for solid state lighting applications that require a high accuracy of color difference, CCT and CRIs.

Table 6.12- Color differences, CCTs, AVR_{.1-14} between measured and simulated spectra of the white PC-LEDs

Name	$u'_{Measure}$	$v'_{Measure}$	u'_{Model}	v'_{Model}	$\Delta u'v'_{Me-Mo} / 10^{-3}$	$CCT_{Me.}$	$CCT_{Mo.}$	$AVR_{.1-14.Me.}$	$AVR_{.1-14.Mo.}$
B2.7K	0.2610	0.5276	0.2609	0.5275	0.14	2730.43	2733.37	73.90	73.83
C3K	0.2521	0.5207	0.2521	0.5206	0.11	2966.26	2967.32	78.88	78.84
C4K	0.2230	0.4941	0.2230	0.4941	0.04	4225.88	4224.00	79.39	79.36
B5K	0.2059	0.4948	0.2060	0.4948	0.07	4949.91	4946.02	58.82	58.79

6.5. General Summary

The chapter 6 plays a very important role in the research progress of this thesis. Consequently, the investigation, analysis and establishment of the electrical and optical transient LED models for both the color semiconductor LEDs and the white PC-LEDs were studied deeply in order to supply the best measures for the optimization and stabilization of some lighting quality aspects of hybrid LED-lamps in high quality solid state lighting applications in Chapter 7.

Therefore, all models were researched thoroughly in order to achieve a comprehensive perception about their physical, chemical and geometrical nature. As well, a big amount of previous publications with diverse mathematical qualifications in varied modeling forms of many different authors was collected and analyzed explicitly so as to identify their advantages, disadvantages, appropriate objects and applicable regions. As a result, some previous achievements were inherited such the diffusion-recombination mechanism for electrical transient LED models, the double GAUSSIAN function for horizontal optical transient LED models of color semiconductor LEDs or the idea of horizontal optical transient LED models with their constants as the three-dimensional functions of forward current and junction temperature.

Successively, the new idea of a usable electrical transient model that is limited in a defined experimental operating region of forward current and temperature junction as well as the new idea of the horizontal and vertical optical transient LED models for both color semiconductor LEDs and white PC-LEDs were investigated and carried out in reality. Then, the spectra of the established models were compared with the measured spectra at the operating points that were not used for the interpolation in the previous LED model establishment so that the evaluation for their accuracy was the most objective and accurate. Moreover, the standard concept of the color differences ($\Delta u'v'$, CIE 1976) was applied to evaluate for the accuracy of color semiconductor LED models and white PC-LED models.

Finally, the achieved results proved that horizontal spectral LED models can be accepted for the solid state lighting applications that do not require very high color accuracy. The vertical spectral LED models with a very high color accuracy should be used for the establishment of optical transient LED models of both color semiconductor LEDs and white PC-LEDs in high quality solid state lighting applications that will be carried out in Chapter 7. Particularly, the optical transient LED models of some deep red, red, green, blue and royal blue semiconductor LEDs of two manufactures B and C described in Figure 6.19 and the warm white PC-LED (3000 K) of Manufacturer C described in Figure 6.23 will be used for the optimization and stabilization in Chapter 7.

7. Optimization and stabilization for some lighting quality aspects of hybrid LED-lamps adapted to color objects

7.1. Motivation and general consideration

7.1.1. Motivation

The demand of high quality solid state lighting applications worldwide such as the film and television lighting, the shop lighting, the architectural lighting and the museum lighting is higher in the last years. Indeed, a high quality solid state lighting system is really necessary to expose completely the worthiness and the beauty of famous paintings drawn by oil colors or by water colors in museums or churches such as the painting “*THE SCHOOL OF ATHENS*” of RAPHAEL in Figure 7.1. Similarly, the one is very important to make the clothes or fruit in fashion or food shops more attractive for customers while it must still ensure the true color of their own skin, hair, textiles or clothes. Otherwise, the managers of shops or museums would pay less money for the energy consumption of the lighting system, although it must still ensure both a high lighting quality and good temperature stability. Thus, in this chapter the above issues are the main motivations of the author to optimize and stabilize some lighting quality aspects of hybrid LED-lamps adapted to color objects in the high quality solid state lighting applications.



Figure 7.1 - RAPHAEL'S “*THE SCHOOL OF ATHENS*”, 1510 - 11, VATICAN palace, ROME published by HAAS, R. in ([109])

7.1.2. General Consideration

In order to realize the above established targets, the general consideration about the optimization and the stabilization some lighting quality aspects of hybrid LED-lamps adapted to color objects in high quality solid state lighting applications is very important. In this context, essential concepts are described and explained as follows,

* **Hybrid LED-lamp and vertical spectral LED models:** The central objects of the solid state lighting solution for the highest quality applications mentioned in this chapter are the hybrid LED-lamps consisting of color semiconductor LEDs and white PC-LEDs that are combined together in the most appropriate form. The name “hybrid LED-lamp” is to reflect this combination. In order to optimize and stabilize their lighting quality aspects, the characteristics of the LEDs must be characterized accurately. The vertical spectral LED model establishment method proved previously in Chapter 6 was the method that achieved the highest accuracy in the characterization for LED spectra. Therefore, in this chapter the vertical spectral LED models, which were established for both the color semiconductor LEDs and the warm white PC-LED described in Figure 6.19 and Figure 6.23 of Chapter 6, will be applied to the optimization and the stabilization of the hybrid LED-lamp.

* **Lighting quality parameters, their limits and proposals for the most appropriate LED combination for the hybrid LED-lamps:** As a background, Section 3.1 of Chapter 3 discussed very specifically about the concepts of the lighting quality in general and the ones in the solid state lighting in particular. In that, the mentioned lighting quality aspects included chromaticity ($u', v', 1976$), correlated color temperature (CCT / K), whiteness ($\Delta u'v'_{CCT}$), color rendering indexes (R_a, R_9 and AVR_{1-14}), color preference, color harmony, color memory, color gamut, light source brightness, object brightness, brilliance, circadian stimulus (CS), scotopic - photopic ratio (S/P), temperature dependence and current dependence. However, in the framework of this chapter not all lighting quality aspects can be investigated concurrently for all lighting applications in general, but only some essential lighting quality aspects for the hybrid LED-lamps in the high quality solid state lighting applications such as chromaticity, correlated color temperature, whiteness, color rendering indexes, luminous flux, luminous efficacy, temperature dependence and current dependence can be considered for the optimization and the stabilization in some particular lighting cases as the methodical demonstration examples. In more detail, based on the practical investigations of the typical color semiconductor LEDs (red, green, blue and orange) and the typical white PC-LEDs (warm white, neutral white and cold white), the achieved results in Chapter 3 confirmed that both the temperature and current dependence of the orange semiconductor LED are very bad; the ones of the red semiconductor LED are much better, and there is a big opposition between the color quality aspects and the energy quality aspect of the white PC-LEDs. Particularly, for excellent CRI LEDs ($R_a > 90$) their luminous efficacy is only around 75 lm/W and most of them have no good temperature stability. Consequently, the orange, yellow or amber semiconductor LEDs should be avoided in the design. In addition, the color rendering indexes should be higher than 90 and the luminous efficacy should be higher than 90 lm/W. As well, the temperature dependence must be stabilized and the current dependence must be taken account into the spectral LED models in order to ensure the highest accuracy in all calculations for the most available combination of the color semiconductor LEDs and the white PC-LEDs in the hybrid LED-lamps.

* **Two methodical demonstration examples and their tasks:** In order to explain the optimization and stabilization principles, meaningfully the optimization and the stabilization should be not carried out for all high quality lighting applications, and their procedures should be not repeated similarly for more than one application. Therefore, the museum lighting will be chosen as the first demonstration

example for the optimization for the average value of the new specific color rendering indexes of the oil color objects (called oil color index) of the hybrid LED-lamp adapted to the oil color objects in the a museum, methodically. And the shop lighting will be selected as the second demonstration example for the optimization and the stabilization for some lighting quality aspects of the hybrid LED-lamp adapted to all red objects of general shop lighting applications. However, the similar procedures of the optimization should be not explained specifically one again in the shop lighting case, but only the stabilization of the correlated color temperature and the whiteness for the best combination case between the color semiconductor LEDs and the white PC-LEDs should be carried out and evaluated in this example. In addition, the color rendering indexes, the luminous efficacy and other subordinate parameters must be ensured as high/stable as possible, besides the stability of the correlated color temperature and the whiteness. Otherwise, about the LED combination and the LED selection of the LED-lamps, both examples will play their own specific roles with different levels. Particularly, the general qualitative criteria will be the main factors in the first example to explain for the most available LED combination. And then the temperature dependence of the color quality parameters, the luminous efficacy and the feasibility of the finished hybrid LED-lamps in its composition and its practical operation in the second example will be used as the supplementary factors for the LED selection in the hybrid LED-lamps.

7.2. Demonstration example of the optimization for some lighting quality aspects of the hybrid LED-lamp adapted to the color objects

Section 7.1 described the motivation and general consideration for the optimization and stabilization of some lighting quality aspects of hybrid LED-lamps in high quality solid state lighting applications. Hence, the museum lighting was assigned as the first demonstration example for the optimization. In addition, the average value of the new specific color rendering indexes of the oil color objects in a museum was determined as the desired lighting quality parameter, which has to be optimized in this example. Consequently, it is called the optimization for LED-lamps adapted to the oil color objects. Successively, in this section the optimization of the oil color index for the hybrid LED-lamp adapted to the oil color objects in the specific museum lighting application will be described and carried out specifically for four correlated color temperatures 3000 K, 4000 K, 5000 K and 6500 K. Particularly, the most available LED combination will be explained based on the general qualitative criteria and the LED selection for that combination will base on the supplement factors described in Section 7.3.1.b. And then, the optimization using the oil color objects will be performed and evaluated for the hybrid LED-lamp. Finally, the new candidate reflectance curves for the museum lighting application will be established and compared with fourteen CIE standard reflectance curves in order to determine the best standard reflectance curves, which can enhance the accuracy of the design, the evaluation and the optimization of the color quality in the museum lighting application.

7.2.1. LED combination and LED selection of the LED-lamps

The temperature dependence of the color quality parameters, the luminous efficacy and the feasibility of the finished hybrid LED-lamps in its composition and its practical operation will be considered more entirely for the LED selection in Section 7.3.1.b. In this section, only the general qualitative criteria are the main factors in the analysis of the most available LED combination and the results of Section 7.3.1.b are used as the complement factors for the LED selection. Finally, the most available solution for both the LED combination and the LED selection will be proposed for the hybrid LED-lamp.

a. Some general qualitative criteria and some LED combination solutions for the LED-lamps

In order to create high quality solid state lighting systems (3000 K, 4000 K, 5000 K and 6500 K), there are many LED combination solutions that can be selected. And some general qualitative criteria of the evaluation for their possibility can be proposed such as the color rendering indexes (R_a , R_9 and AVR_{1-14}), the efficiency (the radiant efficiency and the luminous efficacy), the flexibility (the desired variations of CCT and $CRIs$), the stability (the short term and the long term stability of the color quality parameters, the luminous flux and the luminous efficacy) and the cost of the total LED-lamp with the LED combination solution. Quantitatively, if it is assumed that the mark “1”, “2”, “3” and “4” correspond with “bad”, “acceptable”, “good” and “excellent” levels, respectively and the role of the general quantitative criteria is equal, the evaluation of the LED combination solutions can be described as the following table,

Table 7.1 - Relative quantitative evaluation of some possible LED combinations

Order	Solution	CRI	Efficiency	Flexibility	Stability	Cost	Total
1	R-G-B	1	3	4	1	2	11/20
2	WW-NW-R-G-B	4	1	4	3	1	13/20
3	WW-CW-R-G-B	3	1	3	3	1	11/20
4	NW-CW-R-G-B	3	1	3	3	1	11/20
5	NW-R-G-B	3	2	2	2	3	12/20
6	WW-R-G-B	4	2	4	2	3	15/20
7	WW-CW	4	2	1	4	3	14/20

In Table 7.1, the seven solutions were suggested for possible LED combinations including the case of pure color semiconductor LEDs (called R-G-B ~ order 1), the one of warm white - neutral white PC-LEDs and color semiconductor LEDs (called WW-NW-R-G-B ~ order 2), the one of warm white - cold white PC-LEDs and color semiconductor LEDs (called WW-CW-R-G-B ~ order 3), the one of neutral white - cold white PC-LEDs and color semiconductor LEDs (called NW-CW-R-G-B ~ order 4), the one of neutral white PC-LEDs and color semiconductor LEDs (called NW-R-G-B ~ order 5), the one of a warm white PC-LED and color semiconductor LEDs (called NW-R-G-B ~ order 6) and the one of warm white - cold white PC-LEDs (called WW-CW ~ order 7). Consequently, the results showed that experimentally and quantitatively the sixth solution (WW-R-G-B) should be chosen because of its highest mark (15/20) compared with other cases.

b. Role of componential LEDs and primary proposals for the LED selection

There are many different color semiconductor LEDs and different warm white PC-LEDs belonging to diverse binning groups of varied LED manufacturers in the world, which are possible to be used for the chosen LED combination solution (WW-R-G-B). However, the yellow, amber and orange semiconductor LEDs can be ignored early because their temperature stability and current stability were very bad (See Chapter 3). For other LEDs, many different LEDs such as the royal blue ($\lambda_p \sim 440 \text{ nm} - 450 \text{ nm}$), the blue ($\lambda_p \sim 465 \text{ nm} - 470 \text{ nm}$), the green ($\lambda_p \sim 520 \text{ nm} - 530 \text{ nm}$), the red ($\lambda_p \sim 630 \text{ nm} - 640 \text{ nm}$), the deep red ($\lambda_p \sim 660 \text{ nm} - 670 \text{ nm}$) semiconductor LEDs; and many different warm white PC-LEDs ($CCT \sim 2700 \text{ K} - 3000 \text{ K}$) as well as their combinations of three well-known LED manufacturers on the world (called A, B and C) were used in the practical investigations, which will be

described in more detail in Section 7.3.1.b. Intrinsically, each color semiconductor LED plays its own specific role to compensate partially for the spectral gaps of the original spectrum of the warm white PC-LED. Particularly, the royal blue LED is to complement for the royal blue spectral region in order to enhance the color quality for the blue objects such as blue jeans, the oil royal blue (RO37), the oil Cobalt blue hue (RO39), the oil Phthalate blue (RO43), the oil Cerulean blue (RO44) or the oil Azure blue (RO45). Experimentally, the royal blue LED ($\lambda_p \sim 440$ nm) of the manufacturer A achieved a really good color quality for the CIE twelfth blue test color sample (TCS12). However, unfortunately there are no many good royal blue LEDs with the peak wavelength of 440 nm or shorter on the worldwide market. Similarly, the green LED ($\lambda_p \sim 520$ nm - 530 nm), the red LED ($\lambda_p \sim 630$ nm) and the deep red LED ($\lambda_p \sim 660$ nm) are to fulfill the spectral gaps in the green, the red and the deep red spectral regions in order to increase the color rendering indexes for the green, red or deep red objects, respectively. Especially, the blue LEDs ($\lambda_p \sim 465$ nm - 470 nm) are to adjust the spectral gap between the blue spectral component and the phosphor spectral component of the original spectrum of the warm white PC-LED. Practically, this gap has a special important role in the improvement of the general color rendering index of all hybrid LED-lamps.

c. The secondary LED selection for the most available LED combination of the hybrid LED-lamp

Finally, in the practical performance based on the aspects of the color quality, the temperature stability, the luminous efficacy and the feasibility in the composition and the operation of the hybrid LED-lamps, which will be mentioned in more detail in Section 7.3.1.b, the most available LED-combination between the semiconductor LEDs and the warm white PC-LED for the hybrid LED-lamp can be chosen as follows: Firstly, about semiconductor LEDs, the royal blue ($\lambda_p \sim 450$ nm), the blue ($\lambda_p \sim 470$ nm), the green ($\lambda_p \sim 530$ nm), the red ($\lambda_p \sim 630$ nm) semiconductor LEDs of the manufacturer C and the deep red semiconductor LED ($\lambda_p \sim 660$ nm) of the manufacturer B are the most appropriate choice at this time, because of their temperature stability, their radiant efficiency and their color complement ability reflected by means of the total luminous efficacy, total temperature stability and the color indexes of the hybrid LED-lamp. Secondly, about warm white PC-LEDs, the warm white PC-LED ($CCT \sim 3000$ K) of the manufacturer C is currently the best warm PC-LED for the hybrid LED-lamp, because according to the practical investigations of the author, this warm white PC-LED is the most efficient (105 lm/W at 350 mA and 60 °C illustrated in Figure 1.2 of Chapter 1 and has the best temperature dependence (under 3 MAC ADAM ellipses, the operating temperature is allowed to change from 25 °C to 100 °C in two cases of 350 mA and 700 mA). In addition, the peak wavelength of its phosphor spectral component is about 600 nm, which can replace well the unstable yellow, amber or orange semiconductor LEDs.

7.2.2. The optimization for the oil color index of the hybrid LED-lamp adapted to oil color paintings

Based on the semiconductor LEDs, the warm white PC-LED chosen in Section 7.2.1 and the vertical spectral LED model establishment method with a very high accuracy demonstrated in Chapter 6, their vertical spectral LED models can be established quite easily for the hybrid LED-lamps like the results described in Figure 6.19 and Figure 6.23 of Chapter 6. In this section, the specific museum lighting with oil color paintings will be used as a demonstration example for the optimization principle adapted to the color objects. Particularly, the spectral reflectance curves of the different color objects of the oil color paintings in a museum, the ones of the human skin types, human hair types, textiles and clothes will be measured and quantified by the new color rendering index. Successively, these new specific color rendering indexes will be prioritized following to their importance for the museum lighting. Finally, the average value of the color rendering indexes of the oil color objects will be optimized in

order to have the best color quality of the hybrid LED-lamp. As well, the specific average value of the color rendering indexes of the skin, hair, textiles and clothes will also be kept at the acceptable level (≥ 80).

a. Oil paintings and their specification for museum lighting

In order to satisfy the demand of high quality museum lighting, the optimization of the lighting system should be performed according to the specific oil color paintings. In the specific part of a museum with the oil color paintings, the desired color objects are the oil color objects and the color objects belonging to visitors such as skin types, hair types, textiles and clothes. In this section, these color objects will be measured and discussed for their spectral reflectance curves.

* **Color objects and their spectral reflectance curves in the museum:** Naturally, any oil painting must be drawn by oil inks. Therefore, in Figure 7.2 seventy nine original oil colors of the oil inks, which are usually used by painters, are described. These colors are denoted as RO1-RO79 in this thesis and their real names are listed correspondingly in Appendix C. Otherwise, Figure 7.3, Figure 7.4, Figure 7.5 and Figure 7.6 show the spectral reflectance curves of the human skin types, human hair types, textiles and clothes, respectively. In order to have these results, thirty two candidates were chosen for the investigation. In that, there are four men and twenty eight women coming from different regions in Africa, Europa and Asian and their ages distribute from twenty five to sixty two.



Figure 7.2 - Seventy nine well-known oil colors RO1 - RO79 of the oil paintings ([108])

* **Analysis of the spectral reflectance curves of the color objects:** Based on the measured results in Figure 7.3, it can be recognized, that although the spectral reflectance of the diverse skin types is different depending on gender, age and country, their rising edges are always about at 600 nm. Hence, in order to enhance the color quality for these human skin types, the peak wavelength of the spectral component of the PC-LED or the one of the color semiconductor LEDs in the hybrid LED-lamp should be about 600 nm. Similarly, Figure 7.4 shows the very low reflectance values of different hair types

(under 0.6 in the range of 400 nm - 740 nm). In addition, these spectral reflectance curves are often flat and some of them have the rising edges of about 680 nm of the deep red spectral region or the ones of about 600 nm of the amber/orange spectral region. Consequently, the color quality of the human hair types is usually high for different light sources. Finally, the spectral reflectance of the textiles is also quite low (almost under 0.7 in the range of 400 nm - 740 nm) and their rising edges lie at the high wavelength (about 690 nm) of the deep red spectral region. In contrast, the clothes have quite high spectral reflectance and the distribution of their rising edges is quite wide in the range of 400 nm - 740 nm such as 420 nm, 530 nm, 560 nm, 590 nm or 680 nm of the blue, green, yellow, orange and red spectral regions leading to the demand of the hybrid LED-lamps with the full spectral components.

*** Qualification and prioritization of the color objects for the optimization of museum lighting:** For museum lighting, the colors of seventy nine oil color objects always play the main role and the colors of skins, hair, textiles and clothes only play the subordinate role in the optimization. In order to qualify for these color objects, the standard definitions and equations of the CIE color rendering index (*CRIs* for fourteen CIE standard reflectance curves (TCS1 - TCS14)) are applied to calculate their new specific color rendering indexes. Particularly, when fourteen standard spectral reflectance curves of the CIE test color samples (TCS) are substituted by other spectral reflectance curves of the oil color objects and the skin, hair, textile and clothes types, the color rendering indexes for these color objects can be determined and called as the new specific color rendering indexes. Then these new specific color rendering indexes for seventy nine oil color objects are denoted by RO_1-RO_{79} and their average value is denoted by $AVR_{.01-79}$ (called the oil color index) in this thesis. Likewise, the average value of the skin, hair, textile and clothes color rendering indexes are also called as the skin color index, the hair color index, the textile color index and the clothe color index.

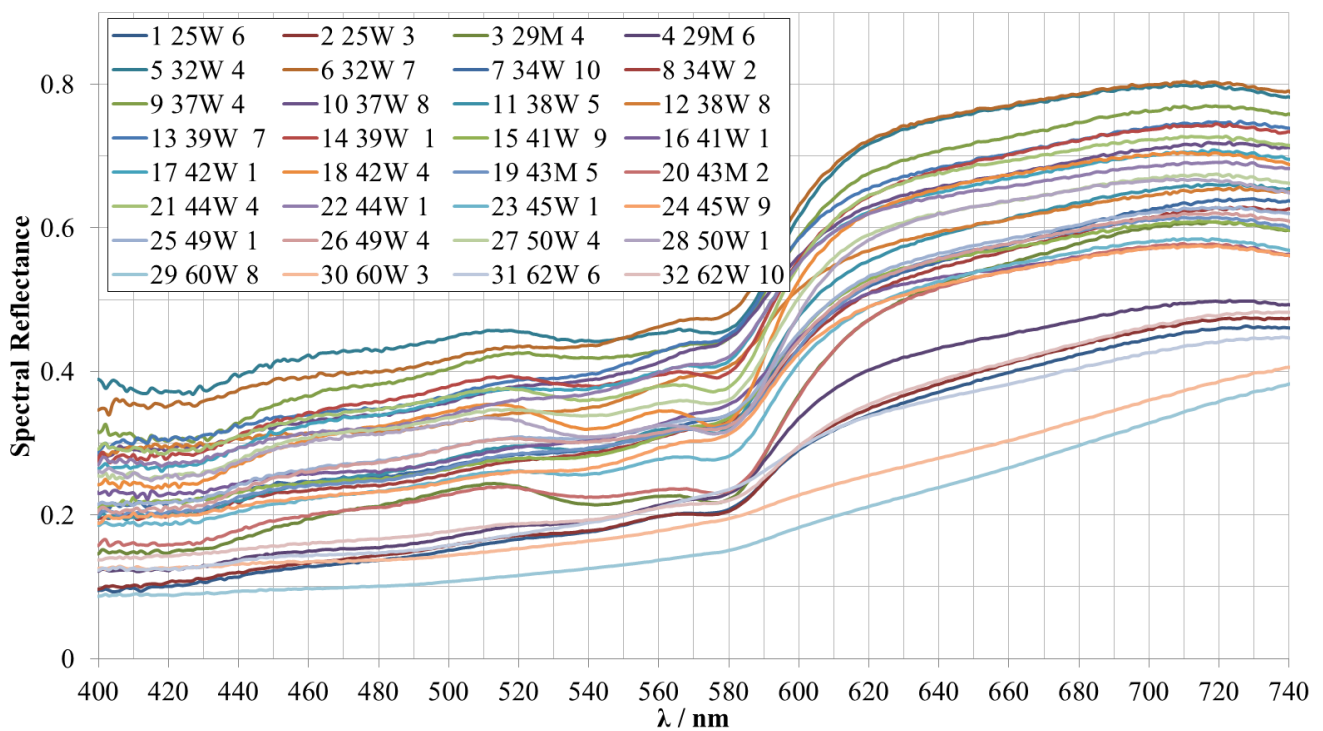


Figure 7.3 - Spectral reflectance curves of some different types of the human skin ([154])

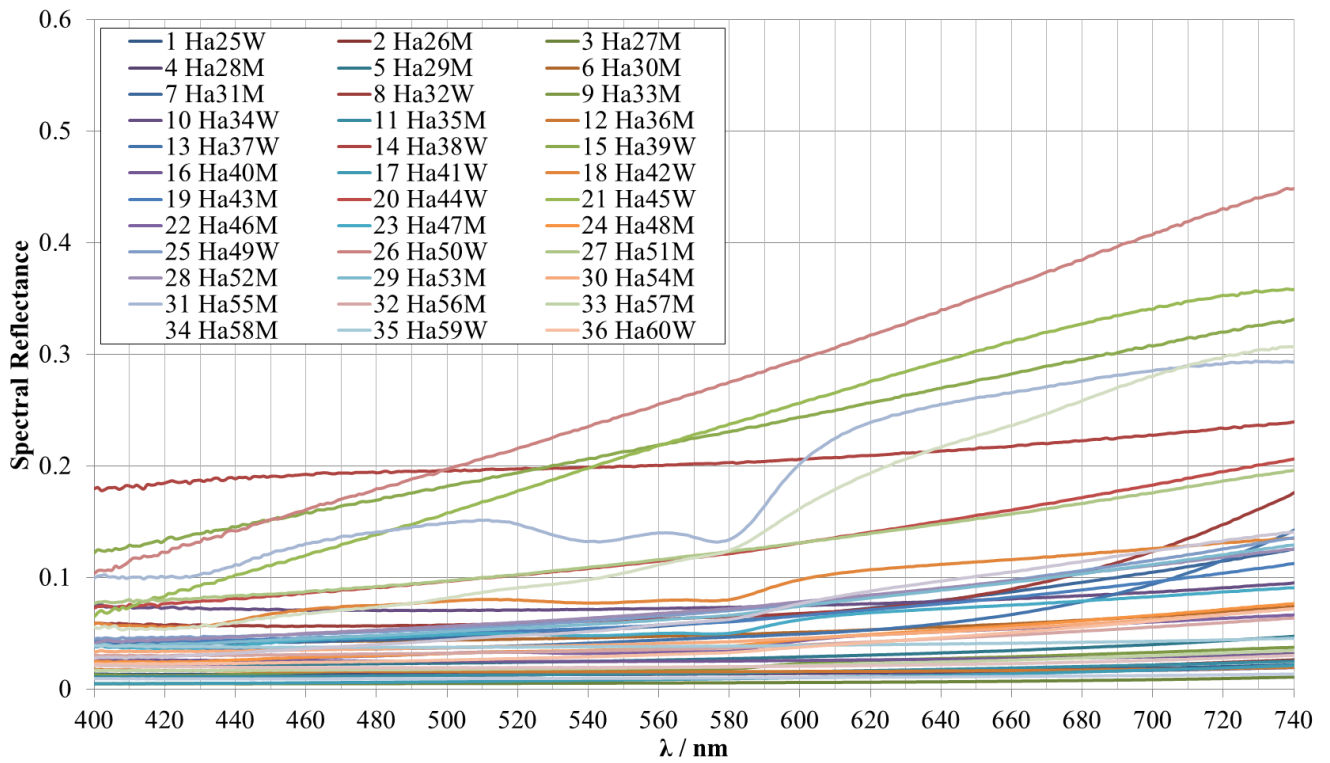


Figure 7.4 - Spectral reflectance curves of some different types of the human hair ([154])

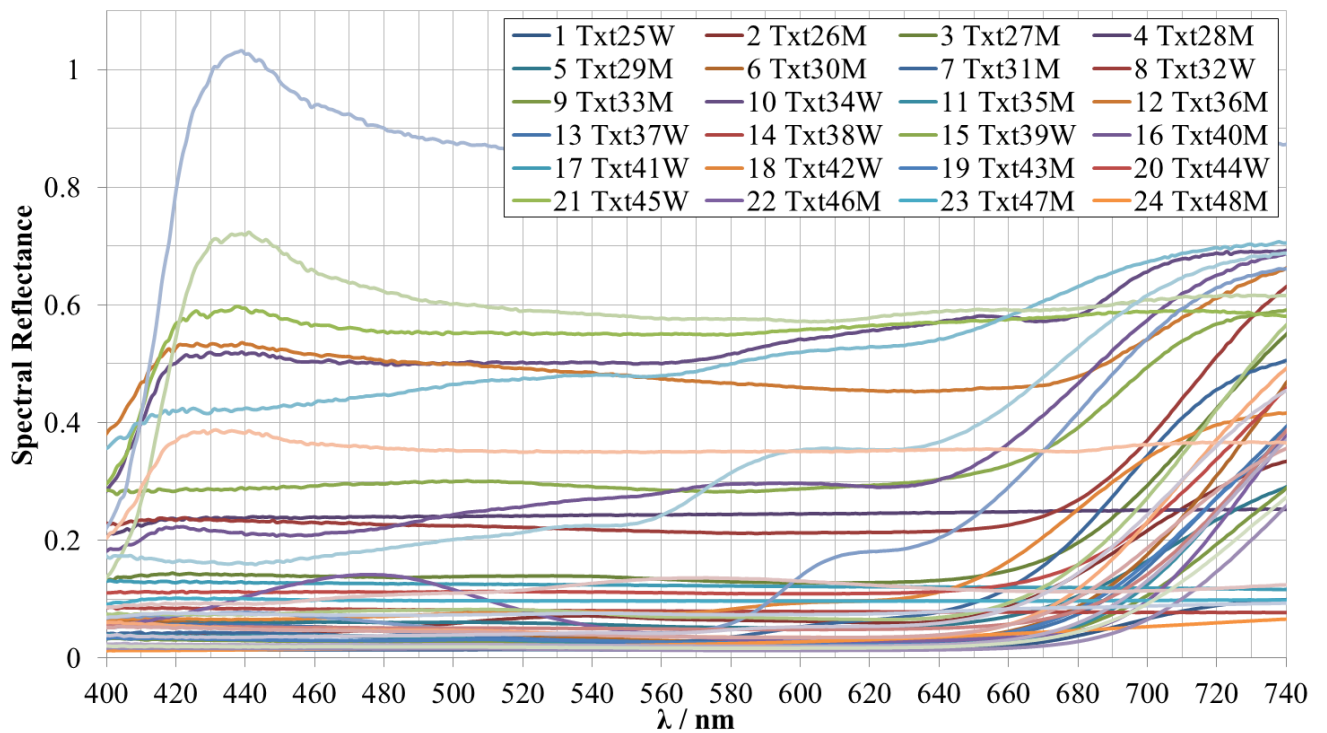


Figure 7.5 - Spectral reflectance curves of some varied colored textiles ([154])

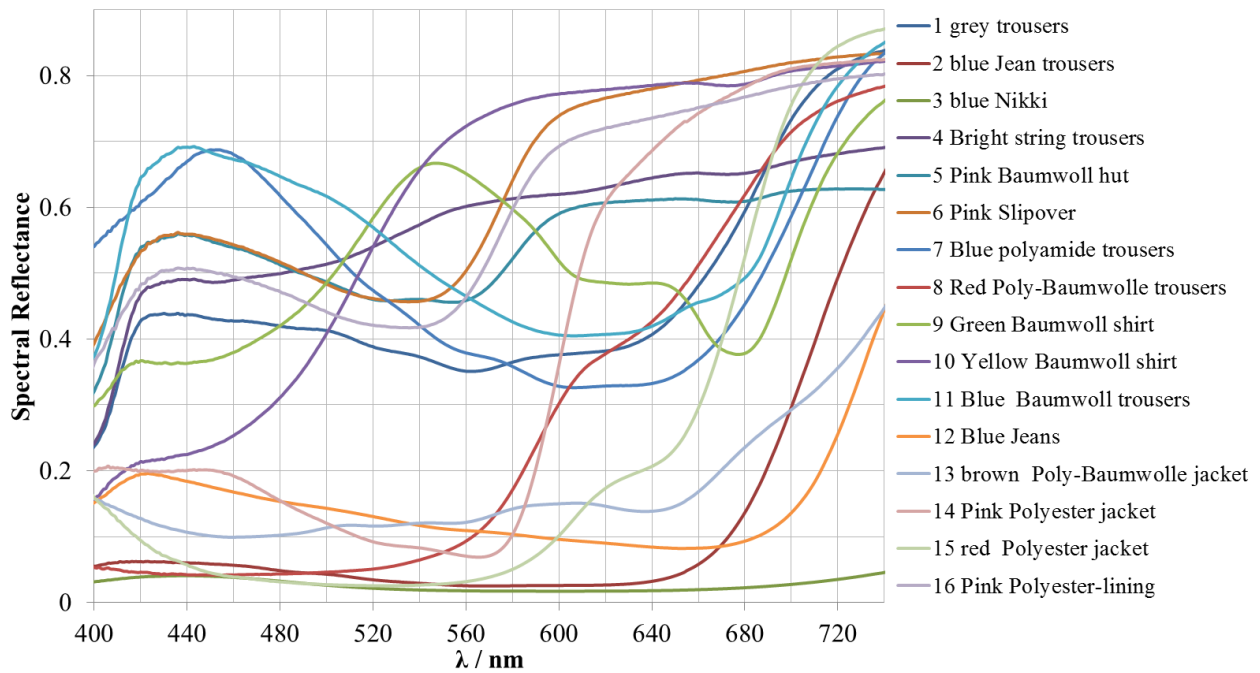


Figure 7.6 - Spectral reflectance curves of some different clothes ([154])

b. Description of the system structure diagram for the optimization

The idea of the control system structure as a multi-input multi-output system (MIMO system) can be applied in case of the hybrid LED-lamps. In that control system structure, the central objects of the MIMO system with its inputs and its outputs (or their set signals and their feedback signals) must be described.

* **Objects of the MIMO system:** In Section 7.2.2.a the color objects were investigated including the oil colors, the skin colors, the hair colors, the textile colors and the cloth colors. The parameters for the identification of these color objects were quantified according to the standard definitions and equations of the CIE color rendering index. Otherwise, the royal blue ($\lambda_p \sim 450$ nm), the blue ($\lambda_p \sim 470$ nm), the green ($\lambda_p \sim 530$ nm) and the red ($\lambda_p \sim 630$ nm) semiconductor LEDs of the manufacturer C, the deep red semiconductor LED ($\lambda_p \sim 660$ nm) of the manufacturer B and the warm white PC-LED ($CCT \sim 3000$ K) of manufacturer B were characterized by their vertical spectral LED models like the results shown in Figure 6.19 (called C-450.Mo.350.80, C-470.Mo.350.80, C-530.Mo.350.80, C-630.Mo.350.80 and B-660.Mo.350.80) and Figure 6.23 (called C3K.Mo.350.80) of Chapter 6, respectively. Thus, in the MIMO system of the hybrid LED-lamp, the vertical spectral LED models of the color semiconductor LEDs and the warm white PC-LED became the central objects of the closed loop control structure illustrated in Figure 7.7 in order to satisfy color quality demands of the color objects.

* **Inputs of the MIMO system:** The main inputs of the MIMO system are the forward currents for all LEDs and the subordinate input is the operating temperature of the entire hybrid LED-lamp. In the optimization process for the hybrid LED-lamp, this subordinate input is just to reflect as the hot binning or the cold binning condition. In addition, in Chapter 4 it was proved that the hot binning at the LED manufacturers is better than the cold binning for the selection and the establishment of LED-luminaires in the manufacturing companies of LED-luminaries. Therefore, the operating temperature in the optimization process in this thesis is always chosen 80°C constantly. Otherwise, the higher the forward current of the warm white PC-LED is, the lower its luminous efficacy is. Consequently, the forward current of 700 mA or lower (about 500 mA) should be selected as the compromise between

the output luminous flux and the luminous efficacy so that the luminous efficacy of the finished hybrid LED-lamp should be always around 90 lm/W as the acceptable limit compared to the other high color rendering index white PC-LEDs that were mentioned in the practical investigation in Chapter 3. Then, in the condition of 80 °C for the operating temperature and 700 mA for the warm white PC-LED forward current, the optimization process is carried out to be able to attain appropriate control laws for the forward currents of the royal blue, the blue, the green, the red and the deep red semiconductor LEDs.

* **Outputs (or the set signals and the feedback signals) of the MIMO system:** Three set main signals including the set correlated color temperature (CCT_{set}), the set whiteness ($\Delta u'v'_{CCT,set}$) and the set average oil color rendering index or the set oil color index ($AVR_{oil,set}$); and four set subordinate signals including the set average skin color rendering index or the set skin color index ($AVR_{skin,set}$), the set average hair color rendering index or the set hair color index ($AVR_{hair,set}$), the set average textile color rendering index or the set textile color index ($AVR_{textile,set}$) and the set clothe color rendering index or the clothe color index ($AVR_{clothe,set}$) must be considered by the optimizing algorithm in the optimization process. If the subordinate parameters such as the skin color index, the hair color index, the textile color index, the clothe color index are only required to fulfill the acceptable limit (higher than 80), the correlated color temperature must be kept at the specific values such as 3000 K, 4000 K, 5000 K or 6500 K as well the whiteness must be kept at its appropriate level (which is lower than $\Delta u'v'=0.001$), and the oil color index must be optimized up to their maximal values as possible. Otherwise, a signal bus for all feedback signals determined from the output spectrum of the hybrid LED lamp is necessary to calculate offsets between the set values and the feedback values (denoted by $Err_{.1} - Err_{.7}$). Finally, based on these errors, the controller of the MIMO system in the control system structure will perform its algorithm to achieve the above specified optimal values.

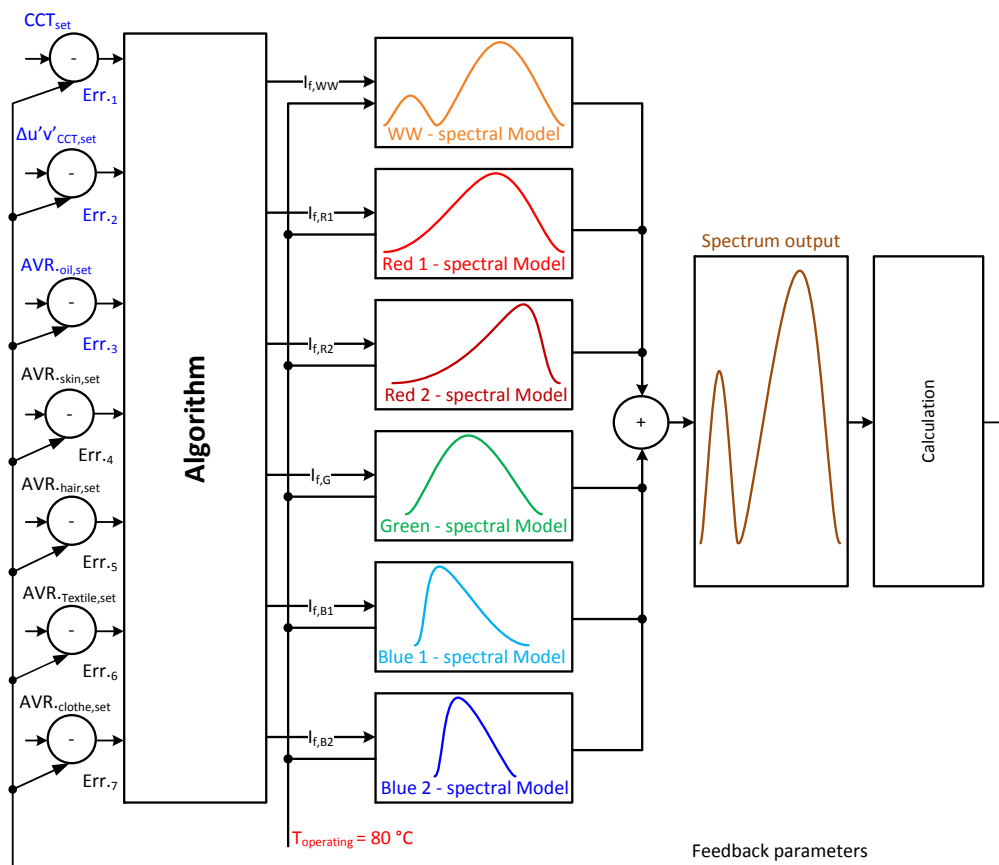


Figure 7.7 - Control system structure for the optimization of the hybrid LED-lamp

c. Optimized spectral power distributions of the hybrid LED-lamps

Figure 7.8 shows four optimized spectra for the cases of 3000 K, 4000 K, 5000 K and 6500 K in museum lighting. In the case of 3000 K, both the red LED and deep red LED play a very important role, whereas the green LED and the blue LED were just included to support color balance and to enhance the gap between the blue spectral component and the phosphor spectral component. The royal blue LED had nearly no influence on this optimization, because its role was substituted by the royal blue, which had existed previously in the warm white PC-LED. Oppositely, in the cases of 5000 K and 6500 K, the royal blue LED has played a very important contribution to the total color mixing, because the spectral amount of the royal blue, which had existed previously in the warm white PC-LED, was not enough for the total color mixing of the hybrid LED-lamp. The green LED and the deep red LED were to support color balance and to increase the color rendering index for the entire spectrum of the hybrid LED-lamp, respectively. Contrarily, the red LED had an inconsiderable role in these cases, because the partial spectrum of the wide phosphor spectrum of the warm white PC-LED replaced its role. Finally, in case of 4000 K the role of the blue royal LED and the red LED became more similar and the weight of the deep red LED and especially the green LED were much more important than others for the total color mixing of the hybrid LED-lamp, because they must enhance both the right and left spectral components of the original spectrum of the warm white PC-LED in order to ensure the correlated color temperature of constant 4000 K. As well, the whiteness was always kept lower than $\Delta u'v'=0.001$ and the oil color index must be maximized.

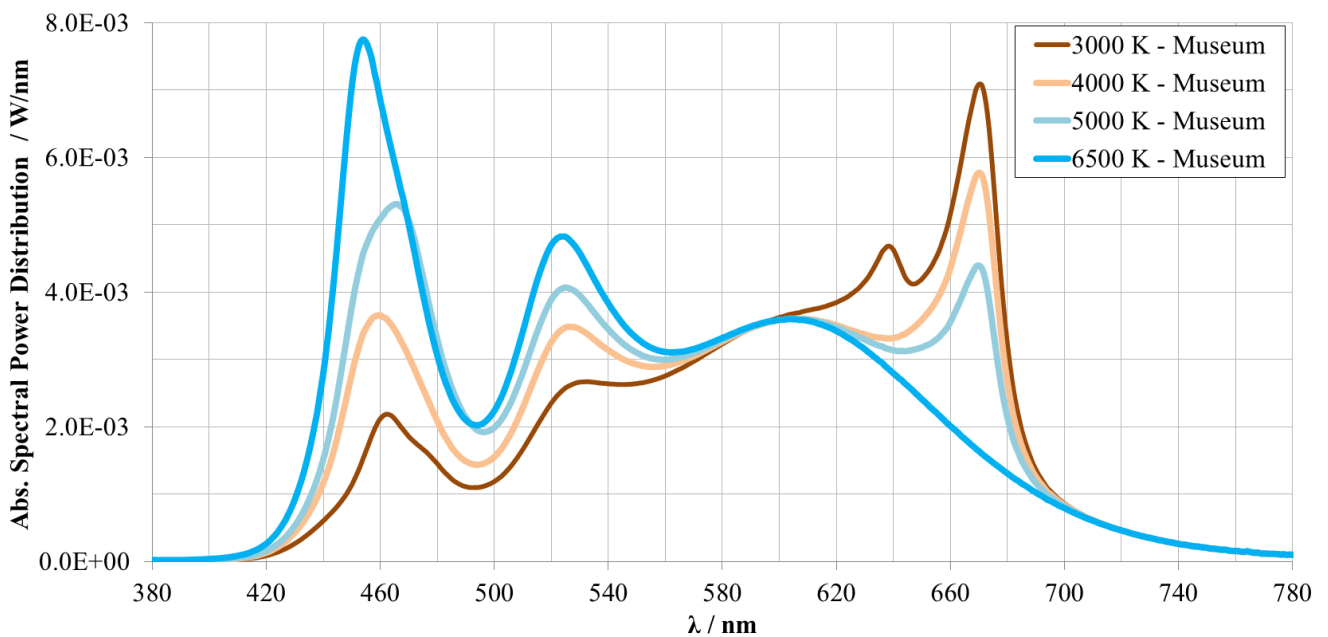


Figure 7.8 - Optimized absolute SPDs of cases 3000 K, 4000 K, 5000 K and 6500 K for the museum lighting

In more detail, the figures 7.9 and 7.10 show the color quality aspects *CRI* and *CQS* of the above optimized cases (3000 K, 4000 K, 5000 K and 6500 K) for the museum lighting. In Figure 7.9, the results showed that the average values of the new specific color rendering indexes of the oil indexes ($AVR_{0.1-79}$) in the role of the main quality parameter have been always higher than 90 in all four cases. And the highest oil color index was achieved in case of 3000 K (about 97). In addition, the subordinate quality parameters such as the skin, hair, textile and clothe color indexes were also always higher than 95 and their highest values were 98, 97, 99 and 97 in case of 3000 K, respectively. Likewise, the average value of fourteen CIE color rendering indexes and the general CIE color rendering index of all

cases were also higher than 93 and they reached the highest value in case of 3000 K. However, the twelfth color rendering index (R_{12}) was only 82, 73, 76 and 68 for cases of 3000 K, 4000 K, 5000 K and 6500 K, respectively, because of using the royal blue LED with the peak wavelength of only 450 nm. This value will be higher if a good royal blue LED with the peak wavelength of about 440 nm is used for the hybrid LED-lamp, while it must still ensure the requirements of other lighting quality parameters such as current stability, temperature stability, luminous efficacy and feasibility of the establishment and the operation of the real hybrid LED-lamp. In addition, the other special CIE color rendering indexes were higher than 90 and their highest values were almost as high as in the case of 3000 K except R_3 and R_{14} (these two CRI s reached the highest value in case of 5000 K).

On the other hand, concerning CQS indexes in Figure 7.10, almost CQS s of the case of 3000 K were the highest values and always higher than 90. Only CQS_4 , CQS_7 and CQS_{11} in the case of 5000 K exceeded those in the case of 3000 K. Therefore, it can be stated that the optimized spectra have satisfied the high color quality demand of oil paintings in the museum lighting; and although the same LED system with the similar combination of the color semiconductor LEDs and the warm white PC-LED was applied in the optimization, the warm white case (3000 K) achieved the highest color quality parameters compared with other cases. Therefore, the warm white solid state lighting system (3000 K) should be designed for high quality solid state museum lighting applications. Furthermore, in all above optimized cases the correlated color temperature and the whiteness were always kept accurately at the determined values (3000 K, 4000 K, 5000 K and 6500 K) and below $\Delta u'v'=0.001$, respectively. As well, their luminous fluxes always achieved approximately about 90 lm/W. And the temperature dependence of these lighting quality parameters was not described in this section, because similar investigations will be described in the second demonstration example in Section 7.3.1.b.

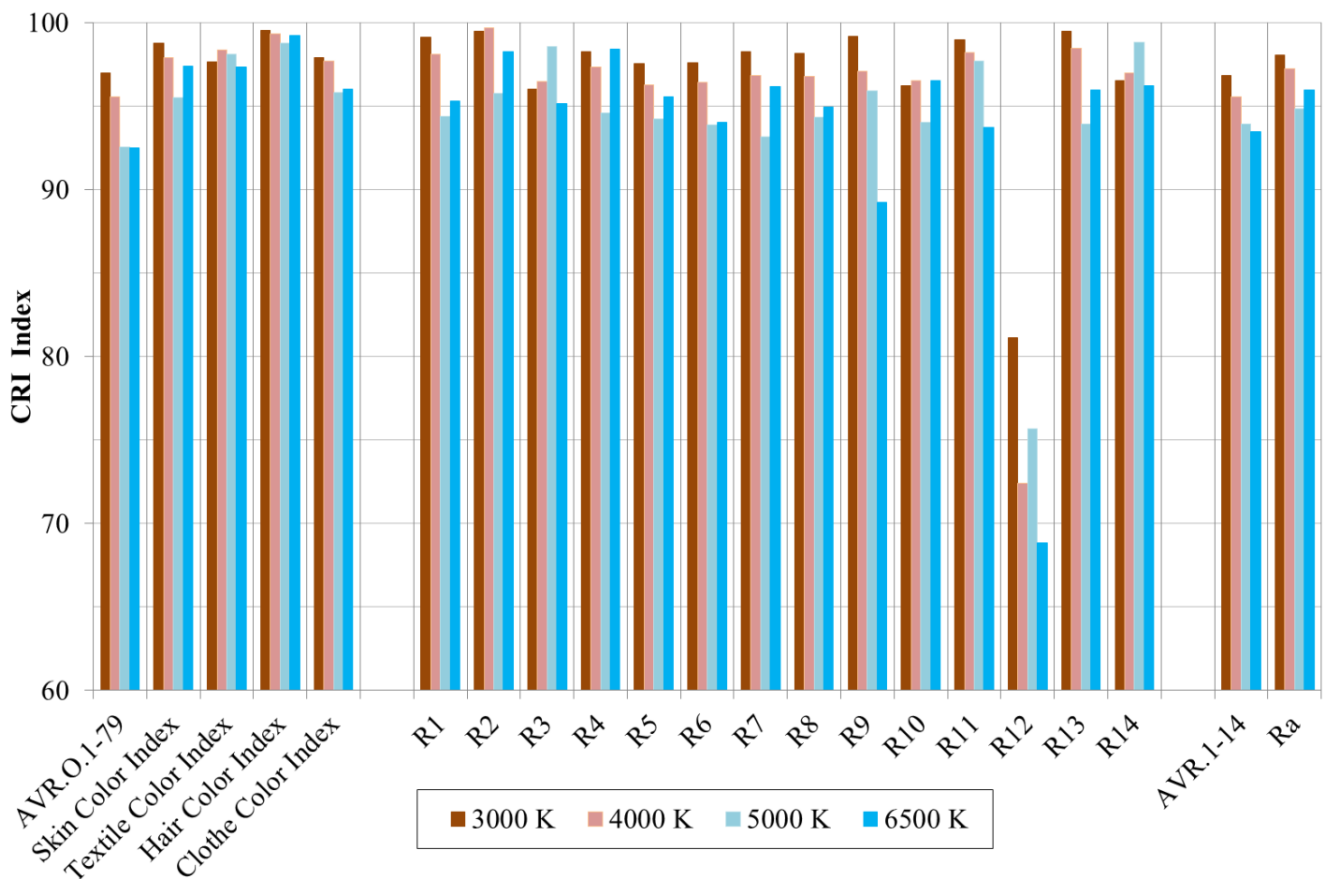


Figure 7.9 - CRI quality of the optimized spectra

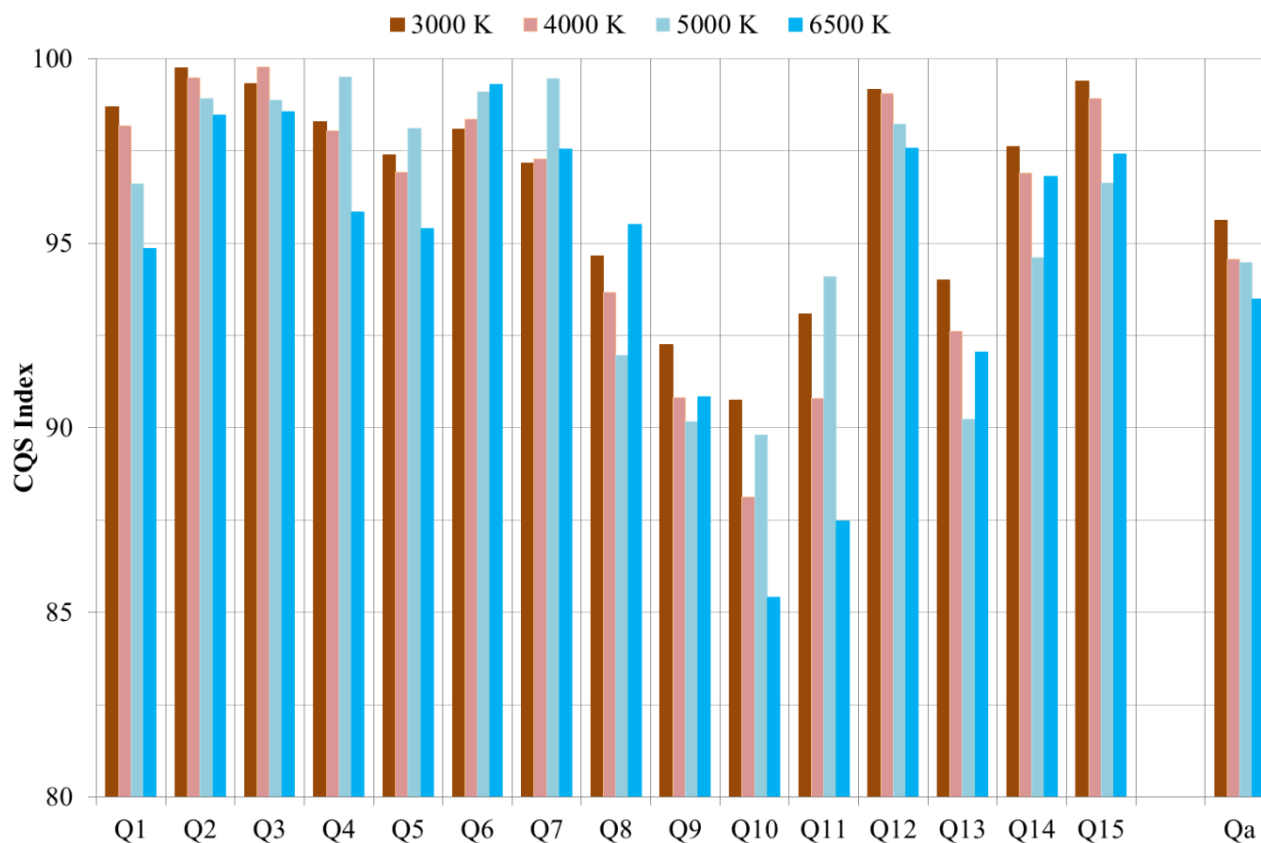


Figure 7.10 - CQS quality of the optimized spectra

7.2.3. Establishment of new standard reflectance curves for the museum lighting

Section 7.2.2 describes the optimization for the oil color index of cases 3000 K, 4000 K, 5000 K and 6500 K of the museum lighting. The best spectra were established and evaluated for different color quality aspects. All of them satisfied high color quality demands for the museum lighting and ensured the available color quality for the other color objects belonging to visitors such as their skin color, hair color, textile color and clothe color. However, in the lighting industry not all designers and applicators can use seventy nine oil color objects in their calculation and design. Therefore, the essential demand can be recognized quite obviously, that fourteen CIE standard reflectance curves should be investigated in order to confirm whether they have a potential ability to describe all oil color objects for the museum lighting or not. And if they cannot do it, a new standard reflectance curve system with an available amount of standard colors is really necessary to be established in order to satisfy the demand in the design and the evaluation of the high color quality lighting systems in the museum lighting.

a. Classification of the oil color objects and primary evaluation for CIE standard test color samples

* **The measures and strategy for the classification:** In order to classify the oil color objects and evaluate the potential of fourteen CIE standard colors primarily, both the new color space (a^* - b^* -J, CAM02-UCS ([115] and [119])) and the spectral reflectance curves of the color oil objects are necessary to be used in the investigation. Coordinately, the chosen standard referent light source for the investigation and the classification is the PLANCK light radiation of the absolute black body (3000 K), because the warm white (3000 K) was proved as the best light source for the museum lighting in Section 7.2.2.c. Therefore, the classification of the oil color objects under the PLANCK light

radiation (3000 K) will make the most accurate evaluation of the color quality parameters focusing on the warm white museum lighting case (3000 K) for later applications.

* **The description of CAM02-UCS color diagram and its range in the use:** Figure 7.11 describes the CIE CAM02-UCS color diagram for seventy nine test oil color samples of a museum (indicated by the solid points with different colors and shapes), fourteen standard test color samples of CIE (indicated by the open blue rectangles marked by numbers 1 - 14) and eight teen new color candidates proposed for the museum lighting (indicated by the open violet rectangles marked by numbers 1 - 18). In order to calculate the parameters (a' and b') for the CIE CAM02-UCS, the spectral reflectance curves must be determined previously. Therefore, the spectral reflectance curves of seventy nine oil color objects were measured at TECHNISCHE UNIVERSITÄT DARMSTADT ([155]), the spectral reflectance curves of fourteen CIE standard colors were published by CIE ([112]) and the ones of eighteen new standard colors will be established by the author in Section 7.2.3.b. As well, they are illustrated together in the figures 7.13 - 7.22. In addition, the color points that placed together in the CAM02-UCS color diagram are not only used to evaluate primarily for the CIE standard test color samples in this section, but also to recognize the difference between the CIE standard test color samples and the new color candidates for the secondary comparison and evaluation in Section 7.2.3.c.

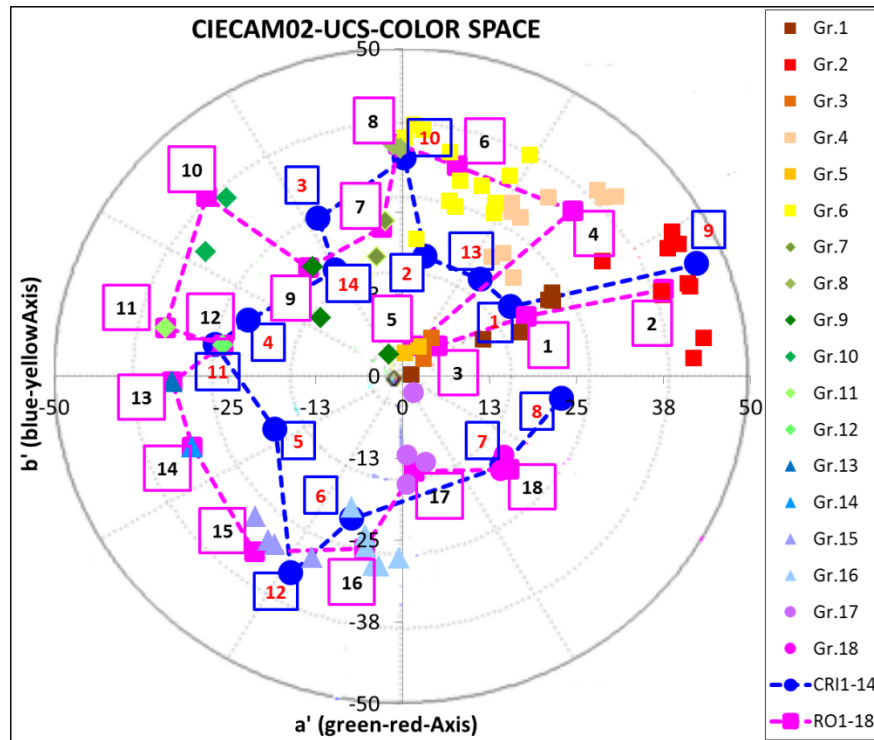


Figure 7.11 - Classification of the oil color objects by CAM02-UCS and comparison with CIE CRIs

* **Classification of the oil objects and primary evaluation for CIE standard test color samples:** In the classification of the oil color objects, seventy nine color points in the CAM02-UCS color diagram corresponding to seventy nine color oil objects play a specially important role. Indeed, the two essential parameters used in the classification are the amplitude (AM) and the tangent of the angle (AG) of the color vectors calculated as follows,

$$AM = \sqrt{a'^2 + b'^2} \quad (7.1)$$

$$AG = tg(\alpha) = \frac{b'}{a'} \quad (7.2)$$

Consequently, the oil color objects can be classified into the specific color regions from the red to the purple based on the angle (AG) with two different saturation levels based on the amplitude (AM). For example, if the red oil color objects have the similar values of the angle in the red region, but have the dissimilar values of the amplitude, they will belong to two different oil color groups including the oil deep red group ($AM > 25$) and the oil light red group ($AM < 25$). In addition, experimentally the oil color objects belonging to the same oil color group must be adjusted many times by the spectral diagrams of their measured spectral reflectance curves described in the figures 7.13 - 7.22 so that these oil color objects have the same color behaviors. It means, that their spectral reflectance curves must have nearly similar spectral shapes and rising / falling edges. By this way, seventy nine oil color objects were classified into eighteen oil color groups (Gr.₁ - Gr.₁₈) like described by color points in Figure 7.11 and by names in Table 7.2. And then, these eighteen oil color groups were compared in general with the matching fourteen CIE standard test color samples as in Table 7.2. Based on the calculated results in Figure 7.11 and the names indicated in more detail in Table 7.2, it can be recognized, that the CIE standard test color samples were impossible to describe the five oil color groups including the color group Gr.₄ (bright skin), Gr.₆ (bright yellow), Gr.₁₀ (permanent green and permanent yellowish-green), Gr.₁₁ (emerald green and Schweinfurt green hue) and Gr.₁₇ (Prussian blue). Oppositely, the CIE standard test color sample TCS8 (light reddish purple) was completely not necessary for the description of the oil color objects.

*Table 7.2 - Eighteen oil color groups with matching oil color objects and fourteen CIE standard TCSs. The 13rd comparison group (Gr*_{.12}) is for the repeated use of the 12nd color group in the comparison with TCS4, because of the near similar positions of TCS4 and TCS11 in the color diagram CAM02-UCS in Figure 7.11*

Order	Names of comparison groups	Names of oil color groups	Names of the average new specific GRI as referent values	Names of matching CRIs	Names of oil color objects belonging to oil color groups	Amount of color objects
1	Gr. ₁	RO _{G1}	AVR _{.Gr.1}	R ₁	RO73, 65, 70, 64, 62, 63	6
2	Gr. ₂	RO _{G2}	AVR _{.Gr.2}	R ₉	RO30, 29, 27, 28, 25, 26, 23, 22, 24, 30, 21, 66, 67	13
3	Gr. ₃	RO _{G3}	AVR _{.Gr.3}	R ₁₃	RO69, 71, 72, 68	4
4	Gr. ₄	RO _{G4}	AVR _{.Gr.4}	-	RO18, 19, 16, 60, 17, 1, 79, 2, 57, 61	11
5	Gr. ₅	RO _{G5}	AVR _{.Gr.5}	R ₂	RO 75, 77	2
6	Gr. ₆	RO _{G6}	AVR _{.Gr.6}	-	RO13, 58,3,6,59, 78, 5, 4, 15, 8, 11, 14	13
7	Gr. ₇	RO _{G7}	AVR _{.Gr.7}	R ₃	RO53, 56	2
8	Gr. ₈	RO _{G8}	AVR _{.Gr.8}	R ₁₀	RO10, 9	2
9	Gr. ₉	RO _{G9}	AVR _{.Gr.9}	R ₁₄	RO76, 55, 54	3
10	Gr. ₁₀	RO _{G10}	AVR _{.Gr.10}	-	RO52, 51	2
11	Gr. ₁₁	RO _{G11}	AVR _{.Gr.11}	-	RO49, 50	3
12	Gr. ₁₂	RO _{G12}	AVR _{.Gr.12}	R ₁₁	RO48	1
13	Gr* _{.12}	RO _{G12}	AVR _{.Gr.12}	R ₄	RO48	1
14	Gr. ₁₃	RO _{G13}	AVR _{.Gr.13}	-	RO47	1
15	Gr. ₁₄	RO _{G14}	AVR _{.Gr.14}	R ₅	RO46	1
16	Gr. ₁₅	RO _{G15}	AVR _{.Gr.15}	R ₁₂	RO40, 45, 44, 43	4
17	Gr. ₁₆	RO _{G16}	AVR _{.Gr.16}	R ₆	RO36, 37, 38, 35, 39, 34	6
18	Gr. ₁₇	RO _{G17}	AVR _{.Gr.17}	-	RO41, 42, 33, 74	3
19	Gr. ₁₈	RO _{G18}	AVR _{.Gr.18}	R ₇	RO31, 32	2

b. Establishment of new candidate reflectance curves and results in the primary comparison

As the early steps, the new color space ($a' - b' - J$, CAM02 UCS) was applied to group the oil color objects into eighteen oil color groups ($Gr_{.1} - Gr_{.18}$) in Section 7.2.3.a and in the performance process they were adjusted again many times by using the spectral diagrams described in Figures 7.13-7.22. Consequently, the gaps as well as the redundant points of fourteen CIE test color samples for the description of the oil color object of the museum lighting could be recognized in Figure 7.11 and Table 7.2 quite obviously. Additionally, the results in Section 7.2.3.a confirmed that fourteen CIE standard reflectance curves could not describe the oil color objects fully and it is necessary to establish new standard reflectance curves. Therefore, in this section the procedures and the method for the establishment of the new standard reflectance curves will be described and carried out. Finally, the desired new standard reflectance curves will be drawn in the same spectral diagrams with the original oil color objects and the CIE standard colors to evaluate the difference between them secondarily.

* **Establishment principle:** Figure 7.12 describes the establishment principle for the color candidates of the color groups. In that, a reference light source was used for both original oil color objects belonging to the same color group (for example, the oil colors 1, 2 ... i denoted by the symbols $RO_1, RO_2 \dots RO_i$ belonging to the same group ROG_1) and the new color candidate (or the proposed new standard reflectance curve for the group ROG_1). Particularly, the chosen referent light source is the optimal warm white (3000 K) that was optimized for the museum lighting in Section 7.2.2.c. Successively, in order to inherit total color behaviors of all the oil color objects belonging to the same group, the proposed new candidate curve for the color group must be established based on all componential spectral reflectance curves by means of constants ($a_1, a_2 \dots a_i$). Then, the average value of $RO_1, RO_2, \dots RO_i$ (called AVR_{ROi}) and new color rendering index ROG_1 for the proposed new candidate curve are used to calculate their offset. As well, this offset is the feedback signal to a controller. Consequently, an optimizing algorithm in the controller is applied to adjust the constants ($a_1, a_2 \dots a_i$) so that the offset is equal zero. Finally, the proposed new standard reflectance candidate curve is established and becomes the representation of the oil color objects of the color group.

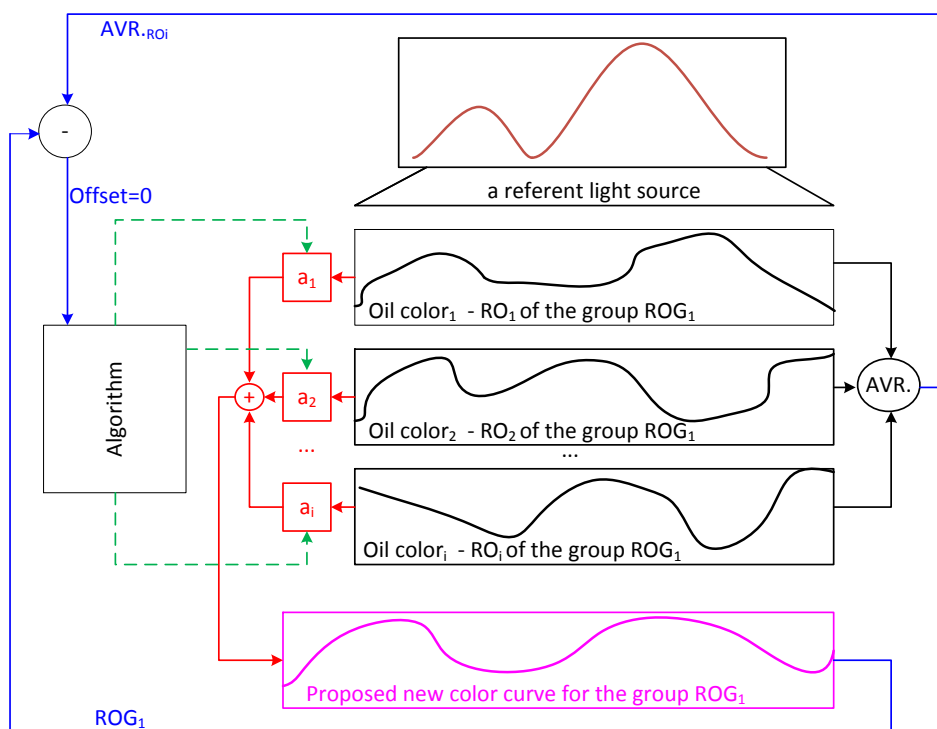


Figure 7.12 - Establishment principle for the new candidate reflectance curve of each color group

* **Results in the primary comparison between CIE standard reflectance curves and new candidate reflectance curves in the same spectral diagrams:** Applying the establishment principle described in Figure 7.12 for eighteen color groups classified in Section 7.2.3.a, eighteen new oil color candidates were established and described in the figures 7.13 - 7.22. In these figures, the spectral reflectance curves of the original oil color objects, the CIE standard test color samples and the new color candidates were drawn in the same spectral diagrams. Thus, based on these spectral diagrams, the difference between the CIE standard test color samples and the new color candidates for the description of the oil color objects of the museum lighting can be compared and recognized visually.

Indeed, the color behaviors of the oil color reflectance spectra such as their spectral shape, position of the rising / falling edges and amplitude are inherited quite fully by the new color candidates (designated by the bold solid curves). Oppositely, these color behaviors could not be reflected fully by the CIE standard test color samples (designated by the bold broken curves). Visually, in the spectral diagrams it can be recognized, that there are always big differences of the representing ability for the oil color objects belonging to the same oil color group between the CIE standard reflectance curves and the new candidate reflectance curves such as the ROG1 and TCS1 curves for the deep red group (the group Gr.₁) in Figure 7.13, the ROG3 and TCS13 curves for light yellowish pink group (the group Gr.₃) in Figure 7.15, the ROG5 and TCS2 curves for the dark grayish yellow group (the group Gr.₅), the ROG7 and TCS3 curves for the strong yellow green group (the group Gr.₇), the ROG₈ and TCS10 curves for the strong yellow group (the group Gr.₈) and the ROG9 and TCS14 curves for the moderate olive green group (the group Gr.₉) in Figure 7.18, the ROG12 and TCS4 or TCS11 curves for the Chromium oxide green group (the group Gr.₁₂), the ROG14 and TCS5 curves for the Cobalt turquoise group (the group Gr.₁₄), the ROG₁₈ and TCS7 curves for the violet group (the group Gr.₁₈) in Figure 7.19, the ROG15 and TCS12 curves for the strong blue group (the group Gr.₁₅) in Figure 7.20 and the ROG15 and TCS6 curves for the light blue group in Figure 7.21. Only in the unique case in Figure 7.14, the spectral shape of the new candidate reflectance curve ROG2 (designated by the bold solid red curve) and the CIE standard reflectance curve TCS9 (designated by the bold broken red curve) is quite similar, although there is still a difference in their amplitude.

Finally, there was no CIE standard reflectance curve matching with the skin color group (the color group Gr.₄ - ROG₄) in Figure 7.16, with the very light yellow group (the color group Gr.₆ - ROG₆) in Figure 7.17, with the permanent green group (the color group Gr.₁₀ - ROG₁₀), with the Emerald green group (the color group Gr.₁₂ - ROG₁₂) and with the Phthalate green group (the color group Gr.₁₃ - ROG₁₃) in Figure 7.19 and with the dark blue group (the color group Gr.₁₇ - ROG₁₇) in Figure 7.22.

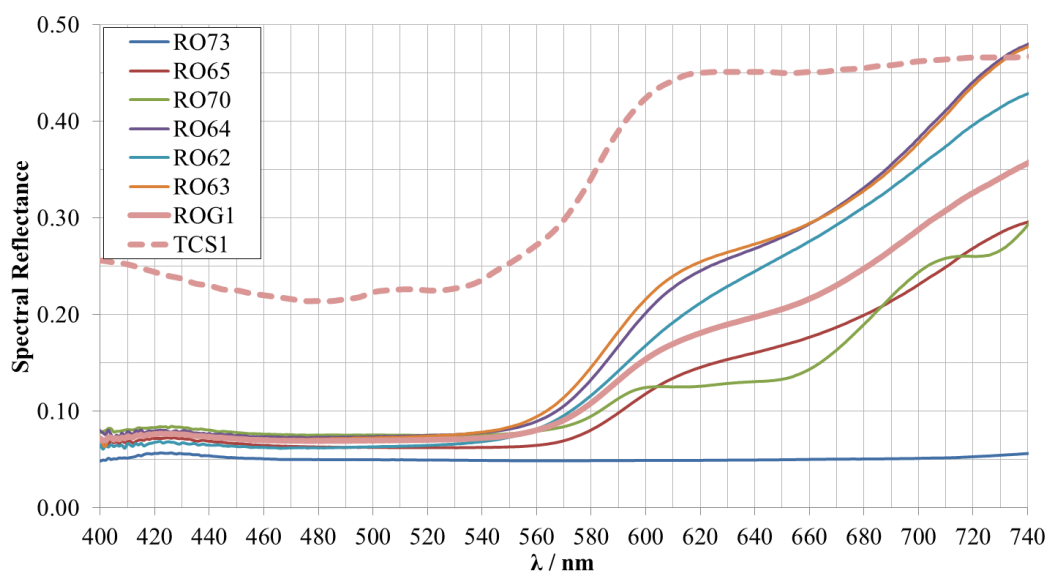


Figure 7.13 - Deep red group, its deep red candidate (ROG1) and the matching R₁ (TCS1)

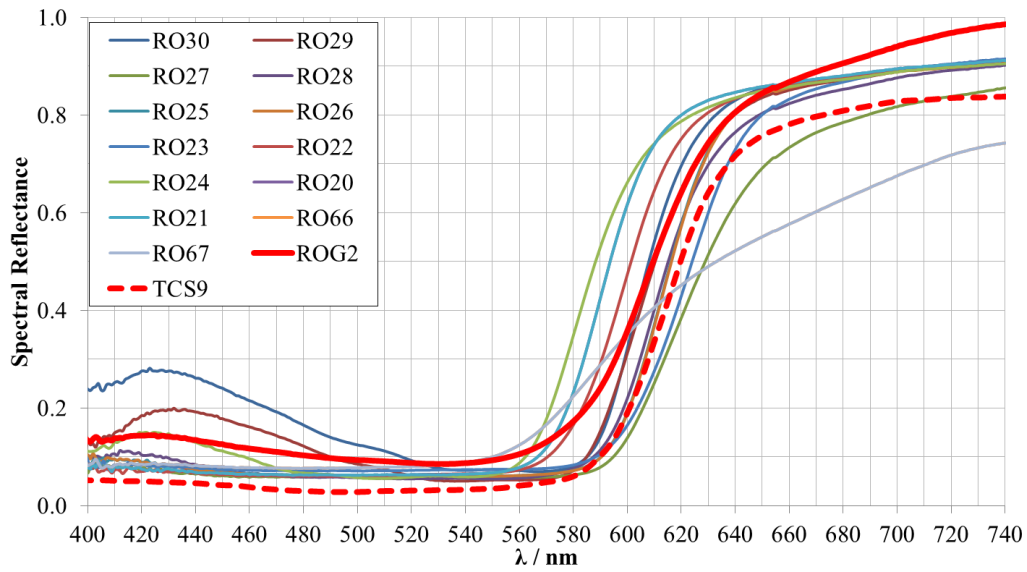


Figure 7.14 - Strong red group, its strong red candidate (ROG2) and matching R_9 (TCS9)

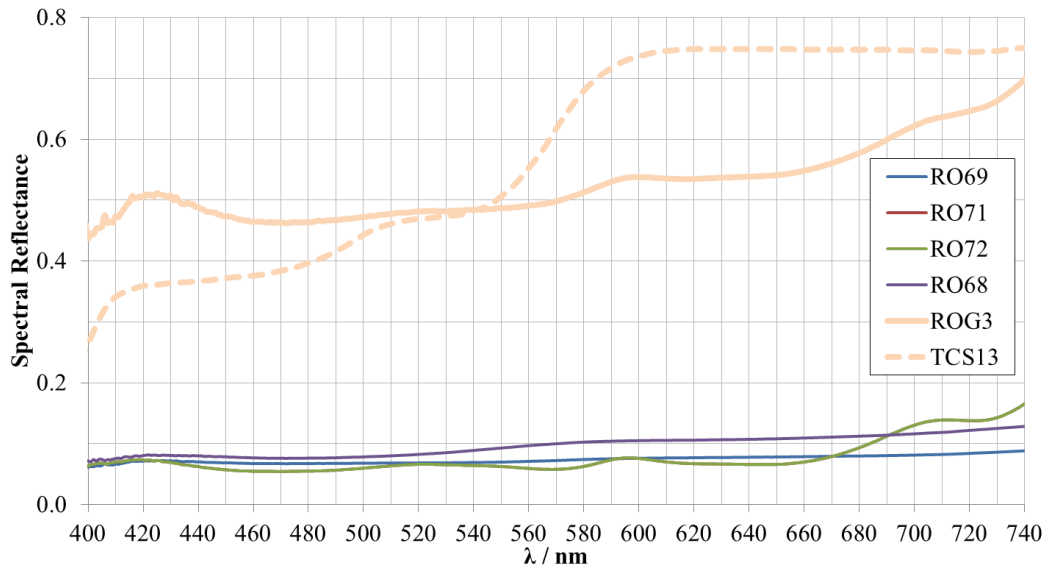


Figure 7.15 - Light yellowish pink group, its light yellowish pink candidate (ROG3) and matching R_{13} (TCS13)

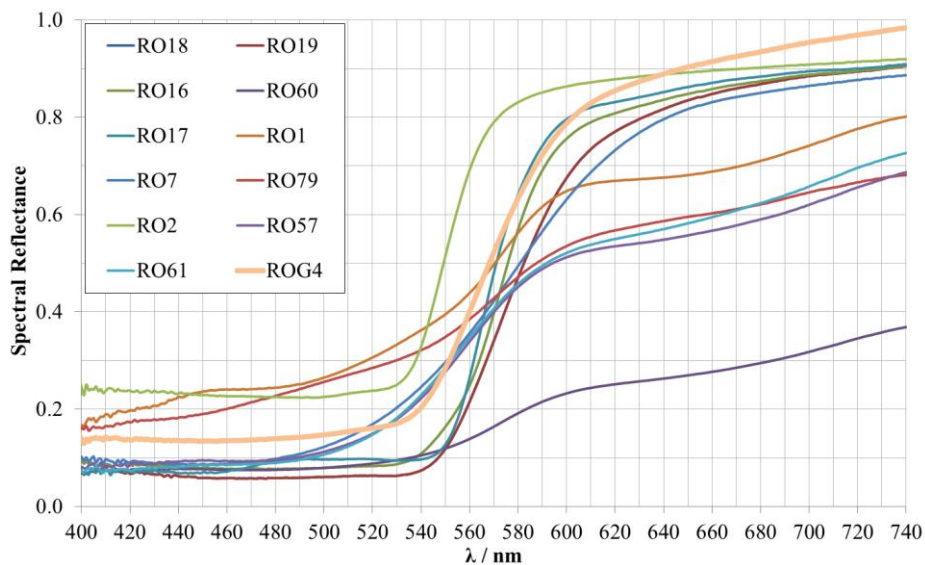


Figure 7.16 - Skin color group, its skin color candidate (ROG4) and no matching CIE TCS

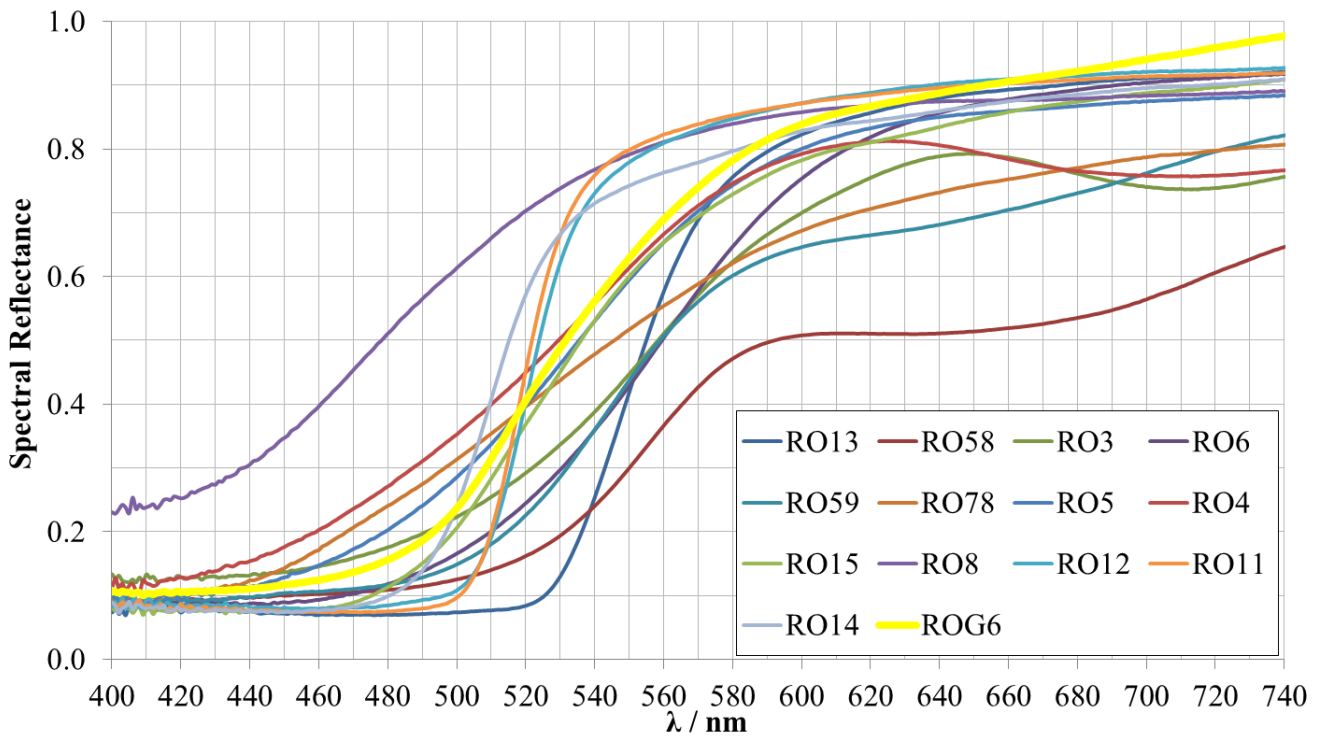


Figure 7.17 - Yellow group, its yellow candidate (ROG6) and no matching CIE TCS

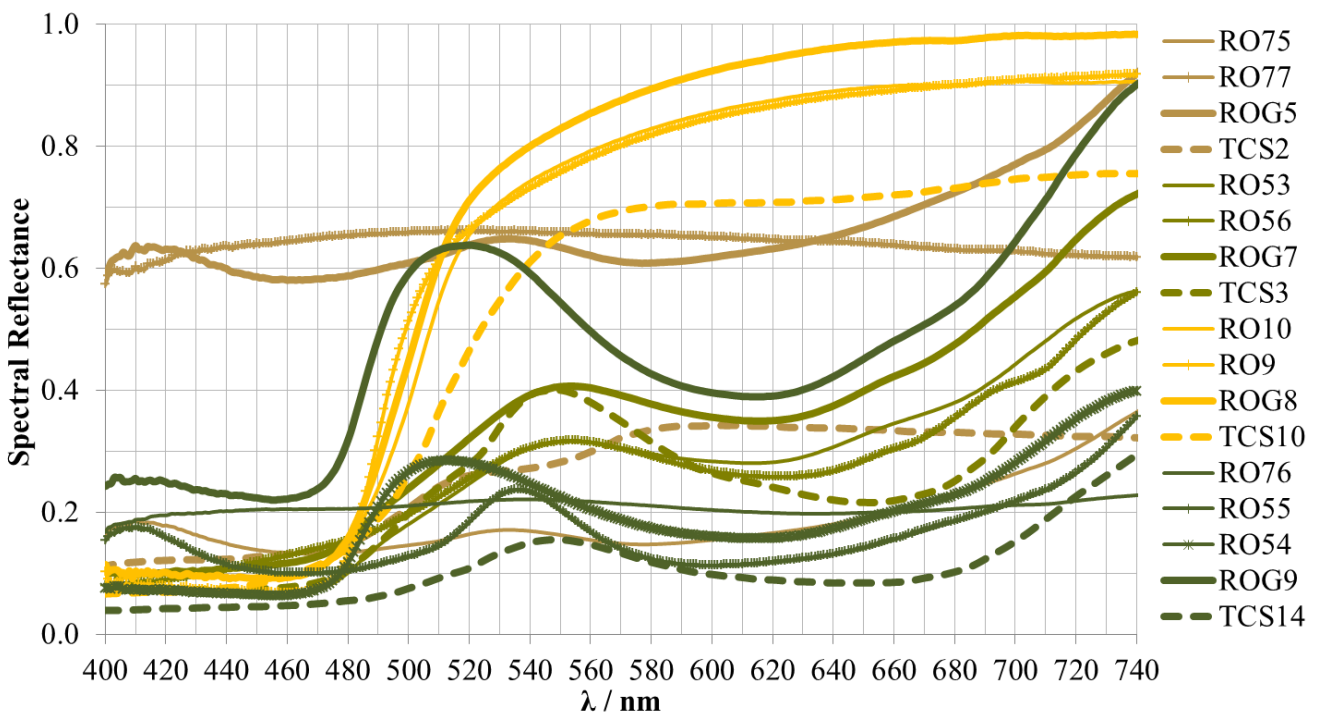


Figure 7.18 - a) Dark grayish yellow group - its candidate (ROG5) - matching R_2 (TCS2), b) Strong yellow green group - its candidate (ROG7) - matching R_3 (TCS3), c) Strong yellow group - its candidate (ROG8) - matching R_{10} (TCS10), d) Moderate olive green group - its candidate (ROG9) - matching R_{14} (TCS14)

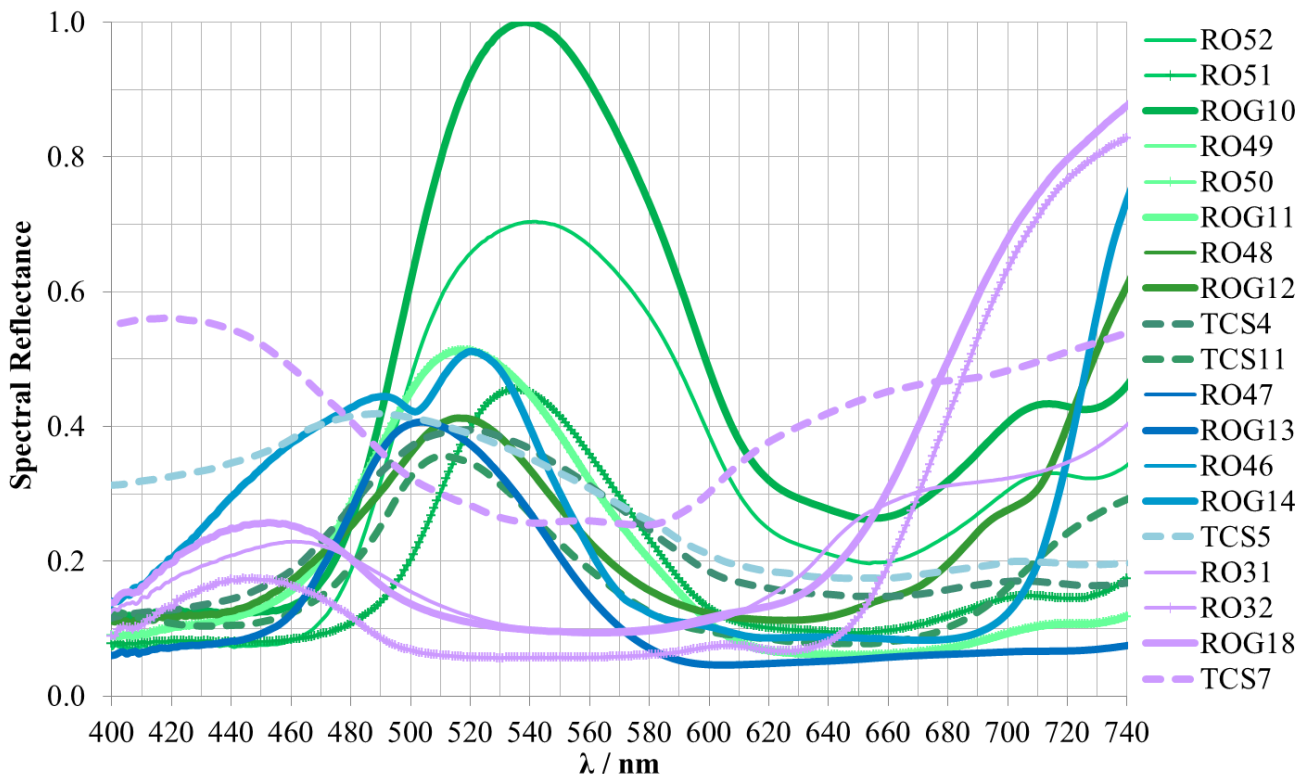


Figure 7.19 - a) Permanent green group - its candidate (ROG10) - No matching CIE TCS, b) Emerald green group - its candidate (ROG12) - No matching CIE TCS, c) Chromium oxide green group - its candidate (ROG12) - R_4 (TCS4) and R_{11} (TCS11), d) Phthalate green group - its candidate (ROG13) - No matching CRI, e) Cobalt turquoise group - candidate (ROG14) - R_5 (TCS5), f) Violet group - its candidate (ROG18) - R_7 (TCS7)

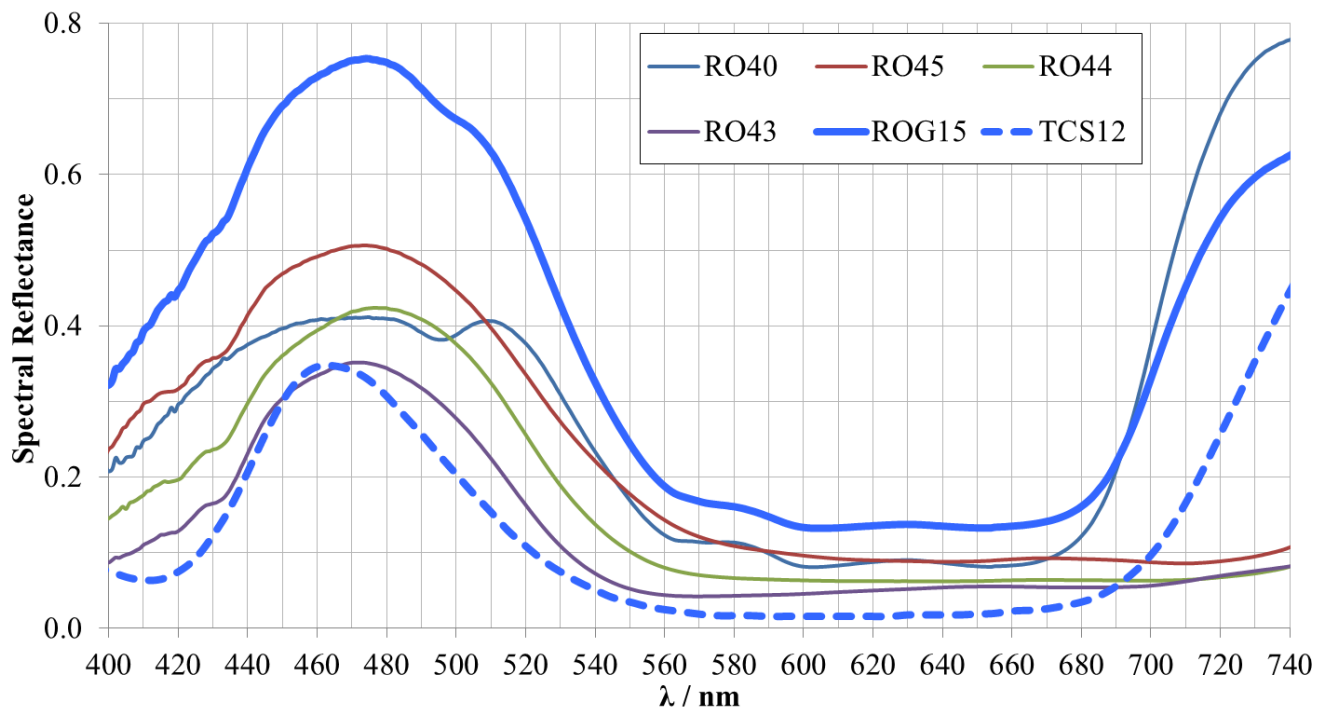


Figure 7.20 - Strong blue group, its strong blue candidate (ROG15) and matching R_{12} (TCS12)

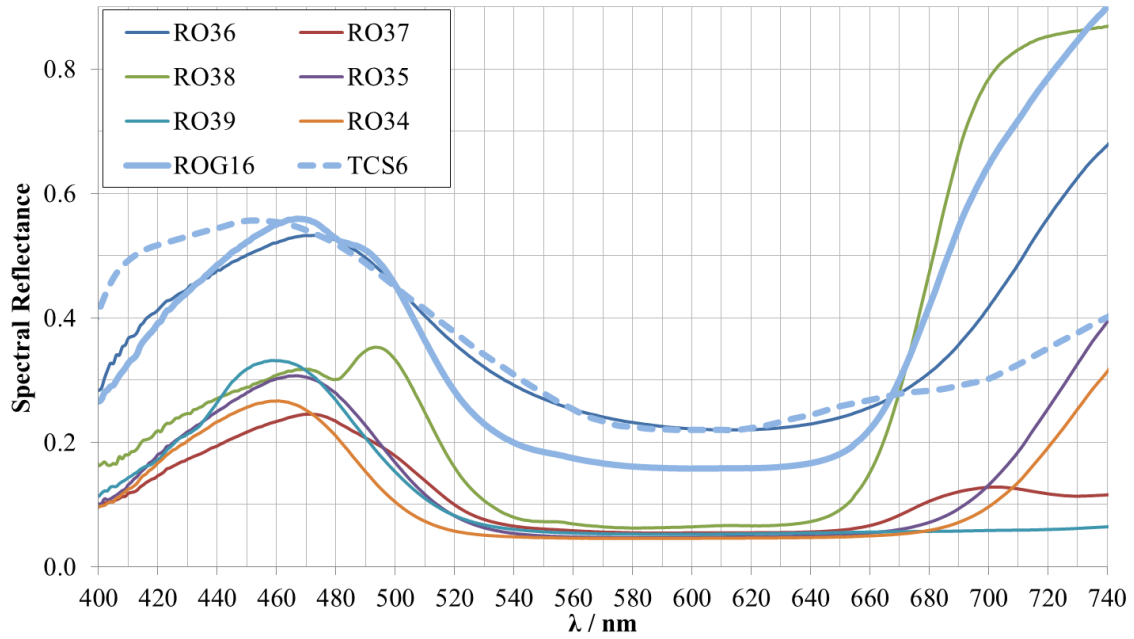


Figure 7.21 - Light blue group, its light blue candidate (ROG15) and matching R_6 (TCS6)

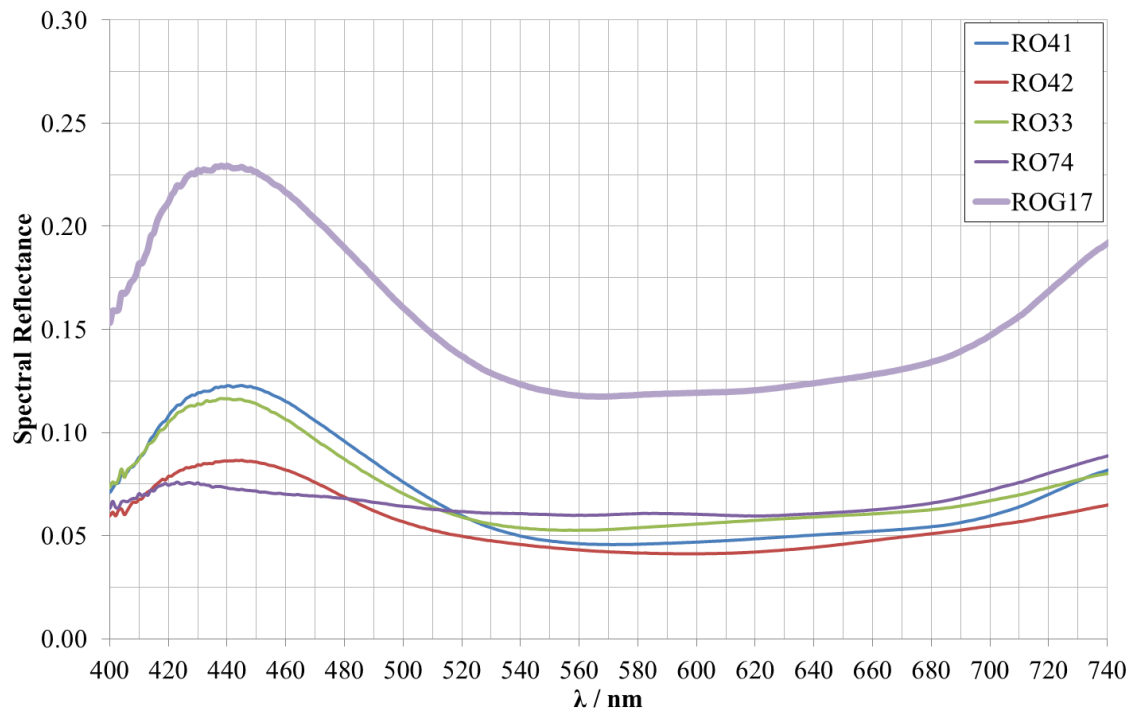


Figure 7.22 - Dark blue group, its dark blue candidate (ROG17) and no matching CIE TCS

c. Secondary comparison and evaluation for reflectance curves in the description for the oil color objects by means of color rendering indexes

* **Determination of color rendering indexes:** Eighteen new candidate reflectance curves were established and compared primarily with the CIE standard reflectance curves in Section 7.2.3.b. In order to compare and evaluate the quality of the CIE standard reflectance curves and the new candidate reflectance curves for the description of the color behaviors of the oil color objects at a sophisticated level, in this section the standard definitions and equations of the CIE color rendering

index are applied to calculate the special color rendering indexes ($R_1 - R_{14}$), the general CRI (R_a) for the first eight CIE standard test color samples and the average CRI (AVR_{1-14}) for all fourteen CIE standard test color samples based on fourteen CIE standard reflectance curves (TCS01 - TCS14) described in Figure 7.23. Similarly, these definitions and equations are used to determine the new specific color rendering indexes for eighteen oil color groups ($ROG_1 - ROG_{18}$) based on eighteen new standard reflectance curves ($Gr_{.1} - Gr_{.18}$) described in Figure 7.24 and the average values of the special new specific color rendering indexes for eighteen oil color groups ($AVR_{Gr.1} - AVR_{Gr.18}$) based on seventy nine spectral reflectance curves measured directly from the oil color objects. Otherwise, the used light sources for all calculations are the optimized spectra (3000 K, 4000 K, 5000 K and 6500 K), which were optimized for the museum lighting in Section 7.2.2.c.

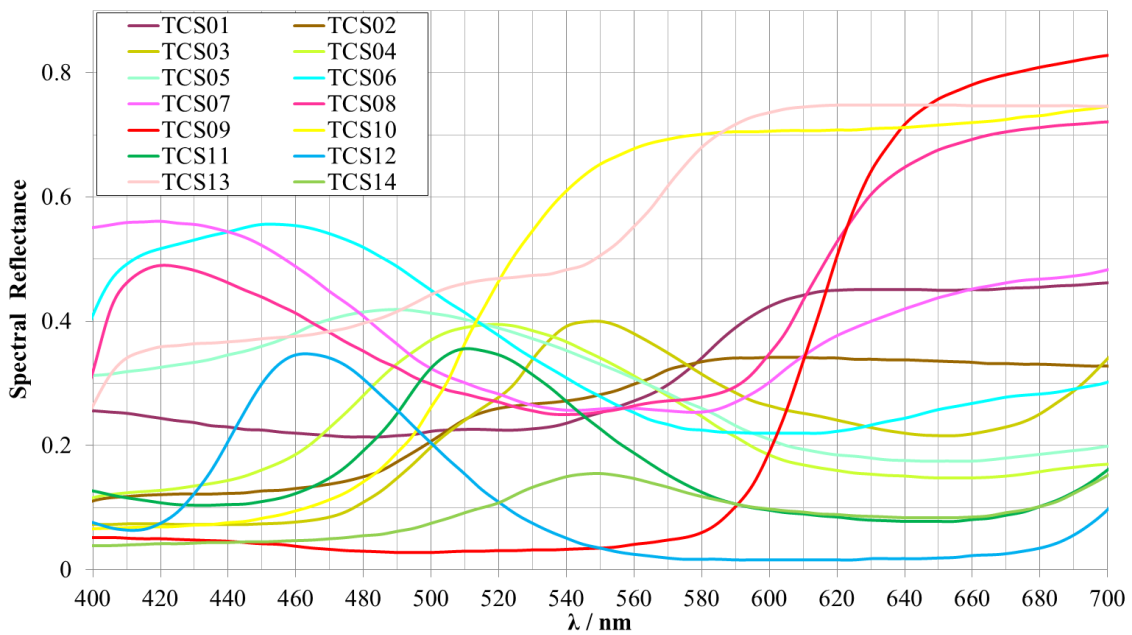


Figure 7.23 - Fourteen CIE standard reflectance curves

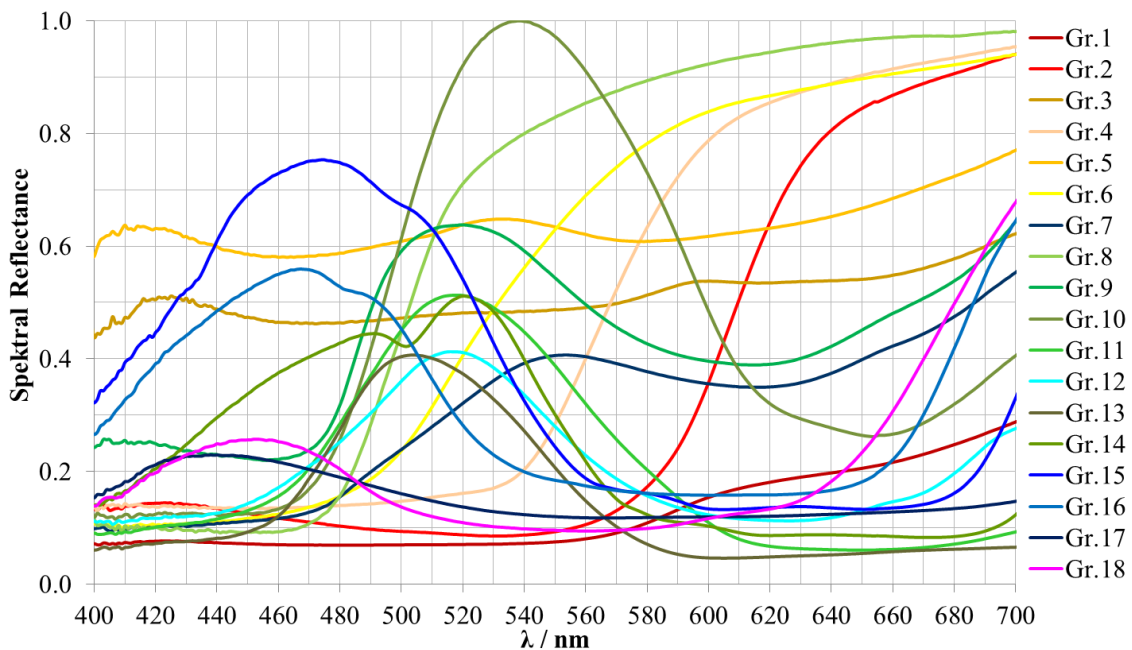


Figure 7.24 - Eighteen new candidate reflectance curves of TECHNISCHE UNIVERSITÄT DARMSTADT

* **Secondary comparison and evaluation for reflectance curves for the description of the oil color objects by means of color rendering indexes:** In this secondary comparison, the reference values are eighteen average values of the new specific CRIs of the oil color objects belonging to eighteen oil color groups (called “*average new specific CRI*”). The first compared objects are the new specific color rendering indexes calculated based on the new candidate reflectance curves (called “*new candidate CRI*”). And the second compared objects are the color rendering indexes calculated based on the standard CIE reflectance curves (called “*CIE standard CRI*”). The comparison and evaluation for the new candidate reflectance curves and the CIE standard reflectance curves for the description of the oil color objects are carried out by the comparison of the offset between the average new specific CRIs and the new candidate CRIs (called “*Offset₁*”) and the one between the average new specific CRIs and the CIE standard CRIs (called “*Offset₂*”).

Particularly, Table 7.3 describes eighteen comparing groups (Gr.₁ - Gr.₁₈) for the first offset (*Offset₁*) between eighteen average new specific CRIs (*AVR_{Gr.1}* - *AVR_{Gr.18}*) of eighteen oil color groups and eighteen new candidate CRIs and for the second offset (*Offset₂*) between eighteen average new specific CRIs and fourteen matching CIE standard CRIs in case of the optimized warm white light source (3000 K). And the 20th - 22nd comparing groups (*AVR_a*, *AVR_b* and *AVR_c*) are to compare between the average values including the average value of eighteen new candidate CRIs (*ROG_a*), the one of eighteen average new specific CRIs (*AVR_{Gr.a}*), the one of seventy nine new specific CRIs (*AVR_{RO1-19}*), the one of eight CIE standard CRIs (*R_a*), and the one of fourteen CIE standard CRIs (*AVR₁₋₁₄*). In addition, the 13rd comparison group (Gr*. ₁₂) is for the repeated use of the 12nd new candidate CRI in the comparison with CIE standard *R₄*, because of the near similar position of *R₄* and *R₁₁* in the color diagram CAM02-UCS described in Figure 7.11. Successively, Figure 7.25 and Figure 7.26 are to describe the first offset and the second offset, respectively not only for the case of the optimized warm white light source (3000 K), but also for the cases of 4000 K, 5000 K and 6500 K. A well, the new candidate CRI, the CIE standard CRI and the average new specific CRI for the cases 3000 K, 4000 K, 5000 K and 6500 K designated by the symbol sets (*ROGi.TUD-3K*, *ROGi.TUD-4K*, *ROGi.TUD-5K* and *ROGi.TUD-65K*), (*Ri.TUD-3K*, *Ri.TUD-4K*, *Ri.TUD-5K* and *Ri.TUD-65K*) and (*AVR.i.TUD-3K*, *AVR.i.TUD-4K*, *AVR.i.TUD-5K* and *AVR.i.TUD-65K*), respectively.

For the results in Table 7.3, it can be recognized, that all first offsets were always equal zero, because eighteen new candidate reflectance curves were established for the case of the optimized warm white light source (3000 K) as the reference light source in Section 7.2.3.b. These offsets will be higher if the applied light source is no the warm white (3000 K), but is 4000 K, 5000 K or 6500 K like described in Figure 7.25. However in all these cases, the first offsets (*Offset₁*) have been also always very much less than the second offsets (*Offset₂*) illustrated by the results in both Figure 7.25 and Figure 7.26. Indeed, there was no gap for the description of the oil color objects in the case of the new candidate CRIs comparing with five gaps above the total eighteen oil color groups (~28%) in case of the CIE standard CRIs. In addition, although the first offsets are higher in cases of the neutral and cold white light sources (4000 K, 5000 K or 6500 K) and at several points (*ROG₂*, *ROG₄* and *ROG₆*), they are always lower than 3. Consequently, this maximal offset value for the first offsets can be accepted for the description of the color objects in the museum lighting applications.

In fact, it is nearly impossible to establish faultless standard reflectance curves that can satisfy for all cases of light sources, but they can be only built in order to minimize the offset as well as possible. Thus, at the best way the evaluation of the color rendering indexes should be performed directly based on all spectral reflectance curves of all color objects or entire color object groups with the average

value of total componential new specific CRIs. However, in the design and evaluation for museum lighting applications, lighting engineers cannot have many spectral reflectance curves such as seventy nine spectral reflectance curves in the above mention, and they need a less amount of the candidates. Therefore, although the candidates cannot be analogous to original color objects perfectly, they should be still established as well as possible so that users can use them easily in their design and evaluation. Hence, the new eighteen standard reflectance curves were established in this opinion and should be used best for the museum lighting with the warm white light source.

Table 7.3 - Eighteen comparing groups (Gr.₁ - Gr.₁₈) for the first offsets (Offset₁) between 18 average new specific CRIs (AVR._{Gr.1} - AVR._{Gr.18}) of 18 oil color groups and 18 new candidate CRIs and for the second offsets (Offset₂) between 18 average new specific CRIs and 14 matching CIE standard CRIs in the case of optimized warm white light source (3000 K).

The 20th-22nd cases (AVR._a, AVR._b and AVR._c) are to compare between average values including the average value of 18 new candidate CRIs (ROG_a), the one of 18 average new specific CRIs (AVR._{Gr.a}), the one of 79 new specific CRIs (AVR._{RO1-79}), the one of 8 CIE standard CRIs (R_a) and the one of 14 CIE standard CRIs (AVR.₁₋₁₄).

Finally, the 13rd comparison group (Gr.^{}₁₂) is for the repeated use of the 12nd new candidate CRI in the comparison with R₄, because of the near similar positions of R₄ and R₁₁ in the color diagram CAM02-UCS described in Figure 7.11.*

Order	Name of Comparison groups	New candidate CRIs		Average new specific CRIs		CIE Standard CRIs		Offsets	
		Name	Value	Name	Value	Name	Value	Offset ₁	Offset ₂
1	Gr. ₁	ROG ₁	99.06	AVR. _{Gr.1}	99.06	R ₁	99,14	0.00	-0.08
2	Gr. ₂	ROG ₂	98.83	AVR. _{Gr.2}	98.83	R ₉	99,17	0.00	-0.34
3	Gr. ₃	ROG ₃	98.69	AVR. _{Gr.3}	98.69	R ₁₃	99,49	0.00	-0.80
4	Gr. ₄	ROG ₄	98.72	AVR. _{Gr.4}	98.72	-	No	0.00	No
5	Gr. ₅	ROG ₅	98.25	AVR. _{Gr.5}	98.25	R ₂	99,47	0.00	-1.22
6	Gr. ₆	ROG ₆	96.98	AVR. _{Gr.6}	96.98	-	No	0.00	No
7	Gr. ₇	ROG ₇	97.08	AVR. _{Gr.7}	97.08	R ₃	95,99	0.00	1.09
8	Gr. ₈	ROG ₈	96.84	AVR. _{Gr.8}	96.84	R ₁₀	81,1	0.00	15.74
9	Gr. ₉	ROG ₉	96.73	AVR. _{Gr.9}	96.73	R ₁₄	97	0.00	0.22
10	Gr. ₁₀	ROG ₁₀	94.93	AVR. _{Gr.10}	94.93	-	No	0.00	No
11	Gr. ₁₁	ROG ₁₁	98.84	AVR. _{Gr.11}	98.84	-	No	0.00	No
12	Gr. ₁₂	ROG ₁₂	98.33	AVR. _{Gr.12}	98.33	R ₁₁	98,98	0.00	-0.65
13	Gr. _{12*}	ROG ₁₂	98.33	AVR. _{Gr.12}	98.33	R ₄	98,24	0.00	0.09
14	Gr. ₁₃	ROG ₁₃	94.49	AVR. _{Gr.13}	94.49	-	No	0.00	No
15	Gr. ₁₄	ROG ₁₄	94.29	AVR. _{Gr.14}	94.29	R ₅	97,56	0.00	-3.27
16	Gr. ₁₅	ROG ₁₅	88.73	AVR. _{Gr.15}	88.73	R ₁₂	81,11	0.00	7.62
17	Gr. ₁₆	ROG ₁₆	91.92	AVR. _{Gr.16}	91.92	R ₆	97,62	0.00	-5.70
18	Gr. ₁₇	ROG ₁₇	99.53	AVR. _{Gr.17}	99.53	-	No	0.00	No
19	G _{R-18}	ROG ₁₈	92.91	AVR. _{Gr.18}	92.91	R ₇	98,24	0.00	-5.33
20	AVR. _a	ROG _a	96.40	AVR. _{Gr.a}	96.40	R _a	98,05	0.00	-1.65
21	AVR. _b	ROG _a	96.40	AVR. _{Gr.a}	96.40	AVR. ₁₋₁₄	96,85	0.00	-0.45
22	AVR. _c	ROG _a	96.40	AVR. _{RO1-79}	96.40	AVR. ₁₋₁₄	96,85	0.00	-0.45

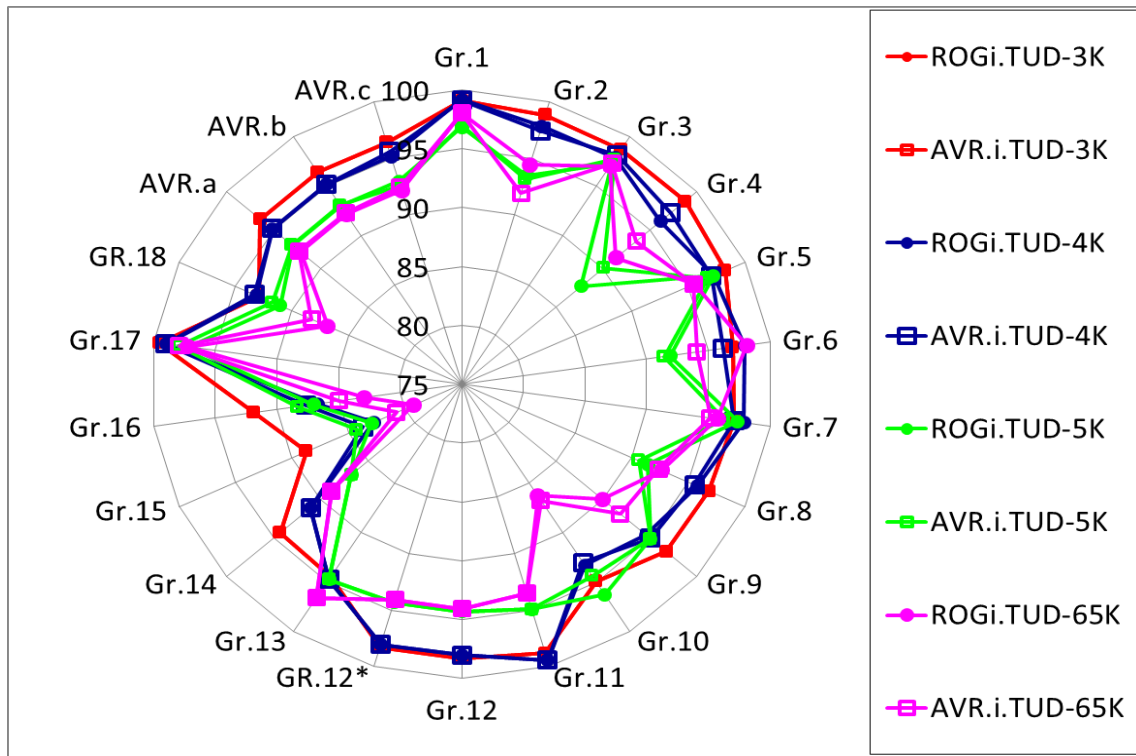


Figure 7.25 - First offset between average new specific CRIs (AVR.i.TUD-3K, AVR.i.TUD-4K, AVR.i.TUD-5K and AVR.i.TUD-65K) and new candidate CRIs (ROGi.TUD-3K, ROGi.TUD-4K, ROGi.TUD-5K and ROGi.TUD-65K) in the cases of 3000 K, 4000 K, 5000 K and 6500 K, respectively

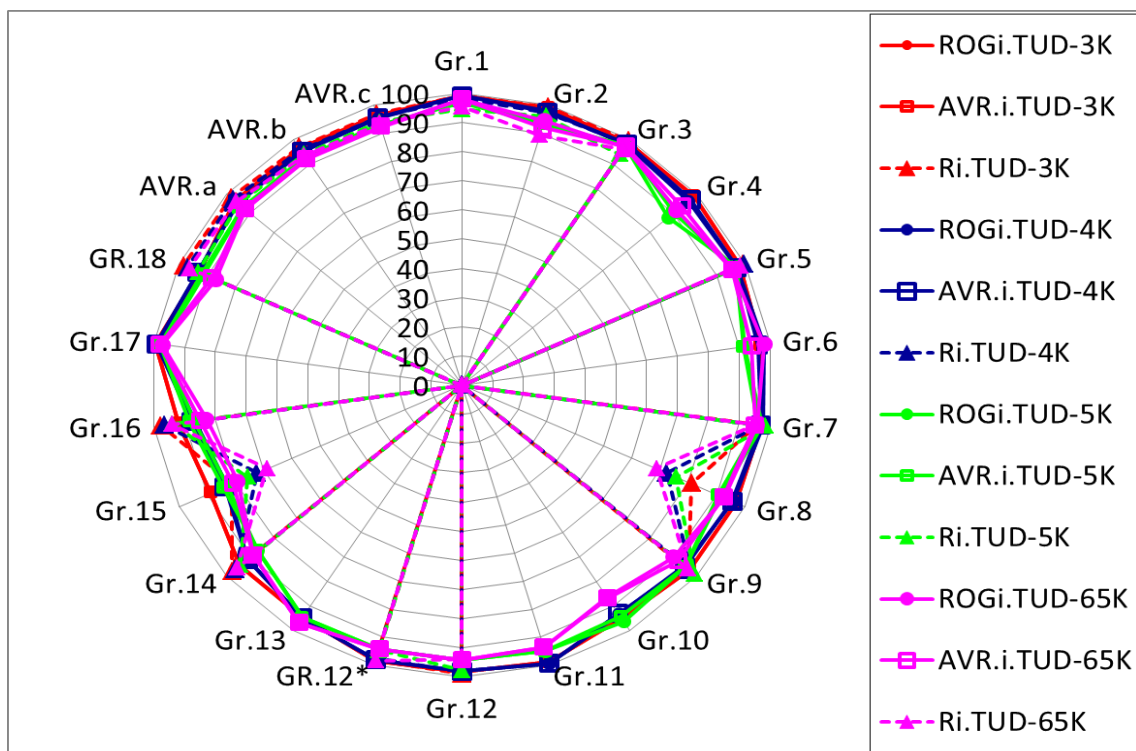


Figure 7.26 - Second offset between average new specific CRIs (AVR.i.TUD-3K, AVR.i.TUD-4K, AVR.i.TUD-5K and AVR.i.TUD-65K) and CIE standard CRIs (Ri.TUD-3K, Ri.TUD-4K, Ri.TUD-5K and Ri.TUD-65K) in the cases of 3000 K, 4000 K, 5000 K and 6500 K, respectively

7.3. Demonstration example of the stabilization for some lighting quality aspects of the hybrid LED-lamp adapted to the color objects

Section 7.2 described the first demonstration example of the optimization for some lighting quality aspects of the hybrid LED-lamp adapted to the color objects. In that, the chosen lighting objects were the specific part of a museum with oil color paintings, the adapted color objects were the oil color objects, and the optimized target was the average new specific oil color rendering index of seventy nine oil color objects in the museum lighting application with cases of 3000 K, 4000 K, 5000 K and 6500 K at the hot binning (80 °C). In fact, normally only in a museum the ambient temperature can be kept constant because of the severe requirements of temperature and humidity for paintings. Unfortunately, the operating temperature of the hybrid LED-lamp in other applications is not always at 80 °C constant, but changes depending on different factors such as the weather, seasons, daytime, nighttime or other operating conditions. When the operating temperature changes, the previous color mixing rate is not correct furthermore causing the total change of all lighting quality parameters of the hybrid LED-lamp such as chromaticity, the correlated color temperature, whiteness, color rendering indexes, luminous flux and luminous efficacy. Therefore, in this section the control system structure, which is similar to that described in Figure 7.7, will be used to optimize the new specific color rendering indexes of the warm white hybrid LED-lamp (3000 K) adapted to all red objects in general shop lighting applications. The hybrid LED-lamp will be established from the varied semiconductor LEDs and the different warm white PC-LEDs of three manufacturers (A, B and C) as well as their combinations at the hot binning (80 °C). Then, the optimized spectra will be investigated at the different operating temperatures so that the change of the lighting quality parameters will be recognized entirely. Finally, the most stable LED-combination system will be chosen for the best hybrid LED-lamp. Successively, the operating temperature must be added as the new feedback signal to the controller in the control system structure and a new control algorithm will be proposed in order to stabilize the correlated color temperature and the whiteness of the hybrid LED-lamp, while its color rendering indexes, luminous flux and luminous efficacy will be still kept in stable/high levels. Consequently, general shop lighting applications will be used as the second demonstration example of the stabilization for some lighting quality aspects of the hybrid LED-lamp adapted to the color objects. The lighting object will be the conventional shop, the adapted color objects will be red objects, the optimized target will be the average value of new specific color rendering indexes of the red objects or the red color index and the stabilized main lighting quality parameters will be the correlated color temperature and the whiteness of the hybrid LED-lamp.

7.3.1. Temperature dependence of some lighting quality parameters of the hybrid LED-lamps

In this section, the main target is to investigate the temperature stability of the different LED-combinations and then the stabilization will be carried out in the case of the most stable LED-combination in Section 7.3.2. However, the optimization adapted to the red objects for all LED-combinations must be performed previously, although the optimization is not the main target in this second demonstration example. Concurrently the adapted red objects of general shop lighting applications are necessary to be described fully.

a. The optimization for the red color index of the warm white hybrid LED-lamp adapted to red objects in general shop lighting applications, evaluation and primary LED selection

* **Description of red objects in general shop lighting applications:** Figure 7.27 describes the spectral reflectance curves of the forty two red objects in general shops such red leaf, pink rose, red

apple, red trousers, Bordeaux pullover, ham, tomato, cherry, strawberry and so on. Based on these reflection curves, it can be recognized, that the rising edge of the reflectance spectra of the red objects distributes from about 610 nm (bright red), 620 nm (red) to about 690 nm (very deep red). In order to quantify for these red colors, the standard definitions and equations of the CIE color rendering index will be applied to calculate their componential new specific color rendering indexes. Then, the average value of all new specific *CRIs* for all red objects (called red color index) will be determined. This value will be established as the most important criterion to optimize for the warm white hybrid LED-lamp in general shop lighting applications. And other subordinate criteria such as the skin color index, the hair color index, the textile color index and the clothe color index will still play their roles similarly to that in Section 7.2.2 for the museum lighting application.

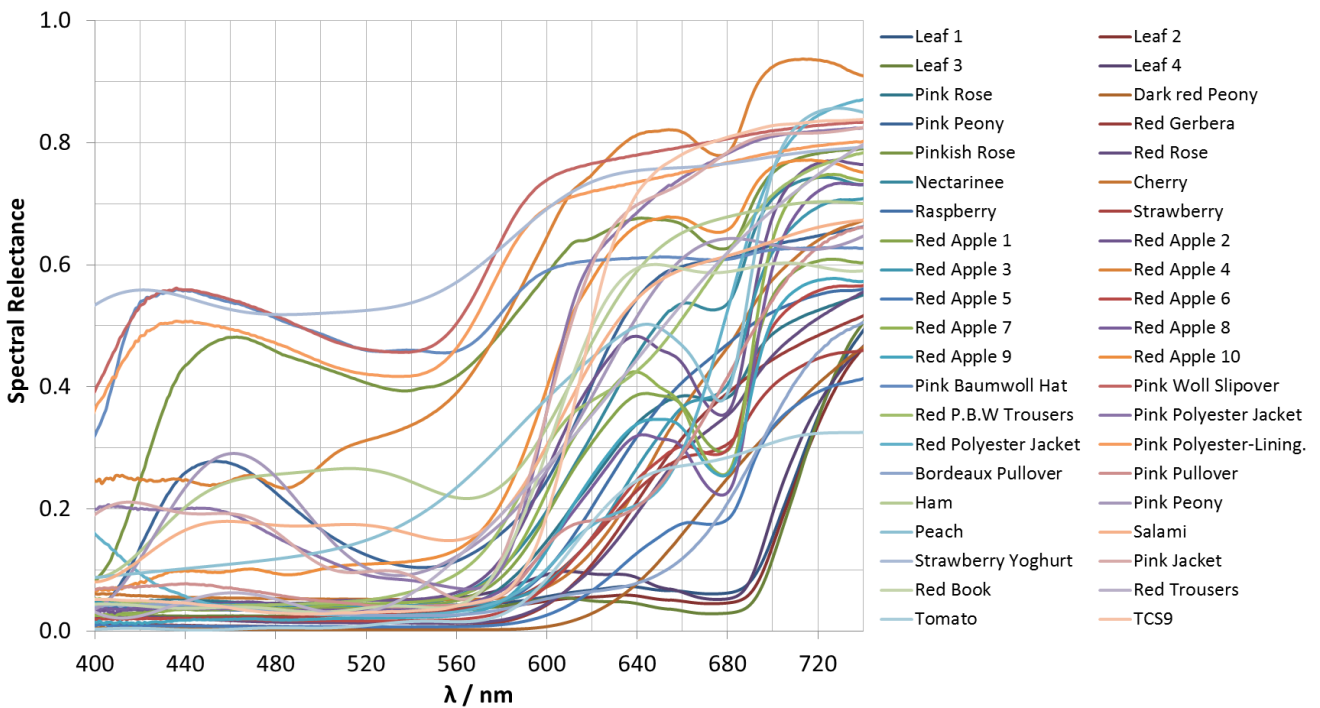


Figure 7.27 - Red objects in general shop lighting applications ([154])

* **Optimization for the red color index of the warm white hybrid LED-lamp (3000 K) with different LED-combinations adapted to red objects in general shop lighting applications:** The control system structure for the optimization is similar to that described in Figure 7.7. In that, the desired *CCT* is 3000 K and the set whiteness is also lower than $\Delta u'v' = 0.001$. However, the average value of the new specific color rendering indexes of all oil color objects ($AVR_{oil.set}$) is replaced by the one for the all red color objects in general shop lighting applications ($AVR_{red.set}$). And the color spectra and the white spectrum in Figure 7.7 are substituted by the different LED spectra of three different manufacturers (A, B or C). Finally, an optimization algorithm is carried out and give out the six optimized spectra for the warm white hybrid LED-lamp (3000 K) with the six LED-combinations described in Figure 7.28 including the optimized spectrum for the pure LEDs of the manufacturer A (called “*OPTM. for Red Color Index. Only A*” or shortly “*Only A*”), the one for the pure LEDs of the manufacturer B (called “*OPTM. for Red Color Index. Only B*” or shortly “*Only B*”), the one for the color semiconductor LEDs of the manufacturer A and the white PC-LED of the manufacturer C (called “*OPTM. for Red Color Index. A-C*” or shortly “*A-C*”), the one for almost color semiconductor LEDs and the warm white PC-LED of the manufacturer C with only the deep red semiconductor LED of the manufacturer B (called “*OPTM. for Red Color Index. B-C1*” or shortly “*B-C₁*”), the one of for all color

semiconductor LEDs of the manufacturer B and only the warm white PC-LED of the manufacturer C (called “OPTM. for Red Color Index. B-C₂” or shortly “B-C2”); and the one for the green semiconductor LED, the red semiconductor LED and the warm white PC-LED of the manufacturer C with the royal blue semiconductor LED and the deep red semiconductor LED of the manufacturer B (called “OPTM. for Red Color Index. B-C₃” or shortly “B-C3”). In addition, the peak wavelength of the royal blue ($\lambda_p \sim 440 \text{ nm} - 450 \text{ nm}$), the blue ($\lambda_p \sim 470 \text{ nm}$), the green ($\lambda_p \sim 530 \text{ nm}$), the red ($\lambda_p \sim 630 \text{ nm}$) and the deep red semiconductor LEDs ($\lambda_p \sim 660 \text{ nm}$) were mentioned in Section 7.2.1. Otherwise, the spectra of three original warm white LEDs of three manufacturers (A, B and C) (called “A.3000K.350mA.80°C”, “B.2700K.350mA.80°C” and “C.3000K.700mA.80°C” or shortly “A.3000K”, “B.2700K” and “C.3000K”, respectively) were also measured and drawn in the same figure 7.28. And visually the results showed, that the spectra of the three original warm white LEDs were impossible to reflect well the color of deep red objects (about 650 nm - 690 nm) compared with the six optimized spectra, because their deep red spectral components were very low.

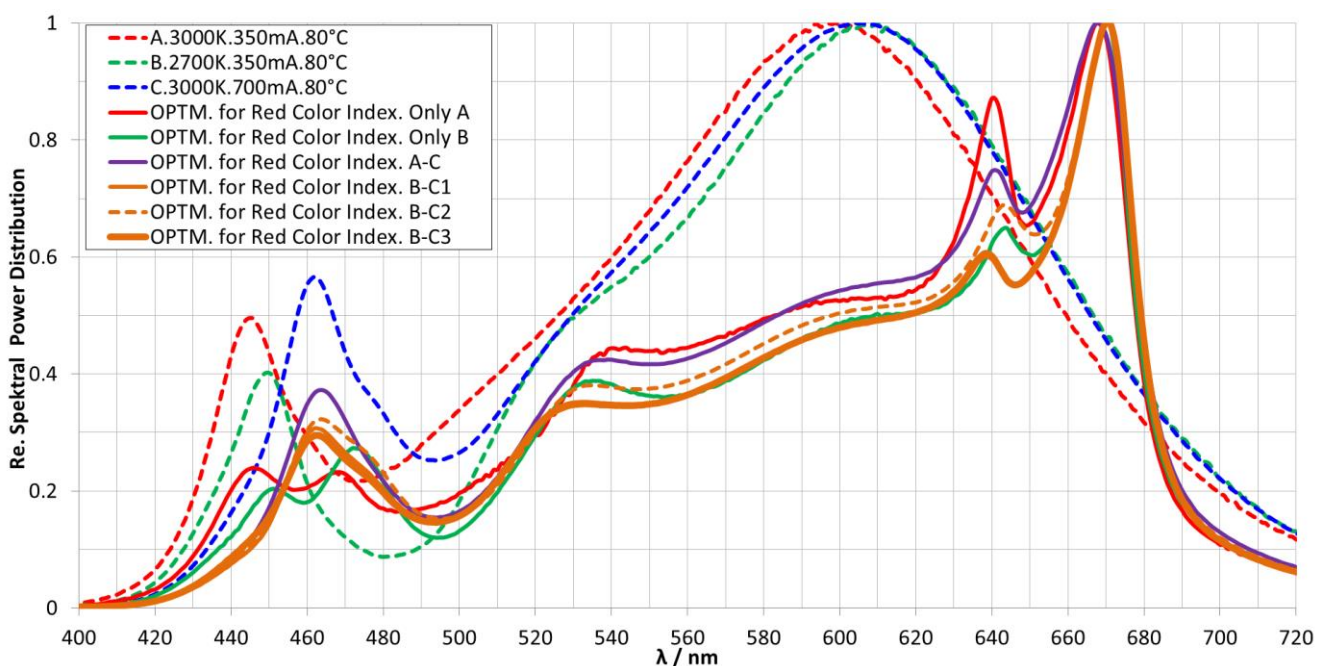


Figure 7.28 - Optimized spectra for the red color index of the warm white hybrid LED-lamp (3000 K) adapted to the red objects in general shop lighting applications with varied LEDs of three different manufacturers (A, B and C) as well as their combinations at 80 °C and 700 mA and three original warm white spectra

* **Evaluation for some lighting quality parameters of the six optimized warm white spectra in the comparison with three original warm white spectra and primary LED selection:** The color quality parameters of the six optimized warm white spectra at 80 °C and 700 mA and the three original warm white spectra at 80 °C and 350 mA (for A.3000K and B.2700K) or at 80 °C and 700 mA (for C.3000K) are described in Figure 7.29. Based on these results, it can be recognized, that the color rendering indexes of the six optimized spectra are higher than that of the three original warm white spectra and always higher than 90, even when they must operate at the forward current of 700 mA, which is two times higher than the forward current of 350 mA of the two original warm white spectra (A.3000K and B.2700K). In more detail, the compared color rendering indexes include some new specific CRIs of some typical red objects (such as red rose, red apple, ham, salami and red tomato) and some CIE standard CRIs (such as R_9 , general R_a and the average CRI AVR_{1-14}). In addition, all average values of the new specific color rendering indexes such the red color index, the skin color index, the hair color index, the textile color index and the clothe color index of the six optimized spectra are also higher

than that of the three original spectra and always higher than 90. In fact, there is nearly no significant difference about the color quality between the six different optimized spectra. Therefore, if only the color quality plays its role as the unique criteria in the LED selection, all color semiconductor LEDs and all the warm white PC-LEDs of three manufacturers (A, B and C) can be chosen equally for general shop lighting applications. However, regarding the energy quality aspect described in Figure 7.30, only cases (A-C, B-C₁, B-C₂ and B-C₃) should be chosen, because their luminous efficacies are about 83, 87, 85 and 87 lm/W, respectively. These values are nearly equal to the desired limit of 90 lm/W proposed in Chapter 3. And their luminous fluxes are nearly similar (about 210 lm). Oppositely, the luminous efficacy of other cases is lower than 73 lm/W and their luminous flux is lower than 110 lm.

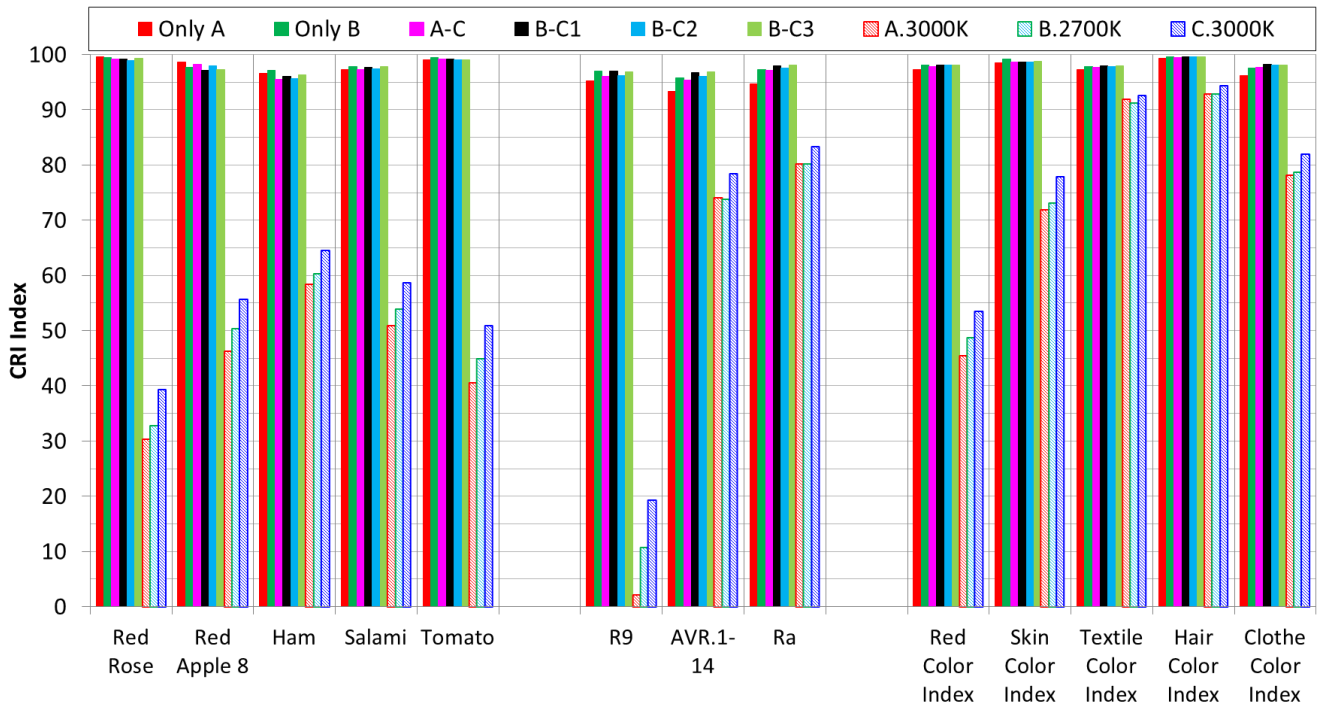


Figure 7.29 - Color quality of six optimized LED-lamps at 80 °C and 700 mA and three original warm white LEDs at 80 °C and 350 mA (A.3000K and B.2700K) or 700 mA (C.3000K)

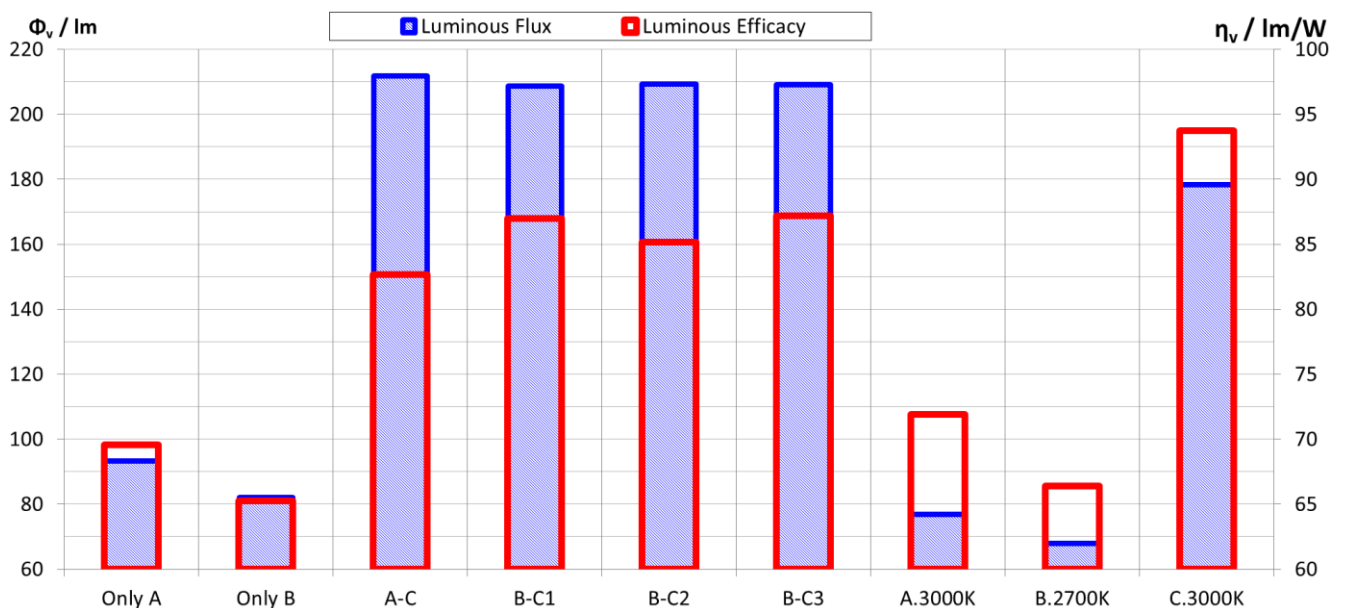


Figure 7.30 - Luminous flux and luminous efficacy of six optimized LED-lamps at 80 °C and 700 mA and three original warm white LEDs at 80 °C and 350 mA (A.3000K and B.2700K) or 700 mA (C.3000K)

b. Temperature stability of six optimized warm white hybrid LED-lamps and secondary LED selection

The investigation in Chapter 3 confirmed that under different operating conditions of temperature and forward current, the stability of LED properties for color LEDs and white PC-LEDs is changed. The properties of the royal blue, blue, green color semiconductor LEDs or the warm white PC-LEDs can be accepted in the quite wide range of forward current and operating temperature, but unfortunately the behaviors of the red or deep red LEDs are under circumstances not really good. Therefore, the total vertical spectral models of the finished LED systems in the six optimized warm white hybrid LED-lamps with the different LED-combinations of five color semiconductor LEDs and one warm white PC-LED must be investigated concurrently so that all changes of their correlated color temperature, whiteness, color rendering indexes, luminous flux and luminous efficacy can be reflected accurately and entirely. Based on these results, color semiconductor LEDs and warm white PC-LEDs can be chosen for the most available LED-combination correctly.

Figure 7.31 describes the correlated color temperature (CCT / K) and the whiteness ($\Delta u'v'_{CCT}$) of six above optimized spectra at operating temperatures of 40 °C, 60 °C and 80 °C. At the hot binning temperature (80 °C), all CCT s and $\Delta u'v'_{CCT}$ are 3000 K and 0.001 for all six cases, respectively. At 60 °C the CCT s of cases “B-C₃”, “B-C₂”, “B-C₁”, “A-C”, “only B” and “only A” are 2951, 2952, 2950, 2900 and 2810 K, and their $\Delta u'v'_{CCT}$ are 2.1, 2, 1.4, 2.5, 3.8 and 4.5 MAC ADAM ellipses, respectively. Hence, it can be recognized, that the cases “only A” and “only B” should be ignored early, because of their relatively big changes at both CCT and $\Delta u'v'_{CCT}$. Successively, if it is assumed that the maximal change of CCT has to be less than 100 K and the operating temperature reduces down to 40 °C, only the case “B-C₂” can satisfy, the cases “B-C₁” and “B-C₃” can be treated as the spare candidates and the case “A-C” should be ignored.

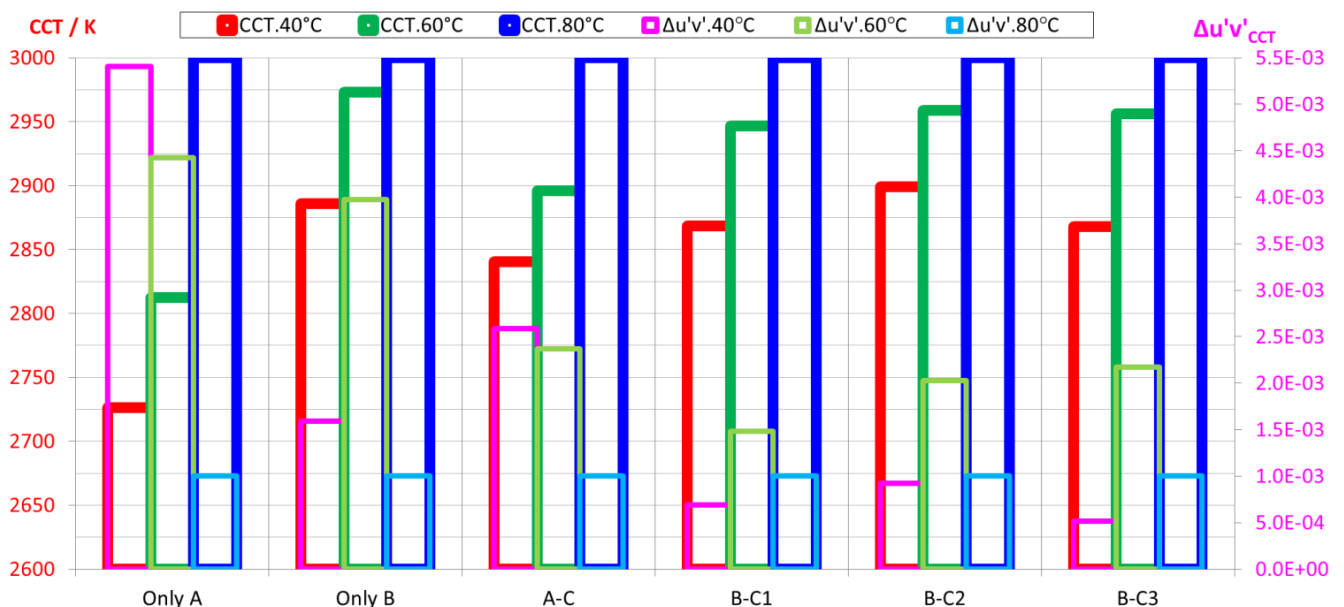


Figure 7.31 - Temperature stability of CCTs and whiteness at different operating temperatures

Otherwise, Figure 7.32 describes the red color index and the CIE standard R_9 of the six optimized spectra at operating temperatures of 40 °C, 60 °C and 80 °C. At the hot binning temperature (80 °C), all red color indexes and R_9 are higher than 95. However, at operating temperature of 60 °C, R_9 of the cases “B-C₃”, “B-C₂”, “B-C₁”, “A-C”, “only B” and “only C” is about 93, 91, 94, 89, 86 and 81, respectively. Therefore, if the lowest limit of R_9 is 90, the cases “only A”, “only B” and “A-C” can be ignored, because the change of their red spectral component too much causes the strong decrement of

the color rendering index R_9 . At the operating temperature of 40 °C, R_9 of the case “B-C₂” is also lower than 90. Finally, two permitted candidates are the cases “B-C₁” and “B-C₃”.

Successively, combining with the results in the figures 7.30 and 7.31, it can be recognized, that on the aspect of the energy quality and the CCT stability both “B-C₁” and “B-C₃” are nearly equal, but on the aspect of the stability of the whiteness and the color rendering indexes, “B-C₁” is better than “B-C₃”. Especially, about the complexity of the composition, “B-C₃” must be mixed by more varied LEDs of two manufacturers (B and C) than “B-C₁” causing the difficulty for substitution and business. Consequently, “B-C₁” is the best selection. However, unfortunately for this best selection, the offset of the CCT between the operating temperatures of 80 °C and 40 °C is nearly 130 K. For high quality lighting applications, this high CCT offset can be not accepted in the real operation. Therefore, the available control structure with the corresponding control algorithm should be investigated and proposed in Section 7.3.2 in order to stabilize both CCT and $\Delta u'v'_{CCT}$ of the hybrid LED-lamp, while its color rendering indexes, luminous flux, luminous efficacy must be still kept on high/stable levels as well as possible.

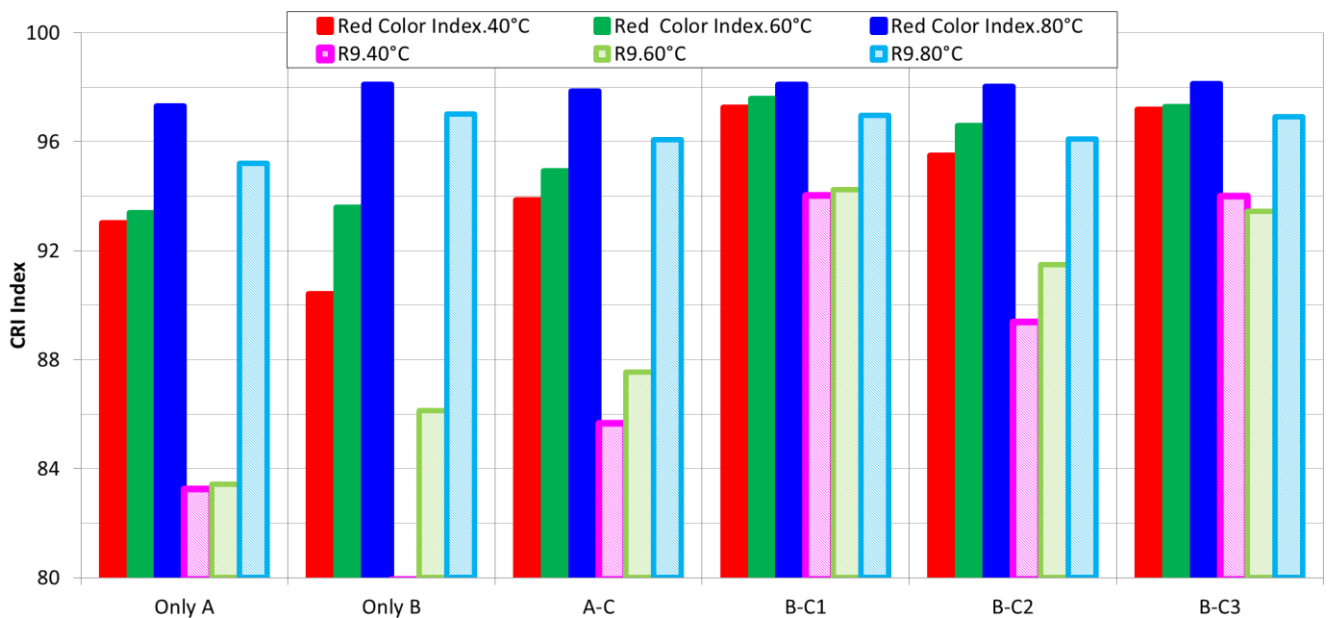


Figure 7.32 - Temperature stability of the red color index and R_9 at different operating temperatures

7.3.2. Description of a control system structure for the stabilization of some lighting quality parameters and the improvement of other lighting quality parameters

Figure 7.33 describes the control system structure diagram to stabilize the correlated color temperature and the whiteness of the hybrid LED-lamp, while it must still keep and improve its color rendering indexes, luminous flux and luminous efficacy at high/stable levels as well as possible, when the operating temperature changes.

* **Limit of the operating temperature:** In the real operation of LED-lamps, the available operating temperature of the hybrid LED-Lamp is usually in the range from about 25 °C to about 80 °C according to the practical investigation of TECHNISCHE UNIVERSITÄT DARMSTADT. In addition, in the modern indoor lighting applications, the temperature in the rooms such as in offices, shops, museums or churches in anywhere in the world is almost about 25 °C, because there are often air-conditioner systems in those rooms and in the own hybrid LED-lamps, their heat sink is always designed very well to transport the thermal power from the inside to the outside. Therefore, the operating temperature of the hybrid LED-lamp is very difficult to exceed 80 °C.

* **Control system structure:** Basically, this control system structure diagram is similar to that described in Figure 7.7. The different points are that the operating temperature becomes the new feedback signal taken into the controller and the average value of seventy nine new specific color rendering indexes of the oil color objects ($AVR_{oil,set}$) is replaced by the one of the forty two new specific color rendering indexes of the red objects in general shop lighting applications ($AVR_{red,set}$). In addition, seven feedback signals are still taken into the feedback bus in order to calculate seven errors ($Err_{.1} - Err_{.7}$) for the controller similarly to that in the control system structure in Figure 7.7. Just the operating temperature feedback signal is taken directly into the controller so that the controller can calculate and select the componential current control law correspondingly to it.

* **Objects of the MIMO system in the control system structure:** The most available LED-combination (“B-C₁”) selected in Section 7.3.1.b due to both its lighting quality and its temperature stability is the best solution for the hybrid LED-lamp. Therefore, for the MIMO system described in Figure 7.33, the hybrid LED-lamp with the LED-combination “B-C₁” is the central object for the stabilization. In that, the forward current for the main component (the warm white PC-LED (3000 K) of the manufacturer C) is not 700 mA like the optimization done in Section 7.3.1.a, but is 500 mA in order to enhance the total luminous efficacy of the hybrid LED-lamp from 87 lm/W up to higher than 90 lm/W determined as the desired limit in Chapter 3. Consequently, the color mixing rate must be established again in the case of 500 mA by the new optimization before the stabilization. In addition, the total luminous flux is not only 210 lm by a single-LED-combination like mentioned in Section 7.3.1.a, but must be enhanced higher than 3000 lm corresponding with the conventional luminous flux of normal luminaries in use by means of the multiple-LED-combination. Coordinately, the LED-arrangement on the circuit board for the optical homogeneity and the energy channel separation must be carried out appropriately for the multiple-LED-combinations like the design samples for the warm white LED-lamp (3000 K) in Appendix D and the neutral white LED-lamp (4000 K) in Appendix E.

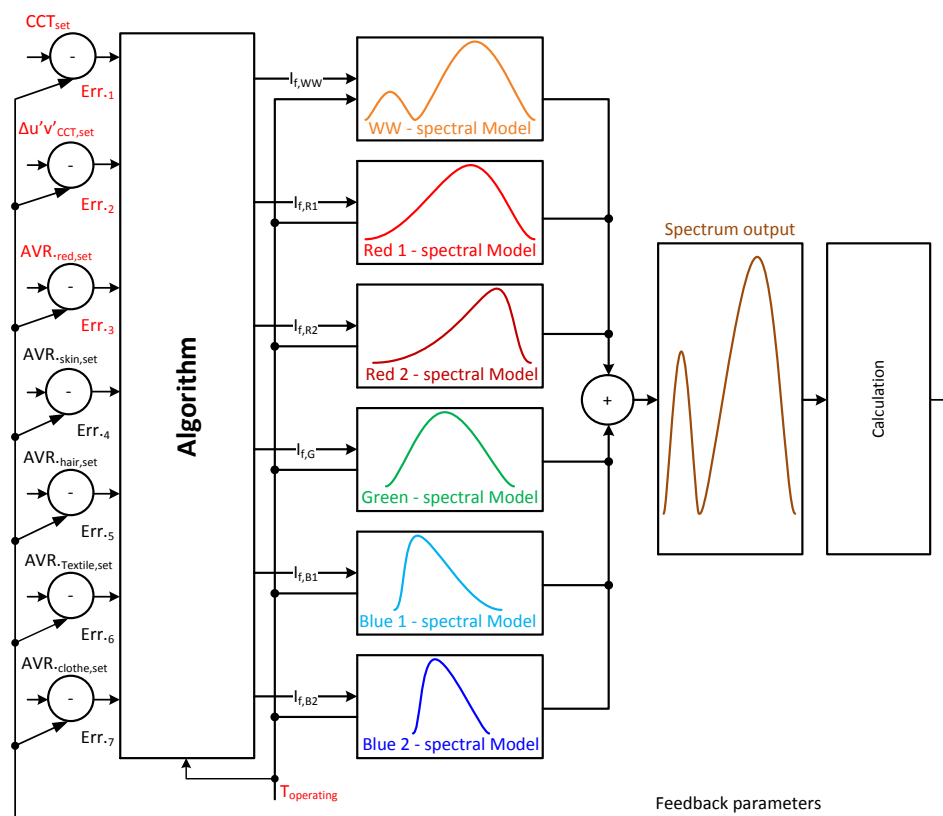


Figure 7.33 - Control system structure to stabilize some lighting quality parameters and improve some other lighting quality parameters of the hybrid LED-lamp

7.3.3. Results

Figure 7.34 illustrated the adjustment of the componential spectra in order to stabilize some lighting quality parameters of the hybrid LED-lamp, when the operating temperature reduces from 80 °C down to 25 °C. In that, the limit 80 °C is the temperature at the hot binning condition for the original optimization in Section 7.3.1.a. In real operating process, this temperature is not always 80 °C constant like that in the binning condition, but it always changes depending on the weather, season, daytime, nighttime and other operating conditions. This change causes many undesired variations of the correlated color temperatures, color rendering indexes and whiteness that were demonstrated in Section 7.3.1.b.

Therefore, based on the control system structure described in Section 7.3.2, the current control laws for each componential LED with the chosen temperature change interval of 5 °C were established. Consequently, by means of the adjustment for the componential currents according to these laws, each spectral component of the hybrid LED-lamp changed appropriately in order to stabilize its correlated color temperature of 3000 K and its whiteness less than $\Delta u'v'=0.001$, while its color rendering indexes, its luminous flux and luminous efficacy were kept at a high and stable level.

In more detail, Table 7.4 describes the lighting quality parameters of the hybrid LED-lamp at different operating temperatures (from 80 °C down to 25 °C) with the matching current control laws. The results showed that, the correlated color temperature and the whiteness were kept constant at 3000 K and 0.1 MAC ADAM ellipses, respectively. In addition, there was nearly no change for the main color rendering indexes such as the red color index for all the red objects, the CIE standard R_9 for the CIE strong red test color sample (TCS09), the average value of the first eight CIE standard test color samples (R_a) and the average value of fourteen CIE standard test color samples (AVR_{1-14}); as well as the subordinate new specific color rendering indexes such as the skin color index, the hair color index, the textile color index or the clothe color index. Moreover, the new specific color rendering indexes sampled for some typical red objects such as red rose, red apple, red ham, red salami and red tomato were also proved, that they were also kept at very high and stable levels.

On the other hand, on energy quality aspect, because of the previous optimization taking place at the hot binning temperature of 80 °C, when the real operating temperature reduced lower than 80 °C, the stabilization for the color quality parameters improved concurrently both the luminous flux and the luminous efficacy of the hybrid LED-lamp. The results in Table 7.4 showed that, when the operating temperature decreased from 80 °C down to 25 °C, the luminous flux and the luminous efficacy of the LED-lamp increased from 3098 lm to 3504 lm and from 91 lm/w to 104 lm/w, respectively. Obviously, these results confirmed, that the proposed current control laws performed very well their two missions including the stabilization for the color quality parameters and the improvement for the energy quality parameters of the hybrid LED-lamp, when the operating temperature changed. Finally, the proposed current control laws really solved the problem of the temperature instability that was mentioned in Section 7.3.1.b for the hybrid LED-lamp.

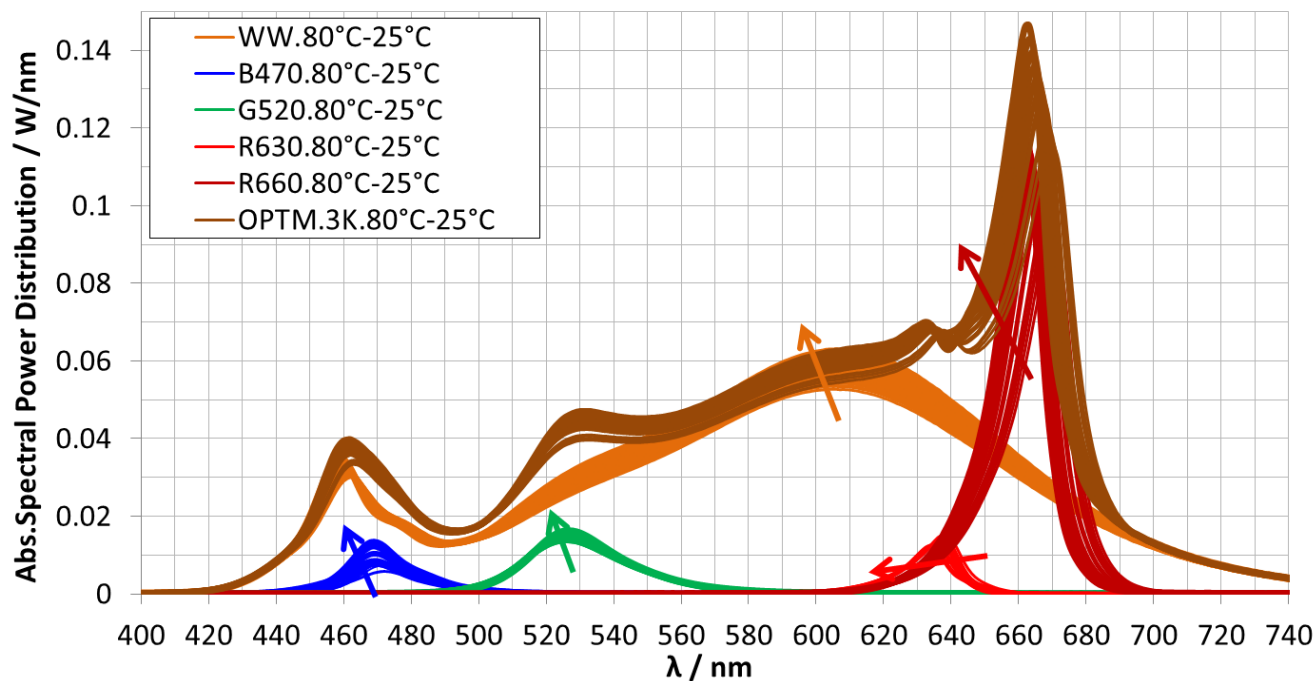


Figure 7.34 - Control of the componential color spectra to stabilize some lighting quality parameters

Table 7.4 - Lighting quality parameters of the hybrid LED-lamp after applying the control algorithm

$T_{\text{operating}} / ^\circ\text{C}$	80	75	70	65	60	55	50	45	40	35	30	25
$R_{\text{Red Rose}}$	99	99	99	99	99	99	99	99	99	99	99	99
$R_{\text{Red Apple 8}}$	97	97	97	98	98	98	98	98	98	98	98	98
R_{Ham}	96	96	96	96	96	96	96	96	96	96	96	96
R_{Salami}	98	98	98	98	98	98	98	98	97	97	97	97
R_{Tomato}	99	99	99	99	99	99	99	99	99	100	100	100
R_g	97	97	97	97	97	97	97	97	97	97	97	97
AVR_{1-14}	97	97	97	96	96	96	96	96	96	96	96	96
R_a	98	98	98	98	98	98	98	98	98	97	97	97
$R_{\text{Red Color Index}}$	98	98	98	98	98	98	98	98	98	98	98	98
$R_{\text{Skin Color Index}}$	99	99	99	99	99	99	99	99	99	99	99	99
$R_{\text{Textile Color Index}}$	98	98	98	98	98	98	98	98	98	97	97	97
$R_{\text{Hair Color Index}}$	100	100	100	100	100	100	100	100	100	100	100	100
$R_{\text{Clothe Color Index}}$	98	98	98	98	98	98	98	98	98	98	97	97
Φ_v / lm	3098	3141	3186	3233	3281	3327	3372	3415	3458	3504	3558	3504
$\eta_v / \text{lm/W}$	91	92	93	94	96	97	99	99	100	100	101	104
CCT / K	3000	3000	3000	3000	3000	3000	3000	3000	3000	3000	3000	3000
$\Delta u'v'_{\text{CCT}}$	10^{-4}	10^{-4}	10^{-4}	10^{-4}	10^{-4}	10^{-4}	10^{-4}	10^{-4}	10^{-4}	10^{-4}	10^{-4}	10^{-4}
Duty-cycle _{ww}	83	83	83	83	83	83	83	83	83	83	83	83
Duty-cycle _{G530}	28	28	28	28	28	29	29	29	28	28	27	28
Duty-cycle _{R630}	41	37	34	32	29	27	25	22	20	17	15	12
Duty-cycle _{R660}	88	88	88	88	88	88	87	87	86	86	86	86
Duty-cycle _{B470}	11	19	22	19	14	9	7	11	20	29	32	20

7.4. Summary

The change of the LED properties such three-dimensional functions of operating temperature and current had become the main consideration from the beginning to the end of this thesis. Thus, the behaviors of both color semiconductor LEDs and white PC-LEDs were investigated specifically in Chapter 3. Consequently, a simple solution for the minimization of the parameter differences between LED manufacturers and the LED-luminaire manufacturers was proposed in Chapter 4. Furthermore, on the sophisticated level thermal - electrical - optical transient LED models were researched and established in Chapter 5 and Chapter 6 so that the LED quality parameters are can be optimized and stabilized in different operating conditions based on these models.

Successively, in this chapter the museum lighting and the shop lighting were studied as two methodical demonstration examples in order to apply the transient LED models in the optimization and the stabilization for some lighting quality aspects of the hybrid LED-lamp at different operating temperatures. As a result, the optimized spectra of cases 3000 K, 4000 K, 5000 K and 6500 K for the oil color objects in the museum lighting were carried out and evaluated. The results proved, that the hybrid LED-lamps were optimized to achieve the highest values of all CRIs (*CRIs* are always higher than 90) and the ones of all *CQSs* (*CQS* are also always higher than 90). As well, they are also stabilized at the *CCT* of 3000 K and the whiteness of below 0.1 MAC ADAM ellipses.

Simultaneously, in the performance progress, the new candidate reflectance curves for the oil color objects in the museum lighting were established and compared with the CIE standard reflectance curves. The results confirmed, that in the description of the oil color objects the new candidate reflectance curves were very good in the case of the warm white museum lighting (3000 K), and the offsets between the *CRIs* calculated based on the new candidate reflectance curves and the average *CRI* value for each color group were quite low (the maximal offset was about 3 at several points) in the cases of the neutral and cold white light sources. Oppositely, fourteen CIE standard reflectance curves were impossible to describe well the oil color objects.

On the other hand, the shop lighting was optimized for all red color objects in the case of warm white lighting (3000 K) with several color semiconductor LEDs and different warm white PC-LEDs of the three manufacturers (A, B and C). Their lighting quality and temperature stability were compared together to determine the best LED-combination of the hybrid LED-lamp. Successively, this LED-combination was investigated to establish the appropriate current control laws for all componential LEDs of the hybrid LED-lamp so that its correlated color temperature and its whiteness can be kept constant, as well its color rendering indexes, luminous flux and luminous efficacy can be also kept at a high and stable level. As a result, all defined tasks for the optimization and stabilization for some lighting quality aspects of hybrid LED-lamps adapted to color objects were carried out completely. Based on the proposed and proved principle in this chapter, the optimization and stabilization can be performed similarly for other cases.

8. Conclusions

In this thesis, the optimization and stabilization of the lighting quality aspects of high qualitative LED-lamps were researched specifically in the chapter 7. In that, the museum lighting and the shop lighting were used as two methodical demonstration examples. The oil color objects and the red color objects were investigated and identified by their spectral reflectance curves. Then, they were used in the closed loop control structure diagrams in order to establish optimized / stabilized algorithms for the controllers of the hybrid LED-lamps in high quality solid state lighting applications. Moreover, the LED selection, the LED combination and the operating forward current selection of the hybrid LED-lamps were studied particularly based on the temperature stability, the compromise between the luminous efficacy and the luminous flux, the feasibility in the real establishment and the total benefit of the entire LED systems. On the other hand, the evaluation of the fourteen CIE standard test color samples for the description of the color oil objects was also carried out. The achieved results showed that these test color samples could not fully describe the oil color objects. Therefore, the new eighteen standard colors were offered in order to support for the design and evaluation of lighting systems in museum lighting.

To achieve the results in Chapter 7, Chapter 6 was a key chapter to investigate, establish and evaluate the electrical transient and the optical transient LED modules. For electrical transient LED models, many models and approaches were summarized in order to recognize their disadvantage, their advantages and their applicability. Hence, the limited electrical transient LED model in a conventional operating region was proposed. For optical transient LED models, the horizontal LED models with some approaches were studied. As a result, their positive points were inherited in the establishment of the horizontal LED models for the semiconductor LEDs and the white PC-LEDs. In addition, the junction temperature and thermal resistance were also determined and integrated into these models. As well, the not high accuracy of the horizontal LED models was recognized. Thus, they should be offered for the solid state lighting applications that do not require the high color accuracy. Finally, the vertical LED models were suggested, established and evaluated for the color semiconductor LEDs and the white PC-LEDs. Their high accuracy was a good reason for the applications in high qualitative hybrid LED-lamps in the chapter 7.

Chapter 5 was used to determine the junction temperature, identify the thermal transient processes and decode the thermal maps of the LEDs with the new measurement system of TECHNISCHE UNIVERSITÄT DARMSTADT in order to supply the thermal parameters for the horizontal LED models in Chapter 6. As well, the different measurement methods were compared by the practical investigations, the classical mathematical background for the thermal circuits was discussed for its applicability and the current well-known identification and decoding method was analyzed for its advantages and disadvantages. As a result, a new identification and decoding method with the application of the exponential interpolation and the EUCLIDEAN algorithm was offered and proved by a simulation example. The achieved results confirmed that the new identification and decoding method was available for real applications because of its accuracy and feasibility. In addition, the thermal maps of the three cold white LEDs (5000 K) were decoded according to the new method as a demonstration example. Moreover, the reasons of the inaccuracy and the improvement approaches were also pointed out in this chapter.

To have the achievements on the advanced level in the chapters 5, 6 and 7, the chapters 1, 2, 3 and 4 were aimed to research important backgrounds. Particularly, the chapter 1 was to review the history of LEDs, classify LEDs and update the state-of-the-art LED technology. Successively, the chapter 2 was to study the basic knowledge on LEDs. The focus of this chapter was the spectral and energy conversions from the electrical energy into the primary blue spectrum of blue chips and then from the primary blue spectrum into the output spectrum of white PC-LEDs. In that, the combination between the semiconductor physics, the quantum physic and the luminescent material chemistry was described with the corresponding mathematical formulations. In the chapter 3, the practical investigations about the optical, radiant and colorimetric properties of LEDs were carried out particularly. Based on the basic knowledge of LEDs in the chapter 2, the experimental results in the chapter 3 were analyzed and explained specifically. As a result, the chapter 3 gave the valuable suggestions of the LED selection and the LED combination as well as the luminous efficacy limit of 90 lm/W for the excellent CRI PC-LEDs for the chapter 7. On the other hand, the chapter 4 offered a simple solution with new three-dimensional characterizations of the properties of LEDs in order to solve the difficulties of LED-luminaire manufacturers and to help the better LED applicability in real performances.

The remaining research problems concentrate mainly in the chapter 5. Particularly, the comparison between the cooling and heating measurement procedures needs a bigger amount of more diverse measured samples in order to have more accurate and persuadable conclusions. Moreover, the measurement system and its software have to be improved better according to the improvement approaches determined in this chapter.

The current well-known identification and decoding method and the new identification and decoding method with the EUCLIDEAN algorithm for the thermal transient processes should be investigated practically together on the same measurement system with a big enough amount of varied measured samples in order to give objective evaluations about these methods. As well, a feasible and accurate measurement system with the full procedure for the junction temperature determination, the transient thermal identification and the thermal map decoding will be better established.

On the other hand, the optimization and stabilization for some lighting quality aspects of high qualitative LED lamps adapted to color objects in the chapter 7 are necessary to be developed furthermore, because the museum lighting and the shop lighting have been just used as methodical demonstration examples. In future, high qualitative hybrid LED-lamps and the optimization and stabilization for them will be carried out for the film and TV lighting, the automotive lighting and other lighting applications.

List of Symbols

SYMBOLS	COMMON UNIT	MEANING
A	m^2	Cross-sectional area
a' and b'	-	Parameters of CAM02-UCS
AG	-	Tangent of the angle of a color vector in CAM02-UCS,
AM	-	Amplitude of a color vector in CAM02-UCS
A_h and A_e	m^2	Cross-sectional area of holes and of electrons
$AVR_{\text{clothe.set}}$	-	Set average CRI of all clothe color objects or set clothe color index
$AVR_{\text{Gr.1}} - AVR_{\text{Gr.18}}$	-	Average CRI of all oil color objects in oil color group 1 to oil color group 18
$AVR_{\text{hair.set}}$	-	Set average CRI of all hair color objects or set hair color index
$AVR_{\text{oil.set}}$	-	Set average CRI of all oil color objects or set oil color index
$AVR_{\text{red.set}}$	-	Set average CRI of all red color objects or set red color index
$AVR_{\text{skin.set}}$	-	Set average CRI of all skin color objects or set skin color index
$AVR_{\text{textile.set}}$	-	Set average CRI of all textile color objects or set textile color index
AVR_{1-14}	-	Average color rendering index for 14 CIE standard test color samples
$AVR_{1-14.Me.}$	-	Average color rendering index for 14 CIE standard test color samples calculated from measured spectra
$AVR_{1-14.Mo.}$	-	Average color rendering index for 14 CIE standard test color samples calculated from simulated spectra
$AVR_{O.1-79} / AVR_{RO1-79}$	-	Average CRI of 79 oil color objects or oil color index
$\Delta AVR_{1-14 Me-Mo}$	-	Average color rendering index offset for 14 CIE standard test color samples between real and simulated LEDs
ΔE	eV	Energy difference
ΔE_C	eV	Energy difference of a conduction band edge
ΔE_V	eV	Energy difference of a valence band edge
$\Delta CCT, \Delta CCT_{Me-Mo}$	K	General correlated color temperature offset and correlated color temperature offset between real and simulated LEDs
$\Delta CCT_{re.}$	%	Offset between measured and calculated relative CCT
$\Delta u'v'_{Me.-Mo.}$	-	Color difference between a measured and model spectrum
ΔE_g	eV	Energy gap difference between an upper confining layer and an active layer
Δn	cm^{-3}	Excess carrier density of n-particles
Δn_0	cm^{-3}	Initial excess carrier density of n-particles
Δp	cm^{-3}	Excess carrier density of p-particles
Δp_0	cm^{-3}	Initial excess carrier density and p-particles
$\Delta \Phi_v$	%	Offset between measured and calculated relative luminous flux
$\Delta T = T_j - T_a$	K	Temperature offset between a junction and ambient
ΔT_i	K	i^{th} temperature difference in a measurement, $i=1 - n$

$\Delta T_{\infty} = \Delta T_0 = \Delta T_{\max}$	K	The amplitude of a temperature offset in transient thermal processes
$\Delta u'v' / \Delta E / Del_E$	-	Color difference, CIE 1976
ΔV	V	Voltage offset
$\Delta u'v'_{\text{CCT}}$ and $\Delta u'v'_{\text{CCT.set}}$	-	Whiteness and its set value
σ	-	Conversion constant between a junction temperature and a carrier temperature
α and β	%	Effective percentage of thermal power of a blue chip and a phosphor on a junction temperature
α_{ch}	-	Coefficient for chemical composition factors
c	m/s	Speed of light ($\sim 3 \times 10^8$ / m/s)
C	J/(kgK)	Specific heat capacity of a material
CCT and $CCT_{\text{.set}}$	K	Correlated color temperature and its set value
$CCT_{\text{.AVR.1-15}}$	K	Average value of correlated color temperatures of the 15 LEDs
$CCT_{\text{.cal.}}$	K	Calculated correlated color temperature
$CCT_{\text{.Me.}}$	K	Measured correlated color temperature
$CCT_{\text{.Mo.}}$	K	Model correlated color temperature
C_j, C_1 and C_2	μF	Junction capacitance and coupling capacitances
$\cos\varphi$	-	Power factor
c_{ph}	%	Phosphor concentration
CRI and $CRI_{\text{.set}}$	-	Color rendering index and its set value
CS	-	Circadian stimulus
C_{th}	Ws/K	Thermal capacitance
$C_{\text{th}i}$	Ws/K	i^{th} thermal capacitance in a measurement, $i=1-n$
$C_{\text{th}\Sigma}$	Ws/K	Total thermal capacitance
$c(x)$	Ws/(Km)	Thermal capacitance per unit length, x is a unit length
D_n and D_p	m^2/s	Diffusion coefficients of n-particles and of p-particles
dZ_{th}/dZ	-	Derivative function of a thermal impedance
e	C	Electric charge e (1.602×10^{-19} / C)
E	eV	Energy
E_A	eV	Energy level of an acceptor
E_c	eV	Energy level of a conduction band
E_D	eV	Energy level of a donor
E_F and E_{Fi}	eV	Fermi energy and Fermi energy in intrinsic semiconductor
E_g	eV	Band-gap energy
$E_{g,\text{ph}}$	eV	Absorbed energy corresponding to a band gap energy of a phosphor
$E_g(T_j)$ and $E_{g,\text{ref}}$	eV	Band gap energy at a junction and a reference temperature
E_m	eV	Radiant transient energy
E_n	eV	n^{th} discrete energy level
$E(T_{\text{ph}})$	eV	Energy difference between an excited state and a ground state at phosphor temperate T_{ph} in K
E_v	eV	Energy level of a valence band
E_0	eV	Initial energy difference at a low phosphor temperature
\bar{E}	V/m	Electric field of a junction region
ε and ε_0	F/m	Dielectric permittivity and vacuum permittivity
f or ν	Hz	Frequency of oscillation of matter waves or frequency of an optical radiation

f_1, f_2, \dots, f_i	K/(Ws)	Inverse values of thermal capacitances with index 1, 2, ...i
$f_B(E)$	W/nm	BOLTZMANN distribution with energy variable
f_{sampling}	Hz	Sampling frequency
$f_{\text{sys.}}$ and $f_{\text{sys.max}}$	Hz	System frequency and its maximal value
G and G'	-	GAUSSIAN spectral matrices
gg_1, gg_2, \dots, gg_i	W/nm	Spectral power distribution element in a spectral matrix, $i=1 - m$
$g(t)$	-	Weighting function
$G(s)$	-	LAPLACE transfer function
g_1, g_2, \dots, g_i	W/K	Inverse values of thermal resistances with index 1,2,...i
η_e and $\eta_{e.\text{set}}$	W/W or %	Radiant efficiency and its set value
η_{ext}	%	External quantum efficiency
$\eta_{\text{extraction}}$	%	Light extraction efficiency
η_i	%	Internal quantum efficiency
$\eta_{\text{inj}}, \eta_{\text{inj.p}}$ and $\eta_{\text{inj.n}}$	%	General injection efficiency, ones of p-particles and n-particles
η_v and $\eta_{v.\text{set}}$	lm/W	Luminous efficiency and its set value
h	$\text{m}^2\text{kg/s}$	PLANCK's constant ($\sim 6.626 \times 10^{-34} / \text{m}^2\text{kg/s}$)
$h(t)$	-	Transient function
h_{tr}	W/(m^2K)	Heat transfer coefficient of a thermal conduction process
\hbar and π	-	PLANCK's constant divided by 2π and constant $\pi \sim 3.14$
I_D and I_{D0}	mA	Diffusion current and its amplitude
I_f	mA	Forward current
I_h and I_e	mA	Hole current and electron current
I_n and I_{n0}	mA	Forward current of electrons and its amplitude
I_{nr}	mA	Non-radiant recombination current
I_p and I_{p0}	mA	Forward current of holes and its amplitude
I_R and I_{R0}	mA	Recombination current (both radiant and non-radiant current) and its amplitude
I_s	mA	Saturated current
I_T and I_{T0}	mA	Tunnel current and its amplitude
J_e and J_h	A/ m^2	Electron current density and hole current density injected
J_f and J_r	A/ m^2	Forward current density and reverse current density
J_T	A/ m^2	Tunneling current density
$k = \frac{2\pi}{\lambda}$	-	Angular wave number or carrier wave number
k_B	J/K	BOLTZMANN's constant ($\sim 1.38 \times 10^{-23} / \text{J/K}$)
$K(x) = \frac{c(x)}{r(x)}$	W ² s/K ²	Material coefficient
L	μm	Length
L_p and L_n	μm	Minority carrier diffusion lengths of p-particles and of n-particles
L_h and L_e	μm	Diffusion lengths of holes and of electrons
L_{skin} and L_s	nH	Skin and bond wire and package inductances
L_{70} and $L_{70.\text{set}}$	Hour	Lifetime of LEDs at 70% luminous flux maintain and its set value
M	-	Number of row vectors of spectral matrices
M_c	-	Number of an equivalent minima in a conduction band

$m_e^* / m_e / m_{en}$	mg	Effective mass of electrons
m_h^* / m_{ep}	mg	Effective mass of holes
m_r^*	mg	General effective mass ($\frac{1}{m_r^*} = \frac{1}{m_e^*} + \frac{1}{m_h^*}$)
m_T	mg	Effective tunneling mass
m_{ph}	mg	Phosphor mass
m_0	mg	Rest mass of particles
N	-	Number of column vectors of spectral matrices
(n, p) and (n_0, p_0)	cm ⁻³	Net concentrations of electrons and holes, and their initial values
N_A and N_D	cm ⁻³	Acceptor and donor concentration
N_C	cm ⁻³	Effective density of states at conduction band edge
N_e and N_h	cm ⁻³	Doping densities of electrons and of holes
$n_i = \sqrt{pn}$	cm ⁻³	Intrinsic concentration
n_{ideal}	-	Ideality factor for a recombination current ($1 < n_{ideal} < 2$)
N_V	cm ⁻³	Effective density of states at valence band edge
n_1 and n_2	-	Refraction indices
P_D	W	The power dissipation
P_e / P_{el}	W	Electrical power
p_e, p_h and p_{ph}	kgm/s	The momentum of electrons, holes and photons
$P_{opt.}$	W	Optical power
$P_{opt.chip}$	W	Optical power of a blue chip
$P_{opt.out}$	W	Output optical power of a PC-LED
$P_{opt.rest.blue}$	W	Rest optical power of blue chips after phosphor absorption
$P_{opt.phosphor}$	W	Optical power radiated by a phosphor layer
p_m	W/nm	m th peak wavelength
$P_{th.chip}$	W	Thermal power of a blue chip
$P_{th.phosphor}$	W	Thermal power radiated by a phosphor layer
P_{thi}	W	i th thermal power in a measurement, $i=1 - n$
$P_{th.in}$	W	Effective thermal power
P_{th-I}, P_{el-I} and $P_{optical-I}$	W	i th thermal power, electrical power, optical power in a measurement
Φ_e and $\Phi_{e.set}$	W	Radiant flux and its set value
$\Phi_{e,\lambda}$	W/nm	Spectral power distribution of LEDs with wavelength variable
Q_{th} and $Q_{th.int}$	J	Thermal energy and its initial value
Φ_v and $\Phi_{v.set}$	Lm	Luminous flux and its set value
$\Phi_{v.AVR.1-15}$	lm	Average value of measured luminous flux of the 15 LEDs
$\Phi_{v.cal}$	lm	Calculated luminous flux
$\Phi_{v.confidence.-0.95}$	lm	Confidence value 95% of luminous flux for the 15 LEDs
R	μm	Distance between a donor and an acceptor involved in a phosphor
R_a / CRI_a	-	Average color rendering index for first 8 CIE standard test color samples
R/G	-	Phosphor rate of a phosphor mixture
R_{nr}	-	Non-radiant recombination rate
ROG_a	-	Average CRI value of new color - candidates
ROG_1-ROG_{18}	-	CRI value of new color - candidates (1 - 18)
R_r	-	Radiant recombination rate

R_{th-i}	K/W	i^{th} thermal resistance in a measurement, $i=1 - n$
R_s	Ω	Series resistance in LEDs
$R_{th.JS}$,	K/W	Thermal resistance between a junction and a solder point
$R_{th.SB}$	K/W	Thermal resistance between a solder point and a board
$R_{th.BA}$	K/W	Thermal resistance between a board and ambient
$R_{th.JA}$	K/W	Thermal resistance between a junction and ambient
$R_{th.Die}$	K/W	Thermal resistance of a Die
$R_{th.Die Attach}$	K/W	Thermal resistance of a Die Attach
$R_{th.Heat sink}$	K/W	Thermal resistance of a Heat sink
$R_{th.Solder point}$	K/W	Thermal resistance of a Solder point
$R_{th\Sigma}$	K/W	Total thermal resistance
$r(x)$	K/W.m	Thermal resistance per unit length, x is a unit length
R_{skin} , R_j and R_s	Ω	Thermal resistance of skin, junction and bond wire and package
R_9	-	Color rendering index of the ninth standard CIE test color sample
s	-	LAPLACE operator
S and \tilde{S}	-	Spectral matrices of LEDs
$S(E)$	W/nm	Spectral power distribution with energy variable
$S_{left}(E)$	W/nm	Left spectral power distribution of LEDs with energy variable
s_m	-	m^{th} row vector of spectral matrix S
S/P	-	Scotopic - photopic ratio
S_p , S'_p and S''_p	W/nm	Peak intensity of spectra, first and second converted peak intensity
$S_p(T_{ph})$ and S_{p0}	W/nm	Peak intensity of phosphor spectra at phosphor temperature T_{ph} °C and its initial peak intensity at a low temperature
$S_{right}(E)$	W/nm	Right spectral power distribution of LEDs with energy variable
ss	μm	Particle shape and size factor in a phosphor mixture
$S(\lambda)$	W/nm	Spectral power distribution with wavelength variable
\tilde{s}_m	-	m^{th} row vector of spectral matrix \tilde{S}
ρ	Kg/m ³	Buck density of a material
$\rho(E)$	W/nm	Joint density distribution of LEDs with energy variable E
t	s	Time
T_a	°C or K	Ambient temperature
(T/T_c) and T_{c0}	°C or K	Temperature and referent temperature of carriers
T_{eff}	°C or K	Effective low temperature for step junctions
Tf_i	-	i^{th} transfer function between a thermal power input and a temperature offset output
Tg_i	-	i^{th} transfer function between a thermal power input and a thermal power output, $i=1 - n$
T_j	°C or K	Junction temperature
T_{j-heat} and T_{j-cool}	°C or K	Junction temperature measured by heating method and by cooling method
T_{ph}	°C or K	Phosphor layer temperature
T_{ref} and $T_{c,ref}$	°C or K	Referent temperature and referent carrier temperature
T_s	°C or K	Sensor temperature is measured by a temperature sensor at a point in a printed circuit board of LEDs
$T_{sampling}$	s	Sampling time
$T_{sys} / \tau_{sys} / T_{sys}$ and T_i	s	Thermal system time constant and the i^{th} thermal system time

		constant, $i=1 - n$
τ	ns	Recombination lifetime
$\tau(T_{ph})$ and τ_0	ns	Luminescence decay time at a phosphor temperature T_{ph} and its initial decay time at a low temperature
τ_n	ns	Electron minority lifetime
τ_{nr}	ns	Non-radiant recombination lifetime
τ_r	ns	Radiant recombination lifetime
$T(x_1, x_2, \dots, x_d)$	-	TAYLOR series with many variables
u', v', u, v, x, y	-	CIE chromaticity
V_A and V_{th}	V	Applied voltage and diffusion voltage / threshold voltage
V_f	V	Forward voltage
V_g and \mathcal{E}_g	eV	Energy gap and height of an energy barrier
ν_p and ν_G	nm	Experimental and GAUSSIAN peak wavelength
V_T	V	Temperature voltage of a junction
V_{vol}	m^3	Volume
$V(\lambda)$	-	Average spectral sensitivity of human visual perception of brightness for photopic vision
$V'(\lambda)$	-	Average spectral sensitivity of human visual perception of brightness for scotopic vision
$V_0 / V_{bi} / V_D$	V	Built-in voltage in a junction layer
ϑ	m/s	Velocity of particles
W	μm	Width
W_D	μm	Width of a depletion region
$\omega=2\pi f$	Rad/s	Angular frequency of oscillation of matter waves
Ψ	W/nm	Intensity of oscillation of matter waves
χ	-	Electric susceptibility of a material
x	μm	A length unit
$Y_{th}=1/Z_{th}$	W/K	Thermal conductance
γ	-	LORENTZ factor
γ_p	-	GAUSSIAN element
$z = \ln(t)$	-	Transfer constant, $t = e^z$
Z_{th}	K/W	Thermal impedance
λ	nm	Wavelength
$\lambda_{FWHM}, \lambda'_{FWHM}$ and λ''_{FWHM}	nm	Full width at half maximum, first and second converted full width at half maximum
λ_p, λ'_p and λ''_p	nm	Peak wavelength, first and second converted peak wavelength
$\xi = \ln(T_i)$	-	The logarithmic value of a thermal system time constant, $T_i = e^\xi$

Abbreviation

ABBREVIATION	EXPLANATION
A	Acceptor
A, B and C	Anonymous names of the three investigated LED manufacturers. Because of many reasons, the author is not allowed to publish their name.
Abs.	Absolute value
AFM	Atomic Force Microscopy
AVR / AVR. / Avr.	Average value
B445 / B-445	Royal blue color semiconductor LED with the peak wavelength of 445 nm
B450 / B-450	Royal blue color semiconductor LED with the peak wavelength of 450 nm
B470 / B-470	Blue color semiconductor LED with the peak wavelength of 470 nm
CAM02	Color Appearance Modeling for Color Management Systems 2002
CIE	COMMISSION INTERNATIONALE DE L'ECLAIRAGE
CQS	Color Quality Scale
CW	Cold White PC-LED
CWEX	Cold White Excellent CRI LEDs
CWG	Cold White Good CRI LEDs
CWVG	Cold White Very Good CRI LEDs
D	Donor
DC	Direct Current
DCM	Dual Current Method
DQW	Double Quantum Well
Em	Radiant transition in a phosphor layer or Emission
ES	Excited State in a phosphor layer
Err.	Error
ETM	Electrical Test Method
Ex	External energy absorption in a phosphor layer
FGLT	FACHGEBIET LICHTTECHNIK
Gr.	Color Group
GS	Ground State in a phosphor layer
G530 / G-530	Green color semiconductor LED with the peak wavelength of 530 nm
Ha.	Hair color
HWEX	High Warm white Excellent CRI LEDs

HWG	High Warm white Good CRI LEDs
HWVG	High Warm white Very Good CRI LEDs
LED	Light-Emitting Diode
LWEX	Low Warm white Excellent CRI LEDs
LWG	Low Warm white Good CRI LEDs
LWVG	Low Warm white Very Good CRI LEDs
M	Man
MCPCB	Metal Core Printed Circuit Board
Me.	Measured value
Mo.	Model Value
MIMO	Multi-Input Multi-Output System
MISO	Multi-Input Single-Output System
MQW	Multiple Quantum Well
MTCS	MAZET True Color Sensor
NW	Neutral White PC-LED
NWEX	Neutral White Excellent CRI LEDs
NWG	Neutral White Good CRI LEDs
NWVG	Neutral White Very Good CRI LEDs
OPM	Optical Test Method
Opt.	Optical
OPTM.	Optimization
Ord.	Order
im	Imaginary
PCB	Printed Circuit Board
PC-LED	Phosphor Converted Light-Emitting Diode
POP	Light Power Method
PWM	Pulse Width Modulation
QW	Quantum Well
RGBWW	Red, Green, Blue, Amber, Warm White , Cold White LED-lamp
Re.	Relative values
RO	CRI of an Oil color object / Oil color object
ROG	CRI of Oil color object Group / Oil color group
R-G-B-O	Red - Green - Blue - Orange color semiconductor LEDs
R630 / R-630	Red color semiconductor LED with the peak wavelength of 630 nm
R660 / R-660	Deep Red color semiconductor LED with the peak wavelength of 660 nm
SISO	Single-Input Single-Output System
SPD	Spectral Power Distribution

Spec. / Spec	Spectrum
SQW	Single Quantum Well
TCS	Test Color Sample
TED	Cross-sectional Transmission Electron Microscopy
Temp.	Temperature
Th. / th	Thermal
Txt.	Textile color
UCS	Uniform Color Scale
W	Woman
WSM	Wavelength Shift Method
WW	Warm White PC-LED
3D	Three dimensional
2.7K	Warm white PC-LED with the correlated color temperature of 2700 K
3K	Warm white PC-LED with the correlated color temperature 3000 K
4K	Neutral white PC-LED with a correlated color temperature 4000 K
5K	Cold white PC-LED with a correlated color temperature 5000 K
65K	Cold white PC-LED with a correlated color temperature 6500 K

Bibliography

- [1] SCHUBERT, E. F.: *“Light Emitting Diodes”*, Cambridge University Press, 2003, pp. 1-112
- [2] ROUND, H. J.: *“A note on Carborundum”*, Electrical World 19 ,1907, pp. 309
- [3] LOSEV, O. V.:*“Telegrafiya i Telefoniya bez Provodov“*, 44, 1927, pp. 485-494
- [4] KHANH, T. Q.: Lectures in TECHNISCHE UNIVERSITÄT DARMSTADT, 2009 - 2013
- [5] DADGAR, A.: *“Crack-Free InGaN/GaN Light Emitters on Si(111)”*, Physical Status Solid (a) 188, 2001, pp. 155-158
- [6] DADGAR, A.; Poschenrieder, M.; Bläsing, J.; Fehse, K.; Diez, A.; Krost, A.: *“Thick, crack - free blue light-emitting diodes on Si (111) using low - temperature AlN interlayers and in situ Si\sub x]N\sub y masking”*, Applied Physics Letters 80, 2002
- [7] OSRAM: *“Success in research: First Gallium - nitride LED chips on silicon in pilot stage”*, www.osram.de, Regensburg, January 12nd, 2012
- [8] Datasheets of Corporations OSRAM (www.osram.de), PHILIPS LUMILEDS (www.philipslumileds.com), CREE (www.cree.com), NICHIA (www.nichia.com), and SAMSUNG (www.samsung.com/global/bussiness/led), 2000 - 2013
- [9] MÜLLER, R.: *“Philips Lumimarc - a new approach in Phosphor converted LEDs”*, Global Phosphor Summit, San Diego, 2008
- [10] BAUMANN, F.: *“Phosphor Solutions for state-of-the-art warm white LEDs”*, Global Phosphor Summit, San Diego, 2010
- [11] SETZER, C.: *“LED und OLED Entwicklung der Technologie und Anwendungen“*, VDE/ZVEI Workshop, OFFENBACH, 2012.
- [12] Energy Star Program Requirements for Solid - State Lighting Luminaires, Eligibility, Version 1.1 - 2008, Version 1.0 - 2010
- [13] RICHMAN, E.: *“Understanding LED tests: IES-79, LM-80 and TM-21”*, DOE SSL Workshop, 2011
- [14] ZUKAUSKAS, A.; SHUR, M. S.; GASKA, R.: *“Introduction to solid state lighting”*, John Wiley & Son, 2002, pp 37-55
- [15] MÜLLER, G.: *“Electroluminescence I - Semiconductors and semimetals”*, Vol. 64, Academic Press, 2000, pp. 61-66
- [16] LIN, C. C.; ZHENG, Y. S; CHEN, H. Y.; RUAN, C.H.; XIAO, G. W.; LUI, R. S.: *“Improving Optical Properties of White LED Fabricated by a Blue LED Chip with Yellow Red Phosphors”*, Journal of The Electrochemical Society, 157 (9), 2010, pp. H900-H903
- [17] LIN, C. C.; LUI, R. S.: *“Advances in Phosphors for Light Emitting Diodes”*, The journal of Physical Chemistry Letters, No.2, 2011, pp. 1268-1277
- [18] RONDA, C. : *“Luminescence - From theory to application”*, Willey-VCH Verlag, 2007, pp. 1-34

- [19] BLACKWELL, H.R.: *“Development of procedures and instruments for visual task evaluation”*. III. Eng. Soc. 65 (1970) 4, pp. 267-291
- [20] DAVIS, W.; OHNO, Y.: *“Color quality scale”*, Optical Engineering 493, 033602, 2010
- [21] GALL, D.: *“Die Kontrastempfindung als Ausgangspunkt für die Beleuchtungsplanung“*, Dissertation B, TECHNISCHE UNIVERSITÄT ILMENAU, 1983
- [22] HENTSCHEL, H. J.: *“Beleuchtungsniveau in betriebswirtschaftlicher Sicht“*, Lichttechnik, 20 (1968), 7, 75A-80A
- [23] UCHIDA, H.: *“A new whiteness Formula”*, Color research & application, John Wiley & Son, 1998, pp. 202-209
- [24] KATAYAMA, I.; MARK, D.: *“Quantitative evaluation of perceived whiteness based on Color Vision Model”*, Wiley Periodicals, 2009, pp. 410-418
- [25] LAM, W. M. C.: *“Perception & Lighting as form givers for architecture”*, Van Nostrand Reinhold, New York, 1992
- [26] LINDNER, H.: *“Beleuchtung und Arbeitsleistung- Systematik experimenteller Grundlagen“*. Z. ges. Hyg. 21, (1975) 2, pp. 101-106
- [27] REA, M. S.; FIGUEIRO, M. G; BIERMAN, A.; BULLOUGH, J. D.: *“Circadian Light”*, Journal of circadian rhythms, 2010
- [28] FAIRCHILD, M. D.; PIRROTTA, E.: *“Predicting the Lightness of Chromatic Object Colours using CIELAB”*, Color Res. Appl. 166, 1991, pp. 385-393
- [29] MUCK, E; BODMANN, H. W.: *“Die Bedeutung des Beleuchtungsniveaus bei praktischer Sehtätigkeit“*, Zts. Lichttechnik 13 (1961) 19, pp. 502
- [30] BODROGI, P.; KHANH, T. Q.; VINH, T.Q.: *“Weiße Hochleistungs-LEDs: Eine umfassende lichttechnische Betrachtung“*, Zeitschrift Licht, Heft 6, 2012, pp. 64-70
- [31] FOTIOS, S.A.; CHEAL, C.: *“Predicting lamp spectrum effects at mesopic levels, Part 1: Spatial brightness”*, Lighting research and technology, Vol.43, 2011, pp. 143-157
- [32] KHANH, T. Q.; BODROGI, *“Farbwiedergabe und Helligkeit, Untersuchungen zu weißen leuchtstoffkonvertierten LEDs“*, Eine wissenschaftliche Publikation zum 80. Jahrestag der CIE-Farbmeterik, Zeitschrift Licht, Pflaum Verlag (München), Heft 10, 2011, pp. 37-43
- [33] VINH, T. Q.; BRÜCKNER, S.; KHANH, T. Q.: *“LEDs-Verhaltens unter Strom- und Temperaturänderung“*, Zeitschrift Licht, Pflaum Verlag (München), Heft 6, 2011, pp. 70-76
- [34] VÖLKER, S.: *„Eignung von Methoden zur Ermittlung eines notwendigen Beleuchtungsniveaus“*, Dissertation, TECHNISCHE UNIVERSITÄT ILMENAU, 1999
- [35] WESTON, H. C.: *“The relation between illumination and visual performance”*, Medical Research Council, Report No. 87 (1945) and Joint Report (1935)
- [36] VINH, T. Q.; KHANH, T. Q.: *“Eine Analyse weißer LEDs - Lichtausbeute, Farbwiedergabe und Farbtemperatur“*, Zeitschrift Licht, Pflaum Verlag (München), Heft 11-12, 2012, pp. 70-75

-
- [37] BIESKE, K.; WOLF, S.; NOLTE, R.: “*Wahrnehmung von Farbunterschieden von Licht-und Körperfarben*“, Vortrag auf der Lichttagung der Deutschsprachigen Länder, Bern, Schweiz, 10 - 13.09.2006, pp. 63-64
- [38] DUNN, T.; STICH, A.: “*Driving The Golden Dragon LED*”, Application Note, OSRAM Opto Semiconductors GmbH, 2007
- [39] KARLICEK, R.: “*The Evolution of LED Packaging*”, Smart Lighting Engineering Research Center, 2012
- [40] HUBER, R.: “*Thermal Management Of Golden Dragon LED*”, Application Note, OSRAM Opto Semiconductors GmbH, 2008
- [41] SIEGAL, B.: “*Practical Considerations in High Power LED Junction Temperature Measurements*”, IEMT, 2006.
- [42] GU, Y.; NADREAN, N.: “*A non - contact method for determining junction temperature of phosphor-converted white LEDs*”, Third SPIE 5187, 2004, pp. 107-114
- [43] CHHAJED, S.; XI, Y.; GESSMANN, TH.; XI, J. -Q.; SHA, J. M.; KIM, J. K., SCHUBERT, E.F.: “*Junction temperature in light-emitting diodes assessed by different methods*”, 2005
- [44] XI, Y.; SCHUBERT, E. F.: “*Junction-temperature measurement in GaN ultraviolet light - emitting diodes using diode forward voltage method*”, Applied Physics Letter, Vol.85, No.12, 2004, pp. 2163-2165
- [45] HULET, J.; KELLY, C.: “*Measuring LED junction temperature*”, Photonics Spectra, 2008, pp. 73-75
- [46] KEPPEM, A.; REYCKAET, W. R.; DECONINCK, G.; HANSELAER, P.: “*High power light - emitting diode junction*”, Journal of applied Physics, 104, 093104, 2008
- [47] ZONG, Y., OHNO, Y.: “*New Practical Method Of Measuring High - Power LEDs*”, CIE expert symposium on Advances in Photometry and Colorimetry, No. CIE x033:2008, 2008, pp. 102-106
- [48] ISUZU OPTICS COPR., *ITR-180 User Manual*, Version 1.0, 2010
- [49] MA, Z.; ZHENG, X.; LIU, W., LIN, X.; DENG, W.: “*Fast thermal resistance measurement of high brightness LED*”, IEEE, 6th International Conference on Electric Packaging Technology, 2005
- [50] VINH, T. Q.; BRÜCKNER, S.; KHANH, T. Q.: “*Accurate measurement of the pn-junction Temperature of HP-LEDs*”, in 9th International Symposium on Automotive Lighting - ISAL, 2011, pp. 809-827 (1088)
- [51] FARKAS, G.; HAQUE, S.; WALL, F.; PAUL, S.; POPPE, A., VADER, Q. V. V, BOGNÁR, G: “*Electric and Thermal Transient Effects in High Power Optical Devices*”, IEEE, 2004
- [52] SZÉKELEY, V.; TRAN, V. B.: “*Fine structure of heat flow path in semiconductor device - A measurement and identification method*”, Solid-State Electronics, Vol.31., No.9, 1988, pp. 1363-1368
- [53] JERRI, A. J.: “*The Shannon Sampling Theorem - Its Various Extensions and Applications: A Tutorial Review*”, IEEE, Vol.65, No.11, 11-1977, pp. 1565-1596

- [54] WESCOTT, T.: “*Sampling: What Nyquist Didn’t say, and What to Do About It*”, Wescott Design Services, www.wescottdesign.com, 2010
- [55] PROTONOTARIOS, E. N.; WING, O.: “*Theory of Nonuniform RC Lines - Part I: Analytic Properties and Realizability Conditions in the Frequency Domain*”, IEEE, 3.1967, pp. 1-12
- [56] PROTONOTARIOS, E. N.; WING, O.: “*Theory of Nonuniform RC Lines - Part II: Analytic Properties in the Time Domain*”, IEEE, Vo.14, No.1, 3.1967, pp. 13-20
- [57] CARLAW, H. S.; JAEGER, J. C.: “*Conduction of Heat in Solids*”, 2nd edition Clarendon, Oxford, 1959
- [58] WEINBERG, L.: “*Network Analysis and synthesis*”, McGraw - Hill, New York, 1962
- [59] GERSTENMAIER, Y. C.; KIFFE, W.; WACHUTKA, G.: “*Combination of Thermal Subsystems Modeled by Rapid Circuit Transformation*”, THERMINIC, 2007
- [60] LEONOWICZ, Z.: “*Selected problems of circuit theory 1*”, Lecture 2008, pp. 11-22
- [61] SCHEITZER, D.; PAPE, H.; CHEN, L.: “*Thermal Resistance Using Structure Functions Chances and Limit*”, IEEE, 24th IEEE SEMI-THERM Symposium, 2008, pp. 191-197
- [62] RENCZ, M.; POPPE, A.; KOLLÁR, E.; RESS, S.; SZÉKELY V.; COURTOIS, B.: “*A Procedure to correct the error in the structure function based thermal measuring methos*”, IEEE, 20th IEEE SEMI-THERM Symposium, 2004
- [63] HEILER, F.; NIMZ, T.: “*Accuracy optimization of True Color Sensor Solutions for LED color control of multiple LED light sources*”, MAZeT Electronic Engineering & Manufacturing Services, www.mazet.de, 2012
- [64] IHRINGER, J.: “*Modellierung moderner Hochleistungs - Leuchtdioden im Pulsebetrieb*”, Master Thesis, TECHNISCHE UNIVERSITÄT DARMSTADT, 2010, pp. 21-35
- [65] NOTTRODT, O.: “*Entwicklung eines Messsystems zur Bestimmung des thermischen Widerstandes*”, Master Thesis, TECHNISCHE UNIVERSITÄT DARMSTADT, 2009, pp. 37-40
- [66] BAUREIS, P.: “*Compact Modeling of electrical, thermal and optical LED behavior*”, University of applied sciences Würzburg, Proceedings of ESSDERC, Grenoble, France, 2005, pp.145-148
- [67] SHOCKLEY, W.; READ, W. T. JR.: “*Statistics of the Recombinations of Holes and Electrons*”, Physical Review, Vo.87, No.5, 1952, pp.835-842
- [68] SHOCKLEY, W.; QUEISSER, H. J.: “*Detailed Balance Limit of Efficiency of pn Junction Solar Cells*”, Journal of Applied Physics, Vol.32, No.3, 1961, pp. 510-519
- [69] ZHE, B.: “*W. SHOCKLEY'S EQUATION and ITS LIMITATION*”, Applied Mathematics and Mechanics, Vol.3, No.6, 1982, pp. 827-832
- [70] KASAP, S. O.: “*pn Junction - The Shockley equation*”, e-Booklet, <http://Materials.Usask.ca>, 2001
- [71] NELSON, D. F.; GERSHENZON, M.; ASHKIN, A.; D'ASORO, L. A.; SARACE, J. C.: “*BANDFILLING MODEL FOR GaAs INJECTION LUMINESCENCE*”, Applied Physics Letters, Vol.2, No.9, 1963, pp. 182-184
- [72] DUMIN, D. J.; PEARSON, G. L.: “*Properties of Gallium Arsenide diodes between 4.2 and 300 K*”, Journal of Applied Physics, Vol.36, No.11, 1965, pp. 3419-3426

- [73] DONNELLY, J. P.; MILNES, A. G; D.Sc.; C.Eng., M.I.E.E.: “Current/voltage characteristics of p-n Ge-Si and Ge-GaAs heterojunctions”, PROC. IEEE, Vol.113, No.9, 1966, pp. 1468-1476
- [74] RIBEN, A.R.; FEUCHT, D. L.: “nGe - pGaAs HETEROJUNCTION“, Solid - State Electronics, Pergamon Press, 1966, pp. 1055-1065
- [75] NELSON, H; DOUSMANIS, G. C.: “EFFECT OF IMPURITY DISTRIBUTION ON SIMULTANEOUS LASER ACTION IN GaAS AT 0.84 AND 0.88 μm ”, Applied Physics Letters, Vol.4, No.11, 1964, pp. 192-194
- [76] CASEY, H. C; MUTH, J.; KRISHNAMKUTTY, S.; ZAVADA, J. M.: “Dominance of tunneling current and band filling in InGaN - AlGaIn double heterostructure blue light - emitting diodes”, Applied Physics Letter.68 (20), 1996, pp. 2867-2869
- [77] FORREST, S. R.; DIDOMENICO, M.; SMITH, R. G.; STOCKER, H. J.: “Evidence for tunneling in reverse-biased III - V photodetector diodes”, Applied Physics Letter. 36(7), 1980, pp. 580-582
- [78] LESTER, S. D.; PONCE, F.A.; CRAFT, M. G.; Steigerwald, D. A.: “High dislocation densities in high efficiency GaN - based light - emitting diodes”, Applied Physics Letters, 66(10), 1995, pp. 1249-1251
- [79] MÁRTIL, I; REDONDO, E.; OJEDA, A.: “Influence of defects on electrical and optical characteristics of blue LEDs based on III - V nitrides”, Journal of Applied Physics, 81 (5), 1997, pp. 2442-2444
- [80] CHEN, Y.; TAHEUCHI, T.; AMANO, H.; AKASAKI, I., YAMADA N.: “Pit formation in GaInN quantum wells”, Applied Physics Letters, 1998, pp.710-712
- [81] HINO, T.; TOMIYA, S., MIYAJIMA, T.; YANASHIMA, K.; HASHIMOTO, S.: “Characterization of threading dislocations in GaN epitaxial layers”, Applied Physics Letters, Vol.76, No.23, 2000, pp.3421-3423
- [82] CHERMS, D.; HENEY, S. J.; PONCE, F. A.: “Edge and screw dislocations as nonradiative centers in InGaIn - GaN quantum well luminescence”, Applied Physics Letters, Vol.78, No.18, 2001, pp. 2691-2693
- [83] MANASREH, O.: “III - Nitride Semiconductors - Electrical, Structural and Defects Properties”, Elsevier Science B.V., 2000, pp.17-45
- [84] HSU, J. W. P.; MANFRA, M. J.; LANG, D. V.; RICHTER, S.; CHU, S.N.G.: “Inhomogeneous spatial distribution of reverse bias leakage in GaN Schottky diodes”, Applied Physics Letters, Vol.78, No.12, 2001, pp. 1685-1687
- [85] CAO, X.A.; TOPOL, K.; SHAHEDIPOUR-SANDVIK, F.; TEETSOV, J.; LEBOEUF, S. F.; EBONG, A.; KRETCHMER, J.; STOKES, E. B.; ARTHUR, S.; KOLOYEROS, A. E. ;WALKER, D.: “Influence of defects on electrical and optical characteristics of GaNInGaIn-based LEDs”, Proceedings of SPEIE Vol. 4776, 2002, pp. 105-113
- [86] CAO, X. A.; STOKES, E. B, SANDVIK, P. M.; LEBOEUF, S. F; WALKER, D.: ”Diffusion and Tunneling Currents in GaN - InGaIn Multiple Quantum Well LEDs”, IEEE, Vol.23, No.9, 2002, pp. 535-537
- [87] PARK, J.; LEE, C. C.: “An Electrical Model With Junction Temperature for Light - Emitting Diodes and Impact on Conversion Efficiency”, IEEE, Vol.26, No.5, 2005, pp. 308-310
- [88] FUCHS, D.; SIGMUD, H.: “ANALYSIS OF THE CURRENT - VOLTAGE CHARACTERISTIC OF SOLAR CELLS”, Solid-State Electronics, Vol.29, No.8, 1986, pp. 791-795

- [89] GRAEME, J. G.: “*Photodiode Amplifiers - OP Amp Solutions*”, McGraw - Hill, 1995, pp. 1-19
- [90] RAY, L. L.; CHEN, Y. F.: “*Equivalent Circuit Model of Light - Emitting - Diode for System Analyses of Lighting Drivers*”, IEEE, 2009
- [91] STRINGFELLOW, G.B.; CRAFT, M. G.: “*High Brightness Light Emitting Diodes*”, Semiconductors and Semimetals, Vol.48, Academic Press, 1966, pp. 83-95
- [92] REN, F.; ZOLPER, J. C.: “*Wide Energy Band - gap Electronic Devices*”, World Scientific Publishing, 2003, pp. 34-108
- [93] PIPREK, J.: “*Optoelectronic Devices - Advanced Simulation and Analysis*”, Springer, 2005, pp. 40-41
- [94] LUMILEDS LIGHTING: “*Advanced Electrical Design Models*”, Application brief AB20-3A, 2002
- [95] CALOW, J. T.; DEASLEY, P. J.; OWEN, S.J. T.; WEBB, P. W.: “*A Review of Semiconductor Heterojunction*”, Journal of Materials Science, Vol. 2, 1967, pp. 86-89
- [96] ANDERSON, R.L.: “*Solid - State Electron*”, 5, 341, 1962
- [97] McAfee, D. B.; RYDER, E. J.; SCHOCKLEY, W. ; SPARKS, M. *Phys. Rev.* 83, 534, 1964
- [98] MOLL, J. L.: “*Physics of Semiconductors*”, MCGraw - Hill Book Company, Inc, New York, 1964
- [99] KELDYSH, L. V.; *Soviet Phys. JETP* 6, 763, 1958; HELDYSH, L. V.; *Soviet Phys. JETP* 7, 665, 1958; Kane, E.O.; *J. Appl. Phys.* 32, 83, 1961
- [100] KEITHLEY INSTRUMENT, *Manual 2651 A*, 2012
- [101] KHANH, T. Q.: “*Ist die LED - Photometrie mit $V(\lambda)$ - Funktion wahrnehmungsgerecht*“, www.lichtnet.de, Licht 06 / 2004
- [102] OHNO, Y.: “*LED Photometric Standards*”, Lecture 1999
- [103] REIFEGERSTE, F.; LIENIG, J.: “*Modeling of the temperature and current dependence of LED spectra*”, TECHNISCHE UNIVERSITÄT DRESDEN, *J. Light & Vis. Env.* Vol.32, 2008, pp. 288-294
- [104] OHNO, Y.: “*Spectral design considerations for white LED color rendering*”, *Optical Engineering* 44(11), 2005
- [105] CHIEN, M. C.; TIEN C.H.: “*Multispectral mixing scheme for LED clusters*”, *Optical Society of America*, Vol.20, No.S2, *OPTICS EXPRESS*, 2012, pp. 245-254
- [106] KEPPENS, A.; RYCKAERT, W. R.; DECONINCK, G.; HANSELAER, P.: “*LED Modeling Spectra and variation with temperature*”, *Journal of Applied Physics*, No.108, 043104, 2010
- [107] JAYASINGHE, L.; DONG, T.; NARENDRAN, N.: “*is thermal resistance coefficient of high power LEDs constant?*”, *SPIE* 6669:666911, 2007
- [108] SCHMINCKE, NORMA PROFESSIONAL, *Feinste Künstler - Ölfarben - Pigment - Übersicht*, GERMANY
- [109] HAAS, R.: “*Raphael's The School of Athens - A Theorem in a Painting*”, *Journal of Humanistic Mathematics*, Vol.2, No.2, 2012, pp. 3
- [110] FROHNAPFEL, A.: “*Psychophysische und physiologische Aspekte der Farbwiedergabe für LED Anwendungen*“, Master thesis, TECHNISCHE UNIVERSITÄT DARMSTADT, 2008, pp. 57 - 60

- [111] CIE COLORIMETRY 1931 - 2006: “*Colorimetry - Understanding the CIE System - CIE Colorimetry 1931 - 2006*”, 2006
- [112] CIE 13.3-1995: “*Method of Measuring and Specifying Colour Rendering Properties of Light Sources*”, 1995
- [113] CIE 18.2 - 1983.: “*The Basis of Physical Photometry*”, 2nd Edition, 1983
- [114] CIE 127:2007 : “*Measurement of LEDs*”, 2nd Edition, 2007
- [115] CIE 159:2004 : “*A colour appearance model for colour management systems - CIECAM02*”, 2004
- [116] CIE 177:2007: “*Colour rendering white LED light sources*”, 2007
- [117] BODROGI, P.: “*Colour Rendering: Past, Present (2004), and Future*”, CIE Expert Symposium on LED Lighting Sources: Physical Measurement and Visual and Photobiological Assessment TOKYO, 2004
- [118] BODROGI, P.: “*Why does the CIE Colour Rendering Index Fail For White RGB Light Source*”, CIE Expert Symposium on LED Lighting Sources: Physical Measurement and Visual and Photobiological Assessment, TOKYO, 2004
- [119] LI, C.; LUO, R.; LI, C.: “*Assessing Colour Rendering Properties of Daylight Sources Part II: A New Colour Rendering Index: CRI-CAM02 UCS*”, 2009
- [120] QUINTERO, J. M.; SUDRIÀ, A.; HUNT, C.E.; CARRERAS, J.: “*Color rendering Map: a graphical metric for assessment of illumination*”, Vo.20, No.5, OPTICS EXPRESS 4939, 2012
- [121] KITAI, A.: “*Luminescent Materials and Application*”, John Wiley & Son, 2008, pp. 1-P18
- [122] ROSENCHER, E.; VINTER, B.: “*Optoelectronics*”, Cambridge University Press, 2002, pp. 1- P28
- [123] BLASSE, G.; GRABMAIER, B.C.: “*Luminescent Materials*”, Springer, 1994, pp. 1-31
- [124] TAKAHASHI, K.; YOSHIKAWA, A.; SANDHU, A.: “*Wide Band - gap Semiconductor - Fundamental Properties and Modern Photonic and Electronic Devices*, Springer-Verlag Berlin Heidelberg, 2007, pp. 97-179
- [125] NAKAMURA, S.; CHICHIBU, S. F: “*Introduction to nitride semiconductor blue lasers and light emitting diodes*”, CRC Press, 1999, pp. 1-25
- [126] BACHMANN, V. B.: “*Studies on Luminescence and Quenching Mechanisms in Phosphor for Light Emitting Diode*”, Doctor Thesis supported by PHILIPS TECHNOLOGIE GMBH, FORSCHUNGLABORATORIEN, AACHEN, GERMANY, 12.9.2007, pp. 87-116
- [127] VINH, T. Q.; KHANH, T. Q.: “*Gefährliche Mischung - Wirkung von Strom und Temperatur auf die LED-Lebensdauer*“, Zeitschrift Licht, Heft 11-12, 2011, pp. 76-80
- [128] VINH, T. Q.; KHANH, T. Q.: “*Kennzeichnung der Strom- und Temperaturverhalten von Hochleistungs - LED*“, Lange - Handbuch für Beleuchtung - 59.Erg.-Lfg.03/13, 2013, I - 6.13.13, pp. 1-6
- [129] VINH, T. Q.; GROH, A.; HAFERKEMPER, N.; KHANH, T. Q.: “*Präzise Bestimmung der thermischen und elektrischen Daten verschiedener Hochleistung - LED - Typen mit verschiedenen Leiterplatten- und Kühlungssystem*“, Licht Tagung - Berlin, 2012, pp. 288-294

- [130] LUO, C. L.; LIN, D. Y.: “Automatic Measurement System for Junction Temperature of Light Emitting Diode”, IEEE, 2010, pp. 276-279
- [131] HUANG, B. J.; TANG, C. W.; WU, M. S.: “System dynamics model of high power LED luminaire”, new energy center, Taiwan, Applied Thermal Engineering, 2008
- [132] BOCHE, H.; MÖNICH, U.: “Recent advances in Shannon Sampling Theory - Fundamental Limits for Digital Signal Processing”, Lecture, Information Theory Winter School, 2009
- [133] WING, O.: “Classical Circuit Theory”, Springer, Columbia University, New York, , 2008, P. 105 - 108
- [134] SZÉKELY, V.; RENCZ, M.: “Thermal dynamics and the time constant Domain”, IEEE, Vol. 23, No.3, 2000, pp. 587-594
- [135] RENCZ, M.; SZÉKELY, V.: “Structure function evaluation of stacked dies“, IEEE, 20th SEMI-THERM Symposium, 2004
- [136] FARKAS, G.; VADER, Q. V. V.; POPPE, A.; BOGNÁR, G.: “Thermal investigation of high power optical devices by transient testing”, 9th Thermionic workshop, 2003, pp.213-218
- [137] SOFIA, J. W.: “Analysis of thermal transient data with synthesized dynamic models for semiconductor devices”, IEEE, 1999, pp. 117-124
- [138] LUO, X.; XIONG, W.; LIU, S.: “A Simplified Thermal Resistance Network Model for High Power LED Street Lamp”, IEEE, 2008
- [139] OHNO, Y.: “Color Rendering and Luminous Efficacy of White LED Spectra”, Proceedings of SPIE, Vo.5530, 2004, pp. 88-98
- [140] NARENDRAN, N.; GU, Y.; HOSSEINZADEH, R.: “Estimating junction temperature of high-flux white LEDs”, Proceedings of SPIE, 5366, 2004, pp.158-160
- [141] POPPE, A.; FARKAS, G.; SZÉKELY, V.; HORVÁTH, G.; RENCZ, M.: “Multi-domain simulation and measurement of power LED-s and power LED assemblies”, IEEE, 2005
- [142] POPPE, A.: “On the standardization of thermal characterization of LEDs”, LED thermal management conference, Luger Research and LED-professional, 2009, pp.22-29
- [143] SCHEEPERS, G.; VISSER, JA: “Detailed Thermal Modeling of High Powered LEDs”, IEEE, 2009, pp. 87-91
- [144] SANJEEV; CHAKRABARTI, P.: “Generic Model of SH - LED for Mid - infrared (2 - 5 μ m) Applications”, IEEE, 2008, pp.453-456
- [145] KUO, S. L.; LIU, C. K.; DAI, M. J.; YU, C. K.; CHIEN, H. C.; HSU, C. Y.: “Characteristics of Thermal Resistance for High Power LEDs”, IEEE, 2008, pp. 149-154
- [146] THORSETH, A.: “Characterization, Modeling, and Optimization of Lighting - Emitting Diode Systems”, Dissertation, Faculty of Science, University of Copenhagen, 2011, pp. 61-77
- [147] LUI, S.; LUO, X.: “LED Packing for Lighting Applications - Designing, Manufacturing and Testing”, John Willey & Son, 2011, pp. 149-164
- [148] BRÜCKNER, S.; VINH, T. Q.; KHANH, T. Q.: “Double-binned LEDs reduce inhomogeneity in rear lamps?”, in 9th International Symposium on Automotive Lighting - ISAL, 2011, pp. 154-163 (1088)
- [149] BRÜCKNER, S.; VINH, T. Q.; KHANH, T. Q.: “Dimming von Hochleistung - LED”, ET Licht, 2012, pp. 20-25
- [150] BRÜCKNER, S.; VINH, T. Q.; KHANH, T. Q.: “Binning - Strategie bei LED”, ET Licht, 2012, pp. 10-15

-
- [151] BRÜCKNER, S.; VINH, T. Q.: *“Binning von Hochleistung-LED”*, Licht, Vol.2011, pp. 44-49
- [152] BRÜCKNER, S.; VINH, T. Q.: *“Binning von Hochleistung-LEDs - Grundlagen, Defizite und Lösungen”*, presented at the VDI - Conference *“Innovative Beleuchtung mit LED”*, Düsseldorf, 2011
- [153] KHANH, T. Q.; BODROGI, P.; VINH, T. Q.: *“Weiße Leuchtstoff-basierte Hochleistungs-LEDs”*, Deutsche Lichttechnische Gesellschaft e.V. (LiTG), presented at Licht und Gesundheit Berlin, LiTG, 15.03 -16.03.2012, pp. 51-59
- [154] KRAUSE, N.; BODROGI, P.; KHANH, T. Q.: *“Bewertung der Farbwiedergabe - Reflexionsspektren von Objekten unter verschieden weißen Lichtquellen“*, Zeitschrift Licht, Heft 5, 2012, pp. 62-69
- [155] PEPLER, W.; KHANH, T. Q.: *“Museumsbeleuchtung - Lichtquellen, Reflexionsspektren, optische Objektschädigung, Teil 1“*, Zeitschrift Licht, Heft 1 - 2, 2013, pp. 70-77
- [156] VINH, T. Q.; BRÜCKNER, S.; KHANH, T. Q.: *“Farb- und lichttechnisches Verhalten von Hochleistungs-LEDs bei Strom- und Temperaturänderung - Auswirkungen auf LED-Binning-Prozesse“*, Lange - Handbuch für Beleuchtung - 56.Erg.-Lfg.06/12, 2012, I - 6.13.11, pp. 1-11

Appendix A - Calculation of CIE Color Rendering Index

Color Rendering Index 1974/1995 ([110], [111])

$\varphi(\lambda) = S(\lambda)\rho(\lambda) \quad (A.1)$ <p>- $S(\lambda)$ is the spectrum of a light source - $\rho(\lambda)$ is the remission factor of a surface</p>	$c = \frac{1}{v}(4 - u - 10v) \quad (A.11)$
$X = k \int_{380}^{780} \varphi(\lambda)\bar{x}(\lambda)d\lambda \quad (A.2)$	$d = \frac{1}{v}(1.078v + 0.404 - 1.481u) \quad (A.12)$
$Y = k \int_{380}^{780} \varphi(\lambda)\bar{y}(\lambda)d\lambda \quad (A.3)$	$u'_{k,i} = \frac{10.872 + 0.404 \frac{c_r}{c_k} c_{k,i} - 4 \frac{d_r}{d_k} d_{k,i}}{16.518 + 1.481 \frac{c_r}{c_k} c_{k,i} - \frac{d_r}{d_k} d_{k,i}} \quad (A.13)$
$z = k \int_{380}^{780} \varphi(\lambda)\bar{z}(\lambda)d\lambda \quad (A.4)$	$v'_{k,i} = \frac{5.520}{16.518 + 1.481 \frac{c_r}{c_k} c_{k,i} - \frac{d_r}{d_k} d_{k,i}} \quad (A.14)$
$k = \frac{100}{\int S(\lambda)\bar{y}(\lambda)d\lambda} \quad (A.5)$ <p>- $\bar{x}(\lambda), \bar{y}(\lambda), \bar{z}(\lambda)$ are the CIE standard curves</p>	<p>- $u'_{k,i}, v'_{k,i}$ - the chromaticity of test color i - u_r, v_r - the chromaticity of reference</p>
$x = \frac{X}{X+Y+Z} \quad (A.6)$	$W^*_{r,i} = 25^3 \sqrt{Y_{r,i}} - 17 \quad (A.15)$
$y = \frac{Y}{X+Y+Z} \quad (A.7)$	$U^*_{r,i} = 13W^*_{r,i}(u_{r,i} - u_r) \quad (A.16)$
$z = \frac{Z}{X+Y+Z} \quad (A.8)$	$V_{r,i} = 13W^*_{r,i}(v_{r,i} - v_r) \quad (A.17)$
$u = \frac{4X}{X+15Y+3Z} = \frac{4x}{3-2x+12y} \quad (A.9)$	$W^*_{k,i} = 25^3 \sqrt{Y_{k,i}} - 17 \quad (A.18)$
$v = \frac{6Y}{X+15Y+3Z} = \frac{6y}{3-2x+12y} \quad (A.10)$	$U^*_{k,i} = 13W^*_{k,i}(u'_{k,i} - u'_k) \quad (A.19)$
	$V_{k,i} = 13W^*_{k,i}(v'_{k,i} - v'_k) \quad (A.20)$
$\Delta E_i = \sqrt{(W^*_{r,i} - W^*_{k,i})^2 + (U^*_{r,i} - U^*_{k,i})^2 + (V^*_{r,i} - V^*_{k,i})^2} \quad (A.21)$	
$R_i = 100 - 4.6\Delta E_i \quad (A.22)$	
$R_a = \frac{1}{8} \sum_{i=1}^8 R_i \quad (A.23)$	

Appendix B - Calculation of CIECAM02

Model CIECAM02 ([110], [111], [119])

$\varphi(\lambda) = S(\lambda)\rho(\lambda) \quad (B.1)$ <ul style="list-style-type: none"> - $S(\lambda)$ is the spectrum of a light source - $\rho(\lambda)$ is the remission factor of a surface 	<ul style="list-style-type: none"> - F_L is the luminance adaptation factor
$X = k \int_{380}^{780} \varphi(\lambda) \bar{x}(\lambda) d\lambda \quad (B.2)$	$n = \frac{Y_b}{Y_w} \quad (B.12)$
$Y = k \int_{380}^{780} \varphi(\lambda) \bar{y}(\lambda) d\lambda \quad (B.3)$	<ul style="list-style-type: none"> - Y_b is the relative background luminance
$z = k \int_{380}^{780} \varphi(\lambda) \bar{z}(\lambda) d\lambda \quad (B.4)$	$N_{bb} = N_{cb} = 0.725 \cdot \sqrt[5]{\frac{1}{n}} \quad (B.13)$
$k = \frac{100}{\int S(\lambda) \bar{y}(\lambda) d\lambda} \quad (B.5)$ <ul style="list-style-type: none"> - $\bar{x}(\lambda), \bar{y}(\lambda), \bar{z}(\lambda)$ are the CIE standard curves 	$z = 1.48 + \sqrt{n} \quad (B.14)$
$\begin{pmatrix} R \\ G \\ B \end{pmatrix} = \begin{pmatrix} 0.7328 & 0.4296 & -0.1624 \\ -0.7036 & 1.6975 & 0.0061 \\ 0.0030 & 0.0136 & 0.9834 \end{pmatrix} \begin{pmatrix} X \\ Y \\ Z \end{pmatrix} \quad (B.6)$	$\begin{pmatrix} R' \\ G' \\ B' \end{pmatrix} = M_{HPE} M_{CAT02}^{-1} \begin{pmatrix} R_C \\ G_C \\ B_C \end{pmatrix} \quad (B.15)$
$D = F \left[1 - \frac{1}{3.6} e^{-\frac{(L_A+42)}{92}} \right] \quad (B.7)$ <ul style="list-style-type: none"> - D is the adaptation grade - L_A is the adaptation luminance of environment - F is the adaptation grade of background luminance 	$M_{HPE} = \begin{pmatrix} 0.38971 & 0.68898 & -0.07868 \\ -0.22981 & 1.18340 & 0.04641 \\ 0.00000 & 0.00000 & 1.00000 \end{pmatrix} \quad (B.16)$
$R_C = R \left[\frac{Y_w D}{R_w} + (1 - D) \right] \quad (B.8)$	$M_{CAT02}^{-1} = \begin{pmatrix} 1.096124 & -0.278869 & 0.182745 \\ -0.454369 & 0.473533 & 0.072098 \\ -0.009628 & -0.005698 & 1.015326 \end{pmatrix} \quad (B.17)$
$G_C = G \left[\frac{Y_w D}{G_w} + (1 - D) \right] \quad (B.9)$	$R'_a = \frac{400 \cdot \left(\frac{F_L R'_0}{100}, 42 \right)}{27.13 + \left(\frac{F_L R'_0}{100}, 42 \right)} + 0.1 \quad (B.18)$
$B_C = B \left[\frac{Y_w D}{B_w} + (1 - D) \right] \quad (B.10)$ <ul style="list-style-type: none"> - X_w, Y_w and Z_w are the standard color values of applied lighting type 	$G'_a = \frac{400 \cdot \left(\frac{F_L G'_0}{100}, 42 \right)}{27.13 + \left(\frac{F_L G'_0}{100}, 42 \right)} + 0.1 \quad (B.19)$
$F_L = 0.2 \cdot \frac{1}{5L_A+1}^4 \cdot 5L_A + 0.1 \left[1 - \frac{1}{5L_A+1}^4 \right]^2 \cdot \sqrt[3]{5L_A} \quad (B.11)$	$B'_a = \frac{400 \cdot \left(\frac{F_L B'_0}{100}, 42 \right)}{27.13 + \left(\frac{F_L B'_0}{100}, 42 \right)} + 0.1 \quad (B.20)$
	$a = R'_a - \frac{12}{11} \cdot G'_a + \frac{1}{11} \cdot B'_a \quad (B.21)$
	$b = \frac{1}{9} \cdot (R'_a + G'_a + 2B'_a) \quad (B.22)$

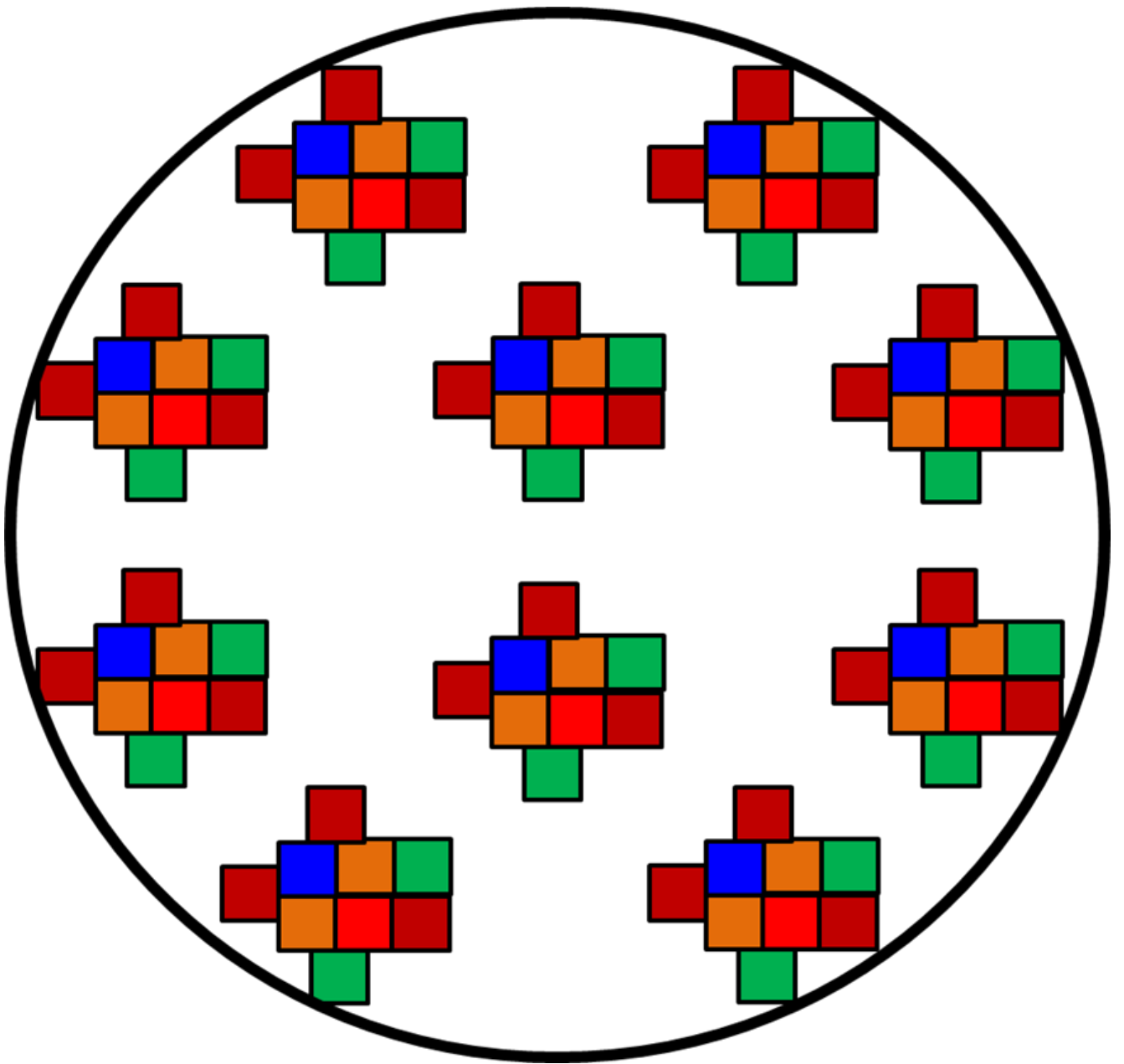
Appendix C - Name of oil color objects

Name of oil color objects ([108])

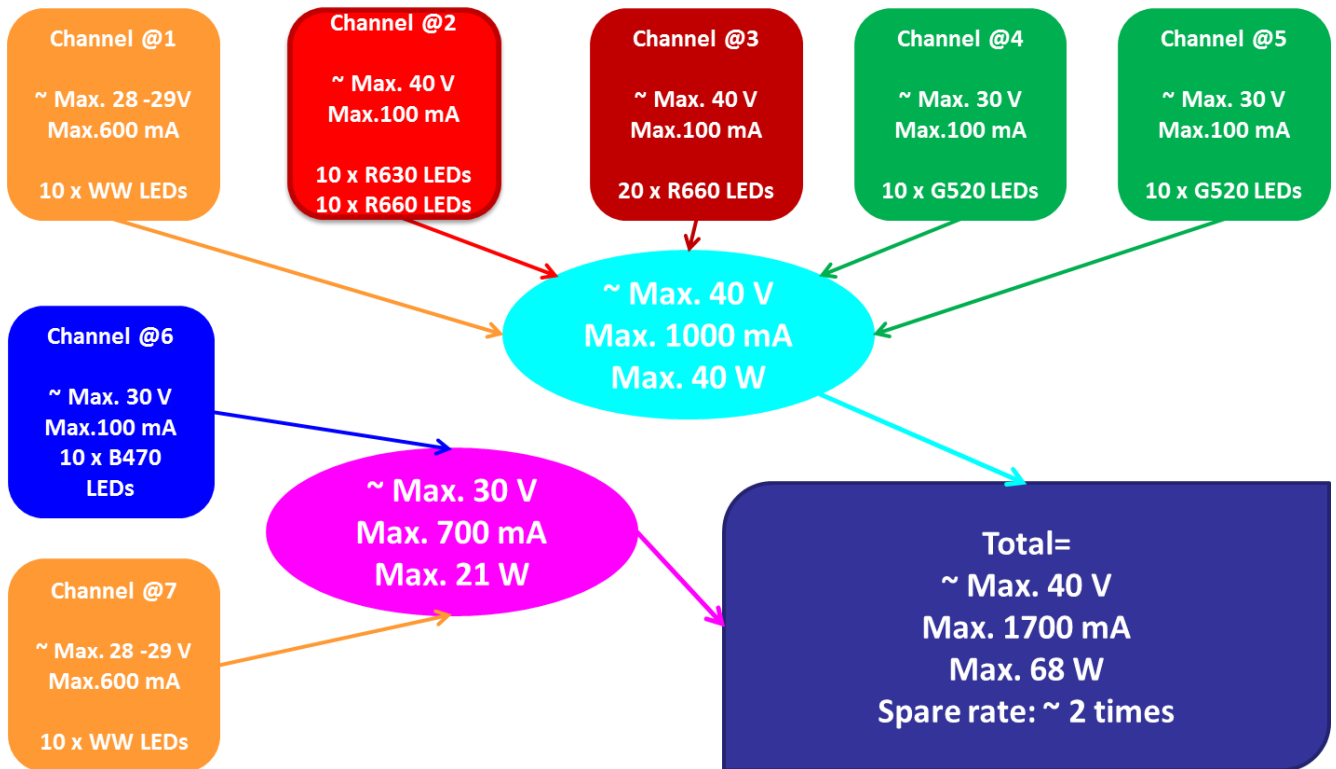
RO1	RO2	RO3	RO4	RO5	RO6	RO7	RO8	RO9
Flesh Tint	Naples Yellow Reddish	Naples Yellow Deep	Naples Yellow Light	Chrome Yellow Hue Light	Chrome Yellow Hue Middle	Chrome Yellow Hue Deep	Brilliant Yellow Light	Lemon Yellow
RO10	RO11		RO12	RO13		RO14	RO15	
Cadmium Yellow Lemon	Cadmium Yellow Mix		Cadmium Yellow Light	Cadmium Yellow Deep		Brilliant Yellow	Indian Yellow	
RO16	RO17		RO18	RO19		RO20	RO21	
Cadmium Orange	Brilliant Orange		Poppy Red	Vermilion Red Light		Vermilion Red Deep	Cadmium Red Light	
RO22	RO23		RO24	RO25	RO26		RO27	RO28
Cadmium Red Mix	Cadmium Red Deep		Madder Light	Madder Red	Madder Ruby		Madder Deep	Carmine Red
RO29	RO30	RO31	RO32	RO33	RO34	RO35	RO36	RO37
Ruby Red	Magenta	Cobalt Violet Hue	Violet Dark	Indanthrene Blue	Ultramarine Blue Deep	Ultramarine Blue Hell	Royal Blue	Cobalt Blue Deep
RO38	RO39		RO40	RO41		RO42	RO43	
Cobalt Blue Light	Cobalt Blue Hue		Cobalt Cerulean Blue	Indigo		Prussian Blue	Phthalate Blue	
RO44		RO45		RO46		RO47		RO48
Cerulean Blue		Azure Blue		Cobalt Turquoise		Phthalate Green		Chromium Oxide Green Brill
RO49		RO50		RO51		RO52		RO53
Emerald Green		Schweinfurt Green Hue		Permanent Green		Permanent Yellowish Green		Olive Green
RO55		RO56	RO57	RO58	RO59	RO60	RO61	RO62
Chromium Oxide Green		Green earth	Raw Light Ochre	Yellow Ochre	Translucent Ochre	Golden Ochre	Raw Sienna	Burnt Sienna
RO63	RO64	RO65	RO66		RO67	RO68	RO69	RO70
English Red	Red Earth	Caput Mortuum	Translucent Red Brown		Agate Brown	Raw Umber	Burnt Umber	Vandyke Brown
RO71	RO72		RO73	RO74	RO75	RO76	RO77	RO78
Neutral Black	Black Iron Oxide		Ivory Black	Pane's Gray	Warm Gray	Cold Gray	Silver	Classic Gold
								RO79
								Bronze

Appendix D - Basic design for the 3000 K hybrid LED-lamp

D1. Design for the optical homogeneity of the 3000 K hybrid LED-lamp



D2. Design for energy channels



D3. Parameters of energy channels

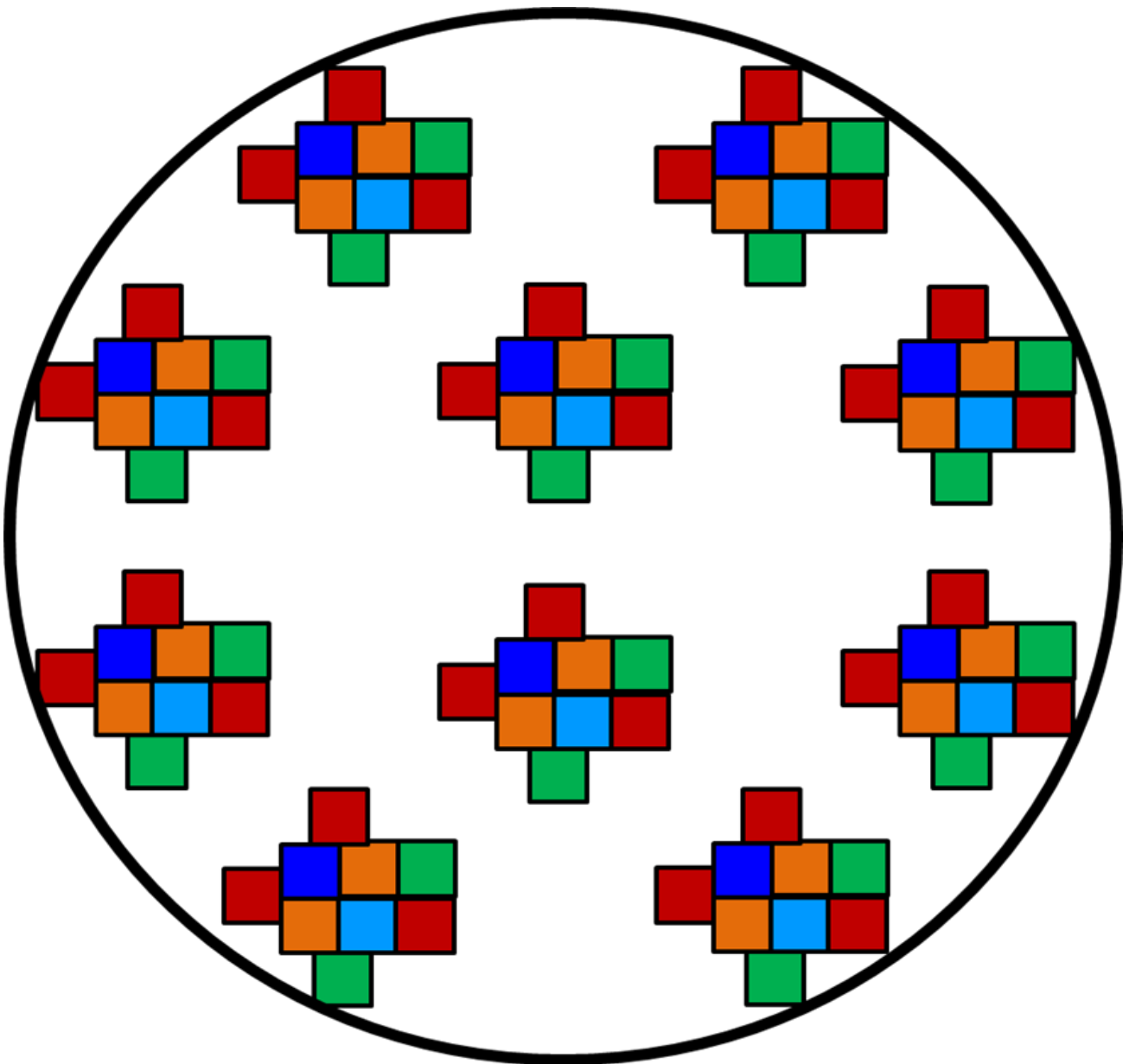
Name	V_f / V	Power / W
Chanel 1 - 10 x WW	26.887	13.444
Channel 2 - 10 x R630 + 10 x R660	34.610	2.223
Chanel 3 - 20 x R660	34.330	3.025
Channel 4 - 10 x G520	25.964	0.738
Channel 5 - 10 x G520	25.964	0.738
Chanel 6 - 10 x B470	25.239	0.277
Chanel 7 - 10 x WW	26.887	13.444
Total Power / W		33.888
Total luminous flux / lm	3098	
Luminous efficacy / lm/W	91.416	

D4. Parameters of the 3000 K hybrid LED-lamp

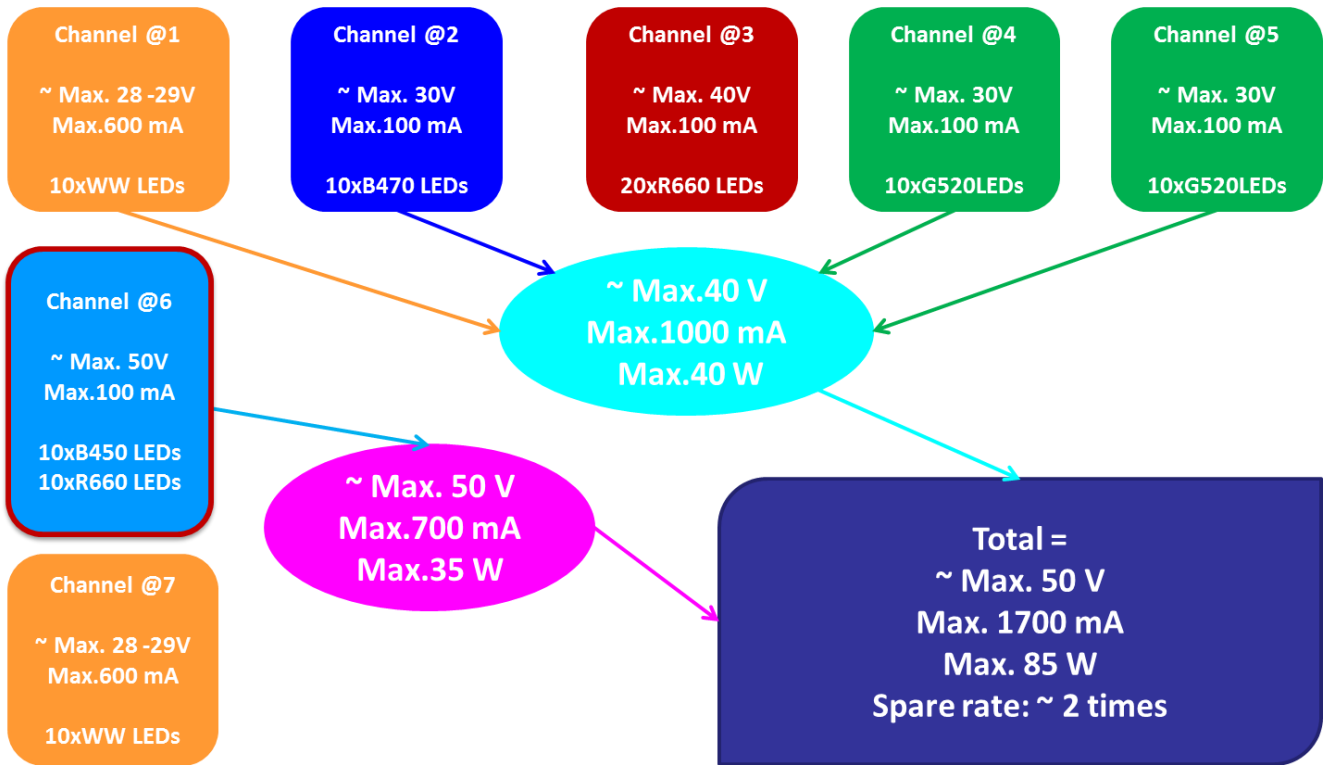
Name	DC Current	Duty cycle	Max. V_f at 25°C. 100% duty cycle	Max. V_f at 80°C. 100% duty cycle
WW. - 3000 K	500 mA	83.3 %	2.81 V ~ 3V	2.68 V
G-520	28.4 mA	28.4%	2.905 V ~ 3V	2.703 V
R-660	88.1 mA	88. 1%	1.887 V ~ 2V	1.772 V
R-630	40.7 mA	40.7%	1.918 V ~ 2V	1.84 V
B-470	10.97 mA	10.97%	2.789 V ~ 3V	2.654 V
Φ_v / Im at 80°C	3098 lm	$R_a=98$	High level for WW.	600 mA
$\eta_v / \text{lm/W}$ at 80°C	~ 90-95 lm/W	$R_g=98$	Low Level for color LEDs	100 mA

Appendix E - Basic design for the 4000 K hybrid LED-lamp

E1. Design for the optical homogeneity of the 4000 K hybrid LED-lamp



E2. Design for energy channels



E3. Parameters of energy channels

Name	V_f / V	Power / W
Chanel 1 - 10 x WW	26.887	13.444
Chanel 2 - 10 x B470	25.457	0.805
Chanel 3 - 20 x R660	33.683	2.207
Channel 4 - 10 x G520	26.260	1.673
Channel 5 -10 x G520	26.260	1.673
Channel 6 -10 x B450 + 10 x R660	42.937	2.250
Chanel 7 - 10 x WW	26.887	13.444
Total Power / W		35.496
Total luminous flux / lm	3364	
Luminous efficacy / lm/W	94.782	

E4. Parameters of the 4000 K hybrid LED-lamp

Name	DC Current	Duty cycle	Max. V_f at 25 °C. 100 % duty cycle	Max. V_f at 80 °C. 100 % duty cycle
WW. - 3000 K	500 mA	83.3 %	2.81 V ~ 3V	2.68 V
G-520	63.7 mA	63.7 %	2.905 V ~ 3V	2.703 V
R-660	65.5 mA	65.5 %	1.887 V ~ 2V	1.772 V
B-450	43.9 mA	43.9 %	2.809 V ~ 3V	2.687 V
B-470	31.63 mA	31.63 %	2.789 V ~ 3V	2.654 V
Φ_v / Im at 80 °C	3364 lm	$R_a=97$	High level for WW.	600 mA
$\eta_v / \text{lm/W}$ at 80 °C	~ 90-95 lm/W	$R_g=98$	Low Level for color LEDs	100 mA

Appendix F - Investigation for neutral white PC-LEDs

F1. Color rendering indices and luminous efficacy of 3500 K - 5000 K PC-LEDs

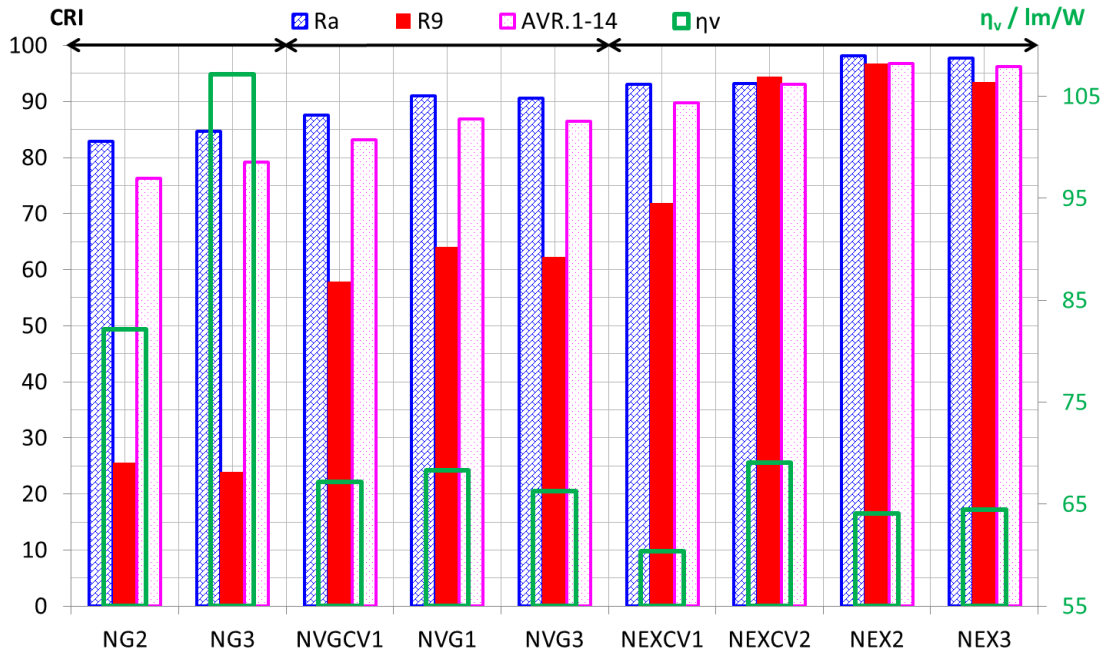


Figure F.1 - R_a , R_9 , AVR_{1-14} , and luminous efficacy some neutral white PC-LEDs at 350 mA and 80 °C

F2. Whiteness of 3500 K - 5000 K PC-LEDs

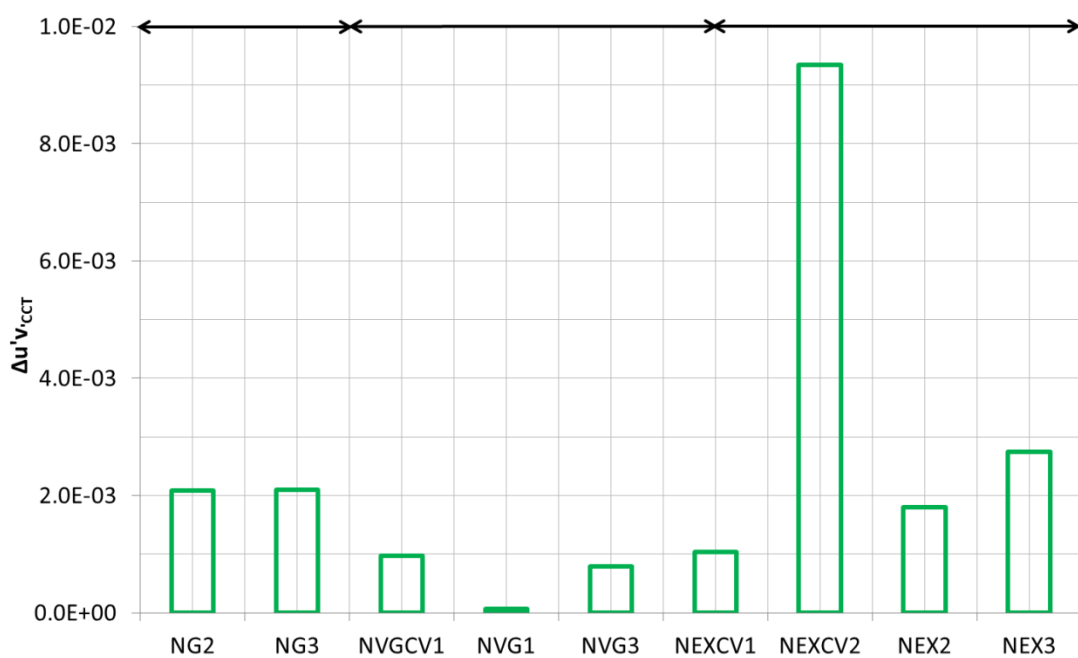


Figure F.2 - Whiteness of some neutral white PC-LEDs at 350 mA and 80 °C

F3. Temperature dependence of the spectra of 3500 K - 5000 K PC-LEDs

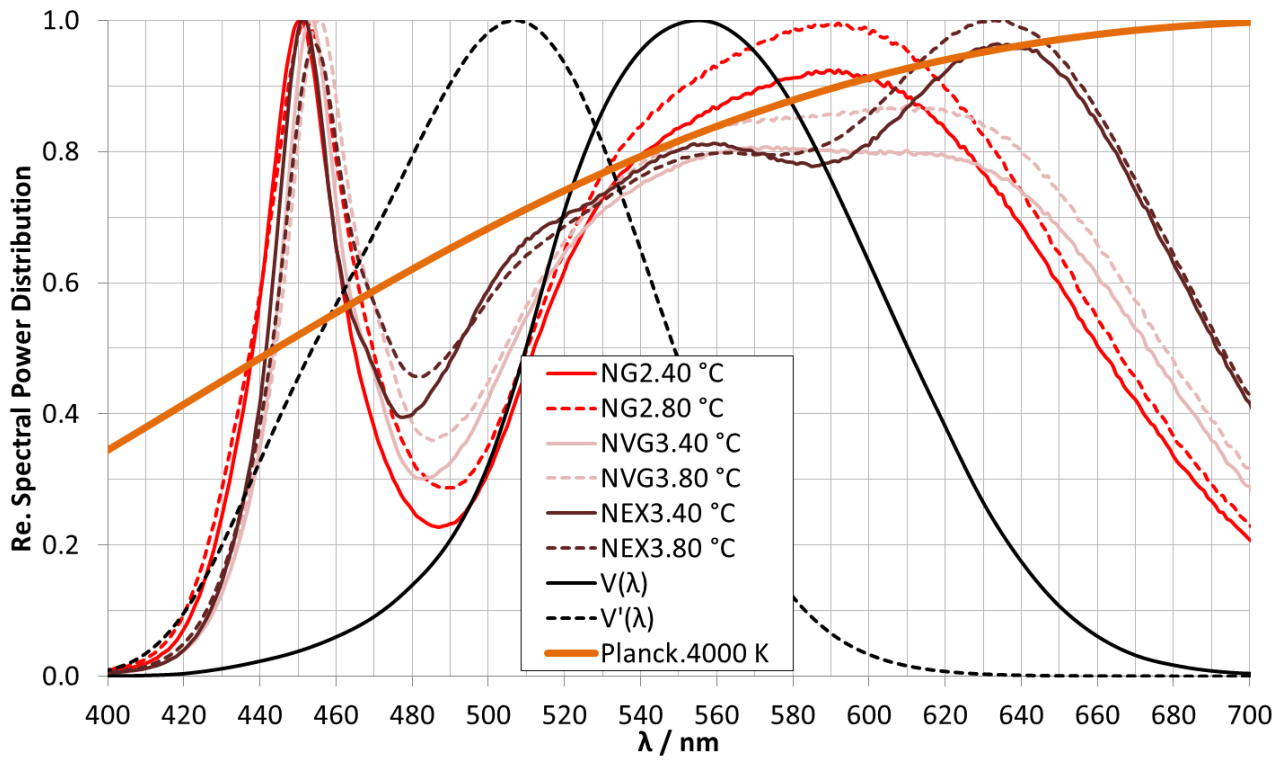


Figure F.3 - Relative spectral change of some neutral white PC-LEDs over operating temperature

F4. Current dependence of the spectra of 3500 K - 5000K PC-LEDs

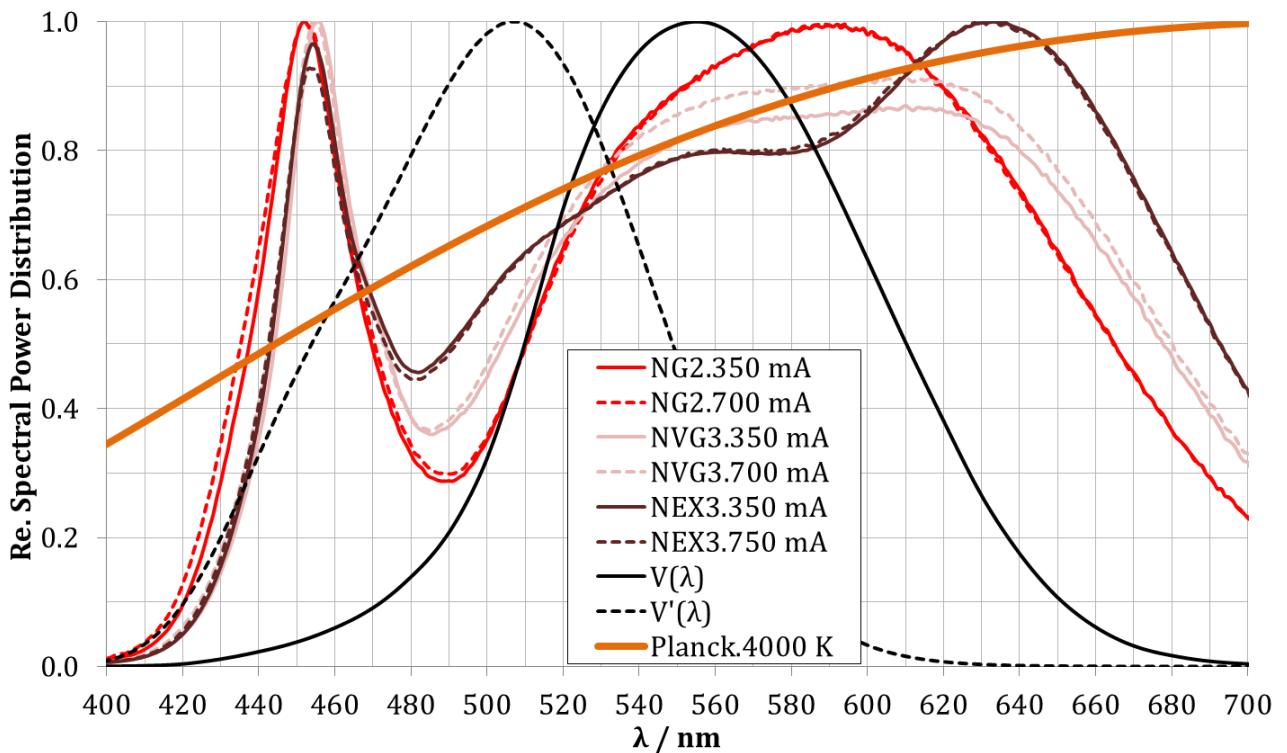


Figure F.4 - Relative spectral change of some neutral white PC-LEDs over forward current

F5. Temperature dependence of the luminous flux and luminous efficacy of 3500 K - 5000 K PC-LEDs

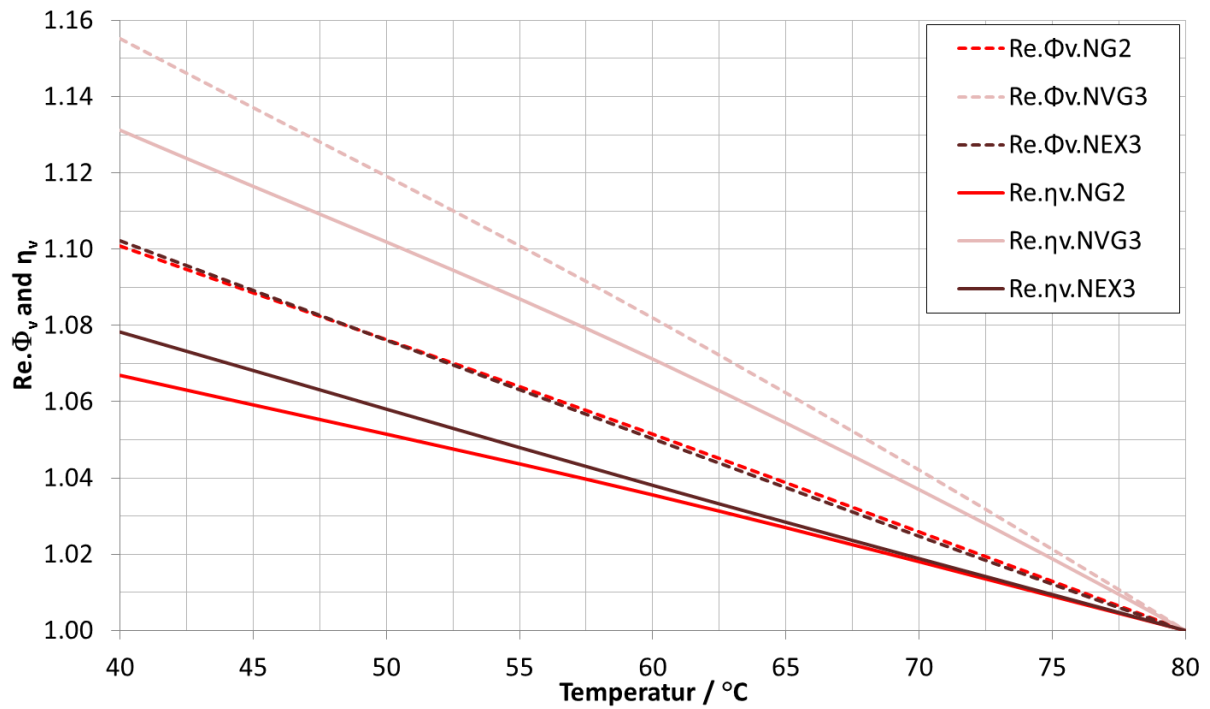


Figure F.5 - Relative Φ_v and η_v change of some neutral white PC-LEDs over operating temperature

F6. Current dependence of the luminous flux and luminous efficacy of 3500 K - 5000 K PC-LEDs

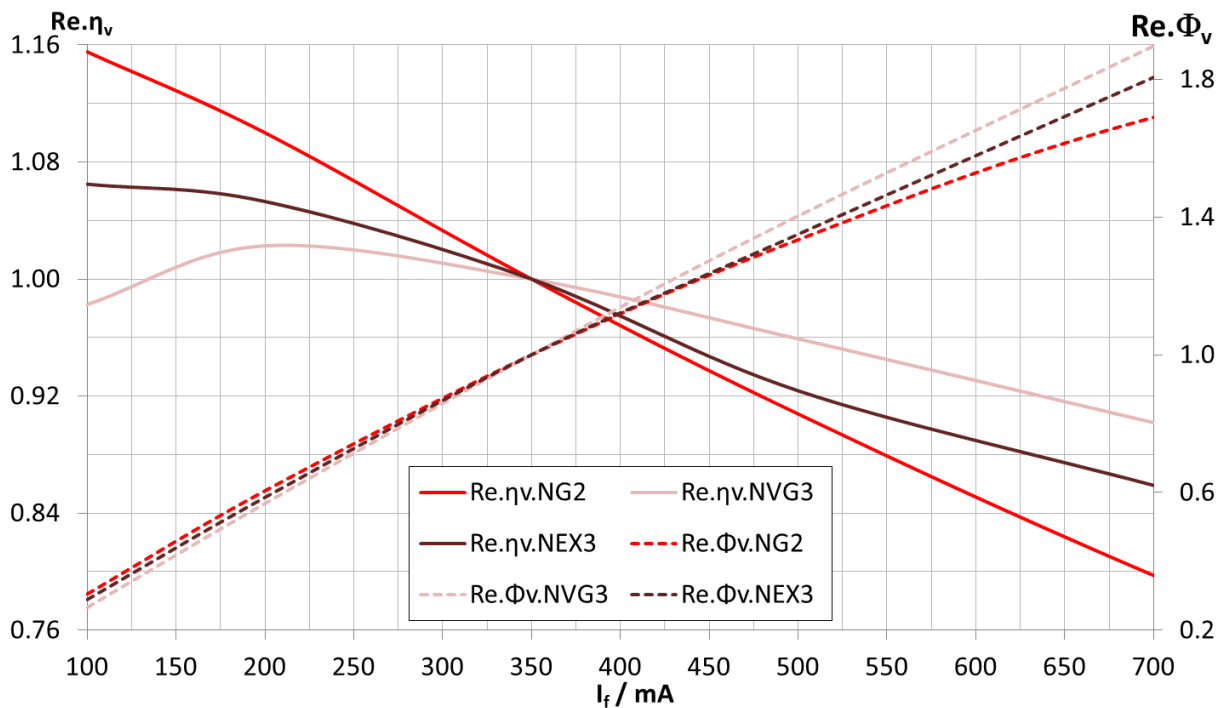


Figure F.6 - Relative Φ_v and η_v change of some neutral white PC-LEDs over forward current

F7. Temperature dependence of the color difference of 3500 K - 5000 K PC-LEDs

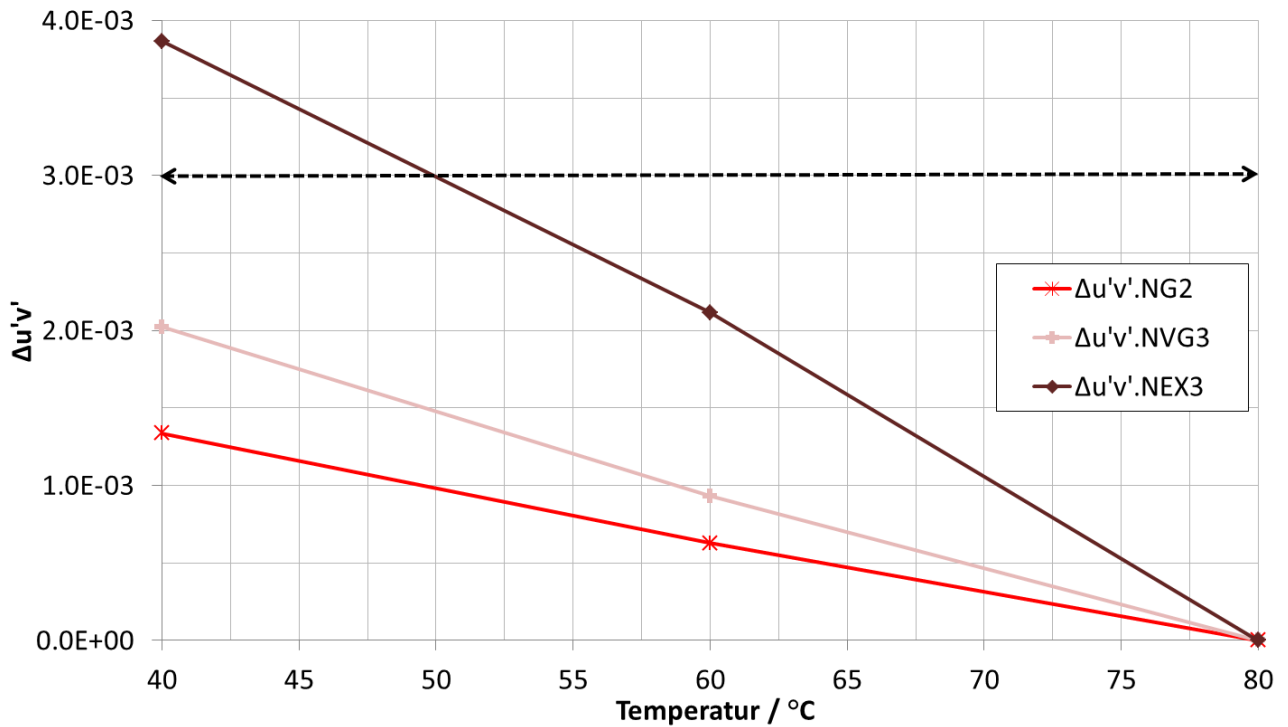


Figure F.7 - Color difference of some neutral white PC-LEDs over operating temperature

F8. Current dependence of the color difference of 3500 K - 5000 K PC-LEDs

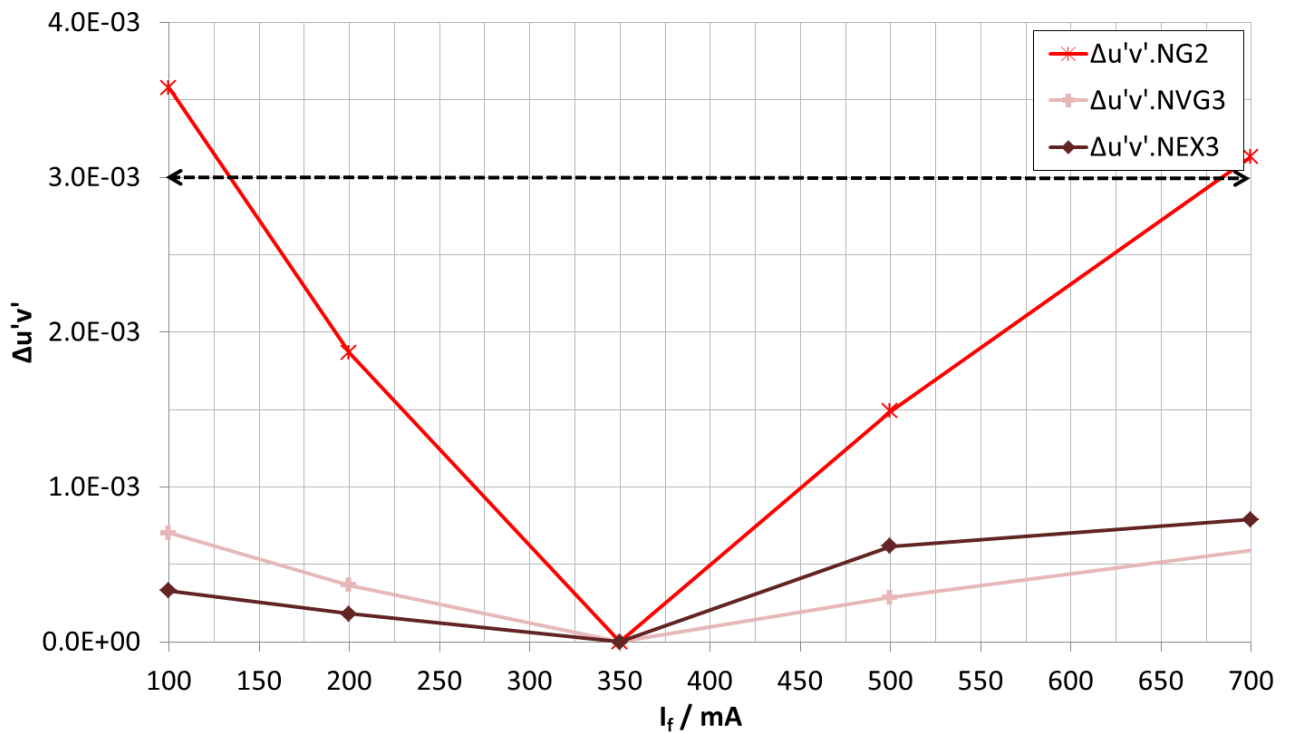


Figure F.8 - Color difference of some neutral white PC-LEDs over forward current

Appendix G - Investigation for cold white PC-LEDs

G1. Color rendering indices and luminous efficacy of 4800 K - 5500 K PC-LEDs

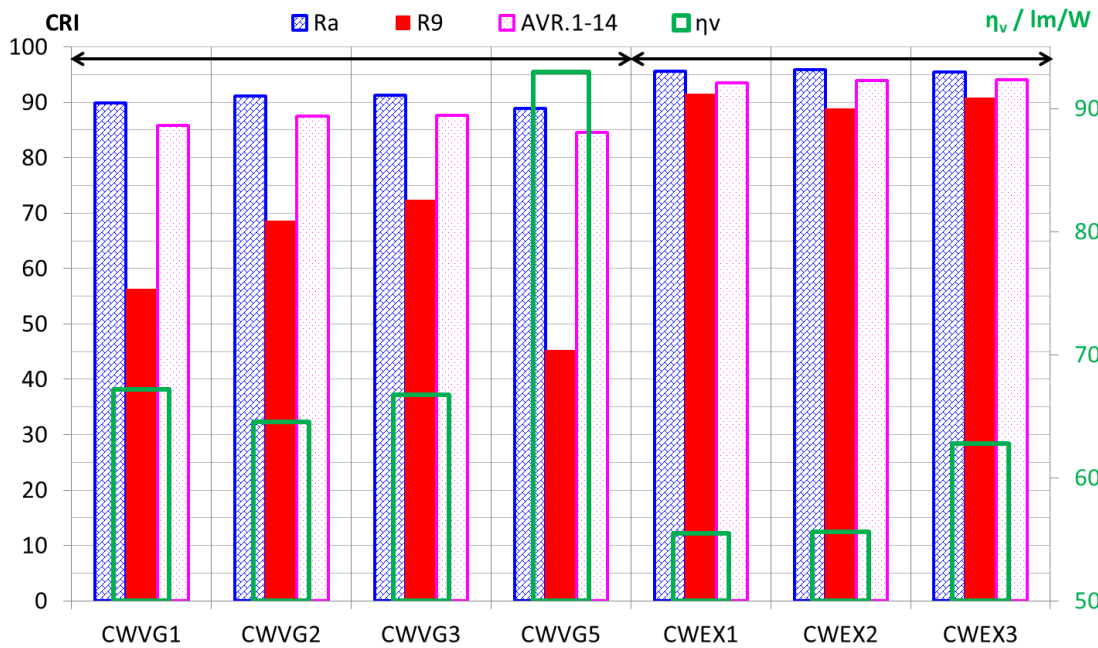


Figure G.1 - R_a , R_9 , AVR_{1-14} and luminous efficacy of some cold white PC-LEDs at 350 mA and 80 °C

G2. Whiteness of 4800 K - 5500 K PC-LEDs

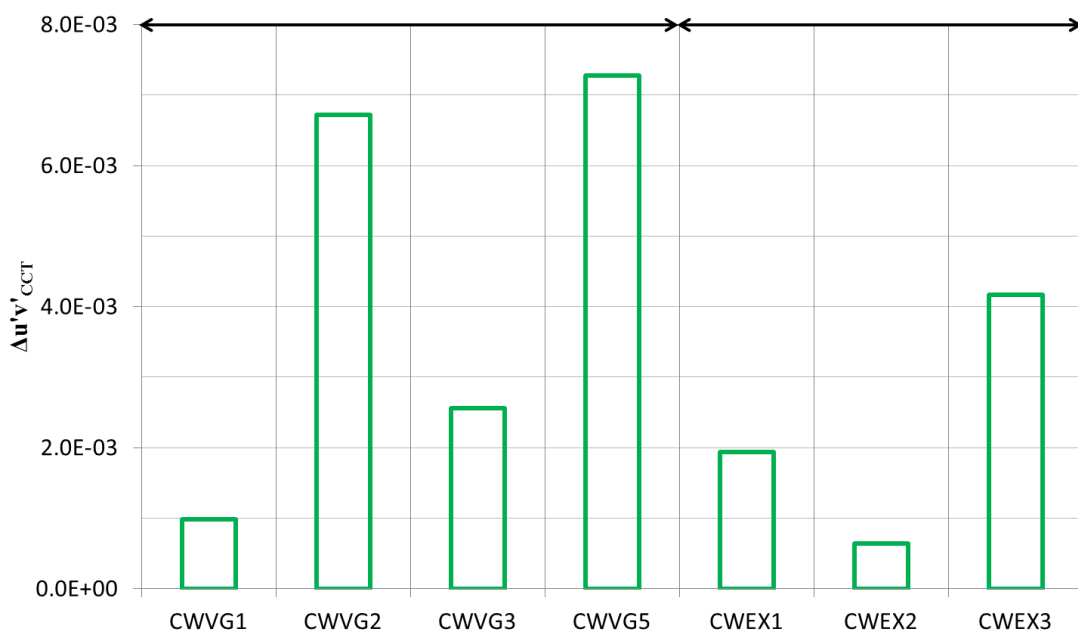


Figure G.2 - Whiteness of some cold white PC-LEDs at 350 mA and 80 °C

G3. Temperature dependence of the spectra of 4800 K - 5500 K PC-LEDs

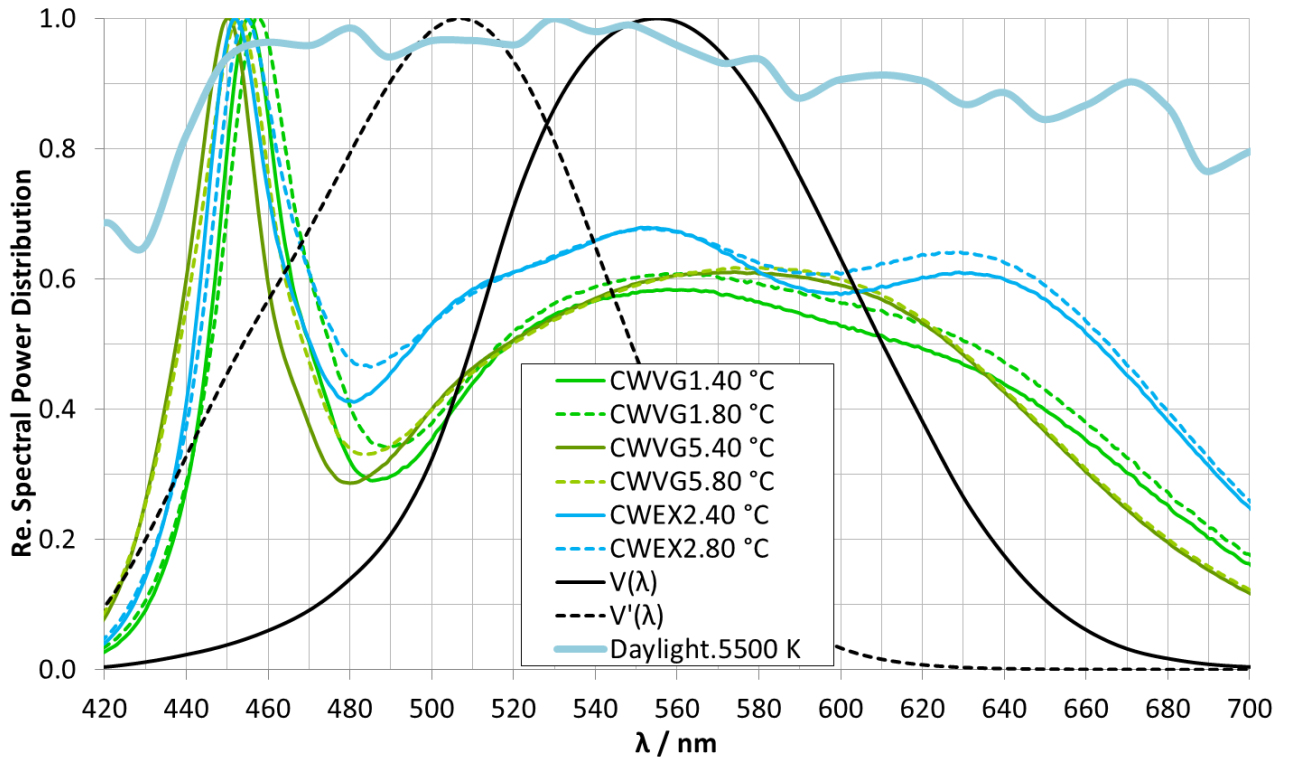


Figure G.3 - Relative spectral change of some cold white PC-LEDs over operating temperature

G4. Current dependence of the spectra of 4800 K - 5500 K PC-LEDs

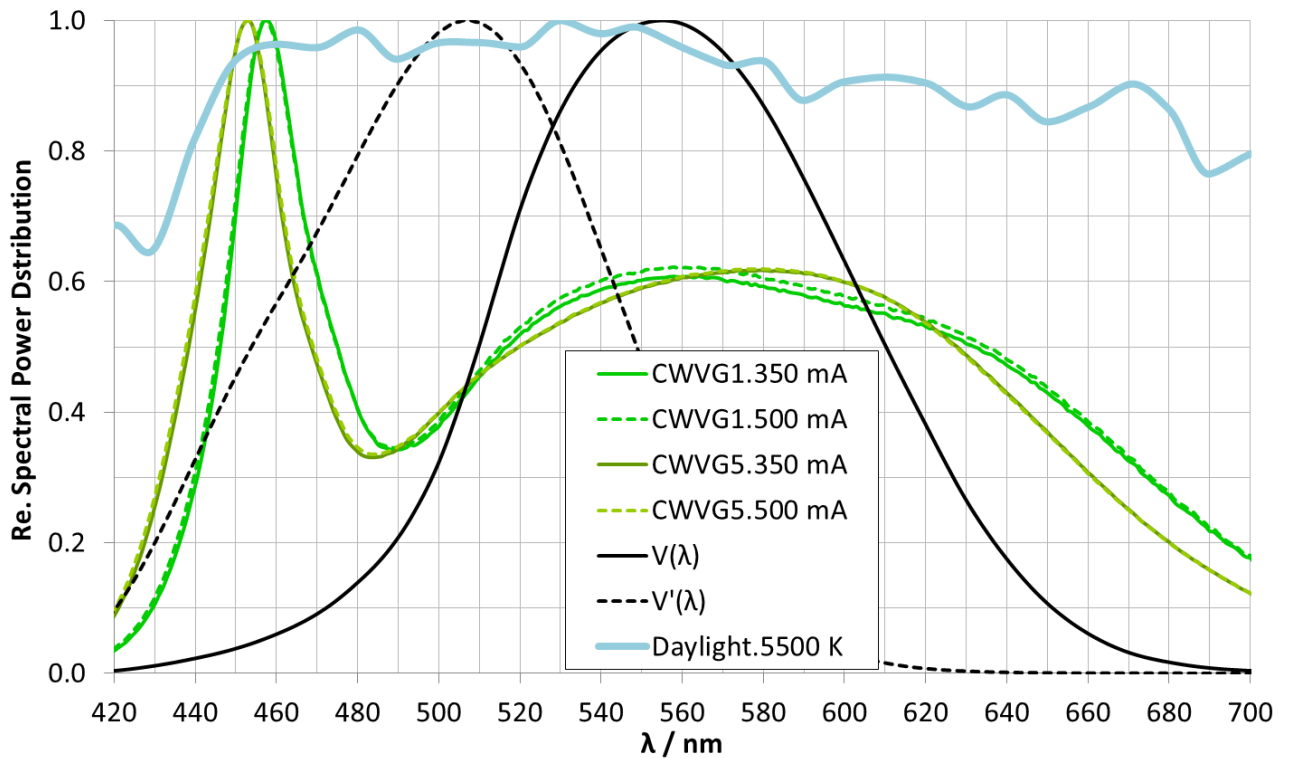


Figure G.4 - Relative spectral change of some cold white PC-LEDs over forward current

G5. Temperature dependence of the luminous flux and luminous efficacy of 4800 K - 5500 K PC-LEDs

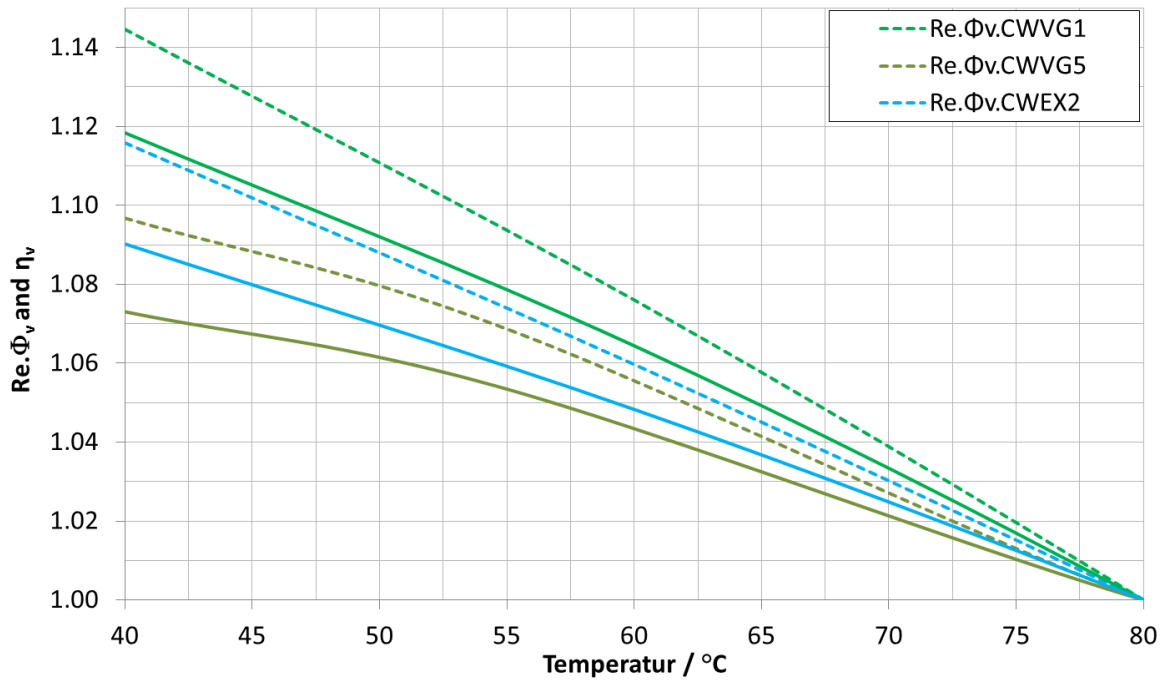


Figure G.5 - Relative Φ_v and η_v change of some cold white PC-LEDs over operating temperature

G6. Current dependence of the luminous flux and luminous efficacy of 4800 K - 5500 K PC-LEDs

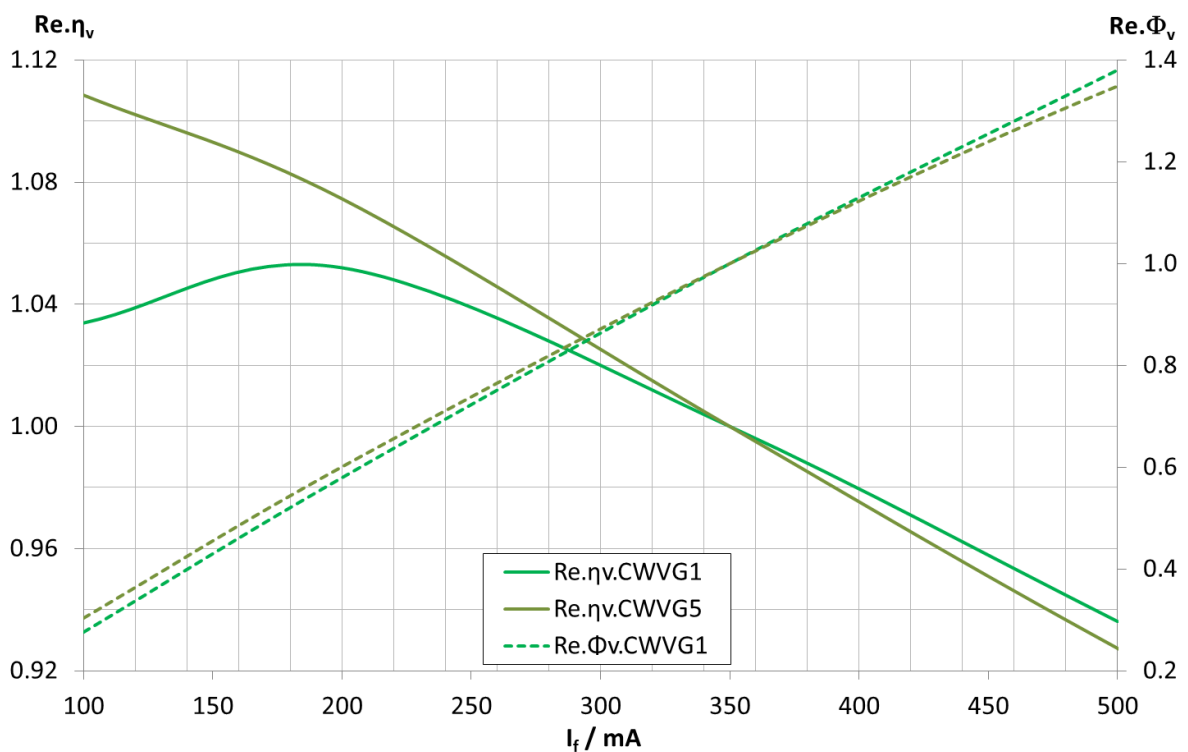


Figure G.6 - Relative Φ_v and η_v change of some cold white PC-LEDs over forward current

G7. Temperature dependence of the color difference of 4800 K - 5500 K PC-LEDs

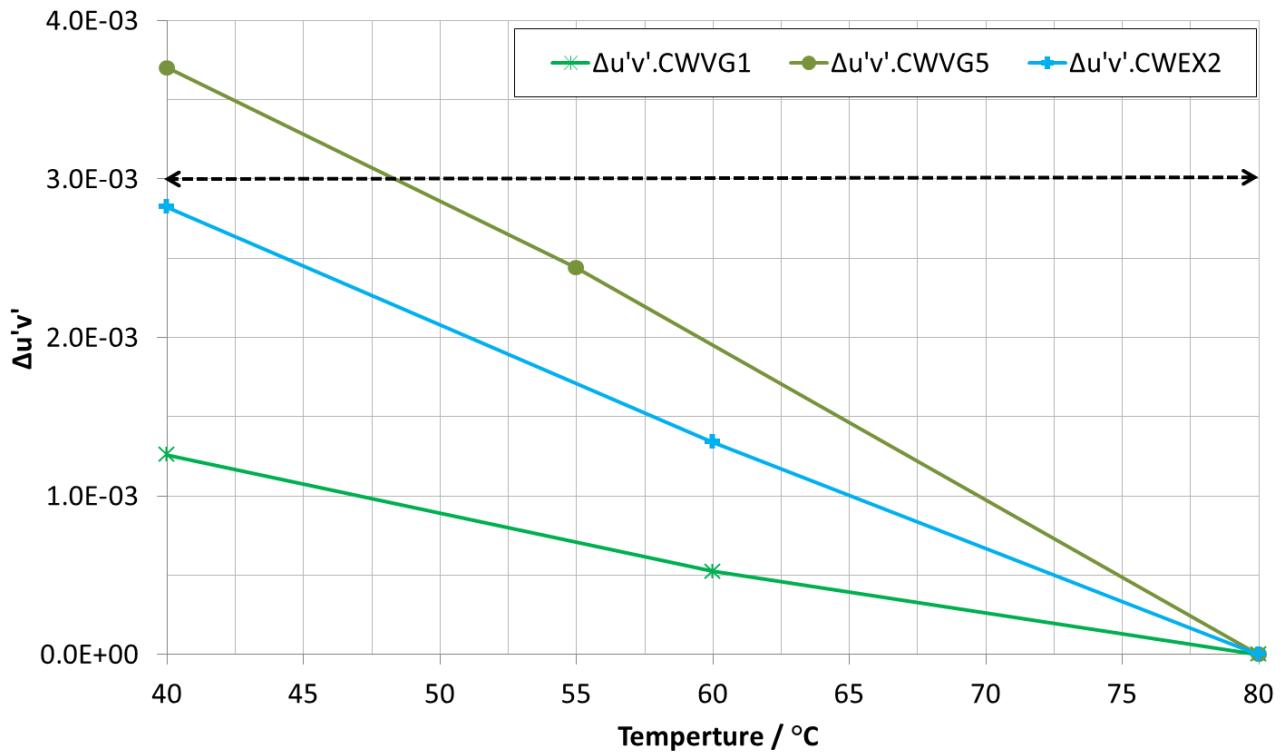


Figure G.7 - Color difference of some cold white PC-LEDs over operating temperature

G8. Current dependence of the color difference of 4800 K - 5500K PC-LEDs

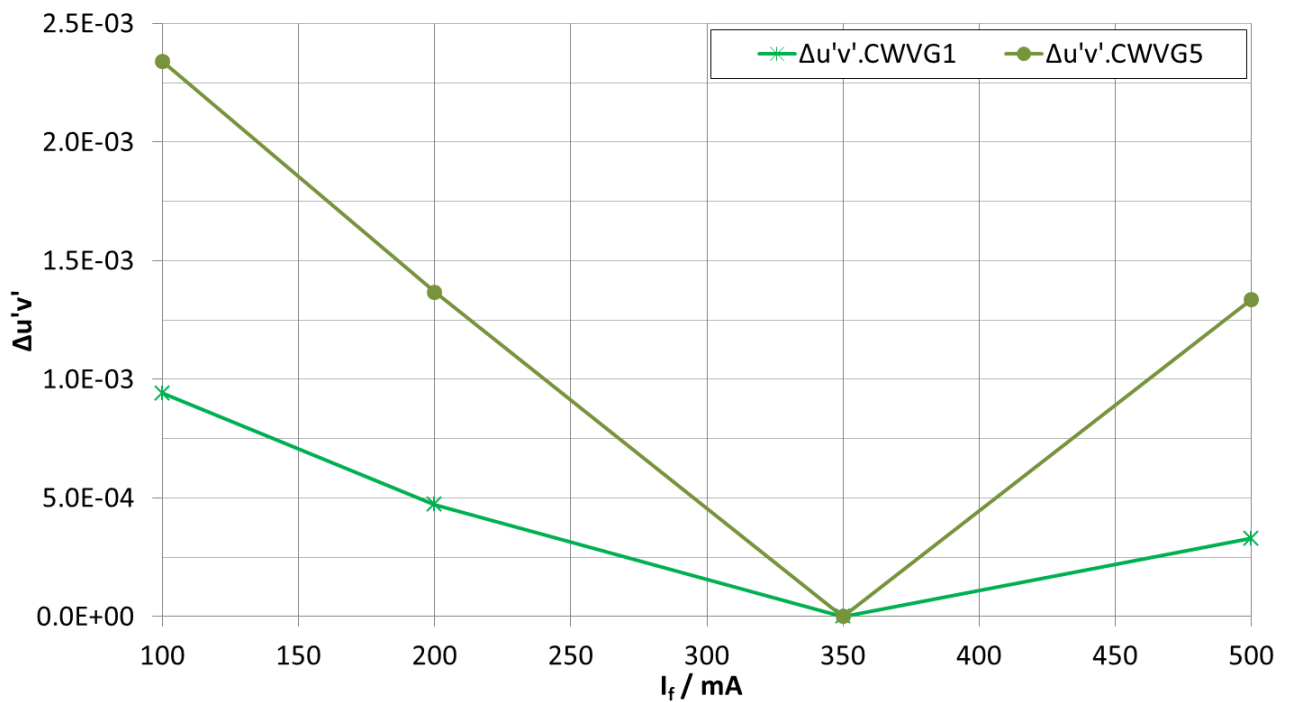


Figure G.8 - Color difference of some cold white PC-LEDs over forward current

Appendix H - Data for the comparison between the cooling and heating procedure

H1. The results of the DC and transient measurement of the cooling procedure

$T_{si} / ^\circ\text{C}$	$V_{f\text{-cooling-beginning}} / \text{V}$	$V_{f\text{-cooling-end}} / \text{V}$	α_0 at 1 mA	$\Delta T / \text{K}$	$T_{j\text{-cool}} / ^\circ\text{C}$	I_{fi} / mA
15	2.556	2.589	-0.0023	14.3	29.3	200
30	2.529	2.560		13.5	43.5	
50	2.486	2.517		13.5	63.5	
70	2.437	2.468		13.5	83.5	
90	2.385	2.417		13.9	103.9	
15	2.575	2.616	-0.0022	18.6	33.6	350
30	2.545	2.587		19.1	49.1	
50	2.503	2.548		20.5	70.5	
70	2.458	2.503		20.5	90.5	
90	2.406	2.452		20.9	110.9	
15	2.560	2.677	-0.021	55.7	70.7	1000
30	2.530	2.645		54.8	84.8	
50	2.489	2.603		54.3	104.3	
70	2.436	2.551		54.8	124.8	
90	2.382	2.517		64.3	154.3	

H2. The direct comparison of the junction temperatures with the same scale and operating area

$T_{si} / ^\circ\text{C}$	$P_{el-i} / ^\circ\text{W}$	$P_{opt-i} / ^\circ\text{W}$	$V_{fi} / ^\circ\text{V}$	$T_{j-heat-i} / ^\circ\text{C}$	$T_{j-cool-i} / ^\circ\text{C}$	$\Delta T_j / ^\circ\text{K}$	$I_{fi} / ^\circ\text{mA}$
15	0.650	0.199	3.251	48.4	29.3	19.1	200
30	0.640	0.194	3.198	66.7	43.5	23.2	
50	0.629	0.187	3.143	85.8	63.5	22.3	
70	0.619	0.180	3.092	103.3	83.5	19.8	
90	0.609	0.171	3.044	119.8	103.9	15.9	
15	1.185	0.326	3.386	54.5	33.6	20.9	350
30	1.166	0.318	3.332	70.8	49.1	21.7	
50	1.147	0.307	3.278	87.3	70.5	16.8	
70	1.130	0.296	3.229	102.0	90.5	11.5	
90	1.114	0.280	3.184	115.6	110.9	4.7	
15	3.741	0.758	3.741	83.4	70.7	12.7	1000
30	3.700	0.739	3.700	94.6	84.8	9.8	
50	3.654	0.709	3.654	106.9	104.3	2.6	
70	3.615	0.673	3.615	117.6	124.8	-7.2	
90	3.580	0.634	3.580	127.0	154.3	-27.3	

H3. The indirect comparison of the properties $V_f(T_S)$ of the cooling model, the heating model and the measured values of ten blue semiconductor LEDs belonging to the same binning group

$T_{si} / ^\circ\text{C}$	$V_f / ^\circ\text{V}$ (Minimal measured value)	$V_f / ^\circ\text{V}$ (Average measured value)	$V_f / ^\circ\text{V}$ (Maximal measured value)	$V_f / ^\circ\text{V}$ (The heating model)	$\Delta V_{f1} / \%$ (*)	$V_f / ^\circ\text{V}$ (The cooling model)	$\Delta V_{f2} / \%$ (*)	I_{fi} / mA
15	3.218	3.248	3.283	3.246	0.062	3.234	0.431	200
30	3.168	3.195	3.227	3.205	-0.313	3.185	0.313	
50	3.112	3.140	3.172	3.147	-0.223	3.126	0.446	
70	3.060	3.089	3.123	3.084	0.162	3.074	0.486	
90	3.011	3.041	3.077	3.016	0.822	3.027	0.460	
15	3.346	3.380	3.420	3.382	-0.059	3.368	0.355	350
30	3.295	3.327	3.364	3.341	-0.421	3.321	0.180	
50	3.241	3.273	3.311	3.282	-0.275	3.264	0.275	
70	3.191	3.225	3.264	3.218	0.217	3.213	0.372	
90	3.144	3.180	3.222	3.148	1.006	3.168	0.377	
15	3.687	3.732	3.783	3.765	-0.884	3.725	0.188	1000
30	3.647	3.691	3.741	3.719	-0.759	3.687	0.108	
50	3.600	3.646	3.698	3.654	-0.219	3.642	0.110	
70	3.559	3.606	3.662	3.584	0.610	3.603	0.083	
90	3.523	3.572	3.632	3.508	1.792	3.57	0.056	

(*). Symbols ΔV_{f1} and ΔV_{f2} denotes the relative voltage offsets between the average measured voltage and the forward voltage of the heating model and the cooling model, respectively.

Veröffentlichungen

Eigene Veröffentlichungen

- [1] VINH, T. Q.; BRÜCKNER, S.; KHANH, T. Q.: *“LEDs-Verhaltens unter Strom- und Temperaturänderung“*, Zeitschrift Licht, Pflaum Verlag (München), Heft 6, 2011, pp. 70-76
- [2] BRÜCKNER, S.; VINH, T. Q.: *“Binning von Hochleistung-LEDs - Grundlagen, Defizite und Lösungen“*, presented at the VDI - Conference *“Innovative Beleuchtung mit LED“*, Düsseldorf, 2011
- [3] VINH, T. Q.; BRÜCKNER, S.; KHANH, T. Q.: *“Accurate measurement of the pn-junction Temperature of HP-LEDs”*, in 9th International Symposium on Automotive Lighting - ISAL, 2011, pp. 809-827 (1088)
- [4] VINH, T. Q.; KHANH, T. Q.: *“Gefährliche Mischung - Wirkung von Strom und Temperatur auf die LED-Lebensdauer“*, Zeitschrift Licht, Heft 11-12, 2011, pp. 76-80
- [5] BRÜCKNER, S.; VINH, T. Q.; KHANH, T. Q.: *“Double-binned LEDs reduce inhomogeneity in rear lamps?”*, in 9th International Symposium on Automotive Lighting - ISAL, 2011, pp. 154-163 (1088)
- [6] BRÜCKNER, S.; VINH, T. Q.; KHANH, T. Q.: *“Dimming von Hochleistung - LED”*, ET Licht, 2012, pp. 20-25
- [7] BRÜCKNER, S.; VINH, T. Q.; KHANH, T. Q.: *“Binning - Strategie bei LED”*, ET Licht, 2012, pp. 10-15
- [8] BRÜCKNER, S.; VINH, T. Q.: *“Binning von Hochleistung-LED”*, Licht, Vol.2011, pp. 44-49
- [9] BODROGI, P.; KHANH, T. Q.; VINH, T. Q.: *“Weiße Hochleistungs-LEDs: Eine umfassende lichttechnische Betrachtung“*, Zeitschrift Licht, Heft 6, 2012, pp. 64-70
- [10] KHANH, T. Q.; BODROGI, P.; VINH, T. Q.: *“Weiße leuchtstoff-basierte Hochleistungs-LEDs“*, Deutsche Lichttechnische Gesellschaft e.V. (LiTG), presented at the conference *“Licht und Gesundheit“*, Berlin, 15.03 - 16.03.2012, pp. 51-59
- [11] VINH, T. Q.; BRÜCKNER, S.; KHANH, T. Q.: *“Farb- und lichttechnisches Verhalten von Hochleistungs-LEDs bei Strom- und Temperaturänderung - Auswirkungen auf LED-Binning-Prozesse“*, Lange - Handbuch für Beleuchtung - 56.Erg.-Lfg.06/12, 2012, I - 6.13.11, pp. 1-11
- [12] VINH, T. Q.; GROH, A.; HAFERKEMPER, N.; KHANH, T. Q.: *“Präzise Bestimmung der thermischen und elektrischen Daten verschiedener Hochleistung - LED - Typen mit verschiedenen Leiterplatten- und Kühlungssystemen“*, Licht Tagung - Berlin, 2012, pp. 288-294
- [13] VINH, T. Q.; KHANH, T. Q.: *“Eine Analyse weißer LEDs - Lichtausbeute, Farbwiedergabe und Farbtemperatur“*, Zeitschrift Licht, Pflaum Verlag (München), Heft 11-12, 2012, pp. 70-75
- [14] VINH, T. Q.; KHANH, T. Q.: *“Kennzeichnung der Strom- und Temperaturverhalten von Hochleistungs - LED“*, Lange - Handbuch für Beleuchtung - 59.Erg.-Lfg.03/13, 2013, I - 6.13.13, pp. 1-6

Lebenslauf

Angaben zur Person

Geburtsdatum und -ort 04.Januar.1982 in Haiphong, Vietnam
Familienstand verheiratet
Staatsangehörigkeit vietnamesisch

Ausbildung

2000 - 2005 Hanoi Technische Universität, Hanoi, Vietnam

- Schwerpunkt: Industrielle Automatisierung
- Titel: Ingenieur Industrieller Automatisierung
- Abschlussarbeit Thema: *„Forschung, Design und Herstellung des automatisierten Geräts für Messung der Feuchtigkeit, Temperatur und des Taupunkts“*
- Note des Abschlusses: sehr gut

2006 - 2009 Hanoi Bergbau- und geologische Universität, Hanoi, Vietnam

- Schwerpunkt: Industrielle Automatisierung für den Bergbau- und Petroläther
- Titel: Master von Engineering in der Automatisierung
- Abschlussarbeit Thema: *„Forschung, Design des speziellen Soft-Starter-Steuergeräts, das für speziellen-Motor in Bergbau-Industrie mit Hochleistung und niedrigen Spannung angewendet wird“*
- Note der Verteidigung : 1,0

2009 - jetzt Doktorand in Fachgebiet Lichttechnik, TU Darmstadt, Deutschland

- Fachbereich: Elektrotechnik und Informationstechnik, TU Darmstadt.
- Schwerpunkte: LED Modellierung - Optimierung, Farbmischung, Leuchtstoffs - Mischung

Berufserfahrung

07.2004 - 06.2005 Mitglied der Forschung, Designs und Herstellung für Verkaufsautomaten, Forschungs- und Entwicklungszentrum der Hoch-Technik, Hanoi Technische Universität, Hanoi, Vietnam, Kontakt - cti@mail.hut.edu.vn

2005 - 2006 Mitarbeiter als Ingenieur in der Instrument Abteilung in der Firma CIMAS; CIMAS Engineering Company Limited is a joint-venture of CTCI Corporation, LILAMA Corporation and SINCERITY Engineering Company, Hanoi, Vietnam, Kontakt - hr@cimas.com.vn

09.2006 - 04.2007 Mitarbeiter in Cosmo-Firma, Hanoi, Vietnam, Kontakt - cosmo@vnn.vn
Tätigkeit: Design des automatisierten Systems, zur Messung, Beobachtung und Steuerung der Temperatur, Feuchtigkeit und des Taupunkts

2006 - 2009 Mitarbeiter in der Ableitung der industriellen Automatisierung für den Bergbau- und Petroläther, Hanoi Bergbau- und geologische Universität, Hanoi, Vietnam, Kontakt - hoptacquocte@humg.edu.vn
Schwerpunkte: Vorlesung, Betreuung und Projekte

2009 - jetzt Mitarbeiter am Fachgebiet Lichttechnik, Technische Universität Darmstadt, Deutschland, Kontakt - office@lichttechnik.tu-darmstadt.de